**University of Southampton**

Faculty of Natural and Environmental Sciences

Centre for Biological Sciences


# Molecular mechanism of nitric oxide-mediated regulation of intracellular cyclic-di-GMP in *Pseudomonas aeruginosa* biofilms

**by**

**Yuming Cai**

Thesis for the degree of Doctor of Philosophy

March 2018

***The great thing however is, in the show of the temporal and the transient to recognize the substance which is immanent and the eternal which is present...But this infinite variety of circumstances which is formed in this element of externality by the light of the rational essence shining in it - all this infinite material, with its regulatory laws - is not the object of philosophy...To comprehend what is, is the task of philosophy: and what is is REASON.——G.W.F.Hegel***

# Table of Contents

# **Academic Thesis:** Declaration of Authorship

I, Yuming Cai, declare that this thesis and the work presented in it are my own and have been generated by me as the result of my own original research.

Molecular mechanism of nitric oxide-mediated regulation of intracellular cyclic-di-GMP in *Pseudomonas aeruginosa* biofilms

I confirm that:

1. This work was done wholly or mainly while in candidature for a research degree at this University;
2. Where any part of this thesis has previously been submitted for a degree or any other qualification at this University or any other institution, this has been clearly stated;
3. Where I have consulted the published work of others, this is always clearly attributed;
4. Where I have quoted from the work of others, the source is always given. With the exception of such quotations, this thesis is entirely my own work;
5. I have acknowledged all main sources of help;
6. Where the thesis is based on work done by myself jointly with others, I have made clear exactly what was done by others and what I have contributed myself;
7. Either none of this work has been published before submission, or parts of this work have been published as:

   Dimerisation induced formation of the active site and the identification of three metal sites in EAL-phosphodiesterases

Signed: Yuming Cai……

Date: …05/03/2018……

# Acknowledgements

My most sincere thanks to Prof. Jeremy Webb and Dr. Ivo Tews for giving me the opportunity to study this project in the University of Southampton and for their inspiration, guidance, discussions and strong support throughout my PhD.

Great thanks to Prof. Zhizhong Wang and Dr. Lei Li for the discussion and the development of novel index Concentration Coefficient. Many thanks to Dr. Catherine Bryant and Dr. Rob Howlin for the guidance and correction during my writing of this thesis. Thanks to Dr. Sandra Wilks and Dr. Caroline Duignan for their detailed guidance and help in the CL2 lab, and to Dr. Curtis Phippen for his hand -by- hand help and guidance on molecular work as well as the fruitful discussions on developing gene knockout methods. Also, many thanks to Dr. Andrew Hutchin from crystallography for the precious collaboration, as well as discussions with Odel Soren for the nitric oxide mechanisms.

Thanks to all the members in Jeremy, Bill and Ivo's groups – for the help and happiness you brought to me during my 4 years in the UoS Microbiology Group. Furthermore, I would like to thank Prof. Martin Feelisch and Diogo Silva for their generosity in allowing me to use the CLD facilitate in Southampton General Hospital, as well as Dr. Eugen Stulz for the extremely kind offer and help in setting up and optimizing the HPLC protocol in his lab. Thanks to Dr. Myron Christodoulides as my internal examiner for providing me lots of valuable and insightful suggestions after my transfer viva, which helped me to improve my content arrangement in the final thesis.

Special thanks to all the friends I made in CfBS – Ibrahim Sayoh, Miguel Ramírez Moreno, Shulan Feng, Tianyu Wu, Benjamin Yarnall and Dave Cook – for the constant warmth and happiness you brought to me. Also thanks to all the friends I made in the hall of residences and back in China for their suggestions, help and support.

Finally, words are not enough for me to express my gratitude to my grandparents for their love, care and support all the time - making me who I am and allowing me to bravely pursue my dreams. This thesis was finished 3 years after my grandfather passed away, but his love and support were with me during the whole PhD, and will be with me for the rest of my life. I hope all my achievements can be deserving of what they were devoted to for so long.

# Abstract

Biofilms are defined as multicellular communities encased by a self-produced extracellular matrix. It is now well understood that most bacteria found in natural, clinical and industrial settings preferentially attach to surfaces or adhere to each other to grow as biofilms, causing serious problems due to their tolerance to conventional antibiotics. Previous studies have shown that low dose nitric oxide (NO) can trigger *Pseudomonas aeruginosa* biofilm dispersal by modulating the level of the intracellular secondary messenger cyclic dimeric guanosine monophosphate (c-di-GMP). Diguanylate cyclase (GGDEF motif) and phosphodiesterase (EAL/HD-GYP motif) activities are responsible for the synthesis and hydrolysis of c-di-GMP, respectively. Various sensor domains have been found to link environmental cues to modulation of GGDEF and EAL/HD-GYP activities, of which PAS and MHYT domains were of our interest due to their potentials to bind NO. In *P. aeruginosa* PAO1, a total of 14 proteins containing either PAS-DGC+/PDE or MHYT-DGC+/PDE were thought to be responsible for the NO-induced biofilm dispersal and were selected as our targets for investigation of their relationships between NO responses and biofilm phenotypes.

To investigate the response of *P. aeruginosa* biofilms to NO, a range of NO donors were first tested for their efficacies, of which 250μM Spermine NONOate (S150) showed outstanding results in dispersing ~60% batch cultured PAO1 biofilms within only 2 hrs. S150 was further applied to some cystic fibrosis *P. aeruginosa* clinical isolates (CF PA) biofilms *in vitro*. The results showed it successfully triggered the dispersal of surface-attached biofilms formed by 14 out of 17 CF PA strains tested, implying its potential for wide applications in clinical settings. However, S150 failed to disperse the non-attached cell aggregates formed by 4 CF PA in aqueous medium, suggesting a different mechanism might exist for clinical isolates to defend the drugs that requires much more attention. In order to facilitate future studies, a quantifying index, Concentration Coefficient, was proposed to evaluate the degree of cell aggregation by simply using one stacked CLSM image for a certain planktonic culture. This index may become widely applied for researchers to compare the cell aggregates more easily and accurately.

For mechanism studies, gene deletion was applied to 14 candidates for phenotypic analysis of mutants. An efficient gene knockout technique that minimizes cloning steps was developed and allowed for rapid generation of mutants. Phenotypic assays for 14

mutants suggested that PA0861 (RbdA) and PA5017 (DipA) play central roles in *P. aeruginosa* PAO1 for reducing intracellular c-di-GMP levels, enhancing swarming motility and triggering biofilm dispersal in response to NO. PA0847 and PA4601 (MorA) are involved in the regulation of biofilm dispersal and swarming/swimming motility, which were suspected to come from localized c-di-GMP pools due to their altered motility phenotypes without changes in intracellular levels. PA0285 and PA4959 (FimX) are responsible for both twitching and swimming motility, which contribute greatly to the 3D structures of the biofilms formed. Deleting either of these two proteins led to much enhanced biofilm dispersal upon NO treatment, providing insight that the deficiency in both Type IV pili and flagella functions may facilitate the elimination of *P. aeruginosa* biofilms.

In summary, evaluation of a broad range of commercially available NO donors showed that S150 was the most effective in dispersing laboratory and clinical *P. aeruginosa* strains in our experimental system. By using S150 and gene-deleted mutants, our research suggested several models whereby different proteins may be responsible for either coarse-tuning on intracellular c-di-GMP pools or fine-tuning on localized ones in response to NO, which collaboratively regulate the motility and biofilm dispersal in PAO1. This work has enhanced our understanding of the NO-c-di-GMP-swarming-dispersal pathway and its regulators in PAO1, shedding light on NO signaling mechanisms and providing potential new targets for therapeutic drug design.

# Abbreviations

| | |
|---|---|
| 3D | Three dimensional |
| $3OC_{12}$-HSL | N-(3-oxododecanoyl)-L-homoserine lactone |
| 5'-UTR | 5′ untranslated region |
| AC | adenylate cyclase |
| AHL | Acyl-homoserine lactone |
| Amp | Ampicillin |
| ATP | Adenosine triphosphate |
| BLUF | sensors of Blue-Light Using FAD (domain) |
| $C_4$-HSL | N-buytryl-L-homoserine lactone |
| CC | Concentration Coefficient |
| CCW | Counter-clockwise |
| CDC | Center for Disease Control |
| c-di-GMP | Cyclic Dimeric Guanosine monophosphate |
| CF | Cystic Fibrosis |
| CFU | Colony forming units |
| cGMP | Cyclic guanosine monophosphate |
| CLD | Chemiluminescence |
| CLSM | Confocal laser scanning microscopy |
| CR | Congo red |
| CV | Crystal violet |
| CW | Clockwise |
| DGC | Diguanylate Cyclase |
| DEACP | Cephalosporin-3'-diazeniumdiolate |
| DEA NONOate | Diethylamine NONOate sodium salt hydrate |
| DMSO | Dimethyl sulfoxide |
| DNase | Deoxyribonuclease |
| dNTP | Deoxynucleotide |
| DUWL | Dental unit waterlines |
| eDNA | Extracellular DNA |
| EDTA | Ethylenediaminetetraacetic acid |
| EPS | Extracellular polymeric substance |

| | |
|---|---|
| FAD | Flavin adenine dinucleotide |
| FWD | Forward (primer) |
| GFP | Green fluorescent protein |
| Gm | Gentamycin |
| GMP | Guanosine monophosphate |
| GSNO | S-nitroso-glutathione |
| GTP | Guanosine Triphosphate |
| HF | High Fidelity |
| H-NOX | Heme-nitric oxide/oxygen binding domain |
| HK | Histidine Kinase |
| HPLC | High-performance liquid chromatography |
| KO | Knockout |
| LB | Lysogeny broth |
| LPS | Lipopolysaccharides |
| MAC | microfluidic agarose channel |
| MAHMA NONOate | Methylamine hexamethylene methylamine NONOate |
| MCP | methyl-accepting chemotaxis proteins |
| MCS | multiple cloning site |
| MQ | Millipore Corporation ultrapure water |
| MV | Membrane Vesicles |
| NMR | Nuclear magnetic resonance |
| NO | Nitric Oxide |
| NO-NSAIDs | NO-Nonsteroidal anti-inflammatory drug |
| NOC-9 | MAHMA NONOate |
| NONOates | Diazeniumdiolates |
| NOS | NO synthase |
| OD | Optical Density |
| PA | *Pseudomonas aeruginosa* |
| PAS | Per-Arnt-Sim domain |
| PBS | Phosphate Buffered Saline |
| PCR | Polymerase chain reaction |
| PDB | Protein Data Bank |
| PDE | Phosphodiesterase |

| | |
|---|---|
| pGpG | Phosphate-Guanosine-Phosphate-Guanosine |
| PIA | Pseudomonas Isolation Agar |
| PKG | Protein kinase G |
| PMN | Polymorphonuclear leukocytes |
| PNA-FISH | Peptide Nucleic Acid Fluorescence In Situ Hybridisation |
| psl | polysaccharide synthesis locus |
| PTIO | Carboxy-PTIO potassium salt |
| Proli NONOate | Disodium 1-[(2-carboxylato)pyrrolidin-1-yl]diazen-1-ium-1,2-diolate methanol |
| PVC | Polyvinyl chloride |
| QS | Quorum Sensing |
| REV | Reverse (primer) |
| RNase | Ribonuclease |
| RR | Response Regulation |
| rSAP | Shrimp Alkaline Phosphatase |
| RSCV | Rugose small colony variant |
| S150 | Spermine NONOate |
| SCV | Small colony variant |
| SDS | Sodium dodecyl sulfate |
| SEM | Scanning electron microscopy |
| SGH | Southampton General Hospital |
| SNAP | S-nitroso-N-acetylpenicillamine |
| SNP | Sodium nitroprusside |
| SOE | Splicing by Overlap Extension |
| Strep | Streptomycin |
| TE | Tris-EDTA buffer |
| TEM | Transmission electron microscopy |
| Tet/Tc | Tetracycline |
| TIM | Triosephosphate isomerase |
| Tm | Melting Temperature |
| Tn | Transposon |
| UV | Ultraviolet |
| WT | Wild Type |

# Chapter 1 - Introduction

For centuries, microbiologists studied microbial cells only in their planktonic state or grown on nutrient agars in laboratories. It was not until 1977 when Harremoës first used the word "biofilm" in his publication[1]. Biofilms can be defined as multicellular communities encased in a self-produced extracellular matrix and attached to the surfaces[2,3]. With increasing research on free-swimming cells and biofilm-state cells developed, it is now widely understood that most of the bacteria found in natural, clinical, and industrial settings, and which cause serious human or medical device-related infection and water contamination, preferentially attach to surfaces[3,4]. These findings have led to intensive research to identify the mechanisms underlying this growth mode, particularly after it was found that they play an important role in tolerance towards antimicrobial compounds. In addition, biofilms can provide a heterogenetic microenvironment that significantly alters gene and protein expression and phenotypes, resulting in strong tolerance to antibiotics mainly due to the existence of persister cells[5,6]. As a consequence, unveiling the knowledge of biofilms should be deemed as urgent as discovering new antibiotics.

Roughly, biofilm development can be separated into five steps: (i) reversible attachment, (ii) irreversible attachment, (iii) maturation-1, (iv) maturation-2, and(v) dispersal[7], among which dispersal is the least understood[8]. Dispersal is an indispensable stage of the biofilm life cycle in which cells return to a planktonic state from biofilm mode leading to biological dispersal, bacterial survival, and the spread of diseases[8]. Such a coordinated manner involves many complex regulatory pathways and thus dispersal becomes a promising area of research which helps us find out novel ways for inhibition and treatment of biofilms in clinical or environmental settings[8].

Although still not fully understood, increasing numbers of studies on biofilm dispersal have been published[8]. One novel strategy for triggering biofilm dispersal involves nitric oxide (NO)[9], but the mechanism behind this needs further studies. This review aims to present some fundamental aspects of biofilm biology, particularly *Pseudomonas aeruginosa* which is extensively used as a model microorganism in biofilm research. Their regulatory pathways serve as the basis for dispersal mechanism studies as well as the progress in NO-mediated dispersal research. Elucidation of dispersal mechanisms

will be of benefits in controlling biofilm and developing new biofilm removal techniques.

# 1.1 Introduction to biofilm biology

## 1.1.1 Extracellular polymeric substance (EPS) of biofilms

One of the most distinct character differences between biofilm and planktonic cells is that biofilms are encased in a complex matrix (as shown in Fig 1.1.1) called extracellular polymeric substance (EPS). EPS is estimated to contain up to 97% water, as well as polysaccharides, proteins, eDNA, surfactants, lipids, some ions and other accessory matrix components. The matrix components of a single biofilm may vary spatially and temporarily in response to environmental changes or due to the growth and metabolism of the cells inside, while the matrix of different bacteria strains have various components. Generally, one or two of the components reach their maximum amounts in the biofilm matrix at a specific stage during biofilm development in combination with supplemental functions from other components[10].

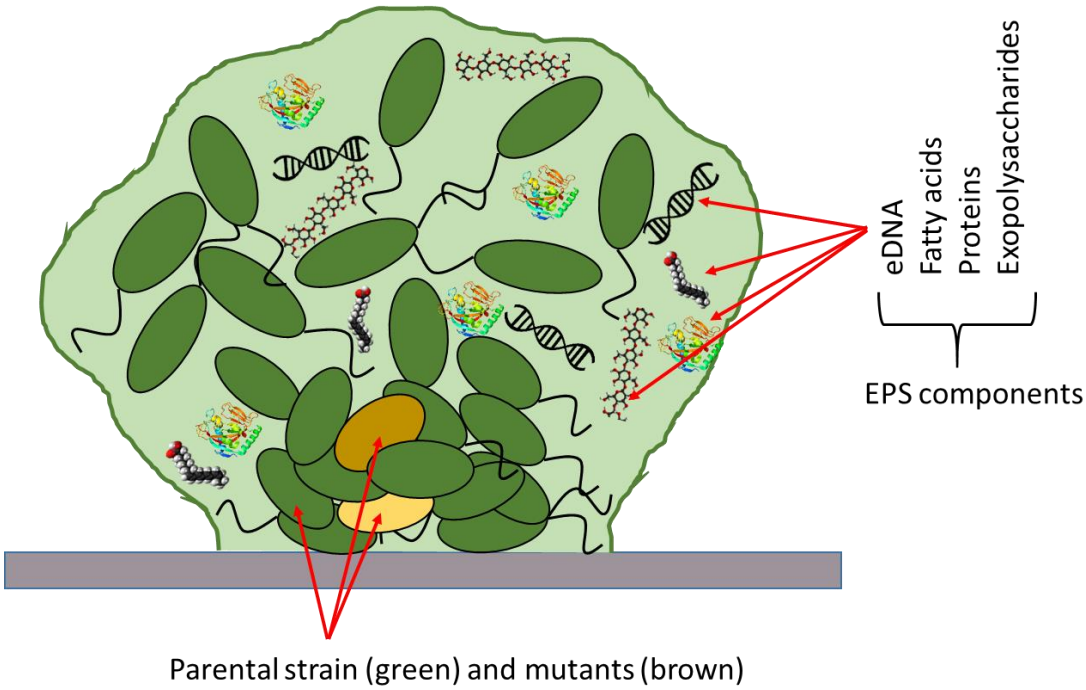


Fig 1.1.1 Typical complex structure of microcolonies in the mature biofilm with an extracellular polymeric substances (EPS) matrix composed of polysaccharides, extracellular DNA (eDNA), proteins, fatty acids etc.

Although it is extremely hard to provide a complete biochemical profile of most EPS samples, especially for carbohydrates due to the diversity in sugar monomers, linkages,

and unique structures, we still have some general ideas of the most frequently seen components within the majority of biofilm EPS concluded as follows:

| Components | Roles involved in biofilms |
|---|---|
| Exopolysaccharides | **a. Adhesion** (Initial and long term attachment)<br>**b. Cell Aggregation** (Increase cell density and cell-cell signalling)<br>**c. Biofilm Cohesion** (Determine biofilm structure and maintain its stability, create hydrated cell-cell interaction network, accumulate enzymes and nutrients)<br>**d. Retention of water** (Create a highly hydrated microenviroment beneficial for bacteria growth)<br>**e. Protective barrier** (Provide strong tolerance to antibiotics and host defences)<br>**f. Nutrient source** (Polysaccharides themselves can be used as nutrients and can absorb nutrients from surroundings) |
| Proteins | **(1) Adhesion** (Binding polysaccharides, facilitate cell–matrix or cell–cell interactions)<br>**(2) Cell Aggregation** (Increase cell density and cell-cell signalling)<br>**(3) Biofilm Cohesion** (Mediating the mechanical stability of biofilms together with polysaccharides)<br>**(4) Protective barrier** (Provide strong tolerance to antibiotics and host defences)<br>**(5) Enzymatic activity** (Digestion of exogenous macromolecules as nutrient and degrade EPS to release cells)<br>**(6) Structural proteins (cell surface-associated and extracellular carbonhydrate-binding proteins)** |
| Extracellular DNA (eDNA) | **a. Biofilm Cohesion** (Influence on the structure of biofilm EPS)<br>**b. Adhesion** (Used as adhesin)<br>**c. Gene exchange** (Horizontal gene transfer)<br>**d. Antimicrobial activities** (Contribute to inducible antibiotic tolerence) |
| Lipids | **Cell components export** (Phospholipids)<br>Lipopolysaccharides (Crucial for the attachment of some strains)<br>Biosurfactants (Influence microcolonies formation and biofilm structures) |

| | |
|---|---|
| Membrane Vesicles (MV) | **Cell components export** (Send enzymes and nucleic acids into the depth of the EPS matrix as "parcel") |
| Flagella, pili and fimbriae | **Initial attachment** (Mediate chemotaxis to enable planktonic cells to swim towards nutrients/signals, mediate motility to enable bacteria to reach and spread along the surface) |
| Dead cells----cell detritus | May have influence on matrix |

**Table 1.1.1** Main components of EPS and their functions **(**Adapted from The biofilm matrix[11])

## 1.1.2. Life cycle of biofilm

According to a relatively refined division, the development of biofilm goes through 5 stages (Fig 1.1.2)[7,12]:

**Stage 1-Initial attachment to the surface**

This step happens when bacteria swim close enough to the surfaces under the control of flagella to allow initial attachment. Forces that mediate this non-specific attachment include Lifshitz-van der Waals, Lewis acid-base, electrostatic forces and hydrophobic interactions[8,13]. At the end of this stage, cells can be easily removed by fluid shear forces[13].

**Stage 2- Irreversible attachment to the surface**

After initial attachment, the interaction between cells and substratum transits from a weak binding to a strong one. Cell clusters commence their development by using pili/fimbriae-mediated motility to propel the locomotion[12] as well as producing extracellular polysaccharides matrix (involving large amount of enzymes) and adhesins located at the surface of the bacterial cells[8,13]. At the end of this stage, the matrix firmly attaches the bacterial mass to the surface and much stronger physical or chemical forces are demanded to remove the cells[13].

**Stage 3-Early development of biofilm structure (maturation-1)**

The irreversibly attached bacterial cells grow and divide by using the nutrients present in the matrix and fluid environment, which leads to the formation of microcolonies that can enlarge to form a layer of cell clusters encased inside the EPS covering the surface[7,14]. This stage can be seen as the transition between initial attachment and

ultimate mature biofilm structure since biofilm development is an adaptive process governed by massive regulatory pathways. Therefore, many experts also put this and following maturation-2 stage together as the maturation stage.

**Stage 4- Maturation of biofilm architecture (maturation-2)**

At this stage, biofilms reach their maximum thickness, resulting in the generation of complex architecture, channels for nutrients exchange and a redistribution of bacteria inside the matrix[12]. Coordinated differentiation and heteromorphy of cell subpopulation also happens during maturation, because different locations of biofilm matrix undergo different microenvironment created by cellular juxtapositions during the earliest stages of biofilm formation[15]. Different cells respond to their specific microenvironmental conditions with different phenotypes or growth patterns[15]. Proteomic analyses and DNA microarray techniques have demonstrated that hundreds of proteins and biofilm-related genes have different expression levels between biofilm mode and planktonic mode[7,16,17,18]. Under these conditions, a mature biofilm with complicated structure gradually develops.

**Stage 5- Dispersal**

At this stage, biofilms release cells to the surrounding for the creation of another biofilm formation cycle at a new site[8]. The result is that the cells originally embedded in the matrix revert to the planktonic mode. After dispersal, cells can go on immigrating to the new niches and attaching to the new substrates, thus commencing another life cycle[8]. The forces that trigger dispersal can be roughly divided into two classes: (i) internal forces initiated by bacteria themselves (active) and (ii) external forces trigger dispersal (passive)[8]. Generally, there are three modes of dispersal recognized so far: (i) Erosion, referring to single cells or small clusters of cells continuously releasing from the matrix during the whole biofilm formation procedure[8]; (ii) Sloughing, referring to large portions of biofilm suddenly detaching during the later stages[19,20] (iii) Seeding dispersal (central hollowing), referring to massive single cells or small cell clusters rapidly releasing from hollow cavities located inside the biofilm[21,22].

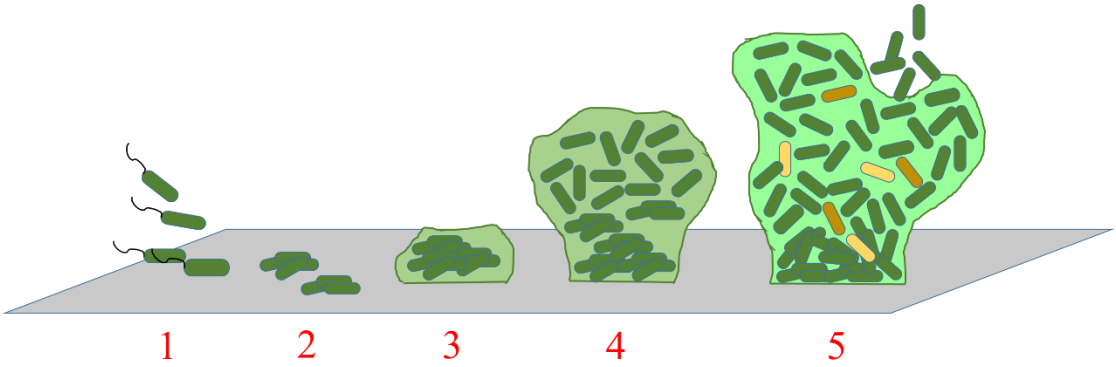

Fig 1.1.2 Five stages of *P. aeruginosa* biofilm development: (1) Initial attachment, (2) Irreversible attachment, (3) Maturation-1, (4) Maturation-2, and (5) Dispersal

## 1.1.3. Physiological heterogeneity in biofilm formation

During the five stages of biofilm formation and dispersal, certain bacteria undergo physiological adaptation and express different phenotypes compared to planktonic forms. Studies have shown that the differences include extracellular polymeric substance production, extracellular organelle production and sometimes distinct cell morphology result from different gene/protein expression or post-translational modification of various enzymes[6]. Due to the diffusional processes and cell metabolism which cause concentration gradients of nutrients, signalling molecules and bacteria waste inside biofilm systems[6], bacteria apply structural, chemical and biological heterogeneity in order to adapt to these various chemical conditions (Fig 1.1.3). As a result, cells in biofilm are not only distinct from planktonic cells, but also different from each other both spatially and temporally[6]. The best studied chemical heterogeneity include oxygen and nutrients concentration which decrease gradually from biofilm exterior to interior[23,24], while on the contrary the metabolic products increase with depth into the biofilm[6]. Moreover, in multispecies biofilm, the waste products from certain species can be used as substrate for another species, leading to a maximum concentration in the intermediate area of biofilm matrix. The concentration gradients of some other solutes such as nitrate, nitrite, carbon dioxide, methane and chlorine dioxide are dependent on the spatial organization of bacteria that consume or produce this solute[25–29].

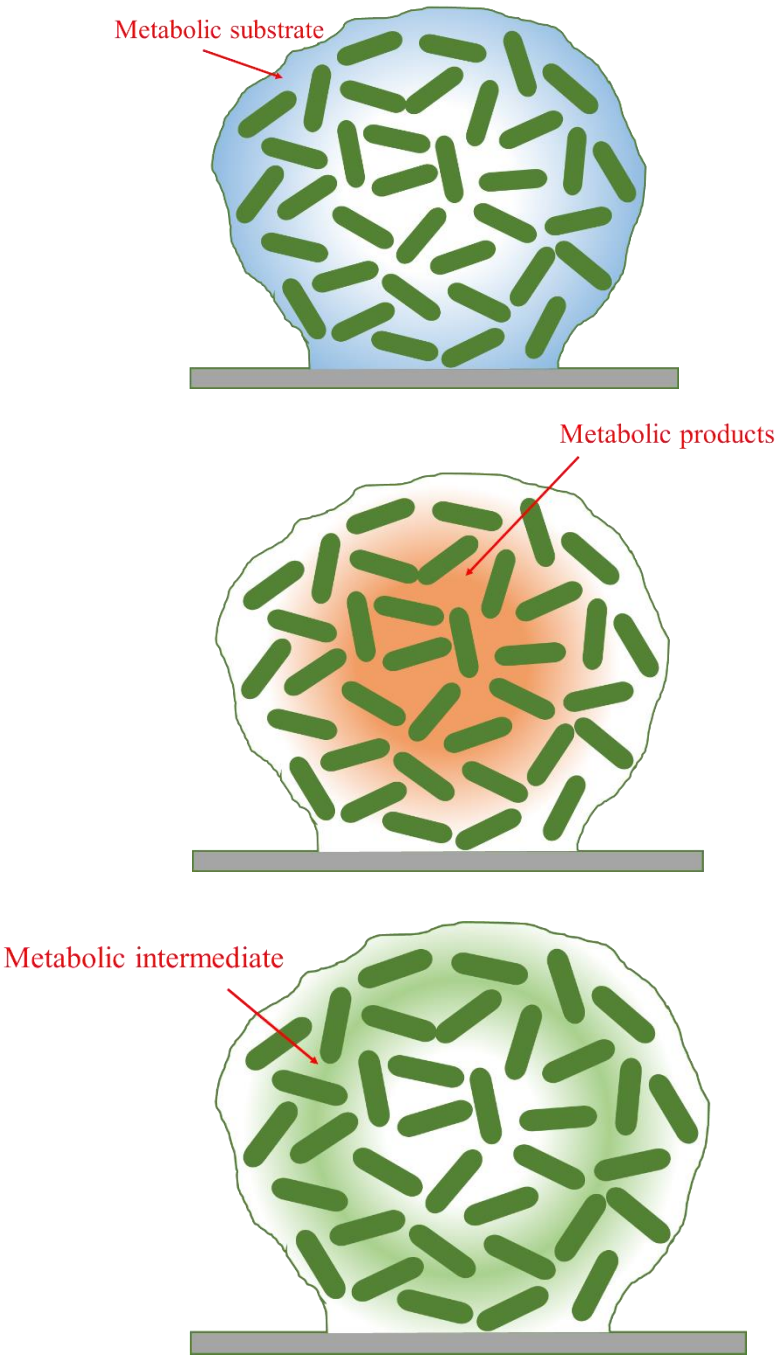


Fig 1.1.3 Chemical heterogeneity in the biofilms. The concentration of a metabolic substrate (a) consumed in the biofilm decreases with depth into the biofilm and distance away from the source. Conversely, the concentration of a metabolic product (b) increases with depth inside the biofilm. A metabolic intermediate (c) both consumed and produced within the biofilm shows concentration profiles that have local maxima.

Apart from displaying different transcriptomic, proteomic profiles as well as physiology characteristics between planktonic and biofilm cells[6] because of a large reservoir of regulatory genes helping bacteria to survive environmental changes, a small percentage of variant subpopulation often emerge during the growth of parent strains in a biofilm driven by mutation or recombination. This might provide insurance against detrimental

environmental changes as diversified population can be more robust than a single parent strain[6]. Provided by a fact that variants constitute 10% or more of a biofilm population during the first few days of biofilm formation[6], it is likely that both genetic rearrangements and natural selection play a part in the accumulation of variants. Also increasing the complexity is stochastic gene expression[30,31]. As this procedure is driven by cells themselves, it is independent from environmental affects and can lead to a broad distribution of expression levels. To sum up, many different factors cause cells' diversities in biofilm systems and benefit their growth and maintenance.

## 1.1.4. Why study biofilms?

Biofilms are found to appear in fossil records dating back to 3.3-3.4 billion years ago[32] and the structure was similar to ones that exist in the modern environment, but biofilm research has only recently begun. It is now demonstrated that most bacteria preferably attach to surfaces and the biofilm matrices provide protection, which make them more difficult to remove using traditional methods for planktonic cells. The significant influence of biofilms on human health and environment make it of high necessity to develop new techniques to fight against biofilms.

### 1.1.4.1. Device-related infections

Modern implant medical devices save millions of lives, but there is always a risk of surface-associated infection during surgeries (Table 1.1.4.1)[33]. The bacteria that are most frequently related to device infections are staphylococci (particularly *S. epidermidis* and *S. aureus*), *P. aeruginosa* and some other opportunistic pathogens coming from the environment. The main reasons why medical devices get infected easily are:

- Hydrophobicity and the electrostatic - Different materials will influence the interactions between the surface of material and cells[33].
- Bacterial surface proteins[33]
- Host molecules - Multiple specific receptors (adhesins) on the cell surface bind to host molecules such as fibronectin, fibrinogen/fibrin, collagen, laminin and vitronectin[33]. Namely, host inflammatory molecules facilitate adhesion to various host cell types as well as some non-biological surfaces coated with host plasma proteins[33].

| Medical devices | Associated species |
|---|---|
| Central venous catheter | *S. epidermidis, S. aureus,* ***P. aeruginosa****, C. albicans, K. pneumoniae* etc[34–38] |
| Prosthetic Heart valves and cardiac pacemaker | *S. epidermidis, S. aureus, Streptococcus* spp., Gram-negative bacilli, diptheroids, enterococci and *Candida* spp[34]. |
| Urinary Catheters | *S. epidermidis, Enterococcus faecalis, E.coli, Proteus mirabilis,* ***P. aeruginosa****, K. pneumoniae* and other Gram-negative bacteria[34] |
| Contact lenses | ***P. aeruginosa****, E. coli, S. aureus, S. epidermidis* and species of *Proteus, Serratia, Candida,* etc[34]. |
| Artificial hip prosthesis | ***P. aeruginosa****, S. aureus, enterococcus* spp[34]. |

**Table 1.1.4.1 Devices-related infections and associated bacteria (**Adapted from Biofilm: Importance and applications[34])

Currently in clinical trials, various antibiotic agents are either imbedded in device materials to reduce the biofilm formation on their surfaces or applied during surgeries to kill bacteria introduced into blood streams[34].

### 1.1.4.2 Biofilm and Pathogenesis

Apart from residing on implant medical devices, bacteria themselves are pathogenic and by forming biofilms, bacteria are easier to grow and resist medication, which in turn causes more serious infections. Below are listed some common diseases caused or complicated by pathogens and their biofilms (Table 1.1.4.2).

| Human Pathogenesis | Associated species |
|---|---|
| Cystic Fibrosis | *S. aureus, H. influenzae,* ***P. aeruginosa***[34] |
| Native Valve Endocarditis | *Streptococcus, Staphylococcus,* Pneumococci, *Candida, Aspergillus* and some Gram-negative species[34]. |
| Otitis Media | *S. pneumomoniae, Haemophilus influenzae, Moraxella catarrhalis, S. epidermidis,* ***P. aeruginosa***[34] |
| Chronic Bacterial Prostitis | *E. coli,* ***P. aeruginosa*** and species of *Klebsiella, Proteus, Serratia, Bacteroides* etc[34] |

| | |
|---|---|
| Periodontitis | *Porphyromonas gingivalis, Fusabacterium nucleatum, Peptostreptococcus micros, Eubacterium timidum, E. brachy, Pseudomonas anerobicus*[34] |

**Table 1.1.4.2 Biofilm-induced pathogenesis and associated bacteria (**Adapted from Biofilm: Importance and applications[34])

Depending on the organisms involved in the infections, different antibiotic treatments can be used. Furthermore, some vaccines are also used to prevent the initial colonization [34].

### 1.1.4.3. Biofilm in industry

#### Food industry

The food processing procedure is often rich in nutrients, wet and warm, which is ideal for the attachment of bacteria and the growth of biofilms. Bacteria that hide within the biofilm matrix escape from sanitizer, which increases the opportunity of microbial contamination. In the dairy industry, improperly cleaned and sanitized equipment and air-borne microflora are considered the major reasons for contamination[14]. EPS produced by existing biofilms offer attachment sites to newly arrived bacteria in a cleaned system[34]. As food contamination is closely related to human health and many severe diseases, even death, it is of high importance to develop reliable and eco-friendly ways to avoid bacteria attachment and biofilm growth. At present, good design of equipment, temperature controlling as well as the reduction of nutrients and water are effective ways to avoid biofilm formation in food industry. Some alkali agents or their combination with sequestrant/chelators are used to clean the potential biofilm growth sites and the sanitizers used in food industry are halogens, acids, peroxygens and quaternary ammonium compounds[34].

#### Paper industry

Process water is an ideal medium for microorganisms due to its high nutrient concentrations and appropriate temperatures ranging from 25 °C to 45 °C[39]. In the production of recycled paper, raw materials are the major sources that introduce bacteria into the system[39]. Volatile compounds produced by microbes (e.g., organic acids, sulphur compounds and amine compounds) and the development of biofilms can significantly lower the quality of the products[39]. Furthermore, increased use of recovered

paper and the closure of the water circuits lead to higher organic loads and water temperatures[39]. Traditional methods used by paper manufacturers include biocides such as chlorine, bromine, isothiazolones and glutaraldehyde as well as dispersants, but these reagents may result in increased resistance to biocides among bacteria and some reagents might not penetrate biofilm effectively. Furthermore, most biocides themselves cause pollution in the environment or have negative influence on paper quality[39]. As a consequence, enzymatic methods that not only reduce biofilm effectively but are also environmentally friendly are of the interest. Studies showed that glycosidases and lipases are not very efficient for biofilm removal, while commercial proteases such as Alcalase or Savinase (both serine type endoproteases) led to a significant reduction of proteins from the EPS matrix, which have great potential on an industrial scale[40].

#### 1.1.4.4. Biofilm and environment

In the environment, some biofilms growing in fast-moving water form filamentous structures while some growing in quiescent water form mushroom or mould-like structures[33]. These robust structures cause continuous contamination in hot springs and freshwater rivers, and the opportunistic pathogens exist in the water might lead to serious human illness if not properly treated. Other scenarios in which biofilms affect water are the deterioration of water quality during storage and in distribution systems[34], as well as dental-unit water systems[41,42].

**Biofilm in water distribution system**

Distribution system is of vital importance because even if the water is treated well, it can be contaminated due to the biofilms that form in the system such as the walls of containers and pipes. Various factors contribute to distribution system biofilm growth, such as pipe material, the disinfectants applied, the temperature and the resistance of biofilm to the disinfectants[34]. Disinfectants, when properly used, can be effective in the removal of microorganisms, but they can also enhance the amount of easily biodegradable substances which serve as nutrient to the biofilm and help microorganisms to re-grow[34]. As a consequence, the disinfectants that can maintain a long residual concentration are needed. Currently the most prevalently used disinfectants are chlorine, chloramines, ozone and hydrogen peroxide[34].

**Biofilm and dental unit waterline**

Dental unit waterlines (DUWL) are an integral part of dental surgery equipment, supplying water as a coolant for air turbine and ultrasonic scalers[43]. Biofilm formation is a universal problem in DUWL and great majority of bacteria that have been identified from DUWL are ubiquitous[43]. As aforementioned, contamination of water distribution systems may contribute to a low number of bacteria in DUWL but they will flourish to biofilms on the lumen surfaces of narrow-bore waterlines in dental units[43]. Patients as well as dentists are both at risk of being infected with opportunistic pathogens by means of cross-infection or aerosol formation from the water[43]. Different actions have been taken to control DUWL transmitted infections such as filtration, drying, biocides, sterile water delivery systems and the use of disinfectants[43].

## 1.2 *P. aeruginosa* biofilm formation and recalcitrance

*Pseudomonas aeruginosa* is a gram-negative bacterium notorious for its environmental versatility, strong disease-causing ability in particularly susceptible individuals and its high resistance to antibiotics. *P. aeruginosa* has the ability to adapt to and survive in many ecological niches, from water and soil to plant and animal tissues by utilizing a wide range of organic compounds as food sources, thus helping it to colonize almost everywhere, even where nutrients are limited. To increase the harm to human beings, *P. aeruginosa* can produce a number of toxic proteins ranging from toxins that kill host cells to degradative enzymes that permanently disrupt the cell membranes and connective tissues in various organs, which not only cause extensive tissue damage, but also interfere with the human immune system's defence mechanisms causing serious disease such as cystic fibrosis complications. At the same time, due to its high capacity to resist the antibiotics, it is very difficult to eradicate. *P. aeruginosa* has long been interested in not only for its ability to cause disease and resist antibiotics, but also its metabolic capability and environmental versatility. In recent years, due to the boost of biofilm research and the fact that *P. aeruginosa* is a good biofilm former, it has been widely used as a model for biofilm research.

With the advanced technologies in genetic research, the whole genome of *P.aeruginosa* was mapped over a decade ago and it is proved to possess a very large bacterial genome (6.3 million base pairs)[44]. Consistent with its large genome size among the bacterial kingdom, *P. aeruginosa* contains a high proportion of regulatory genes and a large number of genes involved in the catabolism, transport, efflux of organic compounds as

well as potential chemotaxis systems[44]. The mapping of *P. aeruginosa* opened the door for scientists all over the world to gain a deeper insight into the mechanisms of *P. aeruginosa* behaviours.

The structured biofilms produced by *P. aeruginosa* in standard flow cell system are described as 'mushroom' shapes and formed in a sequential process involving a non-motile bacterial subpopulation and a migrating bacterial subpopulation. The non-motile bacteria form the "stalks" of mushroom while the migrating bacteria form the "caps" part by climbing the stalks and aggregating on the tops.

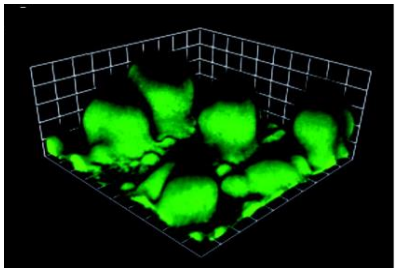

Fig 1.2 Mushroom-like 3D structure of *P. aeruginosa* biofilms observed using CLSM. Image taken from Iron and *Pseudomonas aeruginosa* biofilm formation[45]

## 1.2.1. Early attachment events in *P. aeruginosa* biofilms

### 1.2.1.1. Initial attachment

Biofilm formation begins by bacteria cells sensing the environmental conditions and attaching to surfaces[46]. Various environmental cues can influence biofilm formation, including surface hydration[47], nutrients[48], pH[49], temperature[50], osmolarity[51], iron[45] and oxygen[46]. After sensing the specific environmental conditions that are suitable for settling down, the flagella on the bacteria cell surface promote the swimming of organisms along the surfaces as if they are scanning for a proper location to attach[46], and this kind of attachment is called reversible attachment. Flagella mutants of *P. aeruginosa* that lead to dysfunction of flagella synthesis or rotation result in much impaired cell attachment on different substratum compared with wild type strain. These indicate that both environmental cues and flagella mediated-swimming motility are very important in the biofilm initial attachment stage[52].

### 1.2.1.2. Early attachment events

**Type IV pili-mediated twitching motility**

Once reversible attachment is established, the cells maintain contact with substratum and start irreversibly attachment to develop into 3D structure biofilms. One way for cells transiting to this permanent attachment is mediated by Type IV pili. Time-lapse microscopy indicated that after initial attachment, *P. aeruginosa* cells can continue to move on the surfaces using twitching motility (extend and retract) which absolutely depends on Type IV pili but is ~100 fold slower than swimming mediated by flagella. The formation of cell clusters (microcolonies) is the consequence of individual cells twitching across the surface towards each other, which can also help to strengthen the attachment[52,46].

**Production of EPS**

The mechanisms and regulations of biofilm formation of *P. aeruginosa* cannot be separated from its EPS and the characteristics of the bacteria cells *per se*. The types of EPS components of *P. aeruginosa* are in accordance with those listed in Table 1.1.1. Alginate, Pel and Psl are all *P. aeruginosa* biofilm EPS components, but different strains contain different types and quantities of exopolysaccharides. For example, PA14 is a naturally Psl-deficient strain, while PAO1 can express all three types. In PAO1, confocal laser scanning microscopy showed that mutants deficient in alginate biosynthesis have a decreased proportion of viable cells and decrease susceptibility of biofilms to antibiotic treatment[53], indicating a role of alginate in viability of cells in biofilms[54]. Also, mutants producing only alginate (deficient in both Psl and Pel) lose their ability to form biofilms[54]. Psl is involved in initial attachment of cells. Mutants deficient in Psl showed reduced biomass at an early stage of biofilm development and cannot be compensated by alginate or Pel. The formation of typical mushroom-like structures requires Psl, while the Pel play a role in biofilm cell density and/or the compactness of the biofilm[66]. Psl form a peripheral meshwork covering the cap region of mature mushroom-like microcolonies[22,55], while Pel, together with eDNA, might play a role in cell-to-cell interactions and provide a structural scaffold for the community at early stages of biofilm formation[56]. Furthermore, the deficiency of Psl can enhance the production of Pel, and the absence of Pel increases the production of alginate[54]. Thus, various exopolysaccharides produced at different stages in different species interactively contribute to the biofilm architectures of *P. aeruginosa*.

**LPSs**

Lipopolysaccharides (LPS) are large molecules that consist of a lipid and a polysaccharide composed of O-polysaccharide chain, outer core and inner core (oligosaccharides) joined by a covalent bond. They are found in the outer membrane of Gram-negative bacteria. Many studies showed that whether there is O-polysaccharide chain or not has significant influence on the overall surface charge and hydrophobic character of the Gram-negative cell surface, which also results in changes in attachment behavior[57]. The most heterogeneous portion of LPS is the O-antigen that confers serum resistance to the organisms. *P. aeruginosa* possess two chemically and immunologically distinct types of LPS termed A and B bands. A-band LPS contains a conserved O polysaccharide region with shorter chains mainly composed of D-rhamnose and 2-keto-3- deoxyoctonic acid, while B-band structure varies among 20 O serotypes of *P. aeruginosa*[58].For example, PAO1 (O5 serotype) subunit comprise two uronic acid derivatives and one N-acetylfucosamine residue. Furthermore, B band is significant for the cells to attach to hydrophilic surfaces while the loss of A-band has only mild effects on attachment[57].

### 1.2.2. Quorum-sensing and the development of *P. aeruginosa* biofilms

Following the initial settling down, the bacteria begin constructing a more robust and protective biofilm for them to live in. There are two distinct characteristics in this biofilm maturation stage:

a. EPS synthesis is increased and its structure becomes more complex.
b. The development of antibiotic tolerance.

Both these two changes are related to complicated regulatory pathways, of which Quorum-sensing (QS) is so far the best known. QS is used to describe intercellular signalling pathway in bacteria that involves the synthesis, secretion, and sensing of small chemical molecules called autoinducers such as Acyl-homoserine lactone (AHL)[8,59]. When cell density increases, the concentration of autoinducers increases simultaneously and after reaching a threshold, autoinducers trigger the transcription of biofilm specific genes[8]. Two *P.aeruginosa* quorum sensing systems, LasR-LasI and RhlR-RhlI, were found to involve in the expression of hundreds of genes (315 upregulated and 38 repressed)[60]. The *lasI* gene produces an extracellular signal called N-(3-oxododecanoyl)-L-homoserine lactone ($3OC_{12}$-HSL). The *lasR* product is a transcriptional regulator that responds to sufficient levels of $3OC_{12}$-HSL to activate a number of virulence genes as well as the rhlR-rhlI system. The *rhlI* product directs the

synthesis of another extracellular signal called N-buytryl-L-homoserine lactone (C4-HSL), which is required for both the activation of virulence genes and the expression of the stationary-phase σ factor, RpoS (discussed in next section)[61]. RhlR is a transcription factor that responds to C4-HSL. Both *lasI* and *rhlI* mutants can form biofilm on surfaces, but *lasI* mutant microcolonies are thin, undifferentiated and sensitive to antibiotics compared to wild type and *rhlI* mutant[36]. By adding $3OC_{12}$-HSL to *lasI* mutant the biofilm development can be restored[36]. These all indicate that acyl-HSL mediated QS system is of high significance in biofilm architecture and maturation.

Quorum sensing is related to numerous traits of bacteria activities including surface attachment, biosurfactant synthesis, sporulation, competence, bioluminescence as well as the production of multiple extracellular virulence factors[62–67]. Shrout *et al* showed that QS can control early stages of biofilm development through regulation of swarming motility under certain nutritional conditions[68]. Sakuragi *et al* showed that the transcription of the *pel* operon is greatly reduced in *lasI* and *rhlI* mutants while Davies *et al* demonstrated alginate genes *algC* and *algD* are induced by $3OC_{12}$-HSL and $3OC_4$-HSL, thus connecting QS and the transcription of genes responsible for biofilm matrix biosynthesis[12,69].

## 1.2.3. The recalcitrance of *P. aeruginosa* biofilms

Resistance means the ability of microorganisms to propagate in the presence of a bactericidal or bacteriostatic antimicrobial agent at a concentration that would normally inhibit the growth. In contrast, tolerance means that a microorganism can survive in a bactericidal concentration of antimicrobial agent, but neither grow nor die. In most cases, bacteria in a biofilm employ both resistance and tolerance when facing an antimicrobial challenge, and some researchers use 'recalcitrance' to describe the reduced susceptibility of biofilm cells to antibiotics[70]. Hence, both the resistance of planktonic *P. aeruginosa* and the tolerance of its biofilms are briefly reviewed here.

### 1.2.3.1. Antibiotic resistance in *P. aeruginosa*

The notorious characteristic of *P. aeruginosa* is its high intrinsic resistance to a myriad of common antibiotics, including aminoglycosides, fluoroquinolones and β-lactams compared to many other pathogens. As such, the eradication of *P. aeruginosa* has been more difficult in different settings, leading to vast research ranging from fundamental antibiotic resistance mechanisms to new therapeutic methods.

## Mechanisms of intrinsic resistance

### First line barrier - Low outer membrane permeability

The outer membranes of Gram-negative bacteria work as selective barrier against the uptake of antibiotics through their different sizes of porin channels[71]. Compared to *E. coli*, *P. aeruginosa* bears a much lower (12-100 times) outer membrane permeability[72], which is also thought to be the major character that distinguishes *P. aeruginosa* from other Gram-negative species regarding antibiotic resistance[73]. *P. aeruginosa* outer membrane contains porins that form water channels for diffusion of hydrophilic molecules. The only general porin in *P. aeruginosa* is OprF, which allows for non-specific diffusion of ionic species and small polar nutrients[74], including polysaccharides up to 1.5 kDa in size[75], and possibly some antibiotics[76]. Hence, OprF forms a majority of small channels and a minority of larger channels in *P. aeruginosa* outer membrane[73]. In addition to OprF, some specific porins are in charge of passaging certain types of antibiotics or antibiotic-sized molecules, such as OprD for delivering carbapenem antibiotics, basic amino acids and peptides, while OprB takes up sugars and saccharides[73,77]. Although acting as the first line of defence and decisively reducing drug uptake, equilibration of hydrophilic molecules across the outer membrane can be reached in seconds[78]. Therefore, the following secondary mechanisms – efflux pumps and inducible enzymatic degradation of antibiotics, play more important roles in fighting against different categories of antibiotics.

### Second line barrier – Efflux pumps

Several efflux systems have been identified to markedly contribute to intrinsic antibiotic resistance, such as MexAB-OprM, MexXY-OprM, MexCD-OprJ and MexEF-OprN. They belong to prototype RND (resistance-nodulation-division), containing a cytoplasmic pump protein, a periplasmic linker protein and an outer-membrane protein[73]. MexAB-OprM has the broadest substrate spectrum, removing some β-lactams, chloramphenicol, fluoroquinolones, macrolides, novobiocins, sulfonamides, tetracycline and trimethoprim, as well as various dyes and detergents[79]. MexCD-OprJ extrudes quinolones, erythromycin, tetracycline, chloramphenicol, and expanded-spectrum cephems such as cefpirome[80,81]. MexEF-OprN transports chloramphenicol and quinolones[82]. MexXY-OprM has a primary role in resisting

aminoglycosides and erythromycin[83,84]. Taken together, these efflux systems decisively result in the high resistance of *P. aeruginosa* to a wide range of antimicrobial reagents.

**Adaptive resistance**

The continuous presence of certain antibiotics or environmental stimulus can induce adaptive resistance. β-lactam antimicrobial agents have been most commonly used for bacterial infections and prominently contribute to the resistance to β-lactam antibiotics among Gram-negative bacteria worldwide[85]. β-lactam antibiotics inhibit bacterial cell wall biosynthesis through binding an acylate active site of penicillin-binding protein (PBP), consequently leading to cell lysis and death. However, bacteria can produce an enzyme, β-lactamase, to hydrolyse β-lactam ring and deactivate β-lactam antibiotics[86]. *P. aeruginosa* has an inducible chromosomal AmpC-like β-lactamase encoded by gene *ampC*[73]. Pre-exposure of *P. aeruginosa* to some β-lactam antibiotics can induce the expression of *ampC* gene, resulting in the enzymatic inactivation of the including and many other β-lactams[78]. Different β-lactams differ in their inducing abilities. For instance, some penicillins and cephalosporins such as ampicillin, amoxicillin, cefazolin and cephalothin are both strong inducers and substrates for AmpC β-lactamase. Cefoxitin and imipenem are strong inducers but can be difficult to be hydrolysed. On the contrary, some β-lactams such as ceftazidime, cefepime, piperacillin and aztreonam are weak inducers and weak substrates, and can only be hydrolysed when the enzyme is overproduced[87].

Similarly, genes encoding efflux pumps can be overexpressed under the induction of certain sub-inhibitory concentrations of antibiotics. For example, MexXY pump can be induced by exposure to aminoglycosides, and efflux pump overexpression often leads to upregulated multidrug resistance[88].

**Acquired resistance: horizontal transfer and mutational resistance**

When the intrinsic resistance of *P. aeruginosa* to antibiotics has already caused the remarkable difficulties in its eradication, acquired DNA elements from the environment or other species, such as plasmids, upgrade its barrier. Such external DNA acquisition has been found in *P. aeruginosa* where aminoglycoside modifying enzymes, β-lactamase and even extended-spectrum β-lactamases were transferred and proliferated[78].

Mutational resistance in common *P. aeruginosa* strains can happen spontaneously, although the resistance frequencies between antibiotics vary ranging from $10^{-6}$ to $10^{-9}$. In a background of hypermutator strains that contain mutations in genes involved in the efficient repair of DNA replication errors, the resistance mutation frequency can be increased up to 70-fold[89]. Some key regulatory mutations such as *nalB* (*mexR*), *nfxB*, *nfxC* (*mexT*) and *mexZ* cause the overexpression of four main efflux systems, MexAB-OprM, MexCD-OprJ, MexEF-OprN and MexXY-OprM, respectively[90,91]. These mutations lead to distinct but substantially overlapping multiple antibiotic resistance profiles. In contrast, mutation in *ampD*, an effector of *ampC*, results in the derepression of *ampC* and thus the hyperproduction of β-lactamase targeting lots of different β-lactams[78].

Apart from the systematic upregulation of multi-drugs resistance through the overexpression of efflux pumps or β-lactamase, certain mutations lead to resistance towards specific antibiotics. For instance, mutations in *gryA* and *gryB* (gyrase), as well as *parC* and *parE* (topoisomerase IV) can reduce fluoroquinolone binding affinity[92]. Polycationic antimicrobials pass across the outer membrane by self-promoted uptake, and the *arnBCADTEF* operon can mediate the addition of 4-aminoarabinose to Lipid A of LPS, blocking this uptake and leading to the resistance. Some two-component regulatory systems, PhoPQ, PmrAB and ParRS, were found to be activated in the presence of polymyxins, antimicrobial peptides or colistin and induce *arn* operon, changing the susceptibility to polymyxins and cationic antimicrobial peptides[93,94].

**Common treatments and the mechanisms of resistance in *P. aeruginosa***

| **Class** | **Agents** | **Advantages** | **Disadvantages** | **Resistance mechanisms** |
|---|---|---|---|---|
| **Penicillin** | Ticarcillin<br>Carbenicillin<br>Piperacillin<br>Tazobactam | Synergistic with aminoglycosides against *P. aeruginosa* | May induce β-lactamases in *P. aeruginosa* | Induced chromosomal β-lactamase, overexpression of MexAB-OprM due to *nalB* mutation, and acquired β-lactamase gene externally |

| | | | | |
|---|---|---|---|---|
| **Cephalosporin** | Ceftazidime<br>Cefoperazone<br>Cefepime<br>Cefpirome | Can be used singly in *P. aeruginosa* | May induce β-lactamases in *P. aeruginosa* | Induced chromosomal β-lactamase, overexpression of MexAB-OprM due to *nalB* mutation. For cefepime and cefpirome, overexpression of the MexCD-OprJ due to *nfxB* mutation |
| **Aminoglycoside** | Gentamicin<br>Tobramycin<br>Amikacin | Synergistic with β-lactams against *P. aeruginosa* | Narrow therapeutic/toxic ratio; penetrate poorly into cerebrospinal fluid | Overexpression of the MexXY efflux pump due to a mutation in *mexZ*; acquired modifying enzymes gene externally |
| **Quinolone** | Ciprofloxacin | Oral treatment accessible | Contraindicated in children under 16 years of age | Mutations in *gyrA/gyrB* for topoisomerase subunit inactivation. Mutations in *nalB*, *nfxB* or *nfxC* for overexpression of efflux pumps |
| **Polymyxin** | Colistin | Highly active and without much resistance developed so far | Possible toxicity concerns; used largely in CF patients | PhoP/PhoQ regulatory mutations for LPS changes |
| **Carbapenem** | Imipenem<br>Meropenem | Broad spectrum of activity against Gram-negative bacteria, including *P. aeruginosa* | May induce β-lactamases in *P. aeruginosa*; rapid development of resistance | Mutation in nfxC for reducing OprD and upregulating MexEF-OprN |

Table 1.2.3.1.1. Antibiotics commonly used in the treatment of *P. aeruginosa* infections and the main resistance mechanisms of *P. aeruginosa* to these drugs. Content adapted from Hancock and Speert, Antibiotic resistance in *Pseudomonas aeruginosa*: mechanisms and impact on treatment[73].

## Alternative non-antibiotic therapeutic options

| Class | Agent | Mechanism |
|---|---|---|
| Quorum sensing and quenchers (QSI) | Furanone, lyngbyoic acid, *cis*-2-dodecenoic acid, iberin, PD12, meta-bromo-thiolactone, eugenol, 6-gingerol, ajoene, macrolide antibiotic azithromycin (AZM) | Virulence and biofilm formation of *P. aeruginosa* depend on its quorum sensing system. QSIs inhibit the production of virulence factors such as proteases, pyoverdin, chitinase and exoprotease |
| Lectin inhibitors | Fucose, galactose | LecA and LecB bind to the fucose-specific and galactose-specific receptors of the lung epithelial cells. This binding can be blocked by inhalation of competitive inhibitors fucose and galactose. |
| Iron chelators | Gallium (Ga), gallium exchanged carboxymethyl cellulose, desferrioxamine-gallium (DFO-Ga) complex and gallium maltolate | Iron is essential for growth and the functioning of key enzymes involved in protein and DNA synthesis, electron transport and oxidative stress in *P. aeruginosa* planktonic cells or biofilms. Iron analog and iron chelators disrupt iron metabolism. |
| Efflux pump inhibitors | Phenyl-arginine-β-naphthylamide (PAβN) | Inhibit efflux pump and AmpC β-lactamase |
| Lactoferrin and hypothiocyanite combination | Lactoferrin + hypothiocyanite | CFTR dysfunction prevents airway epithelium to transport thiocyanate ($SCN^-$). $SCN^-$ can be oxidized by $H_2O_2$ in the presence of lactoperoxidase (both $H_2O_2$ and lactoperoxidase secreted at the surface of airway surface) to generate hypothiocyanite with antimicrobial activity. Supplement of Lactoferrin and hypothiocyanite restores the antimicrobial function of airways. |
| Phage | Bacteriophages such as MPK1, MPK6 and PAK-P1 | Lytic bacteriophages can target and kill bacteria even within the biofilms |
| Antimicrobial peptides (AMP) | | AMP binds to LPS with high affinity, causing the displacement of divalent cations that stabilize the outer membrane, self-promoted uptake of the destabilizing compound across the outer membrane, subsequent channel formation in cytoplasmic membrane and cell death |
| Probiotics | Probiotic *Lactobacillus plantarum* whole culture or culture filtrates | Affect quorum-sensing signal molecules (acyl-homoserine-lactones), inhibit elastase |

| | | |
|---|---|---|
| | | production and biofilm formation |
| Vaccines | Mice *in vivo* experiments: Vaccines towards flagella, pili, alginate, outer membrane proteins (OMP) and purified type III translocation protein<br><br>Preclinical trial: PhoB, type IV pilin-exotoxin A toxoid, Octavalent O-polysaccharide-toxin A conjugate, 3-oxo-C12-HSL-carrier protein conjugates, live-attenuated *P. aeruginosa aroA* deletion mutant strain and plasmid vaccine harbouring oprF. | Stimulates the body's immune system to recognize the agent during invasion without causing harm. Immune system destroys the agent, and to further recognize and destroy any of the microorganisms associated with that agent when it encounters afterwards |
| Nanoparticles | Zinc oxide, copper oxide, iron (III) oxide, titanium dioxide, lanthanum calcium manganate (LCMO), ceria ($CeO_2$), gold-functionalized magnetic, silver:gold alloy, dextrose reduced gelatin capped-silver and NO-releasing silica nanoparticles | Tiny particles of size less than 1μm with large surface to mass ratio. Penetrate through the bacteria membrane, causing ROS production that damage cellular components and membrane, inactivation of cellular proteins and enzymes essential for ATP production and DNA replication |

Table 1.2.3.1.2. Non-antibiotic antimicrobial agents as alternative treatments to prevent or solve *P. aeruginosa* antibiotic resistance. Adapted from Chatterjee *et al*, Antibiotic resistance in *Pseudomonas aeruginosa* and alternative therapeutic options[95].

## 1.2.3.2. *P. aeruginosa* biofilm tolerance

### Matrix as barrier

It has now been agreed in the literature that purely insufficient penetration/diffusion is not the major explanation for increased antimicrobial tolerance in biofilms. However, this rule may apply to certain antibiotics, and the diffusion limit varies depending on bacterial strains and biofilm growth experimental setups[70]. So far, the most notable example showing how failure of antibiotic penetration determines *P. aeruginosa* biofilms tolerance is tobramycin. The possible mechanism might be positively charged tobramycin molecule interacts with matrix components, and this hypothesis is reinforced by the fact that given enough exposure, tobramycin can eventually penetrate through[96,97].

As such, certain EPS components may interact with specific antibiotic. Different *P. aeruginosa* strains may produce Psl, Pel and alginate in their matrices, and eDNA plays an important role in EPS structure. Psl was proposed to deactivate antibiotics through

electrostatic interactions, hence contributing to the resistance to colistin, polymyxin B, tobramycin and ciprofloxacin at early stages of *P. aeruginosa* biofilm development[98]. Pel may provide protection against tobramycin and gentamicin as the gene-deleted mutant *ΔpelB* biofilms were more susceptible to these two antibiotics. It has been hypothesized that Pel sequester antibiotics through ionic binding, but the detailed mechanisms needs further investigation[56]. Mulcahy *et al* suggested that sub-inhibitory concentration of eDNA chelates magnesium ion and can create a cation-limited environment in EPS. This depletion can activate PhoPQ-PmrAB two component system and regulate antimicrobial resistance *arn* operon in *P. aeruginosa*. This results in up to 2560-fold increased resistance to cationic antimicrobial peptides and 640-fold increased resistance to aminoglycosides, but does not influence β-lactam and fluoroquinolone resistance[99]. Chiang *et al* further proved that eDNA in EPS, acquired either endogenously or exogenously, acts as an antimicrobial shield by physically binding positively charged aminoglycosides and antimicrobial peptides. In addition to serving a physical role, eDNA may also involve in horizontal transfer as the carrier of antibiotic gene targeting natural recipients[70].

## Physiological heterogeneity - Oxygen depletion and slower metabolism

Gradients of oxygen, nutrient, waste products and signalling factors due to the complex 3D structure of biofilms allow for cells experiencing different micro-environments within the same biofilm. This results in the physiological heterogeneity with different gene expression patterns, metabolic activity and phenotypes, including antimicrobial tolerance[70].

Several reports claimed the steep oxygen gradient exists within biofilms of various species, with the deep layer cells going through hypoxic state[70] and these oxygen-limited cells are more tolerant to antibiotics. For instance, Borriello *et al* showed that bacterial subpopulations growing in oxygen-replete regions within *P. aeruginosa* biofilms tend to be killed more easily by tobramycin, ciprofloxacin, carbenicillin, ceftazidime, chloramphenicol, or tetracycline compared to subpopulations growing in oxygen-limited regions[100]. Similarly, Werner showed that antibiotic-induced cell damage were predominantly at the air-biofilm interface where cells possess higher protein synthetic activity[101]. The ability of certain antibiotics (such as β-lactams) to kill bacteria has long been linked to bacterial growth rate. Hence, the reduced cell

metabolism activity contributed by oxygen limitation may result in selective tolerance to some antibiotics.

Another mechanism may be hypoxia affects multidrug efflux gene expression. For example, *mexEF-oprN* genes are upregulated in oxygen depleted planktonic cells and confer a certain degree of antibiotic resistance. Although not examined in biofilm, this operon may contribute to antibiotic resistance of biofilm subpopulations in area with low oxygen[102,103]. Meanwhile, another major efflux *mexCD-oprJ* was shown to be transcriptionally upregulated in *P. aeruginosa* biofilms grown under low oxygen conditions[104].

Persister cells are a small number of cells in biofilm that are dormant and non-growing. As such, these cells are tolerant to some antibiotics that are effective against actively growing cells and stay persistent. Some early statements demonstrated that the majority of *P. aeruginosa* biofilm cells are equally susceptible compared to planktonic cells, and the increased tolerance of biofilms to antibiotics relies on the higher amounts of persister cells inside[105]. However, many factors mentioned here proved that antibiotic tolerance can be the outcome of the collaboration of many mechanisms in different strains under different conditions. Persister cells may be contributing, but are not fully responsible for the tolerance.

## Stress responses

**General:** Slow growth rate of some cells within the biofilm was thought to be not owing to nutrient or oxygen limitation *per se*, but to a general stress response initiated by growth in a biofilm and centrally regulated by σ factor RpoS. Recently, it was shown that RpoS is required for the induction of another gene, *ndvB*[106]. *ndvB* expression is elevated in biofilms, and encodes a glucosyltransferase enzyme that catalyses the synthesis of periplasmic β-(1→3)-cyclic glucans, which physically binds to cationic aminoglycosides such as kanamycin and tobramycin. This interaction sequesters these antibiotics in the periplasm and prevents them from breaching inner membrane and targeting their cellular targets[5,107].

**Oxidative:** There is one hypothesis highly debated currently, where bactericidal antibiotic kills cells by inducing cellular respiration and the production of lethal levels of ROS[108]. These hydroxyl radicals contribute to cell death by oxidising substrates such

as deoxyguanosine triphosphate and DNA[108,109]. Although still at the stage of hypothesis, it is logical to assume that tackling antibiotic-induced ROS may be one of the mechanisms for biofilm cells to achieve high antibiotic tolerance. For example, even sub-inhibitory concentrations of ciprofloxacin uplifts the ROS level and reduces cellular viability, but can be partially detoxified by an antioxidant catalase, KatA[110]. However, *P. aeruginosa* biofilms contain less catalase activity compared to the planktonic counterpart, suggesting KatA may contribute to the biofilm tolerance due to its antioxidant activity, but is not the prominent factor[111].

**Stringent response:** Amino acid starvation can increase the number of stalled ribosomes carrying deacetylated tRNA molecules, which recruit pppGpp synthesis. pppGpp can be converted into ppGpp, and (p)ppGpp interacts with RNA polymerase. This procedure can lead to many transcriptional changes such as the downregulation of ribosomal protein genes and upregulation of amino acid biosynthetic genes, permitting bacterial survival during starvation[70]. The gradient in biofilms may cause nutrient limitation or depletion in a subset of cells, thus triggering a stringent response. It was proposed that a stringent response contributes to antimicrobial tolerance in biofilms by reducing oxidative stress, as the activation of a stringent response prevents the accumulation of pro-oxidant 4-hydroxy-2-alkylquinolines (HAQs)[112,113]. Furthermore, a stringent response can also upregulate antioxidant catalase such as KatA abovementioned[114]. As such, it is very likely a subpopulation in *P. aeruginosa* biofilm go through nutrient starvation and trigger the stringent response, which increases antimicrobial tolerance by reducing oxidative stress.

## Efflux pumps in biofilms

While efflux pumps play a vital role in planktonic cells antibiotics resistance, they can also affect antimicrobial tolerance in biofilms. Apart from the four major efflux systems mentioned previously, Zhang and Mah identified another biofilm specific multidrug efflux pump encoded by PA1874-1877 operon, which is 10 times more highly expressed in *P. aeruginosa* biofilms compared to planktonic cells. While PA1874 does not show significant influence on antibiotic resistance, deletion of PA1875, PA1876 and PA1877 individually all result in an increase in susceptibility to tobramycin, gentamicin and ciprofloxacin in biofilms, but the susceptibility of planktonic cells was unaffected[115]. Additionally, the resistance of *P. aeruginosa* biofilms to azithromycin

is dependent on the presence of either MexAB-OprM or MexCD-OprJ pumps, suggesting the four major pumps may contribute to the tolerance to some specific antimicrobial agents[116,117].

## Genetic diversity

**Horizontal gene transfer:** In addition to taking up eDNA carrying antibiotic resistance gene from EPS, cells may conduct conjugation and transfer genes between each other within the biofilm community aided by the sessile nature and spatial proximity[70]. Thus, when certain single strains are highly susceptible to some antibiotics, they may acquire antibiotic resistance gene from other species in a multi-species biofilm, leading to an increased subpopulation resistant to antibiotics and more tolerance of the overall biofilm.

**Mutation:** Some reports showed that cells in a biofilm accumulate mutations at higher rates than planktonic cells, of which contribute to elevated antibiotic resistance. For instance, the mutation frequency for ciprofloxacin resistant selection is about 2-log higher in *P. aeruginosa* biofilms cells than in planktonic cells[118]. Apart from increasing mutations towards specific antibiotics, a biofilm lifestyle may increase the emergence of hyper-mutable isolates with defeated methyl mismatch repair or DNA oxidative repair system[119,120]. These isolates can increase the mutation within themselves, including triggering the formation of antibiotic resistant genotypes.

## Different tolerance patterns within biofilms and their application

Conventional antimicrobial agents commonly used for killing *P. aeruginosa* cells, such as ciprofloxacin that interfere with replication, or tetracycline, tobramycin and gentamicin that interfere with translation, were proved to only target metabolically active cells in the outer layer of biofilms[121]. Meanwhile, the cells in the inner layer bearing a lower metabolic activity survive the treatment.

Notable exceptions were found where *P. aeruginosa* in the inner layer of biofilm are susceptible to some membrane-disrupting antimicrobial agents such as colistin, chlorhexidine, EDTA and SDS, and the killing patterns are similar[122]. In contrast, cells in outer layer with high metabolic activity become tolerant to these agents. Colistin-tolerant subpopulations was found to depend on the *pmr*-LPS modification system, as well as on the *mexAB-oprM*, *mexCD-oprJ*, and *muxABC-opmB* efflux systems, but not

*mexPQ-opmE*. Chlorhexidine-tolerant subpopulations were found to depend on the *mexCD-oprJ* genes, but does not depend on the *pmr*, *mexAB-oprM*, *mexPQ-opmE*, or *muxABC-opmB* genes. Metabolically active cells in biofilms are tolerant to SDS and EDTA, but does not depend on any of *pmr*, *mexAB*, *mexCD*, *mexPQ*, or *muxABC* genes. It was suggested that the active subpopulation in *P. aeruginosa* biofilms develop tolerance to membrane-targeting agents through different genetic determinants in correspondence to different compounds[122]. Furthermore, Pamp *et al* stated that planktonic cells at exponential-phase and stationary-phase exhibited equal sensitivity to colistin, highlighting the colistin tolerance is biofilm-specific[117], while Koplen *et al* showed that colistin tolerance in biofilms can be enhanced under anaerobic conditions[123]. It has recently been proposed that hypoxia reduces outer membrane potential in *P. aeruginosa*, thereby conferring tolerance to some conventional antibiotics that rely on an intact membrane potential for transportation[124]. As the outer layer of biofilms are oxic while the inner one tends to be hypoxic, it is possible that that these membrane-targeting antimicrobial agents can be more effective in the slow-growing biofilm subpopulation as their membrane integrity is already compromised[70].

As such, the combination of conventional antibiotics targeting metabolic active cells in the outer layer and the membrane-targeting antimicrobial agents killing metabolic inactive cells in inner layer, would significantly elevate the elimination efficacy of *P. aeruginosa*. Pamp *et al* have shown that by employing ciprofloxacin + colistin and tetracycline + colistin combinations, almost all the cells in *P. aeruginosa* biofilms are killed[125]. Future studies applying different combinations of conventional antibiotics and membrane-targeting agents can be carried out for biofilms formed by different *P. aeruginosa* strains, including CF isolates.

## 1.3 Activities of *P. aeruginosa* during biofilm dispersal

The final stage of biofilm life cycle is the detachment of cells from the biofilm and release into the environment[8]. Usually, the terms “detachment”, “dispersal” and “dispersion” can all be referred to the cell-detachment phase. This stage is essential for bacterial survival as nutrients in biofilms decrease while waste accumulates with time. Dispersal is a complex procedure triggered by many environmental signals, signal transduction pathways and effectors. Dispersal is not completely separated from the

biofilm formation procedures[126] as dispersal happens over the course of biofilm formation and maturation, so a steady state of biofilm is to some degree a balance between new attachment and low level of detachment[127]. The molecular mechanisms of bacterial biofilm dispersal are only beginning to be elucidated and it is a very promising and important field that can promote the development of novel drugs targeting genes responsible for dispersal to reduce biofilm in a wide range of applications.

### 1.3.1. Seeding dispersal – cell death and lysis

Among the three general modes of biofilm dispersal (Erosion, sloughing and seeding) mentioned in 1.1.2, seeding dispersal (also known as central hollowing) has been studied extensively in *P. aeruginosa* biofilms. It is the rapid release of a large number of single cells or small clusters of cells from the interior of microcolonies, leaving behind hollow cavities inside biofilm colonies[19,128]. Hollow cavities formed inside *P. aeruginosa* biofilm are lack of polysaccharide, which involves cells evacuating cell clusters, swimming through openings in colony wall and entering bulk liquid[7,8]. Central hollowing in *P. aeruginosa* appears in sufficiently large cell clusters (>80μm), and is proved to be triggered by an increase in colony size[129]. The mechanism of central hollowing is not fully understood, but evidence suggests that cell death and lysis occur in the biofilms of *P. aeruginosa* during the normal course of development[130]. Similar to apoptosis in higher organisms, *P. aeruginosa* undergoes programmed cell death. Webb *et al* discovered that cell death and lysis mechanisms are related to prophage within the genome of *P. aeruginosa* (Fig 1.3.1.1)[130]. The genome of *P. aeruginosa* contains a filamentous prophage that is closely related to phage Pf1, which is known to be upregulated in *P. aeruginosa* biofilms[16]. In Webb's study, it was demonstrated that a double mutant deficient in both Type IV pili and flagella, did not lead to normal cell death inside microcolonies while a single mutant did, demonstrating that either Type IV pili or flagella is required by cell death[130]. Both Type IV pili and flagella are reported to be the receptors of Pf1[131,132], and by adding purified phage to Type IV pili and flagella double mutant biofilm was not killed while adding phage to both single mutants caused similar killing as wild type[130]. These data illustrated that Pf1 phage produced by *P. aeruginosa* genome itself is involved in the cell killing in *P. aeruginosa* biofilms by acting on Type IV pili or flagella. Cells that survive bacteriophage lysis benefit from the nutrients released from their dead siblings, which promotes their "running away"[130,133].

This result was strengthened by Kirov *et al* demonstrating that the amount of bacteriophage activity paralleled the degree of cell death in the biofilm[134] as well as Rice *et al* proving that deletion of the entire prophage genome from the *P. aeruginosa* chromosome did not lead to cell lysis, central hollowing, or seeding dispersal in biofilms[135]. Furthermore, regarding the proteins involved in cell lysis, two proteins, endolysin and holin, are essential for host lysis by phages. Endolysins are muralytic enzymes that degrade the cell wall and accumulate in the cytosol fully folded. Holins are small membrane proteins making membranes more permeable to the fully folded endolysin with specific timing. Once the endolysins are released, murein is destructed and cell burst immediately[136]. Ma *et al* showed that holins and anti-holins which antagonize holin activity, are responsible for cell lysis. *P. aeruginosa cidAB* gene encoding CidA (putative holin) and *lrgAB* gene encoding LrgA (putative anti-holin) control cell death and lysis, as well as the timing of seeding dispersal[22]. Deletion of either *cidAB* or *lrgAB* causes increased cell death[22]. Also, programmed cell death and lysis contribute to the formation of the Psl matrix cavity, suggesting that the cell autolysis is important for Psl degradation and localization in the microcolonies, which in turn cause the release of cells, namely, dispersal[22].

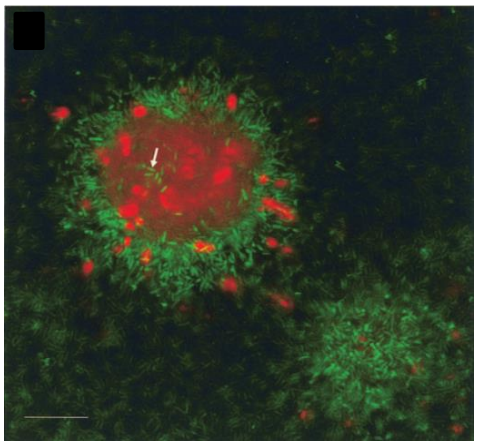

Fig 1.3.1.1. Cell death in microcolonies of mature *P. aeruginosa* biofilms: confocal micrographs of *P. aeruginosa* 7-days-flow cell-biofilm visualized by using the BacLight LIVE/DEAD viability stain. Images taken at the biofilm-substratum interface. Scale bars =50μm. Image courtesy of J.Webb[130].

## 1.3.2. Matrix enzymatic degradation-disruption of EPS

*P. aeruginosa* has a multifactorial system for alginate synthesis, which is beneficial for bacteria to settle down and be protected. However, it would also be meaningful to remove the alginate when it is no longer useful or even detrimental to the bacteria, such as when the detachment of cells from the matrix is needed. *P. aeruginosa* itself can

produce alginate lyase enzyme which is capable of cleaving the bond between two uronic acids to yield two shorter alginate polymers, and further action leads to continuous depolymerization of the alginate to oligosaccharides. Hence, increased expression of alginate lyase promotes the detachment of cells from *P. aeruginosa* biofilms[137].

### 1.3.3. Production of Rhamnolipids-disruption of integrity

As mentioned in 1.2.1, rhamnolipids are one category of the components in *P. aeruginosa* biofilm matrix. Rhamnolipids are glycolipidic surface-active molecules produced by *P. aeruginosa*[138]. They are typically constituted of a dimer of 3-hydroxyfatty acids linked through a beta glycosidic bond to a mono- or di-rhamnose moiety[138]. Rhamnolipid production mainly relies on three genes: *rhlA, rhlB* and *rhlC,* of which *rhlA* and *rhlB* genes are clustered with *rhlR* and *rhlI* from QS regulation system[139,140]. Rhamnolipids have surface-acting properties that decrease the adhesiveness of cell-cell, cell-matrix, and cell-surface interactions due to their amphipathic nature[141]. Inactivation of the *rhlAB* in *P. aeruginosa* biofilms inhibits the central hollowing and cell detachment while over-expression of *rhlAB* or exogenous rhamnolipids in wild-type biofilms increases cell detachment[21,142], indicating that rhamnolipids play a role in central hollowing in *P. aeruginosa* biofilms. The mechanism of rhamnoloipids induced-central hollowing is not known, but most likely they disrupt interactions among various cellular and matrix components within the biofilm colony[8].

### 1.3.4. Enhanced ability of proliferation-regain of motility

Motility is of vital importance during the initial and early stage of biofilm development (see section 1.2.1.2). In mature biofilms cell motility is suppressed as cells stay stably in the matrix, while during the dispersal stage, cells evacuating through cell clusters re-establish motility[7]. It can be inferred that motility is also triggered by some mechanisms at this stage. For example, Barraud *et al* found that low concentration of nitric oxide (NO) which promotes dispersal, enhancing the swarming motility of cells[9].

## 1.4 Mechanisms regulating *P. aeruginosa* biofilm dispersal — — cyclic dimeric GMP

Despite many publications that have described various signal molecules for triggering biofilm dispersal, such as D-amino acid, fatty acid and autoinducers in QS system[143], our interest focus on c-di-GMP, which is involved in many bacterial activities related to biofilm formation and dispersal. c-di-GMP is a secondary messenger used in a wide variety of bacterial species, but not eukaryotes or archaea, to regulate a variety of complex biological processes[144]. The burst of interest in this molecule in recent years led to much progress in understanding how c-di-GMP is regulated, and how c-di-GMP regulates. Cellular functions regulated by c-di-GMP include cell-cell signalling, biofilm formation, motility, differentiation and virulence[144]. Generally speaking, an increase in c-di-GMP level enhances biofilm formation while a decrease leads to dispersal. Two categories of enzymes are involved in the synthesis and degradation of c-di-GMP: diguanylate cyclase (DGC) catalyses the formation of c-di-GMP from two GTP, and phosphodiesterase (PDE) degrades c-di-GMP to 5'-phosphoguanylyl-(3'-5')-guanosine (pGpG) or 2 GMP (Fig 1.4). There are also many sensor domains linked to DGCs and PDEs that have been identified so far. They "translate" environmental signals to changes of c-di-GMP level via manipulating DGC and/or PDE activities, which in turn modulate the expression of genes that are related to biofilm or planktonic mode of life. So far the most studied domains that sense environmental cues as well as connect with DGCs and PDEs are PAS domain that can sense gaseous ligands such as NO and $O_2$, BLUF domains that sense light[143] and MHYT that might sense $O_2$, CO or NO by binding of one or two copper ions[145–147]. With endeavours from scientists all over the world, we now have a relatively clear idea about the synthesis, degradation and regulation mechanisms of this molecule, although still much remains to be elucidated. This section focuses on the regulation mechanisms of c-di-GMP and particularly its connection with biofilm.

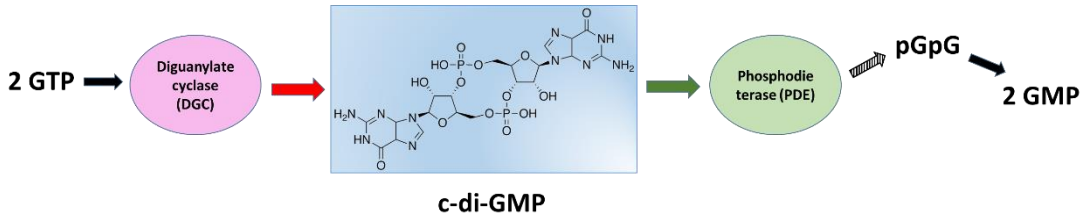


Fig 1.4. One molecule of c-di-GMP is synthesized by the enzyme deguanylate cyclase from 2 molecules of GTP, and is broken down by phosphodiesterase to 2 molecules of GMP through an intermediate pGpG.

## 1.4.1. Making and breaking of c-di-GMP

### 1.4.1.1. Synthesis of c-di-GMP

c-di-GMP is synthesized by a group of enzymes possessing a motif with aa sequence GGDEF (or its variation) named diguanylate cyclase (DGC). GGDEFs catalyse two GTPs into c-di-GMP through a two-step reaction with 5'-pppGpG as intermediate and 2 molecules of pyrophosphate as by-products[148]. One of the best studied DGCs is PleD from *Caulobacter crescentus*. Purified PleD acts in a dimer form that converts GTP into c-di-GMP, while isolated half site GGDEF domain shows no large conformational changes during catalysis[149], resulting in much lower activity. This phenomenon applies to other isolated GGDEF domains too[150]. The crystal structure of PleD (Fig 1.4.1.1) showed this DGC has an active site (A site) which is involved in a GTP binding, an inhibitory site (I site) involved in feedback inhibition as well as a response regulator domain, whose phosphorylation leads to the dimerization of GGDEF[151,152]. The core secondary structure of GGDEF domain is a five-stranded central β-sheet surrounded by helices (βααββαβαβ), for which the topology is identical and the arrangement is similar to adenylate cyclase (AC) that functions as dimer as to the "palm" domain of DNA polymerases[151]. Indeed, GGDEF functionally relates to AC and DNA polymerases in that it catalyzes 3′–5′ phosphodiester formation and the signature motif constituting active site is located to the central β-hairpin. This additional evidence, as well as the dinucleotide nature of c-di-GMP, suggest that GGDEF domains function by two domains coming together as homodimers with active site at dimer interface, not GGDEF *per se*[153].

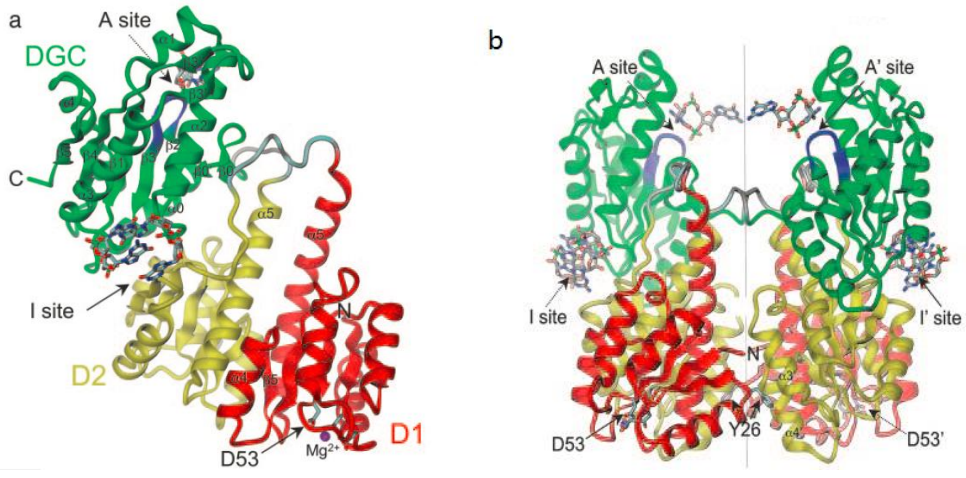


Fig 1.4.1.1 Crystal structure of PleD. (a) The monomer includes three domains. The catalytic DGC domain is shown in green. Domains D1 (red) and D2 (yellow) show the CheY-like fold. D1 carries the phosphoacceptor D53. The GGEEF signature motif is located on the β-hairpin (blue) and constitutes part of the active site (A-site) to which a c-di-GMP molecule is bound. Two c-di-GMP molecules are found at the D2/DGC interface (I-site). Discounting two additional short β-hairpins (β0, β0'and β3', β3'') and the N-terminal helix α0, the core secondary structure of GGDEF is (βααββαβαβ)[151]. (b) The two monomers

of the asymmetric unit form a two-fold dimer. The c-di-GMP molecules in the dimer crosslink A and A' from two monomers. Image taken from Structural basis of activity and allosteric control of diguanylate cyclase (Chan *et al*, 2004)[151].

It is supposed that catalytically active GGDEF are regulated by two mechanisms. The first one is conformational rearrangement of GGDEF in response to changes in the sensory domains linked to GGDEF domain. Apart from PelD, this phosphorylation mechanism is also found conserved in *P. aeruginosa* WspR[154], *B. burgdorferi* Rrp1[150], *P. aeruginosa* PvrR[155], *X. campestris* RpfG[156] and *P. aeruginosa* FimX[157], suggesting that phosphorylation is a common mechanism for GGDEF domain activation. Another mechanism is feedback inhibition (preventing over production of c-di-GMP) that requires a four residue motif constituting I site RxxD positioned five amino acids upstream of GGDEF motif. A base-intercalated dimer of c-di-GMP can bind to this I site leading to the inhibited conformation of protein crystal with coordinating residues either coming from regulatory domain or from GGDEF domain in another protein monomer[157–159]. This binding acts by restricting the movement of GGDEF domains, which blocks the formation of catalytically active homodimer. Further studies also showed that DGCs lacking I sites can still be product inhibited[153].

#### 1.4.1.2. Hydrolysis of c-di-GMP

c-di-GMP is degraded by another group of enzymes named phosphodiesterase (PDE) possessing domains with aa sequences of EAL or HD-GYP. These proteins hydrolyse c-di-GMP into linear di-GMP (5'-pGpG) requiring the presence of either $Mn^{2+}$ or $Mg^{2+}$ but are strongly inhibited by $Ca^{2+}$ and $Zn^{2+}$[153,160]. Subsequently, 5'-pGpG is converted into GMP[161]. The activity of EAL is c-di-GMP specific while the catalytic specificity of other phosphoesters are not clear[153].

#### EAL domain

Isolated, monomeric EAL domains show PDE activity and degrade c-di-GMP rapidly, which lead to the argument that PDEs can function as monomers by some scientists[162,163]. However, the majority of EAL domain PDEs characterized so far form dimers or higher-ordered oligomers *in vitro*[164–167] and the dimeric state appears to be important to activate PDEs through environmental stimulus[153]. Thus, we might infer that dimer is the functional state of the EAL domains involved in c-di-GMP hydrolysis. All structures of EAL domains observed so far display a central barrel composed of 8 β-strands surrounded by 7 α-helices, with a $\alpha\beta(\beta/\alpha)_6\beta$ secondary structure (a variant of the

triosephosphate isomerase (TIM) barrel fold), which is the core structure and is invariable. Variations between different EAL domains are seen in helices and loops[168]. This core barrel is essential to ligand binding, with the c-di-GMP binding site located at the C-terminal end of the β-strands composing the barrel[157]. The residues involved in 5'-pGpG binding located on strands β4, β5, β6 and loops 7 and 8 (Fig 1.4.1.2.1)[168]. With many publications confirming EAL domain uses two-metal catalysis, it is recently found that EAL can use three metal catalysis mechanism[169]. The configurations of EALs suggest that they perform nucleophilic attack on the phosphorus with the bridging solvent molecule[165]. The distance between the two active-site metal ions and their distances to the hydrolytic solvent molecule are important for the success of in-line attack of the phosphorus atom. A tight binuclear metal centre leads to higher activity, while when metal ions are further apart, the coordination is not sufficient for the activation[165].

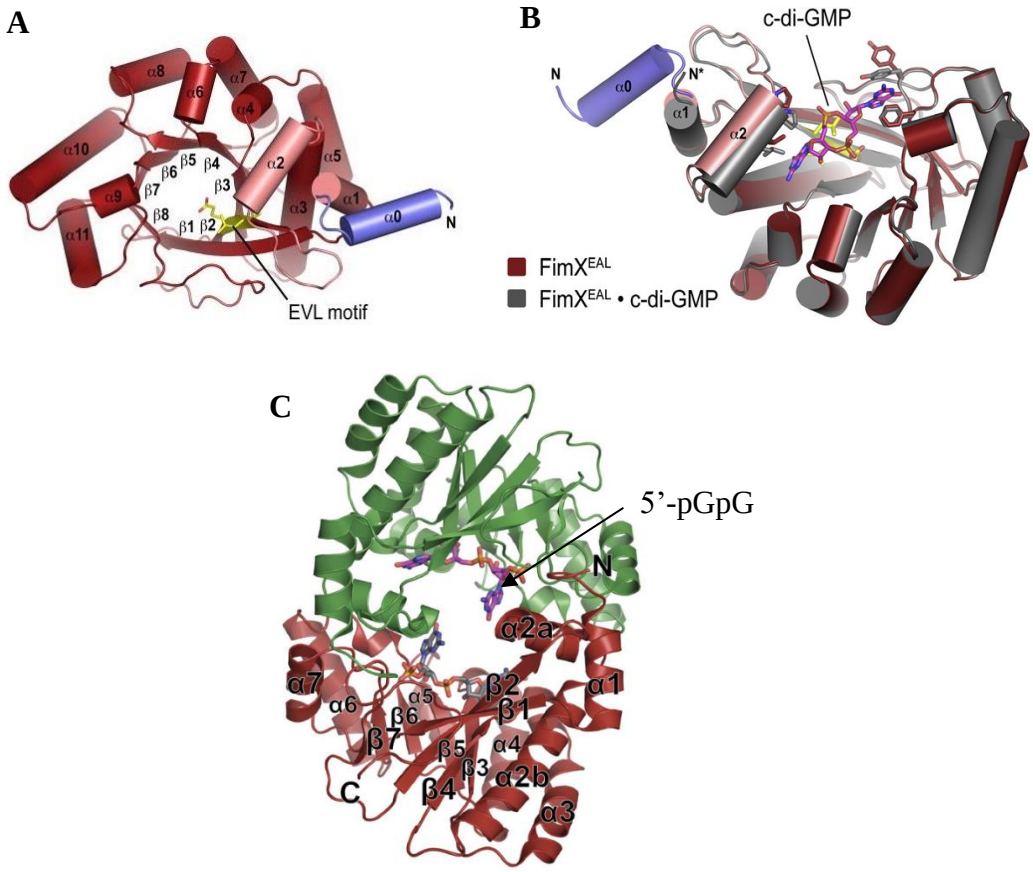


Fig 1.4.1.2.1 (A) αβ(β/α)$_6$β core secondary structure of FimX EAL domain (B) FimX EAL domain homodimer structure with bound c-di-GMP. The c-di-GMP-bound structure of FimX$^{EAL}$ (colored in grey), was superimposed onto the nucleotide-free structure (colored in red).The c-di-GMP binding site of FimX$^{EAL}$ is located at the C-terminal end of the β strands composing the barrel[157] (C) FimX EAL domain structure with bound 5'-pGpG. The interactions between two EAL domains (bound with 5'-pGpG) are

mediated by contacts between ahelices1, 2, 6, 7 and loops α1-β1, β5-α5[168]. Image taken from Structural Analysis of the GGDEF-EAL Domain-Containing c-di-GMP Receptor FimX[157] and Crystal Structure of an EAL Domain in Complex with Reaction Product 5'-pGpG[168].

**HD-GYP domain**

An alternative structure in PDEs is HD-GYP. HD-GYP has long been resisting crystallization and the first structure of HD-GYP domain of Bd1817 from *Bdellovibrio bacteriovorus* was not enzymatically active[170], which hindered the further insight into HD-GYP catalysis mechanism. It is not until recently when Bellini *et al* revealed the first enzymatically active crystal structure of an HD-GYP PDE protein P*m*GH, as well as its complex with c-di-GMP and final product GMP (Fig 1.4.1.2.2)[171]. The study showed that the trinuclear Fe centre, buried at the bottom of the cavity formed by two claws of open chela, was vital for c-di-GMP binding in P*m*GH[171]. By binding the Fe centre, c-di-GMP was hydrolyzed into GMP[171]. Although further studies need to be done to confirm the oxidation state of three Fe ions, a model was purposed estimating that the oxidation state of three Fe ions showing two peripheral sites occupied by Fe(II) and the middle site by Fe(III). Catalysis might involve redox reaction of these Fe ions[172]. As biofilm *per se* owns a gradient of oxygen accessibility and the inside part of biofilm present anerobic characteristics, we can also infer that redox might be responsible for the modulation of c-di-GMP level via changing metal oxidation states. In summary, Bellini's finding of trinuclear Fe centre catalysis is in accordance with the former results and predicts from Lovering *et al* that several conserved residues of HD-GYP group around the binuclear metal centre were with the catalytic metals likely to be either Fe or Mn[170]. Further studies need to be done and HD-GYP may show a new perspective of c-di-GMP controlling system on the basis of redox, perhaps unlike nucleophilic attack as EAL.

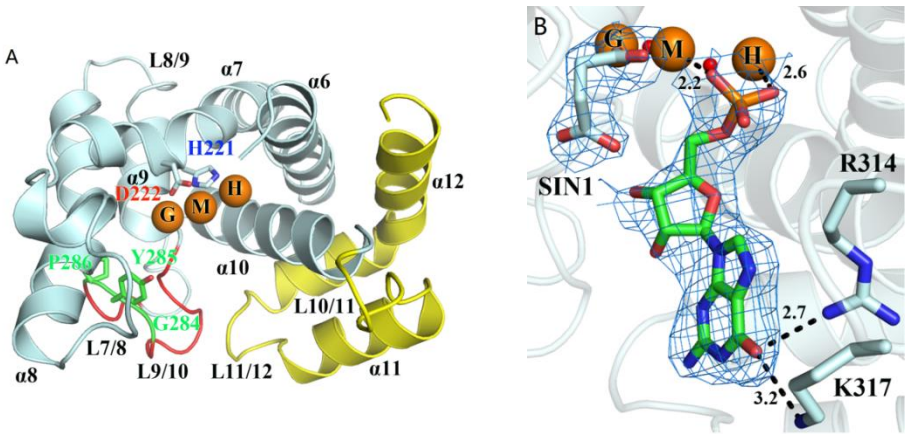

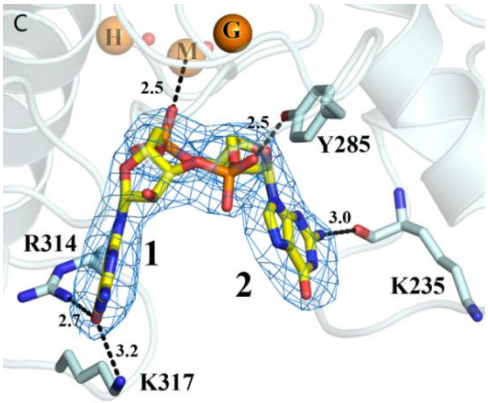


Fig 1.4.1.2.2 (A) Detailed view of the HD-GYP domain of PmGH. The central metal irons are labelled as the middle site (M) and the two flanking metal sites as H and G, to reflect their proximity to the HD and GYP motifs respectively. (B) View of GMP shown in stick mode bound to PmGH. Bonding interactions are represented by dashed lines with distances in Angstroms. (C) View of c-di-GMP bound to a metal depleted subunit of PmGH. Fe atoms occupying the middle (M) and HD (H) sites are shown as semi-transparent spheres as they are not present in the subunit when binding c-di-GMP. Image taken from D.Bellini[171].

### 1.4.1.3. GGDEF and EAL/HD-GYP in tandem

GGDEF and EAL domains are often found on the same polypeptide chain as parts of multi-domain proteins according to genomic analysis. About 1/3 of all GGDEF domains and 2/3 of all EAL domains are found on the same polypeptide in tandem[153]. These proteins fall into three main categories based on their catalytic activity: (1) tandem domain–containing proteins with both DGC and PDE activity; (2) proteins with only one domain active while another one, degenerate and inactive, exhibits a regulatory function; (3) both domains are degenerate and might act as c-di-GMP receptors[173]. Although almost half of all GGDEF-EAL proteins have been reported to have intact active sites, only a few of them are really bifunctional, i.e., both domains have enzymatic activity but only one of them is active under certain circumstance or triggered by specific environmental/intracellular signals and they fall in the first category[164,174]. Examples of this group include BphG1 from *Rhodobacter sphaeroides* whose activity switch involves proteolysis[164], ScrC from *Vibrio parahaemolyticus* whose activity switch involves protein partners[175], MSDGC-1 from *Mycobacterium smegmatis*[176] and Lpl0329 from *Legionella pneumophila*[177]. Recent finding in our group also showed that MorA in *P. aeruginosa* can both synthesize and hydrolyze c-di-GMP. We have described an activity switch involving a secondary structure change of a R helix linking GGDEF and EAL[178]. However, despite this, we have illustrated the structure of full length DGC-PDE of MorA and confirmed both enzymatic activities, only the relationship between the R

helix and the dimerization of the PDE was revealed. Further research on the relationship between DGC and R helix, whether there is a regulatory effect between DGC and PDE as well as under what conditions does MorA switch between DGC and PDE need to be done. Another more commonly found scenario is that one of the two domains is enzymatically inactive [153]. The inactive domain usually presents new functions, including binding (but not processing) the substrate c-di-GMP and protein-protein or protein-RNA interactions[153]. A study showed that the deletion of the enzymatically inactive EAL domain in DgcA1 from *G.xylinus* resulted in the abrogation of DGC activity in the protein, suggesting that the inactive domain might have played an important structural or regulatory role in maintaining the function of the whole protein[153]. The transmembrane protein LapD in *P. fluorescens*[179] and *P. putida*[180] belongs to the third group, containing degenerate GGDEF and EAL domains lack of catalytic activity, but is capable of binding c-di-GMP via its divergent phosphodiesterase domain[181]. It responds to changes in cellular c-di-GMP levels modulated by the availability of inorganic phosphate in the environment and is related to stable cell attachment and biofilm formation[181,182]. With the alteration in c-di-GMP levels, LapD switches between two states: bound off state retards stable biofilm formation and bound on state supports cell adhesion[179,181]. To date, much work has been done to reveal the structure and regulatory mechanisms of GGDEF or EAL *per se*, but little work has been done for the GGDEF-EAL tandems. So far, the dual GGDEF-EAL domain crystal structures available in PDB are FimX and MorA (Fig 1.4.1.3. C,D[178]) from *P. aeruginosa*, as well as LapD from *P. fluorescence* (Fig 1.4.1.3. A,B[173]). Despite the revealed crystal structures, both LapD and FimX showed insufficient catalytic activity of both DGC and PDE, while MorA is the only one with activities of both. Therefore, the mechanism of MorA regulation might be representative of other DGC-PDE tandems that are bifunctional, and might also shed lights on GGDEF-HD-GYP tandem of which no structure of full length tandem was revealed to date.

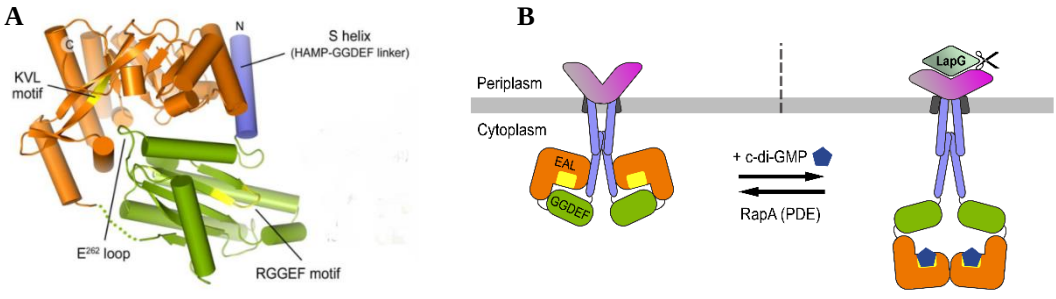

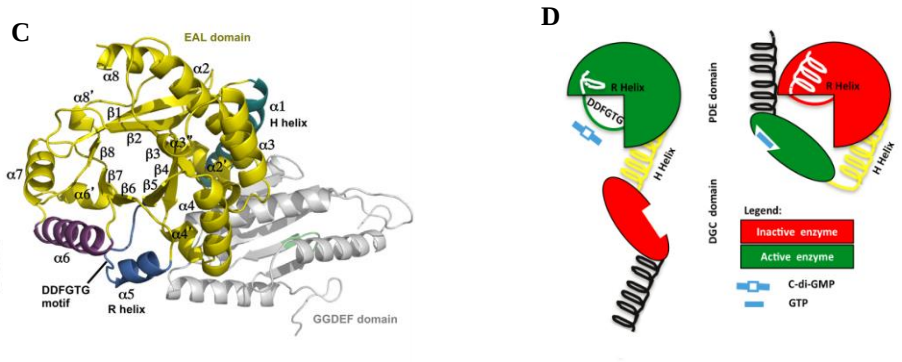


Fig 1.4.1.3. (A) Crystal structure of the dual-domain GGDEF-EAL of apo-LapD in *P. fluorescens*. GGDEF (RGGEF) is shown in green while EAL (KVL) is shown in orange. Image taken from Structural basis for c-di-GMP-mediated inside-out signaling controlling periplasmic proteolysis[173]. (B) Model for how the conformational change of S-helix upon binding LapG change the whole arrangement of GGDEF-EAL tandem and c-di-GMP binding. Image taken Structural basis for c-di-GMP-mediated inside-out signaling controlling periplasmic proteolysis[173]. (C) MorA DGC-PDE tandem highlighting PDE TIM barrel structure. The active site DDFGTG motif and the a5 helix or R helix are highlighted in blue, the a6 helix is shown in purple. The H helix (cyan) links the PDE domain (yellow) to the DGC domain (grey). Alpha helices and beta sheets are labelled (Image taken from Formation and dimerization of the phosphodiesterase active site of the Pseudomonas aeruginosa MorA, a bi-functional c-di-GMP regulator[178]). (D) Supposed model for MorA regulation and activation of both DGC and PDE activities. Key elements of the active states of the PDE domains are the DDFGTG loop and the R helix α5 while the hallmark of an active DGC is formation of the nucleotide recognition helix α2'. (Only when DGC is homo/hetero- dimerised with another DGC domain) (Image courtesy of C.W.Phippen).

### 1.4.1.4. Regulatory sensory domains

Most prokaryotic signal-transduction systems, also known as two-components signal transduction systems, use phosphotransfer schemes. These schemes involve two conserved components, a sensory domain that sense environmental stimuli and a response regulator protein[183]. The changes of sensor domains upon receiving extracellular signal are subsequently transferred to an associated response regulator protein[183], resulting in its activation or inactivation[183] and in turn perform a variety of downstream effects. So far numerous conserved domains have been identified in bacteria (Table 1.4.1.4.).

| Sensor domains | Functions |
|---|---|
| PAS | FAD, heme, and cinnamic acid binding |
| MHYT | metal binding |
| FliY | amino acid binding |
| Cache | small ligand binding |
| GAF | cGMP binding, photopigment binding |
| HAMP | dimerization |
| His Kinase 1 | phosphoacceptor, dimerization |
| His Kinase 2 | Phosphorylation of His kinase 1 domain |

| | |
|---|---|
| Hpt | Phosphoacceptor |
| BLUF | Light-sensing |
| | |
| Response domains | Functions |
| GGDEF | diguanylate cyclase (c-di-GMP production) |
| EAL | Phosphodiesterase (c-di-GMP hydrolysis) |
| HD-GYP | Phosphodiesterase (c-di-GMP hydrolysis) |
| REC (CheY) | phosphoacceptor |
| HTH | DNA binding |
| AAA | $\sigma^{54}$-binding ATPase |

Table 1.4.1.4. Conserved domains of the bacterial signal transduction systems (Adapted from M.Y.Galperin *et al*, Novel domains of the prokaryotic two-component signal transduction systems[184])

The most common sensory domains that are found combining GGDEF, EAL and HD-GYP in cytoplasmic c-di-GMP-metabolizing enzymes are REC, PAS and/or GAF[153]. Another important group of signalling proteins consists of membrane-bound sensors that combine cytoplasmic GGDEF, EAL/HD-GYP domains with periplasmic/extracellular sensory domains, such as MHYT. PAS domain can modulate its activation via binding ligands such as heme and FAD that sense $O_2$, NO, CO, redox potential, or photons, which in turn enables the proteins response to environmental stimuli[185]. It is supposed that PAS domain might influence GGDEF-EAL tandem conformationally by binding NO, which in turn modulates c-di-GMP level and biofilm. Therefore, it is reasonable to infer that PAS-GGDEF-EAL should be of vital importance in NO-mediated biofilm dispersal. More details of PAS domain and NO sensing are discussed later.

## 1.4.2. c-di-GMP receptors

As a second messenger, c-di-GMP serves to integrate information from multiple upstream inputs to influence the rates of synthesis and degradation of itself, and acts on multiple downstream targets, thereby expanding the scope of signal transmission. Naturally, c-di-GMP must have many receptors in bacteria. But so far, much less was known about c-di-GMP receptors than about c-di-GMP metabolizing enzymes due to the difficulty in identifying proteins with great diversity in sequence and structures[153]. Several groups of c-di-GMP protein receptors have been identified including PilZ domain receptors, I-site receptors, inactive EAL domain receptors and likely HD-GYP.

In addition to proteins, two types of riboswitches have also been shown to bind c-di-GMP[153].

### 1.4.2.1. PilZ domain

PilZ is the first identified c-di-GMP receptor originated from *P. aeruginosa* PA2960 and then found in proteins from various bacterial species, such as BcsA from *G. xylinus*[186], YcgR from *E. coli*[187], DgrA from *C. crescentus*[188] and PlzC and PlzD from *Vibrio cholerae*[189]. To date, PilZ appears to have the highest affinities for c-di-GMP compared to the majority of other c-di-GMP receptors[153]. X-ray and NMR studies have demonstrated the structure of PilZ (Fig 1.4.2.1.). Moreover, PilZ domain proteins were found to exist in different states ranging from monomeric to tetrameric[190–193], suggesting potentially different downstream transduction modes. Similar to other domains associated with c-di-GMP, PilZ has active (c-di-GMP binding) and inactive states (lack of c-di-GMP).

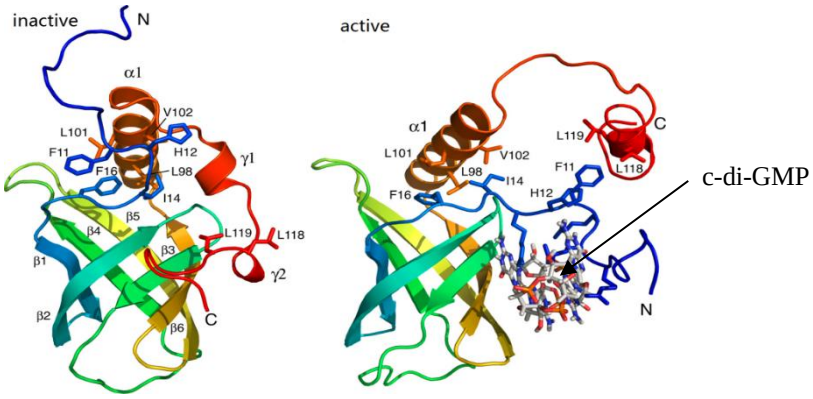


Fig 1.4.2.1. Comparison of overall structure of inactive (lack of c-di-GMP binding) and active (c-di-GMP binding) state of PilZ (PA4608) domain in *P. aeruginosa*. In the inactive form, the c-di-GMP binding side of the β-barrel comprising strands β2, β3, β5 and β6 is partially covered by the C-terminal. Binding of c-di-GMP pushes the C-terminal region away from the β-barrel and causes the unfolding of helix. Image taken from Solution structure of the PilZ domain protein PA4608 complex with cyclic di-GMP identifies charge clustering as molecular readout[190].

### 1.4.2.2. GGDEF I-site and Inactive EAL

Apart from PilZ, there are several other receptors that regulate c-di-GMP level when PilZ is not present *in vivo*. The I-site of inactive GGDEF domain is the most promising candidate. Retiring from its active duty, GGDEF often retains the product-inhibiting I site that has the capacity to bind c-di-GMP, making the catalytically incompetent domains function as a substrate receptor[153]. Thus, I site not only serves to prevent the overproduction of c-di-GMP by DGCs, but also enables proteins that lose the DGC

activities to switch their role to c-di-GMP receptors[153]. Examples include PopA from *C. crescentus*[194], SgmT from *M. Xanthus*[195], CdgA from *B. bacteriovorus*[196], and PelD from *P. aeruginosa*[197]. Following the same principle, inactive EAL domain that lose PDE activities can also retain the ability to bind c-di-GMP. Examples include FimX from *P. aeruginosa*[198], LapD from *P. fluorescens*[199] and YkuI from *B. subtilis*[200]. Although no HD-GYP has been described as c-di-GMP receptor so far, according to its nature HD-GYP is also likely to possess similar characteristics[153]. Whether the binding of c-di-GMP to degenerated DGC/PDEs regulates other proteins and phenotypic outputs, or they mainly bind c-di-GMP as a way to balance the total intracellular level remain unknown so far, which need further investigations.

#### 1.4.2.3. Riboswitches and other receptors

In addition to proteins, c-di-GMP has also been found to bind two kinds of riboswitches[153]. Riboswitches are non-coding segments of mRNA which possess particular secondary structures and bind small molecules[153]. In bacteria, riboswitches frequently occur in the 5' UTRs of mRNAs. The secondary structures of riboswitches change via ligands binding to aptamer part, making the expression platform fold into a terminator stem-loop aborting the transcription[153,201](Fig 1.4.2.3 A). Hence, the binding of c-di-GMP to these riboswitches would regulate the translation of a transcript[202]. Currently there are two categories of riboswitches with a c-di-GMP binding aptamer structure found as shown in Fig 1.4.2.3 (B,C). The first group of riboswitch binding c-di-GMP called GEMM is initially discovered by Breaker *et al* and belongs to c-di-GMP-I aptamer consensus[203,204]. GEMM resides upstream of the DGC and PDE coding regions in some organisms and some genes that are controlled by cyclic di-GMP[204]. Another group of riboswitch (Fig 1.4.2.3 C) belonging to c-di-GMP-II aptamer consensus was also first discovered by Breaker's group. It binds c-di-GMP and regulates the self-splicing in an allosteric group I ribozyme[205]. Riboswitch-binded c-di-GMP induces folding changes at atypical splice site junctions to modulate alternative RNA processing[205].

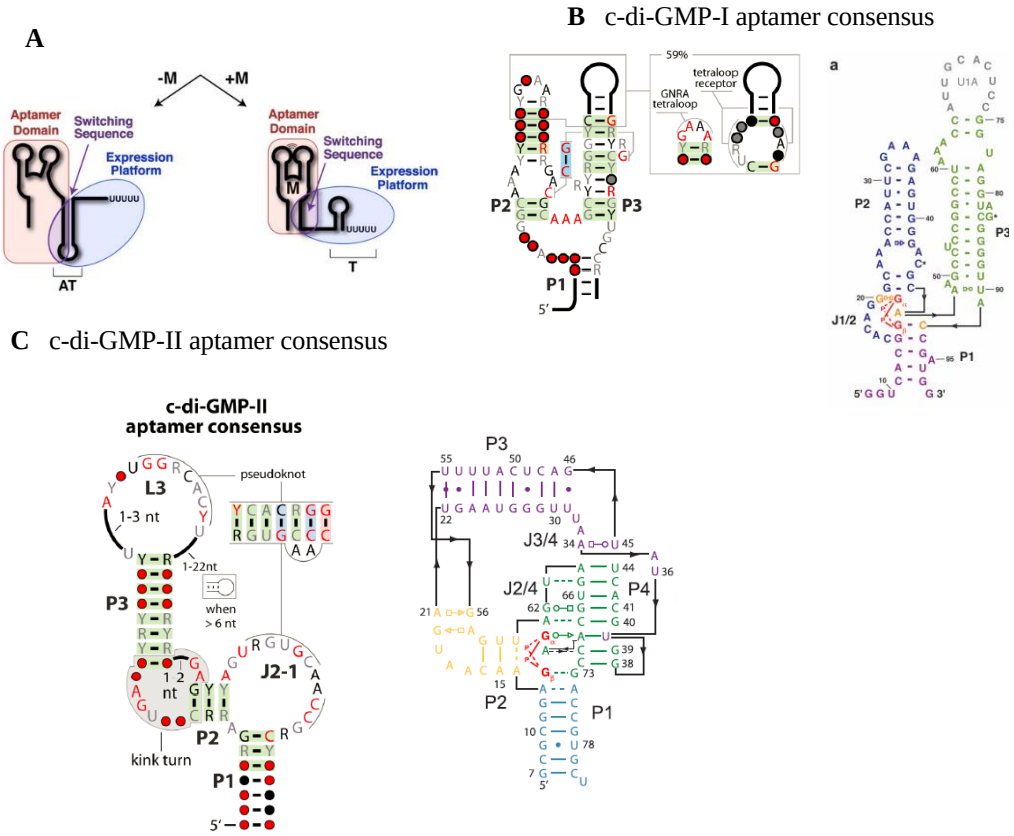


Fig 1.4.2.3. (A) The schematic of a riboswitch that controls transcription. When metabolite is not bound (-M), the expression platform incorporates the switching sequence into an anti-terminator stem-loop (AT) allowing the process of transcription. When metabolite binds (+M), the switching sequence is incorporated into the aptamer domain, and the expression platform folds into a terminator stem-loop (T), causing transcription to abort. Image taken from Riboswitches: A Common RNA Regulatory Element[201]. (B) The consensus sequence and structural model for class I c-di-GMP aptamer (left) and the c-di-GMP bound structure (right, c-di-GMP shown in red). Images taken from An Allosteric Self-Splicing Ribozyme Triggered by a Bacterial Second Messenger[205] and Structural basis of ligand binding by a c-di-GMP riboswitch[206] (C) The consensus sequence and structural model for class II c-di-GMP aptamer (left) and the c-di-GMP bound structure (right, c-di-GMP shown in red). Images taken from An Allosteric Self-Splicing Ribozyme Triggered by a Bacterial Second Messenger[205] and Structural basis of differential ligand recognition by two classes of bis-(3'-5')-cyclic dimeric guanosine monophosphate-binding riboswitches[207]

## 1.4.3. The specificity of c-di-GMP signalling pathway

The redundancy of DGC and PDEs in bacteria raised the doubt in the necessity of the existence of all these proteins, as bacteria always develop the most economical way to metabolize during their evolution. Therefore, it is reasonable to assume that there might be accurate selective regulation of c-di-GMP target outputs by individual c-di-GMP-metabolizing proteins.

Due to the increasing knowledge we have in c-di-GMP-dependent signalling pathways, we now realize that there is a hierarchical logic governing c-di-GMP regulatory systems

with each individual components controlled by specific environmental or intracellular stimuli and in turn serves specific targets[153].

#### 1.4.3.1. Regulation of expression of c-di-GMP-related genes

Differential transcriptional regulation of c-di-GMP-metabolizing proteins directly controls c-di-GMP signalling. The general stress sigma factor RpoS directly or indirectly controls a large amount of genes under various stress conditions such as depleted nutrients, temperature, low pH and osmotic stress, and it is reasonable to suspect RpoS might have influence on c-di-GMP related genes. So far RpoS has been found to be a powerful control of GGDEF/EAL genes expressions in *E. coli* (fimbriae and cellulose synthesis)[208,209], *V. cholera* (biofilm formation and virulence) [210] and *P. putida* (biofilm formation)[211], suggesting a regulation route involving stress response – c-di-GMP – biofilm related phenotypes. Although not deeply studied in *P. aeruginosa*, it is likely that this mechanism is a common trait. Some GGDEF/EAL genes exhibit $\sigma^S$ dependence under more than one stress conditions whereas others show $\sigma^S$ control only under one specific condition[209]. Therefore, these genes might be triggered only in one or a few specific situations, suggesting the specificity in c-di-GMP-metabolizing proteins regulation.

#### 1.4.3.2. DGCs, PDEs and their targets

Apart from the regulation of DGC and PDE genes, specific responses of c-di-GMP targets to individual DGCs and/or PDEs also largely contribute to the specificity of c-di-GMP signalling[153]. Many examples of signalling specificity have been reported in various bacteria. One striking example comes from *P. aeruginosa*, where overexpression of the DGC PA2870 significantly increased c-di-GMP levels without causing changes in biofilm formation and overexpression of SadC (PA4332) results in enhanced biofilm formation without change in c-di-GMP concentration[212]. Similarly, a deletion of the PDE PvrR in *P. aeruginosa* strain PA14 compromised its virulence and biofilm formation but it expressed significant PDE activity[212]. These studies demonstrated that it is the resource of c-di-GMP concentration changes (specificity) over the c-di-GMP amount *per se* that counts for a certain phenotypic change, and that intracellular c-di-GMP concentration is not the only reason for the biofilm formation or dispersal. So far, 39 genes that contain GGDEF and/or EAL domains have been identified in *P. aeruginosa* PA14 and over-expression of them led to different

phenotypes[212], which also to some degree shows that different GGDEF/EAL proteins are specific to different biofilm formation phenotypes. Although Merrit *et al* measured the total cellular levels of c-di-GMP in Δ*roeA* and Δ*sadC* mutants of PAO1 and revealed that the intracellular c-di-GMP level was not correlated to different phenotypic biofilm outputs (swarming motility and EPS production)[213], not all GGDEF/EAL genes in PAO1 were tested yet. Therefore, it is also worth knocking out/overexpressing these different genes individually and analysing the specific genotypic outputs in PAO1 strain background. Additionally, strains in which multi- and/or all DGCs/PDEs are deleted can also be very useful in investigating the specificity of c-di-GMP signalling. By comparing the biofilm formation in all deletion mutants with individual deletion mutant and wild type, we may assign functions to genes/proteins.

## 1.4.4. Biofilm and c-di-GMP

Since the first discovery of c-di-GMP decades ago, important findings of this universal bacterial second messenger kept emerging. Not only did the list of bacteria relying on c-di-GMP signalling grew quickly, but also the phenotypes influenced by c-di-GMP[153]. As shown below, a myriad of phenotypes are regulated by c-di-GMP level (Fig 1.4.4), of which how c-di-GMP influences biofilm formation/dispersal through motility and EPS is reviewed here in details for the project.

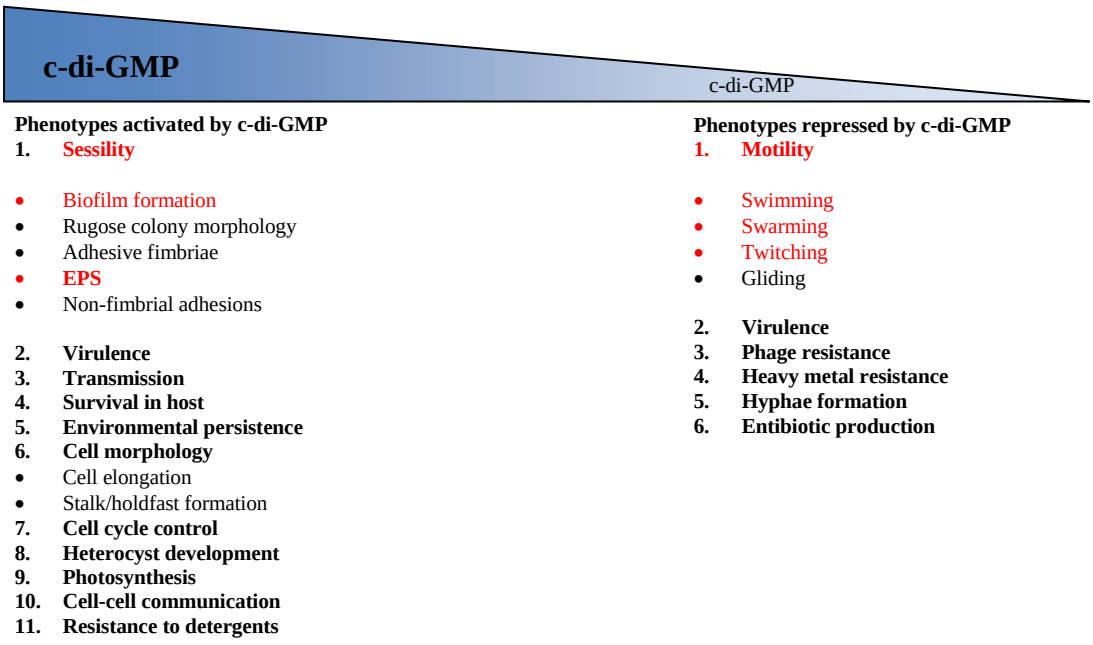


Fig 1.4.4 Phenotypes regulated by c-di-GMP level in bacteria. Image adapted from Cyclic di-GMP: the First 25 Years of a Universal Bacterial Second Messenger[153]

#### 1.4.4.1. Regulation of biofilm via motility and sessility transition

The transition of motile cells to a sessile state involves a drastic lifestyle change, which is usually related to later biofilm formation[153]. A key role of c-di-GMP in the transition between motile and sessile lifestyles of Gram-negative bacteria has been discovered and the underlying molecular mechanisms are beginning to emerge[153]. c-di-GMP mediated motility-to-sessility transition occurs not only when swimming cells approach a surface in the initial stage, but also during biofilm maturation and dispersal. Logically, cell motility should be enhanced when accessing the surface, repressed in mature biofilm and enhanced again for dispersal[153]. Apart from swimming, c-di-GMP also regulates swarming, twitching and gliding motility which are essential during initial and early attachment stages.

**c-di-GMP and fast regulation of flagella**

Swimming capacity conducted by flagella is of vital importance during the initial attachment stage. Flagella mediated motility-to-sessility transition requires rotating flagella not only to get proximity with surfaces, but also to overcome surface repulsion until its successful contact with surfaces and then stop rotating for cells settling down[153]. Flagella are responsive to chemotactic signals, hence posing negative influences on cells that intend to settle down as it increases the chance of swimming away from the surfaces. Therefore, bacteria should benefit from a mechanism that blocks the chemotactic inputs of flagella quickly on the scale of seconds at a posttranslational level during surface attachment[153]. After the permanent attachment occurs, a second, slower mechanism might be involved in turning off rotating flagella/flagellum synthesis[153]. So far the mechanisms of these operations have only been described in enteric bacteria, but it might shed light on the mechanistic study in *P. aeruginosa* whose flagella is also playing a significant role in initial attachment.

In enteric bacteria *E. coli* and *S. enterica*, flagella rotate either in a counter-clockwise (CCW) or a clockwise (CW) direction[153]. The default direction is CCW but chemotactic signals result in changes in rotation direction of one or several flagella from CCW to CW, leading to the tumbling of cells. Later the CCW rotation direction resumes and propels cells in a new random direction, promoting bacterial proliferation. It has been found that c-di-GMP binds to specific receptor that interact with flagella rotor proteins,

which then induces a strong CCW bias in flagellar rotation and inhibits spreading due to its incompetence of switching swimming direction[214,215]. This inhibition of motility and chemotaxis may assist the sessile life of bacteria by disfavoring migration away from a substrate where biofilms might later locate[215]. Apart from the swimming ability in liquid, flagella is also involved in swarming on wet surfaces and high level of c-di-GMP represses swarming. Similar to flagella rotation in *E. coli*, it was proved that in *P. aeruginosa* PA14 two stator complexes, MotAB and MotCD, participate in the rotation of single polar flagellum. When c-di-GMP level is elevated, the MotAB stator that represses swarming motility can displace MotCD from the motor and affect motor function and flagella rotation[216]. The DGCs and PDEs involved in this c-di-GMP – swarming regulation pathway include SadC (DGC) and BifA (PDE)[217–219]. As a result, *sadC* mutation promote surface swarming by increasing the frequency of change of swarming directions while *bifA* results in decreased directional reversal.

**c-di-GMP and transcriptional regulation of flagella behaviour**

In addition to the fast regulation, c-di-GMP can also regulate flagella at a slower transcriptional level. Jyot *et al* have identified the protein FleQ as a c-di-GMP-responsive transcriptional regulator in *P. aeruginosa* that directly interact with flhA, fliE, fliL, and fleSR promoters, which are involved in flagellar export, flagellar basal body MS ring encoding and flagellin synthesis[220]. Similar regulation was also found in other species such as *Xanthomonas* and *V. cholerae* where transcriptional regulators can bind c-di-GMP and repress flagella related genes[221,222]. But all these c-di-GMP-dependent transcription factors only lead to modest control on flagellar genes, indicating that additional molecular mechanisms of motility control need to be discovered[153].

**c-di-GMP and Type IV pili**

Beyond flagellum-mediated swarming and swimming, another important part of motility, type IV pili-mediated twitching in *P. aeruginosa* is also regulated by c-di-GMP. The unique ability of Type IV pili to polymerize and retract confers twitching motility[223,224], which is required both in initial attachment and maturation stage and result in a 3D biofilm architecture[225]. The biogenesis of Type IV pili and its twitching motility are controlled by c-di-GMP, requiring the GGDEF-EAL domain FimX response regulator localized at one cell pole[226]. The GGDEF domain of FimX is degenerate, while the EAL domain binds c-di-GMP with high affinity but only exhibits

weak PDE activity *in vitro*. Although not showing DGC activity, the imperfect GGDEF domain of FimX might serve to activate phosphodiesterase activity and the function of FimX needs the presence of both GGDEF and EAL. The binding of c-di-GMP to EAL domain influences its interaction with PilZ protein required for surface pilin expression and localization. In this way, the dysfunction of FimX results in a pilus assembly defect and the bacterial twitching motility is then impaired[227,228].

#### 1.4.4.2. c-di-GMP and biofilm EPS

Every component of EPS matrix contributes to the biofilm formation, maturation and 3D structure. All these components, including various exopolysaccharides, proteins and eDNA, can be regulated by c-di-GMP on transcriptional, posttranscriptional and posttranslational levels[153].

**Alginate, Pel and Psl as c-di-GMP target in *P. aeruginosa***

Pel and Psl are the major components of biofilm matrix polysaccharides in non-mucoid *P. aeruginosa* while alginate is mainly overproduced in mucoid strains[229]. The role of Pel and Psl in biofilm formation vary drastically from strain to strain. For example, PAO1 relies primarily on Psl while PA14 is more Pel dependent[230]. Most environmental and clinical isolates secrete either Pel or Psl except for some rugose small colony variant (RSCV) clinical isolates that express both the *Psl* and *Pel* operons simultaneously[229].

So far the relationship between c-di-GMP and Pel has been more developed while c-di-GMP is likely to be a poor indicator of Psl[230]. Pel is positively regulated by c-di-GMP on transcriptional level likely via a system containing DGC WspR and YfiN producing c-di-GMP as well as FleQ as the c-di-GMP receptor. WspR is activated by phosphorylation carried out by His kinase WspE, which receives a surface-derived signal from the membrane-bound domain protein WspA[231,232]. WspR clusters form in proximity to FleQ, perhaps due to the necessity of controlling localized c-di-GMP level[153]. When in the absence of c-di-GMP, FleQ forms a complex with ATP-dependent protein FleN, binding two sites up and downstream of the *pel* promoter leading to a bend of DNA and the inhibition of *pel* transcription. In contrast, bending is relieved with the presence of c-di-GMP which results in the activation of *pel* transcription[233].

The biosynthesis of the Pel exopolysaccharide is also regulated by c-di-GMP at the posttranslational level. In addition to widely known c-di-GMP receptor PilZ, the pel

operon encodes another I-site receptor PelD which mediates c-di-GMP regulation of Pel polysaccharide biosynthesis by binding to c-di-GMP directly[234]. Also, some DGCs such as RoeA and PDEs such as BifA in *P. aeruginosa* are involved in c-di-GMP mediated regulation of Pel synthesis although the mechanisms remain unclear[218,213].

Alginate is mainly found in mucoid strains isolated from cystic fibrosis patients. Alg44, possibly part of large alginate synthase complex, is a c-di-GMP receptor containing PilZ domain and is responsible for alginate polymerization or transport[235,236]. Although the mechanism is not clearly elucidated yet, it is supposed that c-di-GMP activates a specific protein-protein interaction within the alginate translocation complex by binding the PilZ domain of Alg44[153]. MucR, a membrane anchored DGC is supposed to activate alginate production through generation of a localized c-di-GMP pool in the vicinity of Alg44 for PilZ to receive c-di-GMP. Thus, more molecular studies are needed to find out the specific determinants allowing DGCs to communicate with specific c-di-GMP targets[153].

**Fimbriae and non-fimbrial adhesins**

Fimbriae are hair-like structures present on the surface of some Gram-negative bacteria. Both pili and fimbriae are bacteria surface structures and are structurally similar to each other but different in size and functions. An individual pilus is usually 0.5 to 7 nm in length and 4 to 6 nm in diameter which is responsible for twitching motility and sexual conjugation, while fimbriae are usually 2-10 nm in diameter and 100-5000 nm in length which facilitates the adhesion to the surfaces and/or host organisms. In *P. aeruginosa*, five fimbrial gene clusters, *cupA,B,C,D,E*, have been identified to date. Although specific functions of fimbriae remain unknown, all of them have been shown to either change adhesive properties of *P. aeruginosa* or relate to biofilm formation[237]. The expression of all Cup fimbriae genes, except for CupE, are reported to be involved in DGC/PDE regulation although the mechanisms remain unknown[153].

Non-fimbrial adhesins also contribute to biofilm formation. Large multi-repeat adhesins often participate in biofilm formation by enhancing cell surface adherence and play a role in stabilizing the extracellular matrix[153]. In *P. aeruginosa*, a putative adhesin CdrA, together with its putative outer membrane transporter CdrB regulated under the same operon, possess a large non-fimbrial β-helical adhesin[238]. The expression of gene cluster cdrAB is elevated under conditions of high intracellular c-di-GMP[238].

## 1.5 Nitric Oxide signalling and biofilm

Free radical nitric oxide was found to be a crucial signalling molecule with wide-ranging functions in the cardiovascular, nervous and immune systems during 1980s and was awarded the curious accolade of "molecule of the year" in 1992[239]. The Nobel Prize in Medicine or Physiology in 1998 was awarded to scientists Robert Furchgott, Louis Ignarro and Ferid Murad for their discoveries concerning nitric oxide as a signalling molecule in the cardiovascular system, which enhanced and expanded the interest in NO among scientists from various fields, resulting in an explosion of investigations in its signalling pathways. So far, the classical NO signalling (cGMP–PKGs), less classical NO signalling (NO binding to cytochrome *c* oxidase in the mitochondria) and non-classical NO signalling (NO-mediated posttranslational modifications) have been deeply studied in mammals[240], but much less is known in bacteria. To date, nitric oxide has been found to be a signalling molecule by interacting with proteins in two distinct pathways: (1) binding ferrous/ferric-haem in proteins that causes 3D structural changes. These signal transduction proteins usually contain an upstream haem-containing sensor domain that binds to gaseous ligands, and a downstream effector domain that generates an output signal[241].(2) binding copper ions in membrane sensor domains, such as MHYT that do not contain haem (Fe)[145,147]. In 2006, Barraud *et al* for the first time discovered that nanomolar scale NO donors led to the biofilm dispersal in *P. aeruginosa* by modulating c-di-GMP level in cells[9,242], which triggered our interest in revealing its mechanisms. Current evidence showed that NO might be involved in both biofilm formation and dispersal though c-di-GMP and/or quorum sensing pathways across a wide range of bacteria species. We focus on how nitric oxide modulates biofilm dispersal and our insights into *P. aeruginosa* biofilm might shed light on other species. The table below summarizes the dispersal of biofilms from different species involving in NO.

| Species | NO resource | Possible mechanism |
|---|---|---|
| *Pseudomonas aeruginosa* | 25nM to 2.5mM SNP[9] | NO binds to PAS/MHYT domains upstream of DGC and/or EAL, resulting in a decrease of intracellular c-di-GMP |
| *Vibrio cholerae* | 25-500nM SNP[243] | NO binds to H-NOX domain that regulate HK-RR for modulation of intracellular c-di-GMP[244,245] |
| *Serratia marcescens* | 25-500nM SNP[243] | Unknown |
| *Escherichia coli* | 25-500nM SNP[243] | NO binds to NsrR which controls the transcription of motility and biofilm related genes[246] |
| *Fusobacterium nucleatum* | 1-10μM SNP[243] | Unknown |
| *Acinetobacter baumannii* | 200ppm gaseous NO[247] | Unknown |

| | | |
|---|---|---|
| *Nitrosomonas europaea* | 30ppm gaseous NO[248] | Unknown |
| *Shewanella woodyii* | 200μM DETA NONOate[249] | NO binds to SwH-NOX that upregulates phosphodiesterase activity and decrease intracellular c-di-GMP[249] |
| *Vibrio harveyi* | 100μM DPTA NONOate[250] | NO binds to H-NOX for the regulation of flagella through LuxU/LuxO/LuxR quorum sensing pathway[250] |
| *Neisseria gonorrheae* | >500nM SNP[251] | Unknown |
| *Shewanella oneidensis* | 50μM DPTA NONOate[252] | Unknown |
| *Bacillus licheniformis* | 100-500nM SNP[243] | Unknown |
| *Staphylococcus epidermidis* | 10μM SNP[243] | Unknown |
| *Staphylococcus aureus* | 200ppm gaseous NO and 1-1000μM DETA NONOate[247,253] | Unknown |

Table 1.5 Effect of Nitric oxide on bacterial biofilms, adapted from Nitric Oxide Regulation of Bacterial Biofilms.[252]

Apparently, despite NO having been proven to trigger dispersal in biofilms from various strains that are closely related to human health, the mechanisms in different strains have not been elucidated yet. From Table 1.5, two main pathways, NO-H-NOX and NO-PAS, are proposed to influence intracellular c-di-GMP level or quorum sensing. However, the studies into them, especially NO-PAS, is only in its infant.

## 1.5.1 NO-haem-H-NOX pathway

### The structure of H-NOX

In prokaryotic organisms, H-NOX serves as NO receptor through its haem binding site. It was originally identified in a bioinformatics search for sequence homologs in bacteria to sGC in mammalian cells. Once NO binds to the ferrous haem cofactor of sGC, the cyclase domain is activated and starts converting GTP to cyclic GMP, the secondary messenger signalling events[254]. So far, it is known that over 250 bacterial species across many phyla possess H-NOX domain, including *Proteobacteria, Firmicutes, Bacteroidetes, Cyanobacteria,* and *Thermotogae.* Certain bacterial classes such as *Actinobacteria* or *Bacilli*, however, do not contain H-NOX domains but are still involved in NO signalling, suggesting the existence of other NO sensors.

H-NOX has one subfamily found in facultative anaerobes that exhibits strict discrimination between $O_2$ and NO, making it a selective receptor that can coordinate low nanomolar NO in the presence of 1000-fold excess $O_2$ in aerobic environment. Another subfamily from obligate anaerobes is capable of binding both $O_2$ and NO with high affinity[255]. These suggest that H-NOX can adapt to different demands of bacterial

respiratory systems and perform different abilities. H-NOX domains are composed of a helical N-terminal subdomain and a C-terminal subdomain as shown below in Fig 1.5.1 (A). The haem cofactor is deeply buried between the two subdomains and the central iron is coordinated axially to a conserved His residue on α-helix F[241,256].

**H-NOX/c-di-GMP pathway**

Among the H-NOX domains discovered so far, the majority (~76%) of bacterial H-NOX domains are encoded as freestanding proteins and the others (~24%) are encoded as part of transmembrane methyl-accepting chemotaxis proteins (MCP)[255]. Freestanding H-NOX domain genes are frequently found involved in diverse signalling pathways, of which the most common one is histidine kinase (HK) – response regulator (RR). Another category of proteins frequently found linked to H-NOX contains DGCs and PDEs. Additionally, some RRs in H-NOX operons also contain HD-GYP (PDE) and GGDEF (DGC). These suggest that within different species, it is very likely that H-NOXs are closely linked to biofilm regulation. Carlson *et al* showed that in *L. pneumophila*, lpg1096 encodes a H-NOX and the adjacent lpg1097 encodes a GGDEF-EAL tandem. NO binding to H-NOX directly inhibits the DGC activity in lpg1097, resulting in reduced biofilm formation. The assays were done by observing biofilm formation phenotype and the *in vitro* diguanylate cyclase assays[257]. In contrast, the H-NOX-DGC/PDE tandem (HaCE) from *Shewanella woodyi* is capable of both the synthesis and degradation of c-di-GMP. Unliganded H-NOX activates the DGC while NO/H-NOX does not; instead NO/H-NOX activates PDE. The switch from DGC to PDE activity in HaCE is then proved to be triggered by NO binding H-NOX, which consequently reduces intracellular c-di-GMP level and biomass[249,258]. The assays were done by observing biofilm formation phenotype, UV−visible spectrum for the detection of $Fe^{2+}$-NO complex of H-NOX and *in vitro* steady-state kinetics analysis of diguanylate cyclase or phosphodiesterase activity with $Fe^{2+}$-NO or $Fe^{2+}$-unligated form of H-NOX[249].

**Interaction between NO and haem bound H-NOX**

So far the most deeply studied H-NOX structure is from *Thermoanaerobacter tengcongensis* due to its well-revealed crystal. However, due to the limitation on direct structural determination of unliganded H-NOX and liganded NO/H-NOX, site-directed mutagenesis was adopted to mimic the conformational changes. One model proposed is NO binding occurs at the open-coordination site of the 5-coordinate Fe(II), forming a

transient 6-coordinate complex. Upon binding, the NO association severely weakens the bond between the Fe(II) and histidine on α-helix F, leading to the dissociation of histidine and the formation of a Fe(II)-NO complex[255] as shown below in Fig 1.5.1 (B). In the inactive (unliganded) state, the haem is held by the coordination of the iron to the histidine on α-helix F. The formation of Fe(II)-NO complex and the subsequent dissociation of the histidine release the haem, allowing it to adopt a more planar geometry. Tight van-der-Waals contacts with residues such as isoleucine in N terminal (I5) and proline in C terminal (P115) are responsible for transferring the conformational haem relaxation to an upward shift and rotational displacement of the entire N-terminal subdomain with respect to α-helix F[255,259]. Although there is a lack of direct evidence, it is deduced that the regulation of H-NOX on its associated effectors (including HK-RR and DGC/PDE) probably comes from this rotational displacement relative to α-helix F, as the effector domains conceivably share the interaction surfaces with H-NOX including α-helix and part of N-terminal subdomain[255].

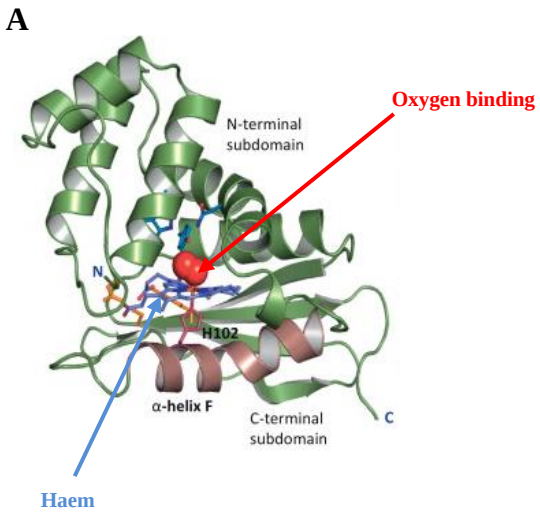

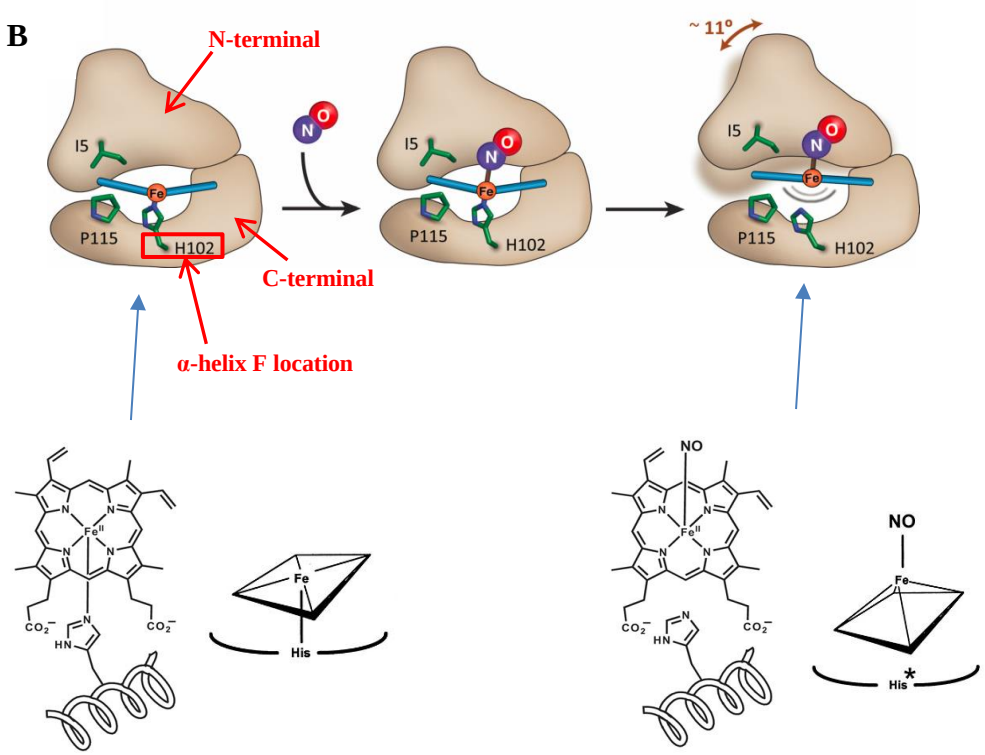


Fig 1.5.1. (A) X-ray crystal structure of *Thermoanaerobacter tengcongensis* (Tt) H-NOX (PDB 1U55). (B) NO/H-NOX activation model and the haem geometry transition from Fe(II)-His to Fe(II)-NO complex. In the unliganded H-NOX state, the haem is highly distorted due to the van-der-Waals interaction between P115 and I5 with two of the haem pyrroles. Initial formation of a six-coordinate Fe(II)-NO complex weakens the Fe-His bond and releases His. Formation of the 5- coordinate Fe(II)-NO complex allows relaxation of the haem into a more planar geometry. Contacts between the N-terminal helix and the haem, in particular through I5, trigger an upward rotational displacement of the N-terminal subdomain relative to the C-terminal subdomain. Image taken from Nitric Oxide-Sensing H-NOX Proteins Govern Bacterial Communal Behaviour[255], A structural basis for H-NOX signaling in *Shewanella oneidensis* by trapping a histidine kinase inhibitory conformation[259] and Nitric oxide signaling in brain: potentiating the gain with YC-1[260].

## 1.5.2. NO-heme-PAS pathway

Among haem-based sensors, PAS domains occur in proteins from all kingdoms of life and are widely utilized by bacteria to sense environmental changes such as NO molecule and transfer signals for adaptation. Examples of signal transduction proteins that are linked to PAS often include histidine kinases (HK), methyl-accepting chemotaxis proteins (MCP) and DGC/PDE in bacteria, which in turn can modulate c-di-GMP levels[185]. Understanding if NO binding to PAS domain can alter the enzymatic activities of DGC/PDEs that are greatly linked to biofilm formation/dispersal is one of the core targets in revealing NO-induced biofilm dispersal mechanisms.

### The structure of PAS domain

The PAS domain was first discovered as a conserved structure in *Drosophila* protein ***per***iod and ***si***ngle-***m***inded as well as vertebrate ***a***ryl hydrocarbon ***r***eceptor ***n***uclear ***t***ransporter, therefore it was named Per-Arnt-Sim or PAS[261,262]. PAS domains can be found as one or several copies within a single protein, and approximately 1/3 of PAS containing proteins possess two or more PAS domains[185]. Sequenced identities for PAS domains are low and lack universally conserved residues[263], with only a common trait of PAS domain containing a conserved core structure - a single antiparallel, five-stranded β-sheet arranged in order 2-1-5-4-3 with intervening α-helices creating a pocket on the β-sheet for ligand binding (Fig 1.5.2.1.)[264]. Signals originated by binding molecules within the conserved core generate structural changes predominantly within the β sheet and then propagate via α-helical and coiled-coil linkers to the covalently attached effector domains[264]. To date, high-resolution structures of more than sixty individual PAS domains have been deposited in Protein Data Bank (PDB)[185].

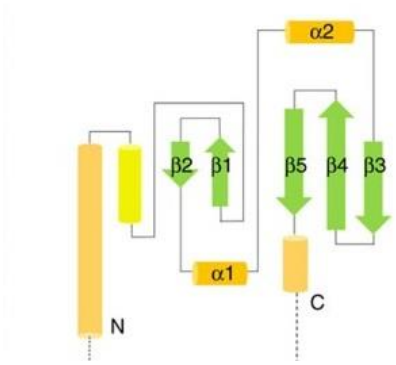


Fig 1.5.2.1. Topology of a core structure of PAS domain with β-strands arranged in the order of 2-1-5-4-3. Image taken from Structure and mechanism of the essential two-component signal-transduction system WalKR in *Staphylococcus aureus*[520].

**Interaction between NO and haem bound PAS**

The most important characteristics of the PAS domain family is that they can bind to a chemically diverse range of small molecules and then perform a variety of functions within signal transduction proteins[185]. It is now clear that NO binds to PAS containing a cofactor ferrous/ferric haem. The interaction between NO and the haem in PAS domain has not been extensively studied, but the primary principle of how NO binds to Fe-haem in PAS domain should be similar to how NO binds to haem in H-NOX proteins. Therefore, it is not reviewed here, but instead, one of our research interests. Two types of haem-PAS binding have been identified: *b*-type haem ligates through a conserved histidine residue[265–267] and *c*-type haem covalently bound through a bi-cysteine ligation site presented on the surface of the PAS domain (outside PAS core)[268,269]. The following

figures show the structure of *b*-type (Fig 1.5.2.2 A and B) and *c*-type (Fig 1.5.2.2 C and D) haem binding PAS in *Alphaproteobacteria* and *Geobacter sulfurreducens.*

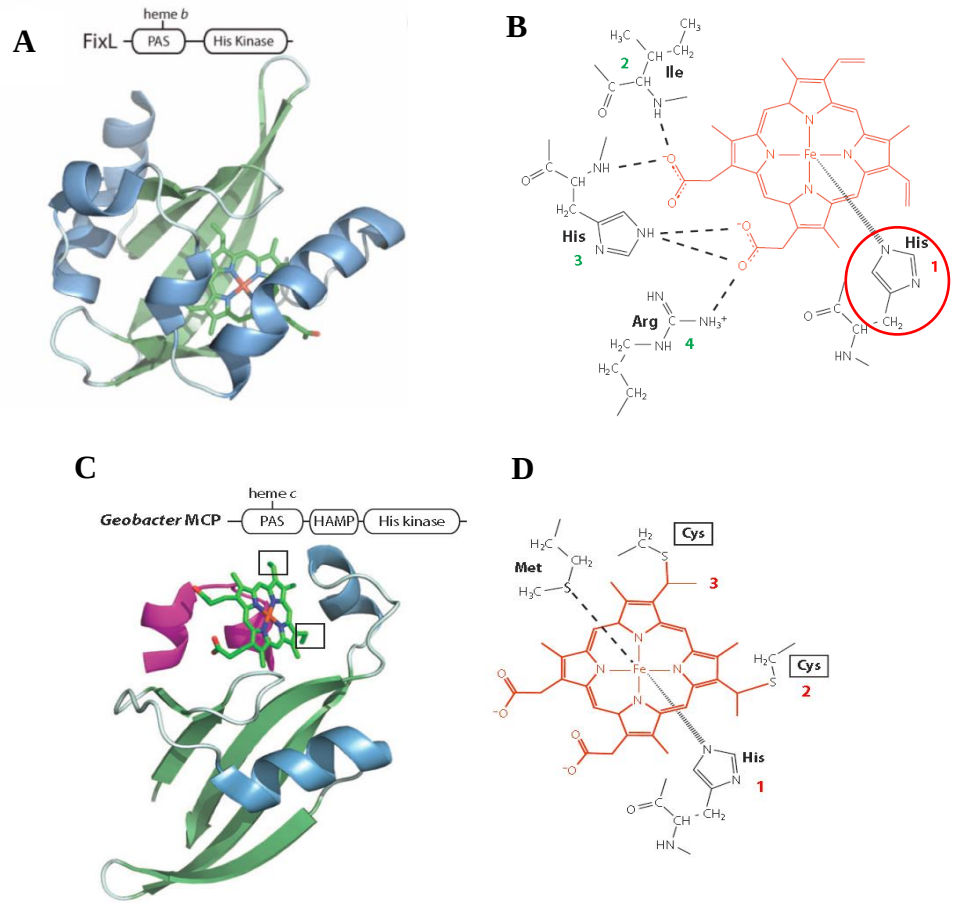


Fig 1.5.2.2. *b*-type and *c*-type heme binding structure. (A) Overall domain architecture and of PAS domain bound to heme *b*. (B)Drawing of protein interactions with the heme *b* cofactor in PAS marked with dotted lines or wedge lines (conserved Histidine residue marked in red circle). (C) Overall domain architecture and of PAS domain bound to heme *c*. (D)Drawing of protein interactions with the heme *c* cofactor in PAS marked with dotted line or wedge lines. Image taken from J.T.Henry *et al*, Ligand-binding PAS domains in a genomic, cellular, and structural context[185].

Despite the detailed studies on PAS domain structures and its frequent occurrence upstream of GGDEF and EAL domains, it is surprising that the research on how PAS modulates DGC and EAL seems very little, to our knowledge. Furthermore, so far there is no direct evidence from the perspective of either crystallography or enzymatic kinase that shows NO binding to PAS domain alters the downstream DGC/PDE activities thus influencing biofilms. Several but very limited studies on how PAS binding to other cofactors manipulates DGC/PDE might shed light on the unknown pathway for NO. Qi *et al* found that the cytoplasmic protein *Ax*DGC2 in *Acetobacter xylinum* regulates cellulose synthesis through modulating intracellular c-di-GMP level. *Ax*DGC2 contains one PAS domain and one GGDEF-EAL tandem, of which PAS domain binds a flavin

adenine dinucleotide (FAD) cofactor noncovalently. The authors showed that the oxidized form FAD increases the DGC catalytic activity[270]. Chang *et al* showed that the binding of $O_2$ to the ferrous haem reduced the PDE enzymatic activity of *Ax*PDEA1 in *Acetobacter xylinum*[271]. An *et al* showed that in *Pseudomonas aeruginosa* RbdA, a mutation in the PAS domain is critical for biofilm dispersal, but the authors did not show the link between PAS and GGDEF/EAL and c-di-GMP[272]. Hence, there is much to study in the future to unveil the detailed structural regulation on NO-PAS-GGDEF/EAL domains and c-di-GMP. Our group is looking into the crystal structure of MorA in *P. aeruginosa* which possesses 4 PAS domains and a GGDEF+EAL domain. If the crystal structure of whole protein and its change upon binding NO can be obtained, it will surely be of significant importance to explain how NO-PAS-GGDEF/EAL works at a structural level and shed light to other similar structures.

### 1.5.3. NO-copper-MHYT pathway

In addition to binding Fe, NO also interacts with copper atoms using three different ways: (1) acts as a ligand for copper atoms (2) engages in redox chemistry and (3) couples with the unpaired electron on $Cu^{2+}$ by an unpaired electron[273]. Model of MHYT domain (Fig 1.5.3) indicates that its conserved residues could coordinate one or two copper ions, thus is assumed to be able to sense NO[145]. MHYT domains are also linked to downstream GGDEF and EAL domain in MucR[147] and NbdA[146] in *P. aeruginosa*. What is the crystal structure of MHYT? How NO interacts with copper in MHYT? How this interaction modulates the structure of MHYT and how this modulation influence GGDEF/EAL domain which in turn affects c-di-GMP level? All these questions are waiting to be answered and have been one of the research directions in our group.

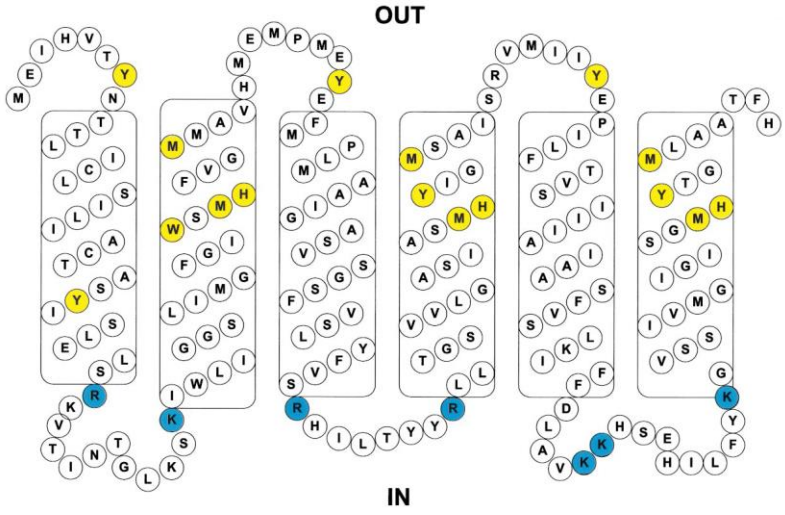

Fig 1.5.3. A model of the membrane orientation of the MHYT domain. Image taken from M.Y.Galperin *et al*, MHYT, a new integral membrane sensor domain[145]

## 1.5.4. Nitric Oxide donors

NO is a free radical with a complex chemistry characteristic, endowing its involvement in various biological actions. The most studied actions of NO are in the cardiovascular and nervous system, while the research of NO and biofilm has just begun. As with the concentration requirement that provide protective effects in cardiovascular and nervous system, the NO concentrations that induce biofilm dispersal are relatively low (in a window of picomolar to nanomolar). Higher concentrations lead to a completely different effect- rather than working as a signal molecule, it will become highly cytotoxic especially under conditions of oxidative stress[239]. Here I review some prevalently used NO donors; despite their usage being majorly based on clinical trials or just at experimental stage, it may be helpful for us to find the best NO donor for biofilm dispersal research.

### 1.5.4.1. Organic Nitrates and Nitrite Esters

The conventional organic nitrate and nitrite esters such as nitroglycerin, amyl nitrite and isosorbide dinitrate have been widely used for their cheap, effective and rapid application in cardiovascular diseases (Fig 1.5.4.1.a, b, c)[274,275]. The basic mechanism of NO release from these kinds of NO donors is the activation of nitrate ester moieties ($-ONO_2$) to liberate NO by some endogenous pathways[275]. The limitations of this class of agents include potentially adverse hemodynamic effects, drug tolerance, lack of selectivity, and limited bioavailability[274]. Most importantly, all of organic nitrate esters are prodrugs that require enzymatic metabolism to generate bioactive NO[274]. Therefore, although widely used in human or animals, it might not be a suitable class of NO donor for microorganism. Since the enzymes involved have not been specifically characterized, probably it is worth trying these agents in biofilm to see the outcomes.

Another clinically relevant NO donor in current use is sodium nitroprusside (SNP) (Fig 1.5.4.1.d). The mechanism of NO release from SNP is complex and has not yet been fully elucidated. SNP can remain stable in aqueous environment without light exposure for up to 6 months and does not release NO spontaneously in the physiological environment; instead, it requires either light or a reducing agent[276]. SNP has been used

in our group but performed inconsistently, at least for *P. aeruginosa* biofilms (data not shown). Hence, different NO donors may be needed to replace SNP in future work.

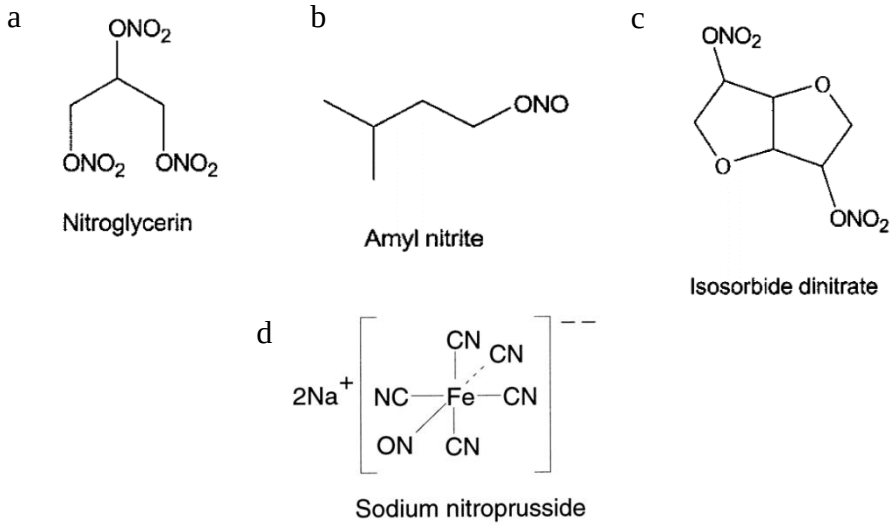


Fig 1.5.4.1. Structures of some conventional organic nitrate and nitrite esters (a, b, c) and SNP (d).

### 1.5.4.2. S-Nitrosothiols

S-nitrosothiols (general formula RSNO) are a class of naturally occurring NO donors that release NO and nitrosonium ($NO^+$) spontaneously from the moiety (-SNO)[274]. However, the effect of these compounds is based on NO as $NO^+$ does not activate guanylate cyclase[274]. Members of this class of agents include S-nitroso-glutathione (GSNO), S-nitroso-N-acetylpenicillamine (SNAP), S-nitroso-albumin, S-nitroso-N-acetyl-L-cysteine, S-nitroso-N-valerylpenicillamine (SNVP) etc (Fig 1.5.4.2.)[277,278]. S-Nitrosothiols are not used in clinical trials currently but only in animal experiments and laboratory studies[239]. Much of the early investigations of S-nitrosothiols in cardiovascular system concentrated on GSNO which is generally used as a powerful antiplatelet agent[275]. The benefit of GSNO is that its by-products are nontoxic compared to cyanide produced by SNP[275]. S-Nitroso-N-acetylpenicillamine (SNAP) is a synthetic S-nitrosothiol highly sensitive to trace copper catalysed decomposition. The limitation of S-nitrosothiols is their unpredictable stability in solution resulting in half-lives vary from milliseconds to hours depending on the R-group, pH and solvent[275]. So far, NO donors belonging to this category that have been tested in our group are GSNO and SNAP, showing the ability to reduce established biofilms (unpublished data). Further optimisation of their concentrations applied in biofilm dispersal is needed.

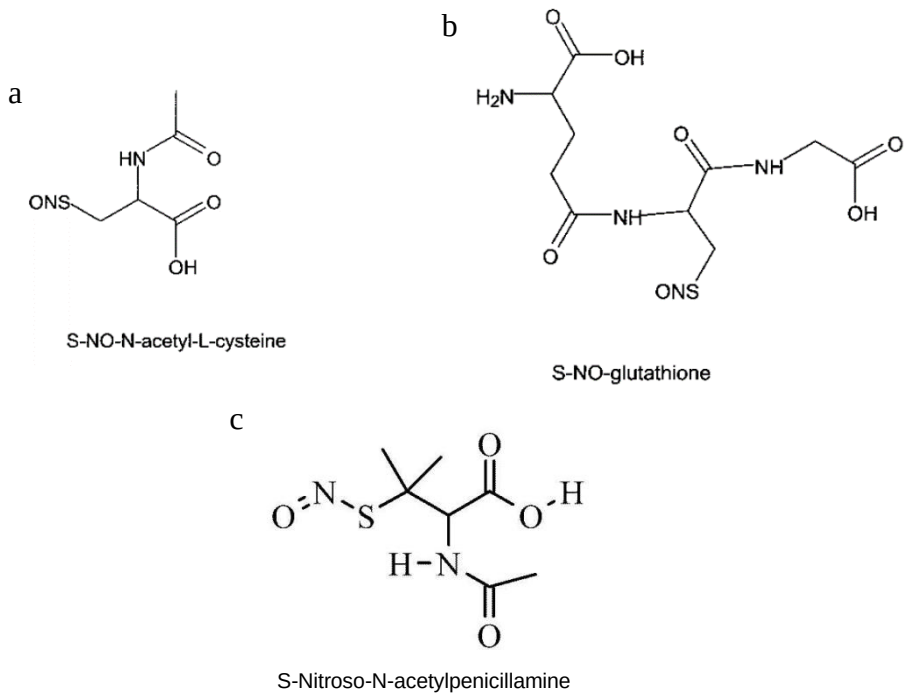


Fig 1.5.4.2. Structures of selected S-nitrosothiols

### 1.5.4.3. Diazeniumdiolates (NONOates)

Diazeniumdiolates have been recognized and synthesized since 1960[279]. However, attentions has been focused on from 1990s when their NO donor properties were considered in biological settings[280]. These compounds consist of a diolate group [N(O-)N=O] bound to a nucleophile adduct via a nitrogen atom[280].The half-lives of a range of NONOates vary from seconds to hours[281], but due to their NO release follows the simple first-order kinetics[281], the rate can be accurately predicted. The most frequently studied NONOates include diethylamine NONOate (DEA/NO), spermine NONOate (SPER/NO or S150), Proli NONOate (PROLI/NO), V-PYRRO/NO and JS-K etc (Fig 1.5.4.3.). Up to now, NONOates have not been used clinically and have only been tested in experimental models for cardiovascular disease research. The most outstanding feature of this class of compounds for biofilm studies is that instead of biologically decomposition, they decompose spontaneously in solution at physiological pH and temperature to generate up to 2 molar equivalents of NO of which the rate is dependent on the structure of the nucleophile[239,282]. This spontaneous reaction significantly reduces the requirement on specific enzymes for triggering NO release, resulting in its potential wide applications in both eukaryotic and prokaryotic cells. Thus, further research about their applications in biofilm dispersal is of high interest.

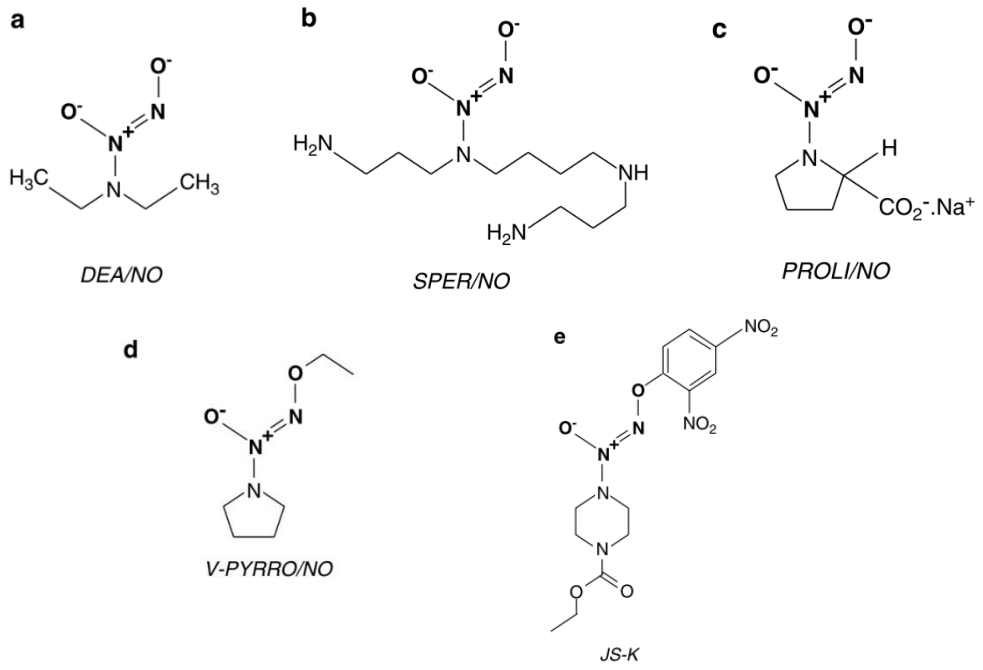


Fig 1.5.4.3 Structures of selected diazeniumdiolate (NONOate)

### 1.5.4.4. NO hybrid drugs - NO-Nonsteroidal anti-inflammatory (NO-NSAIDs)

Hybrid NO donor drugs belong to a broad and novel group of compounds that covers a range of established drugs which are structurally modified to incorporate NO-containing molecules[239].

The high efficacy and low cost of NSAIDs make drugs such as aspirin becoming invaluable in a number of clinical fields. However, prolonged use of aspirin leads to serious side effects in the gastrointestinal tract, which causes ~16000 deaths each year in the USA[239]. NO has a number of effects in the gastrointestinal tract that could counteract the loss of protective prostanoids caused by aspirin[283], leading to the idea of incorporating NO-releasing moieties into aspirin (also called nitroaspirins). This brought up the studies of incorporating different NO moieties into different NSAIDs. Currently NO-NSAID compounds adapted from aspirin to contain a nitrate group are the NicOx compounds, including NCX4016, NCX4018, NCX4215 and NCX4050etc (Fig 1.5.4.4.)[239,284]. The majority of nitroaspirins share the same NO donor moiety and the mechanism of NO release, hence, it is reasonable for scientists to consider new NSAIDs agents with nitrates groups. As a result, paracetamol[285], flurbiprofen[286], naproxen[287], mesalamine[288], gabapentin[289], predisolone and other steroids[290] with nitrate groups came into notice. On the other hand, replacement of nitrate groups with other moieties such as

furoxan[291,292], S-nitroso-[293] and diazeniumdiolate[294] on different NSAIDs has also been described.

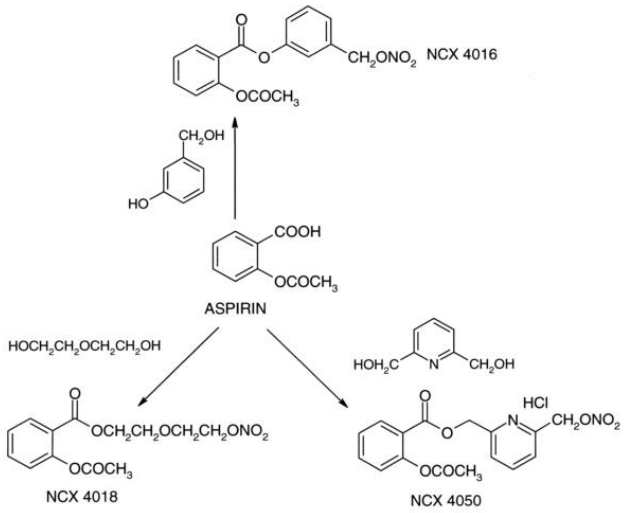


Fig 1.5.4.4. Structures of selected nitric oxide-releasing aspirins

### 1.5.4.5. Biofilm-targeted NO donor

Biofilm-targeted prodrugs appear as ideal NO donors for biofilm since they release NO only after the reaction with a bacteria-specific enzyme. This characteristic can be important and beneficial in clinical trials if applied, as these drugs can localise NO releasing to biofilm infection sites and minimise the exposure of host tissues to NO. Yepuri *et al* for the first time designed cephalosporin-3′-diazeniumdiolate (DEACP) NO-donor prodrug which selectively releases NO upon contact with the bacterial enzyme β-lactamase[295]. By growing the PAO1 biofilms supplied with the sub-inhibitory concentration of imipenem to induce β-lactamase expression, it is shown that DEACP can reduce biofilm significantly at concentrations ranging from 10 μM to 100 μM, thus making it a very promising biofilm-specific NO donor. The mechanism of NO release from DEACP is shown below (Fig 1.5.4.5.)[295].

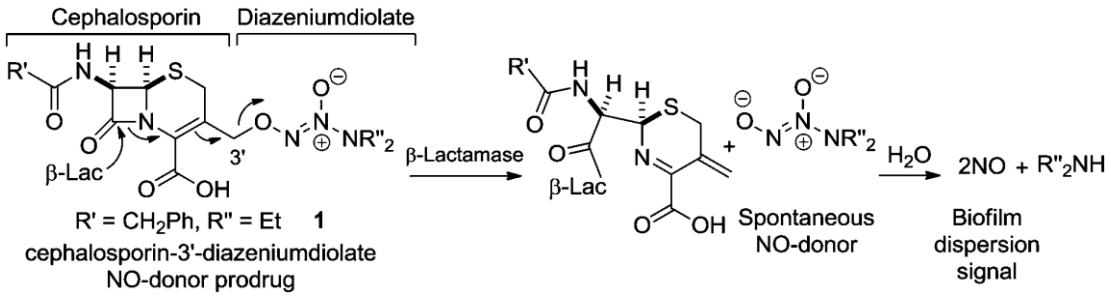


Fig 1.5.4.5. Proposed mechanism of β-lactamase-triggered NO release and biofilm dispersion bycephalosporin-3'-diazeniumdiolates. Image taken from Synthesis of cephalosporin-3'-diazeniumdiolates: biofilm dispersing NO-donor prodrugs activated by β-lactamase[295]

# Aims of the project

I. Sodium nitroprusside has been proved to effectively release NO for decreasing intracellular c-di-GMP in *P. aeruginosa* and dispersing its biofilms. However, SNP needs light exposure or reducing agent to release NO and produces cyanide as a side-product. Hence, it might not be the best NO donor candidate for biofilm treatment in human. Many new NO donors have been found during the last few decades but little studies have been done for their applications on bacteria signaling, especially biofilm dispersal. Thus, my first task is to find out a different and efficient NO donor for triggering *P. aeruginosa* biofilms dispersal.

   (1) 7 NO donors were chosen to disperse PAO1 WT biofilm at different concentrations.

   (2) The most effective donor is then applied to CF PA clinical isolates biofilms/cell aggregates for dispersal assays.

II. In total 39 genes that encode GGDEF and/or EAL domain[212] and 54 genes that encode PAS/MHYT domain are found in *P. aeruginosa* PAO1, among which 13 contain both PAS/MHYT and GGDEF/EAL (Table below) as well as a BdlA containing only PAS but is supposed to interact with another PDE named DipA[296]. GGDEF and EAL domains are responsible for the synthesis and hydrolysis of c-di-GMP respectively, while PAS may potentially bind NO and regulate the activities of GGDEF/EAL domains. Therefore, these 14 genes may participate in NO sensing and intracellular c-di-GMP level modulation, which lead to biofilm formation/dispersal. My second aim is to delete these 14 genes in *P. aeruginosa* PAO1, look into mutants' phenotypes when treated with NO and compare with WT for picking out the most prominent NO sensor(s) for biofilm dispersal.

| | Gene | Name | PAS | MHYT | DGC | PDE | DGC+PDE |
|---|---|---|---|---|---|---|---|
| 1 | PA0285 | -- | + | -- | GGDEF | ESL | GGDEF+ESL |
| 2 | PA0575 | -- | + | -- | GGDEF | EAL | GGDEF+EAL |
| 3 | PA0861 | RbdA | + | -- | GGDEF | ELL | GGDEF+ELL |
| 4 | PA1181 | YegE | + | -- | GGDEF | ELL | GGDEF+ELL |
| 5 | PA4601 | MorA | + | -- | GGDEF | EAL | GGDEF+EAL |
| 6 | PA5017 | DipA | + | -- | ASNEF | EAL | ASNEF+EAL |
| 7 | PA5442 | -- | + | -- | AGDEF | EAL | AGDEF+EAL |
| 8 | PA4959 | FimX | + | -- | GDSIF | EVL | GDSIF+EVL |
| 9 | PA0847 | -- | + | -- | GGDEF | -- | GGDEF |
| 10 | PA0290 | -- | + | -- | GGEEF | -- | GGEEF |
| 11 | PA0338 | -- | + | -- | GGEEF | -- | GGEEF |
| 12 | PA1727 | MucR | -- | + | GGDEF | EAL | GGDEF+EAL |
| 13 | PA3311 | NbdA | -- | + | AGDEF | EAL | AGDEF+EAL |
| 14 | PA1423 | BdlA | + | -- | -- | -- | -- |

(1) Develop an efficient gene knockout method to delete 14 genes in a relatively short time period.

(2) *In vivo* intracellular c-di-GMP levels measurement of PAO1 WT and mutants with/without NO.

(3) Mutants' biofilms dispersal assay with NO.

(4) Colony morphologies and growth curves measurement for 14 mutant strains.

(5) Motility assays (swimming, swarming, twitching) for 14 mutant strains with/without NO.

(6) Biofilm EPS components determination (total exopolysaccharides and total protein) for 14 mutant strains.

N.B. (4), (5) and (6) were tested for their close relationship with biofilm formation and potential regulation pathways under the control of c-di-GMP

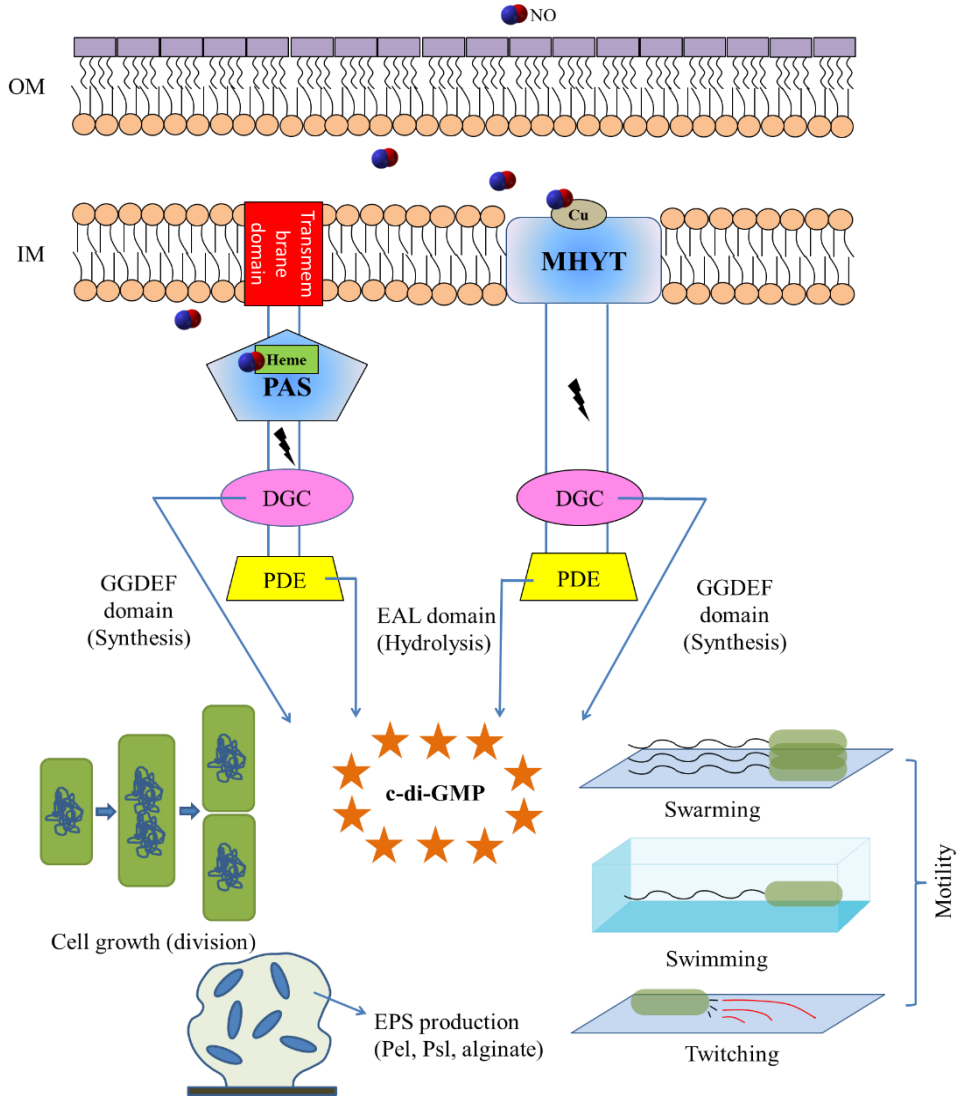


**Hypothetical mechanism of NO influencing DGC/PDEs that modulate intracellular c-di-GMP levels and biofilm related phenotypes**

# Chapter 2 - Materials and Methods

## 2.1. Bacterial strains and culture media

| **Strains and plasmids** | Genotype or phenotypes[a] | Source or reference |
|---|---|---|
| ***E.coli*** | | |
| S17-1(λpir) | *TpR SmR recA, thi, pro, hsdR-M+RP4*: 2-Tc:Mu: Km Tn7 | Biomedal corp. |
| DH5α | *spuE44* Δ*lacU169*(ϕ80*lacZ*ΔM15) *hsdR17* λpir *recA1 endA1 gyrA96 thi-1 relA1* | Lab collection |
| ***P.aeruginosa*** | | |
| PAO1 | Wild-Type | [297] |
| | **PAO1 KO mutants** | |
| Δ*pa0285* | PAO1 mutant (*pa0285::aacCl*); $Gm^R$ | This study |
| Δ*pa0290* | PAO1 mutant (*pa0290::aacCl*); $Gm^R$ | This study |
| Δ*pa0338* | PAO1 mutant (*pa0338::aacCl*); $Gm^R$ | This study |
| Δ*pa0575* | PAO1 mutant (*pa0575::aacCl*); $Gm^R$ | This study |
| Δ*pa0847* | PAO1 mutant (*pa0847::aacCl*); $Gm^R$ | This study |
| Δ*pa0861* | PAO1 mutant (*pa0861::aacCl*); $Gm^R$ | This study |
| Δ*pa1181* | PAO1 mutant (*pa1181::aacCl*); $Gm^R$ | This study |
| Δ*pa1423* | PAO1 mutant (*pa1423::aacCl*); $Gm^R$ | This study |
| Δ*pa1727* | PAO1 mutant (*pa1727::aacCl*); $Gm^R$ | This study |
| Δ*pa3311* | PAO1 mutant (*pa3311::aacCl*); $Gm^R$ | This study |
| Δ*pa4601* | PAO1 mutant (*pa4601::aacCl*); $Gm^R$ | This study |
| Δ*pa4959* | PAO1 mutant (*pa4959::aacCl*); $Gm^R$ | This study |
| Δ*pa5017* | PAO1 mutant (*pa5017::aacCl*); $Gm^R$ | This study |
| Δ*pa5442* | PAO1 mutant (*pa5442::aacCl*); $Gm^R$ | This study |
| | **PAO1 KO mutants with c-di-GMP reporter gfp vector** | |
| PAO1 Tn7CdrA::*gfp* | PAO1 WT with mini-Tn7-$P_{cdrA}$-RBSII-*gfp*(Mut3)-$T_0$-$T_1$;$Gm^R$;$Tet^R$ | This study |
| Δ*pa0285* Tn7CdrA::*gfp* | PAO1 mutant (*pa0285::aacCl*) with mini-Tn7-$P_{cdrA}$-RBSII-*gfp*(Mut3)-$T_0$-$T_1$;$Gm^R$;$Tet^R$ | This study |
| Δ*pa0290* Tn7CdrA::*gfp* | PAO1 mutant (*pa0290::aacCl*) with mini-Tn7-$P_{cdrA}$-RBSII-*gfp*(Mut3)-$T_0$-$T_1$;$Gm^R$;$Tet^R$ | This study |
| Δ*pa0338* Tn7CdrA::*gfp* | PAO1 mutant (*pa0338::aacCl*) with mini-Tn7-$P_{cdrA}$-RBSII-*gfp*(Mut3)-$T_0$-$T_1$;$Gm^R$;$Tet^R$ | This study |
| Δ*pa0575* Tn7CdrA::*gfp* | PAO1 mutant (*pa0575::aacCl*) with mini-Tn7-$P_{cdrA}$-RBSII-*gfp*(Mut3)-$T_0$-$T_1$;$Gm^R$;$Tet^R$ | This study |
| Δ*pa0847* Tn7CdrA::*gfp* | PAO1 mutant (*pa0847::aacCl*) with mini-Tn7-$P_{cdrA}$-RBSII-*gfp*(Mut3)-$T_0$-$T_1$;$Gm^R$;$Tet^R$ | This study |
| Δ*pa0861* Tn7CdrA::*gfp* | PAO1 mutant (*pa0861::aacCl*) with mini-Tn7-$P_{cdrA}$-RBSII-*gfp*(Mut3)-$T_0$-$T_1$;$Gm^R$;$Tet^R$ | This study |
| Δ*pa1181* Tn7CdrA::*gfp* | PAO1 mutant (*pa1181::aacCl*) with mini-Tn7-$P_{cdrA}$-RBSII-*gfp*(Mut3)-$T_0$-$T_1$;$Gm^R$;$Tet^R$ | This study |
| Δ*pa1423* Tn7CdrA::*gfp* | PAO1 mutant (*pa1423::aacCl*) with mini-Tn7-$P_{cdrA}$-RBSII-*gfp*(Mut3)-$T_0$-$T_1$;$Gm^R$;$Tet^R$ | This study |
| Δ*pa1727* Tn7CdrA::*gfp* | PAO1 mutant (*pa1727::aacCl*) with mini-Tn7-$P_{cdrA}$-RBSII-*gfp*(Mut3)-$T_0$-$T_1$;$Gm^R$;$Tet^R$ | This study |
| Δ*pa3311* Tn7CdrA::*gfp* | PAO1 mutant (*pa3311::aacCl*) with mini-Tn7-$P_{cdrA}$-RBSII-*gfp*(Mut3)-$T_0$-$T_1$;$Gm^R$;$Tet^R$ | This study |
| Δ*pa4601* Tn7CdrA::*gfp* | PAO1 mutant (*pa4601::aacCl*) with mini-Tn7-$P_{cdrA}$-RBSII-*gfp*(Mut3)-$T_0$-$T_1$;$Gm^R$;$Tet^R$ | This study |
| Δ*pa4959* Tn7CdrA::*gfp* | PAO1 mutant (*pa4959::aacCl*) with mini-Tn7-$P_{cdrA}$-RBSII-*gfp*(Mut3)-$T_0$-$T_1$;$Gm^R$;$Tet^R$ | This study |
| Δ*pa5017* Tn7CdrA::*gfp* | PAO1 mutant (*pa5017::aacCl*) with mini-Tn7-$P_{cdrA}$-RBSII-*gfp*(Mut3)-$T_0$-$T_1$;$Gm^R$;$Tet^R$ | This study |
| Δ*pa5442* Tn7CdrA::*gfp* | PAO1 mutant (*pa5442::aacCl*) with mini-Tn7-$P_{cdrA}$-RBSII-*gfp*(Mut3)-$T_0$-$T_1$;$Gm^R$;$Tet^R$ | This study |
| PA08 | *P. aeruginosa* clinical isolates from Southampton General hospital CF patients | Sputum samples from 72 patients with CF (median age at informed consent 21 years, range 17-62; UK NHS Research Ethics Reference 08/H0502/1 26 |
| PA10 | *P. aeruginosa* clinical isolates from Southampton General hospital CF patients | |
| PA15 | *P. aeruginosa* clinical isolates from Southampton General hospital CF patients | |
| PA20 | *P. aeruginosa* clinical isolates from Southampton General hospital CF patients | |
| PA21 | *P. aeruginosa* clinical isolates from Southampton General hospital CF patients | |
| PA26 | *P. aeruginosa* clinical isolates from Southampton General hospital CF patients | |
| PA30 | *P. aeruginosa* clinical isolates from Southampton General hospital CF patients | |
| PA37 | *P. aeruginosa* clinical isolates from Southampton General hospital CF patients | |
| PA39 | *P. aeruginosa* clinical isolates from Southampton General hospital CF patients | |
| PA44 | *P. aeruginosa* clinical isolates from Southampton General hospital CF patients | |
| PA49 | *P. aeruginosa* clinical isolates from Southampton General hospital CF patients | |
| PA55 | *P. aeruginosa* clinical isolates from Southampton General hospital CF patients | |
| PA56 | *P. aeruginosa* clinical isolates from Southampton General hospital CF patients | |
| PA57 | *P. aeruginosa* clinical isolates from Southampton General hospital CF patients | |
| PA58 | *P. aeruginosa* clinical isolates from Southampton General hospital CF patients | |
| PA66 | *P. aeruginosa* clinical isolates from Southampton General hospital CF patients | |
| PA68 | *P. aeruginosa* clinical isolates from Southampton General hospital CF patients | |
| | **PAO1 Transposon mutants** | |
| PW1520 (ΔTn*0285 A*) | PAO1 with Transposon ISlacZ/hah inserted after nt 1716 of pa0285; $Tet^R$ | Tn library[298] |
| PW1521 (ΔTn*0285 B*) | PAO1 with Transposon ISphoA/hah inserted after nt 956 of pa0285; $Tet^R$ | Tn library[298] |
| PW1532 (ΔTn*0290 A*) | PAO1 with Transposon ISphoA/hah inserted after nt 131 of pa0290; $Tet^R$ | Tn library[298] |
| PW1531 (ΔTn*0290 B*) | PAO1 with Transposon ISphoA/hah inserted after nt 496 of pa0290; $Tet^R$ | Tn library[298] |
| PW1627 (ΔTn*0338 A*) | PAO1 with Transposon ISphoA/hah inserted after nt 585 of pa0338; $Tet^R$ | Tn library[298] |

| | | |
|---|---|---|
| PW1626 (ΔTn*0338 B*) | PAO1 with Transposon ISlacZ/hah inserted after nt 929 of pa0338; $Tet^R$ | Tn library[298] |
| PW2061 (ΔTn*0575 A*) | PAO1 with Transposon ISphoA/hah inserted after nt 2494 of pa0575; $Tet^R$ | Tn library[298] |
| PW2060 (ΔTn*0575 B*) | PAO1 with Transposon ISphoA/hah inserted after nt 1900 of pa0575; $Tet^R$ | Tn library[298] |
| PW5581 (ΔTn*0575 C*) | PAO1 with Transposon ISlacZ/hah inserted after nt 1586 of pa0575; $Tet^R$ | Tn library[298] |
| PW2543 (ΔTn*0847 A*) | PAO1 with Transposon ISphoA/hah inserted after nt 1026 of pa0847; $Tet^R$ | Tn library[298] |
| PW2544 (ΔTn*0847 B*) | PAO1 with Transposon ISphoA/hah inserted after nt 988 of pa0847; $Tet^R$ | Tn library[298] |
| PW2570 (ΔTn*0861 A*) | PAO1 with Transposon ISphoA/hah inserted after nt 706 of pa0861; $Tet^R$ | Tn library[298] |
| PW2569 (ΔTn*0861 B*) | PAO1 with Transposon ISlacZ/hah inserted after nt 1168 of pa0861; $Tet^R$ | Tn library[298] |
| PW3133 (ΔTn*1181 A*) | PAO1 with Transposon ISlacZ/hah inserted after nt 1757 of pa1181; $Tet^R$ | Tn library[298] |
| PW3134 (ΔTn*1181 B*) | PAO1 with Transposon ISphoA/hah inserted after nt 2959 of pa1181; $Tet^R$ | Tn library[298] |
| PW4044 (ΔTn*1727 A*) | PAO1 with Transposon ISphoA/hah inserted after nt 946 of pa1727; $Tet^R$ | Tn library[298] |
| PW4043 (ΔTn*1727 B*) | PAO1 with Transposon ISlacZ/hah inserted after nt 487 of pa1727; $Tet^R$ | Tn library[298] |
| PW6568 (ΔTn*3311 A*) | PAO1 with Transposon ISphoA/hah inserted after nt 1548 of pa3311; $Tet^R$ | Tn library[298] |
| PW6567 (ΔTn*3311 B*) | PAO1 with Transposon ISlacZ/hah inserted after nt 1578 of pa3311; $Tet^R$ | Tn library[298] |
| PW6569 (ΔTn*3311 C*) | PAO1 with Transposon ISphoA/hah inserted after nt 1850 of pa3311; $Tet^R$ | Tn library[298] |
| PW8754 (ΔTn*4601*) | PAO1 with Transposon ISlacZ/hah inserted after nt 2905 of pa4601; $Tet^R$ | Tn library[298] |
| PW9347 (ΔTn*4959 A*) | PAO1 with Transposon ISphoA/hah inserted after nt 961 of pa4959; $Tet^R$ | Tn library[298] |
| PW9346 (ΔTn*4959 B*) | PAO1 with Transposon ISlacZ/hah inserted after nt 1158 of pa4959; $Tet^R$ | Tn library[298] |
| PW5475 (ΔTn*5017 A*) | PAO1 with Transposon ISphoA/hah inserted after nt 890 of pa5017; $Tet^R$ | Tn library[298] |
| PW9424 (ΔTn*5017 B*) | PAO1 with Transposon ISphoA/hah inserted after nt 1059 of pa5017; $Tet^R$ | Tn library[298] |
| PW9425 (ΔTn*5017 C*) | PAO1 with Transposon ISphoA/hah inserted after nt 1557 of pa5017; $Tet^R$ | Tn library[298] |
| PW10194 (ΔTn*5442 A*) | PAO1 with Transposon ISphoA/hah inserted after nt 1561 of pa5442; $Tet^R$ | Tn library[298] |
| PW10193 (ΔTn*5442 B*) | PAO1 with Transposon ISlacZ/hah inserted after nt 1418 of pa5442; $Tet^R$ | Tn library[298] |
| PW10195 (ΔTn*5442 C*) | PAO1 with Transposon ISphoA/hah inserted after nt 881 of pa5442; $Tet^R$ | Tn library[298] |
| **Plasmids** | | |
| pPS856 | $Ap^R$, $Gm^R$; 0.83-kb blunt-ended SacI fragment from pUCGM | [299] |
| pEX100T | $Ap^R$; $oriT^+$ $sacB^+$ gene replacement vector | [299] |
| pCdrA::*gfp* | pUCP22Not-$P_{cdrA}$-RBSII-*gfp*(Mut3)-$T_0$-$T_1$, $Amp^R$ $Gm^R$ | [300] |

Routine overnight cultures were grown in lysogeny broth (LB) medium with shaking at 37°C, 120rpm for 15 hrs from a single colony on fresh overnight agar plates. Purchased *P. aeruginosa* transposon mutants from Washington library were selected on Cetrimide agar with tetracycline at a final concentration of 60μg/ml and propagated in LB broth with tetracycline at a final concentration of 5μg/ml as suggested by Washington library. Gene-deleted PAO1 KO mutants were selected on Cetrimide agar with gentamicin at a final concentration of 30μg/ml. PAO1 WT with c-di-GMP gauging vector was selected on Cetrimide agar with tetracycline (75μg/ml). Gene-deleted PAO1 mutants with c-di-GMP gauging vector were selected on Cetrimide agar with both gentamicin and tetracycline at final concentration of 30μg/ml and 75μg/ml respectively. Biofilms were grown in standard M9 minimal medium containing 48 mM $Na_2HPO_4$, 22 mM $KH_2PO_4$, 9 mM NaCl, 19 mM $NH_4Cl$, 2 mM $MgSO_4$, 100μM $CaCl_2$, 20mM glucose according to Cold Spring Harbor Protocols[301].

## 2.2. Primers

| Primer | Sequence (5'→3') |
|---|---|
| **KO mutants generation and sequencing** | |
| Δ*pa0285* | |
| PA0285-up-F | ATGC*CCCGGG* CCTGACCGACAATCTCGAC |
| PA0285-up-R | ATGC*GAATTC* GTTCCAGATCTCTCCGCTC |
| PA0285-dn-F | ATGC*AAGCTT* AGTCACCGAAAGCGCGG |
| PA0285-dn-R | ATGC*CCCGGG* TCAGTCTTCCGGCAGCG |
| SeqPA0285-F | GTAACTGCCACCAGTTGC |

| | |
|---|---|
| SeqPA0285-R | CCATCCAGGCTTCTGAG |
| | |
| Δ*pa0290* | |
| PA0290-up-F | ATGC*CCCGGG* GCGAATGGTCTACGTCAGC |
| PA0290-up-R | ATGC*GAATTC* CAGGAACGCCAACGGTATC |
| PA0290-dn-F | ATGC*AAGCTT* GCGACCTGTTCGGGC |
| PA0290-dn-R | ATGC*CCCGGG* TCAGCCCACGACGATG |
| SeqPA0290-F | GTATCGCTCGGCAACTG |
| SeqPA0290-R | CCTTTCTGGCGAGTTACC |
| | |
| Δ*pa0338* | |
| PA0338-up-F | ATGC*CCCGGG* GTGCGGCGCTTACGC |
| PA0338-up-R | ATGC*GAATTC* CTCGGGATGGATGATGC |
| PA0338-dn-F | ATGC*AAGCTT* CCTGTTCGGCCACTCC |
| PA0338-dn-R | ATGC*CCCGGG* TCAGCAACAGGCCACG |
| SeqPA0338-F | CAAGGTGAAGTGGCTGC |
| SeqPA0338-R | CTCCAGCGTGTTCATCG |
| | |
| Δ*pa0575* | |
| PA0575-up-F | ATGC*CCCGGG* GATCATCATCCTGGCACG |
| PA0575-up-R | ATGC*GAATTC* GGACGATGGGAAGACCG |
| PA0575-dn-F | ATGC*AAGCTT* GCCGAGGATTGCGG |
| PA0575-dn-R | ATGC*CCCGGG* CACCGTGAGCTGCATG |
| SeqPA0575-F | GACGAGTGACGAACGAAC |
| SeqPA0575-R | GTTGCCATCAGATAAGGAC |
| | |
| Δ*pa0847* | |
| PA0847-up-F | ATGC*CCCGGG* CCGTCGCCGAGGAC |
| PA0847-up-R | ATGC*GAATTC* GTCGTAGCTGGCATCCC |
| PA0847-dn-F | ATGC*AAGCTT* CGCGCCATGCAGAG |
| PA0847-dn-R | ATGC*CCCGGG* CGCCCAGGCGGTAG |
| SeqPA0847-F | GGAACTTATCCATGCGGTTG |
| SeqPA0847-R | GTGGCTGAACTGCTGCATC |
| | |
| Δ*pa0861* | |
| PA0861-up-F | ATGC*CCCGGG* ATGAGGCAGAACCGGACTC |
| PA0861-up-R | ATGC*GAATTC* AGCTCGATGGCGCG |
| PA0861-dn-F | ATGC*AAGCTT* GGTTGCCAACCTGGCC |
| PA0861-dn-R | ATGC*CCCGGG* CTACCGGAGGTTCTGTCCC |
| SeqPA0861-F | CAGCCACTAGACTCCTACTG |
| SeqPA0861-R | CAGTCGACGATCAGTTGC |
| | |
| Δ*pa1181* | |
| PA1181-up-F | ATGC*CCCGGG* TTCGCGTGCTCTGGG |
| PA1181-up-R | ATGC*GAATTC* AGGCCATCGGCAGGTAC |
| PA1181-dn-F | ATGC*AAGCTT* CTTCGAGCTGACCGAGACG |
| PA1181-dn-R | ATGC*CCCGGG* TCAGCCCAACTCCTGGC |
| SeqPA1181-F | CTGAGCCTGGACGATTC |
| SeqPA1181-R | CTGCACATGAGTTCGCAG |
| | |
| Δ*pa1423* | |
| PA1423-up-F | ATGC*CCCGGG*TCACCGATGCCAATGAG |
| PA1423-up-R | ATGC*GAATTC*CGTGTTCCTGGTGGACG |
| PA1423-dn-F | ATGC*AAGCTT*GCCGAGCAGACCAACC |
| PA1423-dn-R | ATGC*CCCGGG*GAGGGTGCGCGAGAAC |
| SeqPA1423-F | CGAAGACAGGGATGAGC |
| SeqPA1423-R | GCTACATCGGTTACCTGC |
| | |
| Δ*pa1727* | |
| PA1727-up-F | ATGC*CCCGGG* CCATCCTGGCGTCCTACAC |
| PA1727-up-R | ATGC*GAATTC* AGCCACAGCGGGTCG |
| PA1727-dn-F | ATGC*AAGCTT* GCCTGGAGCCCAGCC |
| PA1727-dn-R | ATGC*CCCGGG* TCAGGCGACGCTGGC |
| SeqPA1727-F | GAGCAAGATTCCGCCTG |
| SeqPA1727-R | TTGCTCATGCGAGCCATC |
| | |
| Δ*pa3311* | |
| PA3311-up-F | ATGC*CCCGGG* CGTCGACGGCTACGTG |
| PA3311-up-R | ATGC*GAATTC* GCAGCGATGCCCAG |
| PA3311-dn-F | ATGC*AAGCTT* GGTGGCGGTCAACTGC |
| PA3311-dn-R | ATGC*CCCGGG* GCACCAGCTCGCAATG |

| | |
|---|---|
| SeqPA3311-F | CCATTGAAGCAACTCCTG |
| SeqPA3311-R | CTCAAGGATCTCGATACC |
| | |
| Δ*pa4601* | |
| PA4601-up-F | ATGC*CCCGGG*TTCGCGGACTCTACGACAG |
| PA4601-up-R | ATGC*GAATTC*AACTCGCTACGGGTCTCG |
| PA4601-dn-F | ATGC*AAGCTT*ATCCTGATGAGTGACGTCGC |
| PA4601-dn-R | ATGC*CCCGGG*TCAGCCCTCGTTGAACATG |
| SeqPA4601-F | GACAAAGTGCCTCGAC |
| SeqPA4601-R | GTCAAATCACGGCTGAAC |
| | |
| Δ*pa4959* | |
| PA4959-up-F | ATGC*CCCGGG* CACGTACGACGGCGAAC |
| PA4959-up-R | ATGC*GAATTC* GTTCTCGACTTTCTTCAGCAG |
| PA4959-dn-F | ATGC*AAGCTT* GAGGTGCTCCTGCGC |
| PA4959-dn-R | ATGC*CCCGGG* GGTCCTGGACGAAGGAG |
| SeqPA4959-F | GTTCGAATACCGCTCG |
| SeqPA4959-R | TGGACGGCATCCTCTAC |
| | |
| Δ*pa5017* | |
| PA5017-up-F | ATGC*CCCGGG* CGACTACCCTCTGCGC |
| PA5017-up-R | ATGC*GAATTC* GTGCCGTAGGCTTCGC |
| PA5017-dn-F | ATGC*AAGCTT* GCCGATCGGCAAGTG |
| PA5017-dn-R | ATGC*CCCGGG* CCATGGCGATCACCG |
| SeqPA5017-F | CAATCGGCATAATGCACC |
| SeqPA5017-R | CAGAACCATGGCTCTCG |
| | |
| Δ*pa5442* | |
| PA5442-up-F | ATGC*CCCGGG* ATGACCGTCCATGTCGAG |
| PA5442-up-R | ATGC*GAATTC* CGAACACCAGCACCTGC |
| PA5442-dn-F | ATGC*AAGCTT* CGGCGCAACTGGAGC |
| PA5442-dn-R | ATGC*CCCGGG* TCAACGAGCCTGGCG |
| SeqPA5442-F | GTCGTTGAGGGAGTTCAG |
| SeqPA5442-R | GACCAATCGGGATAGCAG |
| | |
| Gm cassette | |
| Gm-F | ATGC*GAATTC* GAATTGACATAAGCCTGTTCGG |
| Gm-R | ATGC*AAGCTT* GAATTGGCCGCGG |
| | |
| **Transposon mutant PCR confirmation** | |
| PW1520 (ΔTn*0285 A*) | ATGAGCCCCCGCCTGAG |
| PW1521 (ΔTn*0285 B*) | ATGAGCCCCCGCCTGAG |
| PW1532 (ΔTn*0290 A*) | ATGGACGACCTAACCGGCA |
| PW1531 (ΔTn*0290 B*) | TCAGGCGACGCTGGC |
| PW1627 (ΔTn*0338 A*) | TTTCCCCGCAAGCGTATAGAC |
| PW1626 (ΔTn*0338 B*) | TTTCCCCGCAAGCGTATAGAC |
| PW2061 (ΔTn*0575 A*) | CCACGGTATCGACGTCGC |
| PW2060 (ΔTn*0575 B*) | CCACGGTATCGACGTCGC |
| PW5581 (ΔTn*0575 C*) | CCACGGTATCGACGTCGC |
| PW2543 (ΔTn*0847 A*) | ATGGAACCGTCGCCGAG |
| PW2544 (ΔTn*0847 B*) | TCAGGCTGGCGCCTG |
| PW2570 (ΔTn*0861 A*) | ATGAGGCAGAACCGGACTCTC |
| PW2569 (ΔTn*0861 B*) | ATGAGGCAGAACCGGACTCTC |
| PW3133 (ΔTn*1181 A*) | ATGTTCAGTGGCAAAACCGAC |
| PW3134 (ΔTn*1181 B*) | ATGGCGAGATCATCGGCAC |
| PW4044 (ΔTn*1727 A*) | TCAGGCGACGCTGGC |
| PW4043 (ΔTn*1727 B*) | TCAGGCGACGCTGGC |
| PW6568 (ΔTn*3311 A*) | CGTCGACGGCTACGTG |
| PW6567 (ΔTn*3311 B*) | ATTGGCAAGGCCTGCG |
| PW6569 (ΔTn*3311 C*) | CGTCGACGGCTACGTG |
| PW8754 (ΔTn*4601*) | AACCAGGAAGAACTGGCGC |
| PW9347 (ΔTn*4959 A*) | GAAAACCATCCGCCTGCTG |
| PW9346 (ΔTn*4959 B*) | GAAAACCATCCGCCTGCTG |
| PW5475 (ΔTn*5017 A*) | TCAGTGCAGGGTGCGG |
| PW9424 (ΔTn*5017 B*) | ATGAAAAGTCATCCCGATGCC |
| PW9425 (ΔTn*5017 C*) | ATGAAAAGTCATCCCGATGCC |
| PW10194 (ΔTn*5442 A*) | TCAACGAGCCTGGCGC |
| PW10193 (ΔTn*5442 B*) | TCAACGAGCCTGGCGC |
| PW10195 (ΔTn*5442 C*) | ATGACCGTCCATGTCGAGC |
| | |
| ISphoA/hah | CGGGTGCAGTAATATCGCCCT |
| ISlacZ/hah | GGGTAACGCCAGGGTTTTCC |

**N.B. Italic nt with underlines are restriction enzyme cutting sites.**

# 2.3. Biofilm experiments

## 2.3.1. Microtiter plate biofilm batch culture

This method was adapted from George O'Toole[302]. The optical densities of *P. aeruginosa* overnight cultures in 10ml LB were measured in a spectrophotometer at a wavelength of 600nm using plain LB broth as blank. The overnight culture was diluted into fresh M9 media with an initial inoculum of $OD_{600nm}$ 0.01 and 100µl per well was inoculated into microtiter plates. The plates were incubated statically for the desired time at 37°C. To avoid edge effect and evaporation, the edge wells were filled with 200µl sterile PBS to maintain humidity (see Fig 2.3.1) and the plates were placed in a humidified environment by placing wet towels at the bottom of sealed plastic boxes in the incubator.

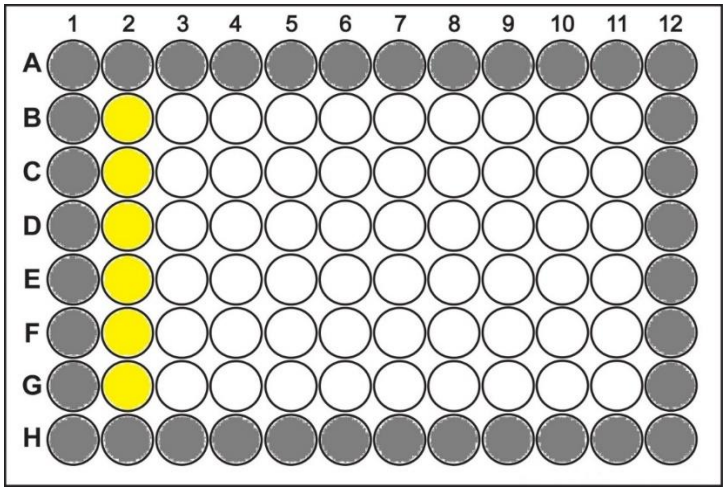


Fig 2.3.1 Arrangement of wells filled with PBS and bacteria culture in microtiter plates. Wells highlighted in grey are filled with 200µl PBS; wells highlighted in yellow represent 6 technical replicates for each bacteria strain.

For NO treatments and dispersal assay, after biofilms were incubated for the desired time periods, spent media was pipetted out and the wells were washed twice with sterile PBS. 150µl plain M9 media pipetted into each well was used as control, while 150µl M9 media with different NO donors at different concentrations in each well were used as experimental groups. After desired time of treatment, the liquid was shaken vigorously onto a stack of blue roll to get rid of all loosely attached bacterial cells. Wells

were washed twice with sterile PBS and stained with 120µl 0.1% (w/v) crystal violet (CV) for 15 mins. After staining, the plates were washed twice and dried overnight. CV was then dissolved in 120µl 30% (v/v) acetic acid for 30 mins and the liquids were transferred into a clean new microtiter plate. The optical density was measured at 584nm in a plate reader using 30% (v/v) acetic acid as a blank.

### 2.3.2. 6 well plate biofilm assay

This method was adapted from E. R. Hendry *et al*[303]. The optical densities of *P. aeruginosa* overnight cultures in 10ml LB were measured in a spectrophotometer at a wavelength of 600nm using plain LB broth as blank. Overnight cultures were diluted into fresh M9 media with an initial inoculum $OD_{600nm}$ 0.01 and plates were inoculated with 4ml inoculum per well. Plates were left at room temperature statically for 1 hr to allow for initial attachment. Then the plates were incubated for 96 hrs at 30℃ with shaking at 50rpm to facilitate biofilm formation and media changed every 24 hrs. For NO treatments, spent media was pipetted out and the wells were washed twice with sterile PBS. 4ml plain M9 media pipetted into each well was used as control, while 4ml M9 media with different NO donors at different concentrations in each well was used as experimental groups. After desired treatment time, spent media was pipetted out of each well and wells were washed with PBS twice. Spent media can be subjected to CFU counts for bactericidal tests.

For crystal violet staining of total biomass, 1ml 0.1% (w/v) CV was added into each well for 15 mins incubation at room temperature. CV was pipetted out and each well was washed with PBS twice. The plates were dried overnight before dissolving CV in 1ml 30% (v/v) acetic acid. The optical densities of solutions were measured in a spectrophotometer at a wavelength of 550nm.

For CFU quantification of total biomass, biofilms in each well were scraped off using a sterile cell scraper (Falcon, Corning) and dissolved in 3ml sterile PBS. Biofilms in PBS were vortexed for 30 s and serial dilutions were made for CFU count of living cells (see 2.5.2 for CFU determination).

### 2.3.3. Confocal laser scanning microscope imaging for biofilm in MatTek plates

MatTek plates are Poly-D-Lysine treated glass bottom culture dishes producing high-resolution microscopic images of cultures growing in standard-size disposable plastic petri dishes. In this study P35G-1.5-14-C plates (From MatTek Corporation, dish diameter 35mm, coverslip diameter 14mm, coverslip thickness 0.170 +/- 0.005 mm) were used for batch-cultured biofilms.

For PAO1 WT as well as its KO/Tn mutants: The optical densities of overnight cultures in 10ml LB were measured in a spectrophotometer at 600nm using plain LB broth as blank. The overnight cultures were diluted into fresh M9 media with an initial inoculum $OD_{600nm}$ 0.01 and 3ml were inoculated into each plate. Plates were left at room temperature statically for 1 hr to allow for initial attachment and then placed under desired temperature (22℃, 30℃ and 37℃). Plates were shaken at 50rpm to create shear force facilitating biofilm formation. Spent media was changed with fresh M9 every 24 hrs until the desired culturing time.

For CF PA clinical isolates: Instead of diluting overnight cultures into M9 to a final $OD_{600nm}$~0.01 and directly incubating this high density cells in MatTek plates, the same amount of cells were first incubated in MatTek for 2 hrs to allow for initial attachment. After 2 hrs, unattached cells were discarded and fresh M9 was added to MatTek plates for incubation. This modification was due to the fact that all those PA clinical isolates were a result of selection and adaption from the first bacteria invading CF lungs and the initial cell density that caused biofilm formation would not be high. All the plates for PA clinical isolates were incubated at 37℃, consistent with body temperature.

Before observation under confocal microscope, the spent media was pipetted out and wells were washed twice with 0.85% (w/v) NaCl. 3µl ingredient A and 3µl ingredient B from LIVE/DEAD® BacLight Bacterial Viability Kits (Invitrogen) were added into 1ml 0.85% (w/v) NaCl and mixed thoroughly as dye. 250µl dye was added to each well and biofilms were stained in dark for 20 mins. After the dye was pipetted out and the wells washed with 0.85% (w/v) NaCl once, the liquid was pipetted out and 1ml 80% glycerol was added onto the surface of biofilms carefully to prevent drying out and damage from laser heating. Wavelengths 488nm and 561nm laser were used for SYTO-9 and Propidium iodide respectively. At least 3 image stacks were taken from random locations in each plate and the biofilms were analysed using COMSTAT[304].

### 2.3.4. Initial attachment and early stage biofilm formation

The optical densities of *P. aeruginosa* overnight cultures in 10ml LB were measured in a spectrophotometer at a wavelength of 600nm using plain LB broth as blank. The overnight culture was diluted into fresh M9 media with an initial inoculum of $OD_{600nm}$ 0.01 or 0.1 as initial inoculum. 100µl of diluted culture per well was inoculated into microtiter plates. The plates were incubated statically for 3 hrs for initial attachment or 24 hrs for early stage biofilm formation at 37°C. For testing the inhibition effect from NO donors, desired concentrations of donors were added with the initial inoculum. After incubation with/without NO donors, the spent media was shaken vigorously onto a stack of blue roll to get rid of all loosely attached bacterial cells. Wells were washed twice with sterile PBS and stained with 120µl 0.1% (w/v) crystal violet for 15 mins. After staining, the plates were washed twice and dried overnight. CV was then dissolved in 120µl 30% (v/v) acetic acid for 30 mins and the liquids were transferred into a clean new microtiter plate. The optical density was measured at 584nm in a plate reader using 30% (v/v) acetic acid as a blank.

## 2.4. Preparation of NO donor/NO scavenger solution

Sodium nitroprusside (SNP), S-Nitroso-N-acetyl-DL-penicillamine (SNAP), S-Nitrosoglutathione (GSNO), MAHMA NONOate (NOC-9), PROLI NONOate, Spermine NONOate (S150), Diethylamine NONOate sodium salt hydrate (DEA NONOate) and Carboxy-PTIO potassium salt (PTIO) were purchased from Sigma Aldrich, UK. All chemicals were first dissolved in fresh M9 media and filter-sterilized as stock solutions and then diluted to desired concentrations. During preparation procedures, all solutions were kept on ice before use and SNP was additionally kept in the dark.

## 2.5. Planktonic cells assays

### 2.5.1. Growth curve of *P. aeruginosa*

Overnight cultures were diluted into fresh, sterile LB media until an OD of 0.001. 100µl of diluted initial inoculums were inoculated into each well of a microtiter plate. The plates were placed in a 37°C shaking plate reader (BMG LABTECH FLUOSTAR) automatically measuring the $OD_{584nm}$ values every 15 mins. 100µl fresh LB was used as blank.

## 2.5.2. CFU count of viable cells on agar

Traditional method of serial dilution and measuring CFU count on agar plates was laborious. The modified Miles and Misra method was used here[305]. Briefly, serial dilutions were made from the cultures in 1ml PBS (1:10, 100µl culture into 900µl PBS) to the desired concentration. Diluted cell cultures were vortexed and at least three 10µl drops were inoculated onto agar plates. Plates were then incubated at 37°C overnight before counting and viable cells were determined as CFU/ml.

## 2.5.3. Growth inhibition test

To test if certain types of NO donors inhibit the growth of *P. aeruginosa*, a modified method from Robert J Barnes[306] was used. 100µl overnight cultures were added into 10ml fresh sterile LB media and incubated at 37°C, 200rpm until an $OD_{600nm}$ around 0.45, indicating that *P. aeruginosa* growth was in the middle of log phase to determine the initial CFU counts. Then stock solutions of NO donors (1mM for S150 and 10mM for SNP) were added into the culture making a desired final concentration, and the tubes were incubated for another desired time (2 hrs or 24 hrs) at 37°C, 200rpm. For the untreated controls, the same amount of PBS was added. Final CFU counts were determined as 2.5.2.

## 2.5.4. Bactericidal test of SNP and S150

To test the toxicity of SNP and S150 to planktonic *P. aeruginosa* cells, a modified method from Robert J Barnes was used[306]. 1ml overnight cultures were centrifuged at 4000×*g* for 30 mins to harvest the cells in micro-centrifuge tubes, washed twice in sterile PBS and re-suspended in 1ml PBS. Dilutions of the cells were made to the desired CFU/ml in PBS (~$10^6$/ml for SNP and ~$10^4$/ml for S150) for treatments. Stock solutions of NO donors (1mM for S150 and 10mM for SNP) were added into the diluted culture making desired final concentrations and the tubes were incubated at 37°C for the desired time (2 hrs or 24 hrs). For the untreated controls, the same volumes of PBS were added. Final CFU counts were determined as 2.5.2.

To test the toxicity of SNP and S150 to *P. aeruginosa* biofilm cells in 6 well plates, biofilms were set up as described in 2.3.2 and incubated for 96 hrs at 30°C. For NO treatments, spent media was pipetted out and the wells were washed twice with sterile PBS. 4ml plain M9 media pipetted into each well was used as control, while 4ml M9

media with SNP/S150 at different concentrations in each well were used as experimental groups. After desired treatment time (2 hrs and/or 24 hrs), all 4ml of spent media in each well was pipetted out into a sterile 10ml falcon tube and vortexed for CFU determination of planktonic cells. The remaining biofilms were washed twice and scraped off for CFU determination as described in 2.3.2.

To test the toxicity of SNP and S150 to *P. aeruginosa* biofilm cells in microtiter plates, biofilms were set up as described in 2.3.1 and incubated for 24 hrs at 37℃. For NO treatments, spent media was pipetted out and the wells were washed twice with sterile PBS. 150µl plain M9 media pipetted into each well was used as control, while 150µl M9 media with SNP/S150 at different concentrations in each well were used as experimental groups. After desired treatment time (2 hrs and/or 24 hrs), all 150µl of spent media in each well was pipetted out into a new microtiter plate for OD measurement and serial dilution for CFU counts. The remaining biofilms were determined using crystal violet stain.

## 2.6. Motility assays

The motility assay methods were modified from M. Harunur Rashid *et al*[307]. Standard swimming, swarming and twitching plates were made as follow. For plates containing SNP, sterilized 10mM SNP stock solution was added to media at temperature below 60°C to the desired concentrations (1µM, 10µM, 100µM) before pouring the plates.

### 2.6.1. Swimming

Media used for swimming assay was tryptone broth [10g/liter tryptone + 5g/liter NaCl] containing 0.3% (wt/vol) agarose. Media were autoclaved at 121℃ for 20 mins and cooled down to 60℃ before pouring. Each petri dish was filled with 20ml media and dried in safety cabinet with constant flow for 20 mins. The surfaces of swim plates were inoculated from a single colony on fresh overnight agar plates with a sterile toothpick. The plates were then wrapped with Parafilm to prevent dehydration and incubated at 30°C for 18 hrs. Image of each plate was taken using G:BOX and GeneSnap software with upper white light source and 5 s exposure time. ImageJ software was used to measure the swimming areas on agar plates by adjusting the over/under threshold of the images to define and calculate the target areas.

### 2.6.2. Twitching

Media used for twitching assay was LB broth solidified with 1% (wt/vol) agar. Media were autoclaved at 121℃ for 20 mins and cooled down to 60℃ before pouring. Each petri dish was filled with 20ml media and dried in safety cabinet with constant flow for 1 hr. The bacteria were stab-inoculated from a single colony on fresh overnight agar plates with a sterile toothpick to the bottom of the petri dish. After incubation at 37°C for 24 hrs, the zone of twitching motility at the agar/Petri dish interface was measured. Image of each plate was taken using G:BOX and GeneSnap software with upper white light source and 5 s exposure time. ImageJ software was used to measure the maximum distance from inoculation point to the edge of twitching zones by adjusting the over/under threshold of the images.

### 2.6.3. Swarming

Swarming patterns varies hugely across different species and even among the different strains within the same species. Dae-Gon Ha *et al* used 0.5-0.8% M8 medium agar supplemented with glucose and casamino acid for *P. aeruginosa* swarming assay and PAO1 WT resulted in a pattern as below[308]. In this assay, I used the same medium as described by Rashid *et al* which consisted of nutrient broth, glucose and 0.5% agar, resulting in the swarm pattern very similar to that seen by Dae-Gon Ha.

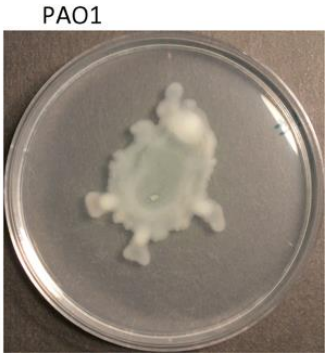


PAO1 WT swarm pattern on M8 medium-supplemented agar. Image taken from Dae-Gon Ha *et al*, Plate-based assay for swarming motility in *Pseudomonas aeruginosa*[308]

Media used for swarming assay contained 0.5% (wt/vol) agar with 8g/liter nutrient broth, to which 5/liter glucose was added. Media were autoclaved at 121℃ for 20 mins and cooled down to 60℃ before pouring. Each petri dish was filled with 20ml media and dried in safety cabinet with constant flow for 40 mins. 3µl overnight culture ($OD_{600nm}$ 1.1-1.3) was inoculated on the surface of agar and plates were incubated at 37 ℃ for 20-22 hrs. It has now been widely accepted that swarming assays lack consistency and reproducibility. Multiple factors were reported to affect the results hugely, even

within different batches for the same strain. Even if all the medium compositions were kept the same, namely, the same pH and agar concentration, the freshness of the bacterial culture, thickness of the plate, plate pouring temperature and humidity (drying time) as well as the location within the same incubator would all affect different batches of swarming plates in the same hand[309]. Therefore, one strain was inoculated per plate and several strains including one WT were inoculated onto the same batch of plates resourced from the same bottle of agar for comparison. Image of each plate was taken using G:BOX and GeneSnap software with upper white light source and 5 s exposure time. ImageJ software was used to measure the swarming area on agar plates by adjusting the over/under threshold of the images to define and calculate the target areas.

## 2.7. DNA manipulation procedure

### 2.7.1. Isolation of genomic DNA from *P. aeruginosa*

*P. aeruginosa* chromosomal DNA was obtained using Wizard® Genomic DNA Purification Kit (Promega, US) according to the manufacturer's protocol. For cell lysis, 1ml overnight culture of *P. aeruginosa* was centrifuged for 2 mins at 16,000×*g*. The supernatant was discarded and 600µl Nuclei Lysis Solution was gently mixed with the pellet by pipetting. The sample was incubated for 5 mins at 80°C. After cooling to room temperature, 3µl of RNase Solution was added to the sample and mixed. The sample was then incubated at 37°C for 60 mins and cooled to room temperature. For protein precipitation, 200µl of Protein Precipitation Solution was added and vortexed before incubating on ice for 5 mins, then centrifuged at 16,000×*g* for 3 mins. For DNA precipitation and rehydration, the supernatant from last step was mixed with 600µl room temperature isopropanol and then centrifuged for 2 mins at 16,000×*g*. The supernatant was decanted and 600µl room temperature 70% ethanol was added. After the same centrifugation step, the pellets were air dried and then rehydrated in 100µl of rehydration solution for 1 hr at 65°C. Concentration of resulting DNA was determined following manufacturers instruction Nanodrop2000 spectrophotometer based on light absorbance optical density at 260nm.

### 2.7.2. Routine PCR

Routine procedures were employed and modified according to Molecular Cloning : a laboratory manual[310] and the manufacturer's protocol. Briefly, 50µl PCR reaction was

applied containing DNase free $H_2O$, 10ng low complexity DNA or 20ng genome DNA, 1×Phusion High-Fidelity buffer, 200μM dNTPs, 0.5μM FWD primer and 0.5μM REV primer, 1.5% DMSO and 1 unit of Phusion High-Fidelity DNA Polymerase (New England Biolabs, UK) for DNA fragment amplifications. Annealing time and extension time were decided based on types of template DNA and the length of target fragments. Primers were designed according to NEB Tm calculator and were all purchased from Eurofins (Ebersberg, Germany). PCR products were checked through gel electrophoresis.

## 2.7.3. Overlap extension PCR

This protocol was modified by Choi *et al* for generating a 'mutant fragment' containing 5'-flanking region and 3'-flanking region amplified from gene of interest with a Gentamicin resistance gene (Gm cassette) in the middle[311].

- *1st round PCR*

Generate 5'-flanking, 3'-flanking regions and Gm cassette following routine PCR procedures.

- *2nd round PCR*

A 50μl PCR reaction was set up containing DNase free $H_2O$, 50ng of purified 5'-flanking, 50ng of 3'-flanking regions and 50ng of Gm cassette prepared during 1st round PCR, 1× Phusion High-Fidelity buffer, 200μM dNTPs, 1.5% DMSO and 1 unit of Phusion High-Fidelity DNA Polymerase. Cycle conditions were 98°C, 3 mins followed by 3 cycles of 98°C for 30 s, 65°C for 30 s and 72°C for 30 s without primers. The third cycle was paused at 15 s of the 72°C extension procedure, each of the primers PAXXXX-up-F and PAXXXX-dn-R (XXXX represents gene number) were added to a final concentration of 0.5μM, and the cycle was then finished by another 15 s at 72°C. The PCR was finished by another 30 cycles of 98°C for 10 s, 65°C for 30 s, 72°C for 2.5 mins and a final extension at 72°C for 5 mins. PCR products were checked through gel electrophoresis.

## 2.7.4. Gel electrophoresis procedure

Routine procedures were employed and modified according to Molecular Cloning : a laboratory manual[247] and the manufacturer's protocol. Briefly, 1% (w/v) agarose gel in 1×TAE buffer and 1kb ladder (Promega, US) were applied. 1μl PCR product, 1μl NEB

purple loading dye and 4µl DNase free $H_2O$ were mixed together and loaded into each well in all experiments. DNA fragments were stained using Gel red (Biotium, UK)

### 2.7.5. Gel extraction for PCR product

When the PCR products showed more than one band on the gel, QIAquick Gel Extraction Kit (Qiagen, Hilden, Germany) was used for extracting the DNA fragments of interest. Briefly, the DNA fragments were excised from the gel and the gel slices were weighed in micro-centrifuge tubes. 3 volumes Buffer QG were added to 1 volume gel and incubated at 50°C until gel slices were completely dissolved. 1 gel volume of isopropanol was added and mixed thoroughly. The samples were applied to the QIAquick column and centrifuged at 17900×$g$ for 1 min. The flow-through was discarded and the columns were placed back into the same tube. The procedure was repeated until all the samples passed through the column. 750µl Buffer PE was added to the column, centrifuged for 1 min and the flow-through discarded. The column was centrifuged at 17900×$g$ once more to remove the residual wash buffer, 50µl Buffer EB (10 mM Tris·Cl, pH 8.5) was added and centrifuged for 1 min to elute DNA into a clean micro-centrifuge tube. Concentration of resulting DNA was determined following manufacturers instruction for Nanodrop2000 spectrophotometer based on light absorbance optical density at 260nm.

### 2.7.6. Simple PCR purification procedure

When the PCR products showed only one clear band on the gel, QIAquick® PCR Purification Kit was used to clean up DNA less than 100bp for further research. According to manufacturer's protocol, 5 volumes Buffer PB were added to 1 volume of the PCR reaction and mixed thoroughly. Samples were applied to the QIAquick column and centrifuged for 1min at 17900×$g$ to bind DNA to the column. The flow-through was discarded, 750µl buffer PE was then added and centrifuged for 1 min at 17900×$g$ to wash DNA. Residual washing buffer was removed by centrifuging for another 1 min and 30µl Buffer EB (10mM Tris·Cl, pH 8.5) was added and centrifuged for 1 min to elute DNA into a clean micro-centrifuge tube. Concentration of resulting DNA was determined following manufacturers instruction for Nanodrop2000 spectrophotometer based on light absorbance optical density at 260nm.

### 2.7.7. Restriction enzyme digestion

20µl reaction containing 10 units of restriction enzyme (for double digestion, 10-20 units for each enzyme and total enzyme volume less than 2µl), 2µl CutSmart® buffer and 500ng target DNA was applied for DNA digestions. Samples were digested for 2 hrs and enzymes were heat inactivated at temperatures according to manufacturer's protocol. All restriction enzymes and CutSmart® buffer were purchased from New England Biolabs, UK. For preventing recircularization and re-ligation of linearized cloning vectors, 1µl Shrimp Alkaline Phosphatase (NEB, UK) was added to the reaction after 2 hrs digestion and incubated at 37°C for another 1 hr for heat inactivation during vector digestion. The digestion products were then checked on gel.

## 2.7.8. Ligation of gene specific amplicons from PCR and digestion

After PAXXXX-up (5'-flanking region of target genes, XXXX represents gene numbers), PAXXXX-dn (3'-flanking region of target genes) and Gm cassette were amplified and properly digested, the following 10µl reactions with different molar ratios were used for three-way sticky end-ligation under room temperature, overnight. T4 DNA ligase and ligase buffer were purchased from NEB, UK.

| | 2:1 | 1:1 | 1:2 | 1:4 |
|---|---|---|---|---|
| PAXXXX-dn | 2µl | 1µl | 1µl | 1µl |
| PAXXXX-up | 2µl | 1µl | 1µl | 1µl |
| Gm | 1µl | 1µl | 2µl | 4µl |
| Buffer | 1µl | 1µl | 1µl | 1µl |
| T4 ligase | 0.5U (0.5µl) | 0.5U (0.5µl) | 0.5U (0.5µl) | 0.5U (0.5µl) |
| $H_2O$ | 3.5µl | 5.5µl | 4.5µl | 2.5µl |

## 2.7.9. Ligation of vectors and inserts

Insert:vector molar ratios of 1:1, 2:1, 3:1 and 5:1 were used for ligating insert ('mutant fragment', PAXXXX-up-Gm-PAXXXX-dn) with vector. After the constructed inserts and vector were properly digested, 20 µl reactions containing 25ng vector, corresponding inserts, 1U T4 ligase and 2 µl ligase buffer were used for blunt end-ligation under room temperature, overnight.

| | 1:2 | 1:1 | 2:1 | 4:1 | 8:1 |
|---|---|---|---|---|---|
| PAXXXX-up-Gm-PAXXXX-dn | 0.5 µl | 1 µl | 2 µl | 4 µl | 8 µl |
| vector | 1 µl | 1 µl | 1 µl | 1 µl | 1 µl |

| | | | | | |
|---|---|---|---|---|---|
| T4 ligase buffer | 1 µl | 1 µl | 1 µl | 1 µl | 1 µl |
| T4 ligase | 0.5U (0.5µl) | 0.5U (0.5µl) | 0.5U (0.5µl) | 0.5U (0.5µl) | 0.5U (0.5µl) |
| $H_2O$ | 7 µl | 6.5 µl | 5.5 µl | 3.5 µl | 0 µl |

## 2.8. Making competent *E. coli* DH5α/S17-λ cells

The method was adapted from Rubidium Chloride Method[312]. *E.coli* DH5α/S17-λ cells were inoculated from a frozen stock into 2ml LB broth and cultured overnight in a shaking incubator at 37°C. 300µl overnight culture was diluted 1:1000 into 300ml fresh LB, incubated in a shaking incubator until $OD_{600nm}$ was ~ 0.4 (log phase). Then the culture was transferred to a centrifuge bottle, chilled on ice for 15 mins and cells were pelleted by centrifugation at 3000rpm for 15 mins at 4°C. After centrifugation, liquid was decanted and the cells re-suspended by gently pipetting in 100ml chilled RF1 buffer (100mM RbCl, 50mM $MnCl_2$, 30mM K acetate, 10mM $CaCl_2$, 15% wt/vol glycerol) until no clumps were visible. The mixed cells and RF1 buffer was then chilled on ice for 60 mins and centrifuged at 3000rpm for 15 mins at 4°C. Liquid was decanted and cells were gently re-suspended in 24ml chilled RF2 buffer (10mM MOPS, 10mM RbCl, 75mM $CaCl_2$, 15% wt/vol glycerol). The cells/RF2 buffer mixtures were incubated on ice for 15 mins and then 200µl was distributed into chilled 1.5ml micro-centrifuge tubes and stored at -80°C.

## 2.9. Transformation of vectors into *E. coli* DH5α/S17-λ competent cells

4µl of ligation products were added into 40µl competent cells thawed on ice in sterile 1.5ml micro-centrifuge tubes. The sample was gently mixed by flipping the mixture and chilled on ice for 15 mins. Cells were heat shocked for 45 s in 42°C water bath and chilled on ice for 3 mins. 200µl fresh LB broth was added into tubes and incubated at 37°C for 1 hr with 200rpm shaking. 200µl cells were plated on desired antibiotic selective agar plates and incubated at 37°C for 24 hrs.

## 2.10. Conjugation of vectors into *P. aeruginosa*

The method was adapted from Claire A. Woodall[313]. Overnight cultures of *E.coli* S17-λ with correct vectors were grown at 37℃ with antibiotics. *P. aeruginosa* PAO1 WT

overnight cultures were grown at 42℃ to suppress restriction systems targeting foreign DNA. Overnight cultures of *E. coli* and *P. aeruginosa* were mixed 1:1 and pipetted onto 0.45μm filter membranes (MF-Millipore Membrane Filter, mixed cellulose esters, Thermo Scientific, UK). A vacuum pump was used to evacuate the liquid on filter membranes and bacterial cells were left very close to each other. The filter membranes were carefully removed and put onto the surface of LB agars with the bacteria side upward. The plates were incubated at 37℃ for 4-5 hrs and then filter membranes were removed into 1ml sterile PBS buffer. All cells on membranes were washed off into buffer by vigorous vortex and plated onto cetrimide agars with desired antibiotics for 24 hrs incubation at 37℃.

## 2.11. EPS extraction and quantification

The method was modified from Robert J. Barnes *et al*[314]. Overnight cultures of *P. aeruginosa* were diluted into fresh M9 media until a final initial inoculum with $OD_{600nm}$ 0.01. 25ml of diluted cultures were inoculated into tissue-culture treated dishes (Corning, UK, D×H 100mm×20mm). After inoculation, dishes were left statically under room temperature for 1 hr to allow for initial attachment before being moved into 30℃ incubator shaking at 50rpm. Media was changed after 24 hrs and biofilms were cultured for 48 hrs. After culturing, plates were washed with sterile 0.85% NaCl twice to get rid of loosely attached cells. Biofilms were scraped off the dishes by cell scrapers and re-suspended into universal tubes with 3ml sterile PBS. Tubes were vortexed 30 s to fully disturb biofilms and 100μl were taken for serial dilution and CFU counts. The remaining bacterial suspensions were centrifuged at 4000×*g* for 40 mins at 4℃ and the supernatants were transferred to clean tubes. For soluble polysaccharide and protein measurement, the supernatants were directly subjected to analysis. For insoluble polysaccharide and protein measurement, 2ml 0.85% NaCl and 12μl 37% formaldehyde (Sigma-Aldrich, UK) were added to the cell pellets after centrifugation. The mixtures were vortexed and incubated at 4℃ for 1 hr, after which 2ml of 1M NaOH and 0.5ml of MQ $H_2O$ were added. The mixtures were further incubated at 4℃ for another 3.5 hrs and then centrifuged at 4000×*g* for 40 mins under 4℃. Supernatants were transferred into clean conical centrifuge tubes and frozen at -80℃. Frozen samples were placed in freeze-dryer to remove all the liquid and formaldehyde. Dried samples were re-dissolved in 3ml sterile MQ water and 80μl concentrated $H_2SO_4$ was added to neutralize NaOH

background. A mixture of all EPS extraction reagents and 80µl concentrated $H_2SO_4$ was used as blank control. The polysaccharide contents were measured by the phenol-$H_2SO_4$ method. Briefly, 2.5ml of concentrated $H_2SO_4$ and 0.5ml 5% phenol were added to 1ml of sample and incubated at room temperature for 10 mins. The absorbance of the solutions were measured at 492nm and compared to a glucose standard curve. The protein contents were measured by the Coomassie (Bradford) Protein Assay kit (Thermo Scientific). 1ml sample was mixed with 1ml working reagent and incubated at room temperature for 10 mins. The absorbance was measured at 595nm and compared to a bovine serum albumin standard curve. In this study, the concentrations of glucose standards were selected as 1µg/ml, 2.5µg/ml, 5µg/ml, 10µg/ml, 25µg/ml, 50µg/ml, 100µg/ml, 250µg/ml and 500µg/ml. The concentrations of protein standards were selected as 25µg/ml, 125µg/ml, 250µg/ml, 500µg/ml, 750µg/ml, 1000µg/ml, 1500µg/ml and 2000µg/ml.

## 2.12. Chemiluminescence-based NO detection

The chemiluminescence-based method was modified from Piknova *et al*[315]. Only free NO gas was detected by chemiluminescence. After NO donor is injected into the system, free NO gas will be purged from the reaction vessel by an inert carrier gas into the chemiluminescence analyser, where it reacts with $O_3$ to form nitrogen dioxide ($NO_2$) in its activated state as below:

$$NO + O_3 \rightarrow NO_2^* + O_2$$

Deactivated $NO_2^*$ emits a photon as below:

$$NO_2^* \rightarrow NO_2 + hv \text{ (photon)}$$

which can be collected by a photomultiplier tube equipped with a long pass filter, detecting only emissions above 600nm. The intensity of emitted light reflects the concentration of NO in the reaction vessel proportionally and after calibration original NO amount can be calculated[315]. In this study, CLD 88Y (EcoPhysics, Duernten, Switzerland) NO analyser was used where $O_3$ was derived from $O_2$ in normal atmospheric conditions. NO standards were prepared by converting sodium nitrite solution to NO using tri-iodide ($I_3^-$) solution as below:

$$NO_2^- + H^+ \Longleftrightarrow HNO_2$$

$$2I^- + 2HNO_2 + 2H^+ \rightarrow 2NO + I_2 + 2H_2O$$

A mixture of KI, $I_2$ and glacial acetic acid were used to generate $I_3$ solution. The standard curve was achieved as follow: For $I_3$ solution, 500mg Potassium iodide (KI) and 379.8mg crystalline iodide ($I_2$) were dissolved in 10ml MQ water to make final concentrations of 301.2 mM and 137.8 mM respectively. The solution was kept from light. This solution was mixed with glacial acetic acid in a 2:7 ratio thoroughly by stirring on magnet plate for 30 mins achieving a brown color. CLD 88Y was connected correctly according to manufacturer's protocol and the system was allowed to warm up to 60℃ with a stable baseline. The carrier gas input line from the gas tank was connected appropriately to reaction vessel. After the carrier gas flow was started, 7.5ml $I_3$ solution was placed into the reaction vessel. The gas flow rate was adjusted until $I_3$ solution bubbled gently but did not over-flow. 100µM sodium nitrite ($NaNO_2$) standard solution was prepared and diluted to 5µM, 7.5µM, 10µM, 15µM and 20µM in MQ water. Using a well-washed gas-tight Hamilton syringe 50µl of each concentration of standards was injected into the $I_3$ solution. Total amount of NO gas released were 50µl×5µM=250pmol, 50µl×7.5µM=375pmol, 50µl×10µM=500pmol, 50µl×15µM=750pmol, 50µl×20µM=1000pmol. 3 biological replicates were performed and the tracings were recorded at a frequency of 4 Hz by PowerChrom® software (eDAQ Pty LtD, Australia) to calculate the areas. For NO donors test, the system was set up as described, 9.5ml of M9 medium was added into the system instead of $I_3$ solution and incubated at 37℃. 500µl of stock NO donor solutions were added into 9.5ml M9 by a well-washed syringe to make a final desired concentration. For light exposure tests on SNP, consistent cold light source from the maximum lightning of Photonic PL®3000 was applied to avoid increasing sample temperature. Foil paper was used to wrap the whole system when light was forbidden in the tests. 3 biological replicates were done and the peaks were recorded by PowerChrom®. Data was plotted by Origin 9 and the areas under peaks were related to the total volume of NO release. Areas were calculated from 0 min to 90 mins for all the samples and compared against areas under standards.

## 2.13 c-di-GMP gauging reporter fluorescence measurement

The method was modified from Morten T. Rybtke *et al*[300] and Wout Overkamp *et al*[316]. A c-di-GMP responsive promoter (CdrA promorter) was infused into GFP expression plasmid with a tetracycline marker on the backbone. The GFP fluorescence levels reflect

the levels of reporter plasmids expression and thus reflect the relative amounts of intracellular c-di-GMP that induce the GFP expression. c-di-GMP reporter was first introduced into *E. coli* S17-λ competent cells and transformed into *P. aeruginosa* as described previously in 2.8 and 2.9. All strains with reporter were checked on agars containing tetracycline (30µg/ml for *E. coli* and 75µg/ml for *P. aeruginosa*). Overnight cultures of *P. aeruginosa::gfp*$^{C}$ strains were first grown in LB broth supplied with 75µg/ml Tet and then diluted into 10ml of M9 media with 75µg/ml Tet to a final $OD_{600nm}$ 0.001, making the positive control groups. For NO treatment groups, the same bacterial initial inoculum was applied and S150 was added to a final concentration of 25µM after 22 hrs incubation and another 2 hrs for treatment. All cultures in M9 were grown in 37℃ at 180rpm prior to analysis. In addition, the *P. aeruginosa* strains without reporter were grown without Tet under the same condition with/without S150 as negative controls for the measurement of background fluorescences. After culturing, all tubes were vortexed vigorously for 30 s before 100µl of bacterial cultures were inoculated into each well of Greiner CELLSTAR® 96 well plates with black polystyrene flat bottom for fluorescence intensity and CELLSTAR® 96 well plates with clear polystyrene flat bottom for cell density. Fluorescence was measured as arbitrary fluorescence intensity units (FIU) from the top of plates using a 485-nm sharp-cut excitation filter and a 520-nm sharp-cut emission filter with a gain of 1500 on BMG LABTECH FLUOSTAR plate reader. OD values were measured at 584nm. Plain M9 and M9 with 75µg/ml Tet were used as medium blanks. Relative fluorescence unit (RFU) values are arbitrary fluorescence intensity units normalized by cell density and were used to analyse relative GFP levels. The calculation used to resolve the levels is as follow for both control and treatment groups:

$$\left(\frac{\mathrm{GFPreporter}-\mathrm{GFPmedium}}{\mathrm{ODreporter}-\mathrm{ODmedium}}\right)-\left(\frac{\mathrm{GFPwt}-\mathrm{GFPmedium}}{\mathrm{ODwt}-\mathrm{ODmedium}}\right)$$

where GFPreporter was the level of fluorescence intensities of the *P. aeruginosa* strains with reporter, GFPwt was the level of fluorescence intensities of the *P.aeruginosa* strains without reporter, GFPmedium was the level of fluorescence intensity in the medium. Same definitions were applied to OD.

PAO1 WT with c-di-GMP reporter plasmids was also tested for biofilm formation in MatTek plates as described in 2.3.3. Biofilms were grown under 22℃, 30℃ and 37℃ with/without 75µg/ml tetracycline for 3 d and subjected to CLSM.

## 2.14. HPLC

This HPLC based quantification of cyclic di-GMP from *P. aeruginosa* was adapted from Ankita B Roy *et al*[317].

- Extraction of c-di-GMP from *P. aeruginosa* cells

Overnight culture was diluted into LB broth 1:100 and grown to mid-exponential phase at 37℃ with 220rpm shaking. The $OD_{600nm}$ was determined by spectrophotometer and 2ml of bacterial culture at $OD_{600nm}$~0.9 was obtained. The culture was centrifuged (4℃, 16000×*g*, 2 mins) and the supernatant was discarded. The cell pellet was washed twice with 1ml ice-cold PBS (4℃, 16000×*g*, 2 mins) and the supernatant was discarded. The cell pellet was re-suspended in 100µl ice-cold PBS and incubated at 100℃ for 5 mins followed by addition of ice-cold ethanol (-20℃) to a final concentration of 65%. The mixture was vortexed vigorously for 15 s. Samples were centrifuged (4℃, 16000×*g*, 2 mins) and the supernatant was removed carefully into a clean micro-centrifuge tube. The extraction steps were repeated from the same bacterial culture twice and the extracts pooled from 3 volumes of sample were combined into one tube. Cell pellets were retained and stored at -20℃ while the combined supernatants containing c-di-GMP were subjected to vacuum concentration. After concentration, the dried c-di-GMP samples should be white pellet and can be stored at -80℃ or dissolved in nanopure water and subjected to HPLC directly. All extraction steps were manipulated on ice to prevent the degradation of c-di-GMP.

- HPLC

Samples were passed through Spectra SYSTEM P4000 HPLC for separation using a reverse-phase $C_{18}$ column (Agilent, Polaris 3 C18-A, 150×4.6mm) at a flow rate of 0.5ml/min. Two solvents were used for eluting c-di-GMP. Solvent A contained 10mM ammonium acetate in nanopure water without adjusting pH. Solvent B contained 10mM ammonium acetate in 100% methanol without adjusting pH. The elution gradient of two solvents was as follow: from 0 to 9 min, 1% B+99% A; from 9 to 14 min, 15% B+85% A; from 14 to 19 min, 25% B+75% A; from 19 to 26 min, 90% B+10% A; from 26 to 40 min, 1% B+99% A. Under this experimental condition the peaks were usually observed at 16-17 mins. Extracted c-di-GMP from *P. aeruginosa* as described above was re-dissolved in 200µl nanopure water and vortexed for 1 min until all white pellets dissolved. The solution was centrifuge at 18,000×*g*, 4℃ and the supernatant was filtered

through 2µm syringe filter (Upchurch Scientific, catalog number: B-100) into a new micro-centrifuge tube. 150µl sample was pipetted into autosamplers (Thermo scientific) and 50µl was injected into HPLC per time. Commercially purchased c-di-GMP (Sigma-Aldrich) dissolved in nanopure water was used as standard for comparison. The standard curve was generated with final concentrations of 1, 2, 5, 10, 20pmol/µl of commercial c-di-GMP and for each batch of HPLC assay, a standard was included along with extracted c-di-GMP to determine peak location due to systematic errors. 2 technical replicates were performed for each sample and solvents were freshly made each time.

## 2.15. Cell aggregates assays

For cell aggregates culture in 6 well plates: The optical densities of *P. aeruginosa* overnight cultures in 10ml LB were measured in a spectrophotometer at a wavelength of 600nm using plain LB broth as blank. Overnight cultures were diluted into fresh M9 media with an initial inoculum $OD_{600nm}$~0.01 and plates were inoculated with 4ml inoculum per well. Plates were incubated at 37℃ with 50rpm shaking for 24 or 48 hrs. Image of each plate was taken using G:BOX and GeneSnap software with upper white light source and 5 s exposure time.

For CLSM images: The optical densities of *P. aeruginosa* overnight cultures in 10ml LB were measured in a spectrophotometer at a wavelength of 600nm using plain LB broth as blank. Overnight cultures of *P. aeruginosa* were diluted into 10ml of fresh M9 in universal tubes to an $OD_{600nm}$~0.005 or 0.01 as initial inoculums. Cell aggregates were then incubated at 37℃ for 24 hrs with 120rpm or 180rpm shaking. After incubation, the bacterial cultures were gently homogenized by inverting the tubes 4-5 times and 200µl was pipetted into a new micro-centrifuge tube using 1ml tips cut at the top to avoid disturbing the aggregates. 1µl of both ingredients A and B from LIVE/DEAD® BacLight Bacterial Viability Kits were added to 200µl of bacterial culture and mixed by flipping the tubes. Cells were stained in dark for 20 mins. Double sided adhesive tapes were cut to leave a ~4mm×4mm hole and stuck to microscope slides. ~50µl stained cell culture was dropped into the hole and a coverslip was placed on the top of liquid drop and also stuck to the rest of the tape. In this way, bacterial cultures were locked on the slide inside of the hole with certain degree of moving freedom to minimize the effect of external pressure on aggregates. The slides were then subjected to CLSM and at least 3 points were selected from each slide. For SNP treatment, desired concentrations of SNP

were added with initial inoculum and exposed to light for 30 mins before incubation, while for S150 treatment planktonic cultures were first incubated for 22 hrs and another 2 hrs after the addition of desired concentrations of S150.

## 2.16. CF sputum collection and *P. aeruginosa* isolation

Sputum samples from 72 patients with CF (median age at informed consent 21 years, range 17-62; UK NHS Research Ethics Reference 08/H0502/126) were obtained by CF physiotherapist-assisted sample expectoration[318,319]. Isolation of *P. aeruginosa* from sputa was carried out by Dr. R Howlin after the samples were transferred to University of Southampton microbiology group on ice. Samples were digested using Mucolyse (Pro-Lab Diagnostics) containing dithiothreitol and phosphate buffer for 15 mins at 37 °C, followed by culture on *P. aeruginosa*-specific cetrimide agar (Sigma-Aldrich). Multiplex PCR was used to confirm *P. aeruginosa* as previously described by De Vos D *et al*[320]. Individual colonies were isolated for overnight culture and purified aqueous cultures were frozen at -80 °C.

## 2.17. The calculation of concentration coefficient based on Gini Index and Lorenz curve

A novel method for determining cells aggregation levels based on the concept of Gini index was developed and described below.

In 1912 Corrado Gini first presented an index, now known as the “Gini Index” and 2 years later he introduced his index and its relation to the Lorenz curve[321]. The Gini Index is now widely and majorly used in the measurement of income inequality in a group of residents. Gini coefficient (G) and Lorenz curve as well as their calculation formula[322] are shown as below in Fig 2.17.1.

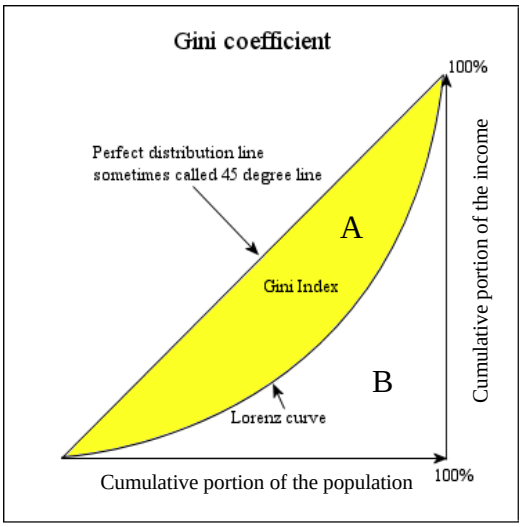


Fig 2.17.1 Gini coefficient and Lorenz curve

With a population portion of 0 to 100%, the income of each resident can be defined as x(t) (t=0 to 1). x(t) is then rearranged into a sequence of values with non-decreasing order (i.e. $x(t_1) \leqslant x(t_2)$ when $t_1<t_2$) prior to the calculation of another variable - cumulative income y(t), which is defined and calculated as

$$y(t) = \int_0^t x(\tau)d\tau$$

The figure curve of y(t) on Cartesian coordinate is called Lorenz curve. As a result, the area in B is

$$B = \int_0^1 y(t)dt$$

Since both horizontal and vertical axis were presented as portion and the maximum is 1 (100%), the area (A+B) = 0.5. Gini Index can then be calculated as

$$G = A/(A+B) = 2A = 1-2B$$

As can be seen, a perfectly equal income distribution would be the one in which every person has the same income, reflecting on the graph as y(t) = t. A perfectly unequal distribution would be the one in which one person has all the income and everyone else has none, reflecting on the graph as y(t) = 0% for all t < 1 and y(1) = 100%. G = A/(A+B) value is between 0 and 1 or can be expressed as a percentage. The higher the G, the more unequal the income distribution is.

In summary, Gini coefficient can be used as an index to measure the income distribution in a defined group of people. This concept is quite similar to cell distribution in a defined CLSM image divided into certain number of pixels. Therefore, a novel index –

concentration coefficient (CC) was developed to depict the cell distribution due to the fact that limited pixel number can only generate Lorenz fold line instead of traditional Lorenz curve, resulting in different calculation formula for the discrete Gini coefficient.

A CLSM image of cell aggregation can be first divided into a certain number pixels with the brightness positively correlate to the amount of cells in each pixel, which is equivalent to the income of a single resident in Gini Index. CC can then be calculated to measure the inequality of cell distribution, namely, the degree (level) of cells aggregation. CC and Lorenz fold line are shown in Fig 2.17.2.

Due to the limited pixel number in a defined CLSM image, the formula to calculate discrete Gini Index is explained as below:

1. Suppose a CLSM image is divided into N pixels with the quantity of bacteria cells in each pixel defined as $X_i$, where i = 1,2,3,...,N. Without losing generality, $X_i$ should be rearranged into a sequence of values with non-decreasing order

$X_1 \leq X_2 \leq \ \ldots\ldots\ \leq X_{N-1} \leq X_N$

Data from each pixel are usually not in a progressive increasing order and a computer program was developed to rearrange the order.

2. Another variable - accumulative number $Y_i$, is defined and calculated as

$$Y_i = \sum_{k=1}^{i} X_k$$

Apparently the total amount of all quantities in the image is $T = Y_N$ .

3. Lorenz fold line is then generated which is equivalent to the Lorenz curve at continuous variables. Similar to the calculation of area B below Lorenz curve, the Sum of all Accumulative Number $Y_i$ (S) is introduced here, i.e.

$S = Y_1 + Y_2 + \ldots\ldots + Y_N$

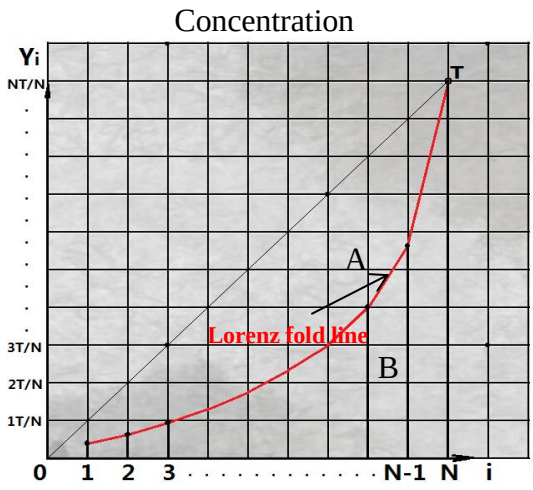


Fig 2.17.2 Concentration Coefficient and Lorenz fold line

The calculation of two extreme situations (perfectly equality and perfectly inequality) in CC are shown as below using N=10 as an example.

1. The maximum value of S occurs when each of the 10 pixels contains the same amounts of cells, i.e. $X_1 = X_2 = \ldots\ldots = X_N = T/N$, $Y_i$ locates at diagonal line.

then $Y_i = i \times \frac{T}{N}$

and $S = \frac{N\times(N+1)}{2} \times \frac{T}{N} = \frac{T\times(N+1)}{2}$

2. The minimum value of S occurs when 9 of the pixels contain no cell and 1 pixel contains T cells, i.e.

$X_1 = X_2 = \ldots\ldots = X_9 = 0$ and $X_{10} = T$

Then $Y_1 = Y_2 = \ldots\ldots = Y_9 = 0$ and $Y_{10} = 100\%T$

As a result, S = T, which is different from normal Gini coefficient where the area B=0 (see Fig 2.17.1)

3. For most common situations, $Y_i$ should locate at Lorenz Fold Line and CC value should be

$$CC = \frac{[T\times\frac{(N+1)}{2} - S]}{[T\times\frac{(N+1)}{2} - T]} = \frac{(N+1-2\times\frac{S}{T})}{(N-1)}$$

Thus, $0 \leq CC \leq 1$. When the cell number in each pixels is equal, CC = 0; when all the cells in one image are concentrated in one pixel, CC = 1.

# Chapter 3 – Determining the optimal NO donor for *P. aeruginosa* biofilm dispersal

## 3.1 *P. aeruginosa* PAO1 WT CFU to OD value

The initial inoculum plays a significant role in batch-cultured biofilm formation characteristics and life cycles. Therefore, it is important to control the initial inoculum cell numbers to ensure the consistency of each experimental replicate in biofilm research. However, it is impossible to measure CFU for inoculation each time as the observation of colonies usually requires overnight culture on agar plates. Consequently, cell optical density (OD value) is performed to quickly determine the number of cells. In order to standardise inoculum cell concentrations, CFUs were taken at different OD values so that cell mass can be correlated with OD (Figure 3.1). CFUs were calculated as described in methods 2.5.2 for 7 time points along with the cell growth up to OD 0.965 (within exponential phase) and were related to OD values. Linear regression analysis was performed with a final $R^2$ value of 0.9823 permitting determination of the OD corresponding to CFU.

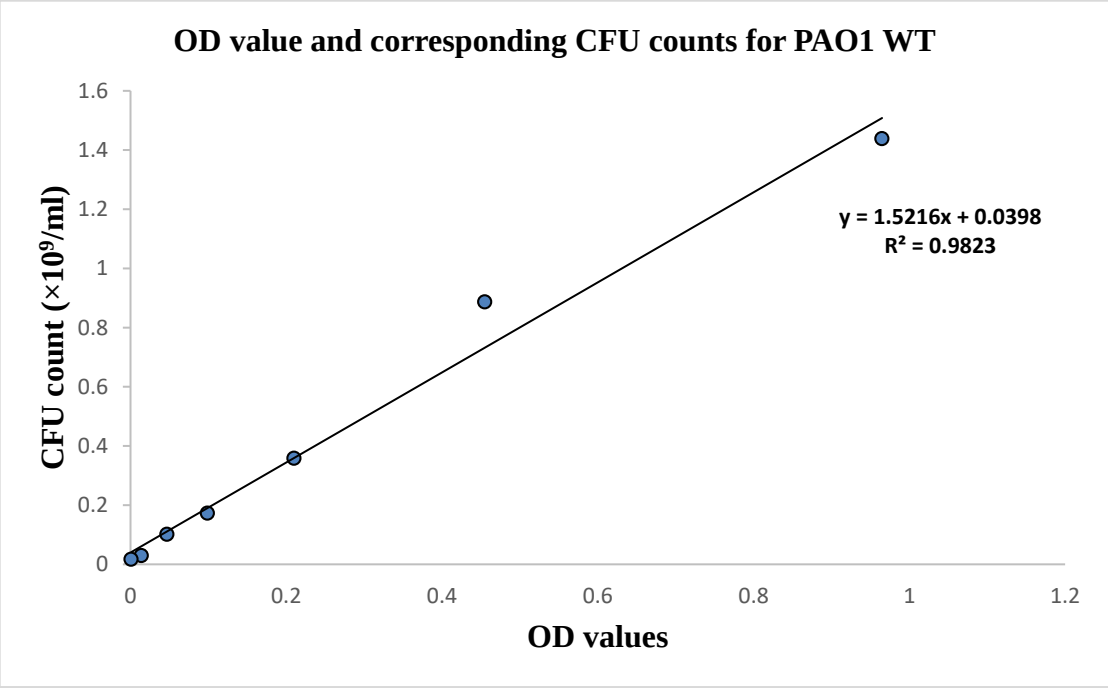


Fig 3.1. The linear relationship between CFU and $OD_{600nm}$ value for PAO1 WT

## 3.2. Biofilm formation in MatTek plates

Previous studies in the lab have determined that an inoculum of $OD_{600nm}$ 0.01 was the optimal condition for growing biofilm in MatTek plates. According to Fig 3.1, an $OD_{600nm}$~0.01 is equivalent to $5.5\times10^7$ cfu/ml which would be used as a standardised inoculum for all future work. Here, two different factors, temperature and time, were tested for their influences on PAO1 biofilm formation and structure.

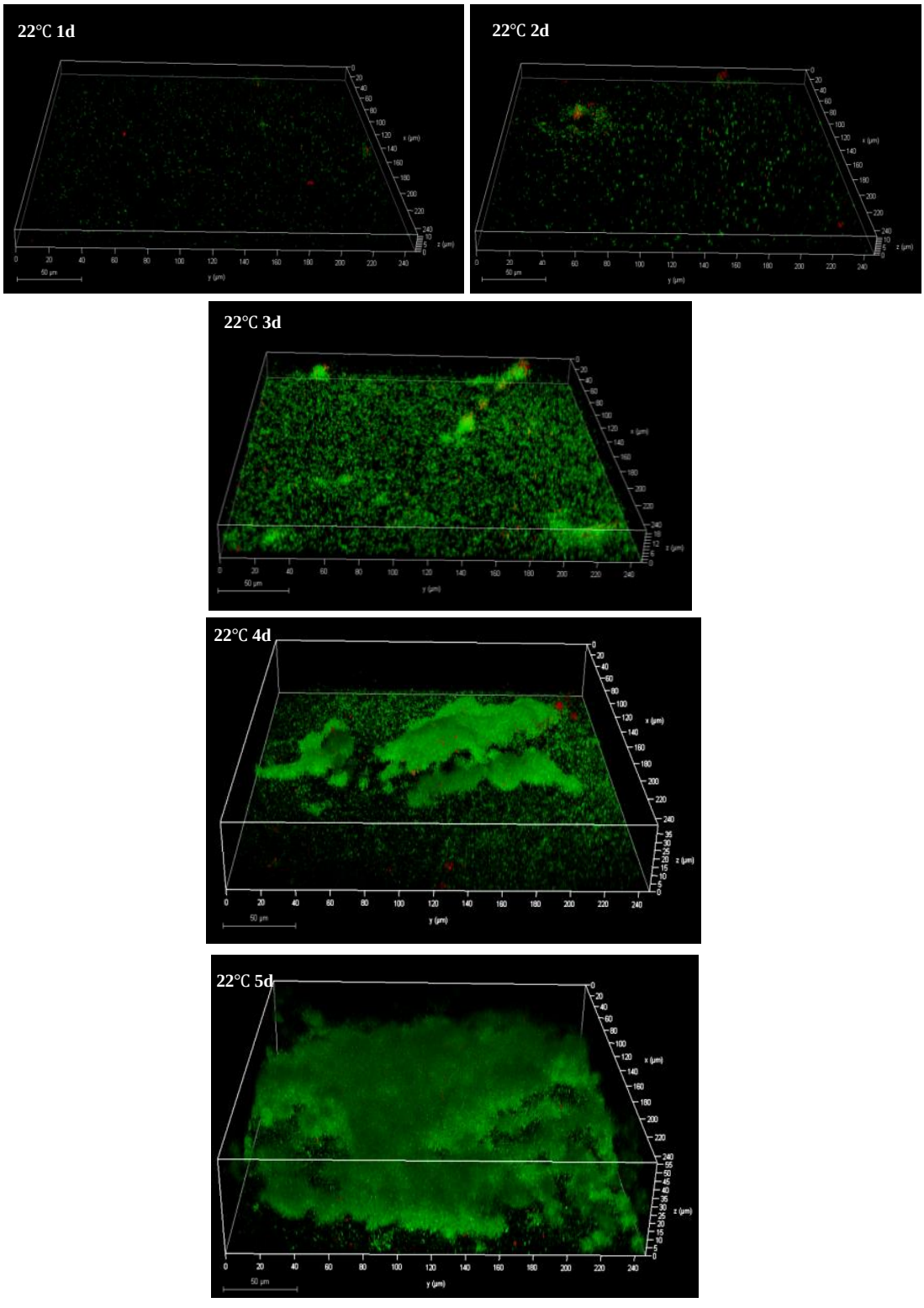

Fig 3.2.1. *P. aeruginosa* PAO1 WT biofilms formation in MatTek plates at 22℃ after 1d, 2d, 3d, 4d, 5d. Initial inoculum was $OD_{600nm}$ 0.01 in M9 medium and MatTek dishes were shaken at 50rpm in 22℃ incubator. 3 fields of view (technical replicates) were chosen randomly from each dish for CLSM and 3 biological replicates were performed.

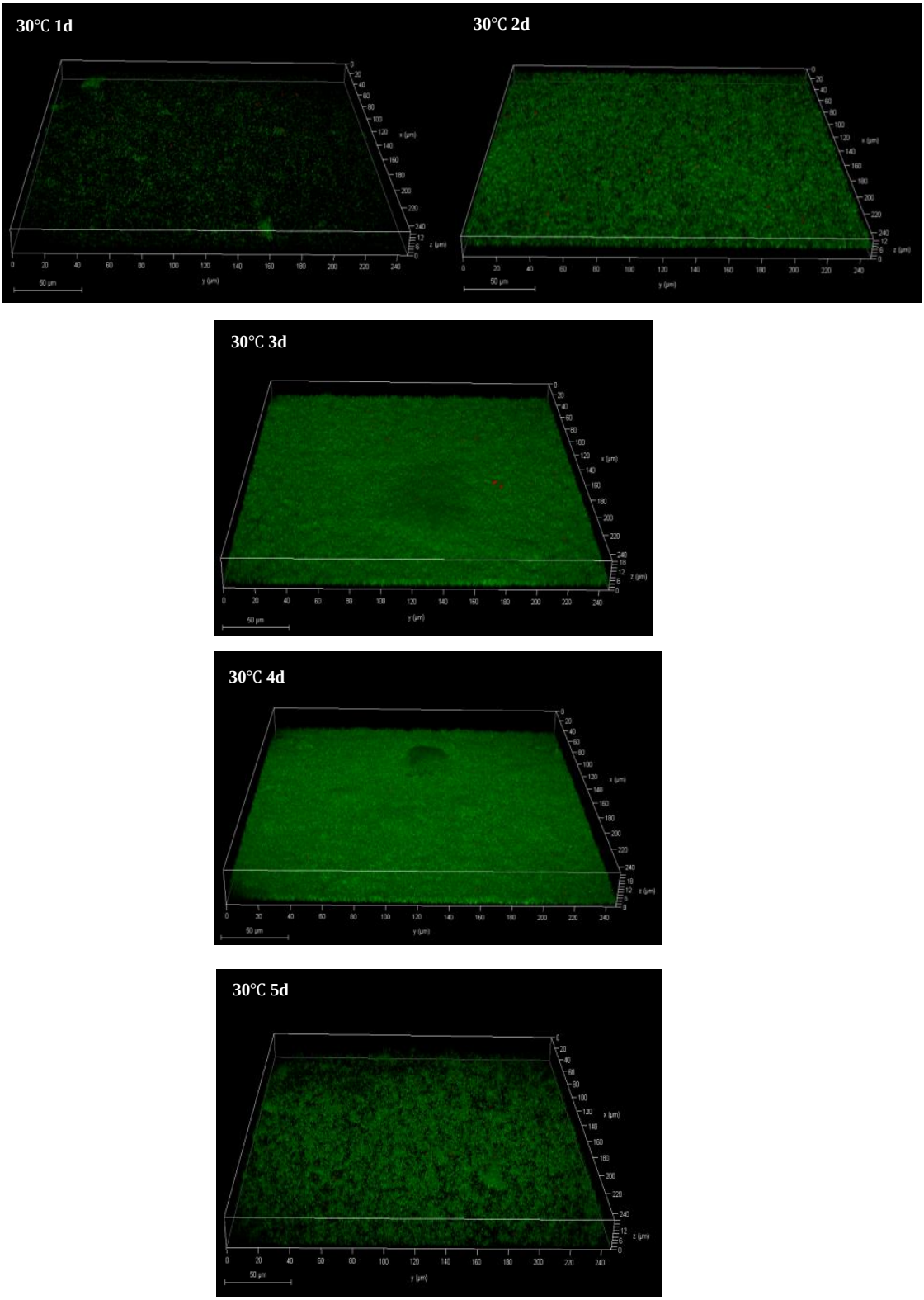


Fig 3.2.2. *P. aeruginosa* PAO1 WT biofilms formation in MatTek plates at 30℃ after 1d, 2d, 3d, 4d, 5d. Initial inoculum was $OD_{600nm}$ 0.01 in M9 medium and MatTek dishes were shaken at 50rpm in 30℃

incubator. 3 fields of view (technical replicates) were chosen randomly from each dish for CLSM and 3 biological replicates were performed.

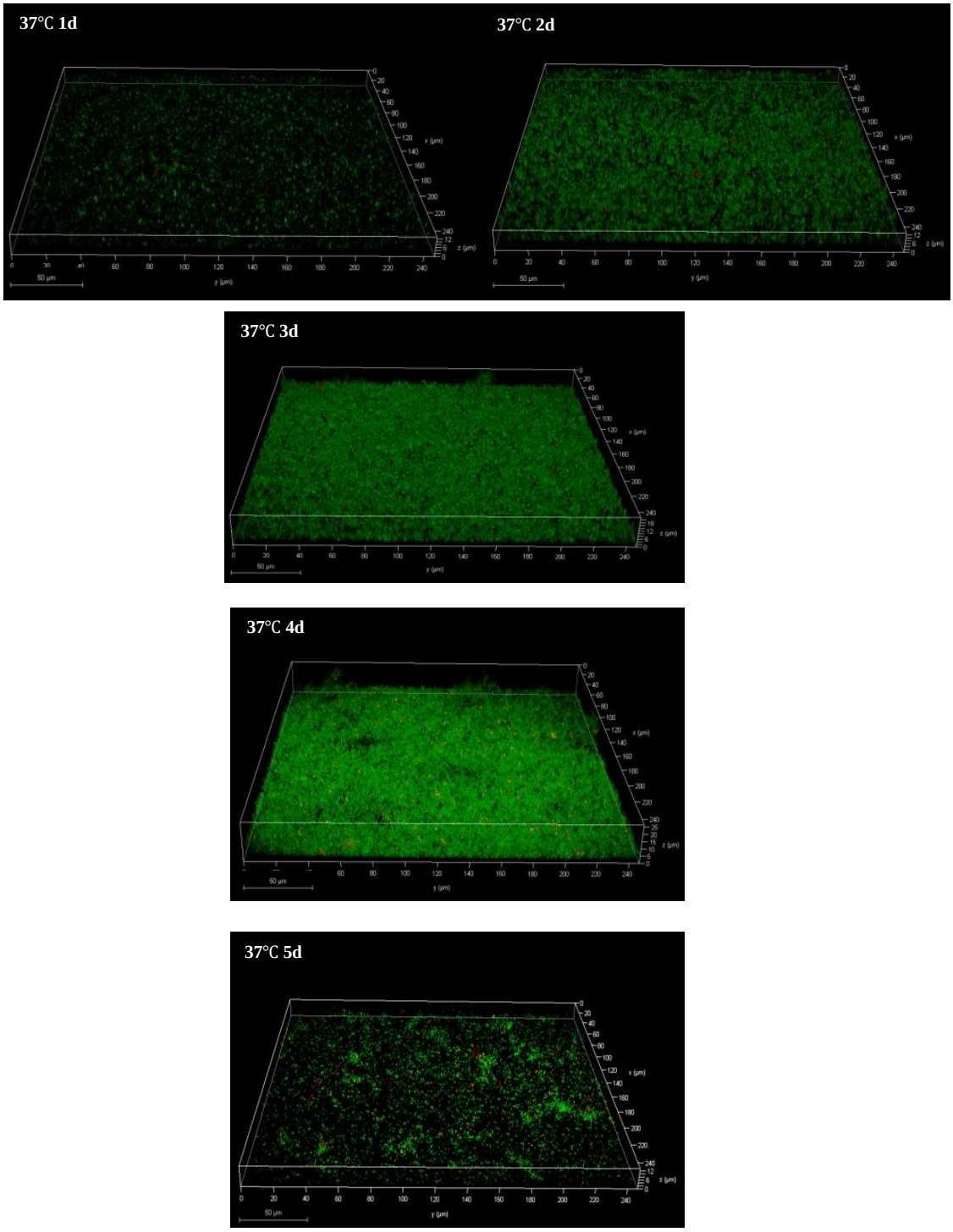


Fig 3.2.3. *P. aeruginosa* PAO1 WT biofilms formation in MatTek plates at 37℃ after 1d, 2d, 3d, 4d, 5d. Initial inoculum was $OD_{600nm}$ 0.01 in M9 medium and MatTek dishes were shaken at 50rpm in 37℃ incubator. 3 fields of view (technical replicates) were chosen randomly from each dish for CLSM and 3 biological replicates were performed.

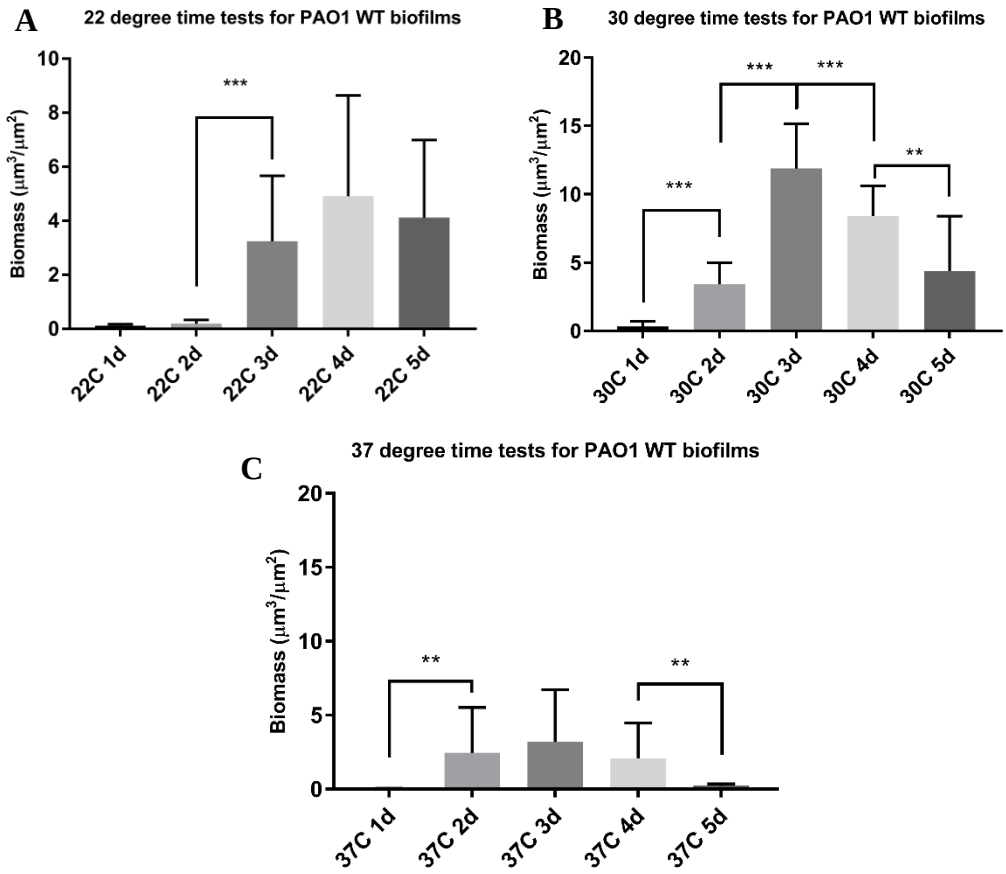


Fig 3.2.4. Biomasses of biofilms at (A) 22℃, (B) 30℃, (C) 37℃ from 1-5 days. Biomass was calculated using COMSTAT[304]. Data represent data means of n=3 of 3 biological replicates. Biomasses of biofilms were compared to one day younger biofilms for investigation of biofilm development under each culture temperatures with Welch T-test. ** represented $0.01<p<0.05$, *** represented $p<0.01$

Fig 3.2.1-3.2.3 showed representative CLSM pictures of biofilms grown at different temperatures and at time periods ranging from 1 d to 5 d. As shown in Fig 3.2.1, from 3-5d, incubation at 22 ℃ resulted in biofilms containing thick 3D-structured microcolonies heterogeneously distributed and attached to the surface while the rest of surfaces rarely had bacteria attached, suggesting the microenvironment and the heterogeneity of the coated coverslips had a marked influence on the biofilm structure. As shown in Fig 3.2.4 (A), total biomass increased significantly from day 2 to day 3 (16.6 fold, $p<0.01$) and standard deviations were very high due to this heterogeneity.

As shown in Fig 3.2.2 and Fig 3.2.4 (B), biofilms cultured at 30℃ formed a uniform, homogeneous monolayer on which several microcolonies developed as mushroom structures. Typical biofilm life cycle was shown in biofilms at 30℃ over 5 d – biomass

kept increasing steadily from day 1 to day 3 reaching its maximum ($p<0.01$ between neighbouring time points) indicating the maturation stages, and kept decreasing from day 3 to day 5 ($p<0.05$ between neighbouring time points) potentially due to the dispersal.

Fig 3.2.3 and Fig 3.2.4 (C) showed that at 37℃, biomasses were generally less than at 30℃ with no substantial three dimensional microcolonies formed on top of the base layer, or irregular cell aggregates compared to 22℃. Biomass significantly increased from day 1 to day 2 (60 fold, $p<0.05$) and decreased from day 4 to day 5 (9.1 fold, $p<0.05$). Furthermore, when performing rinses before staining, it was noted that biofilms under 37℃ were more brittle and easily disrupted by mechanical shear force from pipetting. In summary, 30℃ is regarded as the optimal temperature for biofilm culture in MatTek plates and 2-3 d can be used to observe maturation stages biofilm in future work.

## 3.3. Optimisation of 7 NO donors

Sodium nitroprusside (SNP) has been widely used as an NO donor for *P. aeruginosa* biofilm dispersal and similar effects were also found in other species such as *N. gonorrhoeae*[251] and *S. aureus*[323]. However, the chemical nature of SNP provides certain disadvantages in its use, such as light-induced NO release and cyanide production, which constrain its utilizations in certain settings. During the last decade there has been a steady increase in the production of novel NO donors. Therefore, different kinds of new and commercially accessible NO donors were tested in this study to find an alternative. Their half-lives at 37℃, pH ~7.4 are shown below in Table 3.3.

| | |
|---|---|
| SNP | <2mins |
| SNAP | 6hrs |
| GSNO | 1-3hrs |
| PROLI NONOate | 1.8secs |
| MAHMA NONOate (NOC-9) | 1min |
| Spermine NONOate (S150) | 39mins |
| DEA-NONOate | 2mins |

Table 3.3. Different half-lives of selected NO donors.

Due to various NO releasing mechanisms of different donors, the optimal working concentrations for triggering biofilm dispersal might be different. In this study, the efficacies of 7 donors in M9 medium at 9 concentrations (1μM, 2.5μM, 5μM, 10μM, 25μM, 50μM, 100μM, 250μM and 500μM) and 7 treatment time periods (1 hr, 2 hrs, 4 hrs, 6 hrs, 8 hrs, 12 hrs, 24 hrs) were tested for their abilities to disperse *P. aeruginosa* biofilms under 37℃ using a high-throughput screening microtiter plates assay.

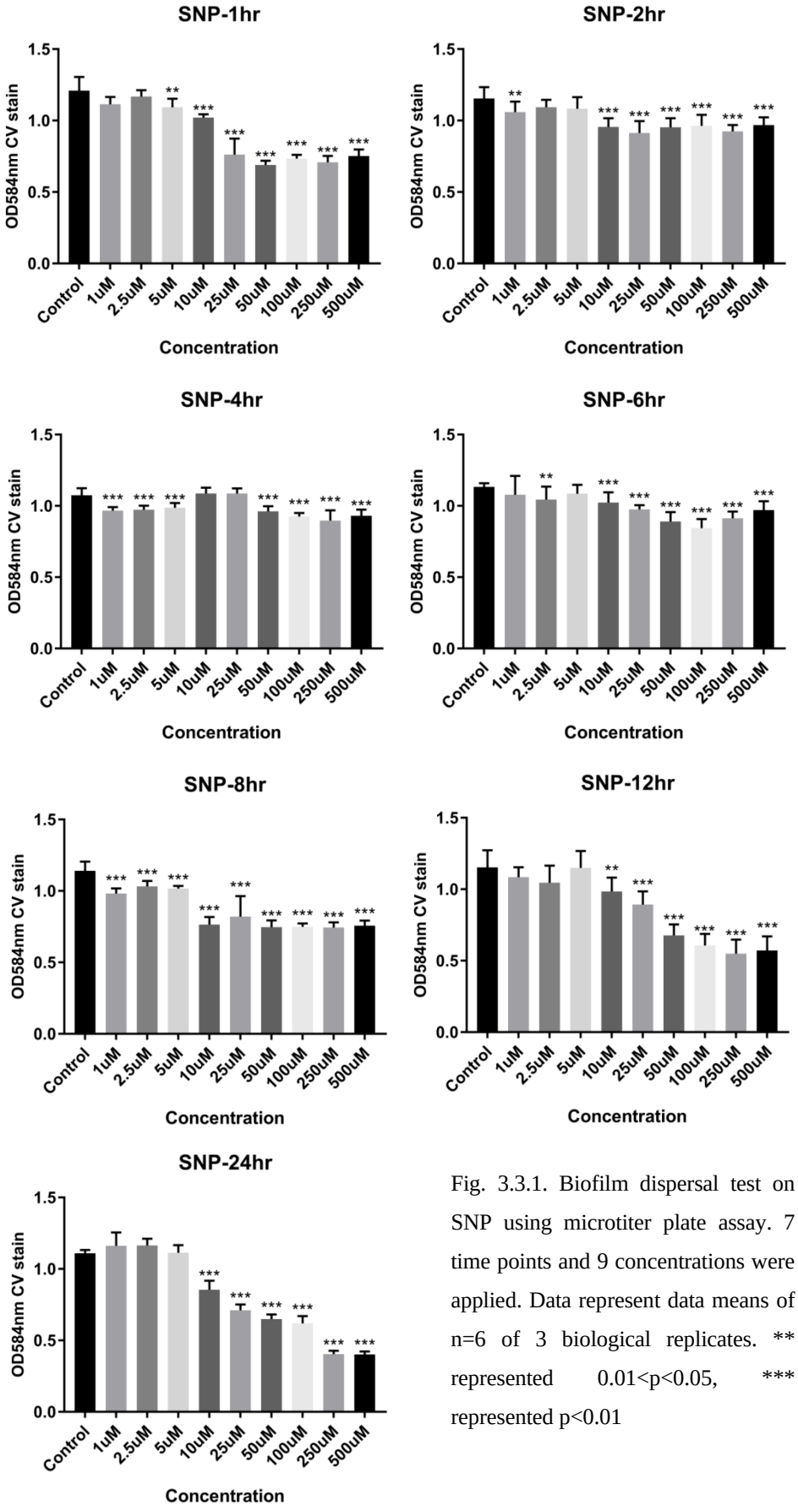


Fig. 3.3.1. Biofilm dispersal test on SNP using microtiter plate assay. 7 time points and 9 concentrations were applied. Data represent data means of n=6 of 3 biological replicates. ** represented $0.01<p<0.05$, *** represented $p<0.01$

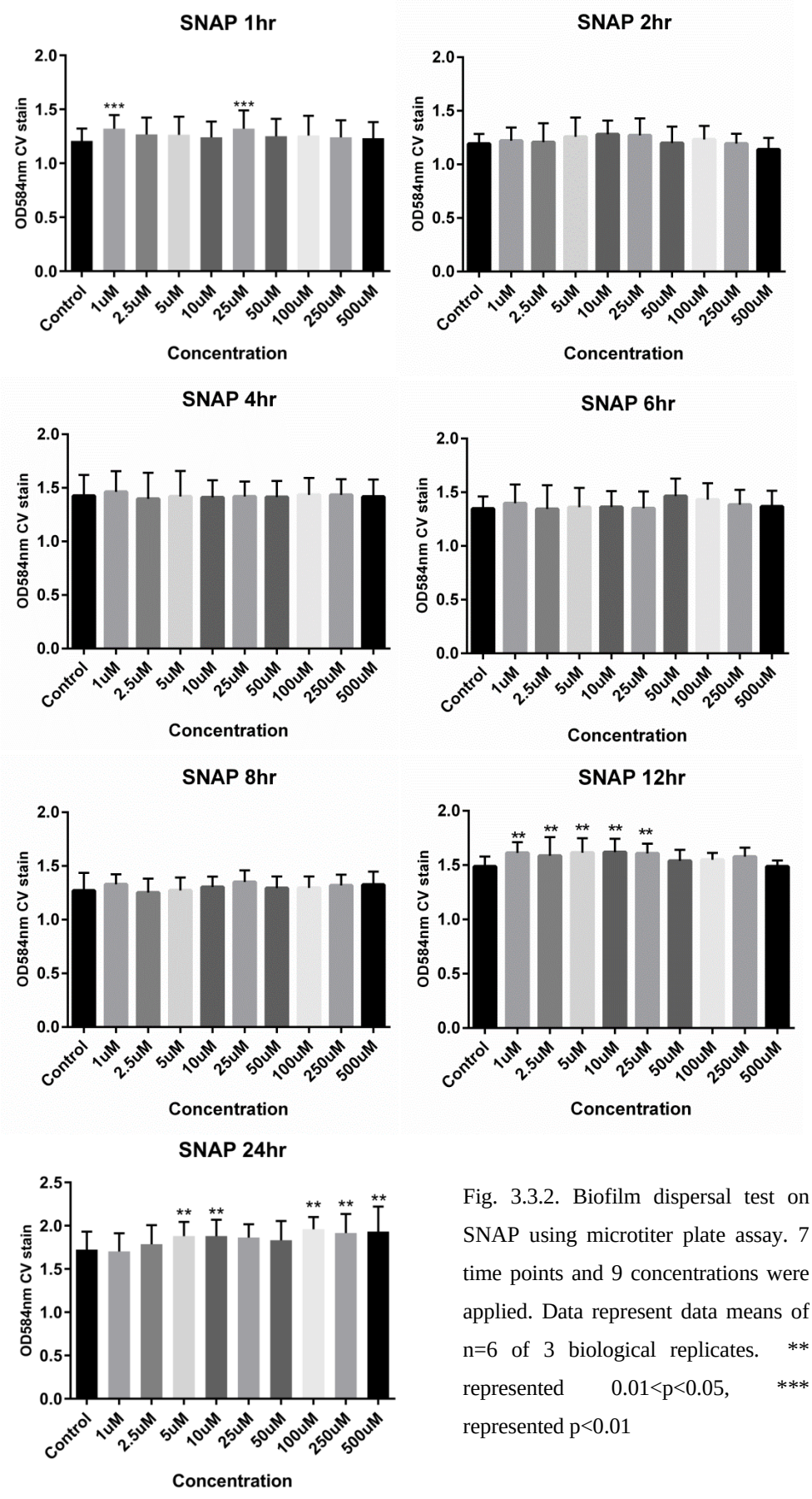


Fig. 3.3.2. Biofilm dispersal test on SNAP using microtiter plate assay. 7 time points and 9 concentrations were applied. Data represent data means of n=6 of 3 biological replicates. ** represented $0.01<p<0.05$, *** represented $p<0.01$

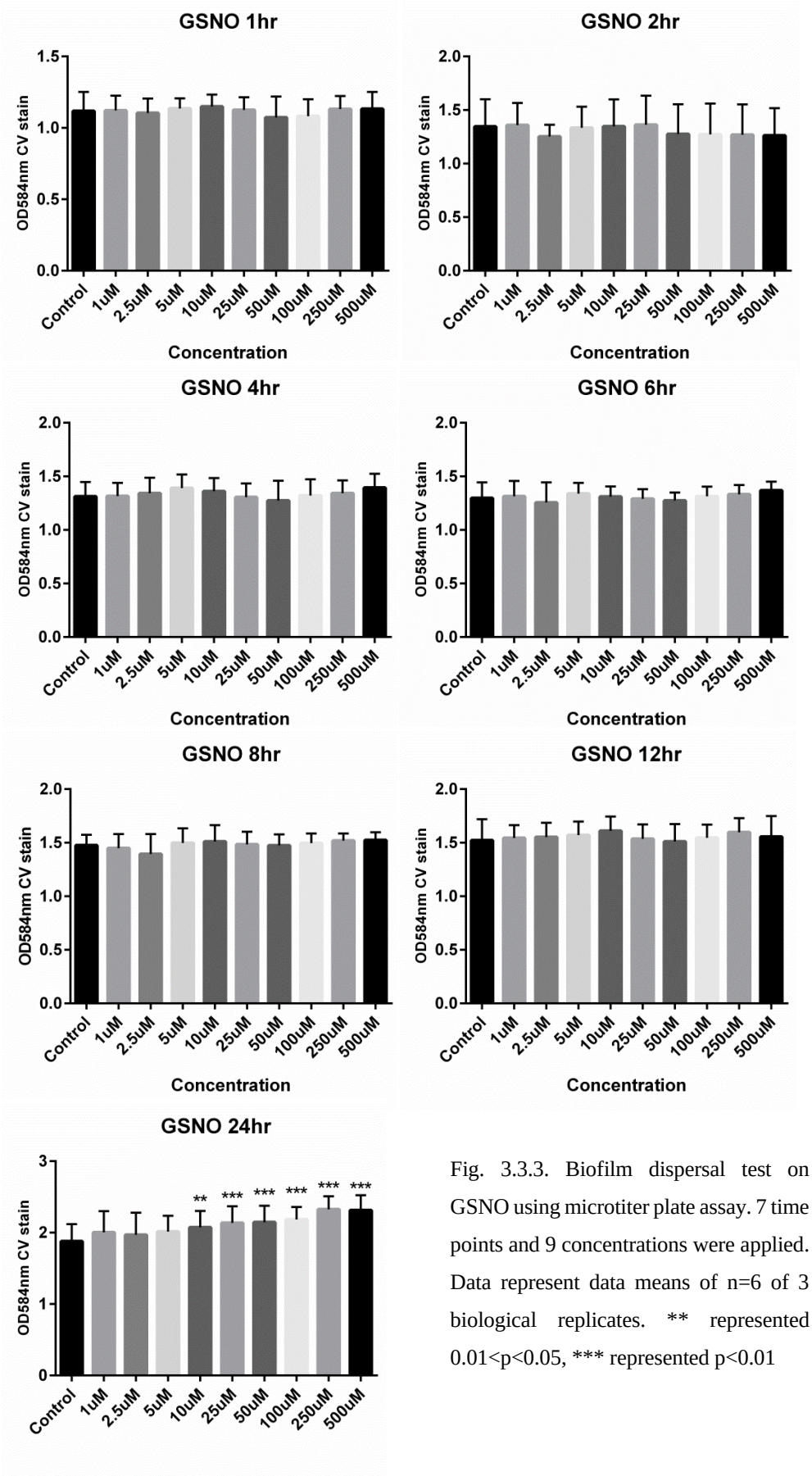


Fig. 3.3.3. Biofilm dispersal test on GSNO using microtiter plate assay. 7 time points and 9 concentrations were applied. Data represent data means of n=6 of 3 biological replicates. ** represented $0.01<p<0.05$, *** represented $p<0.01$

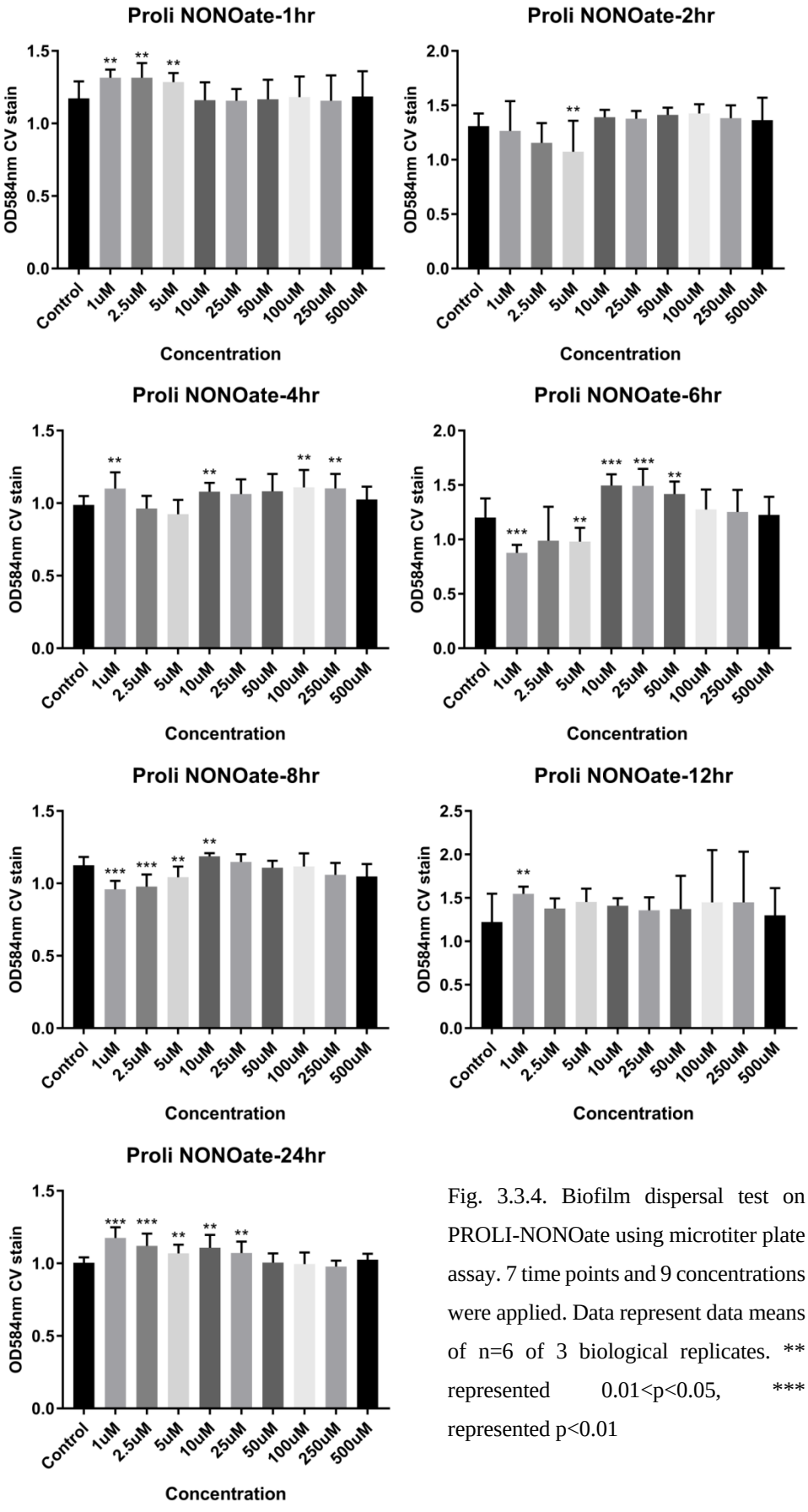


Fig. 3.3.4. Biofilm dispersal test on PROLI-NONOate using microtiter plate assay. 7 time points and 9 concentrations were applied. Data represent data means of n=6 of 3 biological replicates. ** represented $0.01<p<0.05$, *** represented $p<0.01$

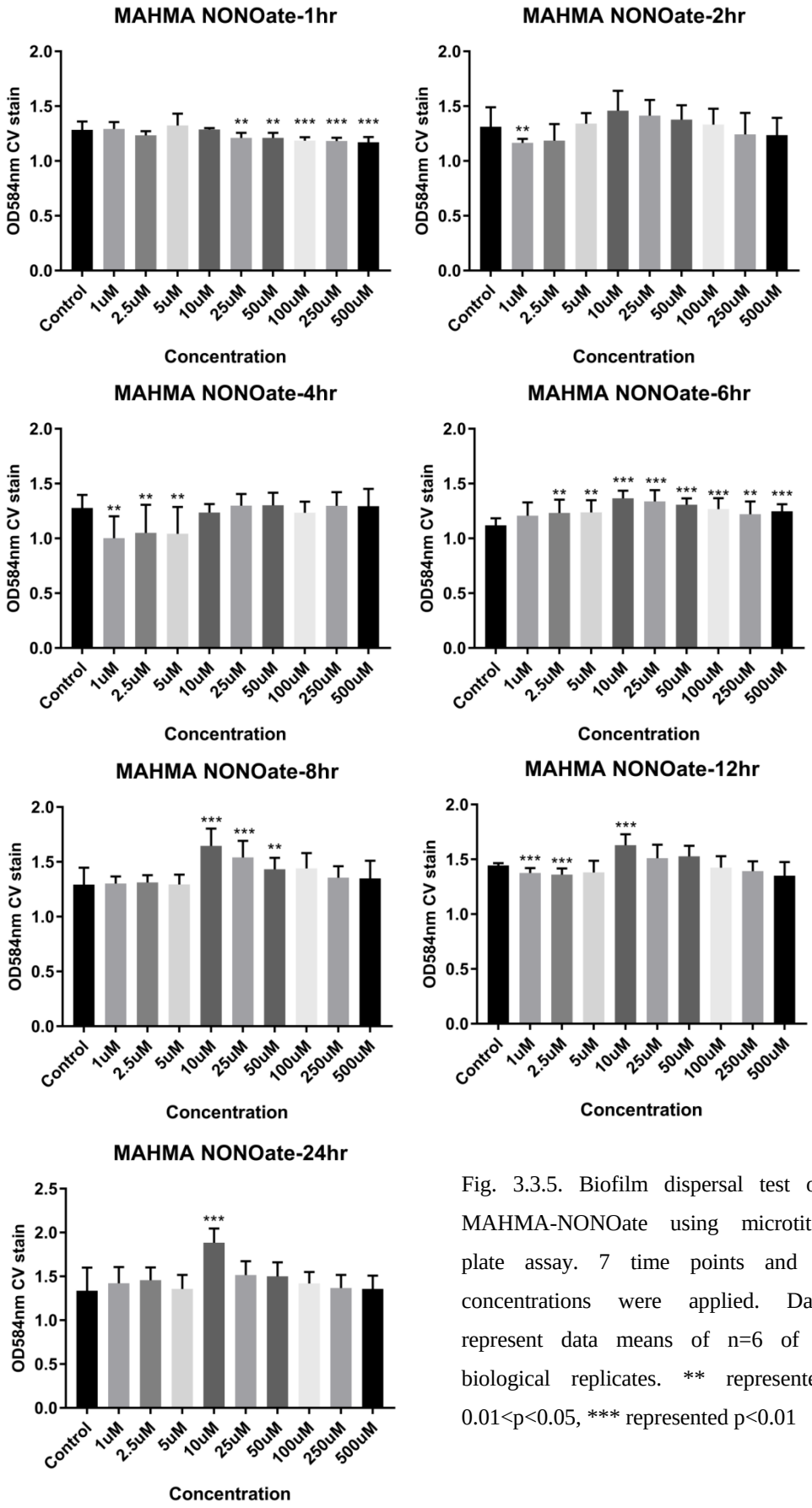


Fig. 3.3.5. Biofilm dispersal test on MAHMA-NONOate using microtiter plate assay. 7 time points and 9 concentrations were applied. Data represent data means of n=6 of 3 biological replicates. ** represented $0.01<p<0.05$, *** represented $p<0.01$

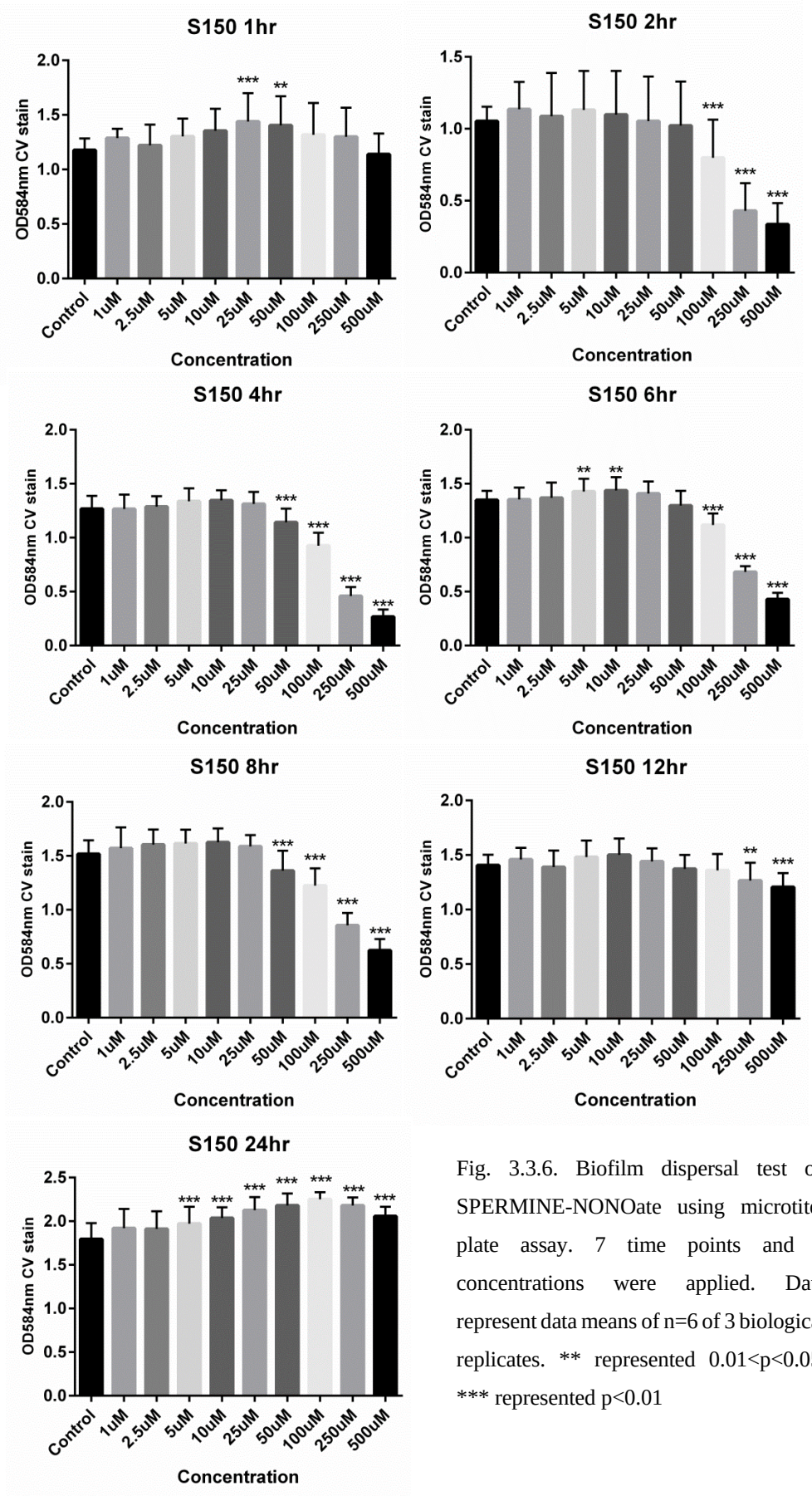


Fig. 3.3.6. Biofilm dispersal test on SPERMINE-NONOate using microtiter plate assay. 7 time points and 9 concentrations were applied. Data represent data means of n=6 of 3 biological replicates. ** represented $0.01<p<0.05$, *** represented $p<0.01$

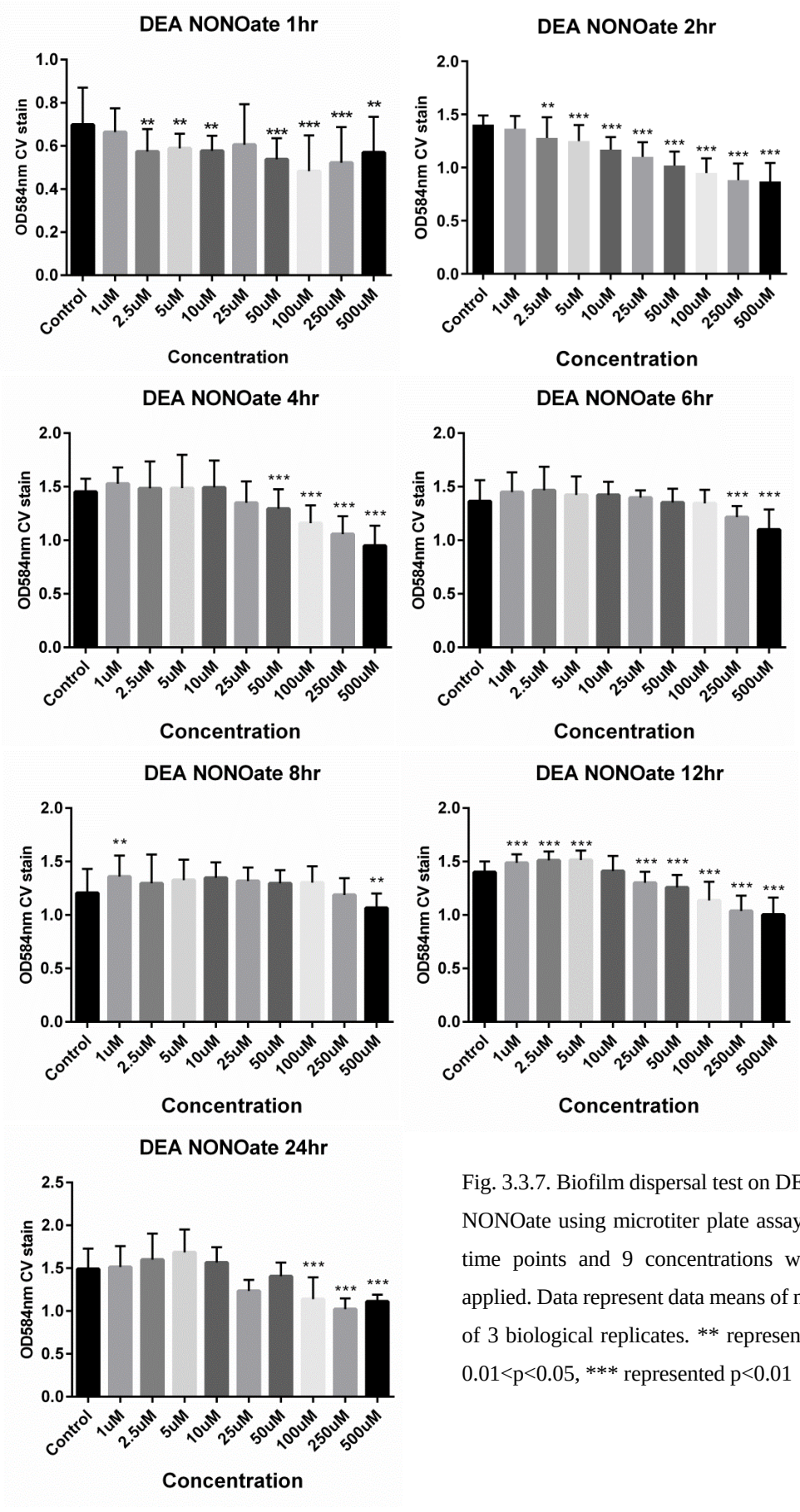


Fig. 3.3.7. Biofilm dispersal test on DEA-NONOate using microtiter plate assay. 7 time points and 9 concentrations were applied. Data represent data means of n=6 of 3 biological replicates. ** represented 0.01<p<0.05, *** represented p<0.01

Among these results, 250 and 500µM SNP reduced biomass by approximately 63% after 24 hrs, while 250 and 500µM S150 reduced biomass up to 60% after 2hrs and 68% after 4 hrs (Fig 3.3.8). However, to minimise the potentials that NO causes stress response rather than the desired signalling effects in cells, 24 hrs 250µM SNP and 2 hrs 250µM S150 treatments were chosen for future work.

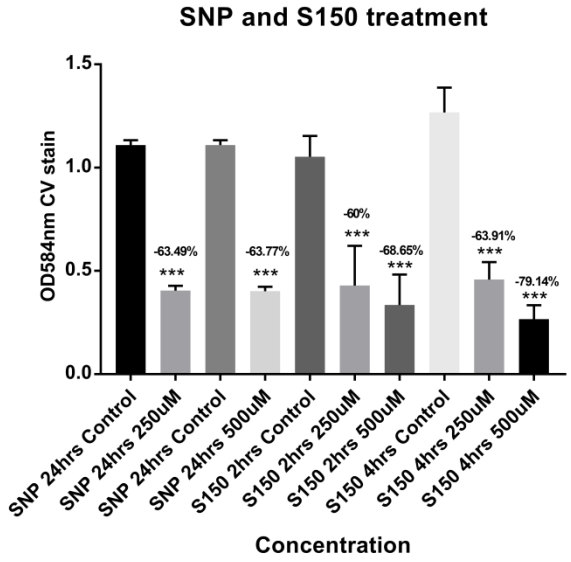


Fig 3.3.8. Comparison of the efficiencies between SNP and S150 on triggering PAO1 WT biofilm dispersal. Data represent data means of n=6 of 3 biological replicates. ** represented $0.01<p<0.05$, *** represented $p<0.01$

## 3.4. Evaluation of the specificity of NO-mediated biofilm dispersal using SNP and S150

As shown in Fig 3.3.8, 250µM was chosen to be the optimal concentration for both SNP and S150 to trigger biofilm dispersal. However, for SNP this concentration was much higher than the 500nM reported previously by Barraud *et al*[9,242] where milimolar range SNP was suspected to have toxic effect. Furthermore, NONOates should generate 2mol of NO per mole of compounds while SNP should only generate 1mol[306]. Hence, 250µM S150 would produce 2 times of NO compared to 250µM SNP. This led to the possibility that dispersal triggered by 250µM SNP and S150 was due to cell death. To determine the dispersal observed was not a result of the toxicity effect of high concentration NO, bactericidal tests on SNP and S150 were carried out. To determine whether the biofilm dispersal effect was from NO release of SNP and S150 or other mechanisms such as the side product/chemical characteristics of NO donors, NO scavenger was applied to eliminate the NO released from NO donors for observing if the biofilm dispersal effect was influenced.

### 3.4.1. NO scavenger test

The widely used PTIO was chosen as NO scavenger for the S150 experiments. A previous study has shown that the dispersal effect of SNP came from NO by using PTIO[9] so it was not re-evaluated here.

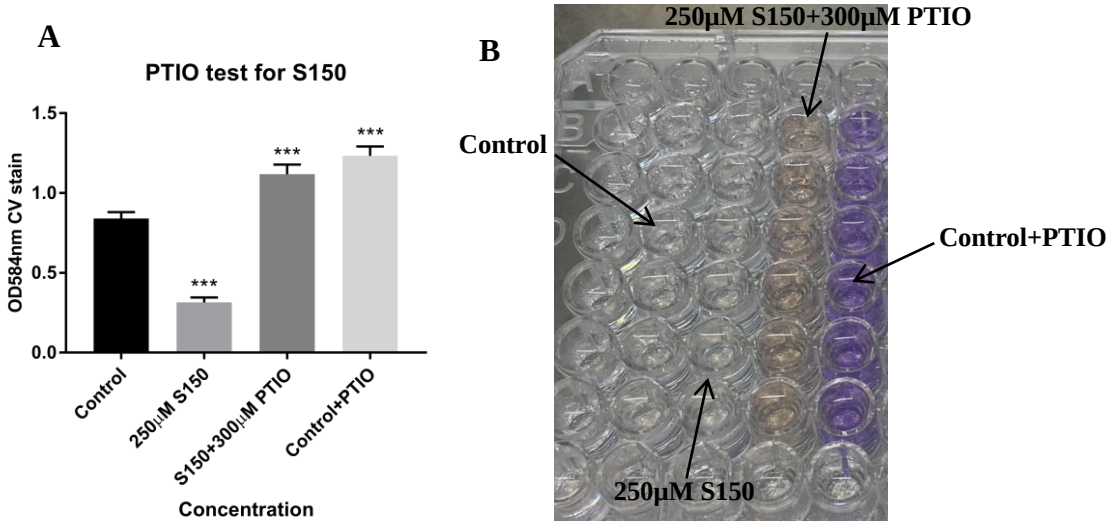


Fig 3.4.1. (A) 2 hrs S150 treatment on pre-established 24 hrs biofilms with or without PTIO. Biofilms with only PTIO was included to eliminate the potential side effect of PTIO (B) Picture of microtiter plate with PTIO. Data represent data means of n=6 of 3 biological replicates. One tailed t-test was applied and ** represented 0.01<P<0.05, *** represented P<0.01.

As shown in Fig 3.4.1 (A), 250μM S150 triggered dispersal after a 2 hrs contact time (62.54%, $p<0.01$). The addition of PTIO in combination with S150 did not elicit dispersal (and even resulted in 33% increase, $p<0.01$). For control + PTIO a larger increase (46.8%, $p<0.01$) was observed. In Fig 3.4.1 (B) the colour of S150+PTIO turned yellow while the wells with only bacteria culture and PTIO remained purple, indicating S150 was reacting with PTIO. In summary, it can be concluded that it was the NO released from S150 that triggered dispersal and the increase of biofilm with PTIO might be due to the inhibition of endogenous NO release from nitrite reductase in the bacteria itself[9].

### 3.4.2. Bactericidal tests

Toxicity of SNP and S150 were tested on (I) planktonic cells in 0.85% (w/v) NaCl after 2 and 24 hrs treatment; (II) 96 hrs biofilms in 6 well plates and their dispersed planktonic cells by CFU counts; (III) 24 hrs biofilms in microtiter plates by crystal violet staining and CFU counts for dispersed planktonic cells.

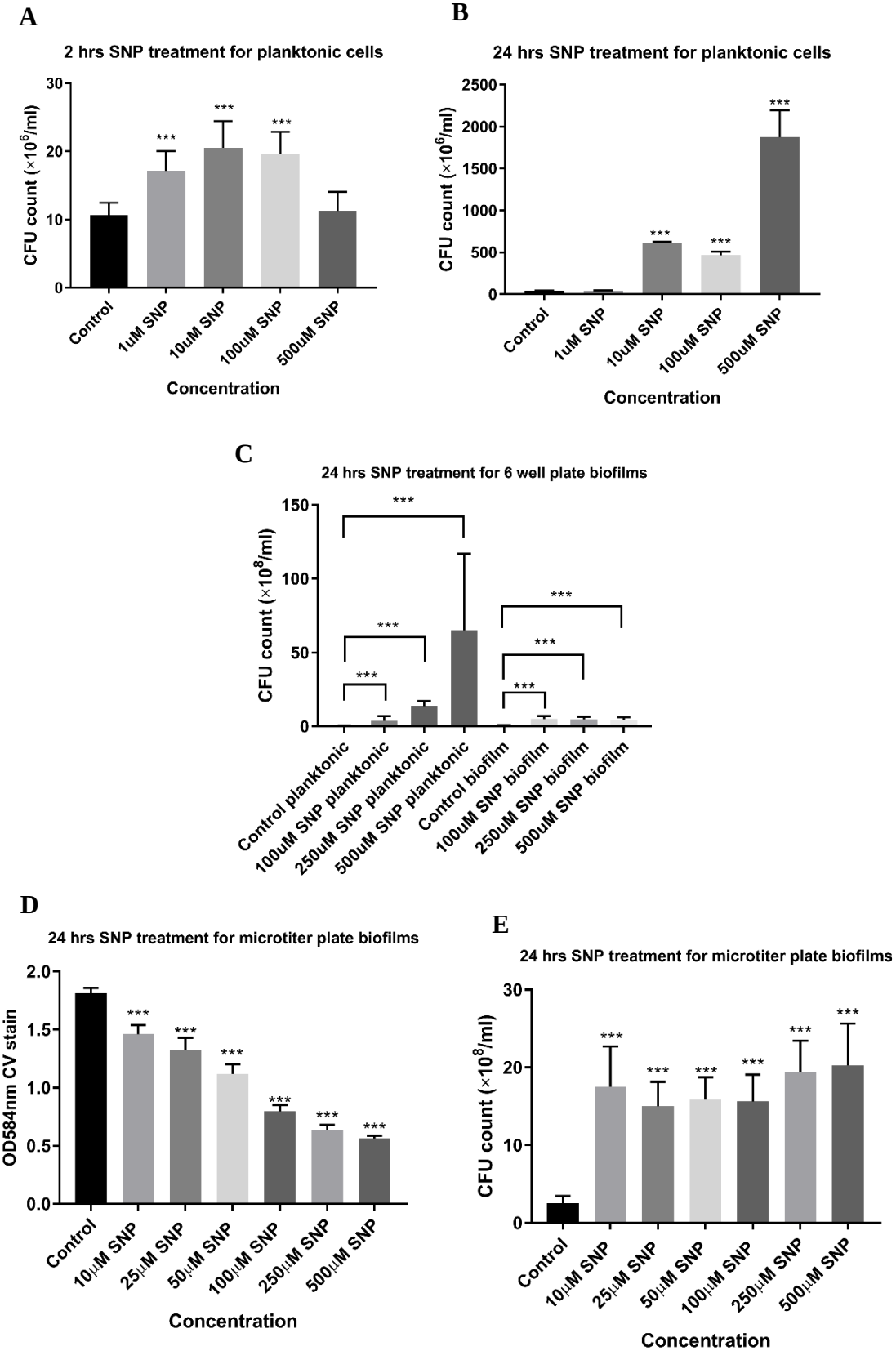
A
2 hrs SNP treatment for planktonic cells
CFU count (×10^6/ml)
30
20
10
0
***
***
***
Control
1uM SNP
10uM SNP
100uM SNP
500uM SNP
Concentration
B
24 hrs SNP treatment for planktonic cells
CFU count (×10^6/ml)
2500
2000
1500
1000
500
0
***
***
***
Control
1uM SNP
10uM SNP
100uM SNP
500uM SNP
Concentration
C
24 hrs SNP treatment for 6 well plate biofilms
CFU count (×10^8/ml)
150
100
50
0
***
***
***
***
***
***
Control planktonic
100uM SNP planktonic
250uM SNP planktonic
500uM SNP planktonic
Control biofilm
100uM SNP biofilm
250uM SNP biofilm
500uM SNP biofilm
D
24 hrs SNP treatment for microtiter plate biofilms
OD584nm CV stain
2.0
1.5
1.0
0.5
0.0
***
***
***
***
***
***
Control
10μM SNP
25μM SNP
50μM SNP
100μM SNP
250μM SNP
500μM SNP
Concentration
E
24 hrs SNP treatment for microtiter plate biofilms
CFU count (×10^8/ml)
30
20
10
0
***
***
***
***
***
***
Control
10μM SNP
25μM SNP
50μM SNP
100μM SNP
250μM SNP
500μM SNP
Concentration

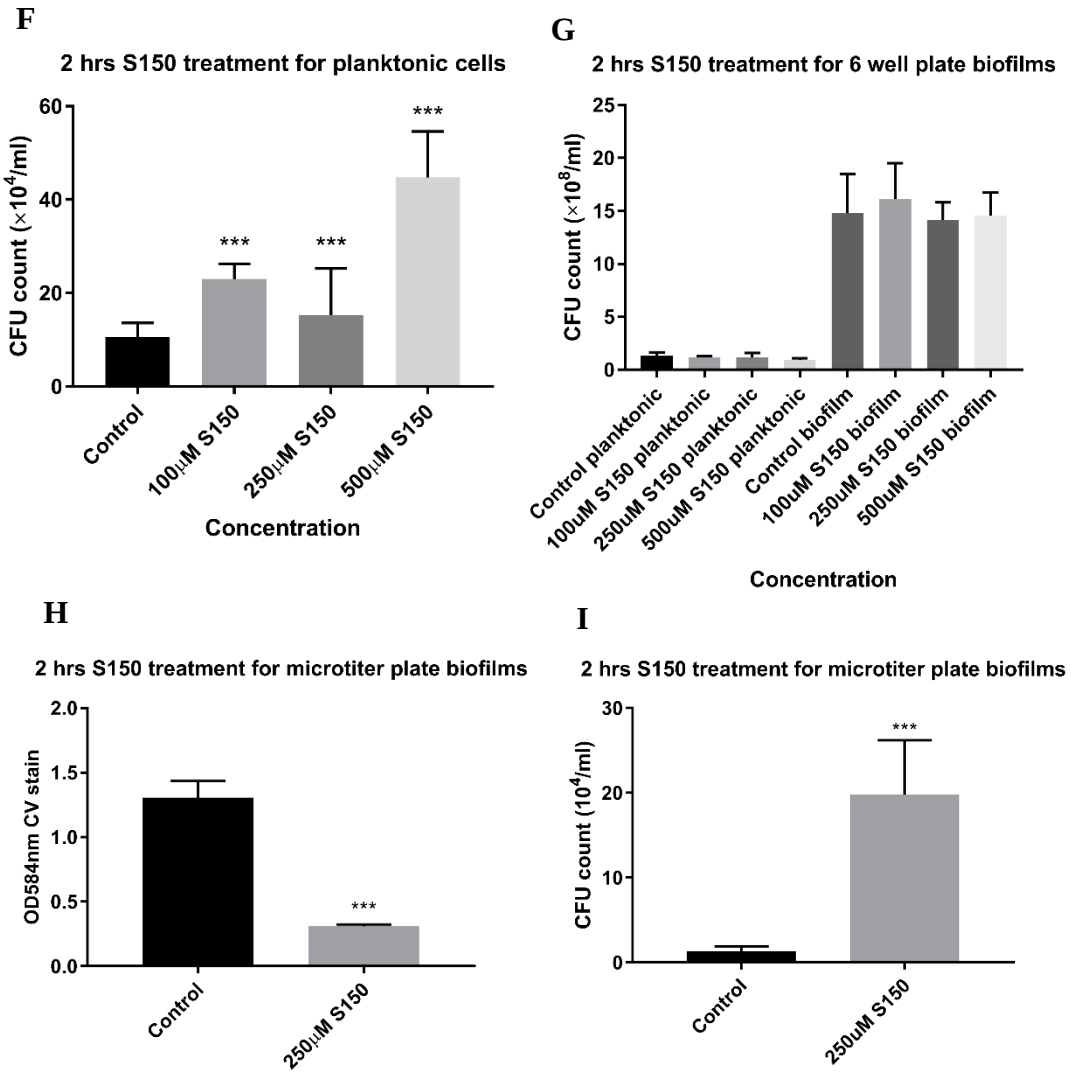


Fig 3.4.2. Bactericidal tests on planktonic and biofilm cells for SNP and S150. (A) Planktonic cells bactericidal tests after 2 hrs SNP treatment. (B) Planktonic cells bactericidal tests after 24 hrs SNP treatment. (C) 6 well plate biofilm bactericidal test after 24 hrs SNP treatment. (D) OD values of crystal violet staining for residual biofilms in microtiter plates after 24 hrs SNP treatment. (E) CFU counts of dispersed planktonic cells in microtiter plates after 24 hrs SNP treatments. (F) Planktonic cells bactericidal tests after 2 hrs S150 treatment. (G) 6 well plate biofilm bactericidal test after 2 hrs S150 treatment. (H) OD values of crystal violet staining for residual biofilms in microtiter plates after 2 hrs S150 treatment. (I) CFU counts of dispersed planktonic cells in microtiter plates after 2 hrs S150 treatment. Data represent data means of n=6 of 3 biological replicates. One tailed t-test was applied and ** represented $0.01<p<0.05$, *** represented $p<0.01$.

As shown in Fig 3.4.2 (A) and (B), SNP surprisingly enhanced planktonic cell growth. After 2 hrs 10 and 100μM SNP increased the CFU up to 2 fold ($p<0.01$) while after 24 hrs 500μM SNP increased CFU up to 90 fold ($p<0.01$). Similar results occurred in (F) where 100μM, 250μM and 500μM S150 enhanced planktonic cells number 2.19, 1.45

and 4.26 fold respectively after only 2 hrs ($p<0.01$). The mechanism of this increase is unknown, but it proved that SNP and S150 do not elicit a toxic effect on the planktonic cells with the concentrations applied in these experiments.

As shown in Fig 3.4.2 (C) and (G), CFU from the scraped remaining biofilms in 6 well plates did not show reduction after the addition of SNP and S150 when compared to control, which was contradictory to the significant dispersal effect in microtiter plates as shown in (D) and (H) or Fig 3.3.8. CFU for remaining biofilms in 6 well plates even increased after the addition of SNP ($p<0.01$). Potential explanations are (1) More biofilm was left after the addition of SNP; (2) Cell density inside biofilm increased after the addition of SNP; (3) Wash step did not flush away all loosely attached planktonic cells and those cells were counted into biofilm cells; (4) Scraped biofilms were not entirely washed into NaCl for CFU.

To eliminate the possible technical errors affecting the results, further tests were carried out using CFU from microtiter plates for dispersed planktonic cells and crystal violet staining for remaining biofilm in each well. Plates were shaken vigorously to get rid of loosely attached cells before CV staining. As shown in Fig 3.4.2 (D), increasing SNP concentrations resulted in statistically significant reductions in $OD_{584nm}$ values following CV staining, indicating biofilm dispersed more when treated with higher concentration of SNP ($0.01<p<0.05$ between neighbouring concentrations). However, the corresponding results in (E) showed that different concentrations of SNP led to similar increase in planktonic CFU ($p>0.05$ between neighbouring concentration from 10-500µM SNP). For example, 10µM and 500µM SNP reduced biofilm CV staining by 19.5% and 71.07% respectively and the OD values were significantly different ($p<0.01$), but the corresponding planktonic cell CFU counts were not significantly different ($p>0.05$). Hence, data here indicated that although SNP did not pose toxicity effect to cells, the increase of planktonic phase cells were not all coming from the dispersed biofilm phase cells. Considering the 24 hrs treatment time, one possible explanation was planktonic cell replication. However, same amount of M9 medium with SNP was added to the same amount of biofilms in each well so the cell replication result from medium should be the same, while more dispersal resulted in more planktonic cells. Combining these two factors, the increase of planktonic cells from 500µM SNP should still be significantly higher than 10µM SNP, which is contradict to the results shown in (E).

As shown in (H) and (I), 250μM S150 reduced biofilm in microtiter plates up to 71.2% ($p<0.01$) while the CFU counts for the planktonic cells suspension increased 15.26 fold ($p<0.01$) within only 2 hrs. Cell replication for PAO1 WT in M9 minimal medium within only 2 hrs should not result in such an obvious increase in planktonic CFU. Hence, S150 did not demonstrate toxicity towards cells, and the remarkable planktonic CFU increase indicated they might be majorly contributed by dispersed biofilm phase cells.

Considering the results in Fig 3.4.2 (A), (B) and (F) where SNP and S150 enhanced planktonic cells, as well as the results in (E) where increased planktonic cells were not convinced to come from dispersed biofilm phase cells and replication, SNP and S150 were supposed to be facilitating planktonic cell growth. Despite the mechanism for this cell growth enhance was not clear, "increased planktonic cell number" cannot be used as statistical evidence of NO-induced dispersed biofilms in future work.

### 3.4.3. Initial attachment and early stage biofilm formation prevention

Apart from triggering dispersal, the prevention of initial attachment and early stage biofilm formation is also important for decreasing biofilms. High levels of c-di-GMP enhance biofilm formation by activating EPS production and inhibiting motility[324], therefore lowering intracellular c-di-GMP level might also prevent the formation of early stage biofilms by adding NO at the initial inoculation point. 3 hrs initial attachment and 24 hrs biofilm formation with added S150/SNP were performed as described in 2.3.4.

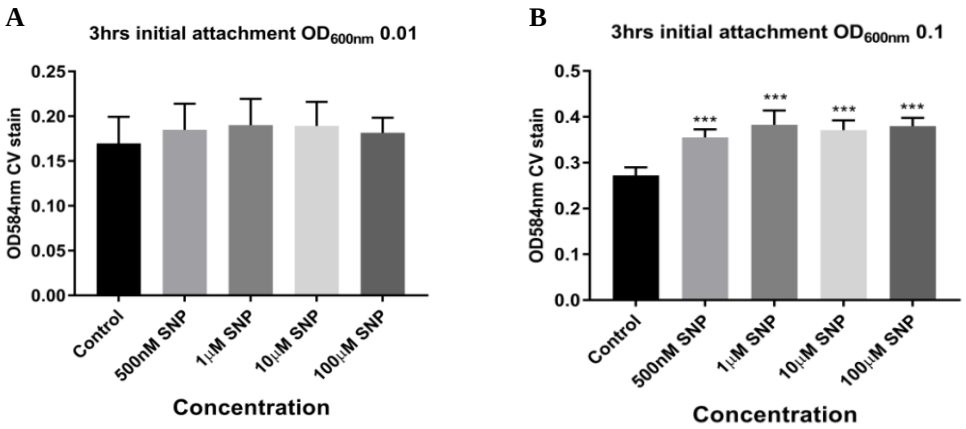

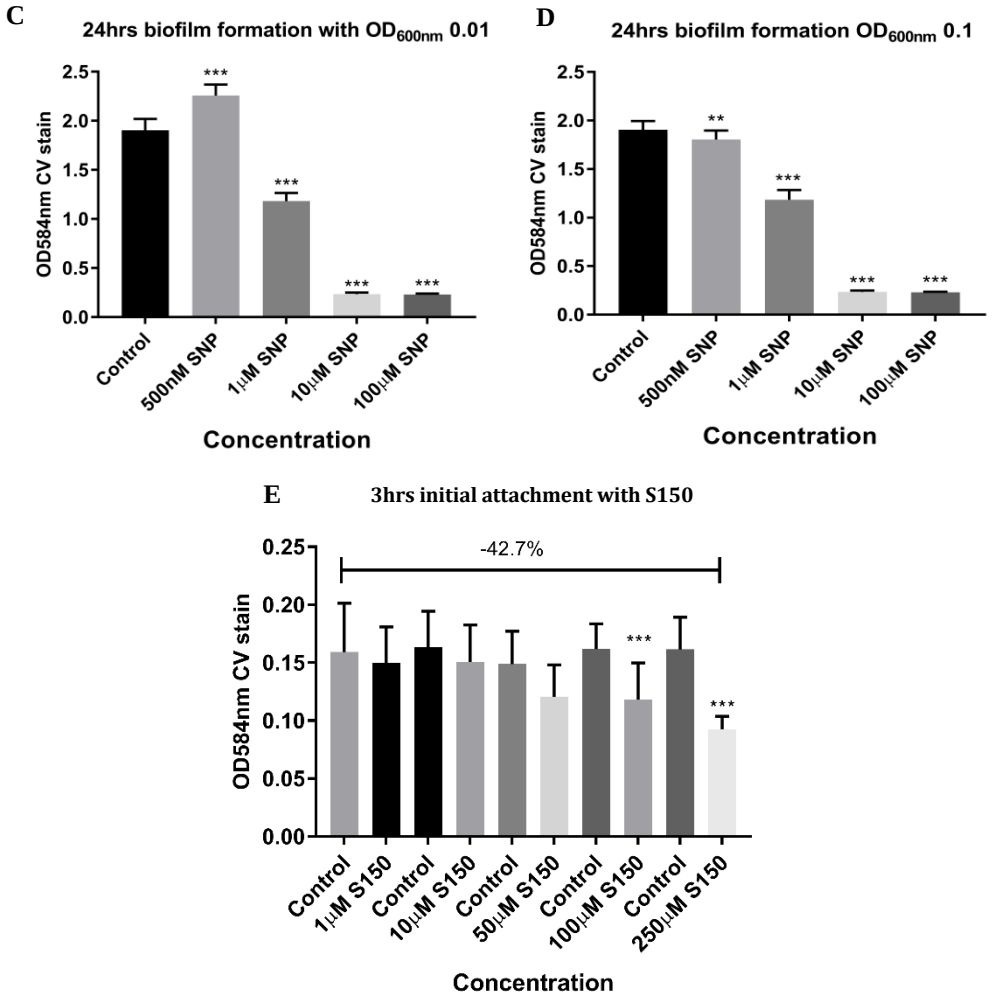


Fig 3.4.3. (A) 3 hrs initial attachment of PAO1 WT with SNP (initial inoculum $OD_{600nm}$ 0.01); (B) 3hrs initial attachment of PAO1 WT with SNP (initial inoculum $OD_{600nm}$ 0.1); (C) 24 hrs early stage biofilm formation of PAO1 WT with SNP (initial inoculum $OD_{600nm}$ 0.01); (D) 24 hrs early stage biofilm formation of PAO1 WT with SNP (initial inoculum $OD_{600nm}$ 0.1). (E) 3 hrs initial attachment of PAO1 WT with S150 (initial inoculum $OD_{600nm}$ 0.1). Data represent data means of n=6 of 3 biological replicates. One tailed t-test was applied and ** represented $0.01<p<0.05$, *** represented $p<0.01$.

SNP did not prevent surface attachment when initial inoculum was $OD_{600nm}$~0.01 (Fig 3.4.3 A, $p>0.05$), and even increased attachment with an initial inoculum of $OD_{600nm}$~0.1 (Fig 3.4.3 B, $p<0.01$). Potential reason for the increase might be the instant stress response of cells to NO or the increased cell inoculum. However, as shown in Fig 3.4.3 (C) and (D), after 24 hrs the early stage biofilm formation significantly decreased after the addition of SNP above 1μM (up to ~88% with 100μM, $p<0.01$) regardless of inoculum cell number. Therefore, low doses SNP can prevent early stage *P. aeruginosa* biofilm formation with a longer (24 hrs) treatment time. As shown in (E), 100μM S150 was able to significantly reduce surface attachment as determined by CV staining, with

250μM further decreasing initial attachment by 42.7% ($p<0.01$) relative to untreated controls. Therefore, S150 can effectively prevent biofilm formation from an initial stage.

### 3.4.4. Inhibition or dispersal?

When treating 24 hrs old pre-established biofilms in microtiter plates as shown in Fig 3.3.1, 100μM SNP caused a reduction of 44.2% ($p<0.01$) in biomass with a treatment time of 24 hrs. However, if mixing 100μM SNP with planktonic cells when they are inoculated into microtiter plates, biofilm formation was significantly inhibited (~88%) within 24 hrs as shown in Fig 3.4.3 (C). Similarly, 250μM S150 reduced 24 hrs old pre-established biofilms in microtiter plate by ~60% ($p<0.01$) within 2 hrs. However, if mixing 250μM S150 with planktonic cells when they are inoculated into microtiter plates, initial attachment was significantly inhibited (42.7%, $p<0.01$). Therefore, it was uncertain whether the reduction of biofilm biomass was the authentic dispersal of pre-established biofilms, or more likely to be a prevention of biofilm formation by planktonic cells. As these two procedures involve different mechanisms, additional assays were required to confirm what concentrations cause a reduction of pre-established biofilms, namely, dispersal.

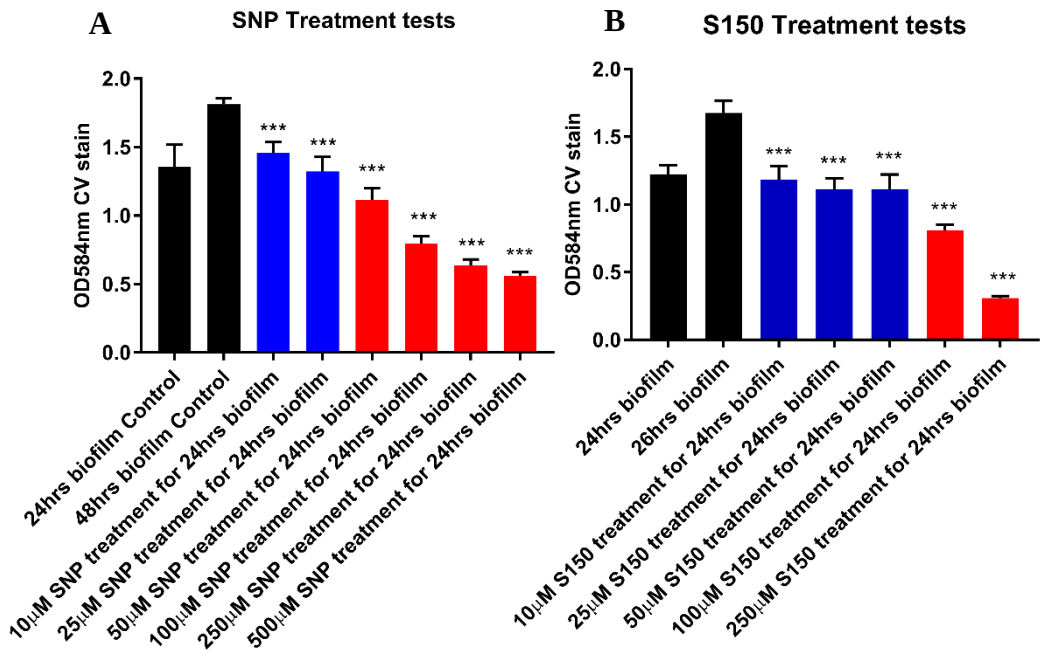


Fig. 3.4.4 (A) 24 hrs SNP treatments for pre-established 24 hrs biofilms. Comparisons of CV OD staining value (residual biofilm mass) between treatment groups and 24 hrs pre-established biofilm or 48 hrs biofilm control were shown. Bars in **blue** represent the CV OD value (residual biofilm mass) were significantly less than 48 hrs biofilm control **but not** 24 hrs pre-established biofilms. Bars in **red** represent

the CV OD values that were significantly less than **both** 48 hrs and 24 hrs biofilms. (B) 2 hrs S150 treatments for pre-established 24 hrs biofilms. Comparisons of CV OD staining value (residual biofilm mass) between treatment groups and 24 hrs pre-established biofilm or 26 hrs biofilm control were shown. Bars in **blue** represent the CV OD value (residual biofilm mass) were significantly less than 26 hrs biofilm control **but not** 24 hrs pre-established biofilms. Bars in **red** represent the CV OD values were significantly less than **both** 26 hrs and 24 hrs biofilms. Data represent data means of n=6 of 3 biological replicates. One tailed t-test was applied and ** represented $0.01<p<0.05$, *** represented $p<0.01$.

For our future work on dispersal mechanisms studies, it is crucial to decide the concentrations of NO donors that generate efficient dispersal rather than prevention. For a dispersal effect in SNP treatment, a significant reduction of biomass should be found after the 24 hrs treatment compared to 24 hrs old pre-established biofilms. If a biomass was found to be only less than 48 hrs biofilm (24 hrs old pre-established + 24 hrs further incubation in M9 corresponding to SNP treatment time) but not 24 hrs old pre-established biofilm, it might be defined as only inhibiting biofilm regrowth or a combination of inhibition and dispersal effect. Similar comparisons were applied to S150 between treated biofilms and 24 or 26 hrs old biofilms (24 hrs pre-established + 2 hrs treatment). From Fig 3.4.4 (A) it could be concluded that at least 50µM of SNP should be used to definitely lessen pre-established 24 hrs biofilm ($p<0.01$), while 10-50µM SNP might be inhibiting new biofilm formation more than triggering dispersal. From Fig 3.4.4 (B) it could be concluded that at least 100µM of S150 should be used to definitely lessen pre-established 24 hrs biofilm within 2 hrs ($p<0.01$), while 10-100µM S150 might be inhibiting new biofilm formation more than triggering dispersal. Hence, 250µM SNP and S150 are suitable for future work as NO donors triggering dispersal.

## 3.5. SNP and S150 treatments on different stages of biofilms

All microtiter plate biofilm assays performed from section 3.3 to 3.4 were targeting 24 hrs old pre-established biofilms. However, longer incubation time in the microtiter plates may lead to the increase of total biomass within a biofilm cycle as shown in the MatTek system (Fig 3.2.1-Fig 3.2.3). Therefore, it was important to investigate whether biofilm biomass and biofilm maturation stages affect the efficacies of NO donors. Here, 1-5 d PAO1 WT biofilms were cultured in microtiter plates for treatments.

**A**

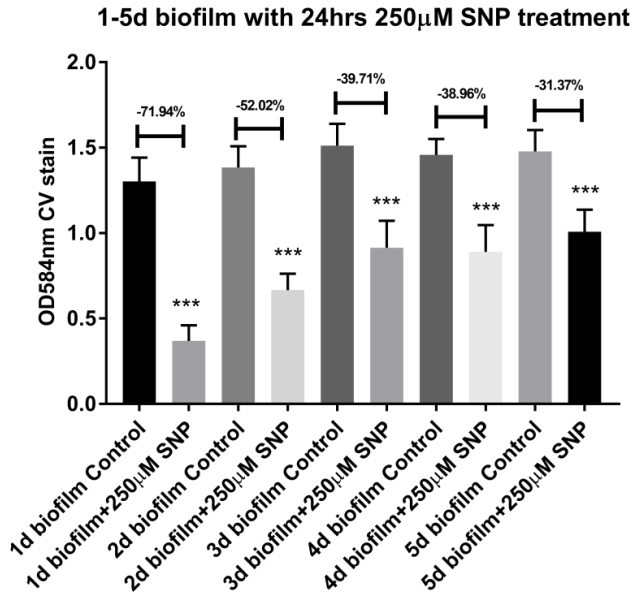
1-5d biofilm with 24hrs 250μM SNP treatment
OD584nm CV stain
2.0
1.5
1.0
0.5
0.0
-71.94%
-52.02%
-39.71%
-38.96%
-31.37%
***
1d biofilm Control
1d biofilm+250μM SNP
2d biofilm Control
2d biofilm+250μM SNP
3d biofilm Control
3d biofilm+250μM SNP
4d biofilm Control
4d biofilm+250μM SNP
5d biofilm Control
5d biofilm+250μM SNP

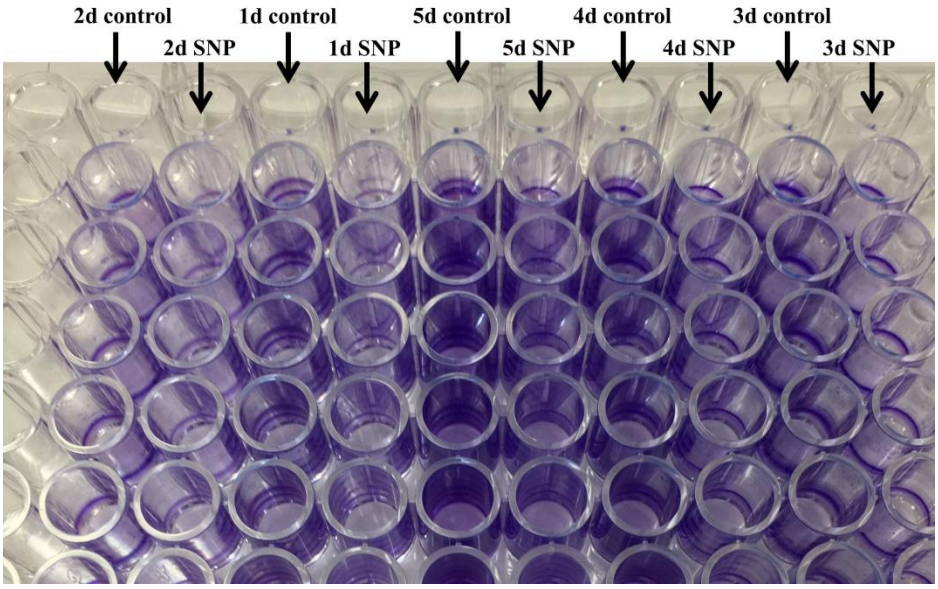
2d control
2d SNP
1d control
1d SNP
5d control
5d SNP
4d control
4d SNP
3d control
3d SNP

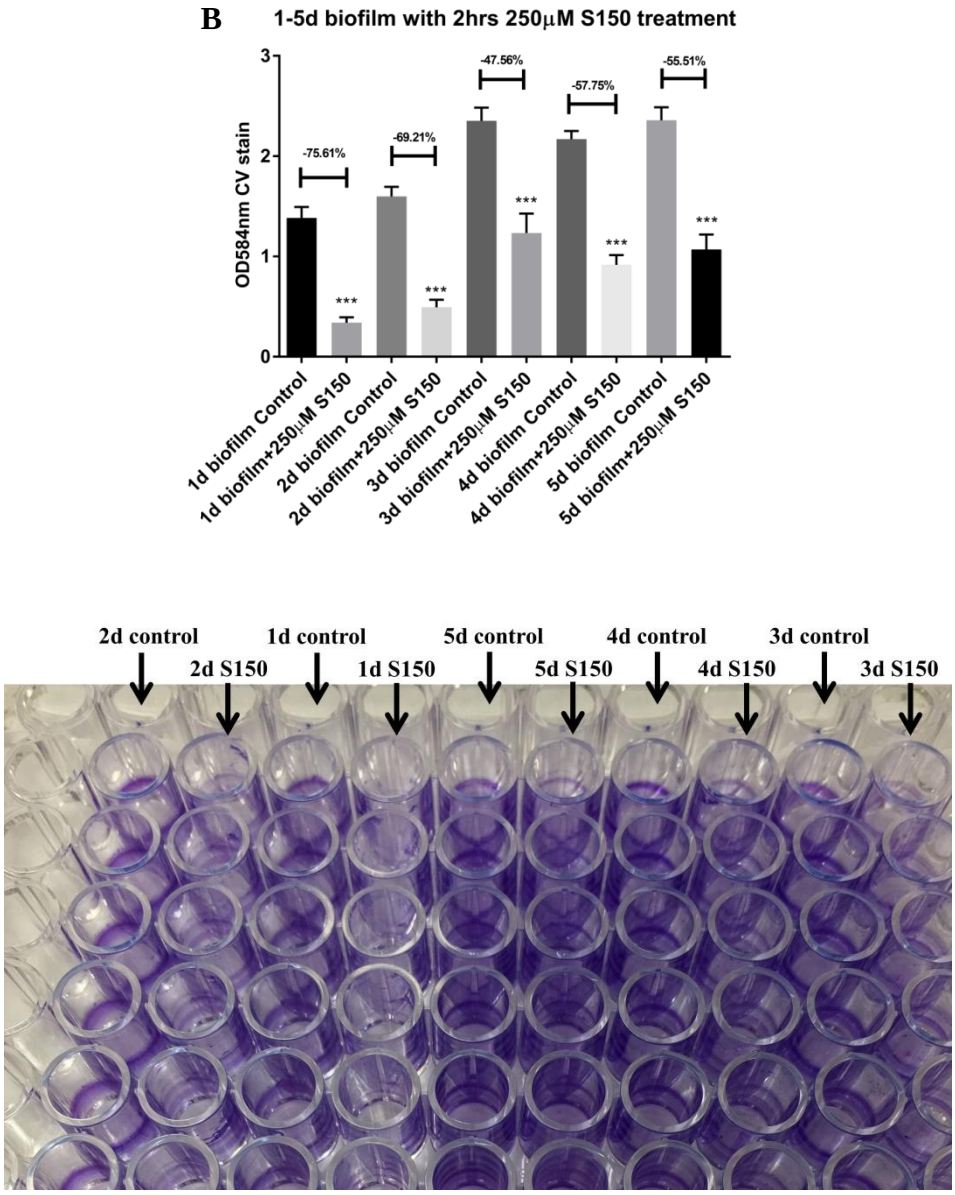


Fig. 3.5 250μM SNP (A) and 250μM S150 (B) treatment on 1-5 d biofilms in microtiter plates. The percentages of biomass reduction after treatments were shown in the bar charts and the representative pictures taken from crystal violet stained plates were shown. Data represent data means of n=6 of 3 biological replicates. One tailed t-test was applied and ** represented $0.01<p<0.05$, *** represented $p<0.01$.

As shown in Fig 3.5, both SNP and S150 can significantly reduce biofilms grown for 1-5 d. The dispersal effect of both donors reached the maximum for 1 d biofilm (>70%, $p<0.01$) and gradually decreased for 2-3 d biofilms reaching the minimum (39.71% for SNP and 47.56% for S150, $p<0.01$). After this point, no difference was observed for 4-5 d biofilms. On the other hand, from 1-3 d, biofilms in the microtiter plates kept growing (up to 1.7 fold, $p<0.01$) while from 3-5 d the total biomass kept the same

($p>0.05$), which was similar to the life cycle of biofilms from initial attachment to maturation stage. In summary, efficacies of the NO donors changes depending on the stage of the biofilm life cycle and this was consistent between both NO donors SNP and S150. Hence it was suggested that the biofilms development stages, cells phenotypic changes inside of biofilms or the biomass itself might have influence on the efficacies of NO donors. Also, by comparing efficiencies of S150 and SNP towards different stages of biofilms shown as bar charts in Fig 3.5 A and B, the efficacy of S150 was constantly higher than SNP for different stages of biofilms, indicating that S150 might be more efficient than SNP in different settings.

## 3.6. Chemiluminescence test for SNP and S150

SNP is supposed to generate 1 mole of NO per mole of compound while NONOates generate 2 mole of NO per mole of compound[306]. Hence, 250µM S150 and 500µM SNP should release equal amount of NO when fully degraded. Indeed, comparable percentage reductions in biofilm biomass were observed between 250µM S150 (60% within 2 hrs) and 500µM SNP (63.77% within 24 hrs) in Fig 3.3.8. However, the same achievement took different contact times for S150 and SNP, leading to the suspicion that SNP releases NO much slower than S150 in these experimental settings despite the fact that the half-life of SNP is much shorter than S150. Therefore, chemiluminescence tests were conducted to directly record NO release curves from SNP and S150. Furthermore, as it was reported SNP can only release NO after exposure to light, NO release from SNP with fixed external light source (cold light source) and in dark (foil paper) were compared. Gas phase chemilluminescence is a sensitive method accessible for quantification of low NO concentrations. Only free NO gas can be detected by chemiluminescence so chemicals should be converted into free NO before quantification. NO signals were recorded and total amount of NO was calculated as described in 2.12.

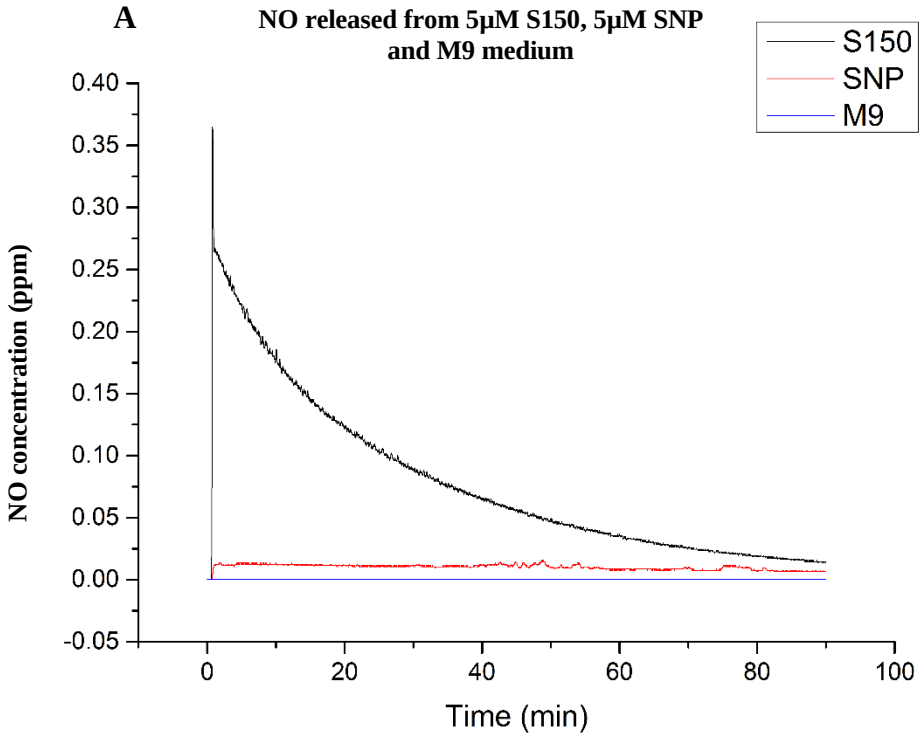
A
NO released from 5µM S150, 5µM SNP and M9 medium
S150
SNP
M9
NO concentration (ppm)
0.40
0.35
0.30
0.25
0.20
0.15
0.10
0.05
0.00
-0.05
0
20
40
60
80
100
Time (min)

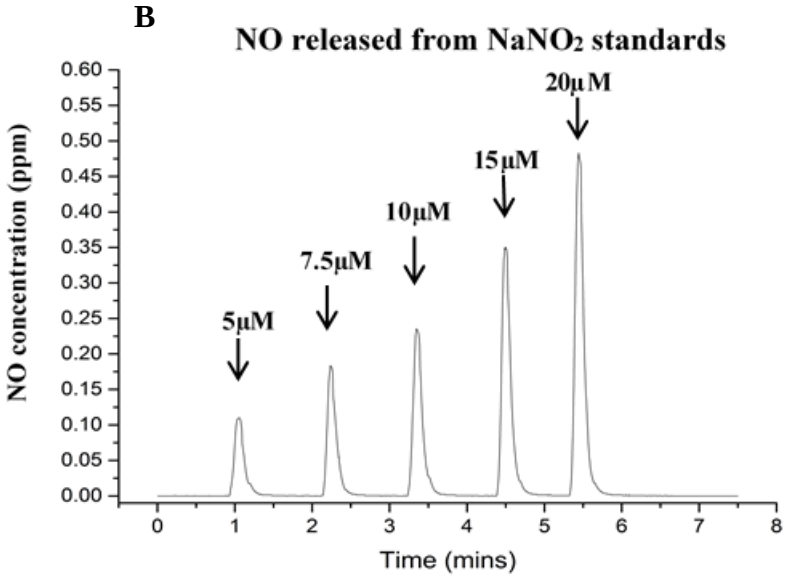
B
NO released from NaNO2 standards
20µM
15µM
10µM
7.5µM
5µM
NO concentration (ppm)
0.60
0.55
0.50
0.45
0.40
0.35
0.30
0.25
0.20
0.15
0.10
0.05
0.00
0
1
2
3
4
5
6
7
8
Time (mins)

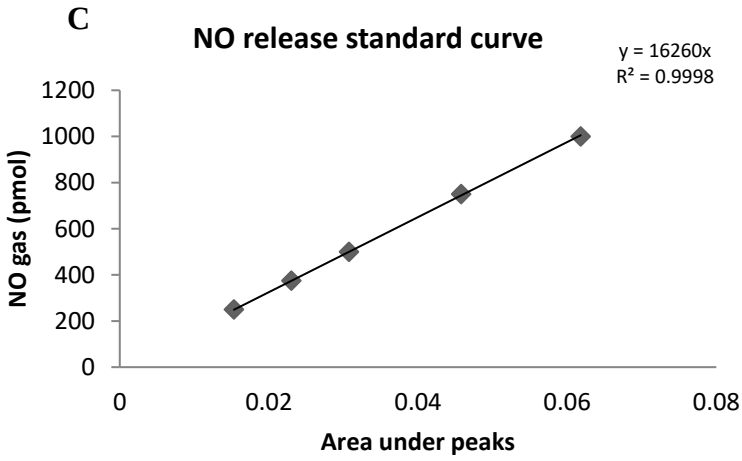
C
NO release standard curve
y = 16260x
R² = 0.9998
NO gas (pmol)
1200
1000
800
600
400
200
0
0
0.02
0.04
0.06
0.08
Area under peaks

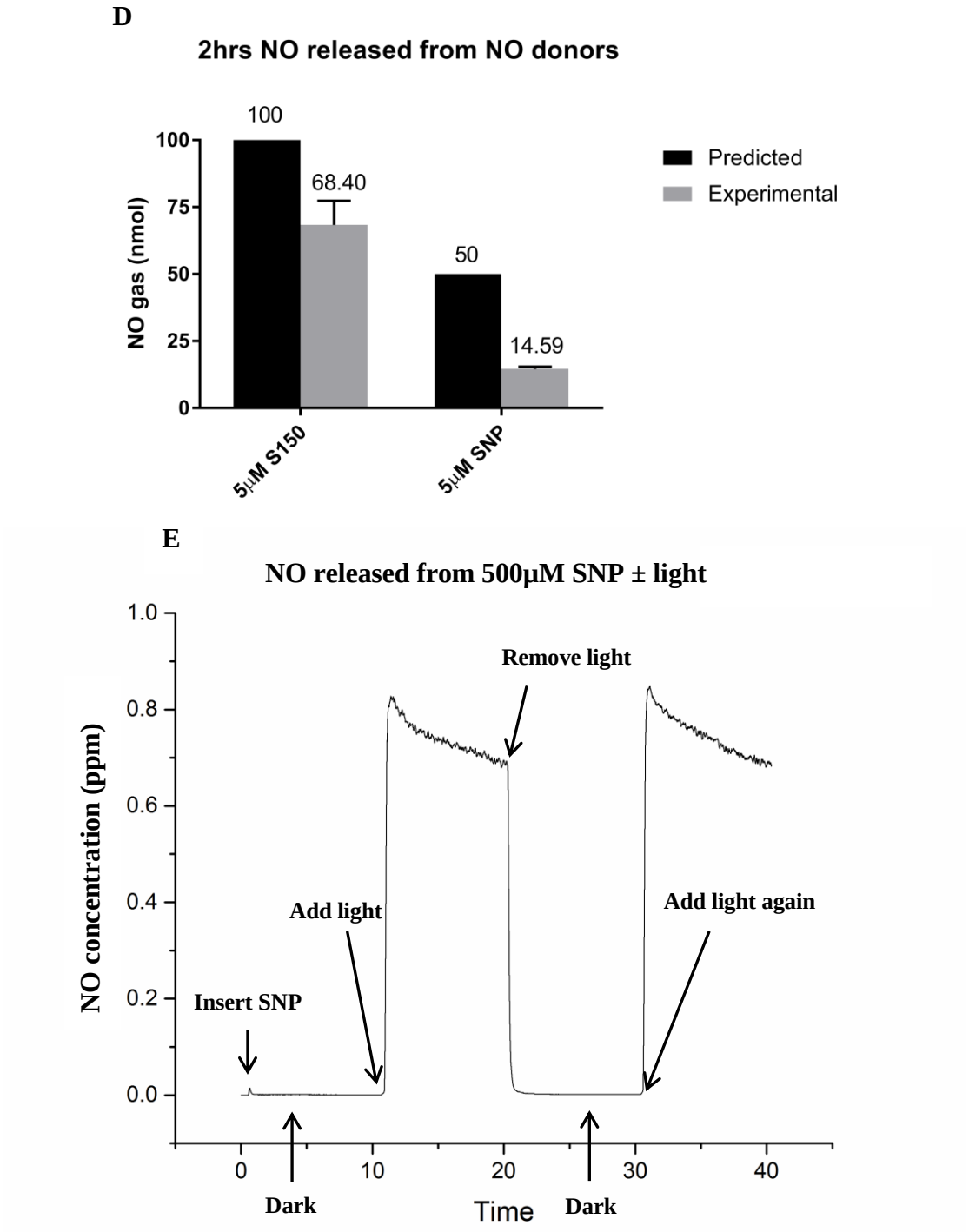


Fig 3.6 (A) Representative NO release curves from CLD tests of 5μM S150, 5μM SNP and plain M9, (B) Standards using 5μM, 7.5μM, 10μM, 15μM, 20μM $NaNO_2$ to generate NO. (C) Standard curve generated using NO gas amount as Y axis and areas under the peak as X axis. One mole of $NaNO_2$ releases one mole of NO. (D) NO amount (nmol) released from 10ml 5μM S150/SNP. Data represent data means of 3 biological replicates and one tailed T-test was applied to compare S150 and SNP. ** represented $0.01<p<0.05$, *** represented $p<0.01$. (E) Representative NO release curve from 500μM SNP with/without cold light source at 37℃ in M9 media. 3 biological replicates were performed.

The precision of NO gas quantification on CLD was confirmed by linear regression curve in Fig 3.6 (D) ($R^2$=0.9998) after area calculation of 3 biological replicates of standards (Fig 3.6 C). From Fig 3.6 (A) it could be concluded that NO release from S150 was much quicker, showing an obvious peak followed by a gradual degradation with time. By contrast, NO release from SNP was much lower relative to S150, peaking at a maximum of 0.0134 ppm and remaining at the concentration approximately 0.012 ppm for the duration of the assay. M9 medium was confirmed not contributing NO to the assays (less than 0.00007 ppm).

5μM was chosen due to the 1ppm maximum measurement limitation of the CLD analyser. After calculation in Fig 3.6 (D), at 37℃ and normal daylight used for biofilm dispersal assays, S150 released 4.69 times more NO than SNP within 1.5 hrs ($p<0.01$). Specific for the amount used in microtiter plates (150μl) and MatTek plates (3ml), 250μM S150 should be releasing around 1.04μmol in each MatTek plate and 51.9nmol NO in each well of microtiter plates after 2 hrs treatment. Therefore, it can be concluded from Fig 3.6 (A) and (D) that at the same concentration, S150 was more effective in releasing NO within a relatively short timeframe.

As shown in Fig 3.6 (A), the signal of NO released from 5μM SNP was constantly low. Hence, 500μM SNP in M9 media at 37℃ was chosen to release more NO in a short timeframe for more obvious signals in light exposure tests. Data shown in Fig 3.6 (E) strongly confirmed that under normal experimental conditions (37℃ in M9 medium), NO release from SNP was dependent on light exposure and rapidly reduced immediately after the removal of light. Therefore, S150 was chosen as an effective NO donor for biofilm dispersal as superior to SNP under certain circumstances and used in most of biofilm dispersal assays in later chapters.

# Discussion

## Batch culture of *P. aeruginosa* PAO1 forms compact mushroom structured biofilms on Poly-L-Lysine surface at 30℃

*Pseudomonas aeruginosa* is an opportunistic pathogen responsible for both acute and chronic infections and is the major cause of death in cystic fibrosis (CF) patients[325]. Biofilms and cell aggregates can be easily formed by different *P. aeruginosa* strains and once they are established, the antibiotic tolerance of *P. aeruginosa* makes it hard to eliminate with conventional therapy methods[326]. Therefore, this bacterium has become a model for biofilm research. The most widely accepted *P. aeruginosa* biofilm growth model is a life cycle starting from individual/small aggregates of cells, which attach to surfaces and grow to a mushroom shape 3D structure mature stage before dispersal. The influences of different growth conditions on *P. aeruginosa* biomass and 3D structures have been discussed in previously published papers. Kannan *et al* showed that biofilms of *P. aeruginosa* (MTCC 2297) grown at 37 ℃ had more biomass, extracellular polysaccharide production, adhesion force and mechanical stability compared to those grown at 28℃, 33℃ and 42℃[327]. However, when Hostacka *et al* used different *P. aeruginosa* clinical isolate strains to grow biofilms at 30℃ and 37℃, some strains produced more biofilm at 30℃ while others produced more at 37℃, indicating optimal growth temperature is strain-specific[328]. Abdallah *et al* grew *P. aeruginosa* CIP 103467 biofilms on stainless steel and polycarbonate at 20℃, 30℃ and 37℃[329]. Thicker and mushroom-structured biofilms were formed at 20 ℃ on both surfaces with the fundamental cell layer thinner on stainless steel, while biofilms formed at 30 and 37 °C formed flat and compact biofilms on both surfaces with 37℃ resulting in the least heterogeneous biofilms. These results showed that both temperature and the surface type significantly affected the three-dimensional (3D) structure of *P. aeruginosa* biofilms. Ghanbari *et al* claimed that mushroom-shaped *P. aeruginosa* biofilms structures formation depended on nutrient levels and the initial inoculation cell density[330]. In summary, strain, temperature, growth medium, attachment surface type and initial inoculum all influence biofilm formation and structures.

Consequently, optimization of these conditions was carried out to set up a standard PAO1 growth conditions for CLSM analysis in this study. The most frequently used biofilm culture methods include: (1) flow cell systems using glass coverslip/silicon

tubing as the attachment surface; (2) Static batch culture using microtiter plates which are normally coated by polystyrene; (3) Shaking batch culture using microscope glass slides in petri dishes. Flow cell and static systems have been the most frequently used for biofilm studies. However, biofilm formation in some natural and clinical settings is quite different from these two forms. For example, in cystic fibrosis patients, a layer of mucus provides an anaerobic or microaerophilic environment to the growth of *P. aeruginosa* and biofilm formation on the layer of airway epithelial cells. This is quite different from the flow cell system where continuous fresh medium provides sufficient nutrition and hydrodynamic conditions to attached cells and also washes away metabolic waste[331,332]. Different batch culture methods were also developed, of which the most frequently used were static culture using microtiter plates and shaking culture using microscope glass slides dipped in petri dishes with bacteria culture. In our lab individual MatTek culture dishes with Poly-D-Lysine treated glass coverslips at the bottom were used to culture biofilms with rotation at a relatively slow speed. Poly-L-lysine has been well known to enhance mammalian cell adhesion to solid surfaces while only a few studies reported it enhanced microbial adhesion in strains such as *E. coli* DH10B[333] and *Mycobacterium tuberculosis*[334]. Here, whether *P. aeruginosa* PAO1 can attach to poly-L-lysine surface in MatTek plates was tested due to their advantage in large scale culturing and direct application to CLSM. Media in MatTek plates were changed at certain time points. Also, these dishes were much easier to handle for mimicking different settings. However, since these culture dishes are very different from the flow cell or batch culture systems mentioned above, optimization for biofilm growth in MatTek plates must be carried out before further applications. Results in 3.2 showed that with an initial inoculum of $OD_{600nm}$~0.01 in M9 medium, biofilms grown at 22℃ contained thick 3D structure microcolonies heterogeneously distributed on the surfaces, with the data highly dependent on the selection of field of view. Biofilms grown at 37℃ formed less biomass without obvious mushroom structures and were easily broken by mechanical shear force from pipetting. Biofilms cultured at 30℃ showed ‘a flat mat’ at the bottom where bacteria attached to the whole area homogeneously, on which several microcolonies developed as mushroom structures. Therefore, it was proved here that with an initial inoculum of $OD_{600nm}$~0.01, *P. aeruginosa* PAO1 formed better biofilms in M9 medium at 30℃ in MatTek plates compared to 22℃ and 37℃. Typical mushroom 3D structures can be obtained under CLSM after 2-3d culture. Research on whether the

modulation of initial inoculums can affect biofilm structures in MatTek plates can be carried out in the future, if necessary.

**S150 is an effective NO donor for PAO1 biofilms dispersal**

Low dose nitric oxide released from sodium nitroprusside (SNP) was first discovered to disperse *P. aeruginosa* biofilms and similar effects were also found in other species such as *N. gonorrhoeae*[251]. However, various studies have reported dispersing *P. aeruginosa* biofilms using different concentrations of SNP ranging from 500nM to 500μM[9,242,243,335–337]. The discrepancy might be due to the fact that SNP can remain stable for 6 months in aqueous solution without light and does not release NO unless after photolysis or the addition of reducing agents[338], resulting in the differences of its efficacy under different light sources. Barnes *et al* found that 20μM SNP even increased biofilm from 1 hr to 12 hrs without triggering dispersal, and the reduction of biomass occurred after exposure for 24 hrs[306]. This long period of time for treatment raised a suspicion that instead of triggering dispersal, this specific concentration of SNP might have been preventing further development of biofilm. In fact, data from Falsetta *et al* showed that 24 hrs-old *N. gonorrhoeae* biofilms with another 24 hrs 500nM NO treatment did have significantly less biomass and smaller average thicknesses than untreated 48 hrs-old biofilms[251]. However, there was no apparent difference in biomass and average thickness for 24 hrs-old biofilms without treatment and biofilms grown for 24 hrs and then treated with SNP for another 24 hrs. This suggests that the addition of SNP did not reduce the original 24 hrs-old biofilms but only prevented further development. Furthermore, cyanide released from SNP as a side product might also cause serious problems to certain patients[339,340]. Therefore, alternative NO donors need to be discovered with high performance on dispersing biofilms without introducing toxicity.

SNAP and GSNO were reported to decrease *P. aeruginosa* biofilms although less effective than SNP[9]. Barnes *et al* reported MAHMA NONOate and PROLI NONOate can effectively disperse wastewater membranes biofilms. However, the half-lives of MAHMA NONOate and PROLI NONOate are 1 min and 1.8 s, respectively[306,341]. Therefore, extra care should be taken to avoid the loss of efficiency during storage and preparation procedures. Diethylamine (DEA) NONOate-cephalosporin prodrug

(DEACP) was reported to release NO after an activation step and effectively dispersed *P. aeruginosa* biofilms[342], but it is strain specific due to the requirement on the existence of β-lactamase. In this study 7 NO donors were tested including SNP, SNAP, GSNO, PROLI NONOate, MAHMA NONOate, DEA-NONOate and Spermine NONOate (S150) with different concentrations and exposure times. Fig 3.3.8 has shown that 24 hrs 250μM SNP treatment and 2 hrs 250μM S150 treatment can effectively disperse *P. aeruginosa* PAO1 WT biofilms in microtiter plates up to ~60%. The dispersal came from NO released by the compounds rather than cytotoxicity or the effect of by-products of compound degradation. However, the efficacies of these two drugs were higher when applied to younger biofilms (1 d) than older biofilms (≥3 d). The possible explanation could be biofilm matrix was acting as a diffusion barrier[343] and Stewart has claimed that diffusion limitation led to gradients in the concentration of reacting solutes, resulting in the failure of diffusion into thick biofilms[344]. *P. aeruginosa* has nitric oxide reductase reacting with added NO and older biofilms normally have thicker and more compact EPS structures. Therefore, it is suspected that lower efficiency of NO donors on older biofilms might be the result of NO diffusion failure. Despite this, the efficacy of S150 was constantly higher than SNP for different stages of biofilms, indicating that S150 might be more efficient in triggering *P. aeruginosa* biofilms dispersal than SNP in different settings.

**S150 is more efficient in releasing NO and the presence of light is essential for NO release from SNP**

Barraud *et al* reported that 5μM SNP can steadily release 5nM NO by using Apollo 4000 NO analyzer for detecting free radicals in solution[9]. Here, gas phase chemiluminescence (CLD) was applied for the quantification of low NO concentrations. CLD results in Fig 3.6 have shown that 50nmol S150 released around 68.4nmol NO within 2 hrs, which was 4.69 times the NO released from the same amount of SNP within the same time frame. Hence, the data is consistent with the hypothesis that (1) NONOates should generate 2mol of NO per mole of compounds while SNP should only generate 1mol and (2) the same amount of NONOate should be releasing NO faster than SNP[306]. This was also consistent with biological data where 250μM S150 resulted in 60% biofilm reduction in 2 hrs only while the same amount of SNP needed 24 hrs to reach the same efficiency. Furthermore, CLD proved that SNP can only generate NO with the presence of light, and the removal of light source immediately stopped NO release in the solution.

These results strongly suggested that (1) even with constant light source, SNP released NO less and slower than S150; (2) SNP cannot be effectively used in patients without reducing agents for biofilm dispersal as expected due to the absence of light *in vivo.* Data also explained the discrepancy of optimal SNP concentrations for *P. aeruginosa* biofilm dispersal reported in different groups, as different light sources might have caused inconsistent SNP performances. Therefore, S150 can be widely used for different applications and the half-life is more desirable (39 mins at pH7.4, 37℃) compared to other short half-life NONOates such as MAHMA NONOates and PROLI NONOates. However, SNP could be a very good NO donor when longer working time is required with access to stable light sources, and it is easier for preparation and storage and more economical in high-dose utilization.

**SNP and S150 enhance *P. aeruginosa* growth in planktonic culture**

As shown in 3.4.2, bactericidal tests of SNP and S150 were carried out in 0.85% (w/v) NaCl for planktonic cell culture of PAO1. Both NO donors significantly enhanced bacterial numbers without additional nutrients added into the solution. An increase in cell number after the addition of SNP and S150 was also found in PBS and M9 media (data not shown). c-di-GMP was reported to be related to cell cycle in *C. crescentus*, but the conclusion was that c-di-GMP promoted cell cycle progression[345]. Since no further research was done for the relationship between intracellular c-di-GMP and cell cycle in *P. aeruginosa*, several hypotheses were raised as follows: (1) NO bound to a certain type of NO sensor and this sensor regulated cell cycle related gene/protein; (2) The chemical breakdown or side products from SNP and S150 influenced gene/proteins related to cell cycle; (3) The chemical breakdown or side products from SNP and S150 acted as nutrients; (4) Cell aggregates exist in the solution and the addition of NO triggered cell aggregates dispersal, resulting in increased CFU count due to the fact that cell aggregates might not be distinguished on agar plates; (5) *P. aeruginosa* is a facultative anaerobe that preferentially uses aerobic respiration. However, previous research has shown that nitrate can support the growth of *P. aeruginosa* in anaerobic/anoxic environment by denitrification[346–348]. Furthermore, supplementing anoxic cultures of PAO1 with $\geq$150μM $NO_3^-$ significantly increased the growth rate[348]. Due to the almost insolubility of NO in $H_2O$, NO rapidly reacted with oxygen in air or dissolved in the solution producing nitrogen dioxide ($NO_2$) [$2 \cdot NO + O_2 \rightarrow 2\ NO_2$]. Nitrogen dioxide reacted

with $H_2O$ to produce nitric acid [$3\ NO_2 + H_2O \rightarrow 2\ HNO_3 + NO$]. Despite the preparation procedures of bactericidal tests being carried out in aerobic condition, the growth of bacterial cultures was in sealed conical centrifuge tubes where 10ml of bacteria occupied the 25ml (maximum volume) tubes and the remainder was normal air. The oxygen level inside the tube was limited once the incubation began. Therefore, the additional $NO_3^-$ might have partially increased the anoxic growth where oxygen access was limited in planktonic culture.

To test these hypotheses in future work, the following experiments might be carried out corresponding to each hypothesis: (1) 0.85% (w/v) NaCl solution purged with pure NO gas before and after the inoculum of bacteria should be tested to determine if CFU/OD increased compared to normal NaCl under experimental conditions. If there is an increase, the planktonic culture from normal NaCl and NaCl + NO should be subjected to transcriptomic and proteomic analysis for the comparison of gene expression and protein expression; (2) SNP and S150 are first dissolved in 0.85% NaCl solution and kept under 37℃ for one day (SNP continuously exposed to light) prior to experiment to release all NO. Solutions are then subjected to CLD to ensure no NO is left before inoculum. The NO free SNP/S150 solution is then used for inoculation to see if CFU/OD increased compared to normal NaCl under experimental conditions. If there is an increase, the planktonic culture from normal NaCl and NaCl + SNP/S150 should be subjected to transcriptomic and proteomic analysis for the comparison of gene expression and protein expression; (3) If hypothesis (1) and (2) showed no change in gene/protein expression, SNP/S150 might act as nutrient resources despite their completely different chemical structures. SNP and S150 are first dissolved in 0.85% (w/v) NaCl solution and kept under 37℃ for one day (SNP continuously exposed to light) prior to experiment to release all NO. Solutions are subjected to CLD to ensure no NO is left before inoculum. Overnight cultures of PAO1 should be totally washed 3 times in 0.85% (w/v) NaCl to get rid of all possible trace nutrients from nutrient broths for overnight cultures prior to inoculation. Washed cells are then inoculated into NaCl and NaCl + NO free SNP/S150 to compare CFU/OD after certain incubation time. If there is an increase with SNP/S150, incubate the cells for more time to consume SNP/S150 breakdown products. Filter sterilize the used NaCl and NaCl + NO free SNP/S150 and repeat the same inoculation procedure again. If SNP and S150 are used as nutrients, they should be consumed at least partially in the first round inoculum.

Therefore there should be no increase or much less increase in the CFU in second round inoculum; (4) Scheleck *et al* reported PAO1 can also grow as cell aggregates in planktonic culture with well shaking[349]. Cell culture in normal 0.85% NaCl and NaCl + SNP/S150 can be subjected to sonication prior to CFU count. If cell aggregates in normal 0.85% NaCl is the reason of lower CFU, it should be increased after sonication; (5) Yoon *et al* reported that PAO1 cells go through elongation during anaerobic respiration[347]. To test if the increase in cell number in NaCl + SNP/S150 solution is a result from partially anaerobic/anoxic culture, samples can be taken from the planktonic culture and observed under CLSM. Furthermore, benchtop dissolved oxygen meter can be used to measure the oxygen concentration in NaCl and NaCl + SNP/S150 cultures[347] while the $NO_3^-$ concentration can be measured by converting the $NO_3^-$ in filter sterilized spent culture into $NO_2^-$ and incubating with Griess Reagent[348]. When necessary, nitrate reductase mutant Δ*narG* and nitrite reductase mutant Δ*nirS* can be used to test if CFU increased after the addition of SNP and S150. If the addition of NO is the reason for increased denitrification, the abolished reductases will impair the denitrification pathway and no increase/much less increase of CFU should be found.

Despite the mechanism of this cell number enhancement after adding SNP/S150 being unknown, it might be beneficial for the adjunctive usage of NO and antibiotic. If cells division times in planktonic/biofilm culture can be shortened after the addition of NO, cells might be more susceptible to antibiotics. This may contribute to the conclusion from previous research showing the increased efficacies of conventional antibiotics when used in combination with NO[9]. Some CF patients' clinical isolates were reported to have higher resistance/tolerance to antibiotics in planktonic forms compared to PAO1. Therefore, studies should be carried on to elucidate the mechanism of this enhancement and at the same time, MBC of different antibiotics with the addition of NO on different *P. aeruginosa* strains should be tested to see if the efficacies of conventional antibiotics are improved by adjunctive usage with NO.

# Chapter 4 – NO triggered CF PA biofilms dispersal and a novel index for cell aggregation quantification

Cystic fibrosis (CF) is a genetically inherited disease occurring with a high frequency in the Caucasian population, with morbidity and mortality a consequence of chronic microbial colonization of patients' lungs and airways[350,325]. *P. aeruginosa* is the most commonly found species and, once chronic infection is established, cannot be eradicated. When bacteria invade healthy individuals, they can be cleared through mucociliary clearance and destroyed by stomach acids after being swallowed. Opportunistic pathogens that overcome mucociliary clearance can be targeted by phagocytic cells and specific opsonizing antibodies[325]. However, in CF patients the dehydrated surface liquid on respiratory epithelium results in defective mucociliary clearance and frustrated phagocytosis due to the impaired opsonisation process, hence contributing to colonization by *P. aeruginosa*[325]. The *P. aeruginosa* strains isolated from CF patients are referred to as CF PA clinical isolates here.

CF PA clinical isolates have major differences in genotypes and phenotypes compared to some reference lab strains such as PAO1 WT. These lead to some outstanding characteristics compared to PAO1 WT including 1: Mucoidy due to the overexpression of alginate[350,351]; 2: Non-motility due to the deficiency in flagellar formation[352]; 3: More progressive antibiotic resistance[353]; 4: CF specific lipopolysaccharide (penta-acylated lipid A)[354]; 5: Deficient lipopolysaccharide O side chain[355]; 6: High frequency of hypermutable genes[119]; 7: High level of persister cells[356]. Consequently, although it is well characterised that some CF PA strains form biofilms in CF lungs, the role of the CF PA biofilm phenotypes in disease pathophysiology however is less well understood.

Singh *et al* reported that the quorum-sensing signals ratio in clinical isolates were similar to PAO1 WT when both were grown in biofilm mode[357]. Images of *P. aeruginosa* in sputum by transmission electron microscope[357] as well as Gram stain and PNA FISH[326] have proved that some mucoid strains form aggregates in CF lungs. As mentioned above, two terms were used to describe cell clusters – cell aggregates and biofilms. The American Center for Disease Control (CDC) defines sessile, aggregated cells as 'an assemblage of microbial cells that is irreversibly associated (not removed by gentle rinsing) with a surface and enclosed in a matrix of primarily polysaccharide material'[358]. This can be referred to as a biofilm growth mode and indeed some literatures describe

cell aggregates as microcolonies in the biofilms or floating biofilms (or biofilm-like aggregates) in the liquid. Also, cells detached from biofilms can be in the form of large cell aggregates[20]. To distinguish these two terms here, in this study cell aggregates are referred to as non-attached/suspended 3D structural cell clusters encased in EPS and grown in liquid media, while biofilm is defined as attached 3D structural bacterial microcolonies encased in EPS.

Aggregated cells have been extensively studied in environmental sciences[359] while in medical research the main focus has been biofilms attached to surfaces. However, the majority of *P. aeruginosa* in CF lung infection are not found attached to pulmonary epithelial surfaces, but form aggregates within the viscous mucus associated with larger airways[360]. Alhede *et al* proved that non-attached *P. aeruginosa* aggregates resemble surface attached biofilms in growth rate, internal structures of the matrix, tolerance to antibiotics and resistance to phagocytes[361]. Furthermore, the tolerance of both biofilms and non-attached aggregates was proved to be reversible by physical disruption[361]. This phenomenon is similar to the fact that the adjunctive usage of conventional antibiotics and NO donors - biofilm structures are dispersed by NO, and the efficacies of antibiotics in eliminating PAO1 WT biofilm cells are enhanced. Therefore, here I tested if NO can disperse the cell aggregates and biofilms formed by clinical isolates. Strains were isolated from CF patients in Southampton General hospital as described in 2.16 and generously provided by Dr. Rob Howlin.

## 4.1. Characterisation of CF PA clinical isolates morphology and biofilm formation

As mucoidy is prevalently found in different CF PA strains and is relevant to biofilm formation, the colony morphologies on agar plates were first observed. It was reported that Pseudomonas isolation agar (PIA) can give a reliable determination as to whether a strain is mucoid or not[325]. Therefore, all the CF clinical isolates from lab collection were plated on PIA for 48 hrs incubation at 37℃. Microtiter plate biofilms were set up as described in 2.3.1 for 1 and 3 d due to their different growth rates (many CF PA clinical isolate strains were reported to possess a relatively slow growth rate[362]).

**A**

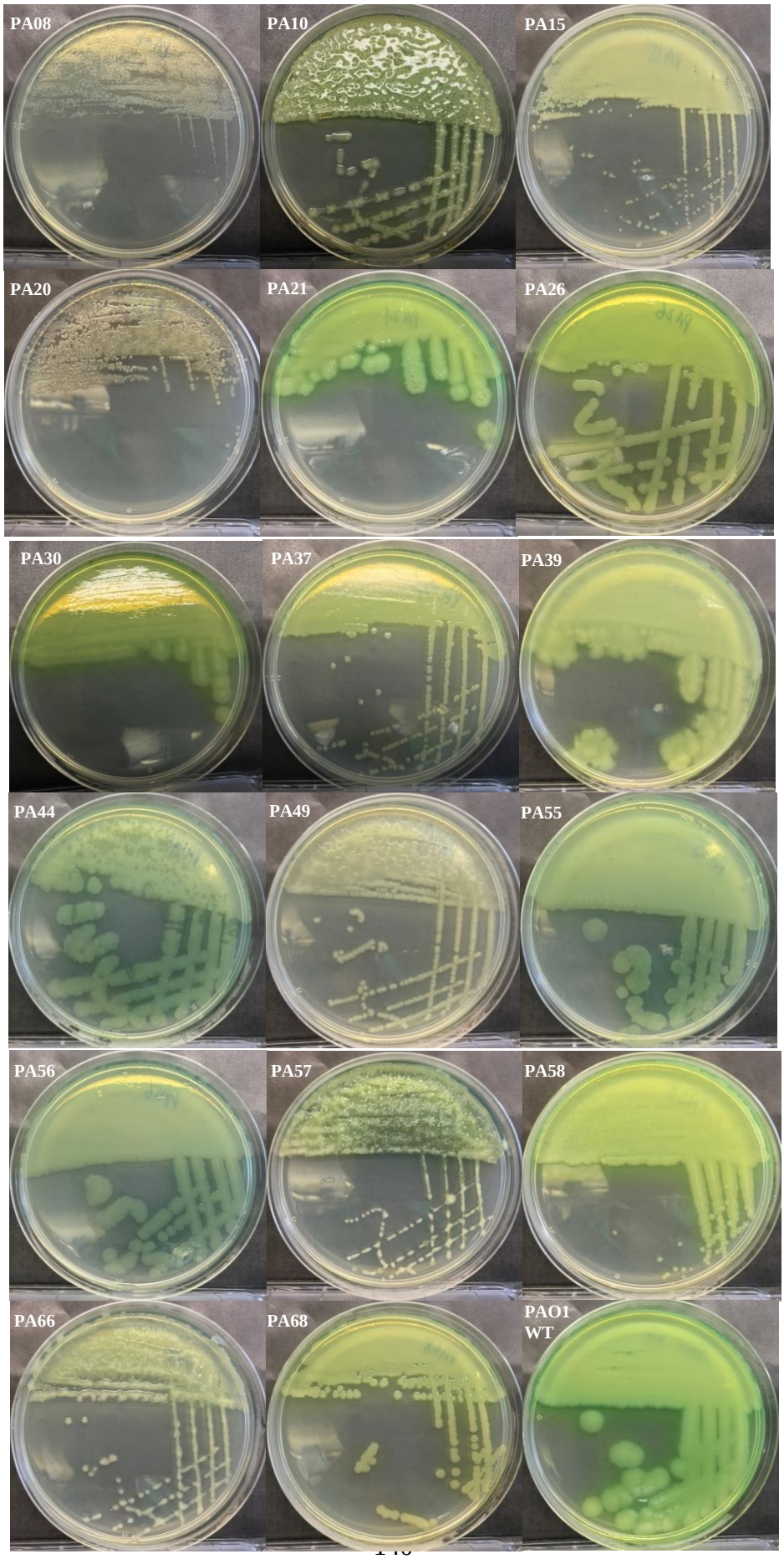
PA08
PA10
PA15
PA20
PA21
PA26
PA30
PA37
PA39
PA44
PA49
PA55
PA56
PA57
PA58
PA66
PA68
PAO1
WT

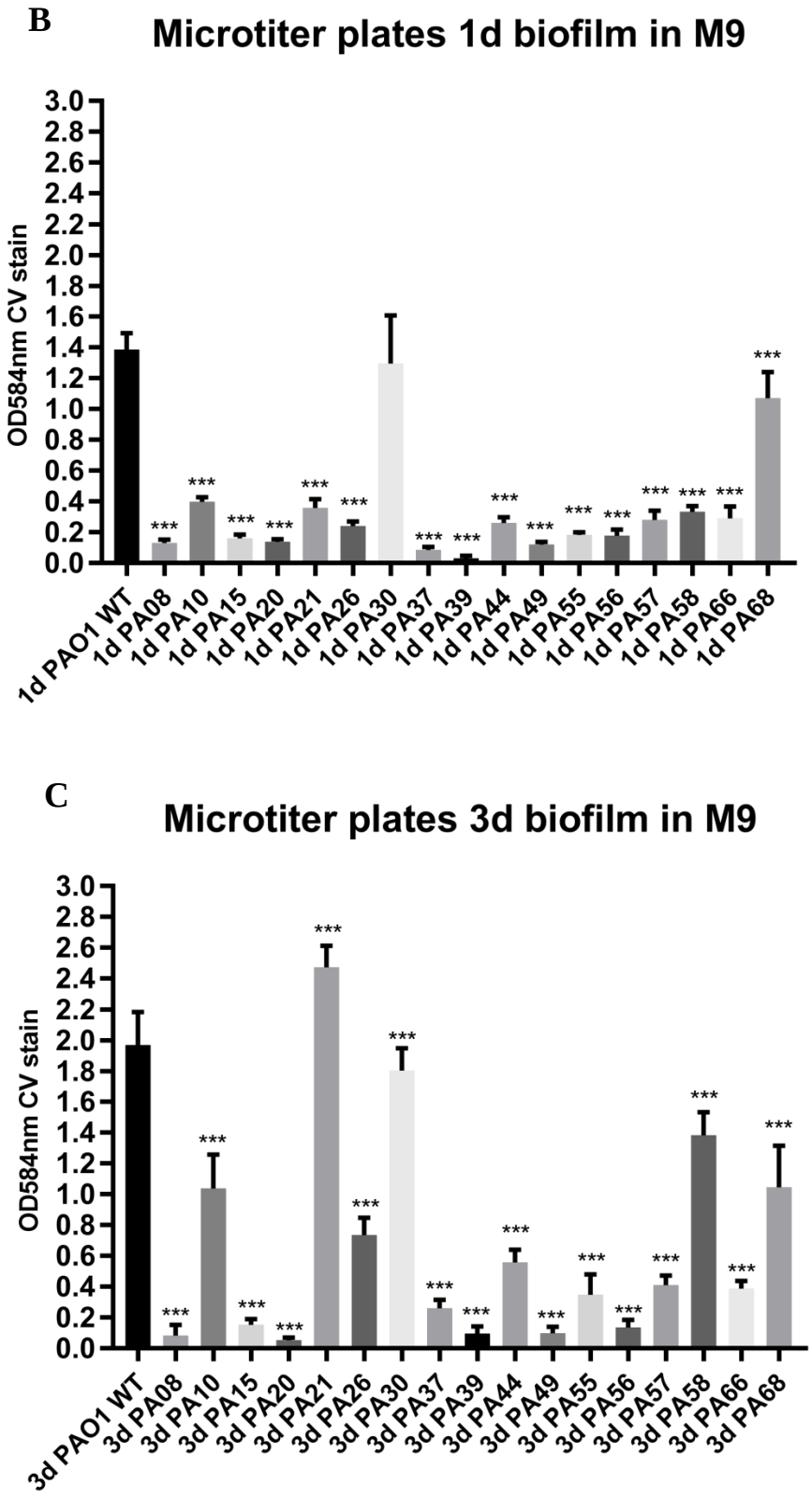


Fig 4.1 (A) Colonies of PA clinical isolates on 20mm *Pseudomonas* isolation agar after 48hrs. (B) and (C) Comparison of 1 d and 3 d biofilm biomass in microtiter plates among PA clinical isolates and PAO1 WT. Welch T-test was applied for comparing PA clinical isolates biomasses and PAO1 WT biomass. Data represent data means of n=6 of 3 biological replicates. *** represents $p<0.01$, ** represents $0.01<p<0.05$.

| | PA08 | PA10 | PA15 | PA20 | PA21 | PA26 | PA30 | PA37 | PA39 |
|---|---|---|---|---|---|---|---|---|---|
| mucoidy | - | + | - | - | - | - | - | - | - |
| biofilm | * | ** | * | * | *** | ** | *** | * | * |
| | PA44 | PA49 | PA55 | PA56 | PA57 | PA58 | PA66 | PA68 | PAO1 |
| mucoidy | - | - | - | - | + | - | + | - | - |
| biofilm | ** | * | ** | * | ** | *** | ** | *** | *** |

Table 4.1 The mucoidy and biofilm formation abilities of 17 CF PA strains and PAO1 WT. – represents non-mucoid strain on PIA agar, + represents mucoid strain on PIA agar. *,** and *** represent the strains form weak, intermediate and extensive biofilm biomasses in microtiter plates by crystal violet staining, respectively.

From the agar plates in Fig 4.1 (A) it can be concluded that the majority of CF isolates appeared to have very different morphologies compared to PAO1 WT as expected. As shown in Fig 4.1 (B), most clinical isolates cultured *in vitro* formed significantly less biofilm than PAO1 WT (97.69% to 71.29% less biomass, $p<0.01$) after 1 d static incubation in M9 minimal medium, except for PA30 and PA68 (highlighted in red, $p>0.05$). By comparing Fig 4.1 (C) to (B), biomass from PA10, PA21 and PA58 hugely increased after 3 d comparing to 1 d (2.61, 6.88, and 4.13 folds respectively, $p<0.01$) when PAO1 increased 1.42 fold ($p<0.01$). This suggested the initiation of biofilm or growth rate was slower in these 3 strains comparing to PAO1 WT, but once established, biofilm could develop well. Generally, from the data, it was determined that PA10, PA21, PA26, PA30, PA58 and PA68 formed significantly more biofilms biomass than other PA clinical isolates tested after 3 d and could be subjected to CLSM analysis of biomass and 3D structures. Table 4.1 summarizes the mucoidy and biofilm formation phenotypes of these 17 CF PA strains.

## 4.2. NO-induced CF PA biofilms dispersal

250μM S150 selected in chapter 3 was applied to CF PA biofilms formed in both microtiter plates and MatTek plates set up as described in 2.3.1 and 2.3.3. For microtiter plates, 1 d and 3 d biofilms of all 17 CF PA strains were subjected to the NO treatment. For MatTek plates only the strains forming extensive biofilm (shown as *** in Table 4.1) were grown for 3 d and treated for observation.

**A**

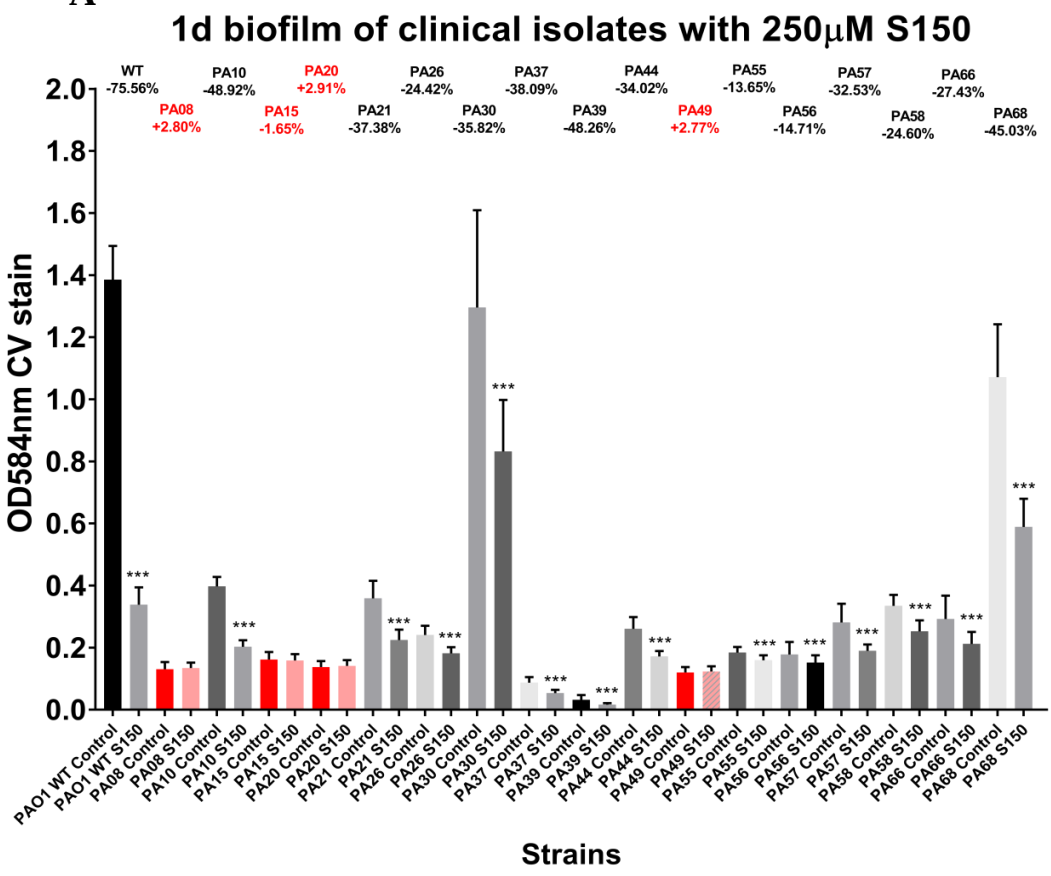
1d biofilm of clinical isolates with 250μM S150
OD584nm CV stain
Strains
WT -75.56%
PA10 -48.92%
PA20 +2.91%
PA26 -24.42%
PA37 -38.09%
PA44 -34.02%
PA55 -13.65%
PA57 -32.53%
PA66 -27.43%
PA08 +2.80%
PA15 -1.65%
PA21 -37.38%
PA30 -35.82%
PA39 -48.26%
PA49 +2.77%
PA56 -14.71%
PA58 -24.60%
PA68 -45.03%

**B**

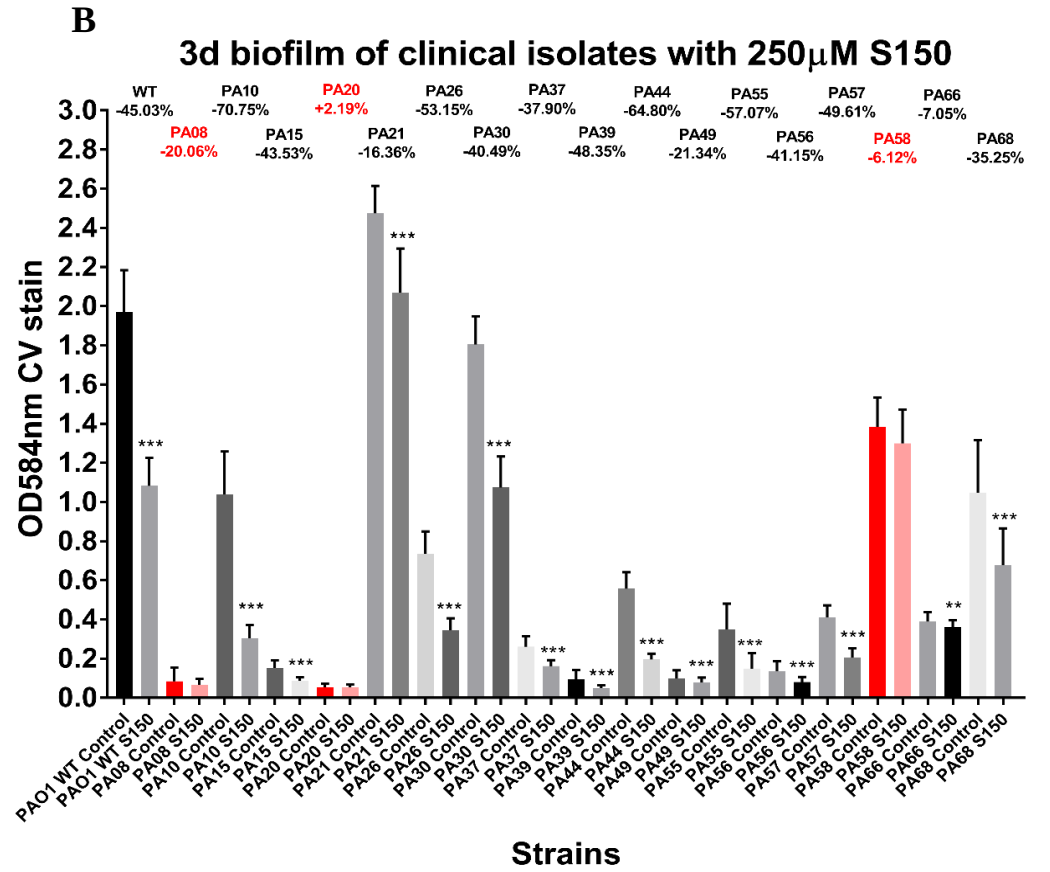
3d biofilm of clinical isolates with 250μM S150
OD584nm CV stain
Strains
WT -45.03%
PA10 -70.75%
PA20 +2.19%
PA26 -53.15%
PA37 -37.90%
PA44 -64.80%
PA55 -57.07%
PA57 -49.61%
PA66 -7.05%
PA08 -20.06%
PA15 -43.53%
PA21 -16.36%
PA30 -40.49%
PA39 -48.35%
PA49 -21.34%
PA56 -41.15%
PA58 -6.12%
PA68 -35.25%

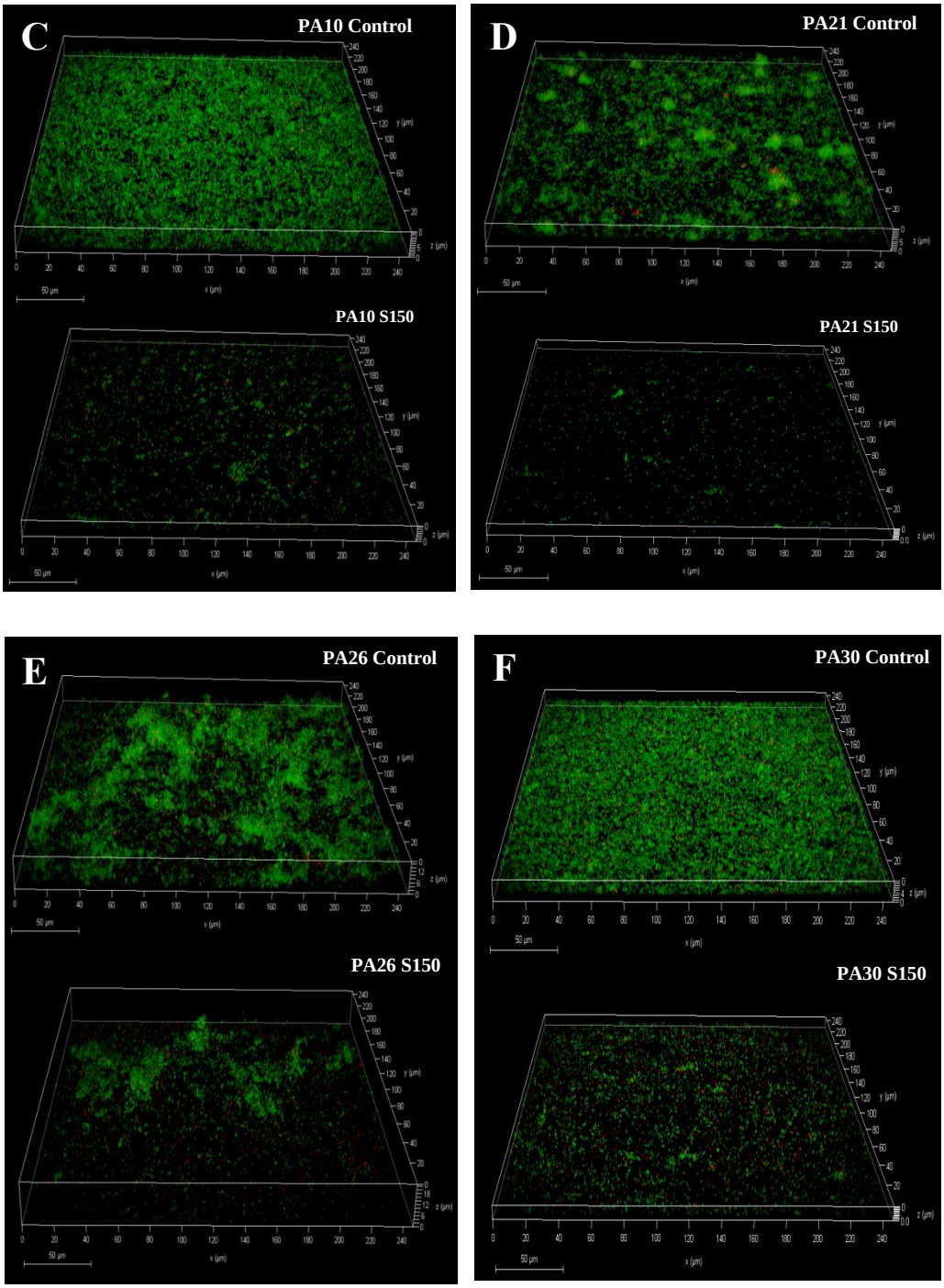
C
PA10 Control
PA10 S150
D
PA21 Control
PA21 S150
E
PA26 Control
PA26 S150
F
PA30 Control
PA30 S150

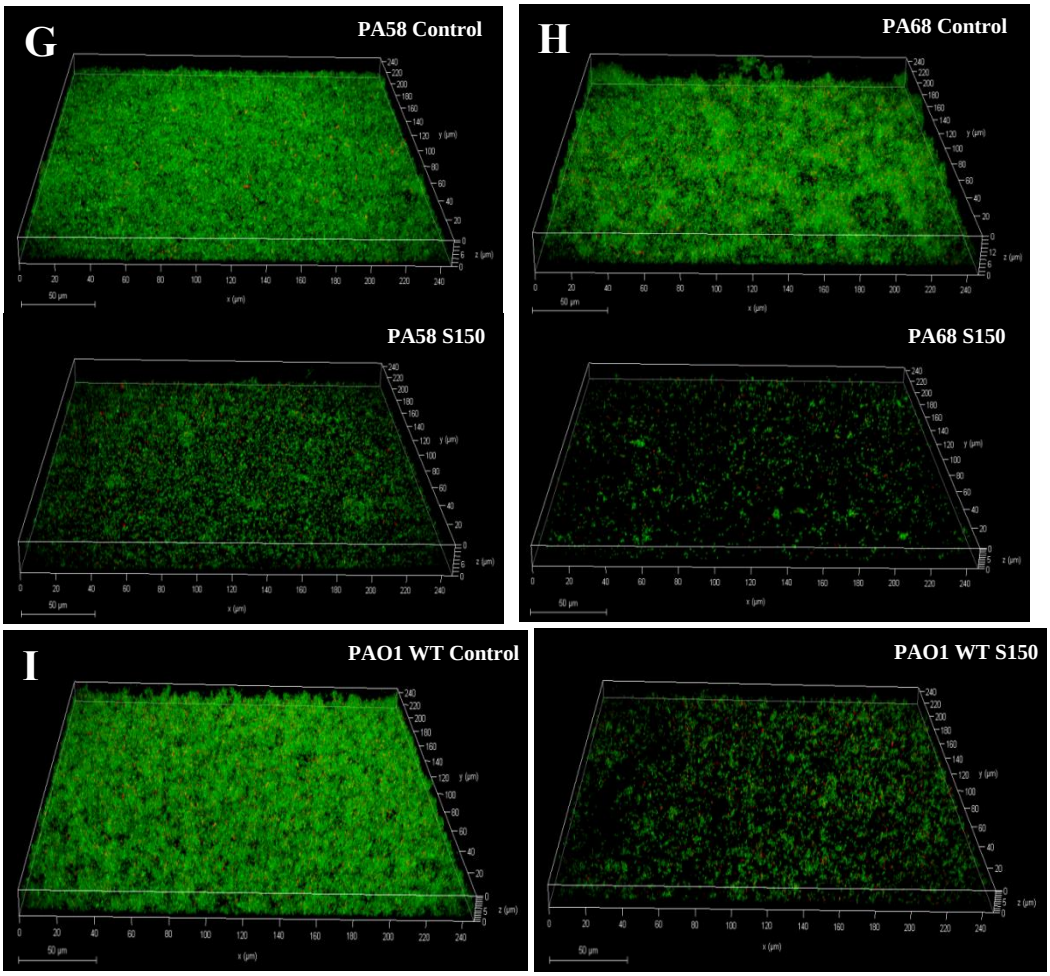


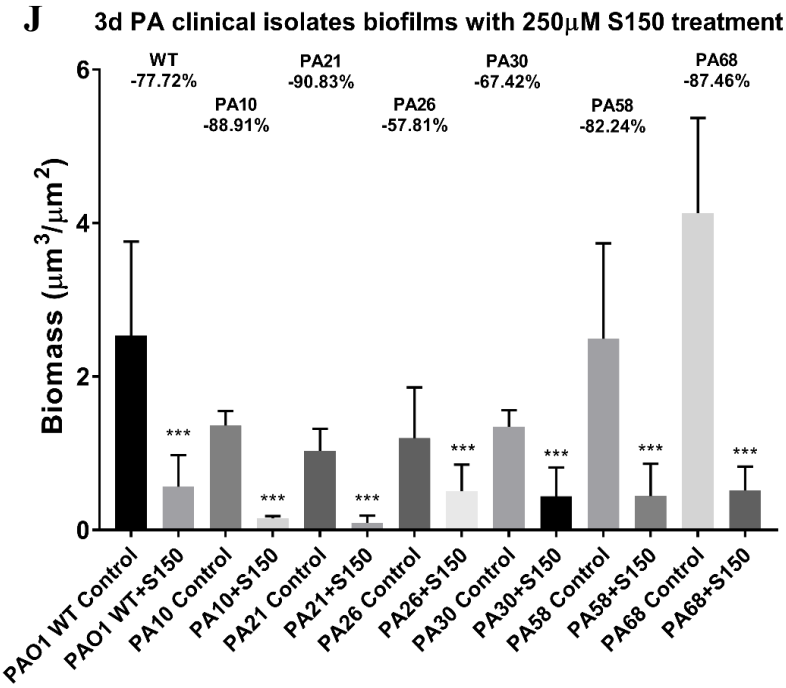


Fig 4.2 (A) and (B) 1 d and 3 d biofilms biomass of PA clinical isolates and PAO1 WT after 2 hrs 250μM S150 treatment. $OD_{584nm}$ was used to measure the crystal violet staining for residual total biomass. Normal

T-test was applied between S150 treatment group and control for each strain. Biomass decrease percentages were marked above bars for each strain. Data represent data means of n=6 of 3 biological replicates. *** represents $p<0.01$, ** represents $0.01<p<0.05$. Selective CLSM pictures of (C) PA10 (D) PA21 (E) PA26 (F) PA30 (G) PA58 (H) PA68 and (I) PAO1 WT biofilm grown at 37℃ with/without S150 treatment. (J) Biomasses of 3 d PA clinical isolates biofilms with/without 250μM treatment analysed by COMSTAT. Welch T-test was applied to compare S150 treatment group and control for each strain. Biomass percentages decreases were marked above bars. Data represent data means of n=3 of 3 biological replicates. *** represented $p<0.01$, ** represented $0.01<p<0.05$.

As shown in Fig 4.2 (A), most of the biofilms cultured for 1 d showed a significant decrease of biomass after S150 treatment (13.65% to 48.95% reduction on biomass, $p<0.01$) except for PA08, PA15, PA20 and PA49 ($p>0.05$). As shown in (B) it can be concluded that 3 d biofilms of PA08, PA20 and PA58 were not significantly disrupted by NO ($p>0.05$). Some strains such as PA15, PA49 and PA58 showed different responses to NO after 1 d and 3 d growth. This might be due to different cell physiology and tolerance to NO, or different biofilm thicknesses that affect NO penetration efficiency. The mechanisms of different NO responses of different strains remain unknown and worth looking into in future work.

As shown in CLSM pictures in Fig 4.2 (C)-(I) and bar chart (J), although different PA clinical isolates formed different biofilm 3D structures in the MatTek plates after 3 d, 250μM showed good dispersal effect (a minimum biomass reduction percentage of 57.81%, $p<0.01$) on all the strains tested in MatTek system. However, biomass of 3 d PA58 biofilm significantly reduced after NO treatment in MatTek plates but not in microtiter plates, and there are some discrepancies on the actual dispersal percentages of the same strains in these two culture systems. The differences might be due to different culturing methods, or COMSTAT measures cell mass thus is more sensitive than the CV staining that measures total biomass. Nevertheless, from both microtiter plate and MatTek plate assays it could be confidently concluded that at least *in vitro*, 250μM S150 can trigger dispersal for 14 out of 17 mature CF PA biofilms. To investigate whether the efficacies are the same *in vivo*, biofilm formation and dispersal under different systems that mimic *in vivo* conditions should be set up and tested in the future.

## 4.3 Cell aggregates from CF clinical isolates

Different methods of acquiring cell aggregates have been reported, such as static or shaking cultures in multiple well plates[361,363]; microfluidic agarose channel (MAC) without shear stress to mimic the thick mucosal layer on the epithelial cells of CF

patients[364]; microfluidic system with vortical flow to mimic microbial conditions at ecologically relevant spatiotemporal scales[365]. Different shaking speeds were reported in published papers such as 160 rpm[366], 200 rpm[367] and 50 rpm[368] with different culture medium. In this study, two different methods – direct visualization in 6 well plate and CLSM images - were used to observe cell aggregates as described in 2.15.

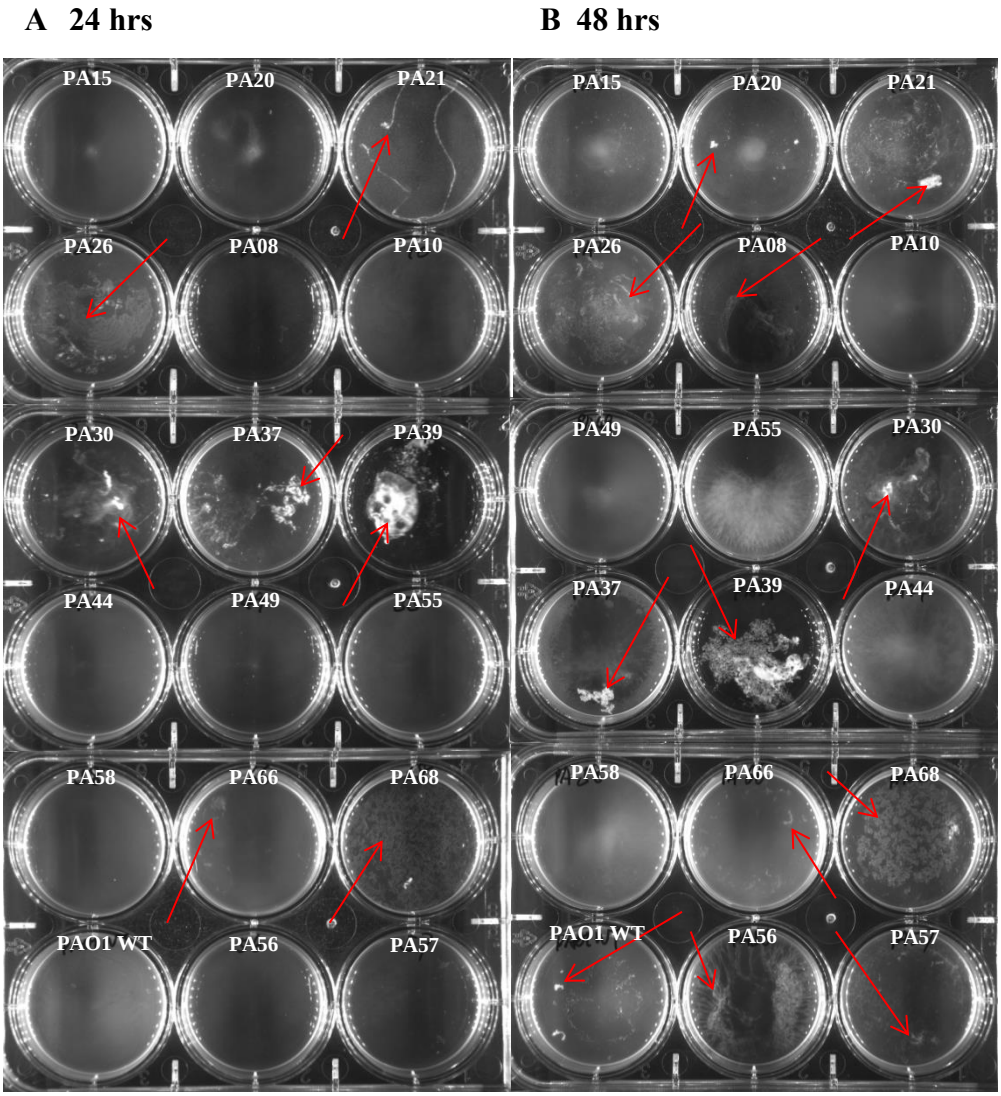

**D**

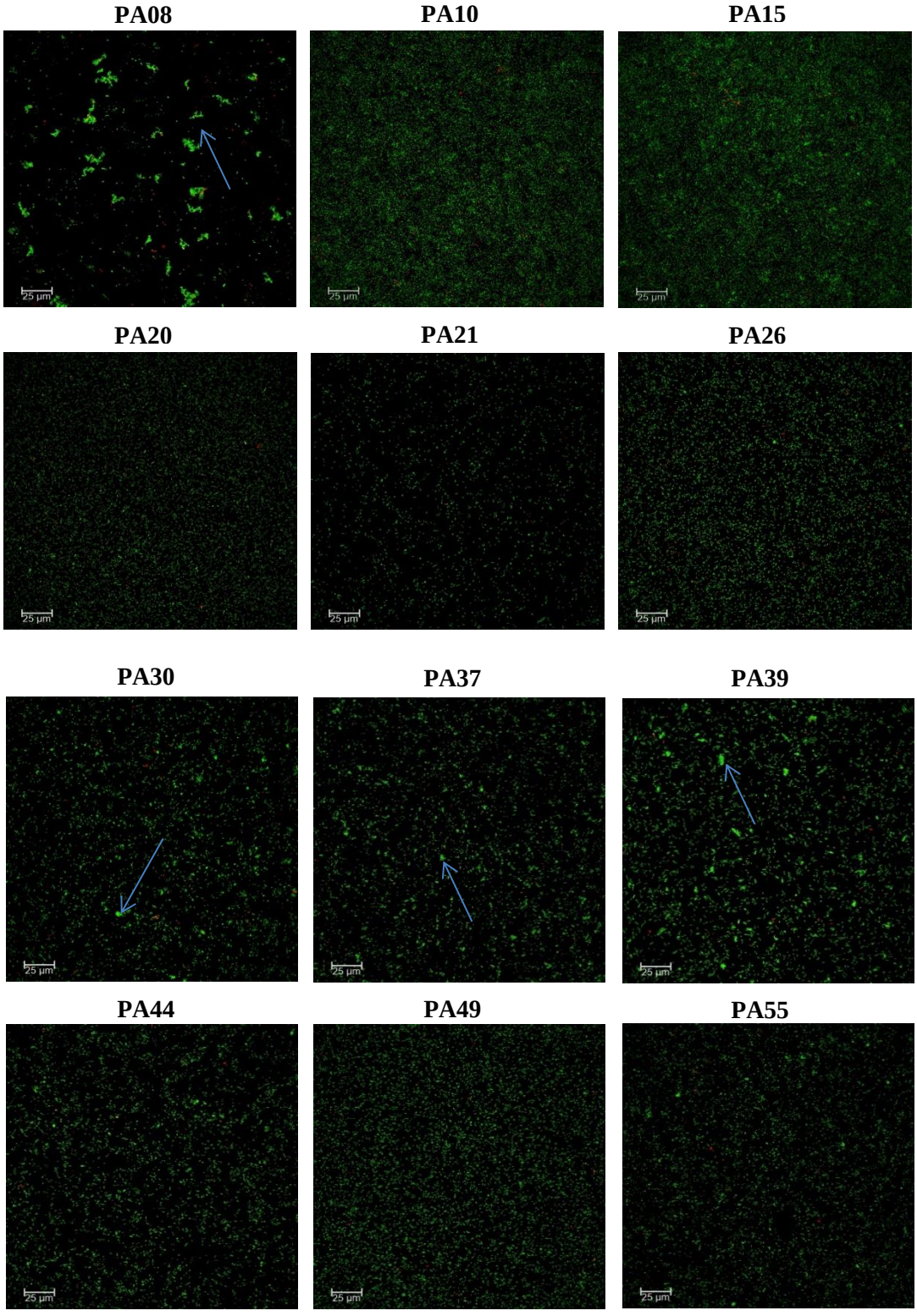
PA08
PA10
PA15
PA20
PA21
PA26
PA30
PA37
PA39
PA44
PA49
PA55
25 µm

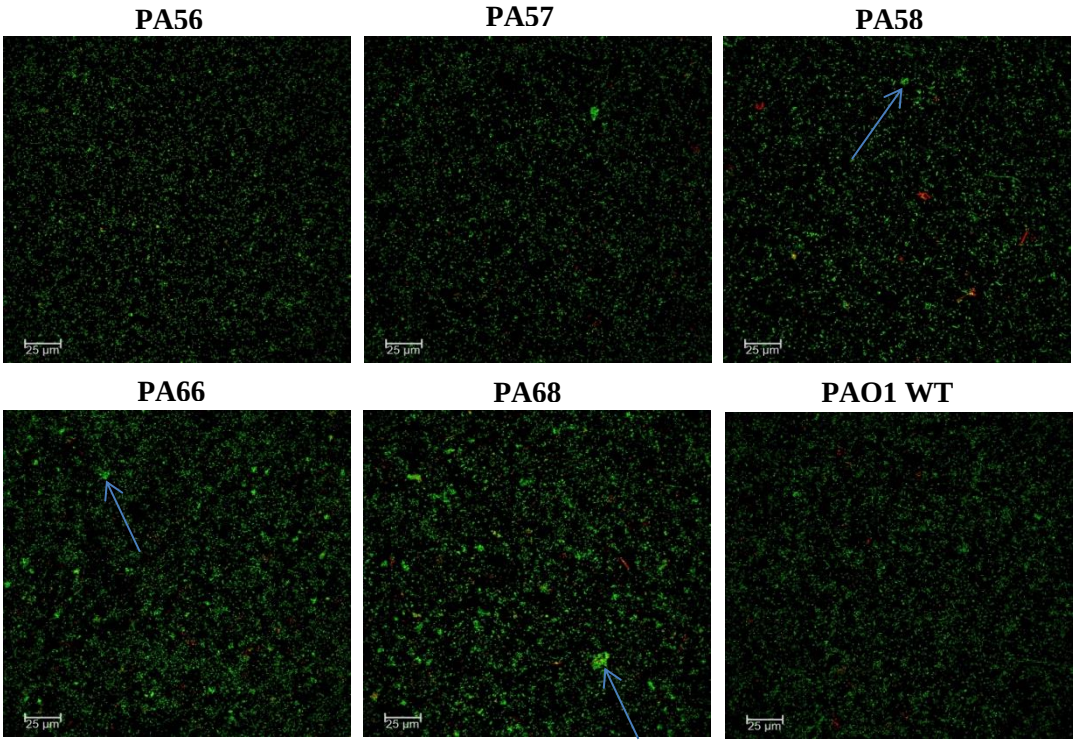


Fig 4.3 Cell aggregation in 6 well plate with an initial inoculum of $OD_{600nm}$~0.01 and incubated at 37℃ with 50rpm shaking after 24 hrs (A) and 48 hrs (B) with M9 media as negative control (C). Red arrows point to cell aggregates in each well. (D) CLSM image for 24 hrs planktonic cells in universal tubes with an initial inoculum of $OD_{600nm}$~0.005 and incubated at 37℃ with 120 rpm shaking. Blue arrows point to cell aggregates and scale bar=25µm

As shown in Fig 4.3 (A) and (B), in 6 well plate with slow shaking and certain shear force, obvious cell aggregates were found in several clinical isolates (red arrows), especially PA39 where nearly the majority of the cells were grown into aggregates leaving the rest of the media the same as blank M9. Some strains (PA08, PA20, PA56, PA57 and PAO1 WT) did not show obvious aggregates after 24 hrs but started aggregating after 48 hrs.

By comparing Fig 4.3 (A) and (D), PA08 appeared to be the strain that aggregated the most under CLSM but not in 6 well plate when directly observed. On the other hand, PA39 was found as the most aggregative in 6 well plates but not in CLSM images, indicating that different culturing methods might result in different cell aggregation status, or some cell aggregations that happened in 6 well plates with gentle shaking can be disrupted by the manually whirling and mixing procedure used in CLSM sampling. In summary, it can be qualitatively concluded that PA08, PA37, PA39, PA66 and PA68

appeared to be “more aggregative” than other strains despite several small aggregates also being found in the majority of the strains cultures.

## 4.4. Gini index and its application in the measurement of cell aggregation – A novel index: Concentration coefficient

The visualized results of cell aggregates in Fig 4.3 cannot quantitatively show the degree of aggregation among different strains, especially when cell sizes and densities were different. As it was shown that CLSM can be used to observe cell aggregates in liquid culture after certain preparation procedures without damaging the structures, a novel index, concentration coefficient (CC), was developed for quantifying aggregation level based on Gini index and CLSM images.

Gini Index was introduced by Corrado Gini in 1912 and is now widely and majorly used in the measurement of income inequality in a group of residents[321]. This concept is quite similar to cell distribution in a defined CLSM image. A CLSM image of cell aggregation can be first divided into a certain number of pixels with the brightness positively correlate to the amount of cells in each pixel (Fig 4.4.1), which is equivalent to the income of a single resident in Gini Index. CC can then be calculated to measure the inequality of cell distribution, namely, the degree (level) of cells aggregation. The details of calculation method is described in 2.17.

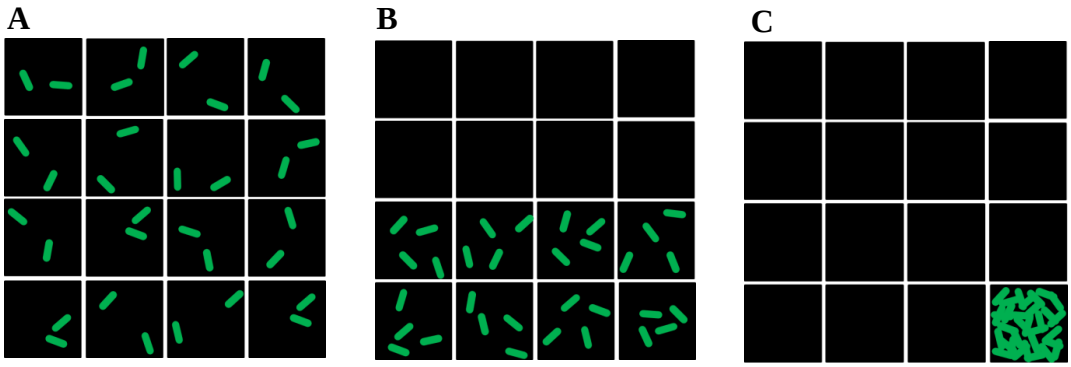


Fig 4.4.1 Three different types of cell distribution in CLSM images with the same total amount of cells. (A) Cells distribute homogeneously into all pixels (equidistribution), (B) Cells distribute heterogeneously into half of the pixels, (C) Totally aggregation of cells into 1 pixel

In Fig 4.4.1, after calculation, CC in (A) is 0, in (B) is 0.533 and in (C) is 1. Therefore, the cells that aggregated more in a sample, the higher is the CC value. Different CC values obtained from various bacterial cultures can then be used to distinguish the different degrees of cell aggregation of different strains. The maximum projection

pictures from stacks of CLSM images taken can be used for analysis and the cell numbers in each pixel can be calculated based on the strength of signals with the same excitation. Thus, CC is used to quantify the aggregation levels in all CLSM images for CF PA clinical isolates grown as described in 2.15 and shown in Fig 4.3 (D)

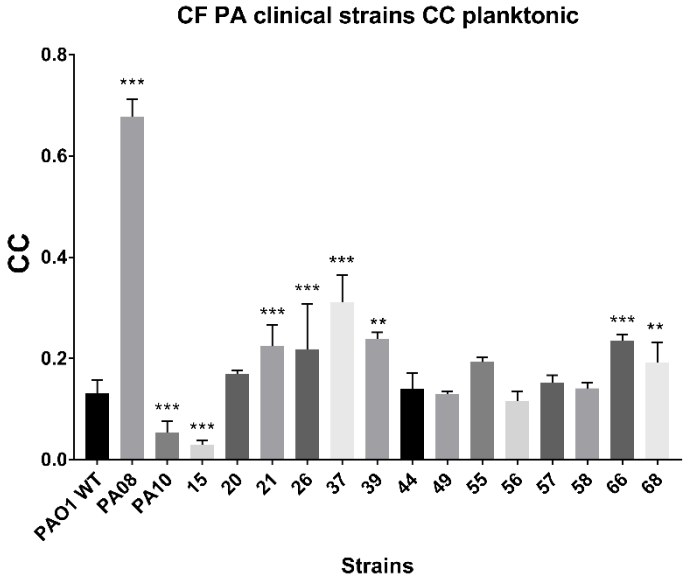


Fig 4.4.2 CC of the CLSM images of all CF clinical isolates sampled from 24 hrs shaking incubation in universal tubes. Welch T-test was applied to compare each CF strain to PAO1 WT. Data represent data means of n=3 of 3 biological replicates. ** represented $0.01<p<0.05$ and *** represented $p<0.01$.

From Fig 4.4.2 it can be concluded that CC of PA08, PA21, PA26, PA37, PA39, PA66 and PA68 were significantly higher than PAO1 WT ($p<0.01$), with PA08 the highest among all (5.18 fold higher than PAO1 WT, $p<0.01$). This corresponded to the visualized judgement from Fig 4.3 (D), proving this method can be a useful tool to reflect and quantify the aggregation levels.

One would assume certain strains might have a preferred mode of growth between planktonic aggregates and surface attached biofilms in the same media (M9 in this study), namely, when biofilm biomass is high, CC might be low and vice versa. Table 4.4 below summarizes the fold changes of cell aggregation level and biofilm biomass of each CF PA strain compared to PAO1 WT.

| Fold changes | PA08 | PA10 | PA15 | PA20 | PA21 | PA26 | PA37 | PA39 |
|---|---|---|---|---|---|---|---|---|
| Biofilm biomass | 0.09 | 0.29 | 0.12 | 0.10 | 0.26 | 0.17 | 0.06 | 0.02 |
| Cell aggregation (CC) | 5.18 | 0.41 | 0.22 | 1.30 | 1.71 | 1.67 | 2.38 | 1.83 |
| | PA44 | PA49 | PA55 | PA56 | PA57 | PA58 | PA66 | PA68 |
| Biofilm biomass | 0.19 | 0.09 | 0.13 | 0.13 | 0.20 | 0.24 | 0.21 | 0.77 |
| Cell aggregation (CC) | 1.07 | 0.99 | 1.48 | 0.89 | 1.17 | 1.08 | 1.80 | 1.47 |

Table 4.4 Fold changes of CF PA strains 24 hrs biofilm biomass in microtiter plates and cell aggregation levels (CC) to PAO1 WT.

From Table 4.4 it is hard to conclude which strain prefer which growth mode. Although 12 out of 16 strains that form much less biofilm than PAO1 WT tended to form more aggregates (biomass fold change<1 and CC fold change>1), PA10, PA15, PA49 and PA56 (highlighted in green) formed much less of both biofilm and cell aggregates compared to PAO1 WT. Nevertheless, PA08, PA37, PA39 and PA66 (highlighted in red) formed significantly more aggregates and less biofilm than PAO1 WT, showing their potential preference of existing as aggregates in M9 media.

## 4.5. Cell aggregates with NO treatment

As shown in 4.2, 250μM S150 effectively triggered the dispersal of CF PA strains biofilms. Can NO also trigger the dispersal of cell aggregates in aqueous environments when preferred by certain strains? To answer this question, PA08, PA37, PA39 and PA66 grown as planktonic cultures were subjected to SNP and S150 treatment for CLSM as described in 2.15.

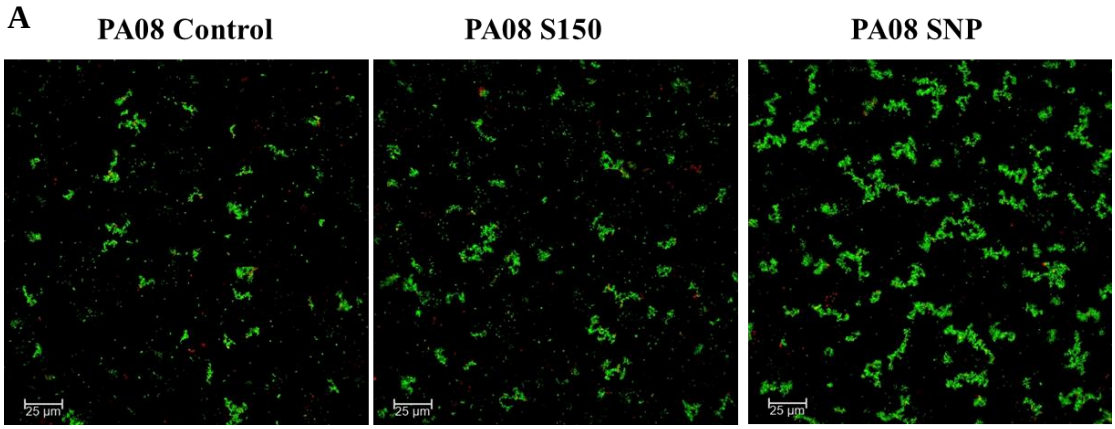

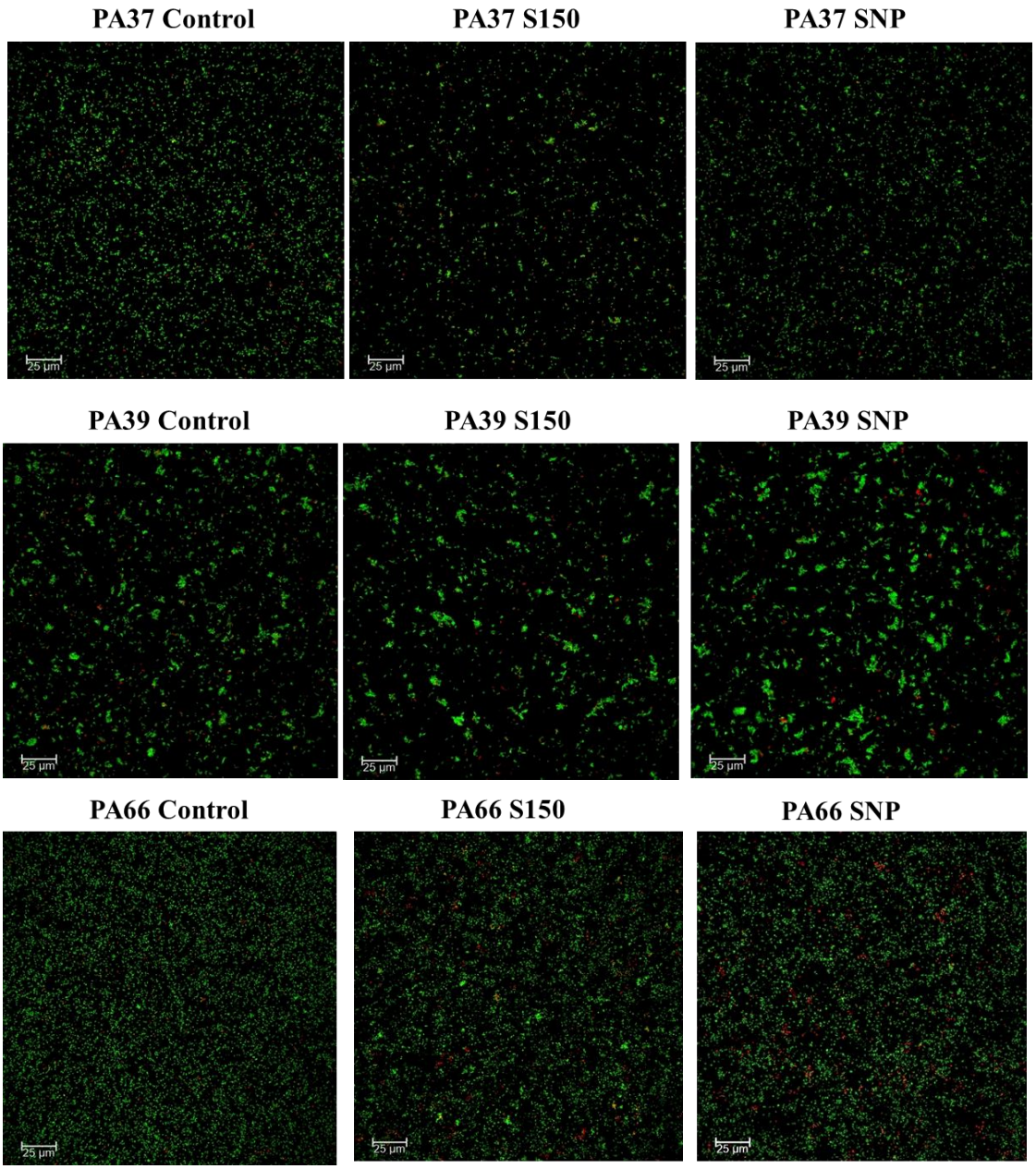
PA37 Control
PA37 S150
PA37 SNP
PA39 Control
PA39 S150
PA39 SNP
PA66 Control
PA66 S150
PA66 SNP
25 µm

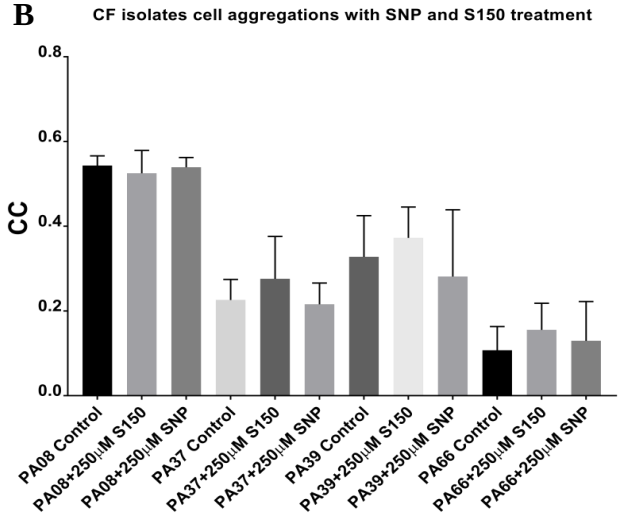
B
CF isolates cell aggregations with SNP and S150 treatment
CC
0.0
0.2
0.4
0.6
0.8
PA08 Control
PA08+250µM S150
PA08+250µM SNP
PA37 Control
PA37+250µM S150
PA37+250µM SNP
PA39 Control
PA39+250µM S150
PA39+250µM SNP
PA66 Control
PA66+250µM S150
PA66+250µM SNP

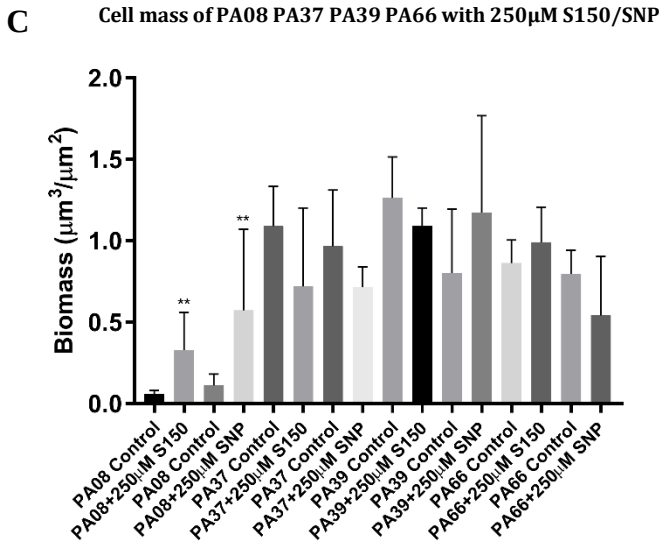


Fig 4.5 (A) CLSM images of cell aggregations of PA08, PA37, PA39 and PA66 with 12 hrs SNP and 2 hrs S150 treatments. Scale bar=25μm. (B) CC of PA08, PA37, PA39 and PA66 with/without 250μM S150 and SNP treatments. (C) Cell masses of PA08, PA37, PA39 and PA66 with/without 250μM S150 and SNP treatments. Data represent data means of n=3 of 3 biological replicates. Welch T-test was applied between control and treatments. ** represents $0.01<p<0.05$ and *** represents $p<0.01$.

From both visualized judgement (CLSM images in Fig 4.5 A) and CC calculation for aggregation levels (Fig 4.5 B), it can be concluded that neither SNP nor S150 decreased the degree of cell aggregation for all strains ($p>0.05$). Thus, the NO treatment effective for dispersal of various CF clinical isolates biofilms on surfaces cannot disperse cell aggregates, at least for these four strains, indicating the EPS or cell signalling mechanisms of these four cell aggregates might be different from biofilms. Further experiments should be carried out to investigate the matrix components and genotypes of these four strains.

Visually judging Fig 4.5 (A), the total cell amounts of PA08 seemed to be significantly increased after the addition of SNP. As SNP and S150 enhanced PAO1 WT cell number after the treatments (See 3.4.2), whether S150 and SNP can enhance the growth of these 4 clinical isolates was tested to see its potential effect on decreasing dispersal efficacy. Since vortex and sonication might not totally separate cell aggregates, there was a risk that CFU counts might not be accurate. Therefore, the cell mass in sampled CLSM images was measured using COMSTAT to represent the amount of cells. As shown in Fig 4.5 (C), 250μM S150 and SNP significantly increased PA08 biomass (5.4 and 5.09 folds respectively, $p<0.05$), but not other 3 strains ($p>0.05$), indicating this enhancement

might be strain specific. Nevertheless, my data showed that 250μM S150 that can disperse PAO1 WT or some clinical isolates biofilms not only cannot disperse cell aggregates of some strains, but might also increase their growth as aggregates. These findings are important for NO therapy in CF patients given that most studies showed the majority of the biofilm-like PA aggregates are not surface associated in CF airway[326,369–371]. Hence, when investigating the optimal NO donor concentration for treating CF PA in the future, it might be more suitable to test the drugs on cell aggregates rather than biofilms on the surfaces of certain strains.

# Discussion

### CF PA clinical isolates can form biofilms and cell aggregates *in vitro*

There are many conflicting reports on whether *P. aeruginosa* adhere to epithelial cells in CF patients or not. Imundo L *et al* reported that tetrasaccharide of αGM is a receptor for *P. aeruginosa* and its increased abundance in the apical membrane of CF epithelia most likely contributes to the *P. aeruginosa* colonization in the CF lung[372]. Hahn further reported that it was the type IV pili of *P. aeruginosa* that was responsible for binding to αGM[373]. Interestingly, *P. aeruginosa* does not avidly bind to normal, uninjured epithelial cell surfaces, but the binding of *P. aeruginosa* to inflamed or injured epithelial cells (CF or mechanically ventilated patients) is significantly higher than to normal cells[374]. Swanson *et al* also developed a high-throughput *in vitro* assay method to analyse the attachment of *P. aeruginosa* to epithelial cells based on microtiter plates[375]. Compared to attachment onto epithelial cells, another theory is that *P. aeruginosa* enters airway epithelial and internalized bacteria acquire biofilm-like characteristics. *P. aeruginosa* formed as clusters within airway cells, favouring its persistence and may contribute to difficulties in the treatment of airway infection[376]. Hassett *et al* claimed that *P. aeruginosa* was never seen localized to the epithelial cell surface in CF airway disease upon microscopic examination of thin sections of airways removed from CF patients[377]. Worlitzsch *et al* found that *P. aeruginosa* is localized in intraluminal material and bound to mucus in freshly excised CF airways, while no *P. aeruginosa* bacteria were observed attached to airway epithelia[370]. Bjarnsholt *et al* only detected bacteria imbedded in the mucus surrounded by PMNs in the conductive zone and there was no bacteria adhered to the bronchial walls or airway epithelia[326]. At the same time, respiratory zones were filled with aggregating bacteria and PMN[326]. These embedded cell aggregations may be

regarded as biofilms formed in mucus or intracellular spaces[377,371]. As shown in Fig 4.2 and 4.3, some of the CF PA strains formed more biofilms (higher biomass) than others in normal microtiter plates and MatTek plates but do not aggregate in liquid cultures, while some formed large cell aggregates in liquid medium but poorly attached to the surfaces. On the other hand, the existence mode for some strains might be neither floating aggregates nor attachment but as separated planktonic cells, while some might both form aggregates and attach to the surfaces. Hence, both non-attached cell aggregates and attached biofilm phenotypes should be tested to confirm their preferred existence mode *in vitro*. Some strains (PA08, PA20, PA56, PA57 and PAO1 WT) did not show obvious aggregates after 24 hrs but started aggregating after 48 hrs. This might be due to the lack of nutrients after a longer period of culture that caused stress responsive aggregation, or when cell density was higher the aggregation became more obvious such as PA08 of which the growth rate was much lower than others on agar plates (Fig 4.1). Therefore, different nutrients conditions should be tested to see if there is specific relationship between nutrients and cell aggregations. Furthermore, the actual situation might not be the same *in vivo* compared to *in vitro* due to the differences in the growth environments, thus other models may be set up in the future to mimic the environment in CF patients' lungs.

**NO can effectively disperse biofilms formed by CF PA clinical isolate strains, but not cell aggregates**

Various publications indicated that exhaled NO from CF patients is reduced compared to that produced by normal patients[378–380]. In human, NO is synthesized from L-arginine by NO synthase (NOS) in three isoforms, of which endothelial NOS and neuronal NOS are constitutively expressed and only produce nanomolar scale of NO. Inducible NOS (iNOS) is expressed maximally following an inflammatory stimulus and produces large, micromolar scale of NO[381]. Gracemann *et al* reported that significant differences between neuronal NOS genotypes were observed among CF patients. A higher repeat number of intronic AAT repeat polymorphism in the neuronal NOS gene was significantly related to low exhaled NO and more *P. aeruginosa* colonization[382]. Inflammation in the respiratory epithelium in patients with asthma and bronchiectasis were found to up-regulate iNOS expression, which correlates with elevated NO concentrations in exhaled air[381]. However, in CF patients' airways with chronic severe

inflammation, the amount of exhaled NO is not increased and the expression of epithelial iNOS is reduced[381]. Darling *et al* reported that NO production reduced *P. aeruginosa* adherence to human bronchial epithelial cells and enhanced killing of internalized bacteria[381]. As described, *P. aeruginosa* attaching to epithelial cells or internalized into them forming large cell aggregates acquire biofilm-like characteristics where the efficacies of antibiotics are impaired. Hence, it is reasonable to deduce that the addition of NO might prevent CF clinical isolate *P. aeruginosa* from colonizing at the surface or aggregating inside of epithelial cells. As discussed in chapter 3, S150 was found to be an efficient NO donor in triggering *P. aeruginosa* PAO1 WT biofilms dispersal. Therefore, 250μM S150 was used to test if the clinical isolate strains that form biofilms *in vitro* can be dispersed. From Fig 4.2 (A) and (B) it can be concluded that different clinical isolates possess different abilities to attach to polystyrene surfaces and growth modes. From the post-dispersal biomass reduction percentages shown in Fig 4.2 (A) and (B) it can be concluded that the efficacies of S150 on different clinical isolate biofilms varied from PAO1 WT biofilm after the same culturing time. This indicated that different genotypic/phenotypic of CF PA strains might result in different responses to NO. Furthermore, 1 d and 3 d biofilms of the same strain in microtiter plates showed different reduction percentages after NO treatment. The explanations remain unknown but some assumptions were proposed. For example, the discrepancy in PA15 and PA49 might result from the different biofilm stages of these two strains when the biofilms after 1d were more robust than 3 d despite the similar biomasses (Fig 4.2 A and B), or the different physiology of the cells inside 1 d and 3 d biofilms and their tolerances to NO. The discrepancy in PA58 might be due to the increased complexity of biofilm or thickness of EPS from 1 to 3 d reflected by significantly increased total biomass (4.13 folds, $p<0.01$). PA08 and PA20 remained tolerant to NO and neither was proved to be mucoid (Fig 4.1 and Table 4.1), therefore the tolerance might not come from lack of penetration of NO into the biofilms due to thick mucoid shield but their specific genotypes/phenotypes.

From Fig 4.2 (C) – (J) it can be concluded that different clinical isolates form different 3D structural biofilms and the efficiency of S150 does not correlate to the structural characters *per se*. The discrepancies on the actual dispersal percentages of the same strains in MatTek and microtiter plates might be due to different culturing methods or biomass measurement methods. For microtiter plate crystal violet was used to stain the

total biomass including live cells, EPS and dead cells, while for MatTek plates only cells were stained and calculated thus is more sensitive. Nevertheless, the results eliminated the assumption in chapter 3 discussion if the decreased effect of NO donors on older biofilms was purely a result of the more mature and complex structure of the older biofilms.

However, data in section 4.5 showed that the same dose treatment of S150 or SNP efficiently did not disperse cell aggregates from certain strains. The reason remain unknown but it is likely that EPS components or cell signalling of the cells that formed aggregates were significantly different from those in biofilms. It might be concluded that in certain circumstances, cell aggregates appear to be even more difficult to eradicate than biofilms. Since many clinical isolates can exist as cell aggregates in *in vitro* assay, it is reasonable to deduce they can exist as cell aggregates in patients as well. When applying NO treatment to some patients with obvious biofilms at certain area (such as medical implants) *in vivo*, data collected from the surface-attached biofilms may show an efficient reduction in biomass, but the aggregates might remain. For those strains that can exist as both biofilms and aggregates, the information might therefore be inaccurate and the lack of focus on aggregates may worsen the situation. Therefore, more attention should be paid to the treatment on CF clinical isolate aggregates besides biofilms. Nevertheless, the success in triggering the dispersal of 14 CF PA biofilms suggested that S150 might act as an efficient NO donor in dispersing pre-established *P. aeruginosa* attached to epithelial cells or other medical implants.

**SNP and S150 have different influences on the growth of different *P. aeruginosa* strains**

As discussed in chapter 3, 5 probabilities were raised to explain why SNP and S150 enhanced the growth of PAO1 WT. One of them is cell aggregates exist in the solution and the addition of NO triggered cell aggregates dispersal, resulting in increased CFU count due to the fact that cell aggregates might not be distinguished on agar plates. However, CLSM images in Fig 4.3 did not show a large amount of cell aggregates in PAO1 WT in our culture method. Furthermore, S150 and SNP did not disperse cell aggregates in the planktonic cultures of the four CF clinical isolate strains as shown in Fig 4.5. Therefore, this explanation for the enhanced growth might be excluded. One of the potential explanations mentioned in chapter 3 was the breakdown products of SNP and S150 can act as nutrients for PAO1. If this is true, they might also be used as energy

resources for other *P. aeruginosa* strains. However, the fact that S150 and SNP only increased the growth of PA08 but not PA37, PA39 and PA66 might indicate that either this explanation is less likely to be true, or the breakdown products may have different influences on different *P. aeruginosa* strains cell cycles. Another assumption is that NO might have different influences on different *P. aeruginosa* strains cell cycles. If the second hypothesis proves to be authentic, the specific concentration of NO should be taken into consideration and strictly controlled as the threshold NO concentration that caused enhanced growth might be different to different strains. The other three explanations described in chapter 3 discussion still need further testing to prove their authenticity.

**A novel index for effective quantification of cell aggregation level**

The levels of cell aggregates have been mainly described in two ways: descriptive and quantifiable. Microscopic or macroscopic images can be directly shown and readers can compare the level of aggregation by eye[383–388]. For quantification, some previously published research used OD value for the measurement. Guo *et al* adopted low speed centrifugation to separate cell aggregates and planktonic cells[388]. Cell aggregates were then collected for vortex and CFU count so that the cell number that went into aggregate was calculated[388]. Baugh *et al* used a static system for cell aggregation and compared the OD value of suspension below the aggregating surfaces. With the same initial inoculum and growth rate, the lower the OD value of suspension (planktonic cells) the more aggregates[385]. However, these methods cannot directly reflect the characters of the cell aggregates themselves. Therefore, other quantification methods were developed to directly measure the sizes of aggregates. Jung *et al* used ImageJ to change the aggregative structures in each image to a binary code and the pixel number was measured to represent the size[364]. Stoodley *et al* used image subtraction to change the grey scale of background and cell aggregation so that the areas and diameters of cell aggregates can be directly measured by image software[20]. The means and standard deviations of the aggregate sizes were calculated to show the differences in the level of cell aggregations. However, the following situation cannot be reflected by this measurement method: suppose image A has 4 aggregates with size of 20, 20, 4, 4 while image B has 4 cell aggregates with sizes of 12, 12, 12, 12. It will be hard to describe the aggregation levels by the same mean but different deviations. Schleheck *et al* used laser diffraction analysis to determine the exact diameters of cell aggregates and different size

ranges were grouped into different catagories[366]. Similar methods include using a coulter counter by measuring electric current change to reflect the size of the particles[389] and a cell counter to count individual cells within cell aggregates[390]. The more cell aggregates belonging to larger cell sizes categories, the more aggregative the cells are. However, this method results in one number for each category and the comparisons need to be done among different categories. In summary, direct visualization cannot quantify the level of aggregation and small but significant differences are hard to describe; OD value cannot give the details of cell aggregates; size measurement is so far the most accurate method to describe the details of cell aggregates, but it is indirect in reflecting the level itself and needs multiple numbers to describe one sample, therefore comparing a large number of samples would be laborious. Here, we introduce a novel index, concentration coefficient (CC), based on the idea of Gini coefficient. CC only gives out one number for each image from a sample and can directly reflect the level of cell aggregation. Briefly, a maximum projection of CLSM image was first divided into a certain number of pixels with the brightness inside each unit standing for the amount of cells in each pixel. CC can then be calculated to measure the inequality of cell distribution, namely, the degree (level) of cells aggregation. As shown in Fig 4.3 and Fig 4.4.2, the calculation of CC corresponded to visualized judgements. CC provides an easy but accurate way to measure the level of cell aggregation, especially to distinguish samples that possess small but significantly different levels of aggregation. Apart from bacterial cell aggregation, CC can also be widely applied to other types of cell aggregation and can be easily used to quantify and compare the efficacies of drug treatments on cell separation in broader fields.

# Chapter 5 – An efficient method for high-throughput gene deletion in *P. aeruginosa*

## 5.0. Introduction

With the whole genome sequence in *P. aeruginosa* strains revealed, manipulation of specific genes became much easier with the help of genetic tools. To elucidate the function of a gene, disruption of a specific gene is one of the most frequently used methods including insertion, deletion and site-directed mutagenesis. In this study, transposon mutants purchased from Washington PAO1 Tn library and Gm marked gene deleted mutants were used for phenotypic analysis. Therefore, here I briefly introduce the knowledge of (1) transposon insertion mutant; (2) conventional gene deletion (gene knockout, KO) methods; (3) an efficient KO method I developed based on conventional ones and (4) the workflow comparison between my newly developed KO method and conventional ones.

### 5.0.1. Transposon (Tn) insertion mutant

Transposable elements (TEs) are DNA sequences that move from one location to a new site on the same or different DNA molecule. This recombination process is termed transposition. Different types of TEs have been identified in all organisms, prokaryotic and eukaryotic. The bacterial transposon Tn5 and its variants have been developed and widely used in genetic engineering by fusing Tn5 into vectors and transforming into different organisms for the random insertion disruption of genes. The structure of Tn5 and its "cut and paste" mechanism are illustrated as below[391].

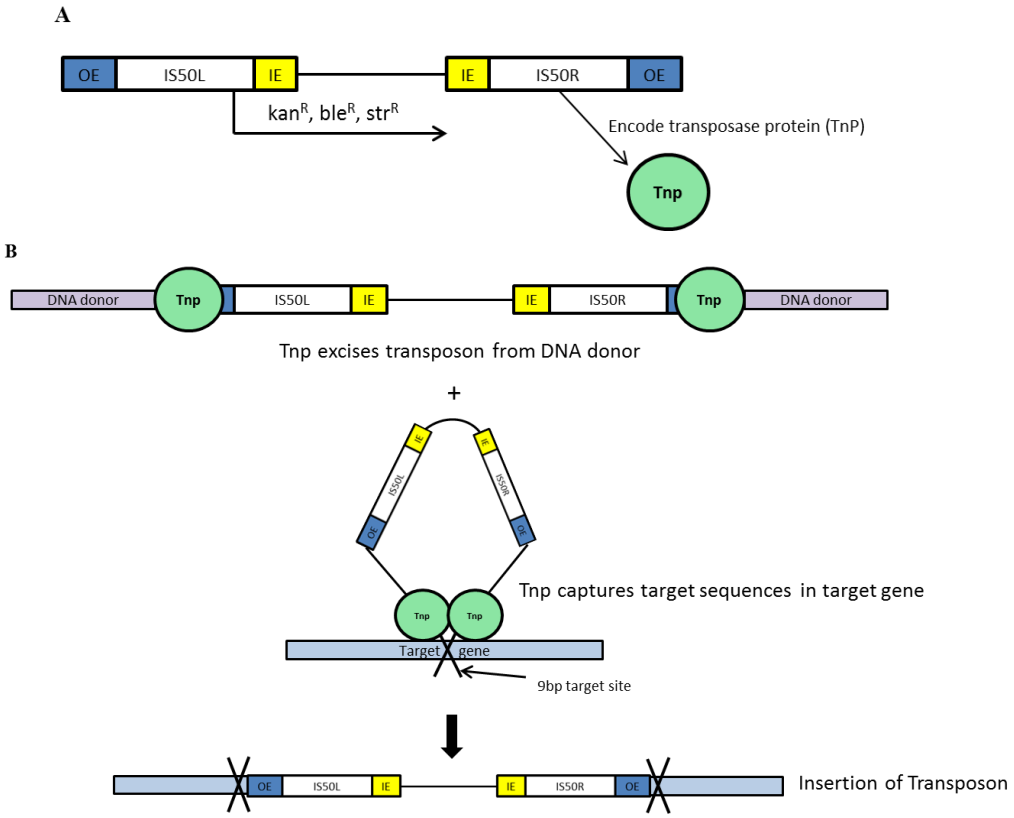


Fig 5.0.1.1 (A) The structure of Tn5 transposon. OE: outside end sequence. IE: inside end sequence. IS50L and IS50R: two inverted, almost identical insertion sequences, with IS50R encoding the transposase protein (TnP). Kan=kanamycin resistance, ble=bleomycin resistance, str=streptomycin resistance (B) The mechanism of Tn5 transposition. The synaptic Tnp excise transposons from DNA donors at end sequences and then capture the 9bp fundamental sequences in target genes. The target for Tn5 is not completely random with modest preferences of certain nucleotides arrangement, but the randomness is sufficient for a large number of random insertions in genomes of large sizes such as in *P. aeruginosa*. After the capture, Tnp catalyzes strand transfer in which the transposon 3' OH groups attack the target DNA in the fundamental 9bp sequence. The strand transfer complex is then disassembled and the two single-strand gaps on either side of the insertion are repaired[391].

With the elucidation of Tn5 structures and the access to a variety of genetic tools, Jacob *et al* developed a transposon mutant library of *P. aeruginosa* PAO1 by using modified transposons[298]. The modifications were mainly in IS50L, generating alkaline phosphatase and β-galactosidase and resulting in the transposons IS*phoA/hah* and IS*lacZ/hah* respectively. These two variations also contain a tetracycline resistance gene which is not among the intrinsic resistances in PAO1. The structures of these two transposons are shown in Fig 5.0.1.2.

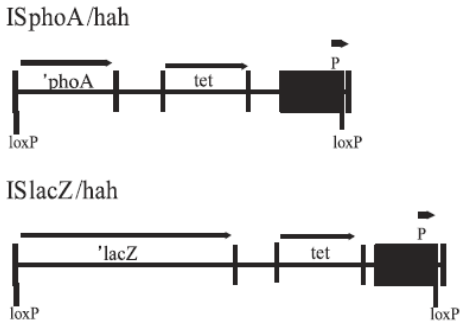


Fig 5.0.1.2 IS*phoA/hah* and IS*lacZ/hah* transposons used in generating *P. aeruginosa* PAO1 insertion mutants library[298].

Insertion of either transposon confers tetracycline resistance when they are positioned in-frame. To confirm a correct insertion in a desired gene two methods can be utilized. (I) Use gene specific flanking primers to test the PAO1 wild type and the Tn insertion strains. A band with the length of the gene should be yielded by PCR when using WT DNA as template, while no band or a band corresponding to a very large product should be yielded when using Tn strains DNA as template. (II) Use a transposon-specific primer in conjunction with one of the gene specific flanking primers to test the PAO1 wild type and Tn insertion strains. There should be no band when using PAO1 WT DNA as template and one band when using Tn strains DNA as template.

## 5.0.2. Gene knockout deletion mutant (KO)

KO is based on allelic exchange between engineered DNA fragment and chromosome by homologous recombination. In most cases, the replacement of WT alleles on the chromosome with plasmid-borne mutations requires the transfer of mutant alleles into bacteria and the integration of this allele into the chromosome in place of WT allele followed by concomitant loss of plasmid sequences[392]. The schematic diagram of the desired double crossover allelic exchange is shown in Fig 5.0.2.1. Endeavours have been made by generations of geneticists to simplify the methods and improve the precision.

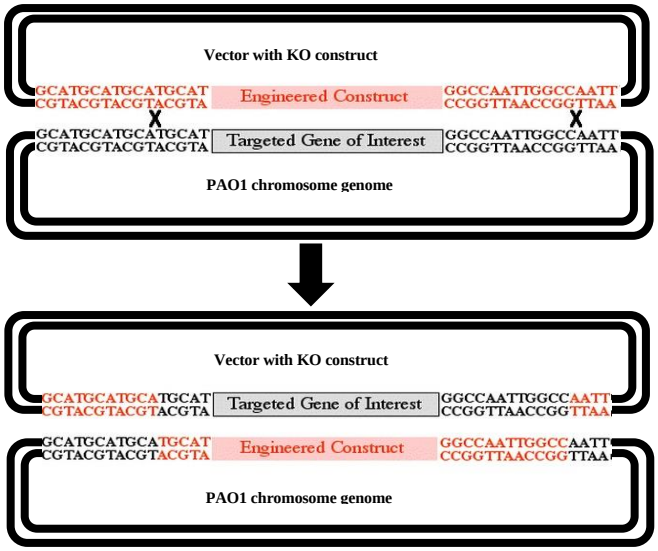


Fig 5.0.2.1 Schematic diagram of allelic exchange with double homologous recombination in gene

## 5.0.3. Specific vector for gene knockout in *P. aeruginosa*

Despite different methods such as transformation or electroporation being used to transfer recombinant plasmids into *P. aeruginosa* strains, conjugation has been the most frequently used one due to the simpler manipulation procedures and the fact that conjugally transferred DNA is less susceptible to host restriction[393]. Therefore, broad-host-range plasmids that can maintain stably both in *E. coli* and *P. aeruginosa* were applied to accomplish conjugation tasks. Also, these vectors should contain multiple cloning sites allowing DNA manipulations and be relatively small-sized to enhance the efficiency of conjugation. Herbert Schweizer has developed several vectors that have been widely used in various labs for genomic modulations in *P. aeruginosa*, among which pEX100T was used in our lab and discussed in details as follows[299].

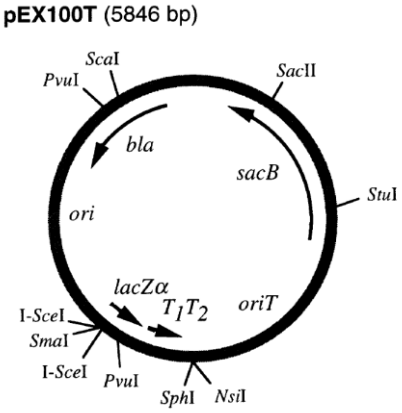


Fig 5.0.3 Physical map of pEX100T vector[299]

The pEX100T vector was developed after several modification steps from the original pUC19 vector[393–396]. As shown in Fig 5.0.3, pEX100T contains (1) *bla*, Ampicillin/Carbenicillin resistant gene. *bla* was used for Carbenicillin in PAO1 WT due to the intrinsic resistance to Ampicillin. (2) *ori*, pMB1(ColE1)-based origin of DNA

replication. pMB1(ColE1)-based plasmid was chosen as ColE1 does not replicate in *P. aeruginosa.* The vector must integrate into the chromosome in order to obtain antibiotic resistance encoded on the vector because it cannot replicate (suicidal properties)[397]. (3) *LacZα* was chosen for reliable blue/white screening of recombinants and minimizing the size of the vector by using α complement gene rather than the whole *LacZ* gene. The smaller the vector size is, the higher the efficiency of conjugation. (4) I-SceI-SmaI-I-SceI cloning site. Instead of using normal multiple cloning sites (MCS), unique cloning sites for SmaI and the rare-cutting meganuclease I-SceI were chosen to give greater access to restriction sites within the cloned fragment. This is particularly useful when the target gene for deletion is relatively small and the cloning parts inevitably contain some restriction sites[299]. (5) *oriT*, origin of transfer from RP4. Self-transmissible IncPα plasmid RP4 mediates DNA transmission by conjugation so *oriT* was inserted to make pEX100T recognizable to RP4 transfer functions provided *in trans*[393,398]. (6) *sacB* gene. The *Bacillus subtilis sacB* gene encodes the enzyme levansucrase, which is a transfructosylase catalyzing sucrose hydrolysis and levan synthesis[399]. In some gram-negative bacteria such as *P. aeruginosa*, expression of *sacB* is lethal in the presence of sucrose[399]. Therefore, *sacB* here served as a positive selection marker for separating double crossover from more frequently occurring merodiploids during allelic exchange[396].

With all these features infused into the pEX100T vector, it can be used to clone and genetically manipulate virtually any DNA fragment from *E. coli* to *P. aeruginosa*[299]. Several modified versions of this vector such as pEX18Gm, pEX18Tc and pEX18Ap were later developed mainly to overcome the drawbacks such as the lack of MCS and the fact that $Amp^R$ is not applicable in many other bacterial species[299].

## 5.0.4. Conventional methods for generating recombinant construct in plasmids

To generate gene deletions, commonly employed protocols[56,307,396,400–404] use amplification of upstream and downstream fragments (ideally 400-500bp) of target gene to ligate these two parts with an optional antibiotic resistance marker interspersed, as summarized in Fig 5.0.4 (A). A variation is using a unique gene-intrinsic restriction site to insert the resistance marker as shown in Fig 5.0.4 (B). Gene splicing by overlap extension PCR (SOE)[405] does away with the requirement of specific restriction sites of

the two previous methods and relies on use of primers complementary to sequence in the gene of interest as summarized in Fig 5.0.4 (C). Several reports have made use of SOE methods in generating variant alleles in *P. aeruginosa*[36,218,272,406–410].

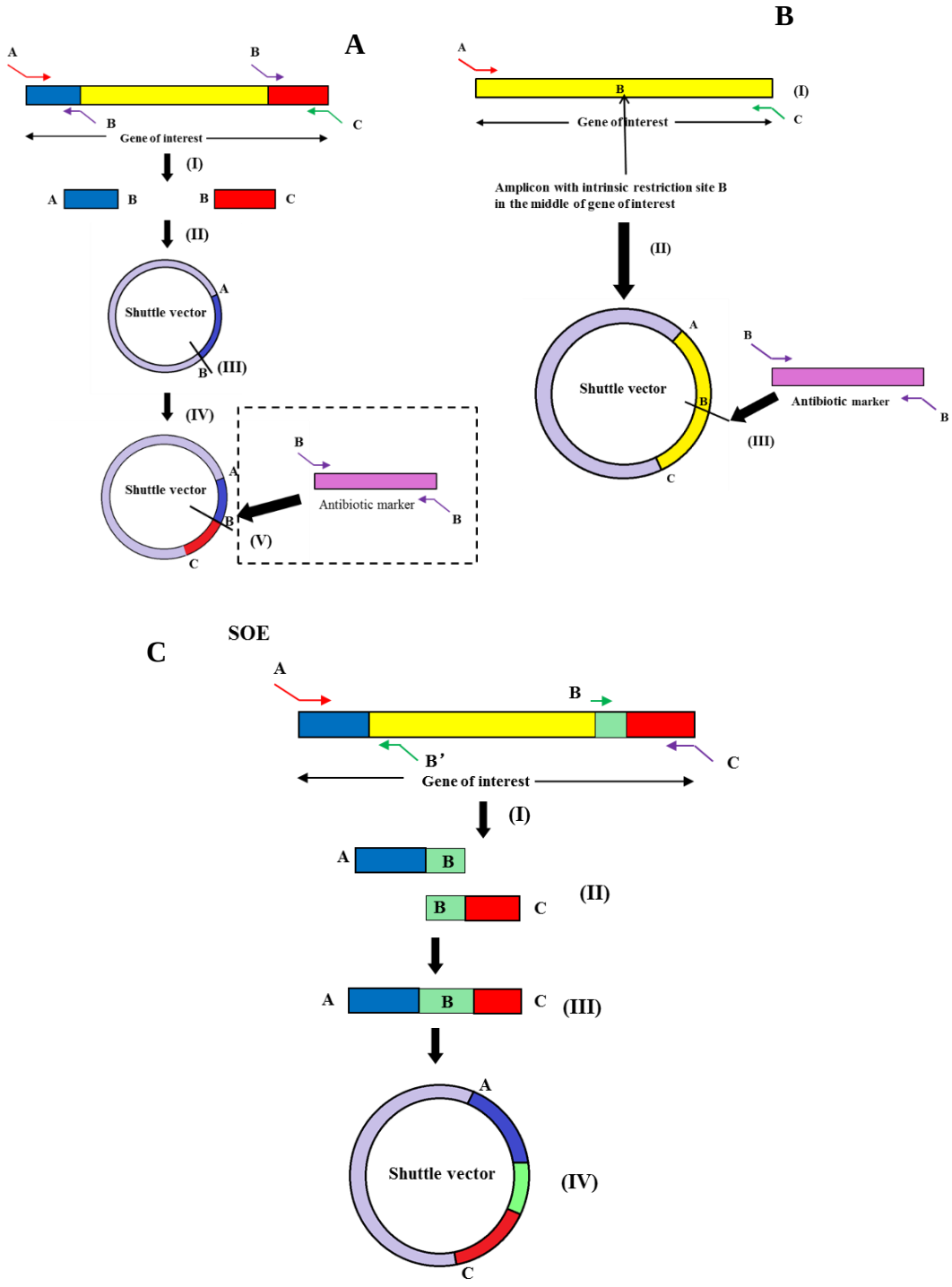


**Fig 5.0.4. Conventional methods for generation of suicide vectors. A.** Introduction of three different restriction sites through primers A, B and C. Upstream (blue) and downstream (red) fragments are ligated consecutively into the shuttle vector. In a subsequent step, the antibiotic resistance gene is amplified, restricted, and ligated into restriction site B. **B.** Genes may also be amplified as a whole, and the resistance marker be inserted *in frame* into a unique restriction site contained in the target gene. **C.** Splicing Overlap Extension (SOE) requires two different restriction sites A and C for upstream (blue) and downstream (red) fragments. The overlapping fragment is generated through specific primer design of primer B' complementary to sequence B in the gene of interest.

### 5.0.5. Gibson Assembly for rapid plasmid construction

A rapid DNA combination method developed by Gibson *et al* in recent years has been adopted by some researchers for the use in cloning and plasmid construction[411–415]. Instead of using restriction enzymes or PCR as mentioned above, 5' T5 exonuclease is applied in Gibson assembly for chewing DNA and the generation of "sticky end" DNA fragments. Ligase and polymerase are added at the same time for the extension and ligation of chewed DNA fragments in the same reaction. So far, only a few papers have reported using this Gibson assembly method for gene deletion in bacteria, including *P. aeruginosa*[416,417], all of which were after we established our KO method for this project (see below). Therefore, it is briefly reviewed here for its marked potential in bacterial gene editing in future. Steps are described below and the schematic illustration of KO vector construction based on Gibson assembly is shown in Fig 5.0.5.

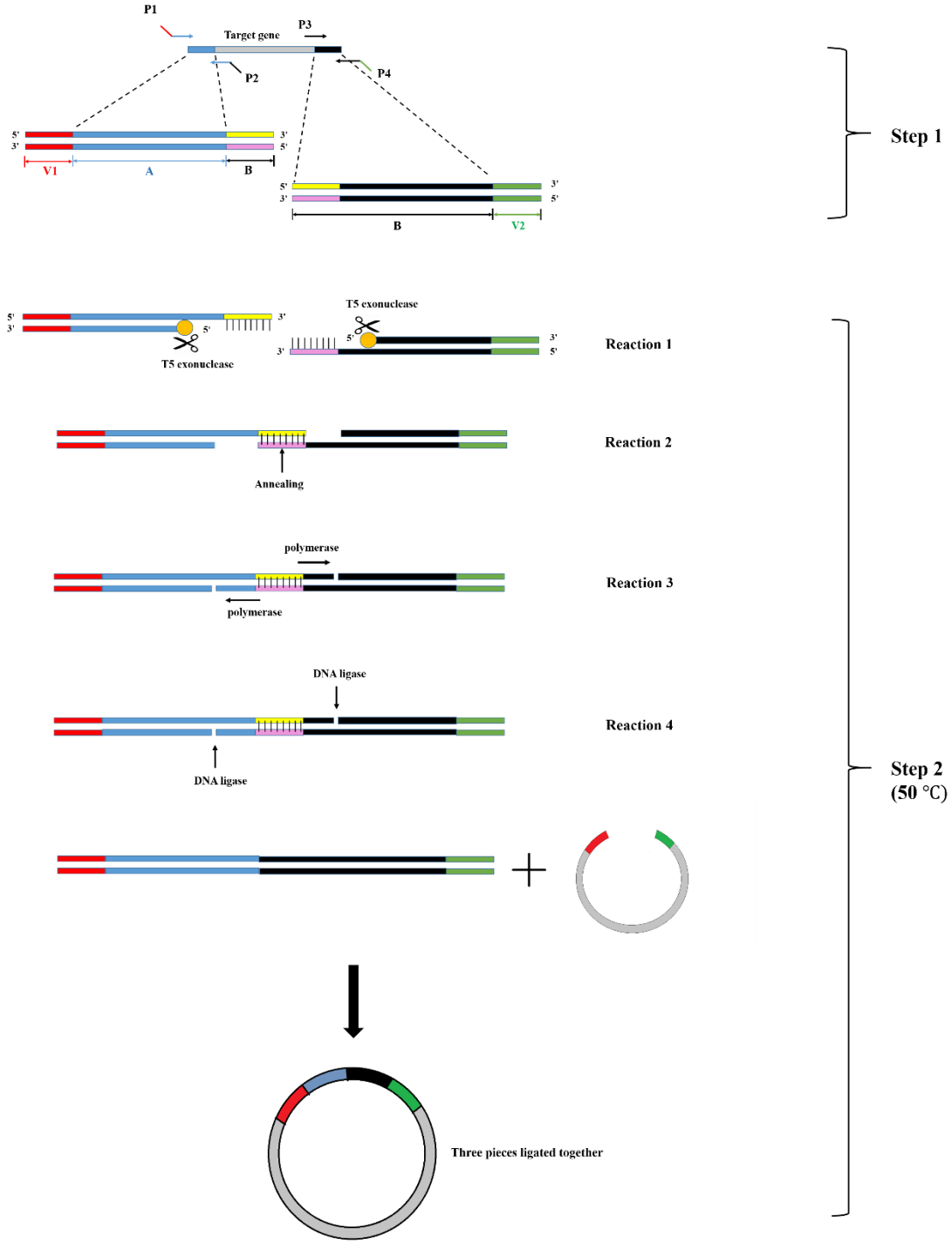


Fig 5.0.5 Schematic of Gibson assembly for KO vector construction

**Step 1:** PCR amplification of DNA fragments upstream (A, blue) and downstream (B, black) of the target gene (grey). Red (v1) and green (v2) parts are introduced by primer design and overlap with desired vector. P1: upstream forward primer contains overlap sequence with the vector (v1). P2: upstream reverse primer contains overlap sequence

with downstream B. P3: normal forward primer for downstream B. P4: downstream reverse primer contains overlap sequence with the vector (v2).

**Step 2:** Purified PCR products A and B from step 1, digested linear vectors, 5' T5 exonuclease, Phusion polymerase and DNA ligase were added into the same tube at specific ratios according to the length of DNA and overlap regions. Exonuclease does not compete with polymerase and all three enzymes can be simultaneously active in a single thermal reaction[411]. The mixture is incubated at 50℃ with several reactions happening sequentially.

**Reaction 1:** According to the length of identical overlap region between A and B (pink and yellow regions), different amounts of T5 exonuclease are added to the reaction. The optimal reaction temperature for exonuclease is 37℃ but the reaction is isothermal at 50℃. Thus, the available unit of exonuclease in the reaction and the ascending temperature of reaction mixture limit the chew back length from 5' to 3'. As T5 exonuclease is heat-liable, it is then inactivated during the 50℃ incubation after accomplishing the desired DNA degradation.

**Reaction 2:** The 3' sequences of dsDNA are exposed after the complementary strain is chewed back by T5 exonuclease. The identical overlapping regions from A and B (yellow and pink) automatically anneal to each other.

**Reaction 3:** Phusion polymerase extend the chewed-back strains with high fidelity from the annealing points, matching the parental strains.

**Reaction 4:** After the DNA extension on both strains, two nicks are left behind. The DNA ligase in the reaction can ligate the nicks and completely join A and B together.

The same reactions are happening in the same tube between fragments and digested vectors at the overlap regions (v1 and v2, red and green). Thus, after step 2, a final product of vector with insertion A and B arranged orderly should be yielded.

Gibson assembly has rapidly becoming a popular choice in molecular cloning, especially when multiple long fragments (>3) are required to be ligated together. It is very time efficient where most of the reactions only take up to 1 hr, especially now New England Biolabs has commercialized a kit containing the pre-made master-mix with three enzymes and optimal buffers. This technique requires longer primers, making it more expensive than conventional approaches, and may increase the chance of synthesis errors, but the outcome is a much simpler workflow and higher efficiency. Up to now, most of the laboratories with well-established *P. aeruginosa* gene deletion protocols still

tend to adopt conventional digestion-ligation or SOE method. Hence, Gibson assembly methods can be an important alternative for large-scale gene deletion or novice researchers.

### 5.0.6 CRISPR-Cas9 for genome engineering

CRISPRs (clustered regularly interspaced palindromic repeats) was first described in 1987 as a series of short direct repeats interspaced with short sequences in the genome of *E. coli*[418] and was later detected in numerous bacteria and archaea[419]. It is now recognized that the RNA-guided enzyme Cas9 with CRISPR sequence consist of CRISPR-Cas9 system for bacterial adaptive immunity[420]. Recent advances in gene-editing using CRISPR-Cas9 have markedly improved the efficiency of precise engineering of the genomic DNA genome[421]. Originally discovered in prokaryotic cells as an adaptive immune system towards invading virus, it has now been widely adopted to edit the genome of mammalian cells since 2013[420]. However, only several studies have been reported to use CRISPR-Cas9 for editing genes in different bacterial species including *Escherichia coli*[422], *Streptococcus pneumoniae*[422], *Streptomyces* species[423], *Corynebacterium glutamicum*[424], *Bacillus smithii*[425], *Pseudomonas putida*[425], *Pectobacterium atrosepticum*[426], *Lactobacillus reuteri*[427] and *Mycobacterium tuberculosis*[428], of which CRISPR-Cas loci have been found in *E. coli*[429], *Streptomyces avermitilis*[430], *Pectobacterium atrosepticum*[431] and *M. tuberculosis*[432]. *P. aeruginosa* has its own CRISPR-Cas9 system that has been found to control bacteriophages resistance and virulence[433–435] and is controlled by quorum sensing[434]. Thus far, no report showed that an engineered CRISPR/Cas system can be used in *in vivo* genomic silence for *P. aeruginosa*, but there is potential for such application. Hence, CRISPR-Cas9 method is briefly reviewed as below.

In Fig 5.0.6.1, the functional CRISPR-Cas loci comprise a trans-activating crRNA (tracrRNA) coding region, a *cas* gene operon encoding Cas enzyme components, and a CRISPR array including some identical repeats intercalated with spacers. The spacers may have been derived from different bacteriophages inserting a foreign DNA fragment into the cells during invasions[420]. Hence, when the foreign DNA with the identical spacer sequence is acquired by bacteria, the precursor crRNA (pre-crRNA) is transcribed from the CRISPR array. With the facilitation by tracrRNA, the pre-crRNA is matured into individual crRNAs mediated by ribonuclease III and Cas9. Each crRNA is composed of one repeat and one spacer from the CRISPR array, which co-complex with a Cas9

protein using mature tracrRNA for binding and stabilizing. The specific Cas protein bearing the complementary spacer RNA to the invading DNA is then directed to the double strain cleavage of this foreign nucleic acid with RuvC and HNH[420].

This intrinsic system in bacteria can be adapted to a gene engineering tool by placing the artificial CRISPR-Cas loci onto a plasmid (Fig 5.0.6.2 A). The plasmid-borne CRISPR-Cas system contains a 20bp artificial spacers designed for any target genes as long as it is immediately upstream of a specific PAM site. The original dual tracrRNA:crRNA naturally generated by bacteria is engineered as a single guide RNA (sgRNA) that retains and links two essential portions: the 20-nucleotide sequence at the 5' end of the sgRNA that determines the DNA target site (artificial crRNA), and the scaffold structure at the 3' end of the sgRNA that binds to Cas9 (modified tracrRNA) (Fig 5.0.6.2 B). When transformed into prokaryotic cells or transinfected into mammalian cells, the cassette will enable the host to assemble the Cas9 complexes with the sgRNA that target the 20bp specific sequence on genomic DNA and generate a dsDNA break. After the detrimental dsDNA break on the genome, cells will either trigger DNA repair in an error-prone non-homologous end joining (NHEJ) pathway automatically, or induce a controlled DNA correction/insertion by using an additional DNA template for homology directed recombination (HDR) (Fig 5.0.6.2 C)[421]. Thus, a random or designed mutation is introduced.

A

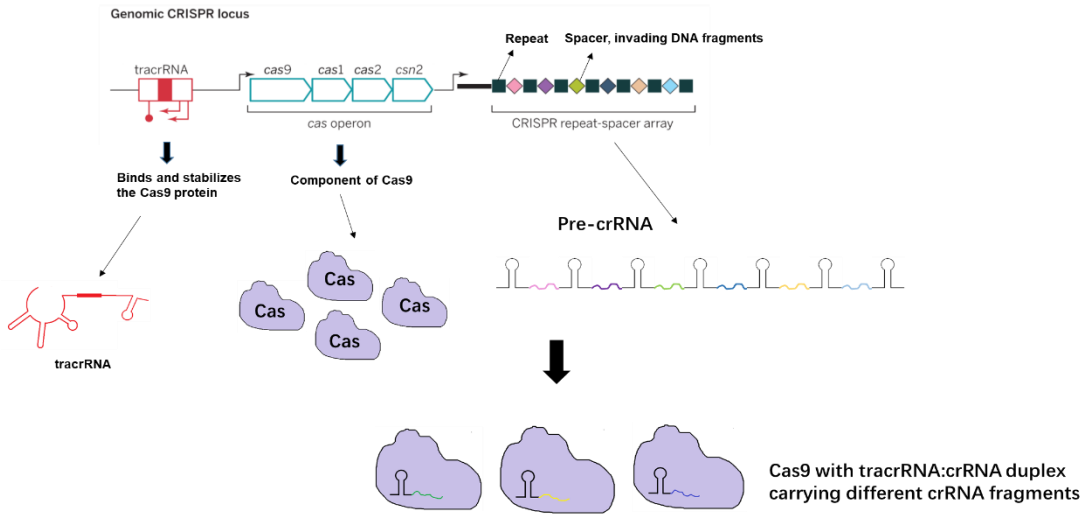

B

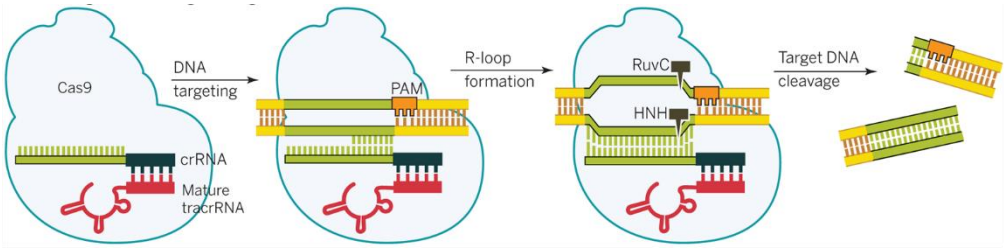


Fig 5.0.6.1 Schematic of natural CRISPR-Cas9 encoding loci (A) and its dsDNA cleavage function after matching to foreign DNA with the complementary sequence to crRNA (B). Figure adapted from Doudna *et al*, The new frontier of genome engineering with CRISPR-Cas9[420].

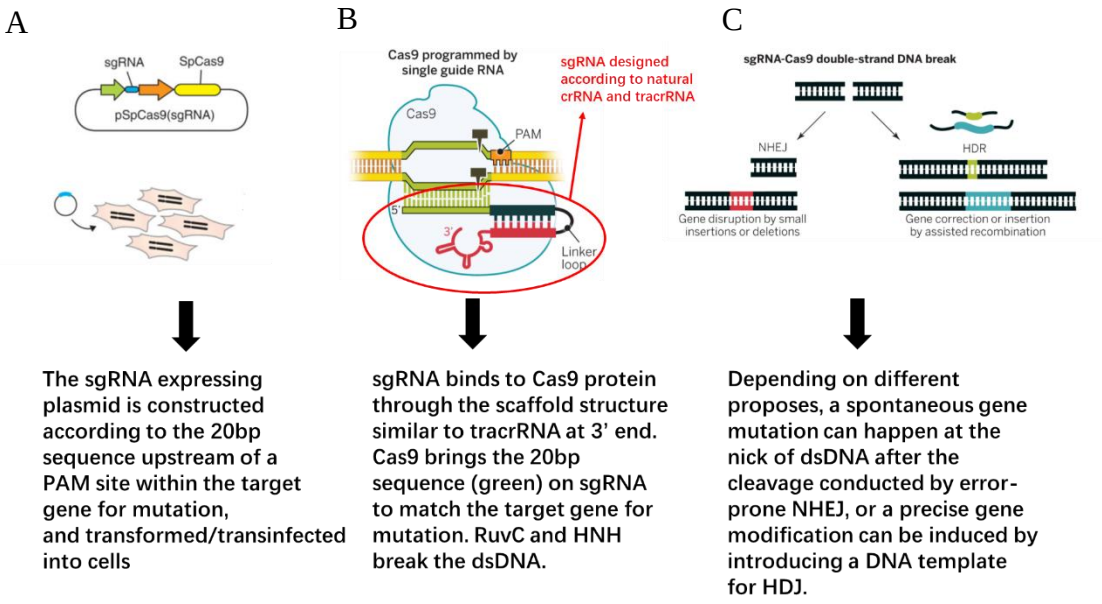


Fig 5.0.6.2 Schematic of CRISPR-Cas9 mediated genome engineering with plasmid-borne CRISPR-Cas9 cassette. Figures adapted from Ran et al, Genome engineering using the CRISPR-Cas9 system[421].

# Results

## 5.1. Modified method for generating recombinant construct in plasmids

Similar to SOE methods where upstream, downstream and resistance markers are ligated all in the same tube[311], I modified the conventional cloning protocols, enabling us to carry out all reactions in a single tube, as shown in Fig 5.1. The comparison of workflow between conventional methods to my modified efficient method is shown in Table 5.1.1. The advantages and drawbacks/challenges of different methods are listed in Table 5.1.2.

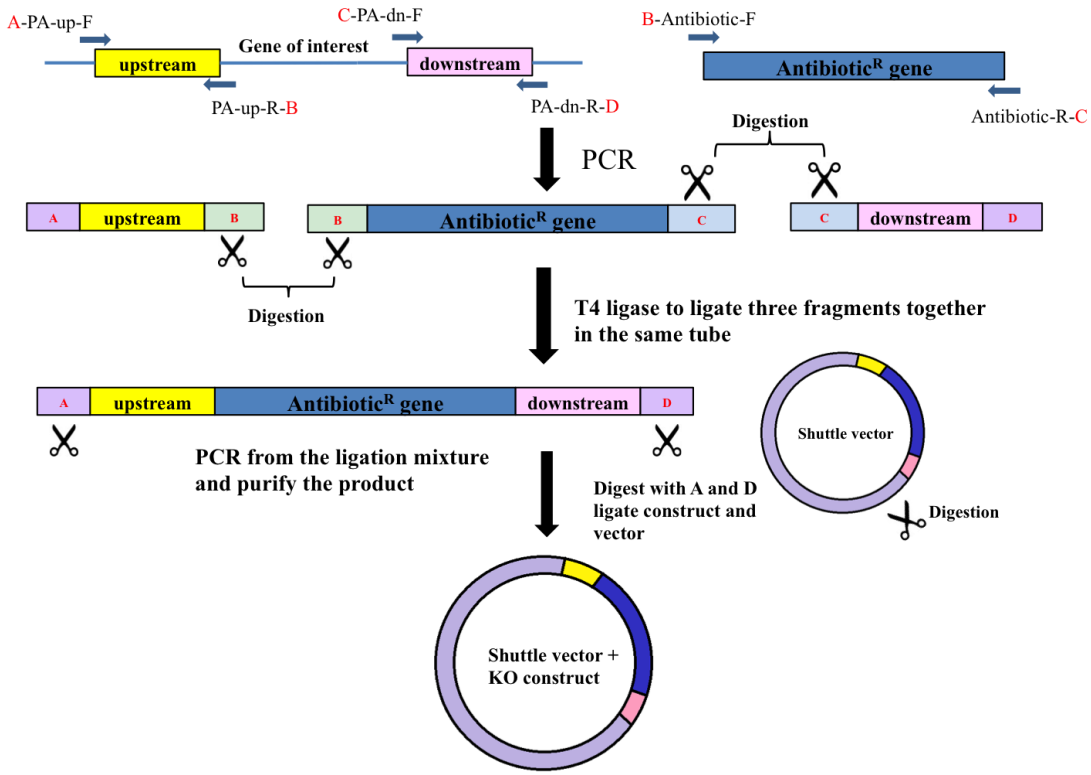


**Fig 5.1.** The modified KO method uses four different restriction sites A, B, C, and D in a three-ways ligation, followed by amplification of the resulting fragment and ligation into the target vector.

| | **Fig 5.0.4 A method 1** | **Fig 5.0.4 B method 2** | **Fig 5.0.4 C SOE** | **Fig 5.1 this study** |
|---|---|---|---|---|
| Preparation | Primer design, *P. aeruginosa* whole genome extraction, restriction enzymes (A, B and C) and T4 ligase purchase. | Primer design, *P. aeruginosa* whole genome extraction, restriction enzymes (A, B and C) and T4 ligase purchase. | Primer design, *P. aeruginosa* whole genome extraction, restriction enzymes (A and C) and T4 ligase purchase. | Primer design, *P. aeruginosa* whole genome extraction, restriction enzymes (A, B, C and D) and T4 ligase purchase. |
| Day 1 | PCR for 3 amplicons: (1) upstream with restriction sites A and B flanking at 5' and 3', (2) downstream with restriction sites B and C flanking at 5' and 3', (3) antibiotic$^{R}$ gene with restriction site B flanking. Check PCR products on gel. PCR products purification. Digestion of upstream fragment and vector with enzyme A and B. Ligation of upstream amplicon and vector. | PCR for 2 amplicons: (1) part/whole of target gene with **intrinsic restriction site B in the middle** and restriction sites A and C flanking at 5' and 3' (2) antibiotic$^{R}$ gene with restriction site B flanking. Check PCR products on gel. PCR products purification. Digestion of target gene and vector amplicon with A and C. Ligation of target gene amplicon and vector. | Two PCR cycles: 1$^{st}$ cycle for 3 separate amplicons: upstream, downstream and antibiotic$^{R}$ gene. 2$^{nd}$ cycle with **optimized** reaction conditions and primers annealing three parts together by denaturation, annealing and extension steps in PCR machine. Check PCR product on gel. PCR products purification. Digestion of annealed amplicon and vector with A and C. Ligation of amplicon and vector. | PCR for 3 amplicons: (1) upstream with restriction sites A and B flanking at 5' and 3', (2) downstream with restriction sites C and D flanking at 5' and 3', (3) antibiotic$^{R}$ gene with restriction site B and C flanking at 5' and 3'. Check PCR products on gel. Digestion of upstream fragment with enzyme A and B; downstream with C and D; antibiotic$^{R}$ gene with B and C. Ligation three amplicons together in one tube. |
| Day 2 | Transformation of vector into *E.coli* DH5α and incubate on antibiotic selective agar (1 antibiotic for correct vector backbone). | Transformation of vector into *E.coli* DH5α and incubate on antibiotic selective agar (1 antibiotic for correct vector backbone). | Transformation of vector into *E.coli* DH5α and incubate on antibiotic selective agar (2 antibiotic for correct vector backbone and inserted antibiotic$^{R}$ gene). | PCR the three-parts-ligated construct using primers with A and D from ligation mixture. Gel check PCR product. Digestion of the amplified amplicons and vector with A and D. Ligation of amplicon and vector. |
| Day 3 | Colony PCR check for the correct vector and vector extraction. | Colony PCR check for the correct vector and vector extraction. | Colony PCR check for the correct vector and vector extraction. | Transformation of vector into *E.coli* DH5α and incubate on antibiotic selective agar (2 antibiotic |

| | | | | |
|---|---|---|---|---|
| | | | | for correct vector backbone and inserted antibiotic$^{R}$ gene). |
| Day 4 | Digest the correct vector from Day 3 and downstream amplicon with B and C. Ligation of the amplicon and vector. | Digest the correct vector from Day 3 and antibiotic$^{R}$ gene with B. Ligation of the amplicon and vector. | Transformation of vector into *E.coli* S17-λ and incubate on antibiotic selective agar (3 antibiotic for correct vector backbone, inserted antibiotic$^{R}$ gene and *E.coli* S17-λ). | Colony PCR check for the correct vector and vector extraction. |
| Day 5 | Transformation of vector into *E.coli* DH5α and incubate on antibiotic selective agar (1 antibiotic for correct vector backbone). | Transformation of vector into *E.coli* DH5α and incubate on antibiotic selective agar (2 antibiotic for correct vector backbone and inserted antibiotic$^{R}$ gene). | Colony PCR check for the correct vector and keep the *E.coli* S17-λ stock strain with the correct vector. | Transformation of vector into *E.coli* S17-λ and incubate on antibiotic selective agar (3 antibiotic for correct vector backbone, inserted antibiotic$^{R}$ gene and *E.coli* S17-λ). |
| Day 6 | Colony PCR check for the correct vector and vector extraction. | Colony PCR check for the correct vector and vector extraction. | Conjugation between *E.coli* S17-λ and *P. aeruginosa*. Conjugants are incubated on *P. aeruginosa* isolation agar with antibiotic. | Colony PCR check for the correct vector and keep the *E.coli* S17-λ stock strain with the correct vector. |
| Day 7 | Digest the correct vector from Day 6 and antibiotic$^{R}$ gene amplicon with B. Ligation of the amplicon and vector. | Transformation of vector into *E.coli* S17-λ and incubate on antibiotic selective agar (3 antibiotic for correct vector backbone, inserted antibiotic$^{R}$ gene and S17-λ). | Potential *P. aeruginosa* mutants on agar are patched onto different selective agars for distinguishing single/double crossover homologous recombinants. | Conjugation between *E.coli* S17-λ and *P. aeruginosa*. Conjugants are incubated on *P. aeruginosa* isolation agar with antibiotic. |
| Day 8 | Transformation of vector into *E.coli* DH5α and incubate on antibiotic selective agar (2 antibiotic for correct vector backbone and inserted antibiotic$^{R}$ gene). | Colony PCR check for the correct vector and keep the *E.coli* S17-λ stock strain with the correct vector. | Colony PCR check for correct mutants and make stock culture. | Potential *P. aeruginosa* mutants on agar are patched onto different selective agars for distinguishing single/double crossover homologous recombinants. |

| | | | | |
|---|---|---|---|---|
| Day 9 | Colony PCR check for the correct vector and vector extraction. | Conjugation between *E.coli* S17-λ and *P. aeruginosa*. Conjugants are incubated on *P. aeruginosa* isolation agar with antibiotic. | Sequence confirm of *P. aeruginosa* mutants | Colony PCR check for correct mutants and make stock culture. |
| Day 10 | Transformation of vector into *E.coli* S17-λ and incubate on antibiotic selective agar (3 antibiotic for correct vector backbone, inserted antibiotic$^{R}$ gene and *E.coli* S17-λ). | Potential *P. aeruginosa* mutants on agar are patched onto different selective agars for distinguishing single/double crossover homologous recombinants. | | Sequence confirm of *P. aeruginosa* mutants |
| Day 11 | Colony PCR check for the correct vector and keep the *E.coli* S17-λ stock strain with the correct vector. | Colony PCR check for correct mutants and make stock culture. | | |
| Day 12 | Conjugation between *E.coli* S17-λ and *P. aeruginosa*. Conjugants are incubated on *P. aeruginosa* isolation agar with antibiotic. | Sequence confirm of *P. aeruginosa* mutants | | |
| Day 13 | Potential *P. aeruginosa* mutants on agar are patched onto different selective agars for distinguishing single/double crossover homologous recombinants. | | | |
| Day 14 | Colony PCR check for correct mutants and make stock culture. | | | |
| Day 15 | Sequence confirm of *P. aeruginosa* mutants | | | |

Table 5.1.1. The workflow comparison among different *P. aeruginosa* gene knockout methods. Here I assume all methods use conjugation and the same vector. With electroporation, the workflow can be much shorter by directly introducing vectors into *P. aeruginosa*. For unmarked deletion, *Flp*-FRT system can be incorporated into antibiotic$^{R}$ gene.

| | Fig 5.0.4 A method 1 | Fig 5.0.4 B method 2 | Fig 5.0.4 C SOE | Fig 5.1 this study |
|---|---|---|---|---|
| Advantages | Can delete nearly any fragment in frame. | Can delete nearly any fragment in frame. Much shorter workflow compared to method 1 with the same concept. | Can delete nearly any fragment in frame. The shortest workflow among all methods. | Can delete nearly any fragment in frame. Much shorter workflow compared to conventional methods 1 and 2 with the same concept. |
| Potential drawback/challenges | Laborious digestion, ligation and PCR check procedures. The longest workflow among 4 methods. | The target gene must have an intrinsic restriction site, while this site may not result in in frame deletion. Even with in frame restriction site, for multiple targets the enzymes needed are different, thus not being cost efficient. | The optimization of primers and PCR reaction annealing three parts together can be challenging, especially for multiple target genes, thus not being cost/time efficient for inexperienced researchers. | Three parts ligation efficiency relies highly on the quality of both restriction enzymes and ligase and may need optimization on DNA quantities/ratio. |

Table 5.1.2 The advantages and drawbacks/challenges of 4 gene deletion methods.

## 5.2. Acquisition of 14 mutant strains

In this project, 14 mutants (gene pa0285, pa0290, pa0338, pa0575, pa0847, pa0861, pa1181, pa1727, pa3311, pa4601, pa4959, pa5017, pa5442 that contain PAS-GGDEF-EAL domains and pa1423 that contains PAS) were required. Transposon mutants were acquired by purchasing from a transposon mutant library and deletion mutants were generated by KO using my modified method as shown in Fig 5.1.

### 5.2.1. PCR confirmation of purchased transposon mutants

Due to the fact that transposon attack normally results in more than one insertion per gene (named as PAXXXX A, B or C), 29 Tn mutants for the 14 genes of interest were purchased from the University of Washington *P. aeruginosa* mutant library. One gene specific primer and one transposon-specific primer for each mutant strain genome and WT genome were used to confirm the correct insertions. After PCR, correct mutants should produce a band (left lane) on the gel while WT should not produce any band (right lane). Primers are listed in 2.2 and PCR was done as described in 2.7.2.

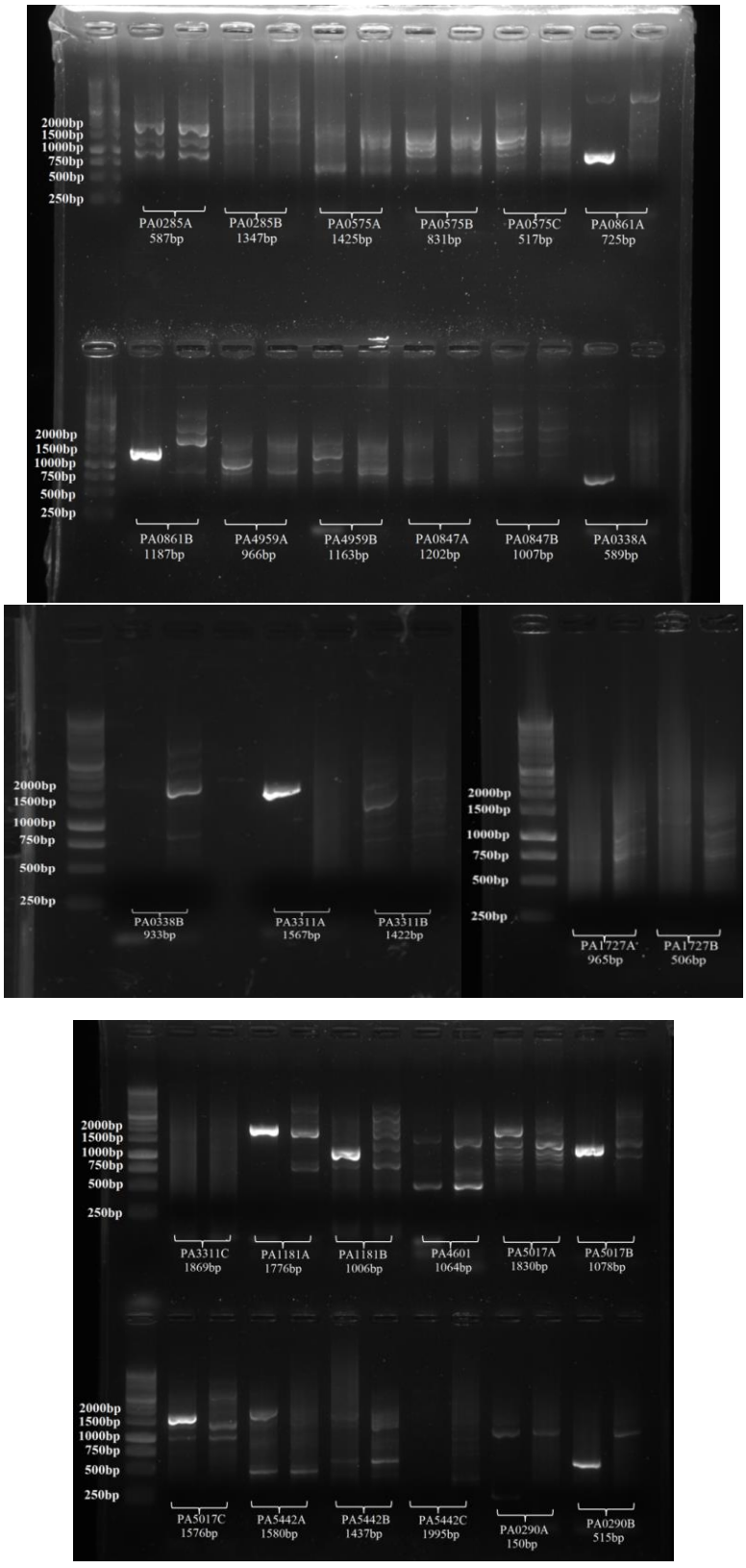


Fig 5.2.1. PCR results for transposon mutants from the University of Washington Library. Within each candidate genes labelled, left lane represents the PCR product amplified from mutant strains genome, right lane represents PCR product amplified from WT genome (negative control).

According to the PCR results, only some of the mutant strains were confirmed to contain the correct transposon insertion including *ΔTn0861A, ΔTn4959A, ΔTn0338A, ΔTn3311A, ΔTn1181A, ΔTn5017C, ΔTn5442A, ΔTn0290B.*

### 5.2.2. *P. aeruginosa* PAO1 gene knockout using the modified vector construction method

Knockout of the pa4601 gene is used here to illustrate the protocol shown in Fig 5.1. Gentamicin resistant gene (*aaaC1*) was chosen as marker and suicide vector pEX100T was chosen for delivery into *P. aeruginosa*[299]. I have used SmaI for restriction sites A and D, EcoRI for restriction site B, and HindIII for restriction site C in Fig 5.1 for constructing the KO vectors. The upstream, downstream and Gm cassette resistance gene (containing ribosome binding site and native promoter) were amplified by routine PCR as described in 2.7.2. PCR products were shown in Fig 5.2.2.1 A. All purified and digested PCR products were subjected to three way sequential ligation in a single reaction as described in 2.7.7 and 2.7.8. The ligation product was re-amplified by a second PCR cycle using the upstream forward and downstream reverse primers, and a product of correct length of 1637 bp was identified in agarose gel electrophoresis as shown in Fig 5.2.2.1 B. After digestion of vector and PCR product with SmaI, the insert was blunt-end ligated into the vector as described in 2.7.9. Vectors resulting from ligation were transformed into *E. coli* DH5α, and resistance selected colonies were subjected to plasmid extraction. Plasmids were then checked by restriction digestion with (1) EcoRI and HindIII for Gm and (2) SmaI for the KO fragment as shown in Fig 5.2.2.1 C.

Positive plasmids were transformed into *E. coli* S17-λ for conjugation with *P. aeruginosa* PAO1 through filter-mating as described in 2.9 and 2.10. Conjugates were plated onto cetrimide agar with 30μg/ml gentamicin to eliminate *E. coli* and select both single and double crossover Δ*pa4601* strains. When only single-crossover event happens generating merodiploids, only PA-up or PA-dn exchange with gene of interest and the whole vector integrates into the chromosome for expressing the sacB and $Amp^R$ genes on the backbone. When double-crossover event happens, both PA-up and PA-dn exchange with original gene replacing the middle part with $Gm^R$ while the plasmid cannot copy into the daughter cell, thus creating the successful deletion. To distinguish single and double crossover mutants, 10% (w/v) sucrose was infused into cetrimide agar

to kill merodiploids due to the presence of *sacB* gene. While sucrose-resistant merodiploids may also arise from mutation in the *sacB* gene[436], all colonies were also patched onto cetrimide agar with 10% (w/v) sucrose and cetrimide agar with 400μg/ml carbenicillin as shown in Fig 5.2.2.1 D. Colonies that grew on sucrose plates but not carbenicillin plates showed that *sacB* gene and $Cb^R$ gene on the plasmid backbone were not integrated into chromosome and expressed, thus eliminating the potential of merodiploids. PCR was used to confirmed the colonies. As shown in Fig 5.2.2.1 E, when using the WT DNA as template, the PCR product of the whole *pa4601* gene was seen (4268bp); when using Δ*pa4601* DNA as template, part of the original gene between allelic exchange positions in PA4601-up and PA4601-dn was replaced by Gm, and hence the PCR band was smaller (1637bp).

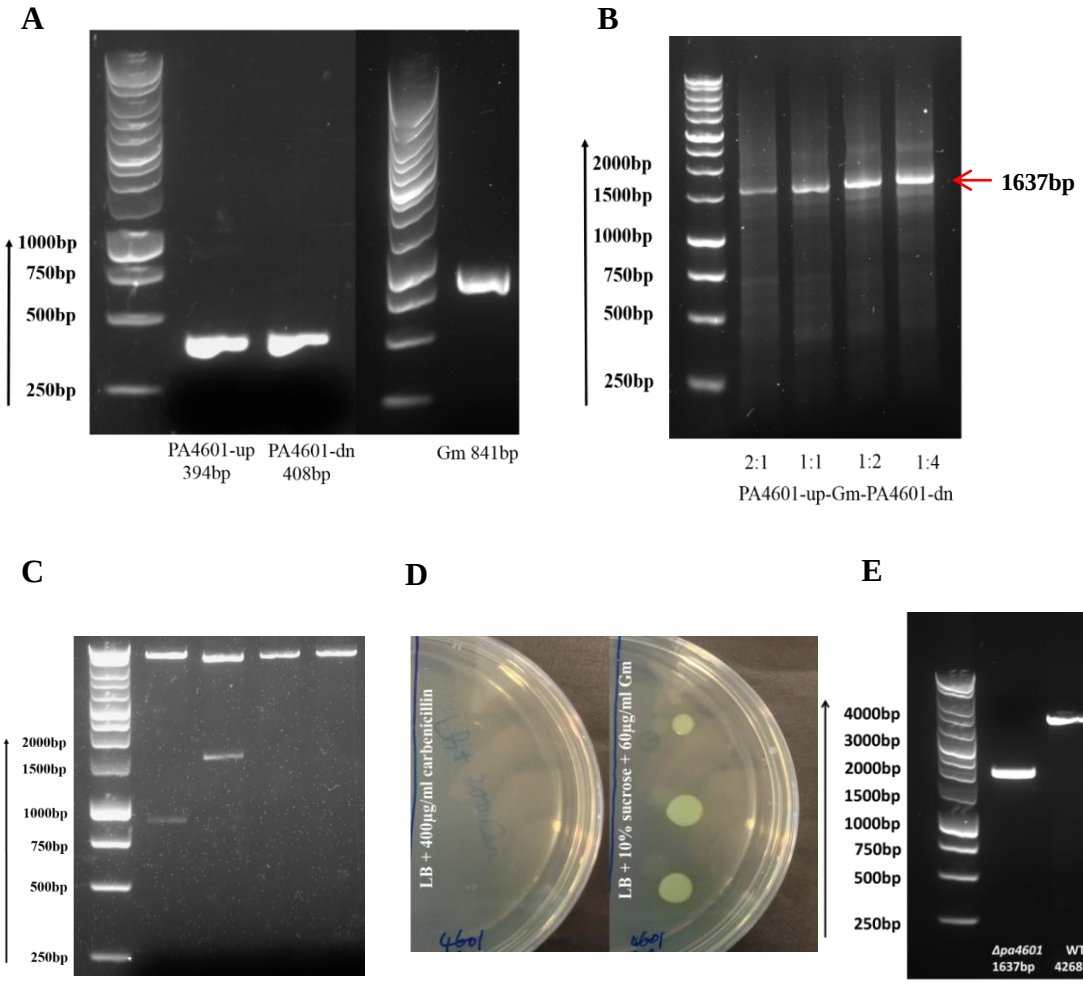


**Fig 5.2.2.1. Generation of the pa4601 deleted mutant. A.** PCR amplification of upstream and downstream fragments, as well as the Gm resistance cassette. **B.** PCR amplification of the three-ways ligation product from A, from ligation mixtures with different fragment ratios (upstream/downstream

fragments *vs.* Gm cassette). **C.** Digestion of purified plasmids. Lane 1: marker; lane 2: EcoRI and HindIII digest excising the Gm cassette; lane 3: SmaI digest excising the entire fragment; lane 4: control digest of pEX100T with SmaI; lane 4: control digest of pEX100T with EcoRI and HindIII. **D.** Potential mutant colonies patched onto carbenicillin and onto sucrose/gentamycin agar plates. **E.** PCR confirmation showing deleted pa4601 gene (lane 2) and WT pa4601 gene (lane 3).

The same procedures were applied to all other 13 genes and 2 PCR runs were done to compare the same gene in corresponding mutants and WT. By using SeqPAXXXX-F and SeqPAXXXX-R (XXXX as gene number) as primer pairs, the deleted genes in mutants and the original genes in WT should present bands of different lengths.

**A**

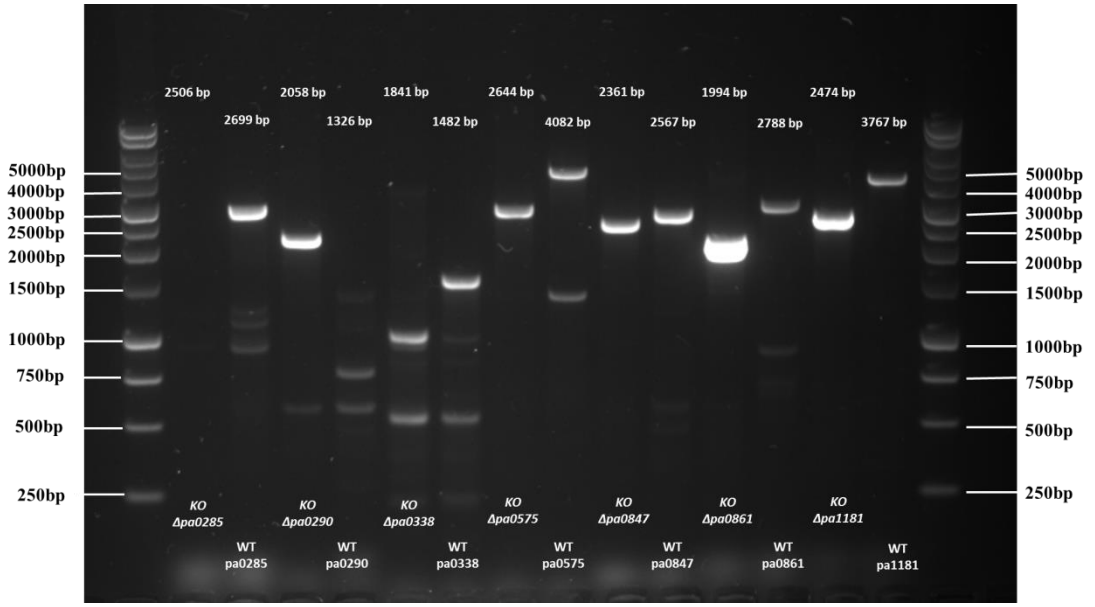


**B**

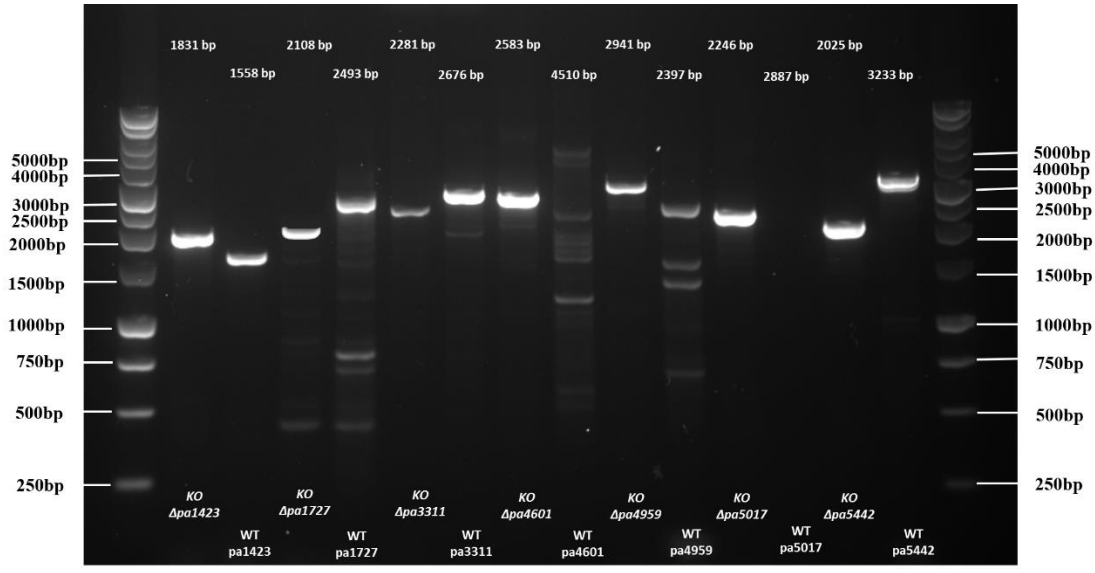

**C**

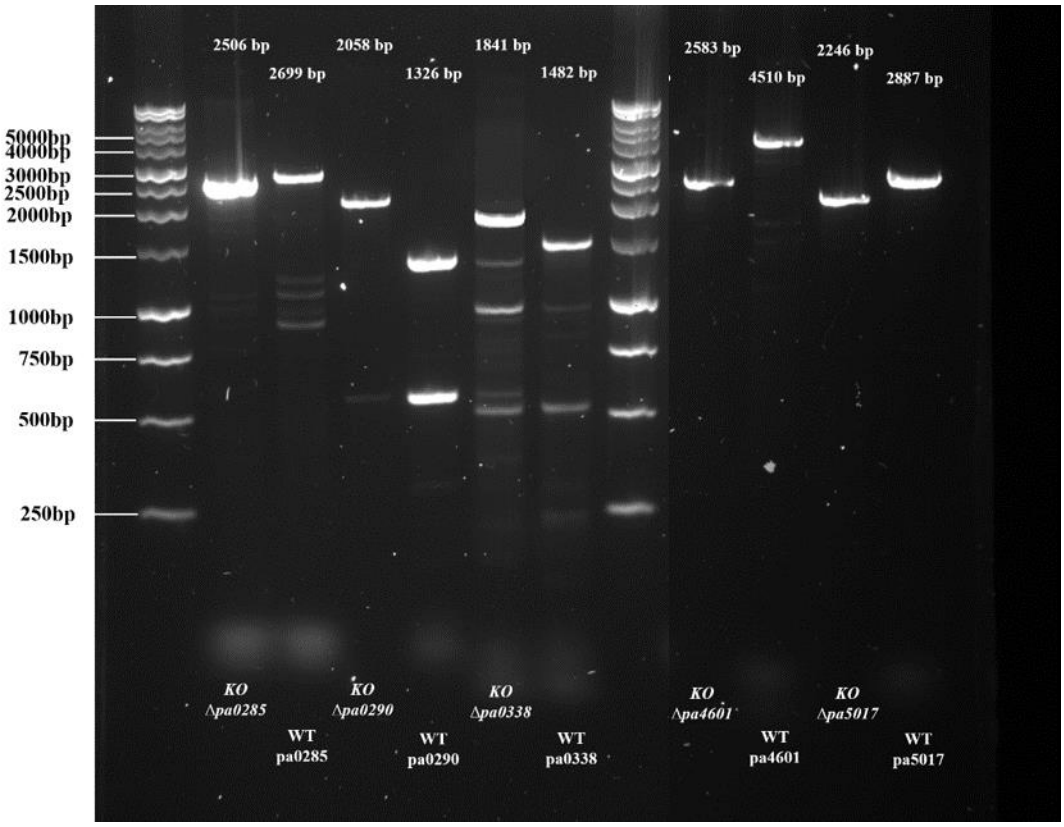


Fig 5.2.2.2 PCR products from KO mutants and WT using the same primer pair SeqPAXXXX-F and SeqPAXXXX-R. PCR products using mutant strain genome DNA as template are shown as KO Δ*paXXXX*, PCR products using WT genome as template are shown as WT paXXXX. The expected product lengths are marked above each lane. (A) and (B) were the first PCR trial. pa0285, pa0290, pa0338, pa4601 and pa5017 did not show expected bands, so the second PCR trial was conducted and the results are shown in (C)

All the mutants were checked by PCR comparing the bands using mutant and WT genome DNA as templates. As shown in Fig 5.2.2.2 (A) and (B), most of the Δ*paXXXX* and paXXXX showed different lengths. pa0285, pa0290, pa0338, pa4601 and pa5017 did not show expected bands either in KO mutants or WT in the first PCR attempt, therefore, a second round PCR was carried out and the results are shown in Fig 5.2.2.2 (C). Multiple bands might have come from unspecific primer binding, but no multiple bands on the gel showed a paXXXX band occurring in the corresponding Δ*paXXXX*, proving the loss of original genes and the purity of the KO strains. SeqPAXXXX-F and SeqPAXXXX-R were used as primer pairs and the products were subjected to sequencing.

# Discussion

### Step-wise protocol of novel method compared to laborious traditional 'cut and paste' method

Despite the mature gene knockout methods in *P. aeruginosa* developed in the past decades, most of the conventional protocols published for vector construction in various papers can be described as Fig 5.0.4 (A) and (B). In Fig 5.0.4 (A), the ligation of PA-up, PA-dn and antibiotic resistance gene are done by multiple rounds of digestions and ligations sequentially between DNA fragments and vectors, thus transformation and plasmid extraction are required every time for checking correct ligations. Method in Fig 5.0.4 (B) is a variation from (A) and seems easier, but it requires the target gene to have at least one restriction site within the whole sequence and the insertion into this site to not cause a frameshift. In a project similar to this one, where a large number of knockout mutants need to be done, it would be very laborious for the researchers, adding up all the PCR, digestion and ligation steps in method (A). Method (B) may not even be approachable in many genes and even if approachable, a variety of restriction enzymes may be involved and it is not economical. Compared to these two well-established methods, the digestion and ligation of all DNA fragments involved can be done at the same time using the modified method decribed here with the transformation into *E. coli* and plasmid extraction needed only once. Besides, the confirmation of successful construct and transformation requires agar plates containing two antibiotics for the marker on the backbone of the vector and within the construct, thus raising the accuracy for positive selection.

### Worry-free PCR protocols in our novel method compared to SOE

SOE method in Fig 5.0.4 (C) has much higher requirements on the primer design and PCR cycle condition optimization than normal PCR to new researchers. In some cases, the design of primer can be constrained by the target sequences, especially when the gene to be knocked out is relatively short and the options are limited. For example, there should not be secondary loop structure formed between the extended tag and main primer sequences while the rules on Tm (Tm of A, B', B and C should all be close), frameshift (no frameshift should exist after deletion) and restriction sites (no restriction site of A and C should exist in two fragment amplified) should also be followed. Therefore, non-optimal primers might result in no amplification products or nonspecific

amplification products[437]. Also, when deleting a large number of genes, the optimal primer Tm and PCR conditions might all be different, thus a large number of PCR cycles and optimizations are needed. Furthermore, the primers used for SOE are normally longer than normal PCR so that the prices are much higher to purchase.

Normally when generating *P. aeruginosa* knockouts, antibiotic resistance genes are included in the constructs for positive selection at least in the first a few steps. Whether this antibiotic resistance gene cassette is excised later or not is dependent on the purpose. If using SOE, two pairs of primers should be designed to meet SOE requirements and anneal two fragments and antibiotic resistance gene in the same tube as described previously[311], resulting in even more difficulties in optimising PCR conditions. Compared to SOE, the requirements on primer design and PCR conditions are much lower in this modified method. All the primers only need to meet the normal criteria for PCR primer design with the addition of enzyme cutting sites to the 5' ends. The PCR runs only need to follow the standard manufacturers' guidance and troubleshooting. There is no need for further optimization of specific DNA amount and annealing temperature in PCR runs, which are critical in a successful SOE as the denatured DNA fragments themselves serve as single primers. For deletion of multiple genes, the primers for all genes can be easily designed with similar Tm and the same restriction site tags. The length of all PA-up and PA-dn can be designed within the same range so many tubes of PCR reaction for PA-ups and PA-dns from different genes can be done at the same time with the same PCR cycle. Besides, because all the PA-up and PA-dn have the same restriction site tags, digestion and ligation steps for annealing three parts together can also be done at the same time. Thus, compared to potential multi-time optimizations in SOE for different genes, this modified method is more straightforward and time-saving when multiple genes need to be done. The only step that needs optimization is the template amount for final amplification of the PA-up-Gm-PA-dn construct, i.e, the amount of ligation mix put into PCR system in Table 5.1.1 day 2. Since the efficiency of T4 ligase varies, the amount of successful ligation as useful template in PCR is difficult to predict. Thus, the quality of restriction enzymes and T4 ligase is crucial for successful ligation of three parts together in one step.

**Alternative choices of suicide vectors and the drawbacks of the modified method**

pEX100T was adopted in this modified method and SmaI was chosen as the ligation site for construct and the vector. Hoang *et al* developed some variants of pEX100T containing MCS and cohesive end cutting sites, which are recommended for the ligation of vector and construct[299]. The option of EcoRI and HindIII were based on the fact that they produce cohesive end cutting sites and HF-EcoRI and HF-HindIII (High-fidelity with reduced star activity) are approachable. Other HF restriction endonucleases can also be chosen for the tasks with the only requirement being these two enzymes should not have corresponding cutting sites anywhere within the rest of vector backbone and the DNA fragments amplified by PCR. HF cohesive end restriction enzymes are always recommended to increase the efficiency of digestion. Despite Choi *et al* developing a gateway system[311], it did not show obvious advantages for deleting genes in one strain. Instead, it introduces more intermediate vectors hence was not applied here. Many studies deleted the antibiotic resistance gene marker after the successful double crossover recombination by using *Flp*-FRT system due to the potential polar effect. Here the Gm marker in mutants was kept for positive selection in later subculture procedures since it was reported that Gm insertion does not create polar effect to downstream genes during gene disruptions[438,439].

In many cases, an unscarred deletion mutant is required when the antibiotic resistance genes cause polar effects or multiple deletions are desired. One of the most frequently used methods is *Flp*-FRT system, which can be infused into antibiotic resistance gene cassette for excision after the confirmation of correct mutants[311]. Hmelo *et al* extensively described a detailed protocol for generating seamless and unscarred deletion mutants without introducing antibiotic resistance gene and *Flp*-FRT system by using SOE[436]. However, using all the conditions given in that protocol, even in experienced hands only ~50% colonies were genuine mutants while the rate is very dependent on the experimental procedures. For novice researchers, large-scale colony PCR may be required to distinguish WT and mutants. Thus, each method for generating deletion mutant has its own benefits and drawbacks shown in Table 5.1.2 and the choices are largely dependent on the purpose and accessibility. My modified method provides a reliable and straightforward way to generate a large number of deletion mutants when seamlessness is not one of the expectations and is particularly useful when the difficulties in optimising SOE are present.

# Chapter 6 – Phenotypic analysis of 14 putative NO-sensing genes in *P. aeruginosa* PAO1 c-di-GMP signaling network

## 6.0. Introduction

Intracellular levels of c-di-GMP strongly influence biofilm characteristics, including cell morphology, motility control, EPS production and cell cycling. Diguanylate cyclase (DGC, GGDEF domain) and phosphodiesterase (PDE, EAL and HD-GYP domain) are responsible for the synthesis and hydrolysis of c-di-GMP, respectively. As many as ~1/3 of all GGDEF domains and ~2/3 of all EAL are found in tandem in all bacterial and archael genera (https://www.ncbi.nlm.nih.gov/Complete_Genomes/c-di-GMP.html)[153]. Kulesekara *et al* reported that PAO1 encodes 17 different proteins with a DGC domain, 5 with a PDE domain, and 16 that contain both of these domains as a fusion (DGC-PDE)[440]. These tandems are frequently found downstream of a sensor domain that transmit environmental cues to these two domains regulating their activities.

### 6.0.1 Genes targeted in this study

As the aim of this study is to reveal through which protein(s) NO modulates intracellular c-di-GMP, the proteins with both sensor domains that potentially bind NO and c-di-GMP modulating domains were therefore selected for investigation. PAS and MHYT domains were chosen as putative NO sensor domains with haem and copper binding sites respectively, despite the function of PAS not being constrained to NO sensing. *In silico* analysis showed that in PAO1, 13 proteins contain both PAS/MHYT and GGDEF and or EAL/HD-GYP domains. Moreover, a protein BdlA that only contains PAS and MA domains was reported to link between sensing environmental cues, c-di-GMP levels and biofilm dispersal[296,441,442]. Therefore, BdlA was also knocked out due to its potential NO sensing ability and its regulation on intracellular c-di-GMP despite the absence of GGDEF/EAL. The KO mutants were then subjected to phenotypic analysis to determine their functions in *P. aeruginosa*. Protein structures and enzymatic activity prediction of these 14 candidates are shown in Figure 6.0.1 using Universal Protein Resource (UniProt) and Simple Modular Architecture Research Tool (SMART).

Some of the candidate genes were named in previously published papers: pa0861 (*rbdA*)[272], pa1181(*yegE*)[208], pa1423(*bdlA*)[443], pa1727(*mucR*)[147], pa3311(*nbdA*)[146], pa4601(*morA*)[404], pa4959(*fimX*)[444], pa5017(*dipA*)[445], of which pa1727 and pa3311 contain MHYT instead of PAS. Here, analysis of biofilm-related phenotypes thought to be regulated by c-di-GMP levels were carried out for the 8 Tn mutants and 14 KO mutants, including (1) direct *in vivo* c-di-GMP level detection; (2) growth curves (cell division cycle); (3) biofilm dispersal with NO; (4) motility (swimming, swarming and twitching) and (5) EPS production.

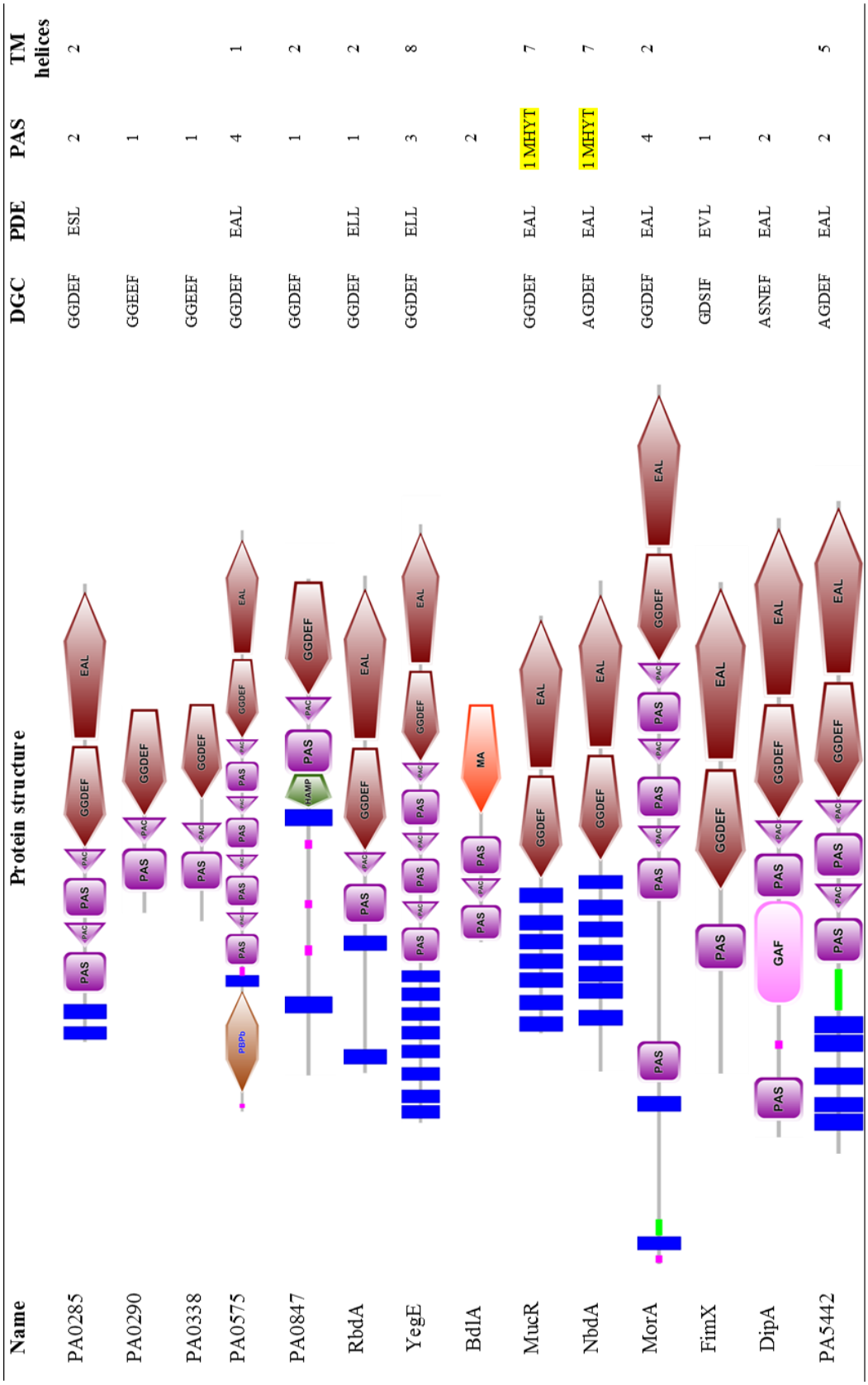


Fig 6.0.1 Protein structures, GGDEF/EAL sequences, the amount of PAS/MHYT domains and transmembrane (TM) helices (blue rectangles) of 14 putative c-di-GMP regulators with NO sensing function.

### 6.0.2 Direct *in vivo* quantification of intracellular c-di-GMP

Two methods are frequently used to determine intracellular c-di-GMP levels in *P. aeruginosa*, including HPLC for whole cell extracts[446] and GFP reporter plasmids with a c-di-GMP responsive promoter[300,447]. HPLC results distinguish c-di-GMP from the whole cell substance and give absolute amount of c-di-GMP in the cells, but the extraction procedures and reagents may cause drastic changes in the global c-di-GMP level[446]. GFP reporter plasmids (PcdrA::*gfp*) were constructed by Rybtke *et al* transcriptionally fusing the cyclic di-GMP-responsive cdrA promoter to GFP genes[300]. As a result, it can only indicate the relative c-di-GMP levels by detecting fluorescence signals rather than calculating the exact concentrations. However, reporter method does not involve disrupting the cell integrity or the addition of reagents so can reveal the real-time c-di-GMP amounts. In this study, GFP reporter was used for real time *in vivo* c-di-GMP gauging in 14 KO mutants and PAO1 WT planktonic cells. NO was also added to the cell culture for observing c-di-GMP level alteration.

### 6.0.3. Cell growth and colony morphologies

c-di-GMP was reported to be related to cell cycle in *C. crescentus*, and the conclusion was c-di-GMP promoted cell cycle progression[345]. So far, no further research reported the relationship between intracellular c-di-GMP and cell cycle in *P. aeruginosa,* which is worth looking into for the importance of cell growth in biofilm formation. Wrinkly colony morphology was found in Pel overexpressed PAO1, and it was well established that *pel* transcription is closely linked to c-di-GMP level[448]. Hence, growth curves of 14 KO strains were compared to WT and their colony morphologies were observed for their potential links to Pel and intracellular c-di-GMP levels.

### 6.0.4. Biofilm dispersal in the presence of NO

NO was reported to be both inhibiting biofilm formation and triggering dispersal of pre-established ones through reducing intracellular c-di-GMP levels[242]. The potential mechanism was proposed where NO binds to NO sensors (PAS or MHYT in this study) located upstream of/in contact with DGCs and PDEs modulating their enzymatic activities, thus changing intracellular c-di-GMP level and biofilm phenotypes. If this hypothesis is correct, at least one of the DGC/PDE candidates chosen in this study should be serving as a NO sensor and triggering c-di-GMP turnover. When this protein

is lost, it will diminish the effect of NO on decreasing intracellular c-di-GMP. To achieve NO induced c-di-GMP level changes *in vivo*, two possible mechanisms are proposed as shown in Fig 6.0.4. If the protein serves as DGC and the addition of NO impairs its activity, this DGC should be highly active *in vivo* so that its inactivation would drastically reduce intracellular c-di-GMP level. If the protein serves as a PDE and the addition of NO activates this PDE, this PDE may be either non or low activate *in vivo*, as the activation/enhancement of its activity causes a drop in intracellular c-di-GMP. In this study, 250μM S150 as suggested in chapter 3 was applied to pre-established biofilms of 14 KO strains and the biofilm reduction percentages were compared to WT. Data were also analysed along with *in vivo* c-di-GMP determination results to reveal the link between NO sensing, c-di-GMP level alteration and biofilm dispersal in these KO strains.

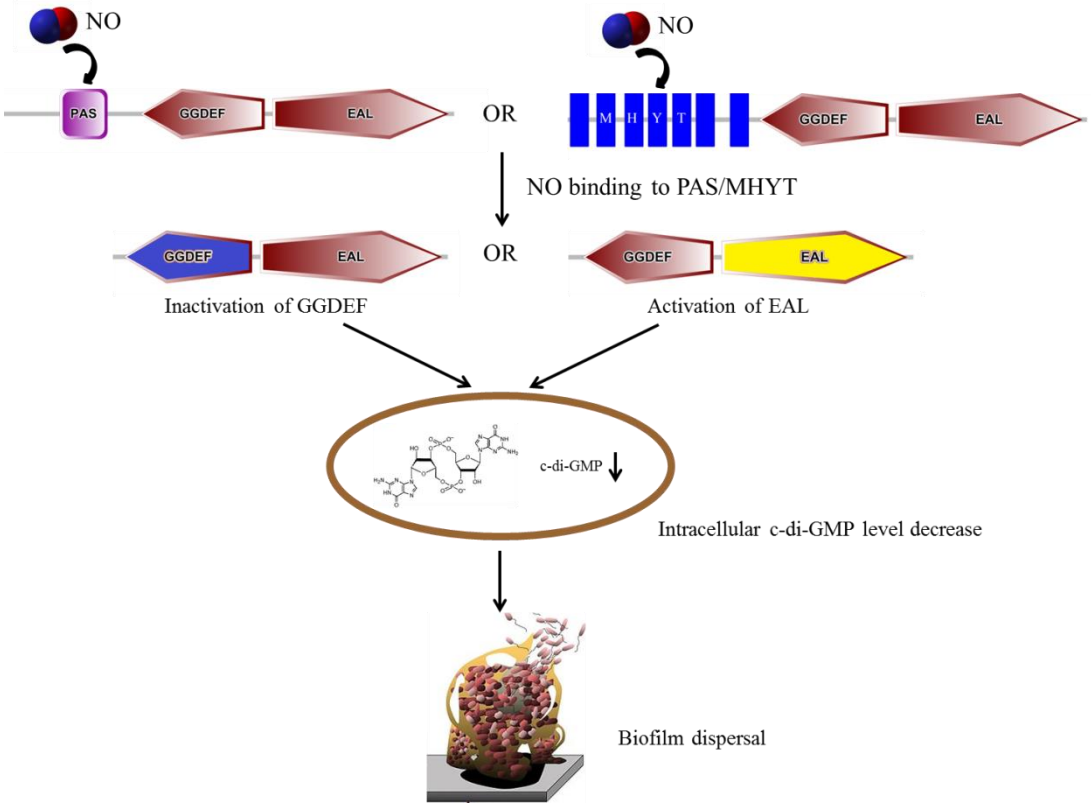


Fig 6.0.4 Two possible mechanisms of NO induced c-di-GMP turnover *in vivo*

## 6.0.5. Motility

Swimming motility is a mode of bacterial movement powered by rotating flagella that takes place as individual cells move in liquid environments, such as 0.3% agar where all

the porous gaps are filled with water[449]. Twitching motility is surface motility powered by the extension and retraction of type IV pili that confers slow cell movement, such as at the bottom of a petri dish with nutrient agar above to supply growth condition[449]. Swarming motility is multicellular bacterial surface movement powered by rotating flagella[449]. Although both powered by rotating flagella, swimming motility in *P. aeruginosa* is a unicellular behaviour that only requires a single polar functional flagellum and can move as few as a single cell, while swarming occurs in multicellular groups that requires coordinated bulk movement. Additionally, the number of flagella on the cell surface can increase during the transition from swimming to swarming. Some species such as *Rhodosprillum centenum* must form multiple peritrichous flagella to conduct swarming when single polar flagellum is sufficient for swimming, while *P. aeruginosa* that swims with a single polar flagellum may produce two polar flagella when swarming[449]. Peritrichous flagella produced by some species during swarming bundle together when they are rotating to increase flagellar stiffness and make force generation more efficient in viscous liquids, while species incapable of producing peritrichous flagella such as *P. aeruginosa* synthesizes an alternative motor specifically required to propel movement on surfaces and through viscous environments[449].

The bulk coordination and additional flagella synthesis controlled by gene expression suggested that apart from the alteration of flagella movement triggered by different viscosities, cell signalling might also be involved in swarming events compared to swimming. Previous reports have demonstrated links between QS signalling[450] and c-di-GMP level[451,452] to swarming behaviour in *P. aeruginosa*. Two proteins that significantly alter intracellular c-di-GMP levels, SadC (DGC) and BifA (PDE), were found to regulate SadB which modulates flagellar reversal rates and affects swarming[218,219,453]. MotAB and MotCD participating in the rotation of *P. aeruginosa* single polar flagellum were linked to c-di-GMP level[216]. MotCD stator is responsible for driving swarming motility and MotAB stator is unable to support swarming. When c-di-GMP level increases, MotAB displaces MotCD from the motor, which in turn promotes the interaction between MotA and FliG, resulting in the repression of swarming[216]. Furthermore, Barraud *et al* proved that the addition of SNP decreased intracellular c-di-GMP level and increased the swarming zone in *P. aeruginosa*[9]. Apart from flagella, several reports also linked Type IV pili (TFP) to swarming patterns[454,455].

However, the role of TFP in swarming and whether the behaviour of pili gene/protein is influenced by c-di-GMP remain unknown.

The best-established relationship between DGC/PDE and twitching motility of PAO1 was through FimX. Huang *et al* first highlighted the involvement of FimX in twitching motility in response to environmental signals[226]. Absence of FimX results in pilus assembly defect, with the surface pilin expression markedly reduced but whole cell pilin remains unchanged[227]. FimX contains PAS-REC-GGDEF-EAL, of which both GGDEF and EAL domains are essential to FimX functions but only PDE activity was presented *in vitro*[228]. However, Jain *et al* found deleting FimX did not influence intracellular c-di-GMP level and FimX is only required for the assembly of pili when intracellular c-di-GMP level is low, while this demand is bypassed if intracellular c-di-GMP level increases[227]. The authors proposed that due to the high-affinity of FimX EVL for c-di-GMP, FimX can promote TFP assembly when intracellular levels of c-di-GMP are low[456]. All these suggested that FimX might not be regulating twitching through altering intracellular c-di-GMP level, but instead its function *in vivo* is influenced by intracellular c-di-GMP. Residues within FimX REC domain are in charge of localizing FimX to the pole as well as the localization of type IV pili at cell surfaces, while the enzymatic activity further restricts FimX to a single pole[444]. This specific localization and the existence of sensor PAS domain suggested the potential models where FimX responses to environmental stimuli and alters twitching through changing localized c-di-GMP pool[227], or the environmental stimuli changes intracellular c-di-GMP through other proteins but affects FimX function locally.

Although c-di-GMP is found to bind to specific receptors that interact with flagella rotor proteins and control the swimming direction in enteric bacteria *E. coli* and *S. enterica*[153,214,215], up to now, no clear mechanism was revealed for the regulation of c-di-GMP on swimming motility in PAO1. Petrova *et al* reported that inactivation of DipA which showed PDE activity significantly reduced the swimming zones[457]. An *et al* reported a reduced swimming motility of Δ*rbdA*[272] with the protein showing PDE activity as well. However, the link between these two proteins and swimming motility cannot confirm a direct link between intracellular c-di-GMP level and swimming pattern as the alteration might be due to gene specific regulation.

In this study, all these three types of motility assays were performed on PAO1 KO strains. Along with the *in vivo* c-di-GMP level quantification, it is possible to provide more information on the relationship between intracellular c-di-GMP level and motility, as well as discover more proteins involved in the regulation apart from previous reported.

### 6.0.6. EPS production

Most frequently found components in *P. aeruginosa* EPS include polysaccharides, proteins and eDNA[10]. Other molecules such as rhamnolipids also contributes to EPS and participates in initial microcolony formation, surface-associated bacterial migration, formation of mushroom-shaped structures, preventing colonization of channels and biofilm dispersion[458].

Although three types of polysaccharides including alginate, Pel and Psl were found in *Pseudomonas aeruginosa* strains, the alginate gene is found abundantly in mucoid strains but not in PAO1 laboratory strain[459]. PAO1 has two loci expressing both Pel and Psl as its EPS components[230,460,461]. Pel is a glucose-rich polysaccharide of which the detailed chemical structure has not been elucidated thus far, whereas Psl consists of a repeating pentasaccharide unit containing D-mannose, D-glucose and L-rhamnose[458,462].

Ueda *et al* and Lee *et al* reported that c-di-GMP stimulated EPS production in PA14 through increasing *pel* expression, and Hickman *et al* further proved that c-di-GMP regulated *pel* transcriptionally through FelQ as a c-di-GMP binder in PAO1[233]. Whitney *et al* reported that PelD is a c-di-GMP receptor that is involved in exopolysaccharide assembly[197]. With lots of evidence showing a clear regulating relationship between c-di-GMP and Pel, however, Colvin *et al* reported that c-di-GMP was a poor indicator of Psl[230].

Apart from polysaccharides, a vast array of proteins also make up of a considerable amounts of EPS component on a mass basis[458], of which enzymes and structural proteins are the two major categories. Most of the enzymes detected in EPS are involved in biodegradation of biopolymers to low-molecular-mass products that can then be taken up and utilized as carbon and energy sources, or further degrade structural EPS to facilitate dispersal procedure[458]. Other enzymes act as virulence factors during infectious processes. These extracellular enzymes can be efficiently retained in the biofilm matrix by interacting with polysaccharides which enhances the thermostability[458]. The structural proteins in the matrix include cell surface-associated and extracellular

carbohydrate-binding proteins (lectins) for crosslinking and structural stability of EPS. As c-di-GMP is involved in regulation of transcription and translation, it is logical to suspect that c-di-GMP level can be linked to some protein expression before their secretion into extracellular matrix. Borlee *et al* reported that CdrA is expressed in response to high c-di-GMP, e.g. in biofilms, which contributes to biofilm structural integrity by maintaining Psl association[238].

eDNA is an integral part of the EPS and biofilm mode of life, which in *P. aeruginosa* biofilms functions as an intercellular connector[463,464]. In *P. aeruginosa* biofilms eDNA and genomic DNA seemed to be identical, which very likely comes from lysed cells although active excretion of DNA cannot be excluded[458,465,466]. Ueda and Wood showed in *P. aeruginosa* PA14, the deletion of a tyrosine phosphatase *tpbA* significantly elevated intracellular c-di-GMP and enhanced cell lysis, which resulted in more eDNA, Their work suggested that intracellular c-di-GMP might be controlling cell lysis but further tests on other DGC/PDEs should be applied. Despite this, thus far to my knowledge there are no other reports proving a link between c-di-GMP and PAO1 bacterial cell lysis, hence the link in PAO1 remains controversial. On the other hand, more evidences were reported suggesting the link between QS and cell lysis in *P. aeruginosa*[467,468,469], and the more cell lysis the more DNA are released into EPS forming eDNA.

Rhamnolipids have been reported to greatly influence biofilms formation. Klausen *et al* claimed that rhamnolipid facilitated swarming motility and thus biofilm establishment[470–472]. An *et al* showed that Δ*RbdA* produced less rhamolipids and swarming zones[272]. Pamp *et al* not only reinforced this finding, but showed that rhamnolipid facilitated twitching motility as well[473]. Furthermore, the authors provided more detailed evidence that the formation of the cap portion of the mushroom-shaped structures in *P. aeruginosa* biofilms is facilitated by biosurfactant production, which is also necessary for the formation of initial microcolonies[473]. However, Shrout *et al* suggested that rhamnolipids are not critical for swarming motility and it was nutrition dependent[68]. The discrepancy of the link between rhamolipids and swarming might have come from different culturing mediums and methods.

Mature biofilms are highly hydrated structures consisting of microcolonies surrounded by large void spaces. These void spaces allow fluids to constantly change the distribution

of nutrients and oxygen as well as remove metabolic end products[474]. When previous studies showed the formation of these void spaces is an active process involving in quorum sensing and motility, Davey *et al* reported that *P. aeruginosa* utilizes rhamnolipid surfactants to actively maintain the void spaces surrounding macrocolonies after channels form, and mutants lacking rhamnolipids production formed much thicker but more homogenous biofilms[474].

Apart from participating in biofilm formation and structure maintenance, rhamolipids was also reported to be involved in "central hollowing" in biofilm dispersal. Boles *et al* reported that the cells at the centre of the biofilm were much more susceptible to externally added rhamnolipids leading to detachment processes compared to biofilm peripheries[21]. Rhamnolipids secreted by peripheral bacteria would induce the separation of cells from the biofilm centre.

It seems that rhamnolipids are involved in nearly all stages of biofilm life cycles and it would be logical to deduce that c-di-GMP might be one of the regulators of rhamnolipids. An *et al* reported that RbdA acted as a phosphodiesterase in *P. aeruginosa* which positively regulates motility and the production of rhamnolipids[272]. However, Ueda *et al* claimed that loss of a phosphodiesterase PA3885 in *P. aeruginosa* PA14 increased intracellular c-di-GMP but did not affect rhamnolipids[475]. Losing a PDE BifA resulted in significantly higher intracellular c-di-GMP but did not exert influences on rhamnolipids production as well[218]. Hence, despite the deep investigations, the link between c-di-GMP level and rhamnolipids production has not been clarified. On the other hand, the link between quorum sensing and rhamnolipid has been well established where three QS molecules 3-oxo-C12-HSL, C4 -HSL and PQS are controlling rhamnolipids production[21,476,477], Therefore, it is suspected that c-di-GMP is not a direct/major indicator of rhamnolipid production, but might be involved in the regulation of certain genes that are involved in rhamnolipids.

In this study, EPS was extracted from KO mutants biofilms followed by determination of their total exopolysaccharides and total protein amount. Data may help to discover more proteins involved in EPS regulation. Due to a large amount of DGC/PDE candidates were tested, it might also shed lights on the potential general/proportional relationship between intracellular c-di-GMP level and EPS compositions.

Various EPS extraction protocols have been developed, including physical methods such as centrifugation, heating, filteration and ultrasonication etc, as well as chemical methods such as EDTA, formaldehyde and formaldehyde plus NaOH and cation-exchange resin etc. However, various conclusions from different publications led to uncertainty and non-comparability of results. For example, Liu and Fang reported that formaldehyde plus NaOH method obtained more EPS from sludge than EDTA and cation exchange resin methods[478]. Comte *et al* claimed that heating induces the hydrolysis of EPS, while chemical reagents strongly affectes the composition of EPS[479]. Zhang *et al* reported that different methods resulted in different yields in carbohydrates and proteins respectively[480]. Therefore, it is clearly extremely difficult to precisely isolate pure and whole EPS components, because some of the EPS fraction remains bound to the bacteria, and most methods inevitably damage cells, causing intracellular material to leak into the matrix. Here, the formaldehyde-NaOH method that has been extensively applied in extracting EPS in *Pseudomonas* sludge[314,478,481] was adopted to extract EPS, while total carbohydrates and protein were chosen for investigation to represent the EPS production ability of different strains[458].

Different methods have been established to quantify exopolysaccharides. Irina Sadovskaya developed a method for quantification of mannose specific to Psl in EPS which is absent in other contaminating carbohydrates[462]. Mannose is quantified by gas chromatography after acid hydrolysis of samples and conversion into volatile alditol acetates using myo-inositol as an internal standard[462]. Due to the lack of knowledge on Pel structure, Pel specific quantification method has not been developed so far. Many researchers used Congo red as the indicator of Pel production[475,482–484]. Congo red binds to amyloid fibers and cellulose and the dye molecule is sandwiched between protein molecules, causing protein oligomerization[485]. Hence, CR is not suitable to be considered as a specific reagent for the quantification of exopolysaccharides[462]. Considering the intention of quantifying total polysaccharides including Pel and Psl in different strains, $H_2SO_4$-phenol method was used in this study. This method detects nearly all classes of carbohydrates, including mono-, di-, oligo-, and polysaccharides. Concentrated $H_2SO_4$ breaks down any polysaccharides, oligosaccharides, and disaccharides to monosaccharides. Pentoses and hexoses are then dehydrated to furfural and hydroxymethyl furfural respectively. These compounds react with phenol to

produce a yellow-gold colour, providing a simple and rapid colorimetric measurement method[486].

Due to the complexity of protein components in *P. aeruginosa* and the lack of necessity to determine specific ingredients in high-throughput screening assay, Bradford protein assay kit was applied for evaluating total protein. It has great variability and compatibility with a range of possible contamination from EPS extraction steps, including reducing agents, chaotropic and chelating agents, metals, protease inhibitors and DNA.

Although eDNA and rhamnolipids are also important EPS components, they were not measured for these 14 KO strains due to the more possible regulation from QS rather than intracellular c-di-GMP. However, our candidate DGC/PDEs might regulate eDNA and/or rhamnolipids in a more genetically specific manner or through modulation of localized c-di-GMP pool. Future work can include the quantification of eDNA using fluorescence dye and rhamnolipids using drop-collapse assays.

# Results

## 6.1. Phenotypic analysis of 14 KO strains

### 6.1.1. *In vivo* intracellular c-di-GMP determination

Planktonic cell culture conditions and GFP fluorescence detection method were described in 2.13. Apart from planktonic cells, PAO1 WT PcdrA*::gfp*$^{Tc}$ biofilms were grown in MatTek plates for real time c-di-GMP level detection in biofilm. Previous experiments showed that biofilms did not grow properly with 75µg/ml tetracycline (data not shown), hence PAO1 WT + c-di-GMP reporter was grown in normal M9 and subjected to CLSM using PAO1 WT as control. Biofilms were grown at 22℃, 30℃ and 37℃ due to their very different biofilm structures and potentially different c-di-GMP levels.

**A**

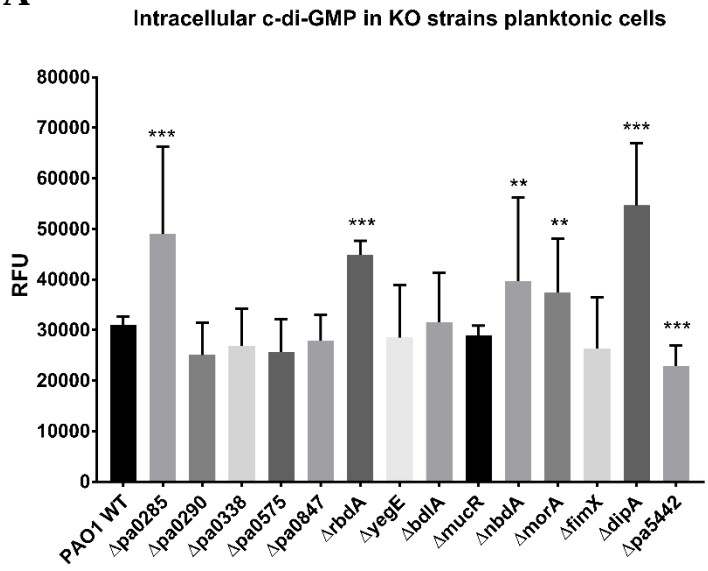


**B**

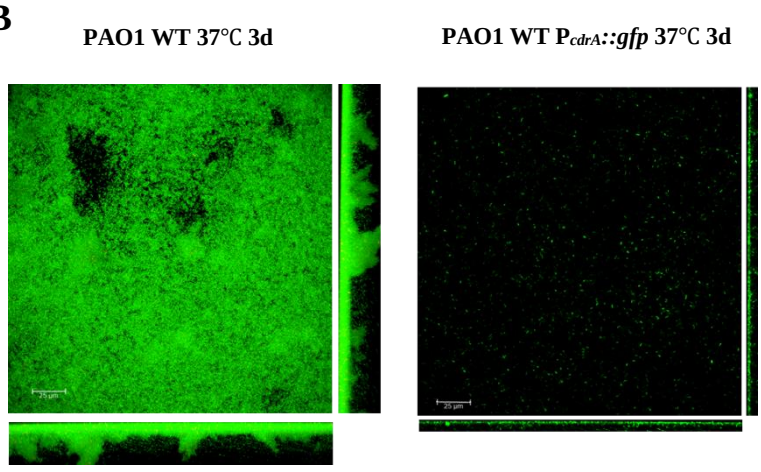

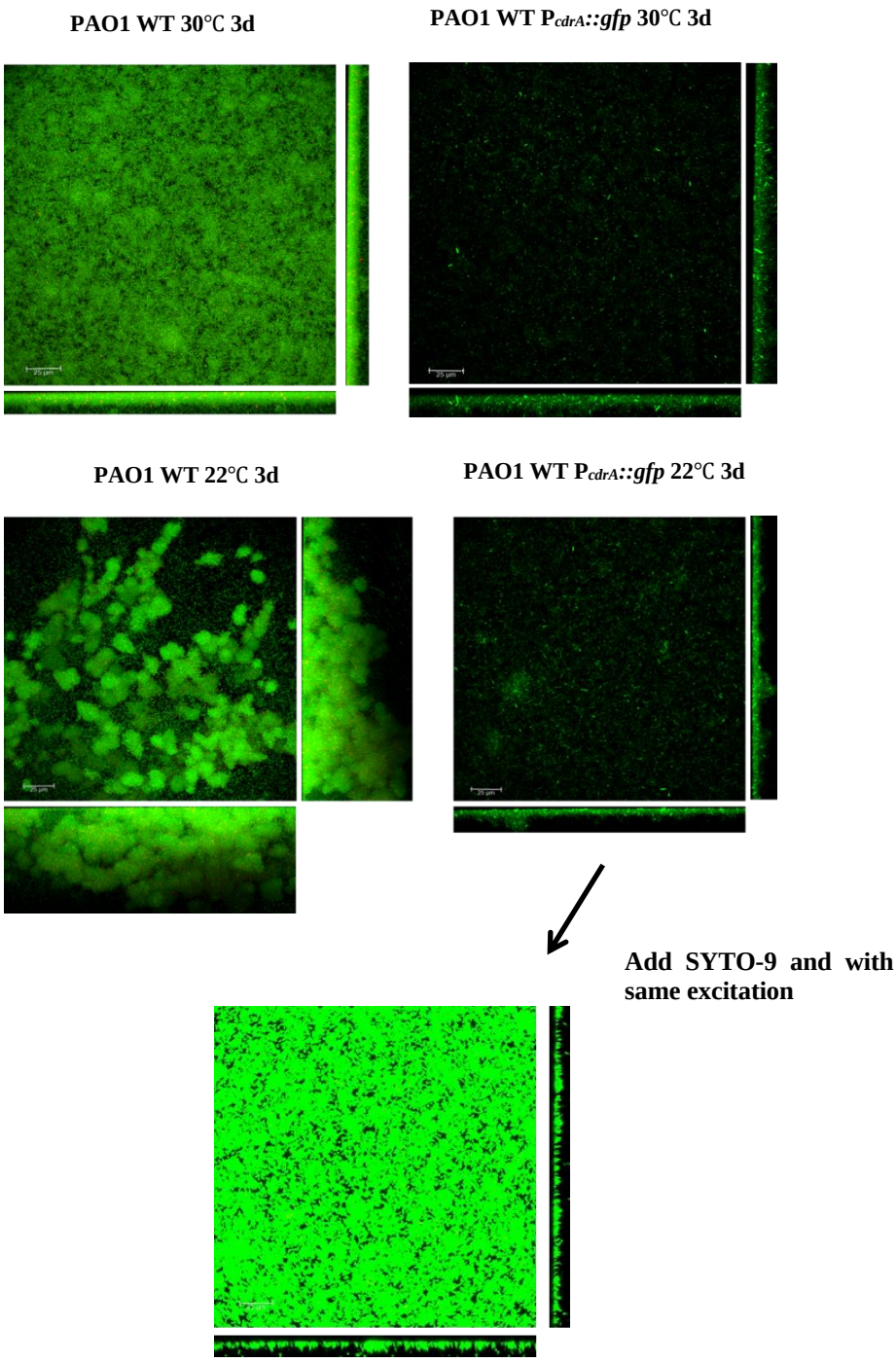


Fig 6.1.1 (A) Comparison of relative intracellular c-di-GMP levels in different KO strains after 24hrs planktonic cultures. The total fluorescence intensity was measured using a 485-nm sharp-cut excitation filter and a 520-nm sharp-cut emission filter with a gain of 1500 on BMG LABTECH FLUOSTAR plate reader and normalized by corresponding OD value of the same culture to obtain relative fluorescence intensity in individual cells. Welch T-test was carried out to compare the PAO1 WT and KO mutants. Data represent data means of n=4 of 3 biological replicates, *** represents $p<0.01$, ** represents $0.01<p<0.05$. (B) Selective CLSM images of 3 d old PAO1 WT biofilms and PAO1 WT P$_{cdrA}$*::gfp* biofilms grown at different temperatures. The excitation intensity applied to PAO1 WT P$_{cdrA}$*::gfp* biofilms was 3 times more than PAO1 WT in order to magnify the signals. Arrow points to the same PAO1 WT P$_{cdrA}$*::gfp* biofilm stained with SYTO-9 but exposed to the same excitation. Scale bar = 25µm.

As shown in Fig 6.1.1 (A), Δ*pa0285,* Δ*rbdA* and Δ*dipA* showed a stronger increase in intracellular c-di-GMP level compared to PAO1 WT (1.58, 1.44 and 1.76 fold respectively, $p<0.01$) while Δ*nbdA* and Δ*morA s*howed less but still a significant increase (1.28 and 1.21 folds respectively, $0.01<p<0.05$). In contrast, Δ*pa5442* showed a decrease in intracellular c-di-GMP level (1.27 fold reduction, $p<0.01$). Other strains exhibited nearly the same cellular c-di-GMP level compared to PAO1 WT.

Fig 6.1.1 (B) demonstrated that generally, PAO1 WT with $P_{cdrA}$*::gfp* reporters exhibited very weak fluorescent signals. However, the excitation intensity applied to PAO1 WT $P_{cdrA}$*::gfp* biofilms was 3 times compared to the control with SYTO-9 staining. There is a possibility that PAO1 WT $P_{cdrA}$*::gfp* form less biofilm compared to WT. Therefore, after the images of 3 d 22℃ PAO1 WT $P_{cdrA}$*::gfp* biofilms were taken under CLSM, the same biofilms were subjected to SYTO-9 staining and observed. The results pointed by the arrow indicated that when using 3 times excitation intensity, over-exposed PAO1 WT $P_{cdrA}$*::gfp* biofilms with SYTO-9 staining clearly showed much less biomass and different architectures compared to WT, indicating the *in trans* reporter plasmid might adversely affect biofilm formation at least under MatTek batch culture system. Therefore, c-di-GMP detection was not carried out for mutants biofilms currently. In order to detect *in situ* c-di-GMP levels in biofilms, other biofilm culture systems should be tested in the future. Furthermore, a dye with different excitation and emission wavelengths compared to GFP fluorescence protein can be used to stain the cell mass so that c-di-GMP signal can be normalized for comparison.

## 6.1.2. Growth curves and colony morphologies

Growth curves were measured in microtiter plates as described in 2.5.1. All the mutants were plated onto Cetrimide *P. aeruginosa* selective agar plates with the same humidity and thickness.

**A**

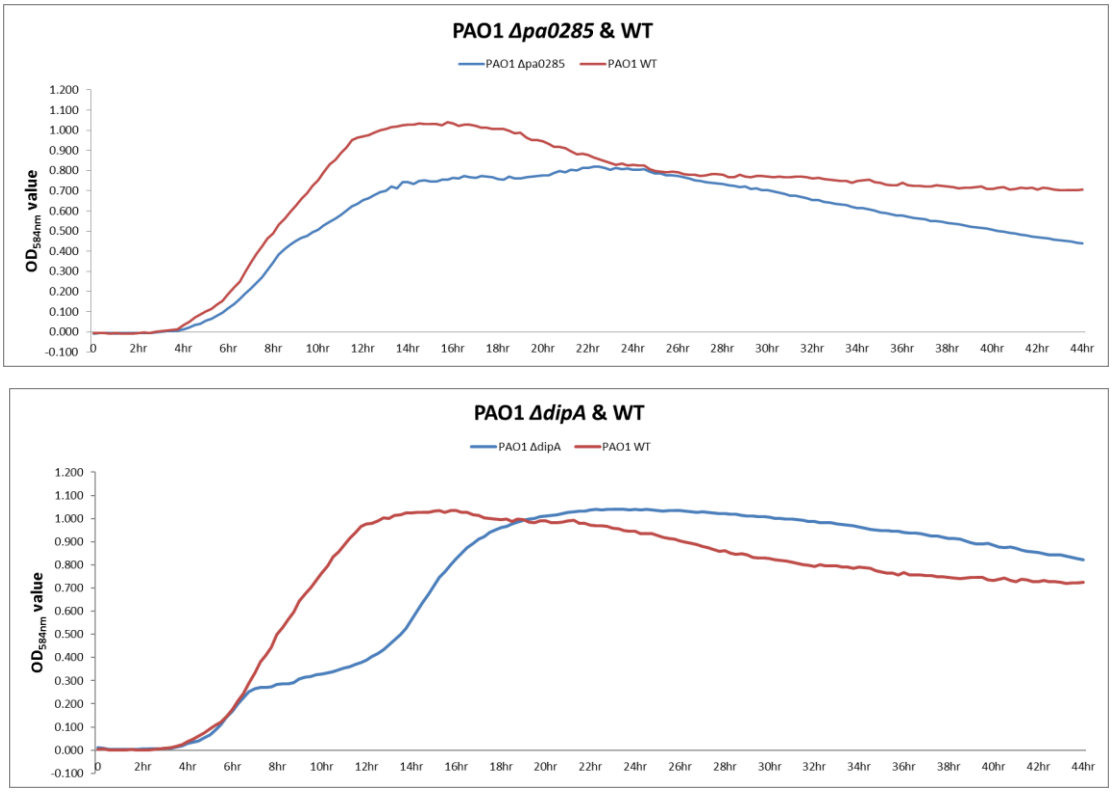


**B**

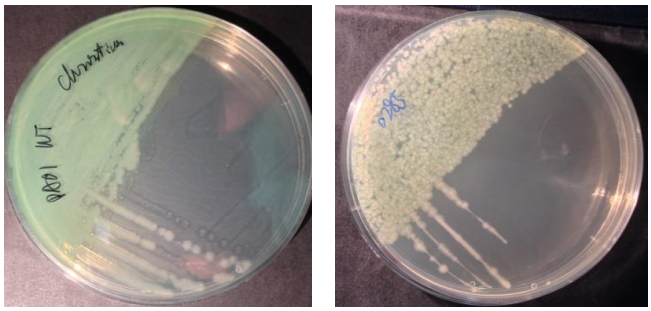

Fig 6.1.2 (A) Growth curves of Δ*pa0285* and Δ*dipA* compared to PAO1 WT. (B) *P. aeruginosa* PAO1 WT and Δ*pa0285* Cetrimide agar plates.

All KO strains growth curves are shown in Appendix Fig A1. 12 out of 14 strains showed similar curves as WT except for Δ*pa0285* and Δ*dipA*. In Fig 6.1.2 (A), they showed significantly different growth curves compared to PAO1 WT, with *Δpa0285* constantly grew slower than WT within exponential phase while *ΔdipA* showed diauxic curves.

All colony morphologies of KO strains on Cetrimide agars are shown in Appendix Fig A2. 13 out of 14 strains showed the same morphologies as WT except for Δ*pa0285*. In Fig 6.1.2 (B), Δ*pa0285* showed smaller and different colony morphology, similar to some CF isolates strains. Furthermore, the pigment of Δ*pa0285* was reduced compared to the obvious green colour of PAO1 WT. Cetrimide enhances the production of

pyocyanin in *P. aeruginosa*, therefore, the lack of pigment in Δ*pa0285* indicated that it might be deficient in pyocyanin synthesis. These data are the first to show the potential link between PA0285 and PAO1 pigment/pyocyanin synthesis.

### 6.1.3. 2 d and 3 d batch cultured KO mutant biofilms

Optimal MatTek culturing conditions for PAO1 WT were determined in chapter 3 where maturation stages with obvious and growing microcolonies occurred after 2-3 d. Hence, KO mutant biofilms were grown in MatTek plates for both 2 d and 3 d in order to observe and compare their 3D structural characteristics. CLSM images were subjected to COMSTAT analysis and four indexes (biomass, mean thickness, surface coverage and roughness coefficient) were calculated to reflect the characteristics.

| **2 d** | **Biomass** | **Mean thickness** | **Surface coverage** | **Roughness coefficient** |
|---|---|---|---|---|
| PAO1 WT | 2.96±2.88 | 4.27±1.79 | 52.60±22.81% | 0.81±0.37 |
| Δ*pa0285* | 4.38±1.53 | **6.33±3.05** | **65.20±11.26%** | 0.56±0.20 |
| Δ*pa0290* | 3.08±0.87 | 5.30±2.45 | 60.41±12.30% | 0.71±0.12 |
| Δ*pa0338* | **1.76±0.82** | 4.06±1.74 | 46.44±26.58% | **1.28±0.28** |
| Δ*pa0575* | **1.55±0.88** | 3.82±1.53 | 42.81±23.36% | **1.29±0.27** |
| Δ*pa0847* | 2.41±1.69 | 4.23±1.89 | 51.69±32.31% | **1.22±0.27** |
| Δ*rbdA* | **6.33±1.82** | **7.50±2.83** | **77.67±17.22%** | 0.66±0.23 |
| Δ*yegE* | 2.26±1.24 | 4.26±0.98 | 48.29±28.95% | **1.26±0.23** |
| Δ*bdlA* | 2.30±1.37 | 3.96±2.49 | 52.66±14.94% | 0.69±0.26 |
| Δ*mucR* | 1.99±1.22 | 3.63±1.92 | 46.02±14.08% | 0.80±0.32 |
| Δ*nbdA* | **1.57±0.72** | 3.39±1.19 | **40.38±12.32%** | 0.86±0.34 |
| Δ*morA* | **1.85±0.94** | 3.94±2.06 | 46.56±10.52% | 0.73±0.26 |
| Δ*fimX* | **1.22±0.81** | 3.96±2.02 | **30.43±17.64%** | 0.96±0.52 |
| Δ*dipA* | 3.63±2.38 | 4.34±1.79 | 64.73±14.67% | **0.46±0.21** |
| Δ*pa5442* | 1.86±1.06 | 3.71±1.18 | **44.99±15.66%** | 0.79±0.39 |

Table 6.1.3 (A) The comparison of biomass, mean thickness, surface coverage and roughness coefficient between 2 d old KO mutants and PAO1 WT. Bold texts with red highlight represent an index is significantly higher than WT. Bold texts with green highlight represent an index is significantly lower than WT.

| **3 d** | **Biomass** | **Mean thickness** | **Surface coverage** | **Roughness coefficient** |
|---|---|---|---|---|
| PAO1 WT | 6.30±1.83 | 6.85±2.43 | 96.76±4.42% | 0.18±0.07 |
| Δ*pa0285* | **3.83±1.13** | **4.37±0.75** | **76.41±8.15%** | **0.53±0.19** |
| Δ*pa0290* | 8.28±2.86 | 6.03±1.35 | 97.88±3.08% | 0.14±0.04 |
| Δ*pa0338* | 7.36±4.39 | 6.23±1.91 | 87.04±19.86% | 0.19±0.03 |
| Δ*pa0575* | 9.23±3.35 | 7.41±2.09 | 99.58±0.85% | 0.20±0.06 |
| Δ*pa0847* | 5.82±3.29 | 6.94±1.08 | 95.22±5.51% | 0.26±0.13 |
| Δ*rbdA* | 7.15±3.58 | 7.73±1.87 | 90.31±11.87% | **0.37±0.15** |
| Δ*yegE* | 9.21±2.47 | 6.98±1.26 | 99.88±0.16% | 0.19±0.05 |
| Δ*bdlA* | 7.42±4.63 | 8.13±2.07 | 92.49±8.18% | 0.26±0.13 |
| Δ*mucR* | 10.08±3.33 | 7.10±1.89 | 98.56±4.20% | 0.19±0.07 |
| Δ*nbdA* | 6.14±3.72 | 8.36±1.63 | 88.64+16.66% | 0.12±0.05 |
| Δ*morA* | 8.79±4.10 | 7.73±0.96 | 98.19±3.39% | 0.19±0.03 |
| Δ*fimX* | **1.74±0.58** | **4.46±1.63** | **45.57±13.52%** | **0.88±0.19** |
| Δ*dipA* | 6.13±2.21 | 6.60±0.76 | 98.59±1.98% | 0.23±0.09 |
| Δ*pa5442* | 5.80±2.63 | 6.60±1.35 | 90.64±13.03% | 0.25±0.13 |

Table 6.1.3 (B) The comparison of biomass, mean thickness, surface coverage and roughness coefficient between 3 d old KO mutants and PAO1 WT. Bold texts with red highlight represent an index is significantly higher than WT. Bold texts with green highlight represent an index is significantly lower than WT.

| 2d - 3d | Biomass | Mean thickness | Surface coverage | Roughness coefficient |
|---|---|---|---|---|
| PAO1 WT | 112.99% | 60.35% | 83.94% | -63.58% |
| Δ*pa0285* | **-12.39%** | **-30.96%** | **17.20%** | **-5.06%** |
| Δ*pa0290* | 168.91% | 48.41% | 62.02% | -80.81% |
| Δ*pa0338* | 318.83% | 53.53% | 87.41% | -82.57% |
| Δ*pa0575* | 494.39% | 94.05% | 132.59% | -88.60% |
| Δ*pa0847* | 141.29% | 63.93% | 84.21% | -89.00% |
| Δ*rbdA* | **13.04%** | **3.01%** | **16.27%** | -72.46% |
| Δ*yegE* | 307.09% | 63.65% | 106.85% | -88.25% |
| Δ*bdlA* | 222.06% | 105.33% | 75.64% | -81.51% |
| Δ*mucR* | 406.74% | 95.52% | 114.15% | -83.42% |
| Δ*nbdA* | 290.30% | 146.51% | 119.53% | -86.29% |
| Δ*morA* | 375.48% | 96.46% | 110.86% | -84.79% |
| Δ*fimX* | **43.38%** | **-14.00%** | **49.40%** | **-10.24%** |
| Δ*dipA* | **68.93%** | 52.07% | **52.32%** | -66.98% |
| Δ*pa5442* | 212.86% | 77.93% | 101.47% | -84.31% |

Table 6.1.3 (C) The development of biomass, mean thickness, surface coverage and roughness coefficient in KO mutants and PAO1 WT biofilms from 2d to 3d. Bold texts with red highlight represent an index is significantly different from WT and unhighlighted strains, suggesting a distinct biofilm formation pattern.

**E**

**2 d PAO1 WT biofilm**

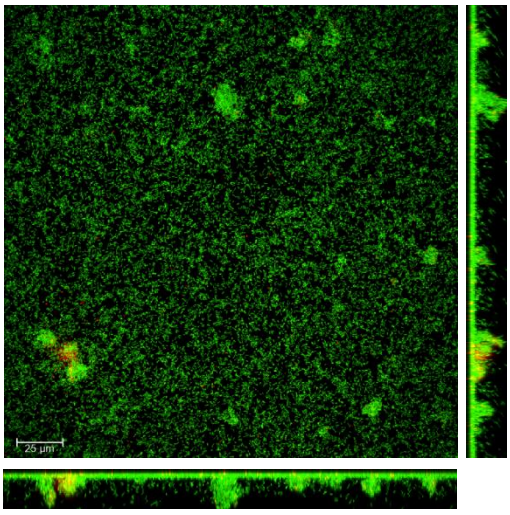


**3 d PAO1 WT biofilm**

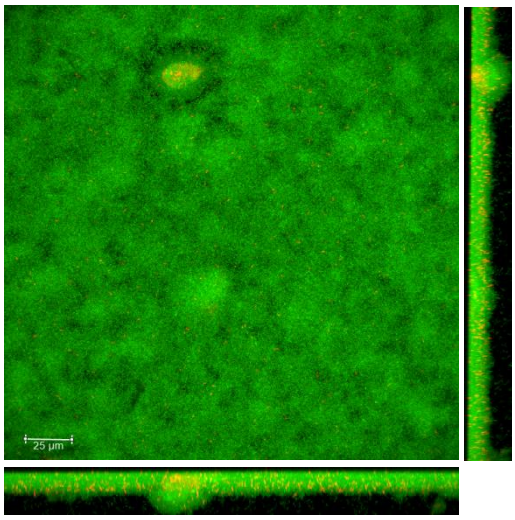


**2 d Δ*pa0285* biofilm**

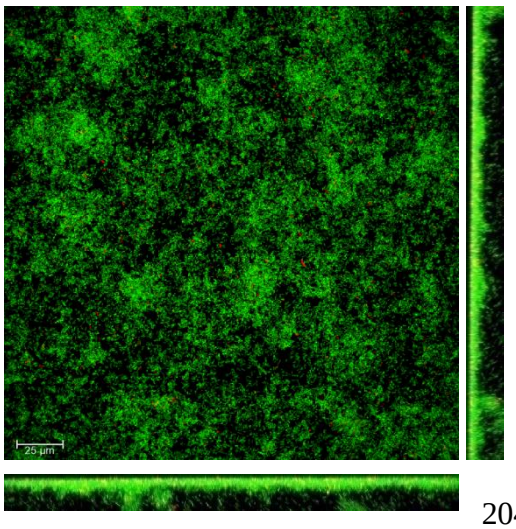


**3 d Δ*pa0285* biofilm**

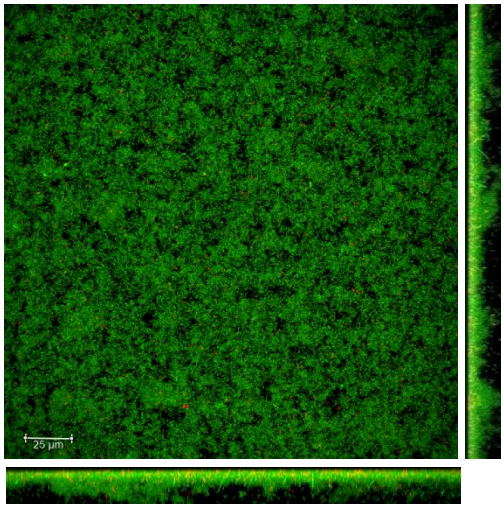

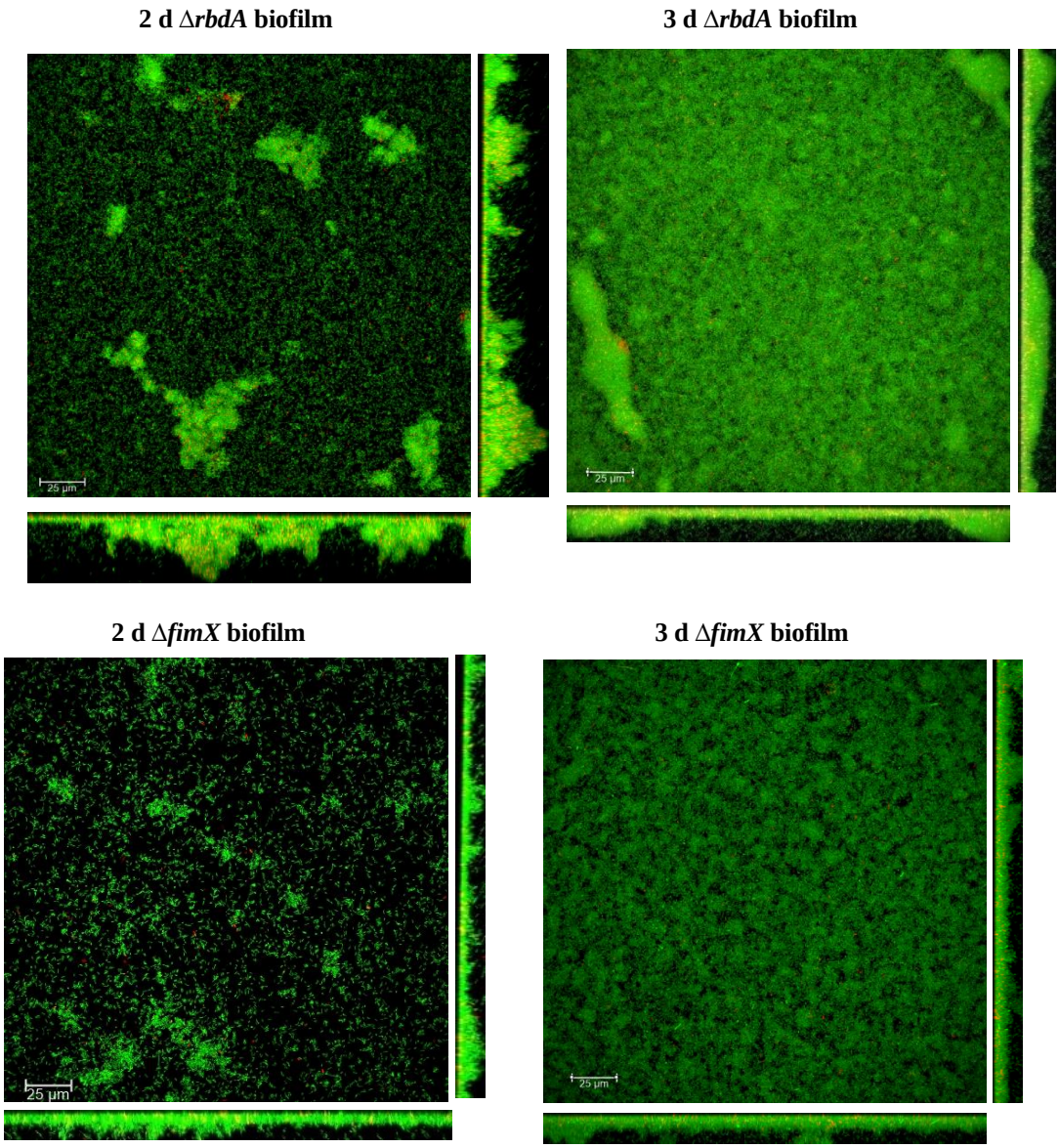


Fig 6.1.3 Selective CLSM images of 2 and 3 d old PAO1 WT, Δ*pa0285,* Δ*rbdA* and Δ*fimX* biofilms in MatTek plates. Scale bar = 25µm.

Representative CLSM images of 2 and 3 d biofilms of Δ*pa0285,* Δ*rbdA* and Δ*fimX* are shown here due to their significantly different biofilm architectures compared to PAO1 WT and other KO mutants. Representative CLSM images of 2 and 3 d biofilms for all the KO mutants were shown in Appendix Fig A3 and A4.

Results in Table 6.1.3 have shown:

(1) Δ*pa0338,* Δ*pa0575,* Δ*nbdA* and Δ*morA* formed significantly less biomasses than WT after 2 d ($p<0.05$), but after 3 d biomasses exhibited no difference from WT ($p>0.05$), suggesting these 4 mutants have the same biofilm formation and maturation abilities as

WT. They might be slower in initial attachment that caused lower biomasses after 2 d, which may or may not be influenced by MatTek plates surfaces. However, once the biofilms started to establish, the mature structure developed well so after 3 d the biomasses were the same as WT ($p>0.05$).

(2) Roughness coefficient reflects structural heterogeneity of biofilms and surface coverage reflects bacterial attachment to surfaces. Δ*pa0338,* Δ*pa0575,* Δ*pa0847,* Δ*yegE* and Δ*dipA* showed significantly different roughness coefficient numbers compared to WT in 2 d biofilms as shown in Table 6.1.3 (A), but no differences after 3 d. Δ*pa5442* only showed a much lower surface coverage after 2 d but not 3 d. Hence, it was suggested these inconsistency might have come from the influences from MatTek plate surfaces micro-niches more than the characteristics of mutants.

(3) Δ*rbdA* might have stronger initial attachment/EPS production abilities so that after 2 d the total biomass, mean thickness and surface coverage were much higher than WT shown in Table 6.1.3 (A). This was supported by visual judgement from Fig 6.1.3 where the microcolonies in Δ*rbdA* biofilms were significantly larger and thicker than WT after 2 d. However, the biofilm might have developed slower afterwards, or some microcolonies started entering dispersal stage while the new attachment continued, so after 3 d these 3 indexes were similar to WT ($p>0.05$). This hypothesis may be supported by Table 6.1.3 (C) where the biomass and surface coverage of Δ*rbdA* biofilms increased much less than WT from 2-3 d, while the mean thickness did not increase ($p>0.05$).

(4) Δ*pa0285* may have similar or even stronger initial attachment ability compared to WT at the early stage of biofilm development. After 2 d the biomasses of Δ*pa0285* and WT showed no difference ($p>0.05$), while the mean thickness and surfaces of Δ*pa0285* were much higher. However, once the biofilms were established, Δ*pa0285* biofilms might have developed slower than WT, or entered dispersal stage earlier than WT, so that after 3 d the biomass, mean thickness and surfaces coverage were significantly lower than WT ($p<0.01$). This hypothesis may be supported by Table 6.1.3 (C) where the biomass and surface coverage of Δ*pa0285* increased much less than WT from 2-3 d, while the mean thickness even decreased ($p<0.01$).

(5) Δ*fimX* biofilms kept showing less biomasses, mean thickness and surface coverage compared to WT after 2 and 3 d as highlighted in Tables. Furthermore, as shown in

Table 6.1.3 (C), the increases in biomass, mean thickness and surface coverage of Δ*fimX* biofilms from 2-3 d were much less than WT, suggesting a slow biofilm development. All these indicated that PAO1 biofilm formation ability may be impaired when losing FimX.

(6) The architectures of mature (3 d) biofilms of Δ*pa0285,* Δ*rbdA* and Δ*fimX* exhibited pronouncing differences compared to WT. Although Table 6.1.3 (B) showed that the roughness coefficient of these three KO mutants were all significantly higher than WT suggesting higher heterogeneities, the CLSM images in Fig 6.1.3 showed that the heterogeneities were contributed by very different 3 D structures. Δ*rbdA* constantly showed larger and thicker microcolonies compared to WT after 2 and 3 d. In contrast, the base layers of Δ*pa0285* and Δ*fimX* biofilms appeared less compact than WT (and other KO mutants, images shown in Appendix Fig A4) with multiple spatial gaps. This visual judgement was supported by their much lower surface coverage percentages compared to WT in Table 6.1.3 (B). Furthermore, when WT showed typical round-shape microcolonies in both 2 and 3 d biofilms, no substantial microcolonies were observed in Δ*pa0285* and Δ*fimX* biofilms.

In summary, 11 out of 14 KO mutants exhibited similar biofilm development abilities compared to PAO1 WT despite the slight discrepancies in initial attachment and development speeds. They kept developing biofilms maturation stages from 2-3 d with significantly increased biomass, mean thickness and surface coverage percentages as shown in Table 6.1.3 (C), while the heterogeneities decreased from 2-3 d. These conclusions were visually supported by CLSM images in Appendix Fig A3 and A4. After 3 d, these 11 KO strains formed very dense base layers that continuously occupied the total field of view on top of which some substantial 3D structured microcolonies developed, while after 2 d the biofilms base layers were not fully occupying the substratum with microcolonies found at random locations. The side views of these CLSM images appeared more uniform after 3 d than after 2 d. These results suggested that during biofilm development in MatTek plates, the first settled down cells started to assemble microcolonies, some of which can be larger and more mature probably due to the variance of attachment surface micro-niches. With maturation, closely located microcolonies grew to join each other and formed a “dense and flat mat”. Exceptions were found for Δ*pa0285,* Δ*rbdA* and Δ*fimX*. Δ*rbdA* showed hyper-biofilm phenotype

forming much larger aggregates during the early biofilm formation stage (< 2 d), but the development slowed down from 2-3 d. Δ*pa0285* and Δ*fimX* showed less ability in forming mature biofilm structures after 3 d and were lack of both condense base layer and substantial microcolonies. This was probably due to the deficiency in surface attachment, as the biofilms of these two mutants showed much lower surface coverage percentages. Therefore, it was concluded that PA0285, RbdA and FimX influence *P. aeruginosa* PAO1 biofilm structural development.

## 6.1.4. Motility of 14 KO mutants

Motility assays were performed as described in 2.6. For swimming and twitching assays, each plate contains two KO mutants and one PAO1 WT to minimize the influence from technical variances. For swarming assays, each plate contains only one strain due to the large surface occupation, but the plates resourced from the same bottle of agar were used for 5 KO mutants and PAO1 WT for comparison. Therefore, a summary of KO mutant motility data compared to PAO1 WT was shown in Table 6.1.4, while the raw data are shown in groups in Appendix Fig A5-A8.

| | **Swimming** | **Swarming** | **Twitching** |
|---|---|---|---|
| PAO1 WT | + | + | + |
| Δ*pa0285* | --- | / **(distinct pattern)** | --- |
| Δ*pa0290* | / | / | / |
| Δ*pa0338* | --- | -- | / |
| Δ*pa0575* | / | / | / |
| Δ*pa0847* | / | / | / |
| Δ*rbdA* | / | -- | / |
| Δ*yegE* | +++ | / | / |
| Δ*bdlA* | / | / | / |
| Δ*mucR* | +++ | / | / |
| Δ*nbdA* | / | / | / |
| Δ*morA* | ++ | / | / |
| Δ*fimX* | --- | +++ **(distinct pattern)** | --- |
| Δ*dipA* | --- | --- | / |
| Δ*pa5442* | / | / | / |

Table 6.1.4. Comparison of swimming, swarming and twitching motilities between KO mutants and WT. The motilities of PAO1 WT were used as control and shown as +. ++ represents significant increase compared to WT ($0.01<p<0.05$), +++ represents significant increase compared to WT ($p<0.01$), -- represents significant decrease compared to WT ($0.01<p<0.05$), --- represents significant decrease compared to WT ($p<0.01$). / represents no difference compared to PAO1 WT.

**A Swimming plates**

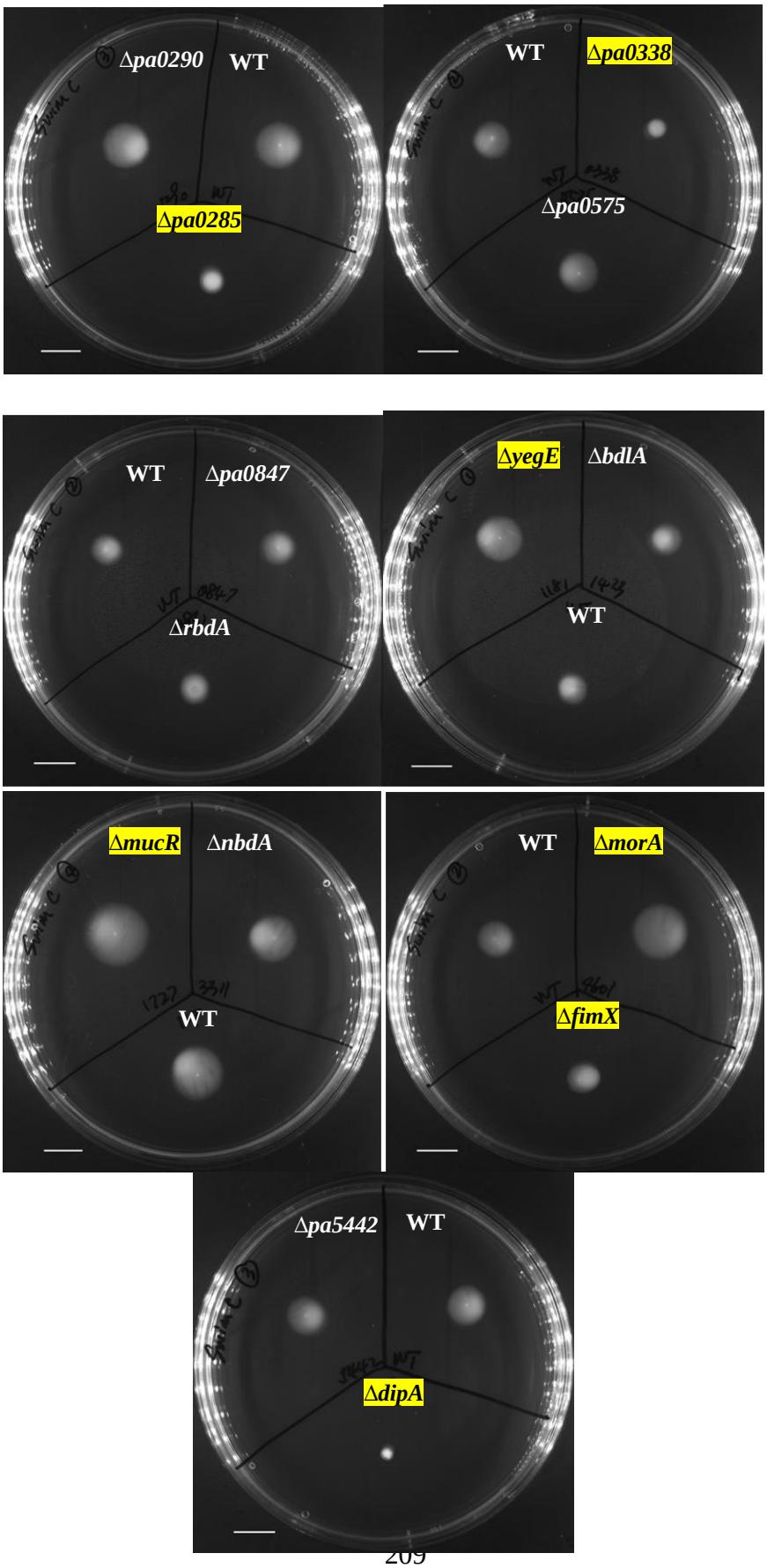

**B Swarming plates**

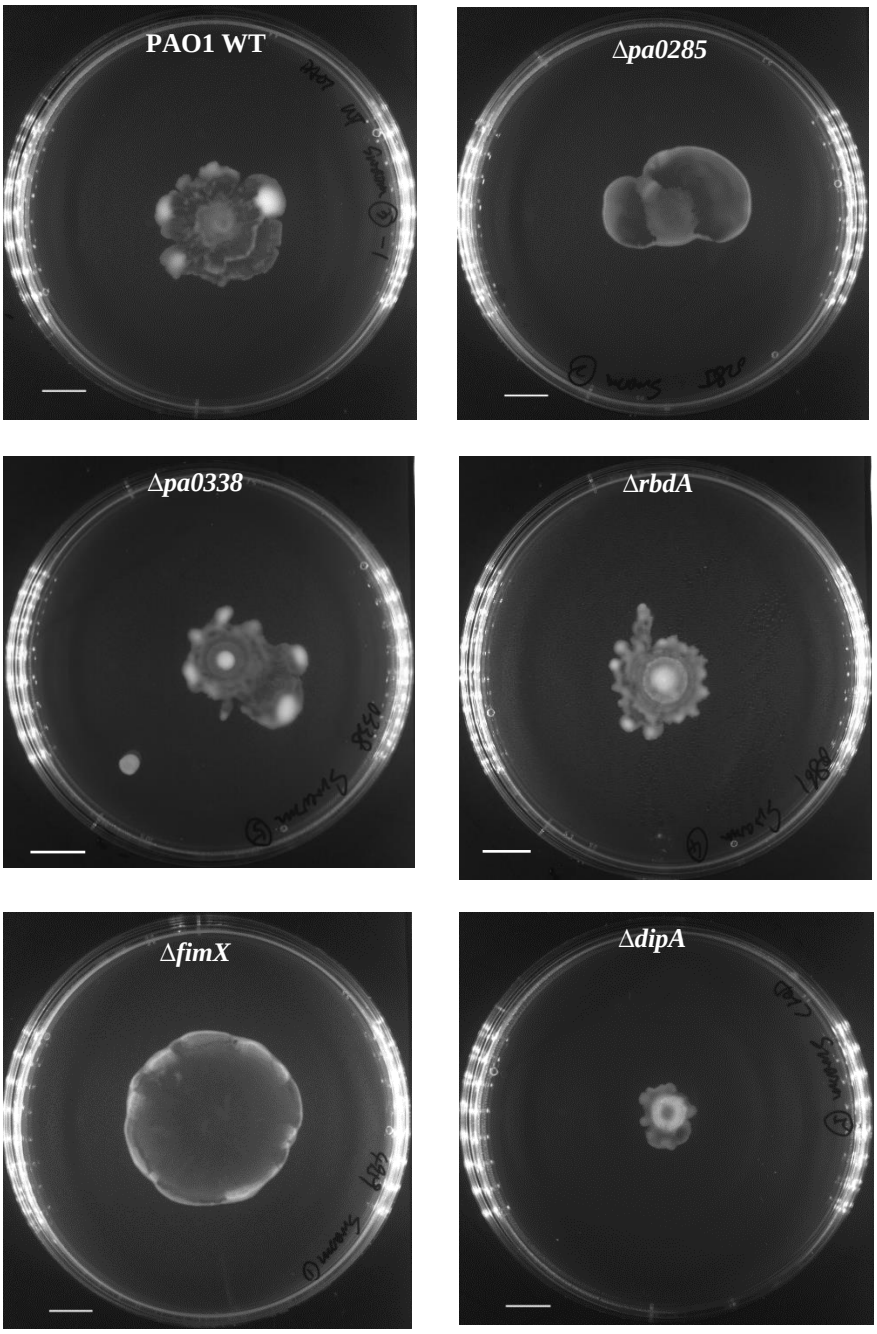

**C Twitching plates**

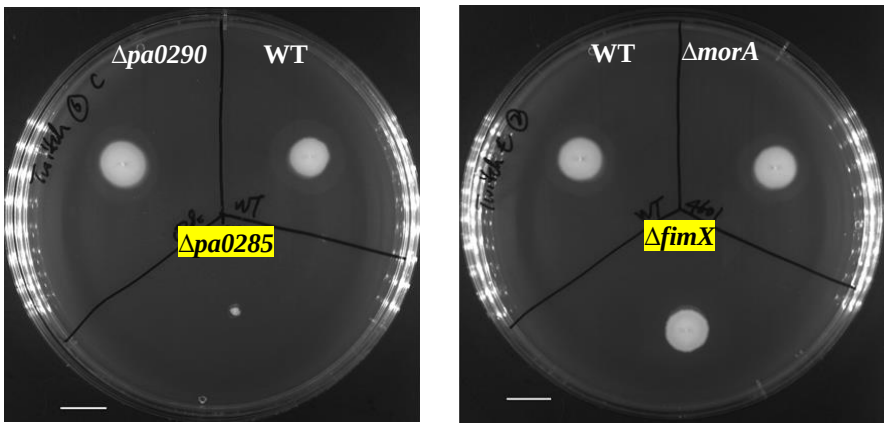


Fig 6.1.4. Selective images of KO mutants swimming agar plates (A), swarming agar plates (B) and twitching agar plates (C). Scale bar = 1cm. KO mutants with distinct motilities compared to WT are highlighted.

Results from both Table 6.1.4 and Fig 6.1.4 showed:

(1) *Δpa0285* and *ΔfimX* both showed significantly reduced swimming motility (~60% reduction on swim areas from both mutants compared to WT, $p<0.01$) and abolished twitching motility, while the swarming patterns were unexpectedly altered. However, Δ*pa0285* was shown in 6.1.2 to have much slower growth rate and smaller colonies sizes compared to WT and other KO strains. Since swimming and twitching plates were consist of nutrient medium, it was possible the reduced swimming and twitching zone came from lower bacteria population rather than the deficiency in motilities. Hence, the conclusion on Δ*pa0285* motility remain controversial and needs further investigations such as TEM for direct flagella/pili observation.

(2) The absence of PA0338 resulted in significantly reduced swimming and swarming, suggesting its regulation on flagella. Swimming agar contains more water than swarming agar that facilitate flagella rotation and bacterial movement, hence swimming assay should be more sensitive in reflecting flagella rotation than swarming. With the swimming decrease in *Δpa0338* more pronounced (-61.22%, $p<0.01$) than swarming (-25.66%, $0.01<p<0.05$) compared to WT, it was then suspected that PA0338 very likely regulates flagella motor proteins so that its presence promotes flagella rotation. In contrast, Δ*dipA* caused remarkable and comparable reduction on both swimming (-85.63%, $p<0.01$) and swarming (-86.32%, $p<0.01$). This hinted that DipA might play a vital role in flagella

assembly/essential function regulations either in a gene-specific manner or through signalling effects.

(3) Δ*rbdA* only caused a significantly reduced swarming zone without altering swimming and twitching motility, suggesting its influence on flagella probably came from cellular signalling modulation that affect flagella behavior rather than through specific regulation on flagella related gene/proteins.

(4) Δ*yegE,* Δ*mucR* and Δ*morA* only enhance swimming motility, suggesting their regulations on flagella assembly/function. However, the role of these three proteins might not be indispensable in flagella production and function and the influences might be minor and more locally, as the swarming motility that is contributed by both flagella rotation and cellular signalling was not affected.

(5) A distinct swarming pattern was found in Δ*pa0285* and Δ*fimX* where there are smooth edges without tendrils and the pattern looked more likely to be just a spread of initial overnight bacteria culture. This swarming pattern was suspected to be similar to the "sliding" pattern mentioned in some previous works[450,455,487] using double mutants lacking both Type IV pili and flagella functions. Δ*pa0285* and Δ*fimX* were also deficient in both swimming and twitching motility, hence added to the evidences of potential sliding motility pattern.

## 6.1.5. EPS components of KO mutants biofilms

The method for EPS extraction as well as determination of total polysaccharides and proteins were described in 2.11.

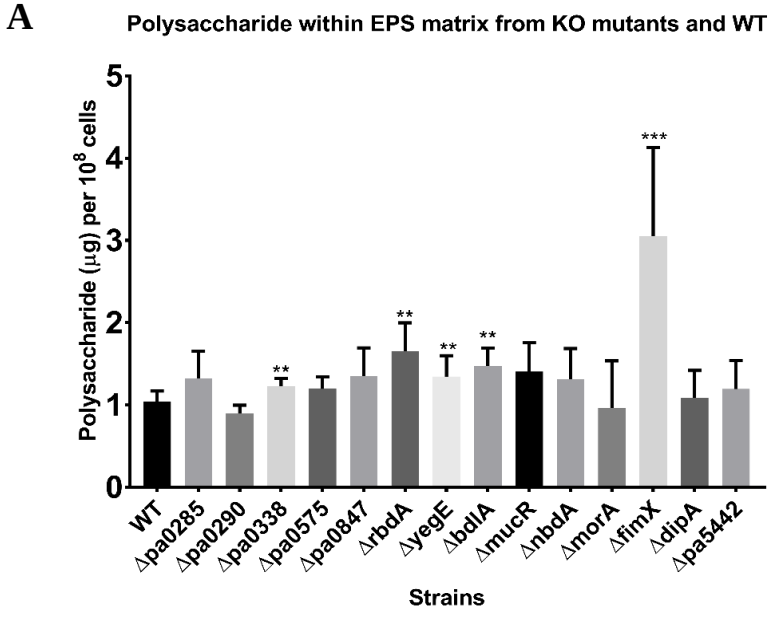

**B**

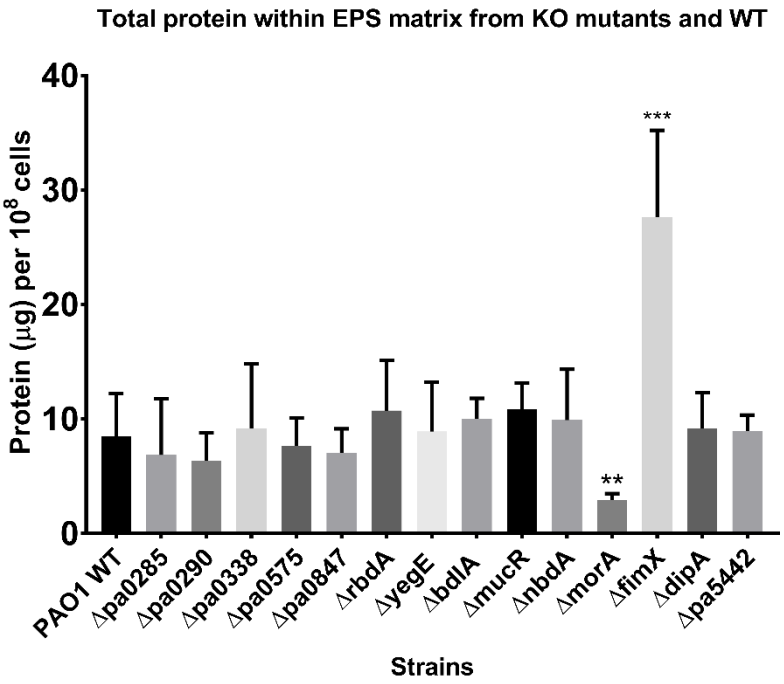


Fig 6.1.5 (A)-(B) Total polysaccharide and total protein concentrations in 2 d KO mutants' biofilms normalized to CFU. Welch T-test was applied to compare KO mutants with PAO1 WT due to large variations. n=4 from 4 individual biological replicates. *** represents $p<0.01$, ** represents $p<0.05$.

From Fig 6.1.5 it can be concluded:

(1) Δ*pa0338,* Δ*rbdA,* Δ*yegE,* Δ*bdlA* and Δ*fimX* produced more polysaccharides compared to WT despite which component was overexpressed remains unknown. While the increases were relatively small in Δ*pa0338,* Δ*rbdA,* Δ*yegE* and Δ*bdlA* (up to 58.74%, $p<0.05$), Δ*fimX* showed a prominent enhancement (192.44%, $p<0.01$).

(2) Δ*morA* showed impaired total protein production compared to WT (-65.74%, $p<0.05$) while Δ*fimX* showed remarkably higher protein amounts (226.24%, $p<0.01$).

# 6.2. The influences of NO on KO mutants phenotypes

## 6.2.1 NO-induced intracellular c-di-GMP reduction in KO mutants

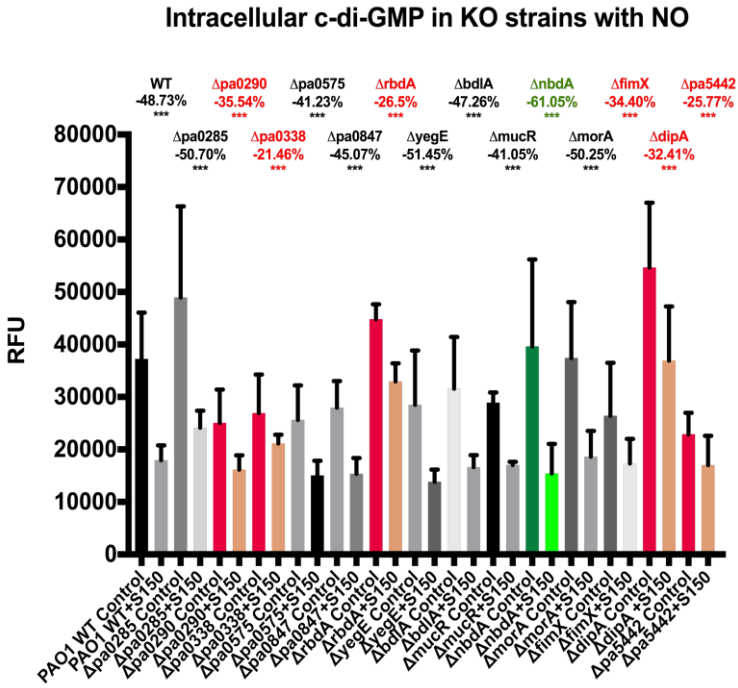


Fig 6.2.1 The influences of 2 hrs 25μM S150 treatment on the relative intracellular c-di-GMP levels in KO mutants. The total fluorescence intensity was measured using a 485-nm sharp-cut excitation filter and a 520-nm sharp-cut emission filter with a gain of 1500 on BMG LABTECH FLUOSTAR plate reader and normalized by corresponding OD value of the same culture to obtain fluorescence intensity in individual cells. Welch T-test was carried out to compare the control and treatment groups. Data represents data means of n=6 of 3 biological replicates, *** represents $p<0.01$, ** represents $0.01<p<0.05$. Relative intracellular c-di-GMP level decrease percentages were marked above bars.

As shown in Fig 6.2.1, PAO1 WT showed a 48.73% decrease in intracellular c-di-GMP level after the addition of NO ($p<0.01$), which was consistent with previous reports[242]. Decrease percentages of 48.73±10% were considered comparable to PAO1 WT due to systematic errors. The most promising NO sensor candidates in charge of the reduction of intracellular pool were RbdA, PA0338 and PA5442 highlighted in red. Deleting these three proteins resulted in a less decrease of intracellular c-di-GMP (around 25% compared to 48.73% in PAO1 WT) upon NO treatment. Δ*pa0290,* Δ*fimX* and Δ*dipA* also had significantly less sensitivity to NO, suggesting their important roles as well.

## 6.2.2 NO-induced biofilm dispersal in KO mutant biofilms

| | 2 d biomass | | 3 d biomass |
|---|---|---|---|
| **PAO1 WT** | -68.56% (***) | > | -57.89% (***) |
| **Δ*pa0285*** | -89.37% (***) | > | -68.54% (***) |
| **Δ*pa0290*** | -62.18% (***) | > | -38.50% (***) |
| **Δ*pa0338*** | -41.50% (***) | | -47.42% (***) |
| **Δ*pa0575*** | -34.84% (**) | | -62.14% (***) |
| **Δ*pa0847*** | -41.87% (**) | > | -31.26% (***) |
| **Δ*rbdA*** | -25.21% (**) | > | -16.09% |
| **Δ*yegE*** | -63.63% (***) | > | -30.40% (***) |
| **Δ*bdlA*** | -57.77% (***) | > | -37.98% (***) |
| **Δ*mucR*** | -55.42% (***) | > | -41.83% (***) |
| **Δ*nbdA*** | -26.55% (**) | | -53.24% (***) |
| **Δ*morA*** | +4.77% | | -13.16% (***) |
| **Δ*fimX*** | -78.05% (***) | | -76.90% (***) |
| **Δ*dipA*** | -34.54% (**) | | -30.88% (***) |
| **Δ*pa5442*** | -17.34% | | -43.50% (***) |

Table 6.2.2. Comparison of NO-induced biomass reduction (dispersal) in 2 d and 3 d biofilms of each KO mutant. Texts highlighted in green represents in both 2 and 3 d old biofilms, the mutants showed more dispersal than WT in contact with NO. Texts highlighted in red represents in both 2 and 3 d old biofilms, the mutants showed less dispersal than WT in contact with NO. ** represents significant biofilm biomass reduction ($p<0.05$). *** represents significant biofilm biomass reduction ($0.01<p<0.05$). > represents 2 d biofilms dispersal is more than 3 d biofilms from the same strains.

As discussed in chapter 3, the same NO treatment resulted in different dispersal percentages on 1-5 d biofilms from the same strain, indicating that the stages of biofilm development may influence NO efficacy. Therefore, only the strains showing an altered dispersal effect both in 2 and 3 d biofilms compared to WT are regarded to be influenced in NO response.

From Table 6.2.2, it can be summarized:

(1) *Δpa0338, Δpa0847, ΔrbdA, ΔbdlA, ΔmucR, ΔmorA, ΔdipA* and *Δpa5442* had impaired NO response to trigger biofilm dispersal (highlighted in red). In contrast, *Δpa0285* and *ΔfimX* showed enhanced NO effect resulting in more dispersal (highlighted in green). Data were also supported by visual judgement from CLSM images in Fig 6.2.2 and Appendix Fig A9 and Fig A11. This suggested that these proteins are involved in biofilm formation and dispersal, as well as NO regulatory network, despite the detailed mechanisms remain unclear.

(2) Despite all these proteins might be involved in NO triggered biofilm dispersal, how much they are involved in and how much they affected the dispersal (biomass reduction percentages) vary. The most prominent dispersal deficiency occurred in *ΔrbdA* and *ΔmorA* 3 d biofilms where they showed no response to NO ($p>0.05$).

*Δpa0847* and *ΔdipA* biofilms also showed consistent and remarkable reduced NO response (more than 26% less reduction of biomass compared to WT) cross 2 and 3 d. Consequently, these four candidates are considered to play major roles in NO-dispersal pathway.

(3) 10 out of 15 strains showed their 2 d biofilms were more sensitive to NO than 3 d biofilms (2 d biomass reduction>3 d biomass reduction). This corresponded to findings in 3.5 showing 3 d PAO1 WT biofilms dispersed less than 2 d ones in microtiter plates. Data from different KO strains suggest and reinforce the hypothesis where maturation stages of biofilms may also affect how NO triggers biofilm dispersal apart from gene/protein specific manners.

## 6.2.3. NO influence on PAO1 WT motilities

Motility assays agar plates needed 20-24 hrs incubation, hence SNP was used as NO donor instead of S150. To investigate the effective SNP concentration, 1µM, 10µM and 100µM SNP were first infused into different agar plates for PAO1 WT and motility assays were performed as described in 2.6.

| **PAO1 WT Swim** | **Swim+1µM SNP** | **Swim+10µM SNP** | **Swim+100µM SNP** |
|---|---|---|---|
| / | / | --- | --- |
| **PAO1 WT Swarm** | **Swarm+1µM SNP** | **Swarm+10µM SNP** | **Swarm+100µM SNP** |
| / | +++ | --- | **/ (pattern altered)** |
| **PAO1 WT Twitch** | **Twitch+1µM SNP** | **Twitch+10µM SNP** | **Twitch+100µM SNP** |
| / | / | / | / |

Table 6.2.3. PAO1 WT motilities alteration with 1µM, 10µM and 100µM SNP. Swimming, swarming and twitching motilities of PAO1 WT were shown as /. +++ represents significant increase ($p<0.01$) compared to control. --- represents significant decrease ($p<0.01$) compared to control. n=12 from individual plates, Welch T-test was applied due to large variations. Raw data are shown in Appendix Fig A13.

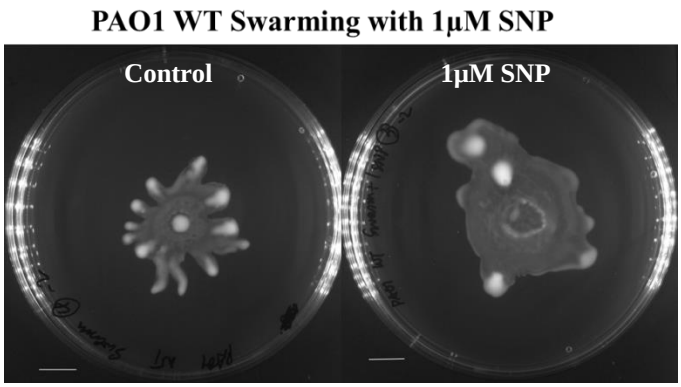


Fig 6.2.3 Selective images of PAO1 WT swarming motility agar plates with 1μM SNP and determination of swarming zone areas using Image J. Representative images of other plates are shown in Appendix Fig A13.

As shown in Table 6.2.3, although SNP was expected to increase the motility, it was found that 1μM SNP significantly promoted swarming motility ($p<0.01$), which was in accordance with previous report[9]. However, it had no influence on swimming and twitching motility ($p>0.05$). On the contrary, 10μM and 100μM significantly inhibited swimming and swarming motilities, while 100μM SNP even altered swarming pattern as shown in Appendix Fig A13. High dose NO may have triggered stress responses in individual cells inoculated on the surfaces of agar plates, which was related to flagella regulation causing inhibition of swimming and swarming. This result was supported by the finding from Barraud *et al* that high concentrations of SNP even promoted biofilm production probably due to the stress response of *P. aeruginosa*[9]. Inhibited swimming and swarming motility may promote the attachment of floating planktonic cells to surfaces, causing increased biofilm formation. Consequently, low dose of SNP (1μM) was chosen to investigate the NO signalling effect on swarming motility of mutant strains, while the swimming and twitching motility were only investigated without SNP to compare the difference among strains.

## 6.2.4 NO influence on the swarming motility of 14 KO mutants

Swarming assays were performed as described in 2.6.3. According to Table 6.2.3, 1μM SNP is the optimal dose for promoting swarming thus was applied to all KO mutants. The increased swarming area of each KO mutant was compared to PAO1 WT and summarized in Table 6.2.4. Representative images of swarming plates are shown in Fig 6.2.4. Raw data are shown in Appendix Fig A14.

| **PAO1 WT** | ***Δpa0285*** | ***Δpa0290*** | ***Δpa0338*** | ***Δpa0575*** | ***Δpa0847*** | ***ΔrbdA*** | ***ΔyegE*** |
|---|---|---|---|---|---|---|---|
| ++ | +++ | ++ | ++ | ++ | + | + | ++ |
| ***ΔbdlA*** | ***ΔmucR*** | ***ΔnbdA*** | ***ΔmorA*** | ***ΔfimX*** | ***ΔdipA*** | ***Δpa5442*** | |
| ++ | ++ | ++ | +++ | +++ | / | ++ | |

Table 6.2.4. NO triggered swarming enhancement on PAO1 WT and 14 KO mutant strains. The swarming increase of PAO1 WT is shown as ++, +++ represents the swarming motility increased more than WT within the same batches of assay ($p<0.05$), + represents the swarming motility increased less than WT within the same batches of assay ($p<0.05$), / represents no increase in swarming was observed after NO addition.

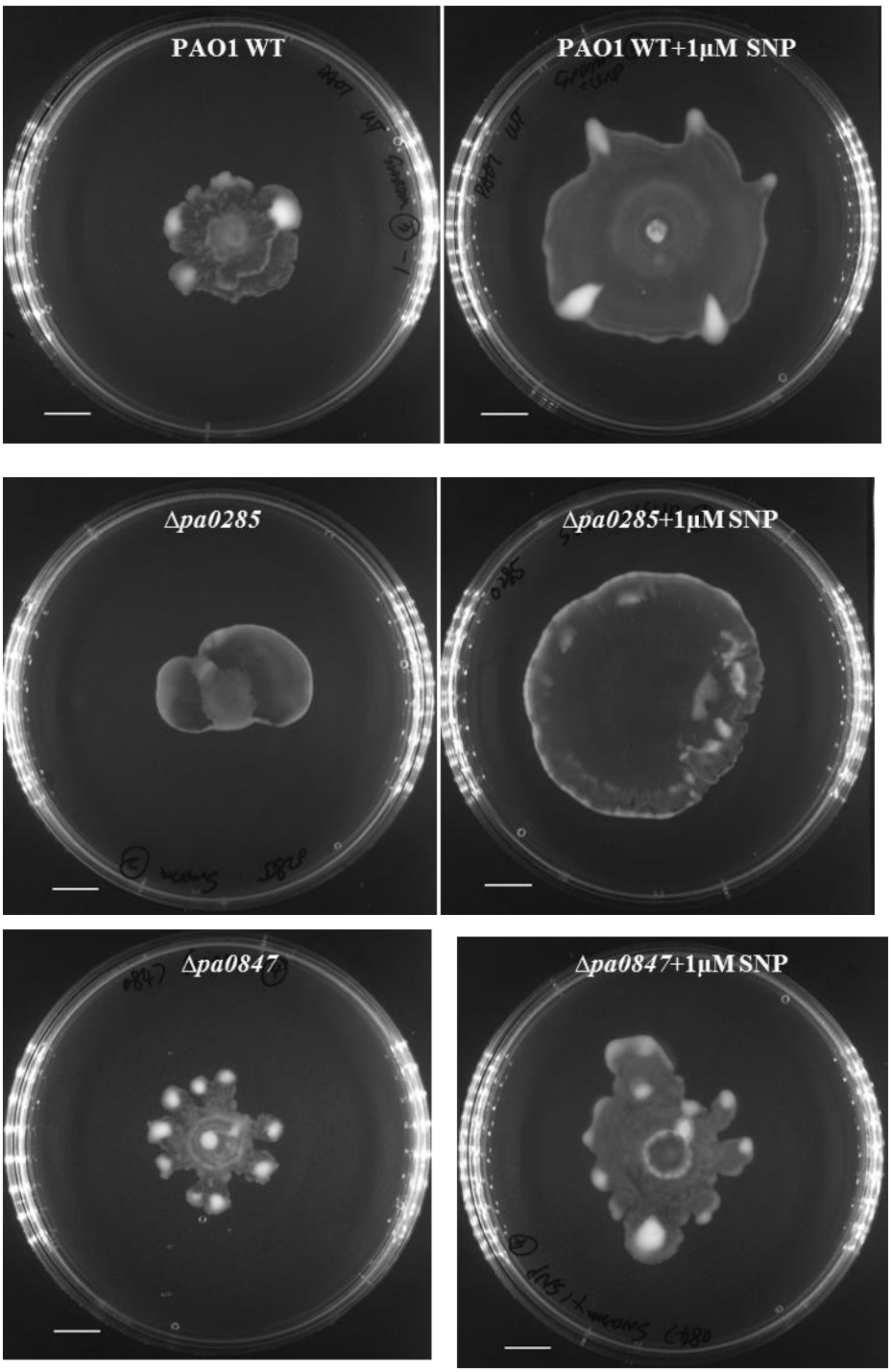

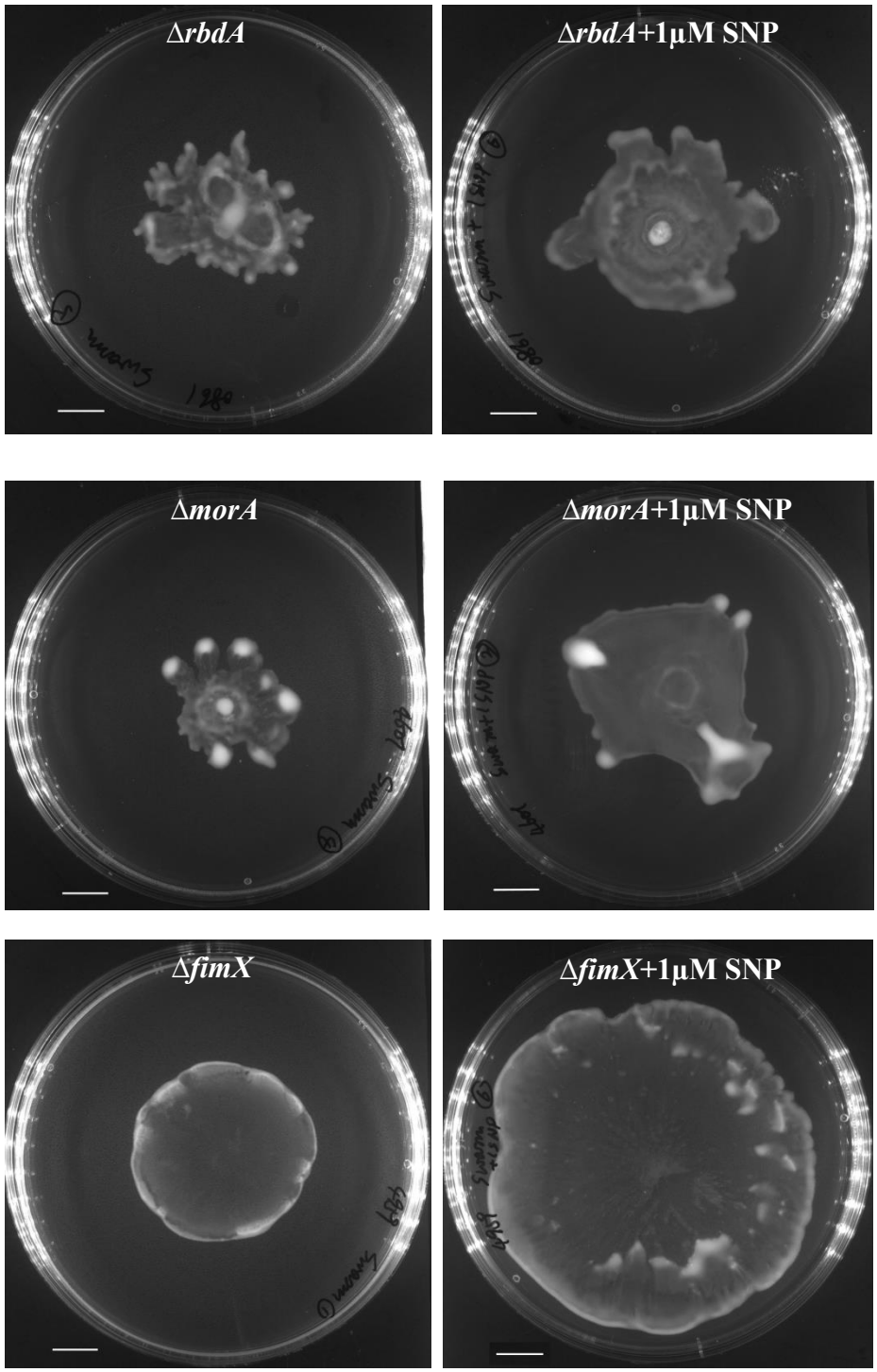
Δ*rbdA*
Δ*rbdA*+1μM SNP
Δ*morA*
Δ*morA*+1μM SNP
Δ*fimX*
Δ*fimX*+1μM SNP

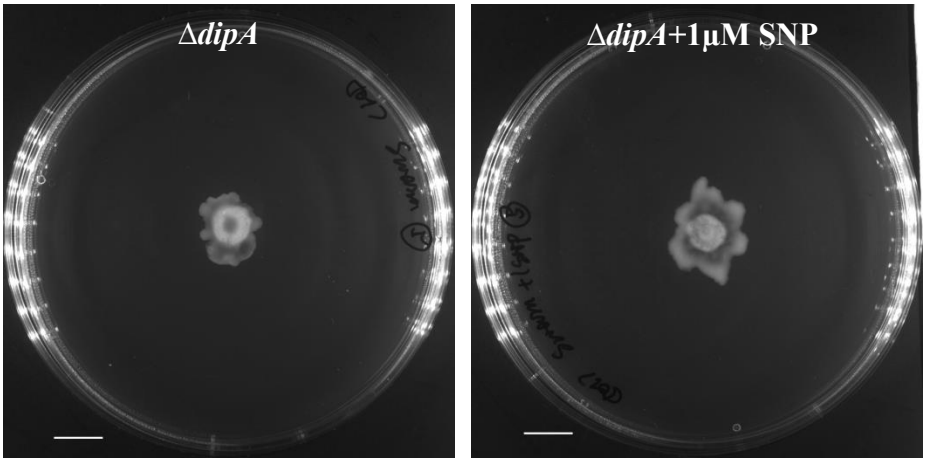


Fig 6.2.4. Representative images of swarming agar with/without 1μM SNP. Scale bar = 1cm.

To my knowledge, apart from Barraud *et al* reporting the addition of NO significantly enhanced swarming motility in PAO1 WT[242], no investigations into how NO affected the swarming motility of our candidate genes were performed. Hence, these data in the current study are the first to report how much NO influences the swarming motilities in all these mutants and compared to WT. It can be concluded that with the addition of NO, *Δpa0285, ΔmorA* and *ΔfimX* showed increased swarming extent compared to WT while the loss of PA0847, RbdA and DipA resulted in impaired swarming enhancement triggered by NO. Data here implicated these proteins are in NO-swarming regulatory pathways in PAO1; however the specific mechanisms wait to be revealed. It is noteworthy that the NO effect on swarming promotion is abolished in *ΔdipA* ($p>0.05$), suggesting its central role in NO-induced swarming alteration.

## 6.3 Phenotypic analysis of Tn transposon mutants

### 6.3.1 Growth curves and colony morphologies of Tn mutants

Growth curves were measured in microtiter plates as described in 2.5.1 and all raw data are presented in Appendix Fig A15.

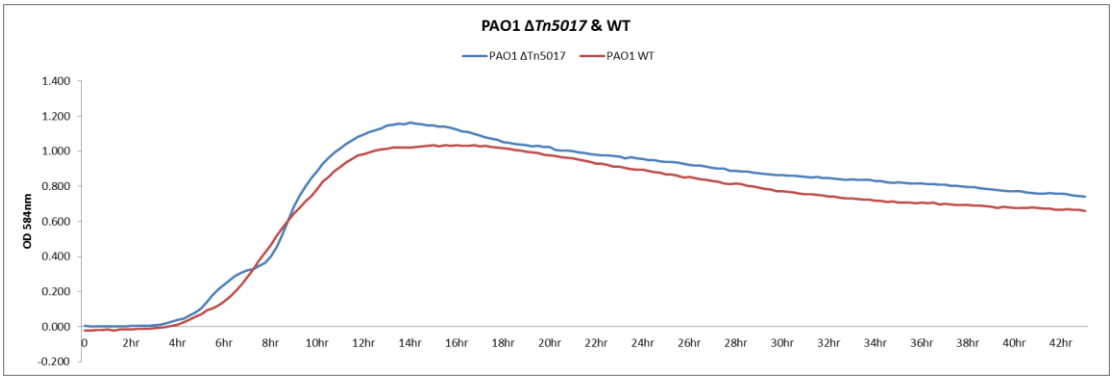


Fig 6.3.1. Growth curves of PAO1 WT and *ΔTn5017 (ΔdipA)*.

5 out of 8 transposon mutants showed the same growth pattern as PAO1 WT until they reached the stationary phase, but then the OD value of Tn mutants decreased more quickly than WT (as shown in Fig 15). Whether this general difference in the growth curve pattern was due to the polar effect of tetracycline resistance gene insertion in these mutants or the transposon insertion itself remained unknown. Δ*Tn5017* showed a slight diauxic pattern although not so obvious as Δ*dipA in* Fig 6.1.2. This consistency proved that pa5017 does have effect on the diauxic-like growth curve. All Tn mutants showed the same colony morphologies (data shown in Appendix Fig A16), which is consistent with data from KO mutants.

### 6.3.2. 2d batch cultured Tn mutants biofilms

**A**

**2d PAO1 WT biofilm**

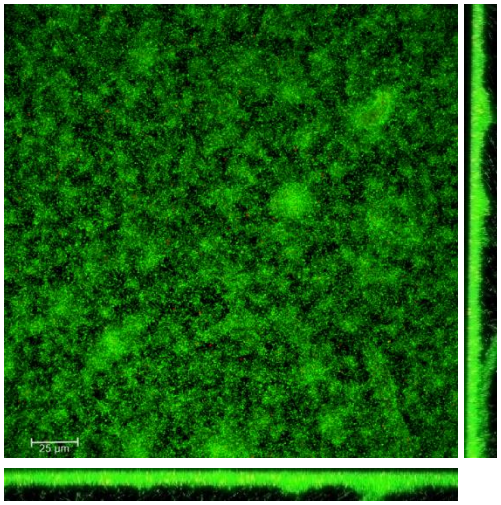

**2d Δ*Tn0290* biofilm**

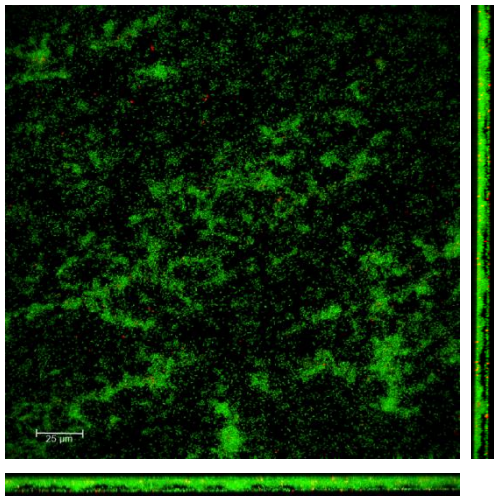

**2d Δ*Tn0338* biofilm**

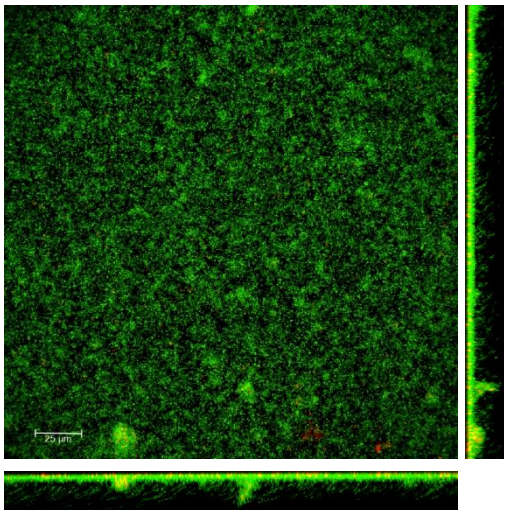

**2d Δ*Tn0861* biofilm**

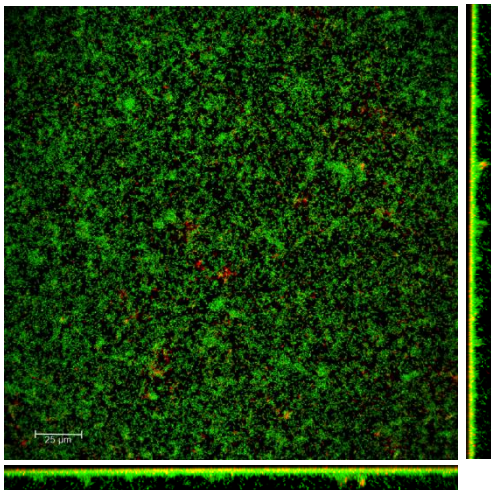

**2d Δ*Tn1181* biofilm**

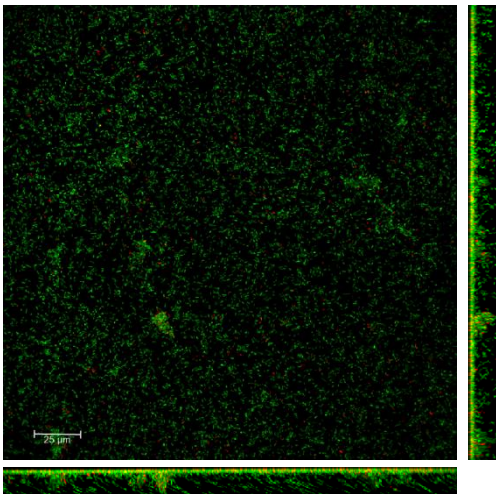

**2d Δ*Tn3311* biofilm**

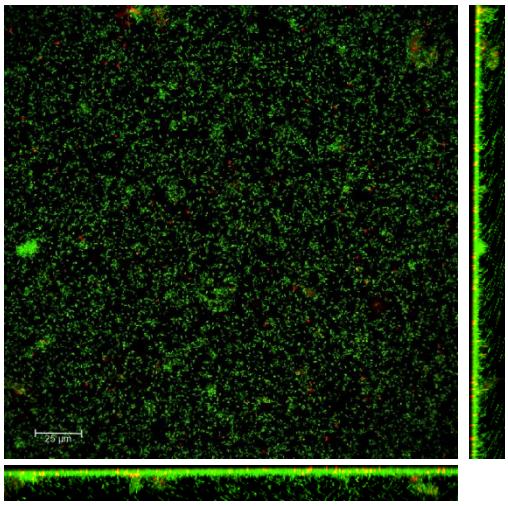

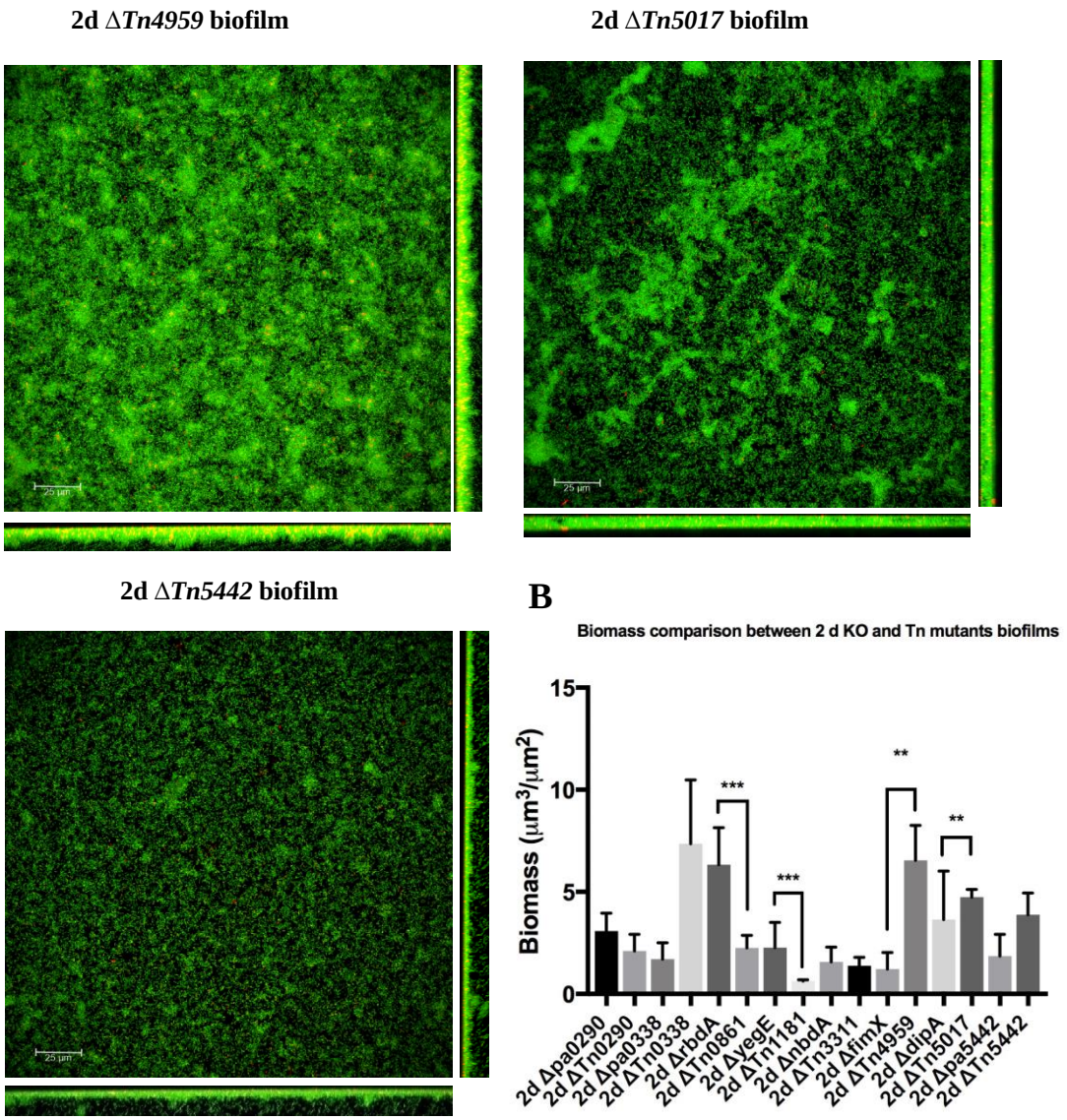


Fig 6.3.2. (A) Selective CLSM images of batch cultured 2d Tn mutants biofilms in MatTek plates. (B) Comparison of biofilm formation abilities (biomass) of Tn mutants with corresponding KO mutants. Welch T-test was carried out to compare the KO and Tn mutants. n=3 from 3 biological replicates, *** represents $p<0.01$, ** represents $0.01<p<0.05$.

Compared to CLSM images in 6.1.2, some Tn mutants showed different biofilm structures compared to the corresponding KO mutants losing the same genes, such as *ΔTn0290, ΔTn0861 (rbdA)* and *ΔTn3311 (nbdA).* As shown in Fig 6.3.2 (B), *ΔrbdA* and *ΔyegE* biofilms showed significantly higher biomasses compared to *ΔTn0861 (rdbA)* and *ΔTn1181 (yegE),* while *ΔfimX* and *ΔdipA* formed significantly less biofilm compared to *ΔTn4949 (fimX)* and *ΔTn5017 (dipA).* Hence, data here showed different gene disruption methods for the same gene resulted in different phenotypic outputs regarding biofilm formation and structures.

*ΔTn5017 (dipA)* showed much more biofilm than WT, which is consistent with previous report[337]. Jain *et al* reported that in a static biofilm model, PAO1*ΔfimX* formed biofilms indistinguishable from those of WT PAO1[227]. Data here showed consistency with this report where *ΔTn4949 (fimX)* formed comparable biomass with WT (see appendix Fig A17), while data from *ΔfimX* (section 6.1.2) showing less biofilm formation disagreed with this finding. However, my data from *ΔrbdA* (section 6.1.2) showing it promoted biofilm formation was consistent with a previous report[488], but *ΔTn0861 (rbdA)* showed much less biofilm than WT (See Appendix Fig A17) and *ΔrbdA*. Hence, it was suspected that *ΔTn0861* biofilm formation might not be able to reflect the authentic influence of RbdA on biofilm formation or structure. No report has shown the relationship between *ΔyegE* the biofilm. In summary, *ΔTn5017* and *ΔTn4959* data agreed with previous finding while *ΔTn0861* did not; *ΔdipA* and *ΔrbdA* data were consistent with previous reports but *ΔfimX* were not. According to Manoil transposon mutants library (http://www.gs.washington.edu/labs/manoil/libraryindex.htm), *ΔTn0861 (rbdA)* and *ΔTn4959 (fimX)* Tn insertion were in frame, while *ΔTn5017 (dipA)* and *ΔTn1181 (yegE)* insertions were not in frame. KO mutants generated in this study were deleted in frame. It is interesting that despite the potential frame shift, *ΔTn5017 and ΔTn4959* data were still consistent with previous research. Therefore, it is difficult to decide which gene disruption method is more likely to reflect the accurate functions of these proteins in biofilm formation.

## 6.3.3. Motility of Tn transposon mutants

Motility assays were performed as described in 2.6.

**A Swimming**

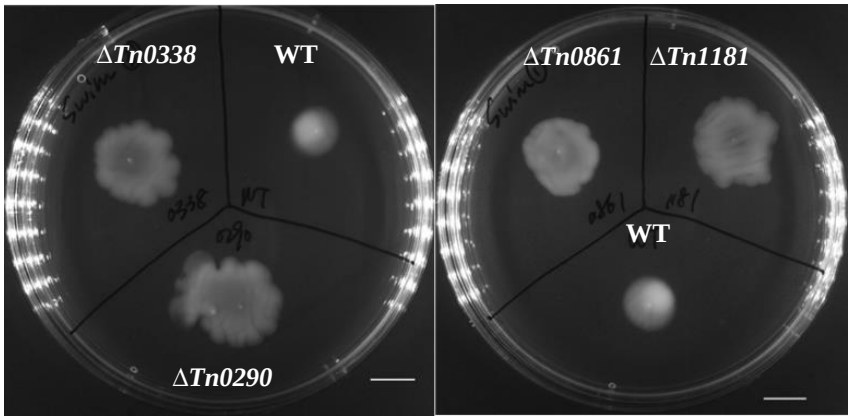

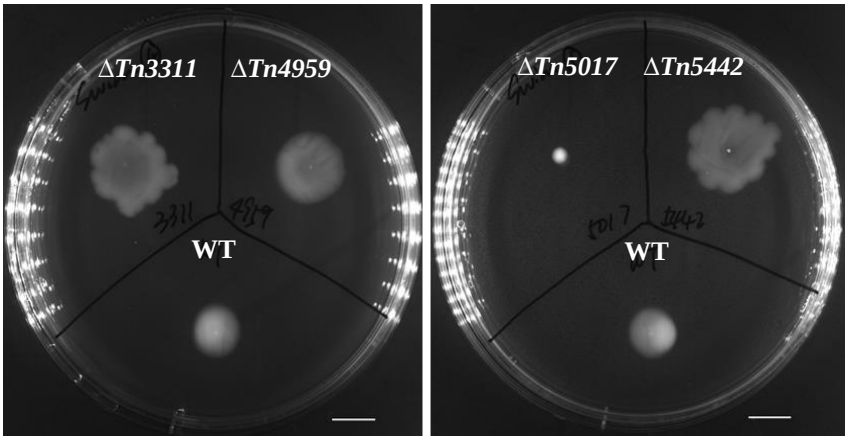


**B Swarming (18 hrs incubation)**

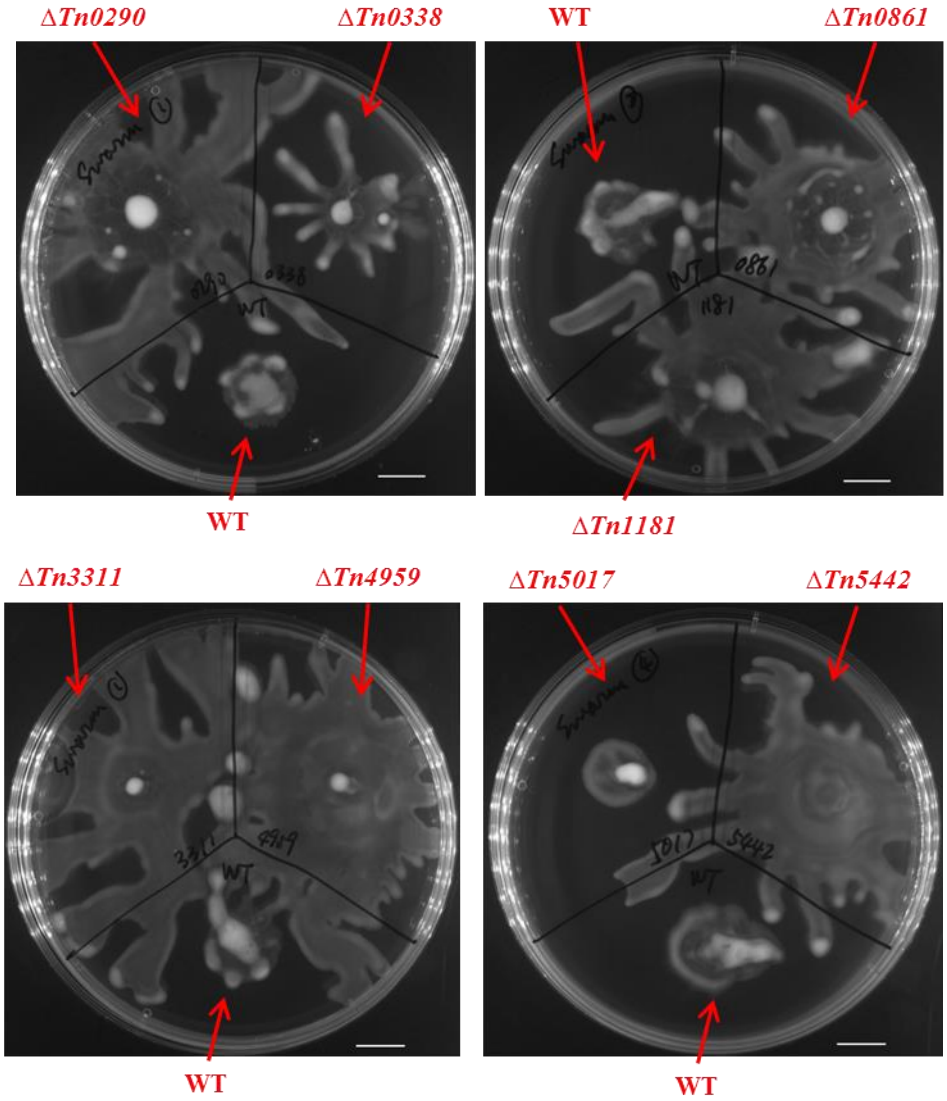

**C Twitching**

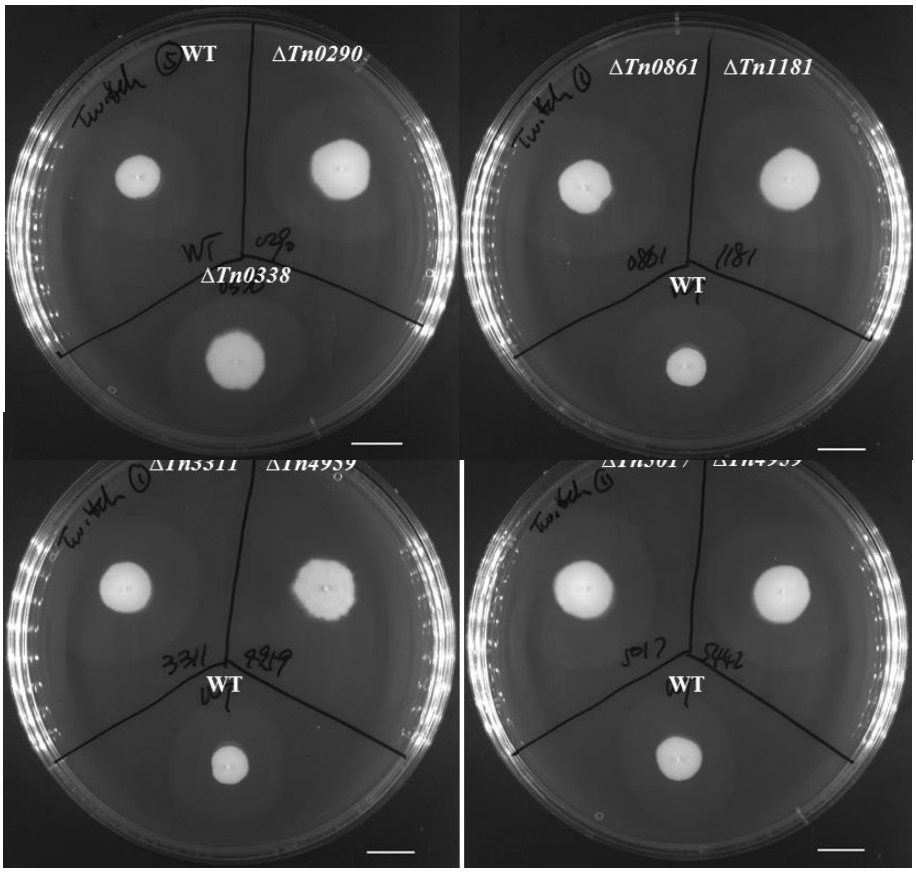


**D**

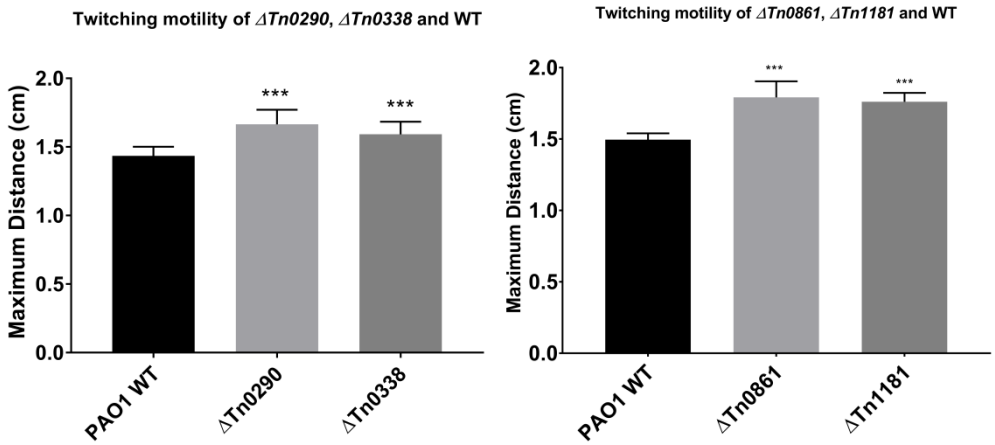

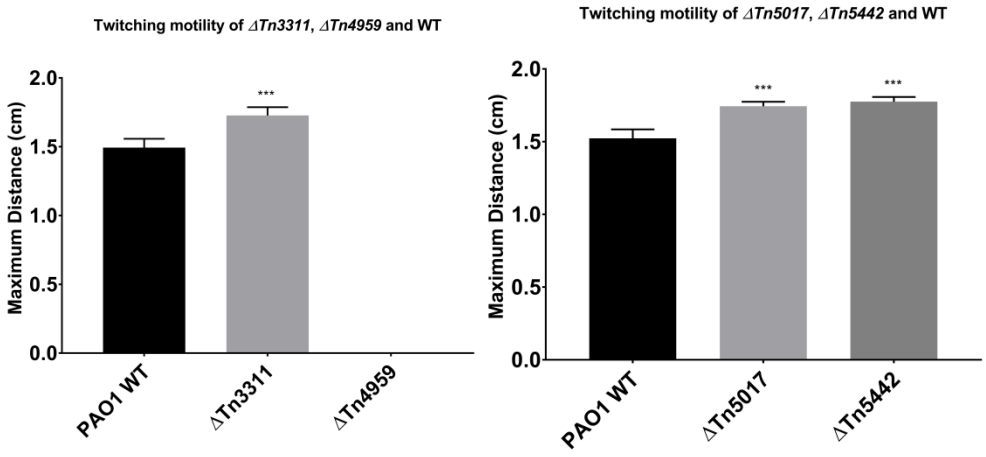


Fig 6.3.3 (A) Selective images of Tn mutants swimming (A), swarming **after 18 hrs incubation** (B) and twitching (C) plates. Scale bar = 1cm. (D) Measurement of twitching zone maximum distances of KO mutants using Image J. n=6 from 6 biological replicates, Welch T-test was applied due to large variations. *** represents 0.01<p<0.05, ** represents p<0.05.

From data shown above it can be concluded:

(1) Apart from *ΔTn4959 (fimX)* and *ΔTn5017 (dipA)*, all Tn mutants exhibited an unusual pattern with irregular swimming zone edges compared to standard radial growth[308], which was not observed in various published PAO1 swimming agars using various media. Among the genes with altered swimming pattern, *ΔTn0861* and *Tn5442* have in frame Tn insertion. Therefore, at least this alteration in these two strains did not come from gene frame shift, and the rest of genes exhibiting abnormal swimming pattern were not likely to be all involved in swimming regulation.

(2) Normally in the swarming assays described here, tendrils only started to appear after 18 hrs incubation for PAO1 WT and all KO mutants at 37℃, and well-developed swarming patterns can only be observed after 24 hrs. However, as shown in Fig 6.3.3 (B), all Tn presented well-developed large swarming patterns after 18 hrs when WT just started to swarm. Furthermore, Δ*Tn0861* and Δ*Tn0338* showed much larger swarming zones compared to WT while *ΔTn5017* showed comparable swarming zone as WT, which was contradictory to what was found in Δ*rbdA*, Δ*pa0338 and ΔdipA* (section 6.1.4). In conclusion, the swarming motility of all Tn mutants pronouncedly differed from corresponding KO mutants in patterns and swarming areas, which was not likely

coming from gene-specific manner. *ΔTn0861, ΔTn4959* and *ΔTn5442* have in frame insertion so again this swarming change should not have been a result of frame shift.

(3) From Fig 6.3.3 (C) and (D) it was concluded that apart from Δ*Tn4959* which showed the same abrogated twitching ability as Δ*fimX* (section 6.1.4), all other Tn mutants resulted in significantly larger twitching zones compared to WT and the corresponding KO mutants. As with the abnormal swarming zones, it was not likely all these genes were involved in twitching ability. Hence, it was suspected that Tn insertion might have caused a polar effect on PAO1 twitching motility.

Taken together, all the Tn mutants exhibited very different motilities compared to KO mutants or WT and it was not likely to be gene-specific or due to frame shift of Tn insertion. Hence, it was suspected that Tn transposon *per se* or the insertion had a polar effect on PAO1 despite the mechanisms remain unknown. However, so far no report has mentioned similar findings. Overhage *et al* reported using mini-Tn5-*luxCDABE* Tn mutant for swarming motility of PAO1 and did not observe unusual swarming patterns, but they were using BM2 swarm agar plates for swarming. Therefore, this effect might be specific to transposon type and experimental conditions[489]. Based on these findings, experiments on Tn mutants with NO were not performed. In general, further studies should be carried out to reveal why this happened and warning should be exerted to all researchers intending to perform motility assays using Tn PAO1 strains from the library.

# Discussion

## *(I) Total intracellular c-di-GMP and phenotypes controlling in P. aeruginosa PAO1*

### (1) Biofilm formation and specific biofilm-related phenotypes are not dependent on the total intracellular c-di-GMP levels

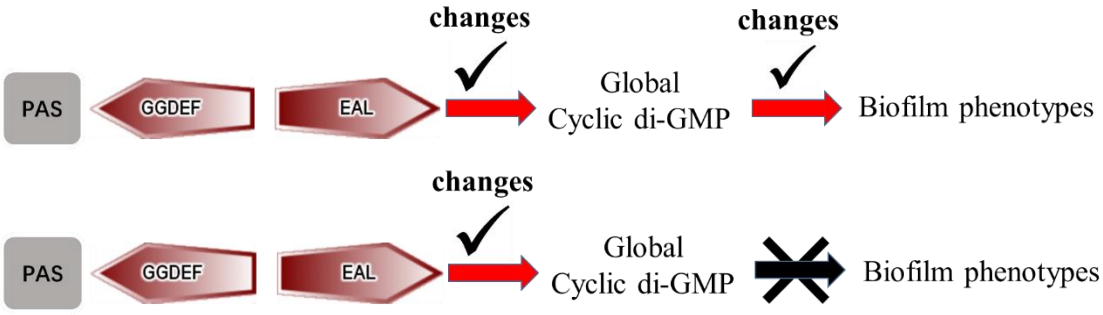


Our hypothesis for the deleted DGC+/PDEs was that they might contribute to intracellular c-di-GMP, which in turn regulate biofilm related phenotypes for the switch between motile and sessile lifestyles. It is shown in Fig 6.1.1 that only PA0285, RbdA, NbdA, MorA, DipA and PA5442 altered the global c-di-GMP level in the cells. PA0285, RbdA and DipA might act as highly active PDEs *in vivo*, or they have high affinity to c-di-GMP and their binding to the molecule decreases intracellular c-di-GMP level. At the same time, MorA and NbdA also contribute to intracellular c-di-GMP pool by acting as PDEs or c-di-GMP binders. On the contrary, PA5442 might act as a highly active DGC *in vivo*, or might exert activity not by itself but by forming heterodimers with another DGC.

Previous reports have shown the *in vitro* phosphodiesterase activities of RbdA[488], MorA[178], and DipA[337], of which DipA was also proved to influence intracellular c-di-GMP level *in vivo*[3]. Furthermore, due to the existence of both GGDEF and EAL domains in tandem (Fig 6.0.1), MorA was shown to exhibit both DGC and PDE activities *in vitro*[178]. The c-di-GMP detection data here supported and added to previous findings on RbdA, MorA and DipA, showing that these proteins reduce intracellular c-di-GMP levels *in vivo*.

Even though *Δpa0285*, *ΔrbdA*, *ΔmorA* and *ΔdipA* all increased global c-di-GMP levels, they are regulating different biofilm-related phenotypes. *Δpa0285* impaired biofilm development but *ΔrbdA* enhanced it, while *ΔmorA* and *ΔdipA* remained comparable to

WT (Table 6.1.3 and Fig 6.1.3). *Δpa0285*, *ΔrbdA* and *ΔdipA* restricted swimming motility, but *ΔmorA* enhanced swimming ability (Fig 6.1.4 and Table 6.1.4). *Δpa0285* resulted in a decreased growth rate as well as smaller and white colony morphology while *ΔdipA* showed a diauxic growth curve, but *ΔrbdA* and *ΔmorA* did not change the growth rate or colony morphology (Fig 6.1.2, Appendix Fig A1-2). *ΔrbdA* increased EPS production while another 3 genes did not (Fig 6.1.5). Results shown here are consistent with previous reports on RbdA[488] and DipA[457], and were the first to report a potential important role of *Δpa0285* in biofilm regulation given it is involved in at least 5 phenotypic outputs. Choy *et al* reported that MorA repressed flagella development and the deletion mutant resulted in increased number of flagella as well as their production time periods in *P. putida*, but not in *P. aeruginosa* PAO1 despite MorA being conserved in these two species[404]. However, data here showed that in PAO1, *ΔmorA* has also significantly increased swimming motility yet not hugely ($0.01<p<0.05$, Fig A5).

Hence, although 6 out of 14 mutants influenced intracellular c-di-GMP levels, only *Δpa0285* and *ΔrbdA* were involved in biofilm formation, but the same elevated intracellular c-di-GMP level exerted the opposite effects. 4 mutants with altered c-di-GMP levels were related to phenotypic outputs tested in this study, but the changes were all different. Therefore, it was suggested that a coarse tuning of total intracellular c-di-GMP level is not the only reason that controls biofilm formation or structures, and so cannot decide a certain phenotype. The complex relationship between c-di-GMP level and biofilm formation cannot be simply summarized as "an increase in intracellular c-di-GMP leads to more biofilm" as was the traditional idea. Future work may use qPCR and proteomic analysis to reveal the profile changes of different mutants with overproduced c-di-GMP by *in trans* expressed DGC and their biofilm formation. If intracellular level on its own affects biofilm formation, the profile changes should be similar in different mutants with the same total amount of c-di-GMP.

It is also noteworthy that in many previous reports, distinct biofilm formation characters were usually found when there was >2 fold difference in intracellular c-di-GMP levels[182,337,443,490,491]. However, the biggest fold change of cellular c-di-GMP level between KO and WT in this study was less than 2 (Fig 6.1.1, *ΔdipA* vs WT). This raised the suspicion whether there is a threshold for c-di-GMP amount to regulate biofilm

formation/dispersal. As such, *Δpa0285* and *ΔdipA* did not enhance c-di-GMP level enough to generate a biofilm promotion as widely observed. To test if there is a minimum of c-di-GMP concentration contributing to biofilms promotion, a defined DGC from another strain may be infused downstream of an IPTG inducible promoter to control the total amount of c-di-GMP. This DGC can then be overexpressed in *P. aeruginosa* with different expression efficiencies and the biofilm formation should be determined to decide if there is a correlation between the c-di-GMP concentration and biomass within the same strain.

**(2) Certain biofilm phenotypes may be decided by certain DGC/PDEs through local c-di-GMP modulation instead of the total amount**


As shown in Fig 6.1.1, *Δpa0338*, *ΔyegE*, *ΔmucR* and *ΔfimX* showed comparable intracellular c-di-GMP amount as WT. Previous reports have shown the *in vitro* phosphodiesterase activities of MucR[146] and FimX[444], of which MucR was also proved to influence intracellular c-di-GMP level *in vivo*[146]. However, Δ*mucR* did not show significantly different c-di-GMP level compared to PAO1 WT, which disagreed with Li *et al* results and the reason remains unknown[146]. Δ*fimX* did not affect intracellular c-di-GMP level, which was in accordance to the findings from Jain *et al* using strain PA103 and was probably due to its specific localization[227].

Despite these 4 genes not affecting total intracellular c-di-GMP levels *in vivo*, they are involved in different biofilm phenotypic regulations. *Δpa0338* and *ΔfimX* both impaired swimming and swarming motility but increased EPS production, while *ΔfimX* also changed swarming pattern and abolished twitching (Fig 6.1.4). In contrast, *ΔyegE* and *ΔmucR* enhanced swimming motility. FimX was reported to be an active phosphodiesterase and involved in twitching motility in *P. aeruginosa*, but not swimming[226,444]. MucR was reported to be an active diguanlyate cyclase that locally regulates alginate production and overexpression affected swarming motility, yet swimming motility was not assessed by the author[147]. Hence, data here first reported the phenotypes of *Δpa0338* and *ΔyegE* in PAO1 WT, and added to the current knowledge of FimX and MucR. *ΔfimX* showed a similar influence on swimming, swarming and twitching motility as *Δpa0285*, but did not change intracellular c-di-

GMP level. *Δpa0338* significantly impaired swimming and swarming as *ΔdipA*, but also had no effect on total c-di-GMP amount. Therefore, it is deduced that some DGC/PDEs may alter c-di-GMP and regulate certain phenotypes locally or under specific circumstances, but is below detection, at least using our plasmid reporter-based method.

In summary, it is suspected that under a certain threshold, it is not the intracellular c-di-GMP level differences *per se* contributing to the variances of biofilm-related phenotypes. More possibly, certain proteins may significantly change intracellular c-di-GMP, but they function through regulating certain compartmentalized c-di-GMP pools that are in vicinity of genes involved in precise regulatory pathways, such as motility or EPS production. In other words, it is the localized c-di-GMP modulation by certain proteins that exert specific regulatory pathways on phenotypic changes, but the DGC/PDE activities or the c-di-GMP binding affinities are so high that at the same time their functions are sufficient to alter the whole intracellular c-di-GMP levels. The situation could also be that certain DGC/PDEs are in charge of c-di-GMP modulation, but the influences are small and restricted to specific locations. This results in phenotypic changes when the proteins are deleted, but the differences of total intracellular c-di-GMP is not detectable using current methods. It is now becoming more widely accepted that the effects of c-di-GMP must be localized subcellularly, being responsible for different phenotypic outputs. Merrit *et al* further proved two different DGCs control discrete outputs despite the same total level of c-di-GMP, which extended the model into one in which localized c-di-GMP signalling might contribute to the coordination of the action of this complex intracellular network[213]. Besides, the redundancy of more than 40 genes in PAO1 responsible for coding DGCs or PDEs with different sensing or anchoring domains may also hint it is not likely they are contributing equally to the c-di-GMP pathway in the cell, either spatially or quantitatively.

On the other hand, the threshold of c-di-GMP level may be very important. For example, the intracellular c-di-GMP level alterations in *ΔdipA* was only <2 fold more than WT and the biofilm formation did not change, seemingly arguing with the traditional concept that increased c-di-GMP causes more biofilms. The *in vivo* overexpression of DipA by 2 fold and 10 fold with an inducible promoter may help to decide whether it

is gene/protein specific or from an intracellular pool. This concentration-dependent phenotypic change model may be supported by Jain *et al* reporting that the assembly of pili at low c-di-GMP concentrations requires FimX, but this demand can be bypassed at high c-di-GMP concentrations[227]. Therefore, the precise amount of c-di-GMP, high or low, and its fine-tuning mechanisms with thresholds might be playing a more important role in certain phenotypic outputs than vague and more relative "high or low levels". When cells have a relatively lower total amount of c-di-GMP, the distribution of this molecule may be controlled in a more economical and beneficial way to bacterial cells. Therefore, it is very likely that under low c-di-GMP levels, the production and allocation of this molecule into different locations and pathways inside the cells are largely dependent on the most urgently required pathways for bacteria survival, or the binding affinities of GGDEF/EAL in different proteins. For regulating a certain phenotype, direct, localized c-di-GMP and remote c-di-GMP may all bind to receptor genes/proteins. However, when the intracellular pool is low but cells need c-di-GMP production to regulate a phenotypic output, it may choose the one that has the best balance between high DGC activity and short distance to receptor. This economical selection may not be needed if there is an overflow of intracellular c-di-GMP either coming from the loss of a PDE or *in trans* overexpression of a DGC. Thus, proteins with different affinities to c-di-GMP work altogether and the final phenotypic outputs is a balance and coordination of all activities.

Hence, the data here potentially adds to the previous concept that it is localized c-di-GMP pools controlling some specific phenotypes (if not all), but probably only under certain background concentrations.

### *(II) How nitric oxide triggers PAO1 biofilm dispersal?*

**Model A: RbdA and DipA are essential PDEs for NO-induced intracellular c-di-GMP reduction, swarming enhancement and biofilm dispersal**

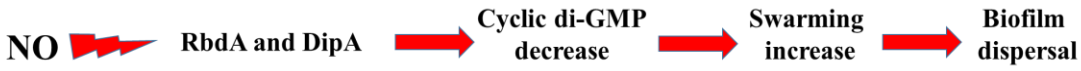


Barraud *et al* showed that NO induces *P. aeruginosa* biofilms dispersal by decreasing intracellular c-di-GMP, while at the same time their results also demonstrated an increased swarming motility of PAO1 WT after NO addition, suggesting a link between

swarming, intracellular c-di-GMP and dispersal[9]. Extensive studies have been conducted to investigate the relationship between swarming motility and biofilm formation[68,492–497], but the relationship between swarming and dispersal is yet to be elucidated, to our knowledge. The three modes of biofilm dispersal identified so far, erosion, sloughing, and seeding, are all involved in the release of cell clusters. Hence, it is reasonable to deduce that swarming, a bulk-translocation behaviour, might contribute to dispersal. Hall-Stoodley observed that *P. aeruginosa* uses swarming mode dispersal with time-lapse microscope[498], which indicated that the increased swarming might cause more dispersal. This suggested one potential pathway where NO-induced dispersal is through reducing cellular c-di-GMP and enhancing swarming, despite that there should be other mechanisms working collaboratively.

*ΔrbdA* and *ΔdipA* were the only two strains that showed impaired NO-induced decrease in intracellular c-di-GMP level (Fig 6.2.1), less biofilm dispersal upon NO treatment (Fig 6.2.2) and the lack of increased swarming zone with the presence of NO (Fig 6.2.4). Linking these three phenotypes together, it seems a pathway where "NO interacts with RbdA and DipA potentially through PAS domains and up-regulates their PDE/c-di-GMP binding activities, resulting in a significant reduction in intracellular c-di-GMP, which in turn enhances swarming motility and facilitates dispersal" can be modelled and fulfils our hypothesis. However, Fig 6.2.1 suggested that PA0290, PA0338 and PA5442 also contributed to NO-induced c-di-GMP decrease, but their swarming motility increased comparably with WT after NO treatment (Table 6.2.4). Hence, it cannot be concluded at this stage that it is intracellular c-di-GMP level alterations *per se* being responsible for the swarming abilities and then dispersal. More likely, the PDE activities of these two proteins are very high so that they influence intracellular c-di-GMP levels, but the actual regulation on swarming relies on compartmentalized c-di-GMP levels.

As such, a refined model was proposed as "NO modulates the protein activities of RbdA and DipA, causing the change in both localized and intracellular c-di-GMP levels, of which the localized one has remarkable impact on swarming motility. At the same time, the remote controls on other bacterial activities from the increased intracellular pool in these two mutants were not sufficient to surpass their site-directed regulations on swarming".

Previous reports showed that BdlA senses NO through its PAS and regulates DipA PDE activity for c-di-GMP modulation, and adding NO to *ΔbdlA* results in less reduction in c-di-GMP compared to WT[242,443]. Data in this study disagreed with this finding where *ΔbdlA* showed the comparable c-di-GMP decrease compared to WT. Instead, DipA itself may have NO sensing ability potentially through its own PAS domain rather than the one from BdlA. Our data on DipA was consistent with Roy *et al*, showing abolished NO-induced dispersal, rendered swarming motility and increased intracellular c-di-GMP level in Δ*dipA*[337], while results on RbdA were consistent with An *et al* showing RbdA was implicated in the regulation of *P. aeruginosa* biofilm dispersal, swarming motility and possessed PDE activity[488]. However, neither group provided direct evidence showing that NO has an impaired effect on decreasing intracellular c-di-GMP and increasing swarming motility in Δ*rbdA* and Δ*dipA*. Hence, data in this study first showed a detailed regulation pathway of NO - c-di-GMP level - swarming - dispersal, which may contribute to one of the regulatory networks where NO modulates dispersal in PAO1.

Currently, we are lacking in experiments to prove PAS domains in RbdA and DipA can bind to NO and modulate their PDE activities, as well as the swarming and dispersal effect. Petrova and Li *et al* suggested the PAS domain BdlA plays a role in environmental cues sensing and together with DipA forms a regulatory network that modulates an intracellular c-di-GMP[296,441,499], while An *et al* proved the PAS domain in RbdA is critical for regulation of biofilm dispersal[488]. Again, neither group showed direct evidence in NO binding to PAS domain that modulates PDE activity. Hence, future studies should focus on (1) *in vitro* analysis through enzymatic activity assay in the presence of NO and crystallography that will show how NO binds to PAS domain, resulting in post-translational modification of EAL domain; (2) site-directed mutagenesis of PAS domain in RbdA and DipA for corresponding phenotype assays with/without NO; (3) GFP tag for the localization of these two proteins *in vivo*; (4) if they are membrane anchored, site-directed mutagenesis of membrane anchored domains for c-di-GMP level quantification, swarming and dispersal assays to determine if it is a localized c-di-GMP pool rather than an intracellular one that affects the phenotypes; (5) Overexpression of RbdA and DipA to see if all the phenotype changes can be restored so that polar effect can be excluded; (6) Overexpression of a PDE from a different strain without membrane anchor or sensor domains, to test if all the phenotypes can be

complemented with the restored intracellular c-di-GMP level. This will shed light on whether the phenotypes come from localized c-di-GMP pools and if they can be bypassed through c-di-GMP regulation on other phenotypes.

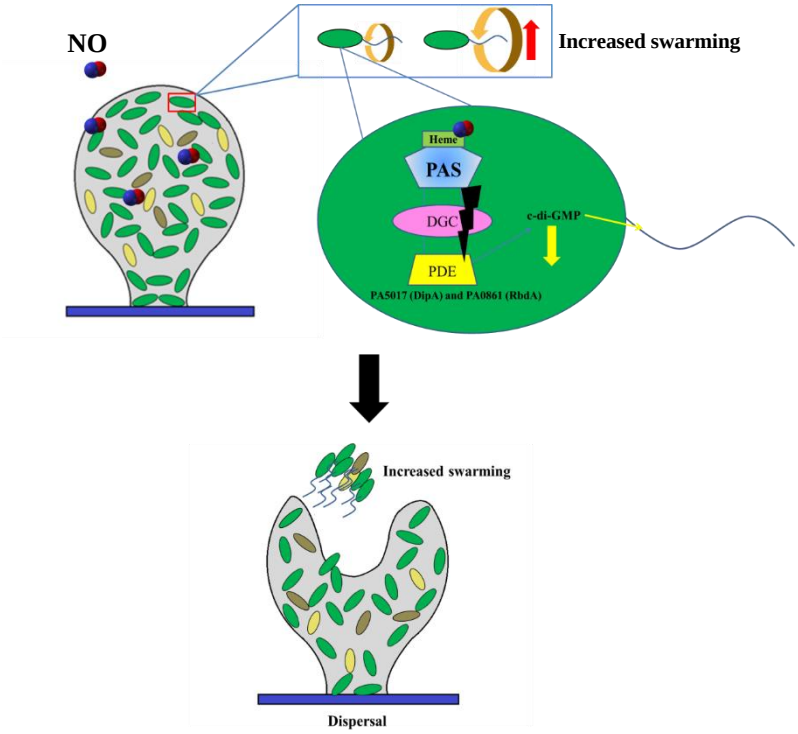


Fig 6 D.1. Hypothetical model of NO-c-di-GMP-swarming pathway for *P. aeruginosa* biofilm dispersal. NO upregulates PDE activity of RbdA and DipA resulting in a significant decrease of both localized and intracellular c-di-GMP level. The localized ones influence the rotation of flagella and increases swarming motility, which plays an important role in bulk cells leaving biofilms and triggering dispersal.

**Model B. Localized c-di-GMP pools changed by NO contribute to dispersal regulation bypass the control from intracellular c-di-GMP**

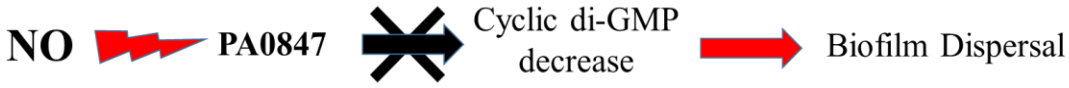


Δ*pa0847* showed less swarming increase after the addition of NO (Table 6.2.4) and impaired dispersal effect compared to WT (Table 6.2.2), but the intracellular c-di-GMP decreased in the same way as WT. As Δ*pa0847* did not show different swimming or swarming pattern compared to WT, it is not likely that PA0847 directly regulates flagella biogenesis or function. Instead, it is suspected that PA0847 contributes to a specific c-di-GMP pool regulating flagella function and swarming motility. If PA0847 exhibits PDE activity but is not sufficient to alter the global level, and the PAS domain binds to NO which sequentially upregulates its PDE activity, it would largely change the local c-

di-GMP pool. If PA0847 locates in vicinity of flagella related gene/proteins regulated by c-di-GMP, the localized c-di-GMP pool near might also regulate swarming motility in a more directed and influential way that bypasses the control from general and remote global c-di-GMP pool. A similar model was proposed by Hay *et al* suggesting MucR generates c-di-GMP that binds to the PilZ of Alg44 in vicinity, thus modulating alginate production[147].

**Model C: Specific cell physiology and biofilm structures influence NO efficacy**

After the addition of NO, the intracellular c-di-GMP decrease and the swarming motility increase in *ΔbdlA* were comparable to WT (Fig 6.2.1 and Table 6.2.4), but *ΔbdlA* biofilms showed impaired dispersal (Table 6.2.2). *ΔbdlA* does not affect the growth rate, but results in more EPS polysaccharide production (Fig 6.1.5). Hence, it is possible that the less biofilm dispersal in *ΔbdlA* was not regulated by a change in intracellular c-di-GMP, but the stronger EPS acting as barrier.

*ΔmorA* increased global c-di-GMP pool (Fig 6.1.1), enhanced swimming motility (Fig 6.1.4) and reduced total protein contents in EPS (Fig 6.1.5) compared to WT. However, NO does not influence global c-di-GMP level through MorA, and the swarming areas of *ΔmorA* increased even more after NO addition (Table 6.2.4). This may be explained by the fact that MorA restricts the *filC* gene[404] and the reduced intracellular c-di-GMP regulates flagella reversal rates[457,500]. Due to the unlocked *filC* gene in *ΔmorA*, the increased expression of FilC promoted the function of flagella in *ΔmorA* so that the effect of c-di-GMP on total reversal rates get pronounced, resulting in a larger swarming zone once the intracellular c-di-GMP pool is significantly reduced by NO. Nevertheless, the increased swarming of *ΔmorA* after NO addition should facilitate its biofilm dispersal, as the enhanced flagella movement should propel bacteria to swim out, while the lack of component in EPS should result in a less robust matrix structure. Interestingly, data showed Δ*morA* biofilm did not disperse effectively as WT upon NO treatment (Table 6.2.2), which is contradictory to what was expected. It can be observed by both visual judgement and COMSTAT analyses that Δ*morA* did not show differences in biofilms mean thickness, roughness coefficient and total biomass compared to WT (Table 6.1.3, Appendix Fig A3-4). If Δ*morA* biofilm EPS matrix has a lack of protein production, while enhanced swimming of Δ*morA* reduced bacteria attachment, how come the biofilms showed no difference compared to WT? Thus, it was suspected that

MorA might also be regulating other pathways that were not tested in this study, and they may compensate for the effect from increased swarming with the presence of NO. Alternatively, the altered swimming motility of Δ*morA* might have changed the texture of the biofilm that forms a barrier to the penetration of NO. Also, Δ*morA* might have resulted in changes of ingredients in polysaccharides or proteins that alter the strength of the matrix, leading to the reduced NO diffusion into bacterial cells. And all these potential regulations did not reduce NO efficacy through global c-di-GMP pathway.

Δ*pa0285* and Δ*fimX* biofilms dispersed far more efficiently than WT and other KO mutants, which was not because of the larger reduction in c-di-GMP after NO treatment according to Fig 6.2.1. It was suggested that the increased sensitivity to NO was due to their significantly different biofilm 3D structures compared to WT, namely, lack of a compact flat mat as foundation and round dense microcolonies (Fig 6.1.3). The cells in microcolonies may be better protected and more tolerant to NO than the thin foundation layers. This hypothesis was similar to some previous reports where *P. aeruginosa* biofilms display differential tolerances to antimicrobial compounds between the cap-forming and the stalk-forming subpopulation of the mushroom-shaped structures[501–504], suggesting that the structure development in biofilms plays a role in their antimicrobial tolerance properties. Furthermore, with spatial gaps within the biofilm structures, NO should diffuse more readily and interact with bacteria cells even at the very bottom more efficiently, hence increasing its efficacy.

It is noteworthy that *Δpa0285* and *ΔfimX* were also the only two strains involved in both twitching and swimming motility, which also contributed to the potential sliding motility on the swarming agar as described by Kohler and Murray et al (Fig 6.1.4)[450,455]. This sliding motility in *Δpa0285* and *ΔfimX* was significantly enlarged with NO as the global c-di-GMP decreased (Table 6.2.4), which was supported by previous reports showing altered intracellular c-di-GMP can change sliding pattern[450,455]. Hence, the increased biofilm dispersal was also possibly coming from increased motility.

Taken together, it was proposed that the enhanced NO-induced dispersal in *Δpa0285* and *ΔfimX* was either because of their less compact biofilm structures that facilitates NO diffusion, or the defeated flagella and pili function resulting in elevated swarming/sliding in response to NO, but not because of the increased global c-di-GMP hydrolysis in these two strains.

**Model D. Mature biofilms develop tolerance to NO**

From Table 6.2.2, it can be concluded that most of the 3d biofilms showed less dispersal than 2d ones even if they were developed from the same strains that rule out gene-specific regulations. As mentioned in 3.5 (chapter 3), the same S150 treatment worked differently on PAO1 WT biofilms cultured with different time periods, with a maximum dispersal percentage around 75% on 1d old biofilm, to a minimum 47% on 3d old biofilm. These suggested that the more mature and compact biofilms are, the less the efficacy of NO treatment. Several explanations can be proposed, as below:

**Cell density**

Older biofilms with higher biomass possess higher cell density. As the amount of NO applied in this study is only constrained to micromolar range and for a signalling effect, it might only be sufficient to be consumed by a certain number of cells. Hence, compared to 2d biofilms, 250μM S150 exerted less dispersal effect on 3d biofilms probably due to a larger number of cells remaining inaccessible to NO.

**Slow or incomplete penetration of the NO into the biofilm**

Even if the NO amount used in this study is sufficient to generate the signalling effect within planktonic cells of high density, EPS may act as a barrier for the contact. So far, the penetration of NO into biofilm has not been elucidated to show the depth of its effective diffusion, but various studies have been done on the diffusion of oxygen and antibiotics. Solely depending on the size, many antibiotics readily permeate bacterial biofilms as the main content in the matrix is water and there is no generic barrier to the diffusion of solutes the size of antibiotics[505,506]. There is a limitation of oxygen penetration into very thick biofilms (>90μm)[23,96,344]. Thus, it is reasonable to suggest that there might also be limitation for NO to penetrate into biofilms. Vanderkooi *et al* calculated the diffusion coefficient of nitric oxide in solution, proteins and membranes by using phosphorescence quenching technique. The authors found that NO and $O_2$ exhibited no marked difference in diffusivity, but NO is slightly less lipophilic resulting in faster diffusion in protein and slower diffusivity in lipid compared to $O_2$[70] . This was also supported by Moller *et al* showing the diffusion rates of $O_2$ and NO in buffer and organic solvents were similar, but NO diffused much slower in liposomes than $O_2$[508]. These reports showed that purely from the perspective of diffusion in aqueous

environment and even compositions of cell membrane, NO might not differ significantly from $O_2$ despite the speed varying.

However, NO· may absorb or react with EPS components, which is found to be the case of many antibiotics with retarded penetration in biofilms[509–511]. For example, positively charged chemicals bind to negatively charged polymers in the biofilm matrix[512]. *P. aeruginosa* biofilm matrix blocked the penetration of charged tobramycin into the biofilm, but not for uncharged ciprofloxacin[97]. Therefore, the active interaction of diffusion agents with matrix components counts hugely in deciding the penetration effect. The lipophilicity of NO results in its accumulation in hydrophobic regions[513], while NO was reported to be able to undergo much more rapid reactions with oxygen when present around the hydrophobic material than aqueous surroundings[514]. As such, NO may be efficiently reacting with EPS component throughout its diffusion, resulting in less penetration.

Furthermore, NO remains a free radical actively reacting with cellular components as well as some enzymes such as the reductases in *P. aeruginosa*, resulting in its lifetime of only seconds in live cells[515]. Thus, the thicker the biofilms are, the more likely the bottom layers are to lack access to NO following consumption in the outer layer.

Taken together, it was speculated that NO might have been reacting with the outer layer of cells in biofilms faster than its diffusion in depth, but detailed investigation should be carried out in the future. In this study the same amount of NO (250μM S150) was added to both 3d and 2d batch cultured biofilms, but 3d biofilms were thicker and contained more biomass. Hence, the diffusion of the same amount of NO to the bottom layer of cells in 3d biofilms might have been less sufficient than in 2d ones due to the fast consumption of NO by cells. This also suggest that in the future when experiments are done to compare the dispersal of different strains, the biomass and thickness of biofilms should also be compared. This is to rule out the possibility that the differences in the NO efficacy mostly come from the structure rather than altered NO response from modified gene/protein profile.

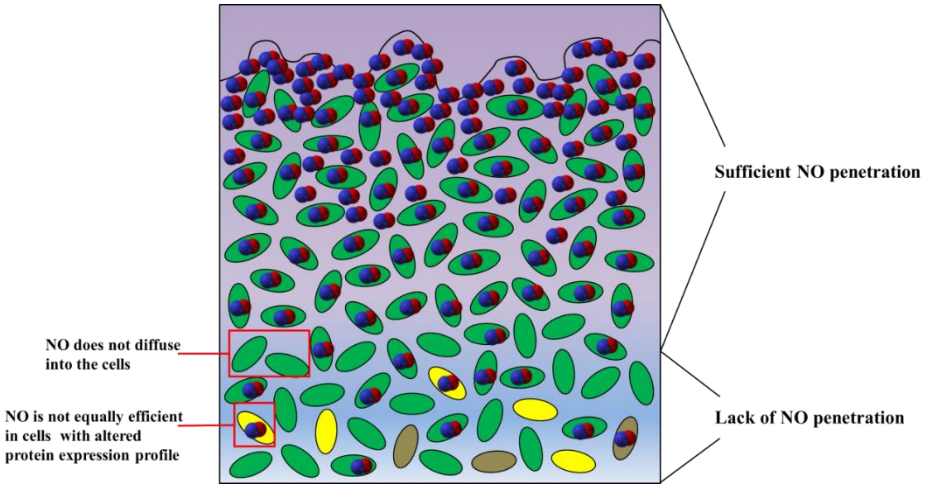


Fig 6 D.2 Two hypothetical mechanisms of less NO efficacy in biofilms: (1) Lack of NO penetration into cell layer and insufficient diffusion into cells. (2) The cells with altered gene/protein expression profile might be less responsive to NO.

**Altered micro-niches within the biofilm for differentiated expression profile**

Microscale gradients in nutrient concentrations, the adaptation to local environmental conditions, altered gene expression and protein profiles, as well as the genotypic variation through mutation and selection within the bacteria cells all contribute to the genetic and physiological heterogeneity within the biofilms[6]. Thus, there is a possibility that apart from artificial mutants without certain DGC/PDEs, the expression of some DGC/PDEs in biofilms might be altered accordingly with the maturation of biofilms and altered micro-niches. Indeed, Kwan *et al* discovered that the increased persistence in mature biofilms was related to the upregulation of a phosphodiesterase, DosP, in *E.coli*[516]. Hence, there might be a subpopulation of cells in *P. aeruginosa* biofilms that altered their gene expression due to the changes of microenvironment and exhibit higher intracellular c-di-GMP level, which might have come from either the upregulation of DGCs or the downregulation of PDEs expression. If the expression of the NO related PDEs has been downregulated, it is reasonable that NO will not be so effectively sensed by a smaller amount of PDEs, resulting in a lack of NO-mediated triggering of PDEs activities and the reduction in c-di-GMP level decrease. Alternatively, if DGCs were hugely upregulated, the decrease of c-di-GMP from PDEs may not be sufficient to support the swarming for dispersal.

In addition, extensive reports have well established that the dormant/persister cells within biofilms are more tolerant to different types of antibiotics[517], but not many investigations have been done for the tolerance of biofilm persister cells to NO. It is

possible that NO does not influence non-dividing cells as much as dividing cells. Isolating persister cells from mature biofilms and exposing them to bactericidal levels of NO can be done in future work.

**Summary**

Taken the 4 models together, the actual efficacy of a certain NO concentration on a biofilm may be relying on several specific factors and is proposed as follow Fig 6.D.3. Further research can be carried on by using newly emerging techniques such as *in situ* c-di-GMP mapping and quantification; knock-out or overexpression of motility related genes; GFP tag for recognition of DGC/PDE cellular locations; isotope $N_2$ labelling in combination with a commercially available NO generator; fluorescence quenching and microelectrodes. These can all be used to further investigate NO-induced dispersal, which can be then applied to promote NO efficacies in different biofilm related settings.

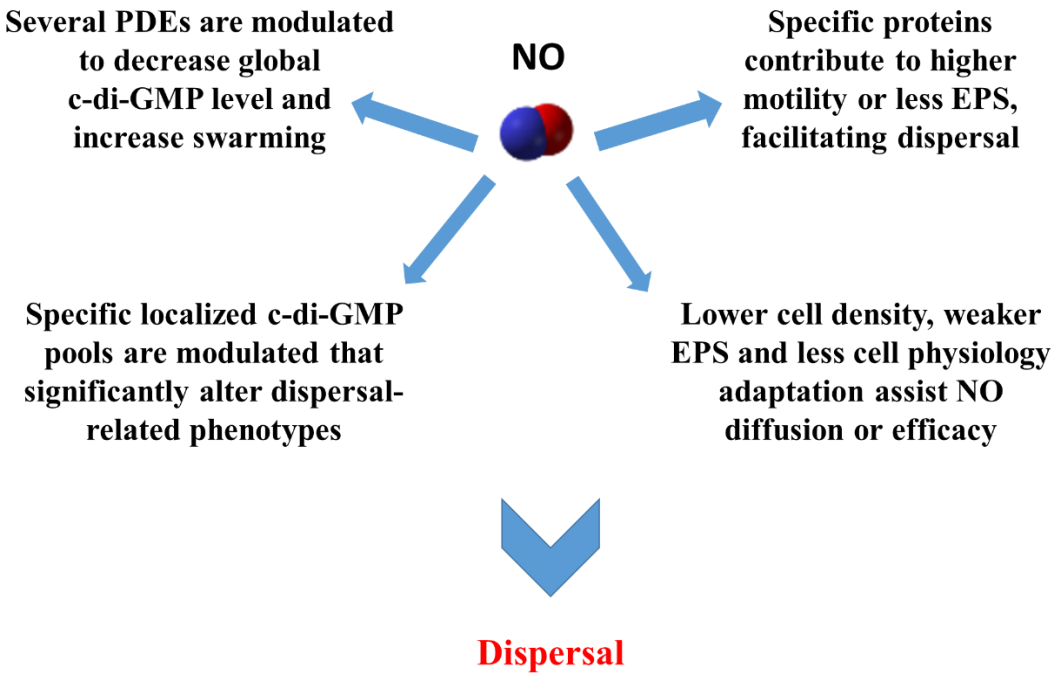


Fig 6.D.3. 4 hypothetical mechanisms that collaboratively contribute to NO-induced biofilm dispersal

# Conclusions

In 2006, Barraud *et al* for the first time discovered that nanomolar concentrations of NO led to biofilm dispersal in *P. aeruginosa* by modulating intracellular c-di-GMP. Moreover, it was proved that when antimicrobial agents such as tobramycin, $H_2O_2$ and SDS were used in adjunct with NO, their efficacies were elevated significantly[9]. NO has been used in the cardiovascular system for its role in regulating blood pressure, vascular tone, platelet aggregation, leukocyte adhesion and smooth muscle cell proliferation[518], as well as in adults with respiratory distress syndrome and persistent pulmonary hypertension for its role in reducing pulmonary artery pressure and vasodilating the blood vessels in ventilated regions[519]. Hence, NO can be used in human at a suitable concentration. The discovery of NO-induced dispersal in biofilms certainly promoted the interest in its application to CF patients, where *P. aeruginosa* plays a significant role in repetitive infection. However, so far the mechanism behind its role has not been fully elucidated yet, which limits further and more efficient applications. Despite it being shown that NO can decrease intracellular c-di-GMP leading to biofilm dispersal[242], the detailed "signal-protein-phenotypic regulation" pathway is not known. Two types of protein, diguanylate cyclase (DGC) and phosphodiesterase (PDE) are responsible for the synthesis and hydrolysis of c-di-GMP in PAO1, respectively. The core motif responsible for DGC enzymatic activity is GGDEF, and the core for PDE is EAL or HD-GYP. For NO binding and signal transfer to GGDEF or EAL domain, two domains in PAO1, PAS (Per-Arnt-Sim) and MHYT, were suspected to be the most probable candidates as they contain cofactor ferrous/ferric haem and copper ion respectively. To our knowledge, no direct evidence in *P. aeruginosa* proteins has shown that PAS binding to NO can modulate the enzymatic activities of downstream DGC/PDEs, as well as the intracellular c-di-GMP level and phenotypic outputs. There are 13 proteins in PAO1 that contain PAS/MHYT-GGDEF/EAL/GGDEF+EAL domains, and one BdlA protein that contains only PAS domain but was reported to regulate another PDE DipA. This project investigates which of these 14 proteins in *P. aeruginosa* PAO1 are the most important in sensing NO that modulates c-di-GMP level; what are the corresponding phenotypic outputs, as well as NO application to some clinical isolates. Apart from the microbiology side, our collaboration with the crystallography group and Diamond Light Source will provide information about conformational changes in the target proteins upon NO

binding to PAS, through protein crystallisation, x-ray diffraction, three-dimensional structure determination and ultrafast spectroscopic techniques.

**1. What is the best growth condition of PAO1 biofilms?**

Individual MatTek culture dishes with Poly-D-Lysine treated glass coverslips at the bottom were applied to batch culture *P. aeruginosa* biofilms in this project. Biofilms were grown with limited nutrients and slow shear-force through rotating the plates at a relatively slow speed with M9 media change every 24 hrs. Three different temperatures (22℃, 30℃ and 37℃) were tested and it was proved that at least in MatTek plates with Poly-D-Lysine surfaces, 30℃ was the most suitable for growing PAO1 biofilms and these exhibited a typical life cycle. The maturation stages were from 2-3d, after which the biofilm can cover the whole substratrum as a flat mat with large microcolonies developing above, making the conditions ideal for high throughput CLSM assays.

**2. What is the best NO donor for PAO1 biofilms?**

Despite the fact that sodium nitroprusside (SNP) has been widely reported in different publications to be able to disperse *P. aeruginosa* biofilms, the concentrations used varied. Previous data from our group also showed the inconsistent performance of SNP. Hence, different NO donors belonging to S-Nirtosothiols and Diazeniumdiolates (NONOates) groups that were relatively newly discovered compared to SNP and have not been clinically applied were tested, including SNAP, GSNO, DEA-NONOate, MAHMA NONOate (NOC-9), PROLI NONOate and Spermine NONOate (S150). The results show that 24 hrs 250μM SNP treatment and 2 hrs 250μM S150 treatment can remarkably reduce *P. aeruginosa* PAO1 WT biofilms, with S150 showing higher efficacy for biofilms at different stages. Furthermore, by using the gas phase chemiluminescence (CLD) for quantification of low NO concentrations, it was shown that the presence of light is essential for NO release from SNP, while S150 released NO spontaneously and much more efficiently, making S150 an ideal donor for treating biofilms where light exposure is not available.

**3. How is the performance of NO donor S150 on other PA clinical strains?**

Despite S150 dispersing PAO1 biofilms very efficiently, the ultimate goal for discovering NO donors is not just eliminating single-species biofilms in laboratory conditions. Proli NONOate was shown to effectively disperse multi-species biofilms in

reverse osmosis membrane biofouling by Barnes *et al*, while SNP was proved by Howlin *et al* to induce biofilm dispersal among biofilms from some CF clinical isolates strains and improve the efficacy of antibiotics[336]. However, as SNP needs light exposure for NO release, it might not work with the same efficacy in patients compared to the lab models. As S150 was identified to be an effective NO donor, it was tested on all the available CF strains in our lab collection. By using crystal violet staining, it was found that S150 can disperse the biofilms formed by 14 out of 17 clinical strains successfully, despite some of them showing less dispersal compared to PAO1 WT. Future work can be carried out to test the adjunctive usage of S150 and antibiotics. For those strains on which S150 performed inferior to others, multi-dose can be tried to enhance the effect.

**4. A novel index for the measurement of cell aggregation**

During my experiments on some PA clinical isolates, it was interesting to find that some of the strains formed large cell aggregates even in normal overnight planktonic cultures. So far the most frequently used methods for describing bacterial cells aggregations are either descriptive or direct counts depending on the aggregate sizes. Neither of the methods can use one simple index to describe "how aggregative" they are, that can be compared directly and easily among different strains. Here, a novel index, concentration coefficient (CC), based on the idea of the Gini coefficient was introduced. By using the maximum projection images from CLSM stacks, the brightness can reflect the number of cells in each pixel of the images. CC can then be calculated to measure the inequality of cell distribution based on the brightness and the division of pixel in each image, namely, the degree (level) of cell aggregation. CC calculations were performed on some CLSM images from clinical isolates and the relative number corresponded to the visual judgements. Thus, CC is expected to be widely applied to other types of cell aggregation in the future.

**5. An efficient method for rapid generating KO mutants in *P. aeruginosa***

Gene knockout methods in *P. aeruginosa* have been widely used in different labs despite the variations, but most of the papers published only involved the deletion of a small number of genes. For high-throughput screening of certain phenotypes within the *P. aeruginosa* genome, one of the most frequently used methods is Tn transposon insertion. From the results in motility assays it was found that PAO1 Tn transposon mutants are not suitable for all swimming, swarming and twitching assays. Although not been tested, their polar effects on other phenotypes might also exist. Therefore, gene deletion is

necessary for this project. Choi *et al* reported a rapid method suitable for large amount of gene deletions using gateway technology[311], but our first trials failed at ligating DNA fragments using the SOE method. Moreover, the gateway technology involves BP and LR clonase reactions as well as the donor vector, resulting in several steps and some by-products vectors before the KO fragment can go into the suicide vector for transformation, thus complicating the whole procedure. Here, an efficient method that only involves 3 major steps to make the gene-knockout vector was developed: PCR amplification – three-way ligation of PA fragments and antibiotic resistant gene – ligation with suicide vector and transformation into *P. aeruginosa*. Repetitive "cut and paste" steps in the traditional cloning methods, as well as the difficulty in optimising SOE for generating KO fragment can both be overcome. This protocol may be popularized in the future for novice researchers facing difficulties generating KO vectors or hoping to delete a large number of genes in *P. aeruginosa*.

**6. Which protein is the most important NO sensor that regulates c-di-GMP level and dispersal?**

The most frequently used methods to investigate the role of a certain gene is either deleting or overexpressing it *in vivo*, of which gene deletion was applied in this project. Quantification of relative intracellular c-di-GMP levels, CLSM observation of NO-induced dispersal, motility assay and EPS measurement were performed to investigate the phenotypic output of each gene. Results showed that among the 14 candidates, PA0861 (RbdA) and PA5017 (DipA) were the most prominent ones that significantly reduced intracellular c-di-GMP levels, enhanced swarming motility and thus triggered dispersal in response to NO. However, the studies so far are not sufficient to reveal the whole pathway. Therefore, future studies should focus on *in vitro* analysis through enzymatic activity assays and crystallography to show if NO binding to PAS domain can lead to the conformational change of EAL domain, as well as site-directed mutagenesis of PAS domain in RbdA and DipA for corresponding phenotype assays.

Apart from the intracellular c-di-GMP levels, localized c-di-GMP pools might be responsible for specific phenotypic outputs that contribute to a dispersal event. The deletion of PA4601 (MorA) led to enhanced swimming motility and did not show any differences in NO sensing, but the biofilm did not disperse as efficiently as WT. Moreover, PA0847 did not show any difference in motility, EPS production or NO-induced c-di-GMP decrease, but after NO treatment the swarming motility was not

enhanced as much as WT and the biofilms showed reduced dispersal in response to NO. It was suspected that PA0847 might be locally regulating swarming related genes/proteins, while MorA might be regulating other phenotypes not tested in this study, such as rhamnolipid production and eDNA production that contribute to the strength of EPS. Alternatively, the altered swimming motility of *ΔmorA* might have changed the texture of biofilm that forms a barrier to the penetration of NO. Further studies on disclosing which genes/proteins pa0847 and morA control by using qPCR/proteomes might help to reveal the possible pathways, while tests on other phenotypes can also be carried out. These suggest that localized c-di-GMP modulations on certain phenotypes might bypass the influence from the general "intracellular c-di-GMP – swarming" pathway and control the dispersal effect specifically.

**7. The loss of two genes makes the dispersal more efficient**

When the loss of our selected proteins was supposed to either inhibit dispersal or show no difference to prove they are or are not involved in NO-induced biofilm dispersal, it was surprising to find the deletion of two proteins, PA0285 and PA4959 (FimX), resulted in much more efficient dispersal compared to all other strains. The loss of these two proteins resulted in variation in biofilm structures that were less compact and aggregated, which might have made them easier to be dispersed by NO. This was probably due to the deficiency in both Type IV pili and flagella function in these two mutants. *Δpa0285* was shown to increase intracellular c-di-GMP while FimX was not, indicating this increased efficacy of NO was not simply coming from the alteration of the intracellular c-di-GMP level. Whether these two proteins contribute to localized c-di-GMP pools that interact with certain c-di-GMP receptors controlling both phenotypes, or these two genes simply regulate the function of pili and flagella through transcriptional/translational/post-translational remains unknown. Investigations such as qPCR, proteomes and pull down assay can be carried out in the future. Nevertheless, the results shown here provided a new insight that the deficiency in both pili and flagella function can promote the efficiency of NO. Some combinations of double knockouts of well-studied flagella and pili related genes can be done in the future to see if the results are similar.

Taken together, our results shed light on the understanding of how NO influences the potential DGCs and PDEs in the c-di-GMP network in PAO1 that leads to biofilm

dispersal. PA0847, PA0861 (RbdA), PA4601 (MorA) and PA5017 (DipA) were selected as several important proteins involved in PAO1 biofilm dispersal. The deficiency in both Type IV pili and flagella after the loss of PA0285 and PA4959 (FimX) leads to the decrease of biofilm compactness, making the mutants easier to be eliminated and providing a new insight into biofilm treatment. Further studies such as complementary overexpression, more phenotypic assays, enzymatic kinase measurement and detailed information from crystallography are needed in the future. Moreover, a novel NO donor, S150, was discovered to be dispersing PAO1 and many CF clinical isolates biofilms very efficiently, providing its potential applications in clinical trials. Some CF clinical isolates form much less surface-attached biofilms compared to others, but they form macro cell aggregates in liquid medium. In order to quantify the aggregation levels, a novel index, Concentration Coefficient (CC) was proposed to calculate from a simple maximum projection CLSM image. Overall, my work provides advanced investigations into both molecular and applied aspects in NO-induced *P. aeruginosa* biofilms, shedding light on wider applications of a commercially available NO donor as well as more in-depth research into the NO signaling mechanisms.

# References


1. Harremoës, P. Biofilm kinetics. in *Water pollution microbiology* 71–109 (John Wiley & Sons Ltd, 1978).
2. López, D., Vlamakis, H. & Kolter, R. Biofilms. *Cold Spring Harb. Perspect. Biol.* **2,** (2010).
3. Davey, M. E. & O'toole, G. A. Microbial Biofilms: from Ecology to Molecular Genetics. *Microbiol. Mol. Biol. Rev.* **64,** 847–867 (2000).
4. Donlan, R. M. & Costerton, J. W. Biofilms: Survival Mechanisms of Clinically Relevant Microorganisms. *Clin. Microbiol. Rev.* **15,** 167–193 (2002).
5. Mah, T.-F., Pitts, B., Pellock, B., Walker, G. C., Stewart, P. S. & O'Toole, G. A. A genetic basis for *Pseudomonas aeruginosa* biofilm antibiotic resistance. *Nature* **426,** 306–310 (2003).
6. Stewart, P. S. & Franklin, M. J. Physiological heterogeneity in biofilms. *Nat Rev Micro* **6,** 199–210 (2008).
7. Sauer, K., Camper, A. K., Ehrlich, G. D., Costerton, J. W. & Davies, D. G. *Pseudomonas aeruginosa* Displays Multiple Phenotypes during Development as a Biofilm. *J. Bacteriol.* **184,** 1140–1154 (2002).
8. Kaplan, J. B. Biofilm Dispersal: Mechanisms, Clinical Implications, and Potential Therapeutic Uses. *J. Dent. Res.* **89,** 205–218 (2010).
9. Barraud, N., Hassett, D. J., Hwang, S.-H., Rice, S. A., Kjelleberg, S. & Webb, J. S. Involvement of Nitric Oxide in Biofilm Dispersal of *Pseudomonas aeruginosa*. *J. Bacteriol.* **188,** 7344–7353 (2006).
10. Mann, E. E. & Wozniak, D. J. Pseudomonas biofilm matrix composition and niche biology. *FEMS Microbiol. Rev.* **36,** 893–916 (2012).
11. Flemming, H. & Wingender, J. The biofilm matrix. *Nat. Rev. Microbiol.* **8,** 623–33 (2010).
12. Stoodley, P., Sauer, K., Davies, D. G. & Costerton, J. W. Biofilms as complex differentiated communities. *Annu Rev Microbiol* **56,** 187–209 (2002).
13. Palmer, J., Flint, S. & Brooks, J. Bacterial cell attachment, the beginning of a biofilm. *J. Ind. Microbiol. Biotechnol.* **34,** 577–588 (2007).
14. Kumar, C. G. & Anand, S. K. Significance of microbial biofilms in food industry: a review. *Int. J. Food Microbiol.* **42,** 9–27 (1998).
15. Costerton, J. W., Lewandowski, Z., Caldwell, D. E., Korber, D. R. & Lappin-Scott, H. M. Microbial biofilms. *Annu Rev Microbiol* **49,** 711–745 (1995).
16. Whiteley, M., Bangera, M. G., Bumgarner, R. E., Parsek, M. R., Teitzel, G. M., Lory, S. & Greenberg, E. P. Gene expression in *Pseudomonas aeruginosa* biofilms. *Nature* **413,** 860–864 (2001).
17. Vilain, S., Cosette, P., Zimmerlin, I., Dupont, J.-P., Junter, G.-A. & Jouenne, T. Biofilm Proteome: Homogeneity or Versatility? *J. Proteome Res.* **3,** 132–136 (2003).
18. Southey-Pillig, C. J., Davies, D. G. & Sauer, K. Characterization of Temporal Protein Production in *Pseudomonas aeruginosa* Biofilms. *J. Bacteriol.* **187,** 8114–8126 (2005).
19. Lappin-Scott, H. M. & Bass, C. Biofilm formation: attachment, growth, and detachment of

microbes from surfaces. *Am J Infect Control* **29,** 250–251 (2001).

20. Stoodley, P., Wilson, S., Hall-Stoodley, L., Boyle, J. D., Lappin-Scott, H. M. & Costerton, J. W. Growth and Detachment of Cell Clusters from Mature Mixed-Species Biofilms. *Appl. Environ. Microbiol.* **67,** 5608–5613 (2001).
21. Boles, B. R., Thoendel, M. & Singh, P. K. Rhamnolipids mediate detachment of *Pseudomonas aeruginosa* from biofilms. *Mol. Microbiol.* **57,** 1210–1223 (2005).
22. Ma, L., Conover, M., Lu, H., Parsek, M. R., Bayles, K. & Wozniak, D. J. Assembly and development of the *Pseudomonas aeruginosa* biofilm matrix. *PLoS Pathog* **5,** e1000354 (2009).
23. de Beer, D., Stoodley, P., Roe, F. & Lewandowski, Z. Effects of biofilm structures on oxygen distribution and mass transport. *Biotechnol. Bioeng.* **43,** 1131–1138 (1994).
24. Xu, K. D., Stewart, P. S., Xia, F., Huang, C.-T. & McFeters, G. A. Spatial Physiological Heterogeneity in *Pseudomonas aeruginosa* Biofilm Is Determined by Oxygen Availability. *Appl. Environ. Microbiol.* **64,** 4035–4039 (1998).
25. De Beer, D., Schramm, A., Santegoeds, C. M. & Kuhl, M. A nitrite microsensor for profiling environmental biofilms. *Appl. Environ. Microbiol.* **63,** 973–977 (1997).
26. Zhang, T. C., Fu, Y.-C. & Bishop, P. L. Competition for substrate and space in biofilms. *Water Environ. Res.* **67,** 992–1003 (1995).
27. Beyenal, H., Davis, C. C. & Lewandowski, Z. An improved Severinghaus-type carbon dioxide microelectrode for use in biofilms. *Sensors Actuators B Chem.* **97,** 202–210 (2004).
28. Damgaard, L. R., Nielsen, L. P. & Revsbech, N. P. Methane microprofiles in a sewage biofilm determined with a microscale biosensor. *Water Res.* **35,** 1379–1386 (2001).
29. Jang, A., Szabo, J., Hosni, A., Coughlin, M. & Bishop, P. Measurement of chlorine dioxide penetration in dairy process pipe biofilms during disinfection. *Appl. Microbiol. Biotechnol.* **72,** 368–376 (2006).
30. Baty, A. M., Eastburn, C. C., Diwu, Z., Techkarnjanaruk, S., Goodman, A. E. & Geesey, G. G. Differentiation of Chitinase-Active and Non-Chitinase-Active Subpopulations of a Marine Bacterium during Chitin Degradation. *Appl. Environ. Microbiol.* **66,** 3566–3573 (2000).
31. Baty, A. M., Eastburn, C. C., Techkarnjanaruk, S., Goodman, A. E. & Geesey, G. G. Spatial and Temporal Variations in Chitinolytic Gene Expression and Bacterial Biomass Production during Chitin Degradation. *Appl. Environ. Microbiol.* **66,** 3574–3585 (2000).
32. Westall, F., de Wit, M. J., Dann, J., van der Gaast, S., de Ronde, C. E. J. & Gerneke, D. Early Archean fossil bacteria and biofilms in hydrothermally-influenced sediments from the Barberton greenstone belt, South Africa. *Precambrian Res.* **106,** 93–116 (2001).
33. Hall-Stoodley, L., Costerton, J. W. & Stoodley, P. Bacterial biofilms: from the Natural environment to infectious diseases. *Nat Rev Micro* **2,** 95–108 (2004).
34. Kokare S，Khopade, A N，Mahadik, K R, C. R. Biofilm: Importance and applications. *Indian J. Biotechnol.* **IJBT Vol.8,** 10 (2009).
35. Costerton, W., Veeh, R., Shirtliff, M., Pasmore, M., Post, C. & Ehrlich, G. The application of biofilm science to the study and control of chronic bacterial infections. *J. Clin. Invest.* **112,** 1466–1477 (2003).

36. Costerton, J. W., Stewart, P. S. & Greenberg, E. P. Bacterial Biofilms: A Common Cause of Persistent Infections. *Science (80-. ).* **284,** 1318–1322 (1999).
37. Raad, I., Costerton, W., Sabharwal, U., Sadlowski, M., Anaissie, E. & Bodey, G. P. Ultrastructural Analysis of Indwelling Vascular Catheters: A Quantitative Relationship between Luminal Colonization and Duration of Placement. *J. Infect. Dis.* **168,** 400–407 (1993).
38. Donlan, R. M. Biofilms and device-associated infections. *Emerg Infect Dis* **7,** 277–281 (2001).
39. Torres, C., Lenon, G., Craperi, D., Wilting, R. & Blanco, Á. Enzymatic treatment for preventing biofilm formation in the paper industry. *Appl. Microbiol. Biotechnol.* **92,** 95–103 (2011).
40. Marcato-Romain, C. E., Pechaud, Y., Paul, E., Girbal-Neuhauser, E. & Dossat-Létisse, V. Removal of microbial multi-species biofilms from the paper industry by enzymatic treatments. *Biofouling* **28,** 305–314 (2012).
41. Whitehouse, R. L. S., Peters, E., Lizotte, J. & Lilge, C. Influence of biofilms on microbial contamination in dental unit water. *J. Dent.* **19,** 290–295 (1991).
42. Walker, J. T., Bradshaw, D. J., Bennett, A. M., Fulford, M. R., Martin, M. V & Marsh, P. D. Microbial Biofilm Formation and Contamination of Dental-Unit Water Systems in General Dental Practice. *Appl. Environ. Microbiol.* **66,** 3363–3367 (2000).
43. I. Liaqat, A. N. S. Biofilm dental unit water and its control. *AFRICAN J. Clin. Exp. Microbiol.* **12(1),** 7 (2011).
44. Stover, C. K., Pham, X. Q., Erwin, A. L., Mizoguchi, S. D., Warrener, P., Hickey, M. J., Brinkman, F. S. L., Hufnagle, W. O., Kowalik, D. J., Lagrou, M., Garber, R. L., Goltry, L., Tolentino, E., Westbrock-Wadman, S., Yuan, Y., Brody, L. L., Coulter, S. N., Folger, K. R., Kas, A., Larbig, K., Lim, R., Smith, K., Spencer, D., Wong, G. K. S., Wu, Z., Paulsen, I. T., Reizer, J., Saier, M. H., Hancock, R. E. W., Lory, S. & Olson, M. V. Complete genome sequence of *Pseudomonas aeruginosa* PAO1, an opportunistic pathogen. *Nature* **406,** 959–964 (2000).
45. Banin, E., Vasil, M. L. & Greenberg, E. P. Iron and *Pseudomonas aeruginosa* biofilm formation. *Proc. Natl. Acad. Sci. U. S. A.* **102,** 11076–11081 (2005).
46. O'Toole, G., Kaplan, H. B. & Kolter, R. Biofilm formation as microbial development. *Annu Rev Microbiol* **54,** 49–79 (2000).
47. Pringle, J. H. & Fletcher, M. Influence of substratum hydration and adsorbed macromolecules on bacterial attachment to surfaces. *Appl. Environ. Microbiol.* **51,** 1321–1325 (1986).
48. O'Toole, G. A., Gibbs, K. A., Hager, P. W., Phibbs, P. V & Kolter, R. The Global Carbon Metabolism Regulator Crc Is a Component of a Signal Transduction Pathway Required for Biofilm Development by *Pseudomonas aeruginosa*. *J. Bacteriol.* **182,** 425–431 (2000).
49. Stanley, P. M. Factors affecting the irreversible attachment of *Pseudomonas aeruginosa* to stainless steel. *Can. J. Microbiol.* **29,** 1493–1499 (1983).
50. Srivastava, S., Yadav, A., Seem, K., Mishra, S., Chaudhary, V. & Nautiyal, C. S. Effect of High Temperature on *Pseudomonas putida* NBRI0987 Biofilm Formation and Expression of Stress Sigma Factor RpoS. *Curr. Microbiol.* **56,** 453–457 (2008).
51. Stanley, N. R. & Lazazzera, B. A. Environmental signals and regulatory pathways that influence biofilm formation. *Mol. Microbiol.* **52,** 917–924 (2004).

52. O'Toole, G. A. & Kolter, R. Flagellar and twitching motility are necessary for *Pseudomonas aeruginosa* biofilm development. *Mol. Microbiol.* **30,** 295–304 (1998).
53. Pier, G. B., Coleman, F., Grout, M., Franklin, M. & Ohman, D. E. Role of alginate O acetylation in resistance of mucoid *Pseudomonas aeruginosa* to opsonic phagocytosis. *Infect Immun* **69,** 1895–1901 (2001).
54. Ghafoor, A., Hay, I. D. & Rehm, B. H. A. Role of exopolysaccharides in *Pseudomonas aeruginosa* biofilm formation and architecture. *Appl. Environ. Microbiol.* **77,** 5238–5246 (2011).
55. Ma, L., Jackson, K. D., Landry, R. M., Parsek, M. R. & Wozniak, D. J. Analysis of *Pseudomonas aeruginosa* Conditional Psl Variants Reveals Roles for the Psl Polysaccharide in Adhesion and Maintaining Biofilm Structure Postattachment. *J. Bacteriol.* **188,** 8213–8221 (2006).
56. Colvin, K. M., Gordon, V. D., Murakami, K., Borlee, B. R., Wozniak, D. J., Wong, G. C. L. & Parsek, M. R. The Pel Polysaccharide Can Serve a Structural and Protective Role in the Biofilm Matrix of *Pseudomonas aeruginosa*. *PLoS Pathog* **7,** e1001264 (2011).
57. Makin, S. A. & Beveridge, T. J. The influence of A-band and B-band lipopolysaccharide on the surface characteristics and adhesion of *Pseudomonas aeruginosa* to surfaces. *Microbiology* **142,** 299–307 (1996).
58. Rocchetta, H. L., Burrows, L. L. & Lam, J. S. Genetics of O-Antigen Biosynthesis in *Pseudomonas aeruginosa*. *Microbiol. Mol. Biol. Rev.* **63,** 523–553 (1999).
59. Parsek, M. R. & Greenberg, E. P. Sociomicrobiology: the connections between quorum sensing and biofilms. *Trends Microbiol.* **13,** 27–33 (2005).
60. Schuster, M., Lostroh, C. P., Ogi, T. & Greenberg, E. P. Identification, timing, and signal specificity of *Pseudomonas aeruginosa* quorum-controlled genes: A transcriptome analysis. *J. Bacteriol.* **185,** 2066–2079 (2003).
61. Davies, D. G., Parsek, M. R., Pearson, J. P., Iglewski, B. H., Costerton, J. W. & Greenberg, E. P. The Involvement of Cell-to-Cell Signals in the Development of a Bacterial Biofilm. *Science (80-. ).* **280,** 295–298 (1998).
62. Passador, L., Cook, J. M., Gambello, M. J., Rust, L. & Iglewski, B. H. Expression of *Pseudomonas aeruginosa* virulence genes requires cell-to-cell communication. *Science (80-. ).* **260,** 1127–1130 (1993).
63. de Kievit, T. R. & Iglewski, B. H. Bacterial Quorum Sensing in Pathogenic Relationships. *Infect. Immun.* **68,** 4839–4849 (2000).
64. Miller, M. B. & Bassler, B. L. Quorum sensing in bacteria. *Annu Rev Microbiol* **55,** 165–199 (2001).
65. Whitehead, N. A., Barnard, A. M. L., Slater, H., Simpson, N. J. L. & Salmond, G. P. C. Quorum-sensing in Gram-negative bacteria. *FEMS Microbiol. Rev.* **25,** 365–404 (2001).
66. Smith, R. S. & Iglewski, B. H. *Pseudomonas aeruginosa* quorum-sensing systems and virulence. *Curr. Opin. Microbiol.* **6,** 56–60 (2003).
67. Nadell, C. D., Xavier, J. B., Levin, S. A. & Foster, K. R. The Evolution of Quorum Sensing in Bacterial Biofilms. *PLoS Biol* **6,** e14 (2008).
68. Shrout, J. D., Chopp, D. L., Just, C. L., Hentzer, M., Givskov, M. & Parsek, M. R. The impact of

quorum sensing and swarming motility on *Pseudomonas aeruginosa* biofilm formation is nutritionally conditional. *Mol. Microbiol.* **62,** 1264–1277 (2006).

69. Sakuragi, Y. & Kolter, R. Quorum-Sensing Regulation of the Biofilm Matrix Genes (pel) of *Pseudomonas aeruginosa*. *J. Bacteriol.* **189,** 5383–5386 (2007).
70. Hall, C. W. & Mah, T.-F. Molecular mechanisms of biofilm-based antibiotic resistance and tolerance in pathogenic bacteria. *FEMS Microbiol. Rev.* **41,** 276–301 (2017).
71. Nicas, T. I. & Hancock, R. E. W. *Pseudomonas aeruginosa* outer membrane permeability: Isolation of a porin protein F-deficient mutant. *J. Bacteriol.* **153,** 281–285 (1983).
72. Hancock, R. E. W. Resistance Mechanisms in *Pseudomonas aeruginosa* and Other Nonfermentative Gram-Negative Bacteria. *Clin Infect Dis* **27,** S93–S99 (1998).
73. Hancock, R. E. & Speert, D. P. Antibiotic resistance in *Pseudomonas aeruginosa*: mechanisms and impact on treatment. *Drug Resist. Updat.* **3,** 247–255 (2000).
74. Yoon, S. S., Hennigan, R. F., Hilliard, G. M., Ochsner, U. A., Parvatiyar, K., Kamani, M. C., Allen, H. L., DeKievit, T. R., Gardner, P. R., Schwab, U., Rowe, J. J., Iglewski, B. H., McDermott, T. R., Mason, R. P., Wozniak, D. J., Hancock, R. E. W., Parsek, M. R., Noah, T. L., Boucher, R. C. & Hassett, D. J. *Pseudomonas aeruginosa* anaerobic respiration in biofilms: Relationships to cystic fibrosis pathogenesis. *Dev. Cell* **3,** 593–603 (2002).
75. Nestorovich, E. M., Sugawara, E., Nikaido, H. & Bezrukov, S. M. *Pseudomonas aeruginosa* porin OprF. Properties of the channel. *J. Biol. Chem.* **281,** 16230–16237 (2006).
76. Bellido, F., Martin, N. L., Siehnel, R. J. & Hancock, R. E. W. Reevaluation, using intact cells, of the exclusion limit and role of porin OprF in *Pseudomonas aeruginosa* outer membrane permeability. *J. Bacteriol.* **174,** 5196–5203 (1992).
77. Dieppois, G., Ducret, V., Caille, O. & Perron, K. The transcriptional regulator CzcR modulates antibiotic resistance and quorum sensing in *Pseudomonas aeruginosa*. *PLoS One* **7,** (2012).
78. Breidenstein, E. B. M., de la Fuente-Núñez, C. & Hancock, R. E. W. *Pseudomonas aeruginosa*: All roads lead to resistance. *Trends in Microbiology* **19,** 419–426 (2011).
79. Poole, K. Multidrug efflux pumps and antimicrobial resistance in *Pseudomonas aeruginosa* and related organisms. *J. Mol. Microbiol. Biotechnol.* **3,** 255–264 (2001).
80. Masuda, N., Sakagawa, E. & Ohya, S. Outer membrane proteins responsible for multiple drug resistance in *Pseudomonas aeruginosa*. *Antimicrob. Agents Chemother.* **39,** 645–649 (1995).
81. Masuda, N., Gotoh, N., Ohya, S. & Nishino, T. Quantitative correlation between susceptibility and OprJ production in NfxB mutants of *Pseudomonas aeruginosa*. *Antimicrob. Agents Chemother.* **40,** 909–913 (1996).
82. Köhler, T., Michéa-Hamzehpour, M., Henze, U., Gotoh, N., Curty, L. K. & Pechère, J. C. Characterization of MexE-MexF-OprN, a positively regulated multidrug efflux system of *Pseudomonas aeruginosa*. *Mol. Microbiol.* **23,** 345–354 (1997).
83. Aires, J. R., Köhler, T., Nikaido, H. & Plésiat, P. Involvement of an active efflux system in the natural resistance of *Pseudomonas aeruginosa* to aminoglycosides. *Antimicrob. Agents Chemother.* **43,** 2624–2628 (1999).
84. Westbrock-Wadman, S., Sherman, D. R., Hickey, M. J., Coulter, S. N., Zhu, Y. Q., Warrener, P.,

Nguyen, L. Y., Shawar, R. M., Folger, K. R. & Stover, C. K. Characterization of a *Pseudomonas aeruginosa* efflux pump contributing to aminoglycoside impermeability. *Antimicrob. Agents Chemother*. **43,** 2975–2983 (1999).

85. Shaikh, S., Fatima, J., Shakil, S., Rizvi, S. M. D. & Kamal, M. A. Antibiotic resistance and extended spectrum beta-lactamases: Types, epidemiology and treatment. *Saudi J. Biol. Sci.* **22,** 90–101 (2015).
86. Zeng, X. & Lin, J. Beta-lactamase induction and cell wall metabolism in Gram-negative bacteria. *Front. Microbiol.* **4,** (2013).
87. Jacoby, G. A. AmpC B-Lactamases. *Clinical Microbiology Reviews* **22,** 161–182 (2009).
88. Hocquet, D., Vogne, C., El Garch, F., Vejux, A., Gotoh, N., Lee, A., Lomovskaya, O. & Plesiat, P. MexXy-OprM efflux pump is necessary for adaptive resistance of *Pseudomonas aeruginosa* to aminoglycosides. *Antimicrob. Agents Chemother.* **47,** 1371–1375 (2003).
89. Tanimoto, K., Tomita, H., Fujimoto, S., Okuzumi, K. & Ike, Y. Fluoroquinolone enhances the mutation frequency for meropenem-selected carbapenem resistance in *Pseudomonas aeruginosa*, but use of the high-potency drug doripenem inhibits mutant formation. *Antimicrob. Agents Chemother*. **52,** 3795–3800 (2008).
90. Germ, M., Yoshihara, E., Yoneyama, H. & Nakae, T. Interplay between the efflux pump and the outer membrane permeability barrier in fluorescent dye accumulation in *Pseudomonas aeruginosa*. *Biochem. Biophys. Res. Commun.* **261,** 452–455 (1999).
91. Muller, C., Plésiat, P. & Jeannot, K. A two-component regulatory system interconnects resistance to polymyxins, aminoglycosides, fluoroquinolones, and β-lactams in *Pseudomonas aeruginosa*. *Antimicrob. Agents Chemother.* **55,** 1211–1221 (2011).
92. Dunham, S. A., McPherson, C. J. & Miller, A. A. The relative contribution of efflux and target gene mutations to fluoroquinolone resistance in recent clinical isolates of P*seudomonas aeruginosa*. *Eur. J. Clin. Microbiol. Infect. Dis.* **29,** 279–288 (2010).
93. McPhee, J. B., Lewenza, S. & Hancock, R. E. W. Cationic antimicrobial peptides activate a two-component regulatory system, PmrA-PmrB, that regulates resistance to polymyxin B and cationic antimicrobial peptides in *Pseudomonas aeruginosa*. *Mol. Microbiol.* **50,** 205–217 (2003).
94. Fernández, L., Gooderham, W. J., Bains, M., McPhee, J. B., Wiegand, I. & Hancock, R. E. W. Adaptive resistance to the 'last hope' antibiotics polymyxin B and colistin in *Pseudomonas aeruginosa* is mediated by the novel two-component regulatory system ParR-ParS. *Antimicrob. Agents Chemother.* **54,** 3372–3382 (2010).
95. Chatterjee, M., Anju, C. P., Biswas, L., Anil Kumar, V., Gopi Mohan, C. & Biswas, R. Antibiotic resistance in *Pseudomonas aeruginosa* and alternative therapeutic options. *International Journal of Medical Microbiology* **306,** 48–58 (2016).
96. Walters, M. C., Roe, F., Bugnicourt, A., Franklin, M. J. & Stewart, P. S. Contributions of Antibiotic Penetration, Oxygen Limitation, and Low Metabolic Activity to Tolerance of *Pseudomonas aeruginosa* Biofilms to Ciprofloxacin and Tobramycin. *Antimicrob. Agents Chemother.* **47,** 317–323 (2003).
97. Tseng, B. S., Zhang, W., Harrison, J. J., Quach, T. P., Song, J. L., Penterman, J., Singh, P. K.,

Chopp, D. L., Packman, A. I. & Parsek, M. R. The extracellular matrix protects *Pseudomonas aeruginosa* biofilms by limiting the penetration of tobramycin. *Environ. Microbiol.* **15,** 2865–2878 (2013).

98. Billings, N., Ramirez Millan, M., Caldara, M., Rusconi, R., Tarasova, Y., Stocker, R. & Ribbeck, K. The Extracellular Matrix Component Psl Provides Fast-Acting Antibiotic Defense in *Pseudomonas aeruginosa* Biofilms. *PLoS Pathog.* **9,** (2013).
99. Mulcahy, H., Charron-Mazenod, L. & Lewenza, S. Extracellular DNA chelates cations and induces antibiotic resistance in *Pseudomonas aeruginosa* biofilms. *PLoS Pathog.* **4,** (2008).
100. Borriello, G., Werner, E., Roe, F., Kim, A. M., Ehrlich, G. D. & Stewart, P. S. Oxygen limitation contributes to antibiotic tolerance of *Pseudomonas aeruginosa* in biofilms. *Antimicrob. Agents Chemother.* **48,** 2659–2664 (2004).
101. Werner, E., Roe, F., Bugnicourt, A., Franklin, M. J., Heydorn, A., Molin, S., Pitts, B. & Stewart, P. S. Stratified growth in *Pseudomonas aeruginosa* biofilms. *Appl. Environ. Microbiol.* **70,** 6188–6196 (2004).
102. Schaible, B., Taylor, C. T. & Schaffer, K. Hypoxia increases antibiotic resistance in *Pseudomonas aeruginosa* through altering the composition of multidrug efflux pumps. *Antimicrob. Agents Chemother.* **56,** 2114–2118 (2012).
103. Van Acker, H. & Coenye, T. The role of efflux and physiological adaptation in biofilm tolerance and resistance. *Journal of Biological Chemistry* **291,** 12565–12572 (2016).
104. Tata, M., Wolfinger, M. T., Amman, F., Roschanski, N., Dötsch, A., Sonnleitner, E., Häussler, S. & Bläsi, U. RNAseqbased transcriptional profiling of *Pseudomonas aeruginosa* PA14 after shortand long-term anoxic cultivation in synthetic cystic fibrosis sputum medium. *PLoS One* **11,** (2016).
105. Spoering, A. L. & Lewis, K. Biofilms and planktonic cells of *Pseudomonas aeruginosa* have similar resistance to killing by antimicrobials. *J. Bacteriol.* **183,** 6746–6751 (2001).
106. Hall, C. W., Hinz, A. J., Gagnon, L. B.-P., Zhang, L., Nadeau, J.-P., Copeland, S., Saha, B. & Mah, T.-F. Expression of the *Pseudomonas aeruginosa* biofilm antibiotic resistance gene ndvB requires the RpoS stationary phase sigma factor. *Appl. Environ. Microbiol.* (2018). doi:10.1128/AEM.02762-17
107. Sadovskaya, I., Vinogradov, E., Li, J., Hachani, A., Kowalska, K. & Filloux, A. High-level antibiotic resistance in *Pseudomonas aeruginosa* biofilm: the ndvB gene is involved in the production of highly glycerol-phosphorylated beta-(1-{\textgreater}3)-glucans, which bind aminoglycosides. *Glycobiology* **20,** 895–904 (2010).
108. Kohanski, M. A., Dwyer, D. J., Hayete, B., Lawrence, C. A. & Collins, J. J. A Common Mechanism of Cellular Death Induced by Bactericidal Antibiotics. *Cell* **130,** 797–810 (2007).
109. Foti, J. J., Devadoss, B., Winkler, J. A., Collins, J. J. & Walker, G. C. Oxidation of the guanine nucleotide pool underlies cell death by bactericidal antibiotics. *Science (80-. ).* **336,** 315–319 (2012).
110. Jensen, P., Briales, A., Brochmann, R. P., Wang, H., Kragh, K. N., Kolpen, M., Hempel, C., Bjarnsholt, T., Høiby, N. & Ciofu, O. Formation of hydroxyl radicals contributes to the

bactericidal activity of ciprofloxacin against *Pseudomonas aeruginosa* biofilms. *Pathog. Dis.* **70,** 440–443 (2014).

111. Hassett, D. J., Ma, J. F., Elkins, J. G., McDermott, T. R., Ochsner, U. A., West, S. E., Huang, C. T., Fredericks, J., Burnett, S., Stewart, P. S., McFeters, G., Passador, L. & Iglewski, B. H. Quorum sensing in *Pseudomonas aeruginosa* controls expression of catalase and superoxide dismutase genes and mediates biofilm susceptibility to hydrogen peroxide. *Mol. Microbiol.* **34,** 1082–1093 (1999).

112. Nguyen, D., Joshi-Datar, A., Lepine, F., Bauerle, E., Olakanmi, O., Beer, K., McKay, G., Siehnel, R., Schafhauser, J., Wang, Y., Britigan, B. E. & Singh, P. K. Active starvation responses mediate antibiotic tolerance in biofilms and nutrient-limited bacteria. *Science (80-. ).* **334,** 982–986 (2011).

113. Schafhauser, J., Lepine, F., McKay, G., Ahlgren, H. G., Khakimova, M. & Nguyen, D. The stringent response modulates 4-hydroxy-2-alkylquinoline biosynthesis and quorum-sensing hierarchy in *Pseudomonas aeruginosa*. *J. Bacteriol.* **196,** 1641–1650 (2014).

114. Khakimova, M., Ahlgren, H. G., Harrison, J. J., English, A. M. & Nguyen, D. The stringent response controls catalases in *Pseudomonas aeruginosa* and is required for hydrogen peroxide and antibiotic tolerance. *J. Bacteriol.* **195,** 2011–2020 (2013).

115. Zhang, L. & Mah, T. F. Involvement of a novel efflux system in biofilm-specific resistance to antibiotics. *J. Bacteriol.* **190,** 4447–4452 (2008).

116. Gillis, R. J., White, K. G., Choi, K.-H., Wagner, V. E., Schweizer, H. P. & Iglewski, B. H. Molecular basis of azithromycin-resistant *Pseudomonas aeruginosa* biofilms. *Antimicrob. Agents Chemother.* **49,** 3858–67 (2005).

117. Pamp, S. J., Gjermansen, M., Johansen, H. K. & Tolker-Nielsen, T. Tolerance to the antimicrobial peptide colistin in *Pseudomonas aeruginosa* biofilms is linked to metabolically active cells, and depends on the pmr and mexAB-oprM genes. *Mol. Microbiol.* **68,** 223–240 (2008).

118. Driffield, K., Miller, K., Bostock, J. M., O'neill, A. J. & Chopra, I. Increased mutability of *Pseudomonas aeruginosa* in biofilms. *J. Antimicrob. Chemother.* **61,** 1053–1056 (2008).

119. Oliver, A., Canton, R., Campo, P., Baquero, F., Blazquez, J., Cantón, R., Campo, P., Baquero, F. & Blázquez, J. High Frequency of Hypermutable *Pseudomonas aeruginosa* in Cystic Fibrosis Lung Infection. *Science (80-. ).* **288,** 1251–1253 (2000).

120. Mandsberg, L. F., Ciofu, O., Kirkby, N., Christiansen, L. E., Poulsen, H. E. & Høiby, N. Antibiotic resistance in *Pseudomonas aeruginosa* strains with increased mutation frequency due to inactivation of the DNA oxidative repair system. *Antimicrob. Agents Chemother.* **53,** 2483–2491 (2009).

121. Harmsen, M., Yang, L., Pamp, S. J. & Tolker-Nielsen, T. An update on *Pseudomonas aeruginosa* biofilm formation, tolerance, and dispersal. *FEMS Immunol. Med. Microbiol.* **59,** 253–268 (2010).

122. Chiang, W. C., Pamp, S. J., Nilsson, M., Givskov, M. & Tolker-Nielsen, T. The metabolically active subpopulation in *Pseudomonas aeruginosa* biofilms survives exposure to membrane-targeting antimicrobials via distinct molecular mechanisms. *FEMS Immunol. Med. Microbiol.* **65,** 245–256 (2012).

123. Kolpen, M., Appeldorff, C. F., Brandt, S., Mousavi, N., Kragh, K. N., Aydogan, S., Uppal, H. A.,

Bjarnsholt, T., Ciofu, O., Høiby, N. & Jensen, P. Increased bactericidal activity of colistin on *Pseudomonas aeruginosa* biofilms in anaerobic conditions. *Pathog. Dis.* **74,** ftv086 (2016).

124. Stewart, P. S. Antimicrobial Tolerance in Biofilms. *Microbiol. Spectr.* **3,** 10.1128/microbiolspec.MB-0010-2014 (2015).
125. Pamp, S. J. & Tolker-Nielsen, T. Multiple Roles of Biosurfactants in Structural Biofilm Development by *Pseudomonas aeruginosa*. *J. Bacteriol.* **189,** 2531–2539 (2007).
126. Karatan, E. & Watnick, P. Signals, regulatory networks, and materials that build and break bacterial biofilms. *Microbiol Mol Biol Rev* **73,** 310–347 (2009).
127. Nadell, C. D., Xavier, J. B. & Foster, K. R. The sociobiology of biofilms. *FEMS Microbiol. Rev.* **33,** 206–224 (2009).
128. Webb, J. S. Differentiation and dispersal in biofilms. *biofilm mode life Mech. Adapt.* 165–174 (2007).
129. Purevdorj-Gage, B., Costerton, W. J. & Stoodley, P. Phenotypic differentiation and seeding dispersal in non-mucoid and mucoid *Pseudomonas aeruginosa* biofilms. *Microbiology* **151,** 1569–1576 (2005).
130. Webb, J. S., Thompson, L. S., James, S., Charlton, T., Tolker-Nielsen, T., Koch, B., Givskov, M. & Kjelleberg, S. Cell Death in *Pseudomonas aeruginosa* Biofilm Development. *J. Bacteriol.* **185,** 4585–4592 (2003).
131. Hill, D. F., Short, N. J., Perham, R. N. & Petersen, G. B. DNA sequence of the filamentous bacteriophage Pf1. *J. Mol. Biol.* **218,** 349–364 (1991).
132. Merino, S., Camprubi, S. & Tomás, J. M. Isolation and characterization of bacteriophage PM3 from *Aeromonas hydrophila* the bacterial receptor for which is the monopolar flagellum. *FEMS Microbiol. Lett.* **69,** 277–282 (1990).
133. Mai-Prochnow, A., Webb, J. S., Ferrari, B. C. & Kjelleberg, S. Ecological Advantages of Autolysis during the Development and Dispersal of *Pseudoalteromonas tunicata* Biofilms. *Appl. Environ. Microbiol.* **72,** 5414–5420 (2006).
134. Kirov, S. M., Webb, J. S., O'May, C. Y., Reid, D. W., Woo, J. K. K., Rice, S. A. & Kjelleberg, S. Biofilm differentiation and dispersal in mucoid *Pseudomonas aeruginosa* isolates from patients with cystic fibrosis. *Microbiology* **153,** 3264–3274 (2007).
135. Rice, S. A., Tan, C. H., Mikkelsen, P. J., Kung, V., Woo, J., Tay, M., Hauser, A., McDougald, D., Webb, J. S. & Kjelleberg, S. The biofilm life cycle and virulence of *Pseudomonas aeruginosa* are dependent on a filamentous prophage. *ISME J* **3,** 271–282 (2008).
136. Wang, I.-N., Smith, D. L. & Young, R. Holins: The Protein Clocks of Bacteriophage Infections. *Annu. Rev. Microbiol.* **54,** 799–825 (2000).
137. Boyd, A. & Chakrabarty, A. M. *Pseudomonas aeruginosa* biofilms: role of the alginate exopolysaccharide. *J. Ind. Microbiol.* **15,** 162–168 (1995).
138. Soberón-Chávez, G., Lépine, F. & Déziel, E. Production of rhamnolipids by *Pseudomonas aeruginosa*. *Appl. Microbiol. Biotechnol.* **68,** 718–725 (2005).
139. Lazdunski, A. M., Ventre, I. & Sturgis, J. N. Regulatory circuits and communication in Gram-negative bacteria. *Nat Rev Micro* **2,** 581–592 (2004).

140. Soberón-Chávez, G., Aguirre-Ramírez, M. & Ordóñez, L. Is *Pseudomonas aeruginosa* Only 'Sensing Quorum'? *Crit. Rev. Microbiol.* **31,** 171–182 (2005).
141. Neu, T. R. Significance of bacterial surface-active compounds in interaction of bacteria with interfaces. *Microbiol Rev* **60,** 151–166 (1996).
142. Dong, Y., Zhang, X.-F., An, S.-W., Xu, J.-L. & Zhang, L.-H. A novel two-component system BqsS-BqsR modulates quorum sensing-dependent biofilm decay in *Pseudomonas aeruginosa*. *Commun Integr Biol* **1,** 88–96 (2008).
143. McDougald, D., Rice, S. A., Barraud, N., Steinberg, P. D. & Kjelleberg, S. Should we stay or should we go: mechanisms and ecological consequences for biofilm dispersal. *Nat Rev Micro* **10,** 39–50 (2012).
144. Tamayo, R., Pratt, J. T. & Camilli, A. Roles of cyclic diguanylate in the regulation of bacterial pathogenesis. *Annu Rev Microbiol* **61,** 131–148 (2007).
145. Galperin, M. Y., Gaidenko, T. A., Mulkidjanian, A. Y., Nakano, M. & Price, C. W. MHYT, a new integral membrane sensor domain. *FEMS Microbiol. Lett.* **205,** 17–23 (2001).
146. Li, Y., Heine, S., Entian, M., Sauer, K. & Frankenberg-Dinkel, N. NO-Induced Biofilm Dispersion in *Pseudomonas aeruginosa* Is Mediated by an MHYT Domain-Coupled Phosphodiesterase. *J. Bacteriol.* **195,** 3531–3542 (2013).
147. Hay, I. D., Remminghorst, U. & Rehm, B. H. A. MucR, a Novel Membrane-Associated Regulator of Alginate Biosynthesis in *Pseudomonas aeruginosa*. *Appl. Environ. Microbiol.* **75,** 1110–1120 (2009).
148. Ross, P., Weinhouse, H., Aloni, Y., Michaeli, D., Weinberger-Ohana, P., Mayer, R., Braun, S., de Vroom, E., van der Marel, G. A., van Boom, J. H. & Benziman, M. Regulation of cellulose synthesis in *Acetobacter xylinum* by cyclic diguanylic acid. *Nature* **325,** 279–281 (1987).
149. Schirmer, T. & Jenal, U. Structural and mechanistic determinants of c-di-GMP signalling. *Nat Rev Microbiol* **7,** 724–735 (2009).
150. Ryjenkov, D. A., Tarutina, M., Moskvin, O. V & Gomelsky, M. Cyclic Diguanylate Is a Ubiquitous Signaling Molecule in Bacteria: Insights into Biochemistry of the GGDEF Protein Domain. *J. Bacteriol.* **187,** 1792–1798 (2005).
151. Chan, C., Paul, R., Samoray, D., Amiot, N. C., Giese, B., Jenal, U. & Schirmer, T. Structural basis of activity and allosteric control of diguanylate cyclase. *Proc. Natl. Acad. Sci. U. S. A.* **101,** 17084–17089 (2004).
152. Paul, R., Weiser, S., Amiot, N. C., Chan, C., Schirmer, T., Giese, B. & Jenal, U. Cell cycle-dependent dynamic localization of a bacterial response regulator with a novel di-guanylate cyclase output domain. *Genes Dev.* **18,** 715–727 (2004).
153. Römling, U., Galperin, M. Y. & Gomelsky, M. Cyclic di-GMP: the First 25 Years of a Universal Bacterial Second Messenger. *Microbiol. Mol. Biol. Rev.* **77,** 1–52 (2013).
154. De, N., Navarro, M. V. A. S., Raghavan, R. V & Sondermann, H. Determinants for the Activation and Autoinhibition of the Diguanylate Cyclase Response Regulator WspR. *J. Mol. Biol.* **393,** 619–633 (2009).
155. Meissner, A., Wild, V., Simm, R., Rohde, M., Erck, C., Bredenbruch, F., Morr, M., Römling, U.

& Häussler, S. *Pseudomonas aeruginosa* cupA-encoded fimbriae expression is regulated by a GGDEF and EAL domain-dependent modulation of the intracellular level of cyclic diguanylate. *Env. Microbiol* **9,** 2475–2485 (2007).

156. Ryan, R. P., Fouhy, Y., Lucey, J. F., Crossman, L. C., Spiro, S., He, Y.-W., Zhang, L.-H., Heeb, S., Cámara, M., Williams, P. & Dow, J. M. Cell–cell signaling in *Xanthomonas campestris* involves an HD-GYP domain protein that functions in cyclic di-GMP turnover. *Proc. Natl. Acad. Sci.* **103,** 6712–6717 (2006).
157. Navarro, M. V. A. S., De, N., Bae, N., Wang, Q. & Sondermann, H. Structural Analysis of the GGDEF-EAL Domain-Containing c-di-GMP Receptor FimX. *Structure* **17,** 1104–1116 (2009).
158. Christen, B., Christen, M., Paul, R., Schmid, F., Folcher, M., Jenoe, P., Meuwly, M. & Jenal, U. Allosteric Control of Cyclic di-GMP Signaling. *J. Biol. Chem.* **281,** 32015–32024 (2006).
159. Wassmann, P., Chan, C., Paul, R., Beck, A., Heerklotz, H., Jenal, U. & Schirmer, T. Structure of BeF3−-Modified Response Regulator PleD: Implications for Diguanylate Cyclase Activation, Catalysis, and Feedback Inhibition. *Structure* **15,** 915–927 (2007).
160. Jenal, U. & Malone, J. Mechanisms of Cyclic-di-GMP Signaling in Bacteria. *Annu. Rev. Genet.* **40,** 385–407 (2006).
161. Orr, M. W., Donaldson, G. P., Severin, G. B., Wang, J., Sintim, H. O., Waters, C. M. & Lee, V. T. Oligoribonuclease is the primary degradative enzyme for pGpG in *Pseudomonas aeruginosa* that is required for cyclic-di-GMP turnover. *Proc. Natl. Acad. Sci. U. S. A.* **112,** E5048-57 (2015).
162. Schmidt, A. J., Ryjenkov, D. A. & Gomelsky, M. The Ubiquitous Protein Domain EAL Is a Cyclic Diguanylate-Specific Phosphodiesterase: Enzymatically Active and Inactive EAL Domains. *J. Bacteriol.* **187,** 4774–4781 (2005).
163. Christen, M., Christen, B., Folcher, M., Schauerte, A. & Jenal, U. Identification and Characterization of a Cyclic di-GMP-specific Phosphodiesterase and Its Allosteric Control by GTP. *J. Biol. Chem.* **280,** 30829–30837 (2005).
164. Tarutina, M., Ryjenkov, D. A. & Gomelsky, M. An Unorthodox Bacteriophytochrome from *Rhodobacter sphaeroides* Involved in Turnover of the Second Messenger c-di-GMP. *J. Biol. Chem.* **281,** 34751–34758 (2006).
165. Barends, T. R. M., Hartmann, E., Griese, J. J., Beitlich, T., Kirienko, N. V, Ryjenkov, D. A., Reinstein, J., Shoeman, R. L., Gomelsky, M. & Schlichting, I. Structure and mechanism of a bacterial light-regulated cyclic nucleotide phosphodiesterase. *Nature* **459,** 1015–1018 (2009).
166. Tchigvintsev, A., Xu, X., Singer, A., Chang, C., Brown, G., Proudfoot, M., Cui, H., Flick, R., Anderson, W. F., Joachimiak, A., Galperin, M. Y., Savchenko, A. & Yakunin, A. F. Structural Insight into the Mechanism of c-di-GMP Hydrolysis by EAL Domain Phosphodiesterases. *J. Mol. Biol.* **402,** 524–538 (2010).
167. Rao, F., Yang, Y., Qi, Y. & Liang, Z.-X. Catalytic Mechanism of Cyclic Di-GMP-Specific Phosphodiesterase: a Study of the EAL Domain-Containing RocR from *Pseudomonas aeruginosa*. *J. Bacteriol.* **190,** 3622–3631 (2008).
168. Robert-Paganin, J., Nonin-Lecomte, S. & Réty, S. Crystal Structure of an EAL Domain in Complex with Reaction Product 5′-pGpG. *PLoS One* **7,** e52424 (2012).

169. Bellini, D., Horrell, S., Hutchin, A., Phippen, C. W., Strange, R. W., Cai, Y., Wagner, A., Webb, J. S., Tews, I. & Walsh, M. A. Dimerisation induced formation of the active site and the identification of three metal sites in EAL-phosphodiesterases. *Sci. Rep.* **7,** 42166 (2017).

170. Lovering, A. L., Capeness, M. J., Lambert, C., Hobley, L. & Sockett, R. E. The structure of an unconventional HD-GYP protein from Bdellovibrio reveals the roles of conserved residues in this class of cyclic-di-GMP phosphodiesterases. *MBio* **2,** (2011).

171. Bellini, D., Caly, D. L., McCarthy, Y., Bumann, M., An, S. Q., Dow, J. M., Ryan, R. P. & Walsh, M. A. Crystal structure of an HD-GYP domain cyclic-di-GMP phosphodiesterase reveals an enzyme with a novel trinuclear catalytic iron centre. *Mol Microbiol* **91,** 26–38 (2014).

172. Brown, I. D. & Altermatt, D. Bond-valence parameters obtained from a systematic analysis of the Inorganic Crystal Structure Database. *Acta Crystallogr. Sect. B* **41,** 244–247 (1985).

173. Navarro, M. V, Newell, P. D., Krasteva, P. V, Chatterjee, D., Madden, D. R., O'Toole, G. A. & Sondermann, H. Structural basis for c-di-GMP-mediated inside-out signaling controlling periplasmic proteolysis. *PLoS Biol* **9,** e1000588 (2011).

174. Seshasayee, A. S. N., Fraser, G. M. & Luscombe, N. M. Comparative genomics of cyclic-di-GMP signalling in bacteria: post-translational regulation and catalytic activity. *Nucleic Acids Res.* **38,** 5970–5981 (2010).

175. Ferreira, R. B. R., Antunes, L. C. M., Greenberg, E. P. & McCarter, L. L. *Vibrio parahaemolyticus* ScrC Modulates Cyclic Dimeric GMP Regulation of Gene Expression Relevant to Growth on Surfaces. *J. Bacteriol.* **190,** 851–860 (2008).

176. Bharati, B. K., Sharma, I. M., Kasetty, S., Kumar, M., Mukherjee, R. & Chatterji, D. A full-length bifunctional protein involved in c-di-GMP turnover is required for long-term survival under nutrient starvation in *Mycobacterium smegmatis*. *Microbiology* **158,** 1415–1427 (2012).

177. Levet-Paulo, M., Lazzaroni, J.-C., Gilbert, C., Atlan, D., Doublet, P. & Vianney, A. The Atypical Two-component Sensor Kinase Lpl0330 from *Legionella pneumophila* Controls the Bifunctional Diguanylate Cyclase-Phosphodiesterase Lpl0329 to Modulate Bis-(3′-5′)-cyclic Dimeric GMP Synthesis. *J. Biol. Chem.* **286,** 31136–31144 (2011).

178. Phippen, C. W., Mikolajek, H., Schlaefli, H. G., Keevil, C. W., Webb, J. S. & Tews, I. Formation and dimerization of the phosphodiesterase active site of the *Pseudomonas aeruginosa* MorA, a bi-functional c-di-GMP regulator. *FEBS Lett.* **588,** 4631–4636 (2014).

179. Hinsa, S. M. & O'Toole, G. A. Biofilm formation by *Pseudomonas fluorescens* WCS365: a role for LapD. *Microbiology* **152,** 1375–1383 (2006).

180. Gjermansen, M., Nilsson, M., Yang, L. & Tolker-Nielsen, T. Characterization of starvation-induced dispersion in *Pseudomonas putida* biofilms: genetic elements and molecular mechanisms. *Mol. Microbiol.* **75,** 815–826 (2010).

181. Newell, P. D., Monds, R. D. & O'Toole, G. A. LapD is a bis-(3′,5′)-cyclic dimeric GMP-binding protein that regulates surface attachment by *Pseudomonas fluorescens* Pf0–1. *Proc. Natl. Acad. Sci.* **106,** 3461–3466 (2009).

182. Monds, R. D., Newell, P. D., Gross, R. H. & O'Toole, G. A. Phosphate-dependent modulation of c-di-GMP levels regulates *Pseudomonas fluorescens* Pf0-1 biofilm formation by controlling

secretion of the adhesin LapA. *Mol. Microbiol.* **63,** 656–679 (2007).

183. Stock, A. M., Robinson, V. L. & Goudreau, P. N. Two-component signal transduction. *Annu. Rev. Biochem.* **69,** 183–215 (2000).

184. Galperin, M. Y., Nikolskaya, A. N. & Koonin, E. V. Novel domains of the prokaryotic two-component signal transduction systems. *FEMS Microbiol. Lett.* **203,** 11–21 (2001).

185. Henry, J. T. & Crosson, S. Ligand-binding PAS domains in a genomic, cellular, and structural context. *Annu Rev Microbiol* **65,** 261–286 (2011).

186. Amikam, D. & Galperin, M. Y. PilZ domain is part of the bacterial c-di-GMP binding protein. *Bioinformatics* **22,** 3–6 (2006).

187. Ryjenkov, D. A., Simm, R., Römling, U. & Gomelsky, M. The PilZ Domain Is a Receptor for the Second Messenger c-di-GMP: The PilZ domain protein YcgR controls motility in Enterobacteria. *J. Biol. Chem.* **281,** 30310–30314 (2006).

188. Christen, M., Christen, B., Allan, M. G., Folcher, M., Jenö, P., Grzesiek, S. & Jenal, U. DgrA is a member of a new family of cyclic diguanosine monophosphate receptors and controls flagellar motor function in *Caulobacter crescentus*. *Proc. Natl. Acad. Sci.* **104,** 4112–4117 (2007).

189. Pratt, J. T., Tamayo, R., Tischler, A. D. & Camilli, A. PilZ domain proteins bind Cyclic Diguanylate and regulate diverse processes in *Vibrio cholerae*. *J. Biol. Chem.* **282,** 12860–12870 (2007).

190. Habazettl, J., Allan, M. G., Jenal, U. & Grzesiek, S. Solution structure of the PilZ domain protein PA4608 complex with cyclic di-GMP identifies charge clustering as molecular readout. *J Biol Chem* **286,** 14304–14314 (2011).

191. Ko, J., Ryu, K.-S., Kim, H., Shin, J.-S., Lee, J.-O., Cheong, C. & Choi, B.-S. Structure of PP4397 reveals the molecular basis for different c-di-GMP binding modes by Pilz domain proteins. *J. Mol. Biol.* **398,** 97–110 (2010).

192. Gentner, M., Allan, M. G., Zaehringer, F., Schirmer, T. & Grzesiek, S. Oligomer Formation of the Bacterial Second Messenger c-di-GMP: Reaction Rates and Equilibrium Constants Indicate a Monomeric State at Physiological Concentrations. *J. Am. Chem. Soc.* **134,** 1019–1029 (2011).

193. Li, T.-N., Chin, K.-H., Fung, K.-M., Yang, M.-T., Wang, A. H. J. & Chou, S.-H. A Novel Tetrameric PilZ Domain Structure from Xanthomonads. *PLoS One* **6,** e22036 (2011).

194. Duerig, A., Abel, S., Folcher, M., Nicollier, M., Schwede, T., Amiot, N., Giese, B. & Jenal, U. Second messenger-mediated spatiotemporal control of protein degradation regulates bacterial cell cycle progression. *Genes Dev.* **23,** 93–104 (2009).

195. Petters, T., Zhang, X., Nesper, J., Treuner-Lange, A., Gomez-Santos, N., Hoppert, M., Jenal, U. & Søgaard-Andersen, L. The orphan histidine protein kinase SgmT is a c-di-GMP receptor and regulates composition of the extracellular matrix together with the orphan DNA binding response regulator DigR in *Myxococcus xanthus*. *Mol. Microbiol.* **84,** 147–165 (2012).

196. Hobley, L., Fung, R. K. Y., Lambert, C., Harris, M. A. T. S., Dabhi, J. M., King, S. S., Basford, S. M., Uchida, K., Till, R., Ahmad, R., Aizawa, S.-I., Gomelsky, M. & Sockett, R. E. Discrete Cyclic di-GMP-dependent control of cacterial predation versus axenic growth in *Bdellovibrio bacteriovorus*. *PLoS Pathog* **8,** e1002493 (2012).

197. Whitney, J. C., Colvin, K. M., Marmont, L. S., Robinson, H., Parsek, M. R. & Howell, P. L. Structure of the Cytoplasmic Region of PelD, a Degenerate Diguanylate Cyclase Receptor That Regulates Exopolysaccharide Production in *Pseudomonas aeruginosa*. *J. Biol. Chem.* **287,** 23582–23593 (2012).

198. Qi, Y., Chuah, M. L. C., Dong, X., Xie, K., Luo, Z., Tang, K. & Liang, Z.-X. Binding of Cyclic Diguanylate in the non-catalytic EAL domain of FimX induces a long-range conformational change. *J. Biol. Chem.* **286,** 2910–2917 (2011).

199. Newell, P. D., Yoshioka, S., Hvorecny, K. L., Monds, R. D. & O'Toole, G. A. Systematic analysis of diguanylate cyclases that promote biofilm formation by *Pseudomonas fluorescens* Pf0-1. *J. Bacteriol.* **193,** 4685–4698 (2011).

200. Minasov, G., Padavattan, S., Shuvalova, L., Brunzelle, J. S., Miller, D. J., Baslé, A., Massa, C., Collart, F. R., Schirmer, T. & Anderson, W. F. Crystal Structures of YkuI and its complex with second messenger Cyclic Di-GMP suggest catalytic mechanism of phosphodiester bond cleavage by EAL Domains. *J. Biol. Chem.* **284,** 13174–13184 (2009).

201. Edwards, A. L. & Batey, R. T. Riboswitches: A common RNA regulatory element. *Nat. Educ.* **3,** 9 (2010).

202. Barrick, J. E. & Breaker, R. R. The distributions, mechanisms, and structures of metabolite-binding riboswitches. *Genome Biol.* **8,** R239 (2007).

203. Weinberg, Z., Barrick, J. E., Yao, Z., Roth, A., Kim, J. N., Gore, J., Wang, J. X., Lee, E. R., Block, K. F., Sudarsan, N., Neph, S., Tompa, M., Ruzzo, W. L. & Breaker, R. R. Identification of 22 candidate structured RNAs in bacteria using the CMfinder comparative genomics pipeline. *Nucleic Acids Res.* **35,** 4809–4819 (2007).

204. Sudarsan, N., Lee, E. R., Weinberg, Z., Moy, R. H., Kim, J. N., Link, K. H. & Breaker, R. R. Riboswitches in Eubacteria sense the second messenger Cyclic Di-GMP. *Science (80-. ).* **321,** 411–413 (2008).

205. Lee, E. R., Baker, J. L., Weinberg, Z., Sudarsan, N. & Breaker, R. R. An allosteric self-splicing ribozyme triggered by a bacterial second messenger. *Science (80-. ).* **329,** 845–848 (2010).

206. Smith, K. D., Lipchock, S. V, Ames, T. D., Wang, J., Breaker, R. R. & Strobel, S. A. Structural basis of ligand binding by a c-di-GMP riboswitch. *Nat. Struct. Mol. Biol.* **16,** 1218–23 (2009).

207. Smith, K. D., Shanahan, C. A., Moore, E. L., Simon, A. C. & Strobel, S. A. Structural basis of differential ligand recognition by two classes of bis-(3'-5')-cyclic dimeric guanosine monophosphate-binding riboswitches. *Proc. Natl. Acad. Sci. U. S. A.* **108,** 7757–7762 (2011).

208. Sommerfeldt, N., Possling, A., Becker, G., Pesavento, C., Tschowri, N. & Hengge, R. Gene expression patterns and differential input into curli fimbriae regulation of all GGDEF/EAL domain proteins in *Escherichia coli*. *Microbiology* **155,** 1318–1331 (2009).

209. Weber, H., Pesavento, C., Possling, A., Tischendorf, G. & Hengge, R. Cyclic-di-GMP-mediated signalling within the σS network of *Escherichia coli*. *Mol. Microbiol.* **62,** 1014–1034 (2006).

210. Schild, S., Tamayo, R., Nelson, E. J., Qadri, F., Calderwood, S. B. & Camilli, A. Genes induced late in infection increase fitness of *Vibrio cholerae* after release into the environment. *Cell Host Microbe* **2,** 264–277 (2007).

211. Matilla, M. A., Travieso, M. L., Ramos, J. L. & Ramos-González, M. I. Cyclic diguanylate turnover mediated by the sole GGDEF/EAL response regulator in *Pseudomonas putida*: its role in the rhizosphere and an analysis of its target processes. *Env. Microbiol* **13,** 1745–1766 (2011).

212. Kulesekara, H., Lee, V., Brencic, A., Liberati, N., Urbach, J., Miyata, S., Lee, D. G., Neely, A. N., Hyodo, M., Hayakawa, Y., Ausubel, F. M. & Lory, S. Analysis of *Pseudomonas aeruginosa* diguanylate cyclases and phosphodiesterases reveals a role for bis-(3′-5′)-cyclic-GMP in virulence. *Proc. Natl. Acad. Sci. U. S. A.* **103,** 2839–2844 (2006).

213. Merritt, J. H., Ha, D.-G., Cowles, K. N., Lu, W., Morales, D. K., Rabinowitz, J., Gitai, Z. & O'Toole, G. A. Specific Control of *Pseudomonas aeruginosa* Surface-Associated Behaviors by Two c-di-GMP Diguanylate Cyclases. *MBio* **1,** (2010).

214. Wolfe, A. J. & Berg, H. C. Migration of bacteria in semisolid agar. *Proc. Natl. Acad. Sci.* **86,** 6973–6977 (1989).

215. Paul, K., Nieto, V., Carlquist, W. C., Blair, D. F. & Harshey, R. M. The c-di-GMP Binding Protein YcgR Controls Flagellar Motor Direction and Speed to Affect Chemotaxis by a 'Backstop Brake' Mechanism. *Mol. Cell* **38,** 128–139 (2010).

216. Kuchma, S. L., Delalez, N. J., Filkins, L. M., Snavely, E. A., Armitage, J. P. & O'Toole, G. A. Cyclic di-GMP-mediated repression of swarming motility by *Pseudomonas aeruginosa* PA14 Requires the MotAB stator. *J. Bacteriol.* **197,** 420–430 (2015).

217. Merritt, J. H., Brothers, K. M., Kuchma, S. L. & O'Toole, G. A. SadC Reciprocally Influences Biofilm Formation and Swarming Motility via Modulation of Exopolysaccharide Production and Flagellar Function. *J. Bacteriol.* **189,** 8154–8164 (2007).

218. Kuchma, S. L., Brothers, K. M., Merritt, J. H., Liberati, N. T., Ausubel, F. M. & O'Toole, G. A. BifA, a Cyclic-Di-GMP Phosphodiesterase, Inversely Regulates Biofilm Formation and Swarming Motility by *Pseudomonas aeruginosa* PA14. *J. Bacteriol.* **189,** 8165–8178 (2007).

219. Caiazza, N. C., Merritt, J. H., Brothers, K. M. & O'Toole, G. A. Inverse Regulation of Biofilm Formation and Swarming Motility by *Pseudomonas aeruginosa* PA14. *J. Bacteriol.* **189,** 3603–3612 (2007).

220. Jyot, J., Dasgupta, N. & Ramphal, R. FleQ, the major flagellar gene regulator in *Pseudomonas aeruginosa*, binds to enhancer sites located either upstream or atypically downstream of the RpoN binding site. *J. Bacteriol.* **184,** 5251–5260 (2002).

221. Lee, M.-C., Weng, S.-F. & Tseng, Y.-H. Flagellin gene fliC of *Xanthomonas campestris* is upregulated by transcription factor Clp. *Biochem. Biophys. Res. Commun.* **307,** 647–652 (2003).

222. Krasteva, P. V, Fong, J. C. N., Shikuma, N. J., Beyhan, S., Navarro, M. V. A. S., Yildiz, F. H. & Sondermann, H. *Vibrio cholerae* VpsT Regulates Matrix Production and Motility by Directly Sensing Cyclic di-GMP. *Science (80-. ).* **327,** 866–868 (2010).

223. Merz, A. J., So, M. & Sheetz, M. P. Pilus retraction powers bacterial twitching motility. *Nature* **407,** 98–102 (2000).

224. Wall, D. & Kaiser, D. Type IV pili and cell motility. *Mol. Microbiol.* **32,** 1–10 (1999).

225. Barken, K. B., Pamp, S. J., Yang, L., Gjermansen, M., Bertrand, J. J., Klausen, M., Givskov, M., Whitchurch, C. B., Engel, J. N. & Tolker-Nielsen, T. Roles of type IV pili, flagellum-mediated

motility and extracellular DNA in the formation of mature multicellular structures in *Pseudomonas aeruginosa* biofilms. *Env. Microbiol* **10,** 2331–2343 (2008).

226. Huang, B., Whitchurch, C. B. & Mattick, J. S. FimX, a Multidomain Protein Connecting Environmental Signals to Twitching Motility in *Pseudomonas aeruginosa*. *J. Bacteriol.* **185,** 7068–7076 (2003).
227. Jain, R., Behrens, A. J., Kaever, V. & Kazmierczak, B. I. Type IV pilus assembly in *Pseudomonas aeruginosa* over a broad range of cyclic di-GMP concentrations. *J. Bacteriol.* **194,** 4285–4294 (2012).
228. Kazmierczak, B. I., Lebron, M. B. & Murray, T. S. Analysis of FimX, a phosphodiesterase that governs twitching motility in *Pseudomonas aeruginosa*. *Mol. Microbiol.* **60,** 1026–1043 (2006).
229. Franklin, M. J., Nivens, D. E., Weadge, J. T. & Howell, P. L. Biosynthesis of the *Pseudomonas aeruginosa* Extracellular Polysaccharides, Alginate, Pel, and Psl. *Front Microbiol* **2,** 167 (2011).
230. Colvin, K. M., Irie, Y., Tart, C. S., Urbano, R., Whitney, J. C., Ryder, C., Howell, P. L., Wozniak, D. J. & Parsek, M. R. The Pel and Psl polysaccharides provide *Pseudomonas aeruginosa* structural redundancy within the biofilm matrix. *Environ. Microbiol.* **14,** 1913–1928 (2012).
231. Hickman, J. W., Tifrea, D. F. & Harwood, C. S. A chemosensory system that regulates biofilm formation through modulation of cyclic diguanylate levels. *Proc. Natl. Acad. Sci. U. S. A.* **102,** 14422–14427 (2005).
232. Irie, Y., Borlee, B. R., O'Connor, J. R., Hill, P. J., Harwood, C. S., Wozniak, D. J. & Parsek, M. R. Self-produced exopolysaccharide is a signal that stimulates biofilm formation in *Pseudomonas aeruginosa*. *Proc. Natl. Acad. Sci.* **109,** 20632–20636 (2012).
233. Hickman, J. W. & Harwood, C. S. Identification of FleQ from *Pseudomonas aeruginosa* as a c-di-GMP-responsive transcription factor. *Mol. Microbiol.* **69,** 376–389 (2008).
234. Lee, V. T., Matewish, J. M., Kessler, J. L., Hyodo, M., Hayakawa, Y. & Lory, S. A cyclic-di-GMP receptor required for bacterial exopolysaccharide production. *Mol. Microbiol.* **65,** 1474–1484 (2007).
235. Merighi, M., Lee, V. T., Hyodo, M., Hayakawa, Y. & Lory, S. The second messenger bis-(3′-5′)-cyclic-GMP and its PilZ domain-containing receptor Alg44 are required for alginate biosynthesis in *Pseudomonas aeruginosa*. *Mol. Microbiol.* **65,** 876–895 (2007).
236. Oglesby, L. L., Jain, S. & Ohman, D. E. Membrane topology and roles of *Pseudomonas aeruginosa* Alg8 and Alg44 in alginate polymerization. *Microbiology* **154,** 1605–1615 (2008).
237. Giraud, C. & de Bentzmann, S. Inside the complex regulation of *Pseudomonas aeruginosa* chaperone usher systems. *Env. Microbiol* **14,** 1805–1816 (2012).
238. Borlee, B. R., Goldman, A. D., Murakami, K., Samudrala, R., Wozniak, D. J. & Parsek, M. R. *Pseudomonas aeruginosa* uses a cyclic-di-GMP-regulated adhesin to reinforce the biofilm extracellular matrix. *Mol. Microbiol.* **75,** 827–842 (2010).
239. Miller, M. R. & Megson, I. L. Recent developments in nitric oxide donor drugs. *Br. J. Pharmacol.* **151,** 305–321 (2007).
240. Martínez-Ruiz, A., Cadenas, S. & Lamas, S. Nitric oxide signaling: Classical, less classical, and nonclassical mechanisms. *Free Radic. Biol. Med.* **51,** 17–29 (2011).

241. Pellicena, P., Karow, D. S., Boon, E. M., Marletta, M. A. & Kuriyan, J. Crystal structure of an oxygen-binding heme domain related to soluble guanylate cyclases. *Proc. Natl. Acad. Sci. U. S. A.* **101,** 12854–12859 (2004).

242. Barraud, N., Schleheck, D., Klebensberger, J., Webb, J. S., Hassett, D. J., Rice, S. A. & Kjelleberg, S. Nitric Oxide Signaling in *Pseudomonas aeruginosa* Biofilms Mediates Phosphodiesterase Activity, Decreased Cyclic Di-GMP Levels, and Enhanced Dispersal. *J. Bacteriol.* **191,** 7333–7342 (2009).

243. Barraud, N., Storey, M. V, Moore, Z. P., Webb, J. S., Rice, S. A. & Kjelleberg, S. Nitric oxide-mediated dispersal in single- and multi-species biofilms of clinically and industrially relevant microorganisms. *Microb. Biotechnol.* **2,** 370–378 (2009).

244. Plate, L. & Marletta, M. A. Nitric Oxide Modulates Bacterial Biofilm Formation through a Multicomponent Cyclic-di-GMP Signaling Network. *Mol. Cell* **46,** 449–460 (2012).

245. Wu, G., Liu, W., Berka, V. & Tsai, A. L. The selectivity of vibrio cholerae h-nox for gaseous ligands follows the 'sliding Scale Rule' Hypothesis. Ligand interactions with both ferrous and ferric Vc H-NOX. *Biochemistry* **52,** 9432–9446 (2013).

246. Partridge, J. D., Bodenmiller, D. M., Humphrys, M. S. & Spiro, S. NsrR targets in the *Escherichia coli* genome: new insights into DNA sequence requirements for binding and a role for NsrR in the regulation of motility. *Mol. Microbiol.* **73,** 680–694 (2009).

247. Sulemankhil, I., Ganopolsky, J. G., Dieni, C. A., Dan, A. F., Jones, M. L. & Prakash, S. Prevention and treatment of virulent bacterial biofilms with an enzymatic nitric oxide-releasing dressing. *Antimicrob. Agents Chemother.* **56,** 6095–6103 (2012).

248. Schmidt, I., Steenbakkers, P. J. M., op den Camp, H. J. M., Schmidt, K. & Jetten, M. S. M. Physiologic and proteomic evidence for a role of nitric oxide in biofilm formation by *Nitrosomonas europaea* and other ammonia oxidizers. *J. Bacteriol.* **186,** 2781–2788 (2004).

249. Liu, N., Xu, Y., Hossain, S., Huang, N., Coursolle, D., Gralnick, J. A. & Boon, E. M. Nitric Oxide Regulation of Cyclic di-GMP Synthesis and Hydrolysis in *Shewanella woodyi*. *Biochemistry* **51,** 2087–2099 (2012).

250. Henares, M. B., Xu, Y. & Boon, M. E. A Nitric Oxide-Responsive Quorum Sensing Circuit in *Vibrio harveyi* Regulates Flagella Production and Biofilm Formation. *International Journal of Molecular Sciences* **14,** (2013).

251. Falsetta, M. L., Bair, T. B., Shan, C. K., Vanden Hoven, R. N., Steichen, C. T., McEwan, A. G., Jennings, M. P. & Apicella, M. A. Transcriptional profiling identifies the metabolic phenotype of gonococcal biofilms. *Infect. Immun.* **77,** 3522–3532 (2009).

252. Arora, D. P., Hossain, S., Xu, Y. & Boon, E. M. Nitric Oxide Regulation of Bacterial Biofilms. *Biochemistry* **54,** 3717–3728 (2015).

253. Jardeleza, C., Foreman, A., Baker, L., Paramasivan, S., Field, J., Tan, L. W. & Wormald, P.-J. The effects of nitric oxide on *Staphylococcus aureus* biofilm growth and its implications in chronic rhinosinusitis. *Int. Forum Allergy Rhinol.* **1,** 438–444 (2011).

254. Derbyshire, E. R. & Marletta, M. A. Biochemistry of soluble guanylate cyclase. *Handb. Exp. Pharmacol.* 17–31 (2009). doi:10.1007/978-3-540-68964-5_2

255. Plate, L. & Marletta, M. A. Nitric oxide-sensing H-NOX proteins govern bacterial communal behavior. *Trends in Biochemical Sciences* **38,** 566–575 (2013).

256. Nioche, P. Femtomolar Sensitivity of a NO Sensor from *Clostridium botulinum*. *Science (80-. ).* **306,** 1550–1553 (2004).

257. Carlson, H. K., Vance, R. E. & Marletta, M. A. H-NOX regulation of c-di-GMP metabolism and biofilm formation in *Legionella pneumophila*. *Mol. Microbiol.* **77,** 930–942 (2010).

258. Liu, N., Pak, T. & Boon, E. M. Characterization of a diguanylate cyclase from *Shewanella woodyi* with cyclase and phosphodiesterase activities. *Mol. Biosyst.* **6,** 1561–1564 (2010).

259. Erbil, W. K., Price, M. S., Wemmer, D. E. & Marletta, M. A. A structural basis for H-NOX signaling in *Shewanella oneidensis* by trapping a histidine kinase inhibitory conformation. *Proc. Natl. Acad. Sci. U. S. A.* **106,** 19753–19760 (2009).

260. Bredt, D. S. Nitric oxide signaling in brain: potentiating the gain with YC-1. *Mol. Pharmacol.* **63,** 1206–1208 (2003).

261. Hoffman, E. C., Reyes, H., Chu, F. F., Sander, F., Conley, L. H., Brooks, B. A. & Hankinson, O. Cloning of a factor required for activity of the Ah (dioxin) receptor. *Science (80-. ).* **252,** 954–958 (1991).

262. Nambu, J. R., Lewis, J. O., Wharton Jr, K. A. & Crews, S. T. The Drosophila single-minded gene encodes a helix-loop-helix protein that acts as a master regulator of CNS midline development. *Cell* **67,** 1157–1167 (1991).

263. Holm, L., Ouzounis, C., Sander, C., Tuparev, G. & Vriend, G. A database of protein structure families with common folding motifs. *Protein Sci.* **1,** 1691–1698 (1992).

264. Möglich, A., Ayers, R. A. & Moffat, K. Structure and Signaling Mechanism of Per-ARNT-Sim Domains. *Structure* **17,** 1282–1294 (2009).

265. Gilles-Gonzalez, M. A., Ditta, G. S. & Helinski, D. R. A haemoprotein with kinase activity encoded by the oxygen sensor of *Rhizobium meliloti*. *Nature* **350,** 170–172 (1991).

266. Gong, W., Hao, B., Mansy, S. S., Gonzalez, G., Gilles-Gonzalez, M. A. & Chan, M. K. Structure of a biological oxygen sensor: A new mechanism for heme-driven signal transduction. *Proc. Natl. Acad. Sci.* **95,** 15177–15182 (1998).

267. Delgado-Nixon, V. M., Gonzalez, G. & Gilles-Gonzalez, M.-A. Dos, a Heme-Binding PAS Protein from *Escherichia coli*, Is a Direct Oxygen Sensor†. *Biochemistry* **39,** 2685–2691 (2000).

268. Londer, Y. Y., Dementieva, I. S., D'Ausilio, C. A., Pokkuluri, P. R. & Schiffer, M. Characterization of a c-type heme-containing PAS sensor domain from *Geobacter sulfurreducens* representing a novel family of periplasmic sensors in Geobacteraceae and other bacteria. *FEMS Microbiol. Lett.* **258,** 173–181 (2006).

269. Yoshioka, S., Kobayashi, K., Yoshimura, H., Uchida, T., Kitagawa, T. & Aono, S. Biophysical Properties of a c-Type Heme in Chemotaxis Signal Transducer Protein DcrA†. *Biochemistry* **44,** 15406–15413 (2005).

270. Qi, Y., Rao, F., Luo, Z. & Liang, Z. X. A flavin cofactor-binding PAS domain regulates c-di-GMP synthesis in AxDGC2 from *Acetobacter xylinum*. *Biochemistry* **48,** 10275–10285 (2009).

271. Chang, A. L., Tuckerman, J. R., Gonzalez, G., Mayer, R., Weinhouse, H., Volman, G., Amikam,

D., Benziman, M. & Gilles-Gonzalez, M. A. Phosphodiesterase A1, a regulator of cellulose synthesis in *Acetobacter xylinum*, is a heme-based sensor. *Biochemistry* **40,** 3420–3426 (2001).

272. An, S., Wu, J. & Zhang, L. H. Modulation of *Pseudomonas aeruginosa* biofilm dispersal by a cyclic-di-gmp phosphodiesterase with a putative hypoxia-sensing domain. *Appl. Environ. Microbiol.* **76,** 8160–8173 (2010).
273. Torres, J. & Wilson, M. T. The reactions of copper proteins with nitric oxide. *Biochim. Biophys. Acta - Bioenerg.* **1411,** 310–322 (1999).
274. Napoli, C. & Ignarro, L. J. Nitric oxide-releasing drugs. *Annu Rev Pharmacol Toxicol* **43,** 97–123 (2003).
275. Megson, I. L. & Webb, D. J. Nitric oxide donor drugs: current status and future trends. *Expert Opin Investig Drugs* **11,** 587–601 (2002).
276. Butler, A. R. & Megson, I. L. Non-heme iron nitrosyls in biology. *Chem Rev* **102,** 1155–1166 (2002).
277. Ewing, J. F., Young, D. V, Janero, D. R., Garvey, D. S. & Grinnell, T. A. Nitrosylated bovine serum albumin derivatives as pharmacologically active nitric oxide congeners. *J Pharmacol Exp Ther* **283,** 947–954 (1997).
278. Ignarro, L. J., Napoli, C. & Loscalzo, J. Nitric oxide donors and cardiovascular agents modulating the bioactivity of nitric oxide: an overview. *Circ Res* **90,** 21–28 (2002).
279. Drago, R. S. & Paulik, F. E. The Reaction of Nitrogen(II) Oxide with Diethylamine. *J. Am. Chem. Soc.* **82,** 96–98 (1960).
280. Maragos, C. M., Morley, D., Wink, D. A., Dunams, T. M., Saavedra, J. E., Hoffman, A., Bove, A. A., Isaac, L., Hrabie, J. A. & Keefer, L. K. Complexes of .NO with nucleophiles as agents for the controlled biological release of nitric oxide. Vasorelaxant effects. *J. Med. Chem.* **34,** 3242–3247 (1991).
281. Morley, D. & Keefer, L. K. Nitric oxide/nucleophile complexes: a unique class of nitric oxide-based vasodilators. *J Cardiovasc Pharmacol* **22 Suppl 7,** S3-9 (1993).
282. Hrabie, J. A., Klose, J. R., Wink, D. A. & Keefer, L. K. New nitric oxide-releasing zwitterions derived from polyamines. *J. Org. Chem.* **58,** 1472–1476 (1993).
283. Brown, J. F., Keates, A. C., Hanson, P. J. & Whittle, B. J. Nitric oxide generators and cGMP stimulate mucus secretion by rat gastric mucosal cells. *Am J Physiol* **265,** G418-22 (1993).
284. Burgaud, J.-L., Ongini, E. & Del Soldato, P. Nitric Oxide-Releasing Drugs. *Ann. N. Y. Acad. Sci.* **962,** 360–371 (2002).
285. Marshall, M., Keeble, J. & Moore, P. K. Effect of a nitric oxide releasing derivative of paracetamol in a rat model of endotoxaemia. *Br. J. Pharmacol.* **149,** 516–522 (2006).
286. Fujihara, C. K., Malheiros, D. M. A. C., Donato, J., Poli, A., De Nucci, G. & Zatz, R. Nitroflurbiprofen, a new nonsteroidal anti-inflammatory, ameliorates structural injury in the remnant kidney. *Am. J. Physiol. - Ren. Physiol.* **274,** F573–F579 (1998).
287. Young, D. V, Cochran, E. D., Dhawan, V., Earl, R. A., Ellis, J. L., Garvey, D. S., Janero, D. R., Khanapure, S. P., Letts, L. G., Melim, T. L., Murty, M. G., Shumway, M. J., Wey, S.-J., Zemtseva, I. S. & Selig, W. M. A comparison of the cyclooxygenase inhibitor-NO donors (CINOD), NMI-

1182 and AZD3582, using in vitro biochemical and pharmacological methods. *Biochem. Pharmacol.* **70,** 1343–1351 (2005).

288. Wallace, J. L., Vergnolle, N., Muscará, M. N., Asfaha, S., Chapman, K., McKnight, W., Soldato, P. Del, Morelli, A. & Fiorucci, S. Enhanced anti-inflammatory effects of a nitric oxide–releasing derivative of mesalamine in rats. *Gastroenterology* **117,** 557–566 (1999).
289. Wu, W.-P., Hao, J.-X., Ongini, E., Impagnatiello, F., Presotto, C., Wiesenfeld-Hallin, Z. & Xu, X.-J. A nitric oxide (NO)-releasing derivative of gabapentin, NCX 8001, alleviates neuropathic pain-like behavior after spinal cord and peripheral nerve injury. *Br. J. Pharmacol.* **141,** 65–74 (2004).
290. Tallet, D., Del Soldato, P., Oudart, N. & Burgaud, J.-L. NO–Steroids: Potent Anti-inflammatory Drugs with Bronchodilating Activity in Vitro. *Biochem. Biophys. Res. Commun.* **290,** 125–130 (2002).
291. Cena, C., Lolli, M. L., Lazzarato, L., Guaita, E., Morini, G., Coruzzi, G., McElroy, S. P., Megson, I. L., Fruttero, R. & Gasco, A. Antiinflammatory, Gastrosparing, and Antiplatelet Properties of New NO-Donor Esters of Aspirin. *J. Med. Chem.* **46,** 747–754 (2003).
292. Turnbull, C. M., Cena, C., Fruttero, R., Gasco, A., Rossi, A. G. & Megson, I. L. Mechanism of action of novel NO-releasing furoxan derivatives of aspirin in human platelets. *Br. J. Pharmacol.* **148,** 517–526 (2006).
293. Bandarage, U. K., Chen, L., Fang, X., Garvey, D. S., Glavin, A., Janero, D. R., Letts, L. G., Mercer, G. J., Saha, J. K., Schroeder, J. D., Shumway, M. J. & Tam, S. W. Nitrosothiol Esters of Diclofenac: Synthesis and Pharmacological Characterization as Gastrointestinal-Sparing Prodrugs†,‡. *J. Med. Chem.* **43,** 4005–4016 (2000).
294. Velázquez, C., Praveen Rao, P. N. & Knaus, E. E. Novel Nonsteroidal Antiinflammatory Drugs Possessing a Nitric Oxide Donor Diazen-1-ium-1,2-diolate Moiety: Design, Synthesis, Biological Evaluation, and Nitric Oxide Release Studies. *J. Med. Chem.* **48,** 4061–4067 (2005).
295. Yepuri, N. R., Barraud, N., Mohammadi, N. S., Kardak, B. G., Kjelleberg, S., Rice, S. A. & Kelso, M. J. Synthesis of cephalosporin-3[prime or minute]-diazeniumdiolates: biofilm dispersing NO-donor prodrugs activated by β-lactamase. *Chem. Commun.* **49,** 4791–4793 (2013).
296. Petrova, O. E. & Sauer, K. PAS domain residues and prosthetic group involved in bdladependent dispersion response by *Pseudomonas aeruginosa* biofilms. *J. Bacteriol.* **194,** 5817–5828 (2012).
297. Holloway, B. W. Genetics of Pseudomonas. *Bacteriol. Rev.* **33,** 419–443 (1969).
298. Jacobs, M. A., Alwood, A., Thaipisuttikul, I., Spencer, D., Haugen, E., Ernst, S., Will, O., Kaul, R., Raymond, C., Levy, R., Chun-Rong, L., Guenthner, D., Bovee, D., Olson, M. V & Manoil, C. Comprehensive transposon mutant library of *Pseudomonas aeruginosa*. *Proc. Natl. Acad. Sci.* **100,** 14339–14344 (2003).
299. Hoang, T. T., Karkhoff-Schweizer, R. R., Kutchma, A. J. & Schweizer, H. P. A broad-host-range Flp-FRT recombination system for site-specific excision of chromosomally-located DNA sequences: application for isolation of unmarked *Pseudomonas aeruginosa* mutants. *Gene* **212,** 77–86 (1998).
300. Rybtke, M. T., Borlee, B. R., Murakami, K., Irie, Y., Hentzer, M., Nielsen, T. E., Givskov, M.,

Parsek, M. R. & Tolker-Nielsen, T. Fluorescence-based reporter for gauging cyclic Di-GMP levels in *Pseudomonas aeruginosa*. *Appl. Environ. Microbiol.* **78,** 5060–5069 (2012).

301. M9 minimal medium (standard). *Cold Spring Harb. Protoc.* **2010,** pdb.rec12295 (2010).
302. O'Toole, G. A. Microtiter dish biofilm formation assay. *J Vis Exp* (2011). doi:10.3791/2437
303. Hendry, E. R., Worthington, T., Conway, B. R. & Lambert, P. A. Antimicrobial efficacy of eucalyptus oil and 1,8-cineole alone and in combination with chlorhexidine digluconate against microorganisms grown in planktonic and biofilm cultures. *J. Antimicrob. Chemother.* **64,** 1219–1225 (2009).
304. Heydorn, A., Nielsen, A. T., Hentzer, M., Sternberg, C., Givskov, M., Ersboll, B. K. & Molin, S. Quantification of biofilm structures by the novel computer program COMSTAT. *Microbiology* **146,** 2395–2407 (2000).
305. Miles, A. A., Misra, S. S. & Irwin, J. O. The estimation of the bactericidal power of the blood. *Epidemiol. Infect.* **38,** 732–749 (1938).
306. Barnes, R. J., Bandi, R. R., Wong, W. S., Barraud, N., McDougald, D., Fane, A., Kjelleberg, S. & Rice, S. A. Optimal dosing regimen of nitric oxide donor compounds for the reduction of *Pseudomonas aeruginosa* biofilm and isolates from wastewater membranes. *Biofouling* **29,** 203–212 (2013).
307. Rashid, M. H. & Kornberg, A. Inorganic polyphosphate is needed for swimming, swarming, and twitching motilities of *Pseudomonas aeruginosa*. *Proc. Natl. Acad. Sci.* **97,** 4885–4890 (2000).
308. Ha, D. G., Kuchma, S. L. & O'Toole, G. A. Plate-based assay for swarming motility in *Pseudomonas aeruginosa*. *Methods Mol. Biol.* **1149,** 67–72 (2014).
309. Ramos, J.-L. & Filloux, A. *Pseudomonas*. *Springer* (2010). doi:10.1007/978-90-481-3909-5
310. Green, M. R. & Sambrook, J. *Molecular cloning : a laboratory manual*. (Cold Spring Harbor Laboratory Press, 2012).
311. Choi, K.-H. & Schweizer, H. P. An improved method for rapid generation of unmarked *Pseudomonas aeruginosa* deletion mutants. *BMC Microbiol.* **5,** 30 (2005).
312. Swords, W. E. Chemical transformation of E. coli. *Methods Mol. Biol. (Totowa, NJ, U. S.)* **235,** 49–53 (2003).
313. Woodall, C. A. DNA Transfer by Bacterial Conjugation. in *E. coli Plasmid Vectors: Methods and Applications* (eds. Casali, N. & Preston, A.) 61–65 (Humana Press, 2003). doi:10.1385/1-59259-409-3:61
314. Barnes, R. J., Bandi, R. R., Chua, F., Low, J. H., Aung, T., Barraud, N., Fane, A. G., Kjelleberg, S. & Rice, S. A. The roles of *Pseudomonas aeruginosa* extracellular polysaccharides in biofouling of reverse osmosis membranes and nitric oxide induced dispersal. *J. Memb. Sci.* **466,** 161–172 (2014).
315. Piknova, B. & Schechter, A. N. Measurement of nitrite in blood samples using the ferricyanide-based hemoglobin oxidation assay. *Methods Mol. Biol.* **704,** 39–56 (2011).
316. Overkamp, W., Beilharz, K., Weme, R. D. O., Solopova, A., Karsens, H., Kovács, Á. T., Kok, J., Kuipers, O. P. & Veening, J. W. Benchmarking various green fluorescent protein variants in *Bacillus subtilis*, *Streptococcus pneumoniae*, and *Lactococcus lactis* for live cell imaging. *Appl.*

*Environ. Microbiol.* **79,** 6481–6490 (2013).

317. Manuscript, A. NIH Public Access. *Changes* **29,** 997–1003 (2012).
318. Blau, H., Linnane, B., Carzino, R., Tannenbaum, E. L., Skoric, B., Robinson, P. J., Robertson, C. & Ranganathan, S. C. Induced sputum compared to bronchoalveolar lavage in young, non-expectorating cystic fibrosis children. *J. Cyst. Fibros.* **13,** 106–110 (2014).
319. Aaron, S. D., Kottachchi, D., Ferris, W. J., Vandemheen, K. L., St. Denis, M. L., Doucette, S. P., Saginur, R., Chan, F. T. & Ramotar, K. Sputum versus bronchoscopy for diagnosis of *Pseudomonas aeruginosa* biofilms in cystic fibrosis. *Eur. Respir. J.* **24,** 631–637 (2004).
320. De Vos, D., Lim, A., Pirnay, J. P., Struelens, M., Vandenvelde, C., Duinslaeger, L., Vanderkelen, A. & Cornelis, P. Direct detection and identification of *Pseudomonas aeruginosa* in clinical samples such as skin biopsy specimens and expectorations by multiplex PCR based on two outer membrane lipoprotein genes, oprI and oprL. *J. Clin. Microbiol.* **35,** 1295–1299 (1997).
321. Ceriani, L. & Verme, P. The origins of the Gini index: extracts from Variability and Mutability by Corrado Gini. *J. Econ. Inequal.* **10,** 421–443 (2012).
322. Gastwirth, J. L. The Estimation of the Lorenz Curve and Gini Index. *Rev. Econ. Stat.* **54,** 306–316 (1972).
323. Schlag, S., Nerz, C., Birkenstock, T. A., Altenberend, F. & Götz, F. Inhibition of staphylococcal biofilm formation by nitrite. *J. Bacteriol.* **189,** 7911–7919 (2007).
324. Ueda, A. & Wood, T. K. Connecting quorum sensing, c-di-GMP, pel polysaccharide, and biofilm formation in *Pseudomonas aeruginosa* through tyrosine phosphatase TpbA (PA3885). *PLoS Pathog.* **5,** (2009).
325. Govan, J. R. W. & Deretic, V. Microbial pathogenesis in cystic fibrosis: mucoid *Pseudomonas aeruginosa* and *Burkholderia cepacia*. *Microbiol. Rev.* **60,** 539–574 (1996).
326. Bjarnsholt, T., Jensen, P. Ø., Fiandaca, M. J., Pedersen, J., Hansen, C. R., Andersen, C. B., Pressler, T., Givskov, M. & Høiby, N. *Pseudomonas aeruginosa* biofilms in the respiratory tract of cystic fibrosis patients. *Pediatr. Pulmonol.* **44,** 547–558 (2009).
327. Kannan, A. & Gautam, P. A quantitative study on the formation of *Pseudomonas aeruginosa* biofilm. *Springerplus* **4,** 379 (2015).
328. Hoštacká, A., Čižnár, I. & Štefkovičová, M. Temperature and pH affect the production of bacterial biofilm. *Folia Microbiol. (Praha).* **55,** 75–78 (2010).
329. Abdallah, M., Khelissa, O., Ibrahim, A., Benoliel, C., Heliot, L., Dhulster, P. & Chihib, N. E. Impact of growth temperature and surface type on the resistance of *Pseudomonas aeruginosa* and *Staphylococcus aureus* biofilms to disinfectants. *Int J Food Microbiol* **214,** 38–47 (2015).
330. Ghanbari, A., Dehghany, J., Schwebs, T., Müsken, M., Häussler, S. & Meyer-Hermann, M. Inoculation density and nutrient level determine the formation of mushroom-shaped structures in *Pseudomonas aeruginosa* biofilms. *Sci. Rep.* **6,** 32097 (2016).
331. Moreau-Marquis, S., Stanton, B. A. & O'Toole, G. A. *Pseudomonas aeruginosa* biofilm formation in the cystic fibrosis airway. *Pulm. Pharmacol. Ther.* **21,** 595–9 (2008).
332. Tolker-Nielsen, T. & Sternberg, C. Methods for studying biofilm formation: flow cells and confocal laser scanning microscopy. *Methods Mol. Biol.* **1149,** 615–29 (2014).

333. Cowan, S. E., Liepmann, D. & Keasling, J. D. Development of engineered biofilms on poly-L-lysine patterned surfaces. *Biotechnol. Lett.* **23,** 1235–1241 (2001).

334. Verschoor, J. A., Meiring, M. J., van Wyngaardt, S. & Weyer, K. Polystyrene, poly-L-lysine and nylon as adsorptive surfaces for the binding of whole cells of *Mycobacterium tuberculosis* H37 RV to ELISA plates. *J. Immunoassay* **11,** 413–428 (1990).

335. Chua, S. L., Liu, Y., Yam, J. K. H., Chen, Y., Vejborg, R. M., Tan, B. G. C., Kjelleberg, S., Tolker-Nielsen, T., Givskov, M. & Yang, L. Dispersed cells represent a distinct stage in the transition from bacterial biofilm to planktonic lifestyles. *Nat. Commun.* **5,** 4462 (2014).

336. Howlin, R., Cathie, K., Hall-Stoodley, L., Niehaus, L., Connett, G., Legg, J., Daniels, T., Carroll, M., Jefferies, J., Clarke, S. C., Stoodley, P., Webb, J. & Faust, S. N. Nitric oxide-mediated dispersal and enhanced antibiotic sensitivity in *Pseudomonas aeruginosa* biofilms from the cystic fibrosis lung. *Arch. Dis. Child.* **96,** 45 (2011).

337. Roy, A. B., Petrova, O. E. & Sauer, K. The phosphodiesterase DipA (PA5017) is essential for *Pseudomonas aeruginosa* biofilm dispersion. *J Bacteriol* **194,** 2904–2915 (2012).

338. Kowaluk, E. a, Seth, P. & Fung, H. L. Metabolic activation of sodium nitroprusside to nitric oxide in vascular smooth muscle. *J. Pharmacol. Exp. Ther.* **262,** 916–922 (1992).

339. Rindone, J. P. & Sloane, E. P. Cyanide toxicity from sodium nitroprusside: Risks and management. *Annals of Pharmacotherapy* **26,** 515–519 (1992).

340. Arnold, W. P., Longnecker, D. E. & Epstein, R. M. Photodegradation of sodium nitroprusside: Biologic activity and cyanide release. *Anesthesiology* **61,** 254–260 (1984).

341. Barnes, R. J., Low, J. H., Bandi, R. R., Tay, M., Chua, F., Aung, T., Fane, A. G., Kjelleberg, S. & Rice, S. A. Nitric oxide treatment for the control of reverse osmosis membrane biofouling. *Appl. Environ. Microbiol.* **81,** 2515–2524 (2015).

342. Barraud, N., Kardak, B. G., Yepuri, N. R., Howlin, R. P., Webb, J. S., Faust, S. N., Kjelleberg, S., Rice, S. A. & Kelso, M. J. Cephalosporin-3'-diazeniumdiolates: Targeted NO-donor prodrugs for dispersing bacterial biofilms. *Angew. Chemie - Int. Ed.* **51,** 9057–9060 (2012).

343. Romeo, T. *Bacterial Biofilms. Current opinion in biotechnology* **322,** (2008).

344. Stewart, P. S. GUEST COMMENTARIES Diffusion in Biofilms Why is diffusion an important process. *J. Bacteriol.* **185,** 1485–1491 (2003).

345. Duerig, A., Abel, S., Folcher, M., Nicollier, M., Schwede, T., Amiot, N., Giese, B. & Jenal, U. Second messenger-mediated spatiotemporal control of protein degradation regulates bacterial cell cycle progression. *Genes Dev.* **23,** 93–104 (2009).

346. Fang, H., Toyofuku, M., Kiyokawa, T., Ichihashi, A., Tateda, K. & Nomura, N. The Impact of Anaerobiosis on Strain-Dependent Phenotypic Variations in *Pseudomonas aeruginosa*. *Biosci. Biotechnol. Biochem.* **77,** 1747–1752 (2013).

347. Yoon, M. Y., Lee, K. M., Park, Y. & Yoon, S. S. Contribution of cell elongation to the biofilm formation of *Pseudomonas aeruginosa* during anaerobic respiration. *PLoS One* **6,** (2011).

348. Line, L., Alhede, M., Kolpen, M., Kühl, M., Ciofu, O., Bjarnsholt, T., Moser, C., Toyofuku, M., Nomura, N., Høiby, N. & Jensen, P. Ø. Physiological levels of nitrate support anoxic growth by denitrification of *Pseudomonas aeruginosa* at growth rates reported in cystic fibrosis lungs and

sputum. *Front. Microbiol.* **5,** (2014).

349. Schleheck, D., Barraud, N., Klebensberger, J., Webb, J. S., McDougald, D., Rice, S. A. & Kjelleberg, S. *Pseudomonas aeruginosa* PAO1 preferentially grows as aggregates in liquid batch cultures and disperses upon starvation. *PLoS One* **4,** (2009).
350. Gilligan, P. H. Microbiology of airway disease in patients with cystic fibrosis. *Clin.Microbiol.Rev.* **4,** 35–51 (1991).
351. Boucher, J. C., Yu, H., Mudd, M. H. & Deretic, V. Mucoid *Pseudomonas aeruginosa* in cystic fibrosis: characterization of muc mutations in clinical isolates and analysis of clearance in a mouse model of respiratory infection. *Infect. Immun.* **65,** 3838–3846 (1997).
352. Mahenthiralingam, E., Campbell, M. E. & Speert, D. P. Nonmotility and phagocytic resistance of *Pseudomonas aeruginosa* isolates from chronically colonized patients with cystic fibrosis. **62,** 596–605 (1994).
353. Saiman, L., Mahar, F., Niu, W. W., Neu, H. C., Shaw, K. J., Miller, G. & Prince, A. Antibiotic susceptibility of multiple resistant *Pseudomonas aeruginosa* isolated from patients with cystic fibrosis, including candidates for transplantation. *Clin.Inf.Dis.* **23,** 532–537 (1996).
354. Ernst, R. K., Yi, E. C., Guo, L., Lim, K. B., Burns, J. L., Hackett, M. & Miller, S. I. Specific lipopolysaccharide found in cystic fibrosis airway *Pseudomonas aeruginosa*. *Science* **286,** 1561–5 (1999).
355. Hancock, R. E. W., Mutharia, L. M., Chan, L., Darveau, R. P., Speert, D. P. & Pier, G. B. *Pseudomonas aeruginosa* isolates from patients with cystic-fibrosis - A class of serum-sensitive, nontypable strains deficient in lipopolysaccharide O-side-chains. *Infect. Immun.* **42,** 170–177 (1983).
356. Mulcahy, L. R., Burns, J. L., Lory, S. & Lewis, K. Emergence of *Pseudomonas aeruginosa* strains producing high levels of persister cells in patients with cystic fibrosis. *J. Bacteriol.* **192,** 6191–6199 (2010).
357. Singh, P. K., Schaefer, A. L., Parsek, M. R., Moninger, T. O., Welsh, M. J. & Greenberg, E. P. Quorum-sensing signals indicate that cystic fibrosis lungs are infected with bacterial biofilms. *Nature* **407,** 762–764 (2000).
358. Donlan, R. M. Biofilms: Microbial life on surfaces. *Emerg. Infect. Dis.* **8,** 881–890 (2002).
359. Bossier, P. & Verstraete, W. Triggers for microbial aggregation in activated sludge? *Appl. Microbiol. Biotechnol.* **45,** 1–6 (1996).
360. Hall-Stoodley, L., Stoodley, P., Kathju, S., Høiby, N., Moser, C., William Costerton, J., Moter, A. & Bjarnsholt, T. Towards diagnostic guidelines for biofilm-associated infections. *FEMS Immunol. Med. Microbiol.* **65,** 127–145 (2012).
361. Alhede, M., Kragh, K. N., Qvortrup, K., Allesen-Holm, M., van Gennip, M., Christensen, L. D., Jensen, P. Ø., Nielsen, A. K., Parsek, M., Wozniak, D., Molin, S., Tolker-Nielsen, T., Høiby, N., Givskov, M. & Bjarnsholt, T. Phenotypes of non-attached *Pseudomonas aeruginosa* aggregates resemble surface attached biofilm. *PLoS One* **6,** (2011).
362. Moskowitz, S. M., Foster, J. M., Emerson, J. & Burns, J. L. Clinically Feasible Biofilm Susceptibility Assay for Isolates of *Pseudomonas aeruginosa* from Patients with Cystic Fibrosis

Clinically Feasible Biofilm Susceptibility Assay for Isolates of *Pseudomonas aeruginosa* from Patients with Cystic Fibrosis. *J. Clin. Microbiol.* **42,** 1915–1922 (2004).

363. Klebensberger, J., Rui, O., Fritz, E., Schink, B. & Philipp, B. Cell aggregation of *Pseudomonas aeruginosa* strain PAO1 as an energy-dependent stress response during growth with sodium dodecyl sulfate. *Arch. Microbiol.* **185,** 417–427 (2006).
364. Jung, Y. G., Choi, J., Kim, S. K., Lee, J. H. & Kwon, S. Embedded biofilm, a new biofilm model based on the embedded growth of bacteria. *Appl. Environ. Microbiol.* **81,** 211–219 (2015).
365. Yazdi, S. & Ardekani, A. M. Bacterial aggregation and biofilm formation in a vortical flow. *Biomicrofluidics* **6,** 1–9 (2012).
366. Schleheck, D., Barraud, N., Klebensberger, J., Webb, J. S., McDougald, D., Rice, S. A. & Kjelleberg, S. *Pseudomonas aeruginosa* PAO1 preferentially grows as aggregates in liquid batch cultures and disperses upon starvation. *PLoS One* **4,** e5513 (2009).
367. Klebensberger, J., Lautenschlager, K., Bressler, D., Wingender, J. & Philipp, B. Detergent-induced cell aggregation in subpopulations of *Pseudomonas aeruginosa* as a preadaptive survival strategy. *Environ. Microbiol.* **9,** 2247–2259 (2007).
368. Caceres, S. M., Malcolm, K. C., Taylor-Cousar, J. L., Nichols, D. P., Saavedra, M. T., Bratton, D. L., Moskowitz, S. M., Burns, J. L. & Nick, J. A. Enhanced in vitro formation and antibiotic resistance of nonattached *Pseudomonas aeruginosa* aggregates through incorporation of neutrophil products. *Antimicrob. Agents Chemother.* **58,** 6851–6860 (2014).
369. Hassett, D. J., Cuppoletti, J., Trapnell, B., Lymar, S. V, Rowe, J. J., Yoon, S. S., Hilliard, G. M., Parvatiyar, K., Kamani, M. C. & Wozniak, D. J. Anaerobic metabolism and quorum sensing by *Pseudomonas aeruginosa* biofilms in chronically infected cystic fibrosis airways: rethinking antibiotic treatment strategies and drug targets. *Adv. Drug Deliv. Rev.* **54,** 1425–1443 (2002).
370. Worlitzsch, D., Tarran, R., Ulrich, M., Schwab, U., Cekici, A., Meyer, K. C., Birrer, P., Bellon, G., Berger, J., Weiss, T., Botzenhart, K., Yankaskas, J. R., Randell, S., Boucher, R. C. & Döring, G. Effects of reduced mucus oxygen concentration in airway Pseudomonas infections of cystic fibrosis patients. *J. Clin. Invest.* **109,** 317–325 (2002).
371. Anderson, G. G., Palermo, J. J., Schilling, J. D., Roth, R., Heuser, J. & Hultgren, S. J. Intracellular bacterial biofilm-like pods in urinary tract infections. *Science* **301,** 105–7 (2003).
372. Imundo, L., Barasch, J., Prince, A. & Al-Awqati, Q. Cystic fibrosis epithelial cells have a receptor for pathogenic bacteria on their apical surface. *Proc. Natl. Acad. Sci. USA* **92,** 3019–3023. (1995).
373. Hahn, H. P. The type-4 pilus is the major virulence-associated adhesin of *Pseudomonas aeruginosa* - A review. in *Gene* **192,** 99–108 (1997).
374. De Bentzmann, S., Roger, P. & Puchelle, E. *Pseudomonas aeruginosa* adherence to remodelling respiratory epithelium. *European Respiratory Journal* **9,** 2145–2150 (1996).
375. Swanson, B., Savel, R., Szoka, F., Sawa, T. & Wiener-Kronish, J. Development of a high throughput *Pseudomonas aeruginosa* epithelial cell adhesion assay. *J. Microbiol. Methods* **52,** 361–366 (2003).
376. Garcia-Medina, R., Dunne, W. M., Singh, P. K. & Brody, S. L. *Pseudomonas aeruginosa* acquires biofilm-like properties within airway epithelial cells. *Infect. Immun.* **73,** 8298–8305 (2005).

377. Hassett, D. J., Cuppoletti, J., Trapnell, B., Lymar, S. V., Rowe, J. J., Yoon, S. S., Hilliard, G. M., Parvatiyar, K., Kamani, M. C., Wozniak, D. J., Hwang, S. H., McDermott, T. R. & Ochsner, U. A. Anaerobic metabolism and quorum sensing by *Pseudomonas aeruginosa* biofilms in chronically infected cystic fibrosis airways: Rethinking antibiotic treatment strategies and drug targets. *Advanced Drug Delivery Reviews* **54,** 1425–1443 (2002).

378. Elphick, H. E., Demoncheaux, E., Ritson, S., Higenbottam, T. W. & Everard, M. L. Exhaled nitric oxide is decreased in infants with cystic fibrosis. *Thorax* **54,** (1999).

379. Jobsis, Q., Raatgeep, H. C., Schellekens, S. L., Kroesbergen, A., Hop, W. C. & de Jongste, J. C. Hydrogen peroxide and nitric oxide in exhaled air of children with cystic fibrosis during antibiotic treatment. *Eur. Respir. J.* **16,** 95–100 (2000).

380. Mhanna, M. J., Ferkol, T., Martin, R. J., Dreshaj, I. A., van Heeckeren, A. M., Kelley, T. J. & Haxhiu, M. A. Nitric oxide deficiency contributes to impairment of airway relaxation in cystic fibrosis mice. *Am. J. Respir. Cell Mol. Biol.* **24,** 621–626 (2001).

381. Darling, K. E. & Evans, T. J. Effects of nitric oxide on *Pseudomonas aeruginosa* infection of epithelial cells from a human respiratory cell line derived from a patient with cystic fibrosis. *Infect Immun* **71,** 2341–2349 (2003).

382. Grasemann, H., Knauer, N., Buscher, R., Hubner, K., Drazen, J. M. & Ratjen, F. Airway nitric oxide levels in cystic fibrosis patients are related to a polymorphism in the neuronal nitric oxide synthase gene. *Am.J.Respir.Crit Care Med.* **162,** 2172–2176 (2000).

383. Wessel, A. K., Arshad, T. A., Fitzpatrick, M., Connell, J. L., Bonnecaze, R. T., Shear, J. B. & Whiteley, M. Oxygen limitation within a bacterial aggregate. *MBio* **5,** 1–9 (2014).

384. Foulston, L., Elsholz, A. K. W., DeFrancesco, A. S. & Losick, R. The extracellular matrix of *Staphylococcus aureus* biofilms comprises cytoplasmic proteins that associate with the cell surface in response to decreasing pH. *MBio* **5,** 1–9 (2014).

385. Baugh, S., Phillips, C. R., Ekanayaka, A. S., Piddock, L. J. V & Webber, M. A. Inhibition of multidrug efflux as a strategy to prevent biofilm formation. *J. Antimicrob. Chemother.* **69,** 673–681 (2014).

386. Zeng, G., Vad, B. S., Dueholm, M. S., Christiansen, G., Nilsson, M., Tolker-Nielsen, T., Nielsen, P. H., Meyer, R. L. & Otzen, D. E. Functional bacterial amyloid increases Pseudomonas biofilm hydrophobicity and stiffness. *Front. Microbiol.* **6,** 1–14 (2015).

387. Jagmann, N., Henke, S. F. & Philipp, B. Cells of *Escherichia coli* are protected against severe chemical stress by co-habiting cell aggregates formed by *Pseudomonas aeruginosa*. *Appl. Microbiol. Biotechnol.* **99,** 8285–8294 (2015).

388. Guo, A., Xu, Y., Mowery, J., Nagy, A., Bauchan, G. & Nou, X. Ralstonia insidiosa induces cell aggregation of *Listeria monocytogenes*. *Food Control* **67,** 303–309 (2016).

389. Zhang, W., McLamore, E. S., Garland, N. T., Leon, J. V. C. & Banks, M. K. A simple method for quantifying biomass cell and polymer distribution in biofilms. *J. Microbiol. Methods* **94,** 367–374 (2013).

390. Dastghey, S., Parvizi, J., Shapiro, I. M., Hickok, N. J. & Otto, M. Effect of biofilms on recalcitrance of staphylococcal joint infection to antibiotic treatment. *J. Infect. Dis.* **211,** 641–650

(2015).

391. Reznikoff, W. S. Transposon Tn 5. *Annu. Rev. Genet.* **42,** 269–286 (2008).

392. Schweizer, H. P. & de Lorenzo, V. Molecular Tools for Genetic Analysis of Pseudomonads. in *Pseudomonas: Volume 1 Genomics, Life Style and Molecular Architecture* (ed. Ramos, J.-L.) 317–350 (Springer US, 2004). doi:10.1007/978-1-4419-9086-0_10

393. Schweizer, H. P. Alielic exchange in *Pseudomonas aeruginosa* using novel ColE1-type vectors and a family of cassettes containing a portable oriT and the counter-selectable *Bacillus subtilis* sacB marker. *Mol. Microbiol.* **6,** 1195–1204 (1992).

394. Schweizer, H. P. Escherichia-Pseudomonas shuttle vectors derived from pUC18/19. *Gene* **97,** 109–112 (1991).

395. West, S. E. H., Schweizer, H. P., Dall, C., Sample, A. K. & Runyen-Janecky, L. J. Construction of improved Escherichia-Pseudomonas shuttle vectors derived from pUC18/19 and sequence of the region required for their replication in *Pseudomonas aeruginosa*. *Gene* **148,** 81–86 (1994).

396. Schweizer, H. P. & Hoang, T. T. An improved system for gene replacement and xylE fusion analysis in *Pseudomonas aeruginosa*. *Gene* **158,** 15–22 (1995).

397. Flynn, J. L. & Ohman, D. E. Use of a gene replacement cosmid vector for cloning alginate conversion genes from mucoid and nonmucoid *Pseudomonas aeruginosa* strains: algS controls expression of algT. *J. Bacteriol.* **170,** 3228–3236 (1988).

398. Grahn, A. M., Haase, J., Bamford, D. H. & Lanka, E. Components of the RP4 Conjugative Transfer Apparatus Form an Envelope Structure Bridging Inner and Outer Membranes of Donor Cells: Implications for Related Macromolecule Transport Systems. *J. Bacteriol.* **182,** 1564–1574 (2000).

399. Jager, W., Schafer, A., Puhler, A., Labes, G. & Spring, S. ~ E. **174,** 5462–5465 (1992).

400. Kato, F. & Sugai, M. A simple method of markerless gene deletion in *Staphylococcus aureus*. *J. Microbiol. Methods* **87,** 76–81 (2011).

401. Déziel, E., Gopalan, S., Tampakaki, A. P., Lépine, F., Padfield, K. E., Saucier, M., Xiao, G. & Rahme, L. G. The contribution of MvfR to *Pseudomonas aeruginosa* pathogenesis and quorum sensing circuitry regulation: Multiple quorum sensing-regulated genes are modulated without affecting IasRI, rhIRI or the production of N-acyl-L-homoserine lactones. *Mol. Microbiol.* **55,** 998–1014 (2005).

402. Masuda, N., Sakagawa, E. & Ohya, S. Substrate Specificities of MexAB-OprM , Pumps in *Pseudomonas aeruginosa* Substrate Specificities of MexAB-OprM , MexCD-OprJ , and MexXY-OprM Efflux Pumps in *Pseudomonas aeruginosa*. *Antimicrob. Agents Chemother.* **44,** 3322–3327 (2000).

403. Klausen, M., Heydorn, A., Ragas, P., Lambertsen, L., Aaes-Jørgensen, A., Molin, S. & Tolker-Nielsen, T. Biofilm formation by *Pseudomonas aeruginosa* wild type, flagella and type IV pili mutants. *Mol. Microbiol.* **48,** 1511–1524 (2003).

404. Choy, W.-K., Zhou, L., Syn, C. K.-C., Zhang, L.-H. & Swarup, S. MorA Defines a New Class of Regulators Affecting Flagellar Development and Biofilm Formation in Diverse Pseudomonas Species. *J. Bacteriol.* **186,** 7221–7228 (2004).

405. Horton, R. M., Hunt, H. D., Ho, S. N., Pullen, J. K. & Pease, L. R. Engineering hybrid genes without the use of restriction enzymes: gene splicing by overlap extension. *Gene* **77,** 61–68 (1989).

406. Ferrández, A., Hawkins, A. C., Douglas, T., Harwood, C. S., Ferra, A. & Summerfield, D. T. Cluster II che Genes from *Pseudomonas aeruginosa* Are Required for an Optimal Chemotactic Response. **184,** 4374–4383 (2002).

407. Dietrich, L. E. P., Price-Whelan, A., Petersen, A., Whiteley, M. & Newman, D. K. The phenazine pyocyanin is a terminal signalling factor in the quorum sensing network of *Pseudomonas aeruginosa*. *Mol. Microbiol.* **61,** 1308–1321 (2006).

408. McKnight, S. L., Iglewski, B. H. & Pesci, E. C. The Pseudomonas Quinolone Signal Regulates rhl Quorum Sensing in *Pseudomonas aeruginosa*. *J. Bacteriol.* **182,** 2702–2708 (2000).

409. O'Loughlin, C. T., Miller, L. C., Siryaporn, A., Drescher, K., Semmelhack, M. F. & Bassler, B. L. A quorum-sensing inhibitor blocks *Pseudomonas aeruginosa* virulence and biofilm formation. *Proc. Natl. Acad. Sci.* **110,** 17981–17986 (2013).

410. Güvener, Z. T. & Harwood, C. S. Subcellular location characteristics of the *Pseudomonas aeruginosa* GGDEF protein, WspR, indicate that it produces cyclic-di-GMP in response to growth on surfaces. *Mol. Microbiol.* **66,** 1459–1473 (2007).

411. Gibson, D. G., Young, L., Chuang, R. Y., Venter, J. C., Hutchison, C. A. & Smith, H. O. Enzymatic assembly of DNA molecules up to several hundred kilobases. *Nat. Methods* **6,** 343–345 (2009).

412. Gibson, D. G., Smith, H. O., Hutchison, C. A., Venter, J. C. & Merryman, C. Chemical synthesis of the mouse mitochondrial genome. *Nat. Methods* **7,** 901–903 (2010).

413. Wang, J. W., Wang, A., Li, K., Wang, B., Jin, S., Reiser, M. & Lockey, R. F. CRISPR/Cas9 nuclease cleavage combined with Gibson assembly for seamless cloning. *Biotechniques* **58,** 161–170 (2015).

414. Siuti, P., Yazbek, J. & Lu, T. K. Synthetic circuits integrating logic and memory in living cells. *Nat. Biotechnol.* **31,** 448–452 (2013).

415. Polstein, L. R. & Gersbach, C. A. A light-inducible CRISPR-Cas9 system for control of endogenous gene activation. *Nat. Chem. Biol.* **11,** 198–200 (2015).

416. Wang, Y., Zhang, Z. T., Seo, S. O., Choi, K., Lu, T., Jin, Y. S. & Blaschek, H. P. Markerless chromosomal gene deletion in *Clostridium beijerinckii* using CRISPR/Cas9 system. *J. Biotechnol.* **200,** 1–5 (2015).

417. Huang, W. & Wilks, A. A rapid seamless method for gene knockout in *Pseudomonas aeruginosa*. *BMC Microbiol.* **17,** (2017).

418. Ishino, Y., Shinagawa, H., Makino, K., Amemura, M. & Nakata, A. Nucleotide sequence of the iap gene, responsible for alkaline phosphatase isozyme conversion in *Escherichia coli*, and identification of the gene product. *J. Bacteriol.* **169,** 5429–5433 (1987).

419. Mojica, F. J. M., Díez-Villaseñor, C., Soria, E. & Juez, G. Biological significance of a family of regularly spaced repeats in the genomes of Archaea, Bacteria and mitochondria. *Molecular Microbiology* **36,** 244–246 (2000).

420. Doudna, J. A. & Charpentier, E. The new frontier of genome engineering with CRISPR-Cas9. *Science* **346,** (2014).

421. Ran, F. A., Hsu, P. D., Wright, J., Agarwala, V., Scott, D. A. & Zhang, F. Genome engineering using the CRISPR-Cas9 system. *Nat Protoc* **8,** 2281–2308 (2013).

422. Jiang, W., Bikard, D., Cox, D., Zhang, F. & Marraffin, L. A. CRISPR-assisted editing of bacterial genomes. *Nat biotechnol* **31,** 233–239 (2013).

423. Cobb, R. E., Wang, Y. & Zhao, H. High-Efficiency Multiplex Genome Editing of Streptomyces Species Using an Engineered CRISPR/Cas System. *ACS Synth. Biol.* **4,** 723–728 (2015).

424. Jiang, Y., Qian, F., Yang, J., Liu, Y., Dong, F., Xu, C., Sun, B., Chen, B., Xu, X., Li, Y., Wang, R. & Yang, S. CRISPR-Cpf1 assisted genome editing of *Corynebacterium glutamicum*. *Nat. Commun.* **8,** (2017).

425. Mougiakos, I., Mohanraju, P., Bosma, E. F., Vrouwe, V., Finger Bou, M., Naduthodi, M. I. S., Gussak, A., Brinkman, R. B. L., Van Kranenburg, R. & Van Der Oost, J. Characterizing a thermostable Cas9 for bacterial genome editing and silencing. *Nat. Commun.* **8,** (2017).

426. Vercoe, R. B., Chang, J. T., Dy, R. L., Taylor, C., Gristwood, T., Clulow, J. S., Richter, C., Przybilski, R., Pitman, A. R. & Fineran, P. C. Cytotoxic Chromosomal Targeting by CRISPR/Cas Systems Can Reshape Bacterial Genomes and Expel or Remodel Pathogenicity Islands. *PLoS Genet.* **9,** (2013).

427. Oh, J. H. & Van Pijkeren, J. P. CRISPR-Cas9-assisted recombineering in Lactobacillus reuteri. *Nucleic Acids Res.* **42,** (2014).

428. Singh, A. K., Carette, X., Potluri, L.-P., Sharp, J. D., Xu, R., Prisic, S. & Husson, R. N. Investigating essential gene function in *Mycobacterium tuberculosis* using an efficient CRISPR interference system. *Nucleic Acids Res.* gkw625 (2016). doi:10.1093/nar/gkw625

429. Pougach, K., Semenova, E., Bogdanova, E., Datsenko, K. A., Djordjevic, M., Wanner, B. L. & Severinov, K. Transcription, processing and function of CRISPR cassettes in *Escherichia coli*. *Mol. Microbiol.* **77,** 1367–1379 (2010).

430. Qiu, Y., Wang, S., Chen, Z., Guo, Y. & Song, Y. An active type I-E CRISPR-cas system identified in *Streptomyces avermitilis*. *PLoS One* **11,** (2016).

431. Przybilski, R., Richter, C., Gristwood, T., Clulow, J. S., Vercoe, R. B. & Fineran, P. C. Csy4 is responsible for CRISPR RNA processing in *Pectobacterium atrosepticum*. *RNA Biol.* **8,** 517–528 (2011).

432. He, L., Fan, X. & Xie, J. Comparative genomic structures of Mycobacterium CRISPR-Cas. *J. Cell. Biochem.* **113,** 2464–2473 (2012).

433. Cady, K. C., Bondy-Denomy, J., Heussler, G. E., Davidson, A. R. & O'Toole, G. A. The CRISPR/Cas adaptive immune system of *Pseudomonas aeruginosa* mediates resistance to naturally occurring and engineered phages. *Journal of Bacteriology* **194,** 5728–5738 (2012).

434. Høyland-Kroghsbo, N. M., Paczkowski, J., Mukherjee, S., Broniewski, J., Westra, E., Bondy-Denomy, J. & Bassler, B. L. Quorum sensing controls the *Pseudomonas aeruginosa* CRISPR-Cas adaptive immune system. *Proc. Natl. Acad. Sci. U. S. A.* 201617415 (2016). doi:10.1073/pnas.1617415113

435. Wiedenheft, B. & Bondy-Denomy, J. CRISPR control of virulence in *Pseudomonas aeruginosa*. *Cell Res.* **27,** 163–164 (2017).

436. Hmelo, L. R., Borlee, B. R., Almblad, H., Love, M. E., Randall, T. E., Tseng, B. S., Lin, C., Irie, Y., Storek, K. M., Yang, J. J., Siehnel, R. J., Howell, P. L., Singh, P. K., Tolker-Nielsen, T., Parsek, M. R., Schweizer, H. P. & Harrison, J. J. Precision-engineering the *Pseudomonas aeruginosa* genome with two-step allelic exchange. *Nat. Protoc.* **10,** 1820–41 (2015).

437. Mergulhão, F. J., Kelly, A. G., Monteiro, G. A., Taipa, M. A. & Cabral, J. M. Troubleshooting in gene splicing by overlap extension: a step-wise method. *Mol. Biotechnol.* **12,** 285–287 (1999).

438. Jain, S. & Ohman, D. E. Role of an alginate lyase for alginate transport in mucoid P*seudomonas aeruginosa*. *Infect. Immun.* **73,** 6429–6436 (2005).

439. Robles-price, A., Wong, T. Y., Sletta, H., Valla, S. & Schiller, N. L. AlgX Is a Periplasmic Protein Required for Alginate Biosynthesis in *Pseudomonas aeruginosa*. *J. Bacteriol.* **186,** 7369–7377 (2004).

440. Kulesekara, H., Lee, V., Brencic, A., Liberati, N., Urbach, J., Miyata, S., Lee, D. G., Neely, A. N., Hyodo, M., Hayakawa, Y., Ausubel, F. M. & Lory, S. Analysis of *Pseudomonas aeruginosa* diguanylate cyclases and phosphodiesterases reveals a role for bis-(3′-5′)-cyclic-GMP in virulence. *Proc. Natl. Acad. Sci. United States Am.* **103,** 2839–2844 (2006).

441. Li, Y., Petrova, O. E., Su, S., Lau, G. W., Panmanee, W., Na, R., Hassett, D. J., Davies, D. G. & Sauer, K. BdlA, DipA and Induced Dispersion Contribute to Acute Virulence and Chronic Persistence of *Pseudomonas aeruginosa*. *PLoS Pathog.* **10,** (2014).

442. Petrova, O. E. & Sauer, K. Dispersion by *Pseudomonas aeruginosa* requires an unusual posttranslational modification of BdlA. *Proc. Natl. Acad. Sci.* **109,** 16690–16695 (2012).

443. Morgan, R., Kohn, S., Hwang, S.-H., Hassett, D. J. & Sauer, K. BdlA, a Chemotaxis Regulator Essential for Biofilm Dispersion in *Pseudomonas aeruginosa*. *J. Bacteriol.* **188,** 7335–7343 (2006).

444. Kazmierczak, B. I., Lebron, M. B. & Murray, T. S. Analysis of FimX, a phosphodiesterase that governs twitching motility in *Pseudomonas aeruginosa*. *Mol. Microbiol.* **60,** 1026–1043 (2006).

445. Roy, A. B., Petrova, O. E. & Sauer, K. The phosphodiesterase DipA (PA5017) is essential for *Pseudomonas aeruginosa* biofilm dispersion. *J. Bacteriol.* **194,** 2904–2915 (2012).

446. Roy, A. B., Petrova, O. E. & Sauer, K. Extraction and Quantification of Cyclic Di-GMP from P. aeruginosa. *Bio-protocol* **3,** e828 (2013).

447. Nair, H. A. S., Periasamy, S., Liang, Y., Kjelleberg, S. & Rice, S. A. Real Time, Spatial and Temporal Mapping of the Distribution of c-di-GMP During Biofilm Development. *J. Biol. Chem.* jbc.M116.746743 (2016). doi:10.1074/jbc.M116.746743

448. Hickman, J. W. & Harwood, C. S. Identification of FleQ from *Pseudomonas aeruginosa* as a c-di-GMP-responsive transcription factor. *Mol. Microbiol.* **69,** 376–389 (2008).

449. Kearns, D. B. A field guide to bacterial swarming motility. *Nat Rev Microbiol* **8,** 634–644 (2010).

450. Köhler, T., Curty, L. K., Barja, F., van Delden, C. & Pechère, J.-C. Swarming of *Pseudomonas aeruginosa* Is Dependent on Cell-to-Cell Signaling and Requires Flagella and Pili. *J. Bacteriol.* **182,** 5990–5996 (2000).

451. Simm, R., Morr, M., Kader, A., Nimtz, M. & Römling, U. GGDEF and EAL domains inversely regulate cyclic di-GMP levels and transition from sessility to motility. *Mol. Microbiol.* **53,** 1123–1134 (2004).

452. Kuchma, S. L., Ballok, A. E., Merritt, J. H., Hammond, J. H., Lu, W., Rabinowitz, J. D. & O'Toole, G. A. Cyclic-di-GMP-mediated repression of swarming motility by *Pseudomonas aeruginosa*: The pilY1 gene and its impact on surface-associated behaviors. *J. Bacteriol.* **192,** 2950–2964 (2010).

453. Merritt, J. H., Brothers, K. M., Kuchma, S. L. & O'Toole, G. A. SadC reciprocally influences biofilm formation and swarming motility via modulation of exopolysaccharide production and flagellar function. in *Journal of Bacteriology* **189,** 8154–8164 (2007).

454. Leech, A. J. & Mattick, J. S. Effect of Site-Specific Mutations in Different Phosphotransfer Domains of the Chemosensory Protein ChpA on *Pseudomonas aeruginosa* Motility . *J. Bacteriol.* **188,** 8479–8486 (2006).

455. Murray, T. S. & Kazmierczak, B. I. *Pseudomonas aeruginosa* exhibits sliding motility in the absence of type IV pili and flagella. *J. Bacteriol.* **190,** 2700–2708 (2008).

456. Jain, R., Sliusarenko, O. & Kazmierczak, B. I. Interaction of the cyclic-di-GMP binding protein FimX and the Type 4 pilus assembly ATPase promotes pilus assembly. *PLoS Pathog.* **13,** (2017).

457. Petrova, O. E., Cherny, K. E. & Sauer, K. The *Pseudomonas aeruginosa* diguanylate cyclase GcbA, a homolog of *Pseudomonas fluorescens* GcbA, promotes initial attachment to surfaces, but not biofilm formation, via regulation of motility. *J. Bacteriol.* **196,** 2827–2841 (2014).

458. Flemming, H.-C. & Wingender, J. The biofilm matrix. *Nat Rev Micro* **8,** 623–633 (2010).

459. Wozniak, D., Wyckoff, T., Starkey, M., Keyser, R., Azadi, P., O'Toole, G. & Parsek, M. Alginate is not a significant component of the extracellular polysaccharide matrix of PA14 and PAO1 *Pseudomonas aeruginosa* biofilms. *Proc. Natl. Acad. Sci. U. S. A.* **100,** 7907–12 (2003).

460. Jackson, K. D., Starkey, M., Kremer, S., Parsek, M. R., Wozniak, D. J., Jackson, K. D., Starkey, M., Kremer, S., Parsek, M. R. & Wozniak, D. J. Identification of psl , a Locus Encoding a Potential Exopolysaccharide That Is Essential for *Pseudomonas aeruginosa* PAO1 Biofilm Formation Identification of psl , a Locus Encoding a Potential Exopolysaccharide That Is Essential for Pseudomonas aeruginosa . **186,** 4466–4475 (2004).

461. Ha, D.-G. & O'Toole, G. A. c-di-GMP and its Effects on Biofilm Formation and Dispersion: a *Pseudomonas aeruginosa* Review. *Microbiol. Spectr.* **3,** MB-0003-2014 (2015).

462. Sadovskaya, I. Exopolysaccharide quantification. *Methods Mol. Biol.* **1149,** 347–357 (2014).

463. Molin, S. & Tolker-Nielsen, T. Gene transfer occurs with enhanced efficiency in biofilms and induces enhanced stabilisation of the biofilm structure. *Current Opinion in Biotechnology* **14,** 255–261 (2003).

464. Yang, L., Barken, K. B., Skindersoe, M. E., Christensen, A. B., Givskov, M. & Tolker-Nielsen, T. Effects of iron on DNA release and biofilm development by *Pseudomonas aeruginosa*. *Microbiology* **153,** 1318–1328 (2007).

465. Steinberger, R. E. & Holden, P. A. Extracellular DNA in single- and multiple-species unsaturated biofilms. *Appl. Environ. Microbiol.* **71,** 5404–5410 (2005).

466. Ueda, A. & Wood, T. K. Tyrosine phosphatase TpbA of *Pseudomonas aeruginosa* controls extracellular DNA via cyclic diguanylic acid concentrations. *Environ. Microbiol. Rep.* **2,** 449–455 (2010).

467. D'Argenio, D. A., Calfee, M. W., Rainey, P. B. & Pesci, E. C. Autolysis and autoaggregation in *Pseudomonas aeruginosa* colony morphology mutants. *J. Bacteriol.* **184,** 6481–6489 (2002).

468. Heurlier, K., Dénervaud, V., Haenni, M., Guy, L., Krishnapillai, V. & Haas, D. Quorum-sensing-negative (lasR) mutants of *Pseudomonas aeruginosa* avoid cell lysis and death. *J. Bacteriol.* **187,** 4875–4883 (2005).

469. Spoering, A. L. & Gilmore, M. S. Quorum sensing and DNA release in bacterial biofilms. *Current Opinion in Microbiology* **9,** 133–137 (2006).

470. Klausen, M., Aaes-Jørgensen, A., Molin, S. & Tolker-Nielsen, T. Involvement of bacterial migration in the development of complex multicellular structures in *Pseudomonas aeruginosa* biofilms. *Mol. Microbiol.* **50,** 61–68 (2003).

471. Caiazza, N. C., Shanks, R. M. Q. & O'Toole, G. A. Rhamnolipids modulate swarming motility patterns of *Pseudomonas aeruginosa*. *J. Bacteriol.* **187,** 7351–7361 (2005).

472. Tremblay, J., Richardson, A. P., Lépine, F. & Déziel, E. Self-produced extracellular stimuli modulate the *Pseudomonas aeruginosa* swarming motility behaviour. *Environ. Microbiol.* **9,** 2622–2630 (2007).

473. Pamp, S. J. & Tolker-Nielsen, T. Multiple Roles of Biosurfactants in Structural Biofilm Development by *Pseudomonas aeruginosa*. *J. Bacteriol.* **189,** 2531–2539 (2007).

474. Davey, M. E., Caiazza, N. C. & O'Toole, G. A. Rhamnolipid Surfactant Production Affects Biofilm Architecture in *Pseudomonas aeruginosa* PAO1. *J. Bacteriol.* **185,** 1027–1036 (2003).

475. Ueda, A. & Wood, T. K. Connecting Quorum Sensing, c-di-GMP, Pel Polysaccharide, and Biofilm Formation in *Pseudomonas aeruginosa* through Tyrosine Phosphatase TpbA (PA3885). *PLoS Pathog* **5,** e1000483 (2009).

476. Pearson, J. P., Pesci, E. C. & Iglewski, B. H. Roles of *Pseudomonas aeruginosa las* and *rhl* quorum-sensing systems in control of elastase and rhamnolipid biosynthesis genes. *J. Bacteriol.* **179,** 5756–67 (1997).

477. Rahman, P., Dusane, D., Zinjarde, S., Venugopalan, V., McLean, R. & Weber, M. Quorum sensing: implications on rhamnolipid biosurfactant production. *Biotechnol. Genet. Eng. Rev.* **27,** 159–184 (2010).

478. Liu, H. & Fang, H. H. P. Extraction of extracellular polymeric substances (EPS) of sludges. *J. Biotechnol.* **95,** 249–256 (2002).

479. Comte, S., Guibaud, G. & Baudu, M. Effect of extraction method on EPS from activated sludge: An HPSEC investigation. *J. Hazard. Mater.* **140,** 129–137 (2007).

480. Zhang, X., Bishop, P. L. & Kinkle, B. K. Comparison of extraction methods for quantifying extracellular polymers in biofilms. in *Water Science and Technology* **39,** 211–218 (1999).

481. Liu, Y. & Fang, H. H. P. Influences of Extracellular Polymeric Substances (EPS) on Flocculation, Settling, and Dewatering of Activated Sludge. *Crit. Rev. Environ. Sci. Technol.* **33,** 237–273 (2003).

482. Vasseur, P., Vallet-Gely, I., Soscia, C., Genin, S. & Filloux, A. The pel genes of the *Pseudomonas aeruginosa* PAK strain are involved at early and late stages of biofilm formation. *Microbiology* **151,** 985–997 (2005).

483. Ghafoor, A., Hay, I. D. & Rehm, B. H. A. Role of Exopolysaccharides in *Pseudomonas aeruginosa* Biofilm Formation and Architecture. *Appl. Environ. Microbiol.* **77,** 5238–5246 (2011).

484. Spiers, A. J., Bohannon, J., Gehrig, S. M. & Rainey, P. B. Biofilm formation at the air-liquid interface by the *Pseudomonas fluorescens* SBW25 wrinkly spreader requires an acetylated form of cellulose. *Mol. Microbiol.* **50,** 15–27 (2003).

485. Khurana, R., Uversky, V. N., Nielsen, L. & Fink, A. L. Is Congo Red an Amyloid-specific Dye? *J. Biol. Chem.* **276,** 22715–22721 (2001).

486. Nielsen, S. S. Phenol-Sulfuric Acid Method for Total Carbohydrates. in *Food Analysis Laboratory Manual* 103–113 (2010). doi:10.1007/978-1-4419-1463-7

487. Henrichsen, J. Bacterial surface translocation: a survey and a classification. *Bacteriol. Rev.* **36,** 478–503 (1972).

488. An, S., Wu, J. & Zhang, L. H. Modulation of *Pseudomonas aeruginosa* biofilm dispersal by a cyclic-Di-GMP phosphodiesterase with a putative hypoxia-sensing domain. *Appl Env. Microbiol* **76,** 8160–8173 (2010).

489. Overhage, J., Lewenza, S., Marr, A. K. & Hancock, R. E. W. Identification of genes involved in swarming motility using a *Pseudomonas aeruginosa* PAO1 mini-Tn5-lux mutant library. *J. Bacteriol.* **189,** 2164–2169 (2007).

490. Moscoso, J. A., Mikkelsen, H., Heeb, S., Williams, P. & Filloux, A. The *Pseudomonas aeruginosa* sensor RetS switches Type III and Type VI secretion via c-di-GMP signalling. *Environ. Microbiol.* **13,** 3128–3138 (2011).

491. Jones, C. J., Newsom, D., Kelly, B., Irie, Y., Jennings, L. K., Xu, B., Limoli, D. H., Harrison, J. J., Parsek, M. R., White, P. & Wozniak, D. J. ChIP-Seq and RNA-Seq Reveal an AmrZ-Mediated Mechanism for Cyclic di-GMP Synthesis and Biofilm Development by *Pseudomonas aeruginosa*. *PLoS Pathog.* **10,** (2014).

492. Caiazza, N. C., Merritt, J. H., Brothers, K. M. & O'Toole, G. A. Inverse regulation of biofilm formation and swarming motility by *Pseudomonas aeruginosa* PA14. *J. Bacteriol.* **189,** 3603–3612 (2007).

493. Pehl, M. J., da Jamieson, W., Kong, K., Forbester, J. L., Fredendall, R. J., Gregory, G. A., McFarland, J. E., Healy, J. M. & Orwin, P. M. Genes that influence swarming motility and biofilm formation in variovorax paradoxus EPS. *PLoS One* **7,** (2012).

494. Verstraeten, N., Braeken, K., Debkumari, B., Fauvart, M., Fransaer, J., Vermant, J. & Michiels, J. Living on a surface: swarming and biofilm formation. *Trends in Microbiology* **16,** 496–506 (2008).

495. Chelvam, K. K., Chai, L. C. & Thong, K. L. Variations in motility and biofilm formation of *Salmonella enterica* serovar Typhi. *Gut Pathog.* **6,** 2 (2014).

496. Chow, S., Gu, K., Jiang, L. & Nassour, A. Salicylic acid affects swimming, twitching and

swarming sotility in *Pseudomonas aeruginosa*, resulting in decreased biofilm formation. *J. experimantal Microbiol. Immunol.* **15,** 22–29 (2011).

497. Murray, T. S., Ledizet, M. & Kazmierczak, B. I. Swarming motility, secretion of type 3 effectors and biofilm formation phenotypes exhibited within a large cohort of *Pseudomonas aeruginosa* clinical isolates. *J. Med. Microbiol.* **59,** 511–520 (2010).
498. Hall-Stoodley, L. & Stoodley, P. Biofilm formation and dispersal and the transmission of human pathogens. *Trends Microbiol.* **13,** 7–10 (2005).
499. Petrova, O. E. & Sauer, K. Dispersion by *Pseudomonas aeruginosa* requires an unusual posttranslational modification of BdlA. *Proc. Natl. Acad. Sci.* **109,** 16690–16695 (2012).
500. Kulasekara, B. R., Kamischke, C., Kulasekara, H. D., Christen, M., Wiggins, P. A. & Miller, S. I. c-di-GMP heterogeneity is generated by the chemotaxis machinery to regulate flagellar motility. *Elife* **2013,** (2013).
501. Bjarnsholt, T., Jensen, P. Ø., Burmølle, M., Hentzer, M., Haagensen, J. A. J., Hougen, H. P., Calum, H., Madsen, K. G., Moser, C., Molin, S., Høiby, N. & Givskov, M. *Pseudomonas aeruginosa* tolerance to tobramycin, hydrogen peroxide and polymorphonuclear leukocytes is quorum-sensing dependent. *Microbiology* **151,** 373–383 (2005).
502. Banin, E., Brady, K. M. & Greenberg, E. P. Chelator-Induced Dispersal and Killing of *Pseudomonas aeruginosa* Cells in a Biofilm. *Appl. Environ. Microbiol.* **72,** 2064–2069 (2006).
503. Haagensen, J. A. J., Klausen, M., Ernst, R. K., Miller, S. I., Folkesson, A., Tolker-Nielsen, T. & Molin, S. Differentiation and distribution of colistin- and sodium dodecyl sulfate-tolerant cells in *Pseudomonas aeruginosa* biofilms. *J. Bacteriol.* **189,** 28–37 (2007).
504. Pamp, S. J., Gjermansen, M., Johansen, H. K. & Tolker-Nielsen, T. Tolerance to the antimicrobial peptide colistin in *Pseudomonas aeruginosa* biofilms is linked to metabolically active cells, and depends on the pmr and mexAB-oprM genes. *Mol. Microbiol.* **68,** 223–240 (2008).
505. Stewart, P. S. & Costerton, J. W. Antibiotic resistance of bacteria in biofilms. *Lancet* **358,** 135–138 (2001).
506. Stewart, P. S. A review of experimental measurements of effective diffusive permeabilities and effective diffusion coefficients in biofilms. *Biotechnology and Bioengineering* **59,** 261–272 (1998).
507. Vanderkooi, J. M., Wright, W. W. & Erecinska, M. Nitric oxide diffusion coefficients in solutions, proteins and membranes determined by phosphorescence. *Biochim. Biophys. Acta (BBA)/Protein Struct. Mol.* **1207,** 249–254 (1994).
508. Möller, M., Botti, H., Batthyany, C., Rubbo, H., Radi, R. & Denicola, A. Direct measurement of nitric oxide and oxygen partitioning into liposomes and low density lipoprotein. *J. Biol. Chem.* **280,** 8850–8854 (2005).
509. Anderl, J. N., Franklin, M. J. & Stewart, P. S. Role of Antibiotic Penetration Limitation in *Klebsiella pneumoniae* Biofilm Resistance to Ampicillin and Ciprofloxacin. *Antimicrob. Agents Chemother.* **44,** 1818–1824 (2000).
510. Kumon, H., Tomochika, K., Matunaga, T., Ogawa, M. & Ohmori, H. A sandwich cup method for the penetration assay of antimicrobial agents through Pseudomonas exopolysaccharides.

*Microbiol. Immunol.* **38,** 615–619 (1994).

511. Shigeta, M., Tanaka, G., Komatsuzawa, H., Sugai, M., Suginaka, H. & Usui, T. Permeation of antimicrobial agents through *Pseudomonas aeruginosa* biofilms: a simple method. *Chemotherapy* **43,** 340–345 (1997).
512. Gordon, C. A., Hodges, N. A. & Marriott, C. Antibiotic interaction and diffusion through alginate and exopolysaccharide of cystic fibrosis-derived *Pseudomonas aeruginosa*. *J. Antimicrob. Chemother.* **22,** 667–674 (1988).
513. Hughes, M. N. Chemistry of Nitric Oxide and Related Species. *Methods in Enzymology* **436,** 3–19 (2008).
514. Liu, X., Miller, M. J., Joshi, M. S., Thomas, D. D. & Lancaster, J. R. Accelerated reaction of nitric oxide with O2 within the hydrophobic interior of biological membranes. *Proc. Natl. Acad. Sci. U. S. A.* **95,** 2175–9 (1998).
515. Poole, R. K. Globins and other nitric oxide-reactive proteins. Preface. *Methods in enzymology* **437,** (2008).
516. Kwan, B. W., Osbourne, D. O., Hu, Y., Benedik, M. J. & Wood, T. K. Phosphodiesterase DosP increases persistence by reducing cAMP which reduces the signal indole. *Biotechnol. Bioeng.* **112,** 588–600 (2015).
517. Wood, T. K. Combatting bacterial persister cells. *Biotechnology and Bioengineering* **113,** 476–483 (2016).
518. Naseem, K. M. The role of nitric oxide in cardiovascular diseases. *Molecular Aspects of Medicine* **26,** 33–65 (2005).
519. Rossaint, R., Falke, K. J., Lopez, F., Slama, K., Pison, U. & Zapol, W. M. Inhaled nitric oxide for the adult respiratory distress syndrome. *N. Engl. J. Med.* **328,** 399–405 (1993).
520. Ji, Q., Chen, P. J., Qin, G., Deng, X., Hao, Z., Wawrzak, Z., Yeo, W.-S., Quang, J. W., Cho, H., Luo, G.-Z., Weng, X., You, Q., Luan, C.-H., Yang, X., Bae, T., Yu, K., Jiang, H. & He, C. Structure and mechanism of the essential two-component signal-transduction system WalKR in *Staphylococcus aureus*. *Nat. Commun.* **7,** 11000 (2016).

# Appendix

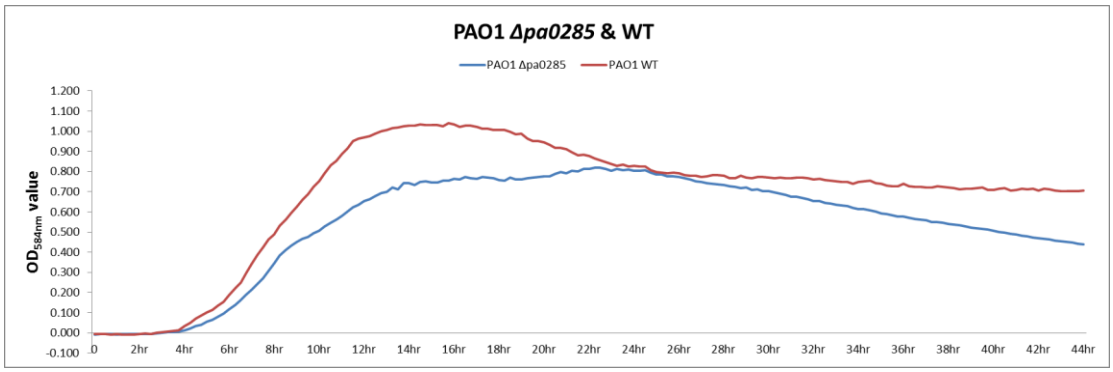
PAO1 Δpa0285 & WT
PAO1 Δpa0285
PAO1 WT
OD584nm value
1.200
1.100
1.000
0.900
0.800
0.700
0.600
0.500
0.400
0.300
0.200
0.100
0.000
-0.100
0 2hr 4hr 6hr 8hr 10hr 12hr 14hr 16hr 18hr 20hr 22hr 24hr 26hr 28hr 30hr 32hr 34hr 36hr 38hr 40hr 42hr 44hr

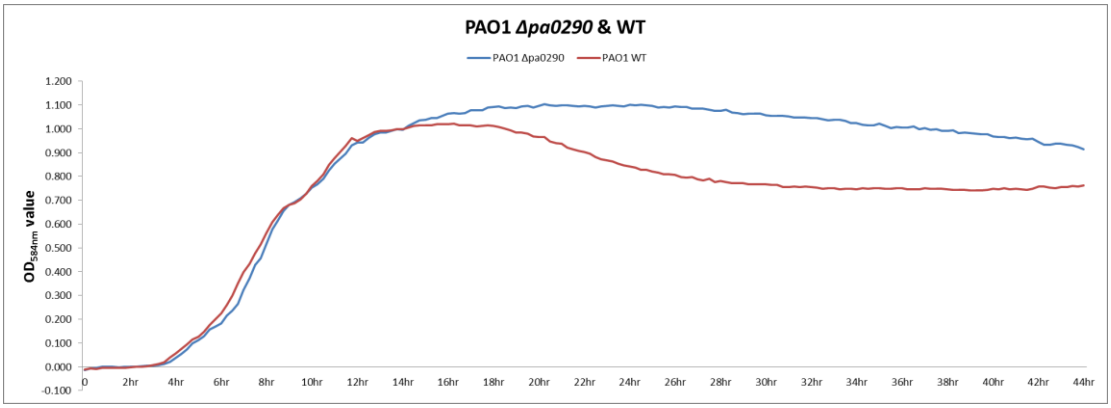
PAO1 Δpa0290 & WT
PAO1 Δpa0290
PAO1 WT
OD584nm value
1.200
1.100
1.000
0.900
0.800
0.700
0.600
0.500
0.400
0.300
0.200
0.100
0.000
-0.100
0 2hr 4hr 6hr 8hr 10hr 12hr 14hr 16hr 18hr 20hr 22hr 24hr 26hr 28hr 30hr 32hr 34hr 36hr 38hr 40hr 42hr 44hr

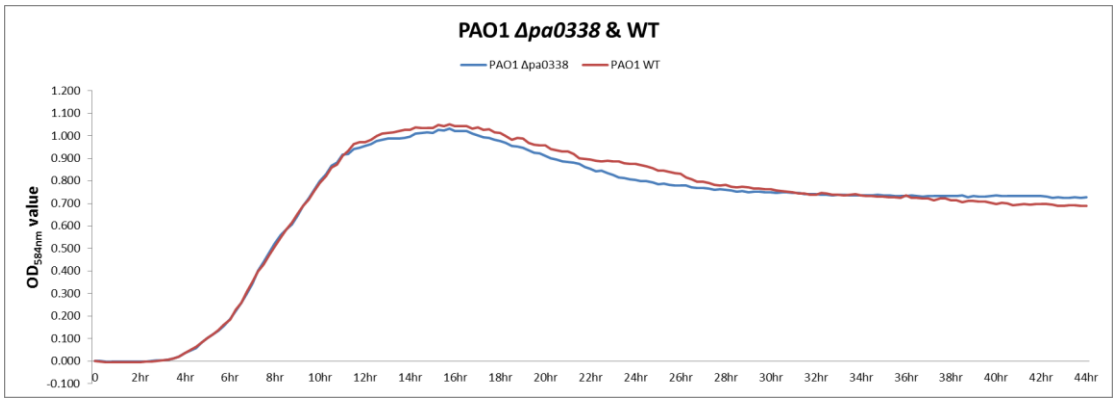
PAO1 Δpa0338 & WT
PAO1 Δpa0338
PAO1 WT
OD584nm value
1.200
1.100
1.000
0.900
0.800
0.700
0.600
0.500
0.400
0.300
0.200
0.100
0.000
-0.100
0 2hr 4hr 6hr 8hr 10hr 12hr 14hr 16hr 18hr 20hr 22hr 24hr 26hr 28hr 30hr 32hr 34hr 36hr 38hr 40hr 42hr 44hr

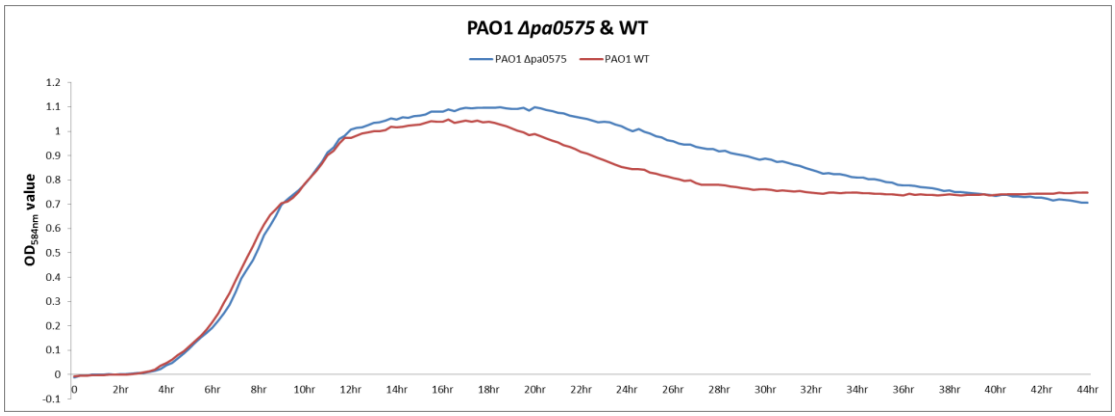
PAO1 Δpa0575 & WT
PAO1 Δpa0575
PAO1 WT
OD584nm value
1.2
1.1
1
0.9
0.8
0.7
0.6
0.5
0.4
0.3
0.2
0.1
0
-0.1
0 2hr 4hr 6hr 8hr 10hr 12hr 14hr 16hr 18hr 20hr 22hr 24hr 26hr 28hr 30hr 32hr 34hr 36hr 38hr 40hr 42hr 44hr

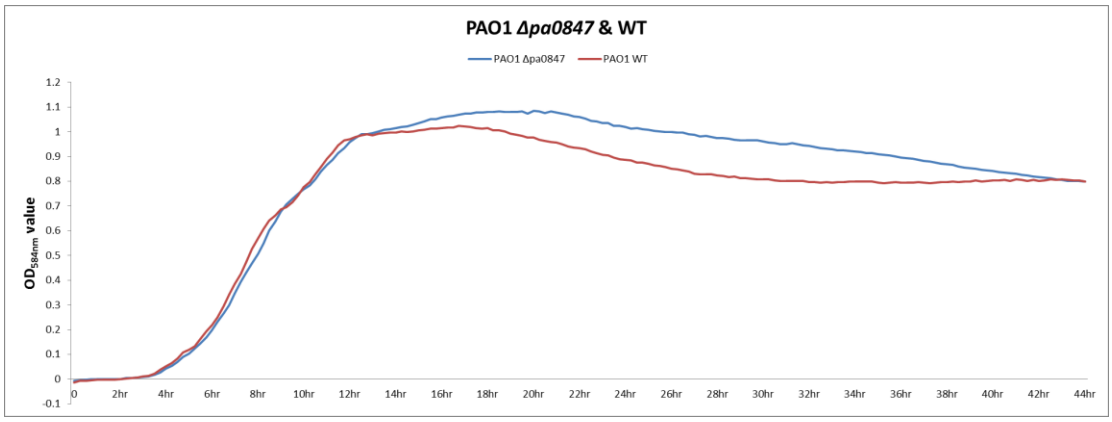
PAO1 Δpa0847 & WT
PAO1 Δpa0847
PAO1 WT
OD584nm value
1.2
1.1
1
0.9
0.8
0.7
0.6
0.5
0.4
0.3
0.2
0.1
0
-0.1
0 2hr 4hr 6hr 8hr 10hr 12hr 14hr 16hr 18hr 20hr 22hr 24hr 26hr 28hr 30hr 32hr 34hr 36hr 38hr 40hr 42hr 44hr

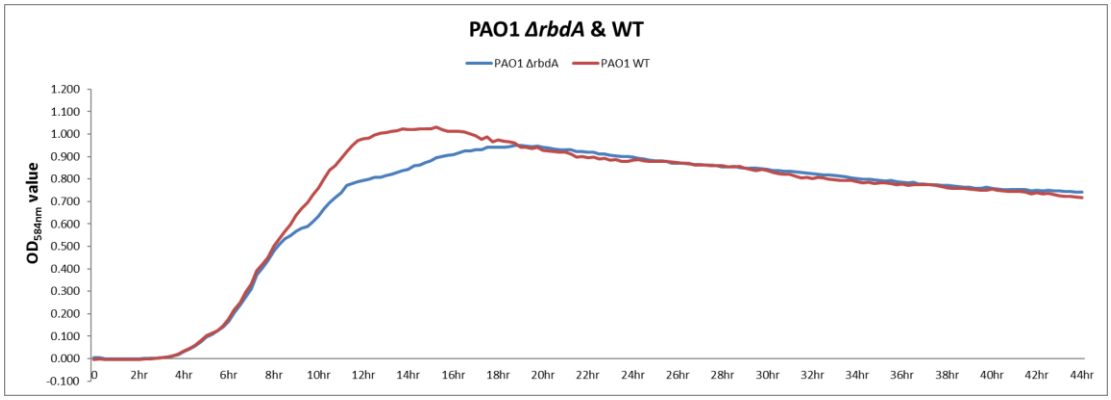
PAO1 ΔrbdA & WT
PAO1 ΔrbdA
PAO1 WT
OD584nm value
1.200
1.100
1.000
0.900
0.800
0.700
0.600
0.500
0.400
0.300
0.200
0.100
0.000
-0.100
0 2hr 4hr 6hr 8hr 10hr 12hr 14hr 16hr 18hr 20hr 22hr 24hr 26hr 28hr 30hr 32hr 34hr 36hr 38hr 40hr 42hr 44hr

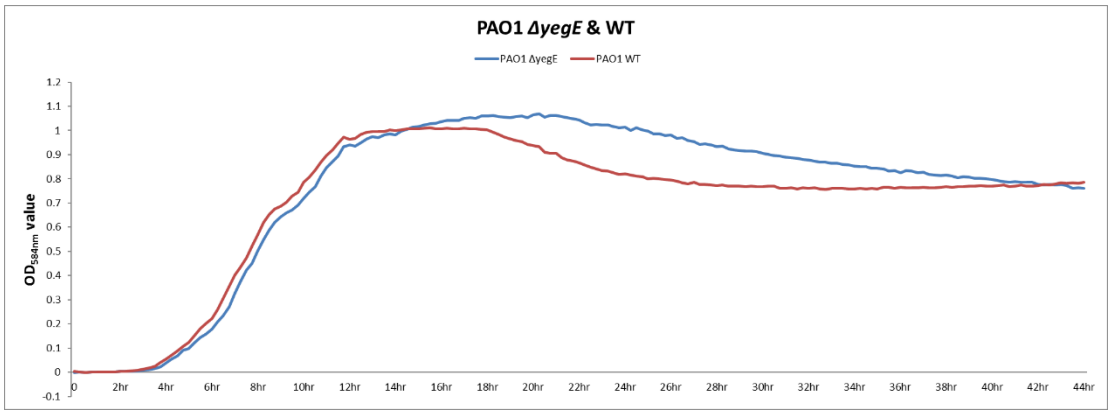
PAO1 ΔyegE & WT
PAO1 ΔyegE
PAO1 WT
OD584nm value
1.2
1.1
1
0.9
0.8
0.7
0.6
0.5
0.4
0.3
0.2
0.1
0
-0.1
0 2hr 4hr 6hr 8hr 10hr 12hr 14hr 16hr 18hr 20hr 22hr 24hr 26hr 28hr 30hr 32hr 34hr 36hr 38hr 40hr 42hr 44hr

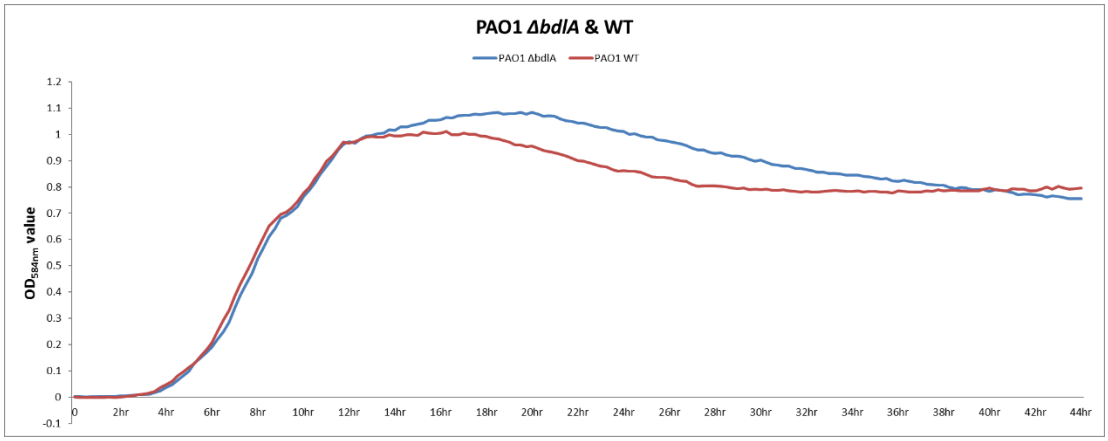
PAO1 ΔbdlA & WT
PAO1 ΔbdlA
PAO1 WT
OD584nm value
1.2
1.1
1
0.9
0.8
0.7
0.6
0.5
0.4
0.3
0.2
0.1
0
-0.1
0 2hr 4hr 6hr 8hr 10hr 12hr 14hr 16hr 18hr 20hr 22hr 24hr 26hr 28hr 30hr 32hr 34hr 36hr 38hr 40hr 42hr 44hr

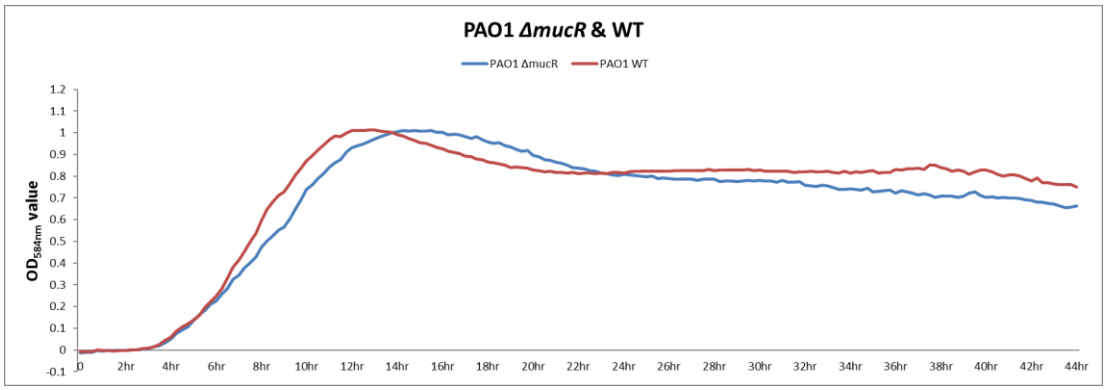
PAO1 ΔmucR & WT
PAO1 ΔmucR
PAO1 WT
OD584nm value
1.2
1.1
1
0.9
0.8
0.7
0.6
0.5
0.4
0.3
0.2
0.1
0
-0.1
0 2hr 4hr 6hr 8hr 10hr 12hr 14hr 16hr 18hr 20hr 22hr 24hr 26hr 28hr 30hr 32hr 34hr 36hr 38hr 40hr 42hr 44hr

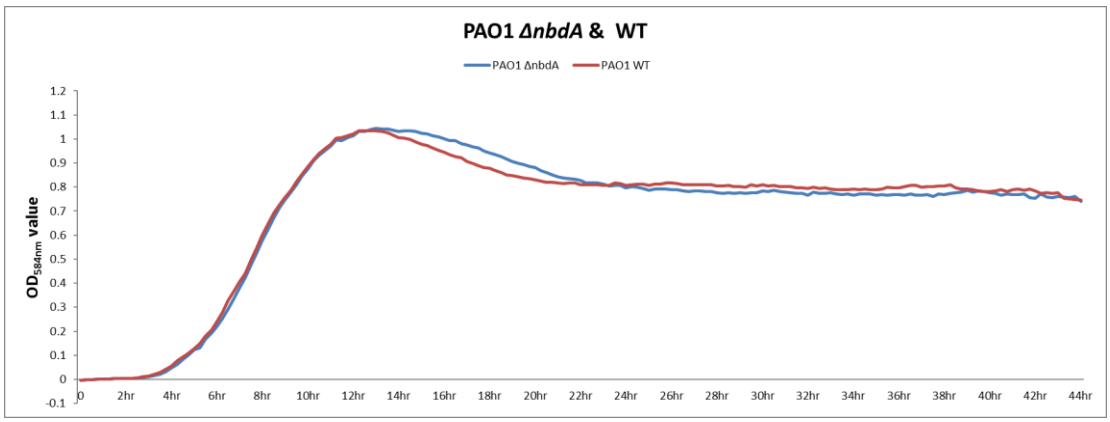
PAO1 ΔnbdA & WT
PAO1 ΔnbdA
PAO1 WT
OD584nm value
1.2
1.1
1
0.9
0.8
0.7
0.6
0.5
0.4
0.3
0.2
0.1
0
-0.1
0 2hr 4hr 6hr 8hr 10hr 12hr 14hr 16hr 18hr 20hr 22hr 24hr 26hr 28hr 30hr 32hr 34hr 36hr 38hr 40hr 42hr 44hr

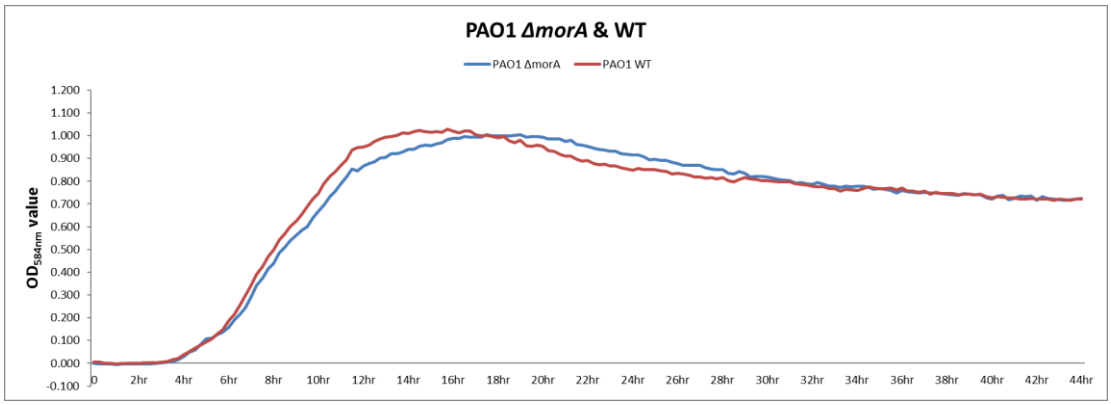
PAO1 ΔmorA & WT
PAO1 ΔmorA
PAO1 WT
OD584nm value
1.200
1.100
1.000
0.900
0.800
0.700
0.600
0.500
0.400
0.300
0.200
0.100
0.000
-0.100
0 2hr 4hr 6hr 8hr 10hr 12hr 14hr 16hr 18hr 20hr 22hr 24hr 26hr 28hr 30hr 32hr 34hr 36hr 38hr 40hr 42hr 44hr

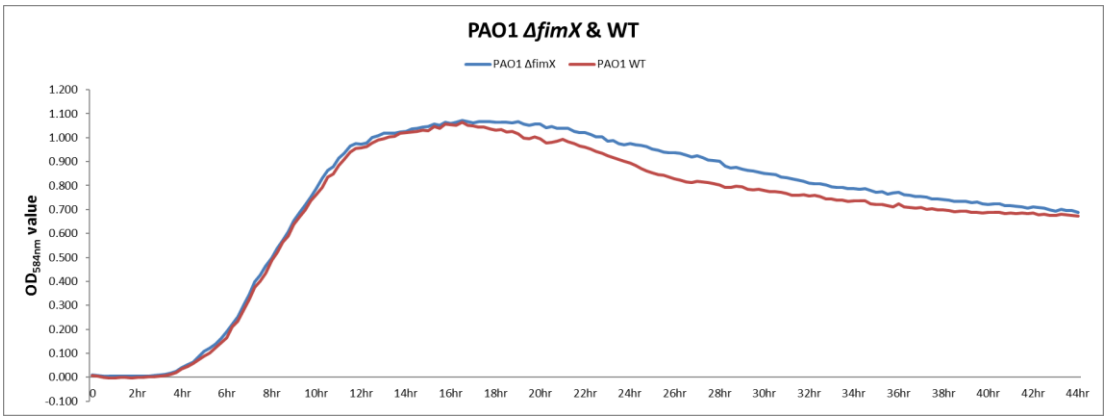
PAO1 ΔfimX & WT
PAO1 ΔfimX
PAO1 WT
OD584nm value
1.200
1.100
1.000
0.900
0.800
0.700
0.600
0.500
0.400
0.300
0.200
0.100
0.000
-0.100
0 2hr 4hr 6hr 8hr 10hr 12hr 14hr 16hr 18hr 20hr 22hr 24hr 26hr 28hr 30hr 32hr 34hr 36hr 38hr 40hr 42hr 44hr

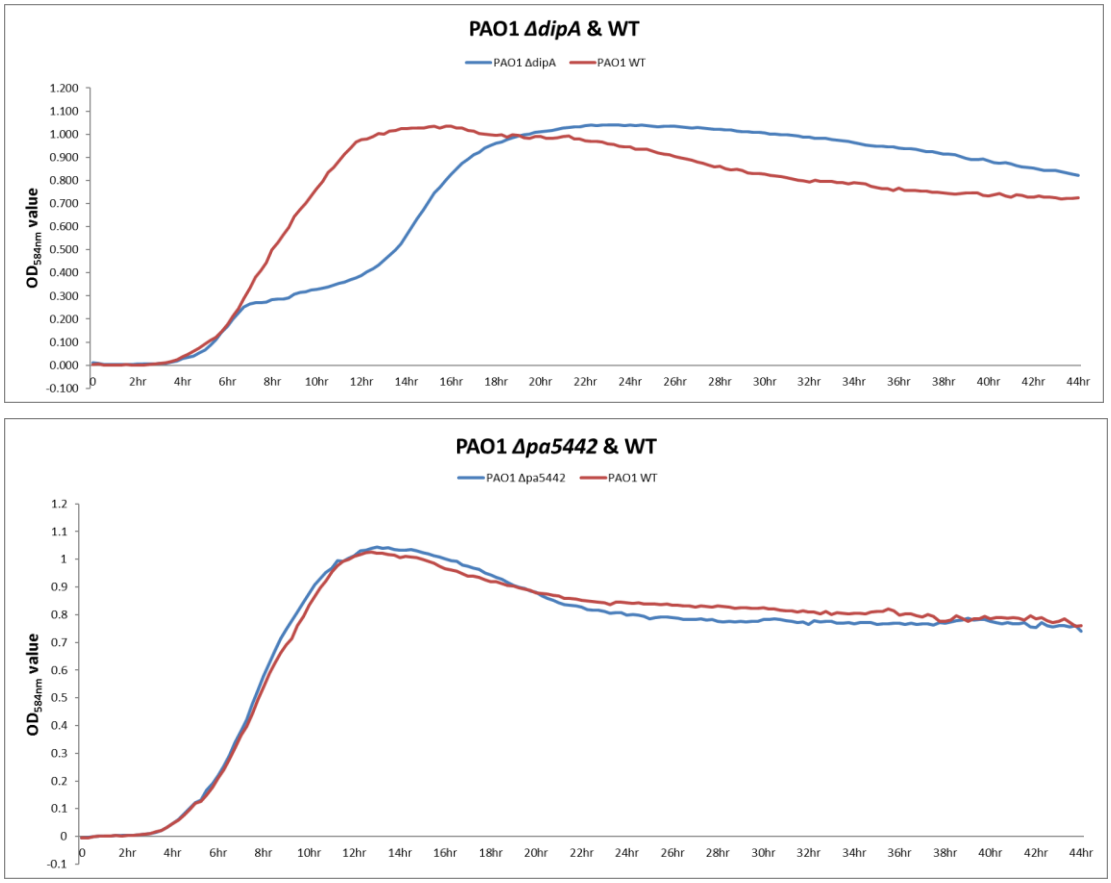


Fig A1. The growth curves of 14 KO mutants in LB broth

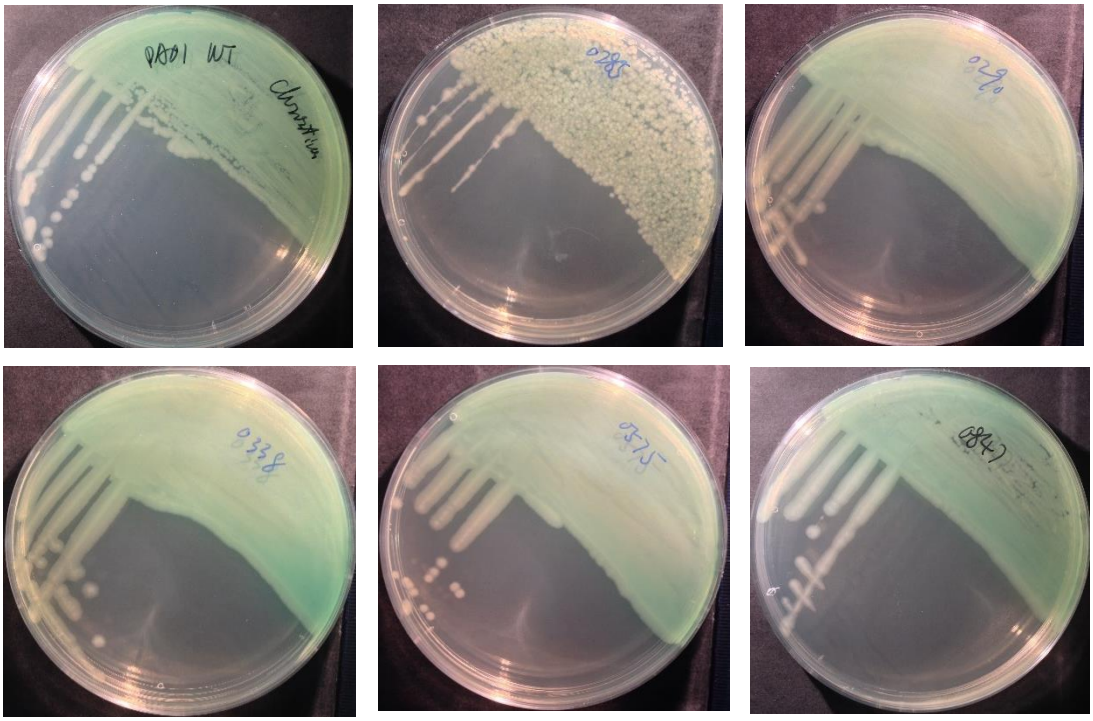

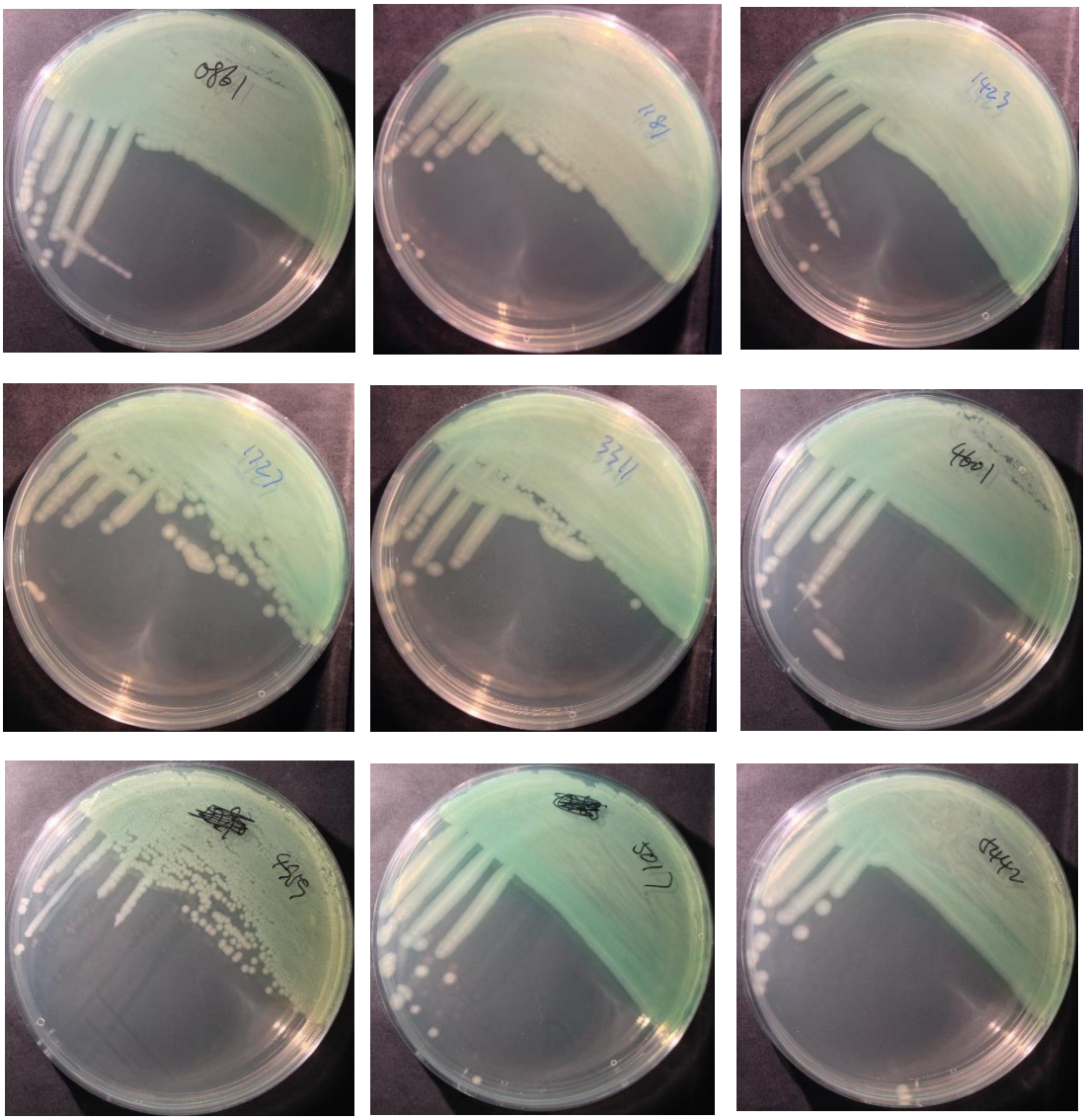

Fig A2. The colony morphologies of 14 KO mutants on Cetrimide agar plates. Plates were incubated at 37℃ for 24 hrs.

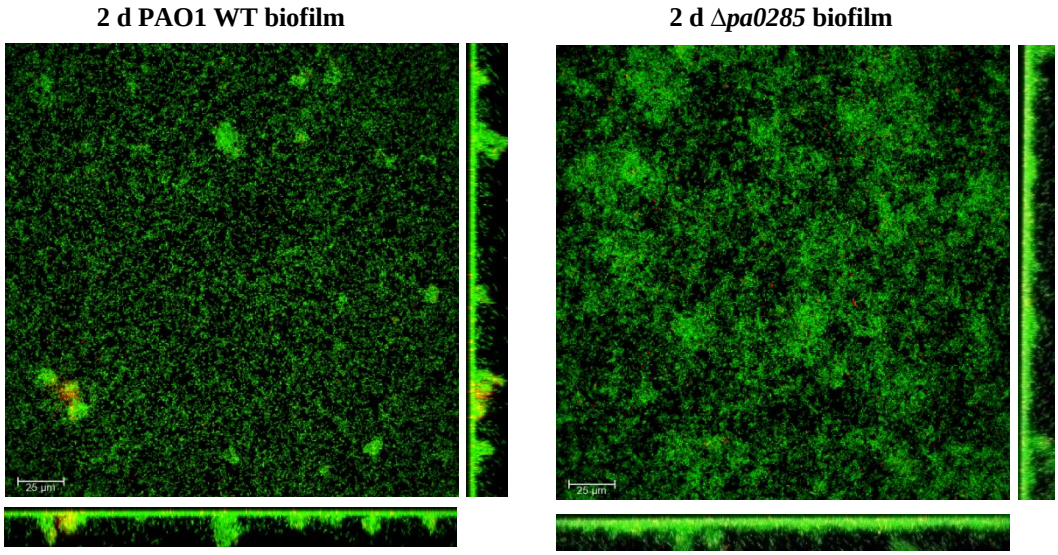

**2 d Δ*pa0290* biofilm**

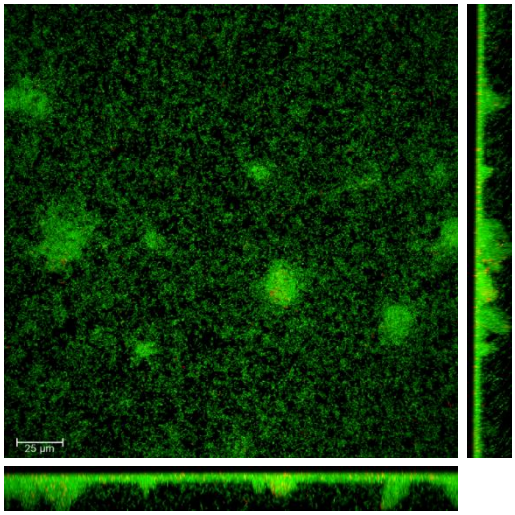


**2 d Δ*pa0338* biofilm**

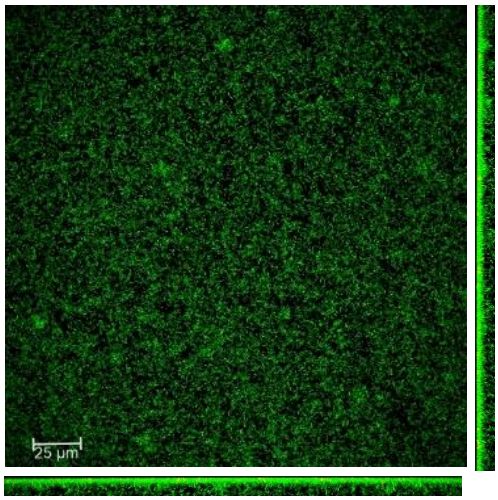


**2 d Δ*pa0575* biofilm**

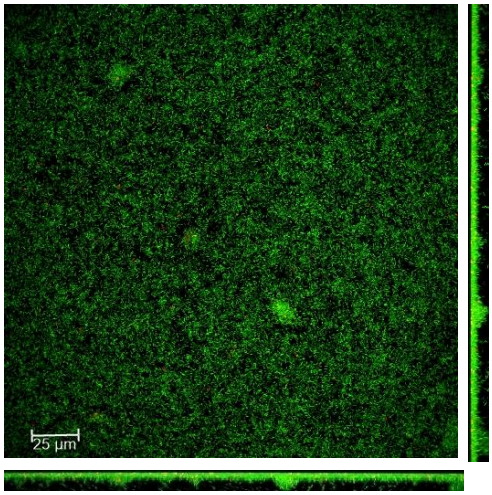


**2 d Δ*pa0847* biofilm**

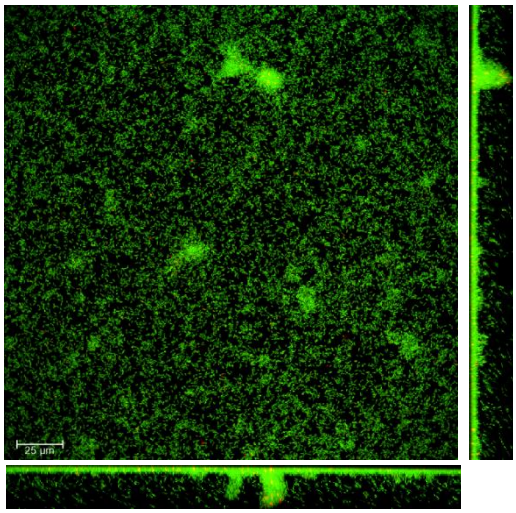


**2 d Δ*rbdA* biofilm**

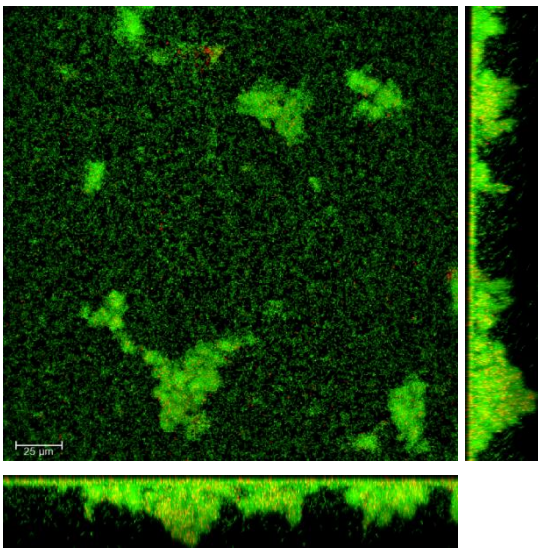


**2 d Δ*yegE* biofilm**

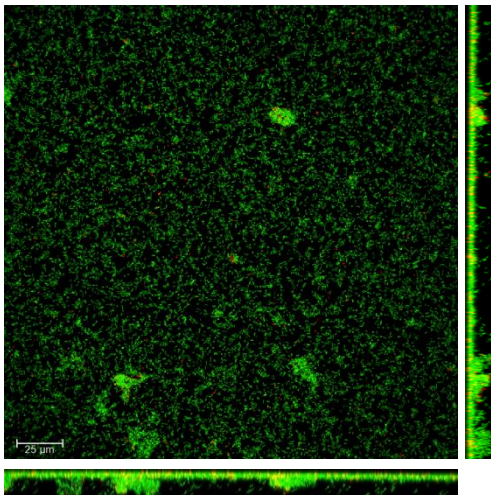

**2 d Δ*bdlA* biofilm**

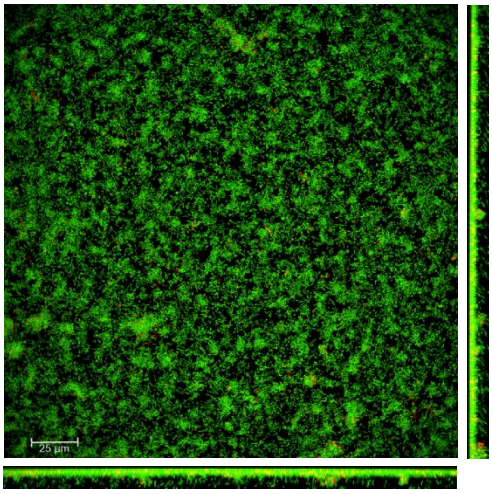


**2 d Δ*mucR* biofilm**

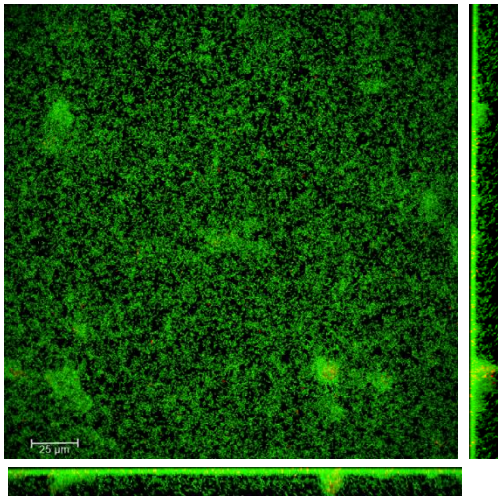


**2 d Δ*nbdA* biofilm**

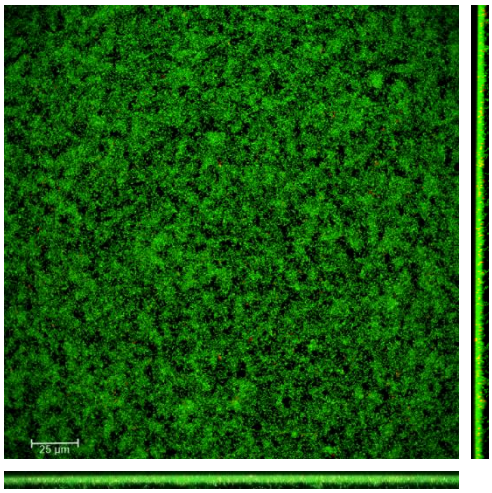


**2 d Δ*morA* biofilm**

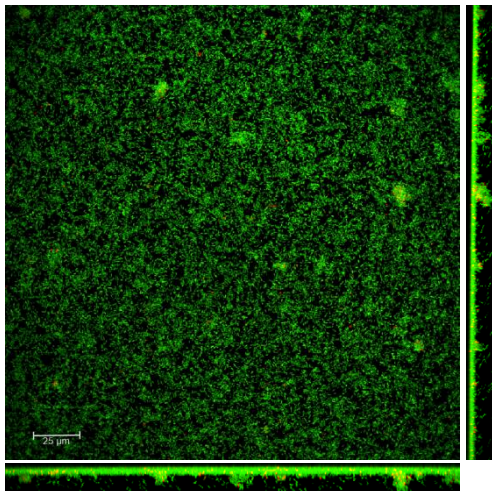


**2 d Δ*fimX* biofilm**

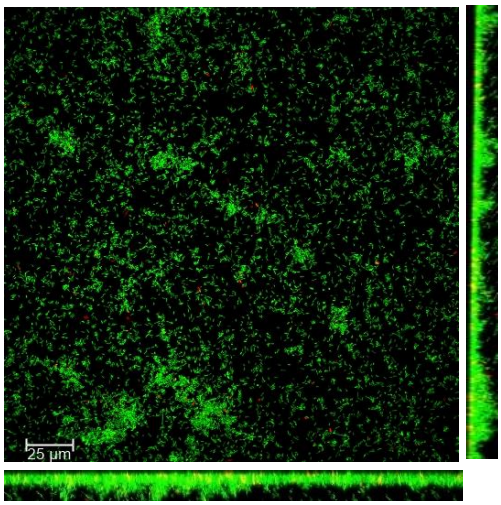


**2 d Δ*dipA* biofilm**

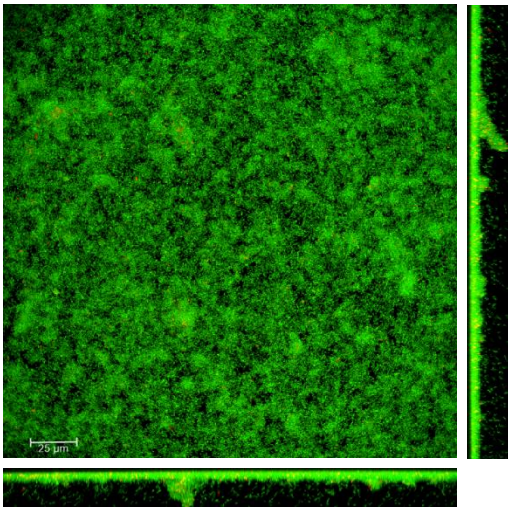

**2 d Δ*pa5442* biofilm**

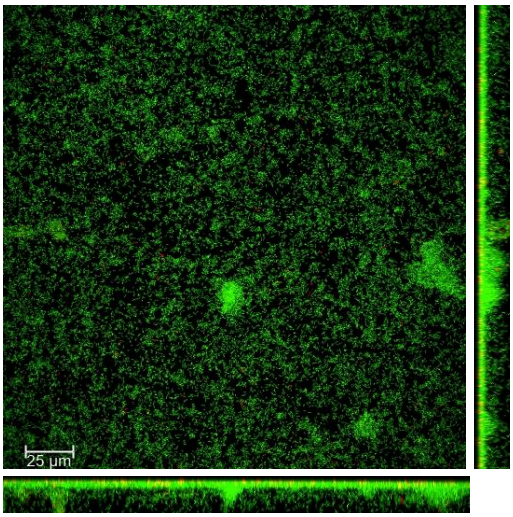


Fig A3. Representative CLSM images of 2 d KO mutants' biofilms. Biofilms are stained using LIVE/DEAD™ *Bac*Light™ Bacterial Viability Kit. Scale bar = 25µm

**3 d PAO1 WT biofilm**

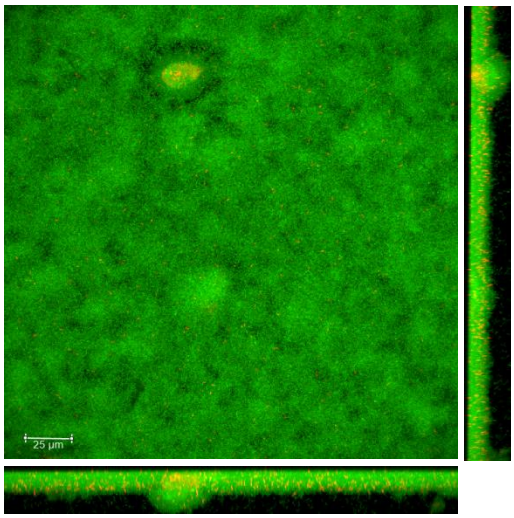


**3 d Δ*pa0285* biofilm**

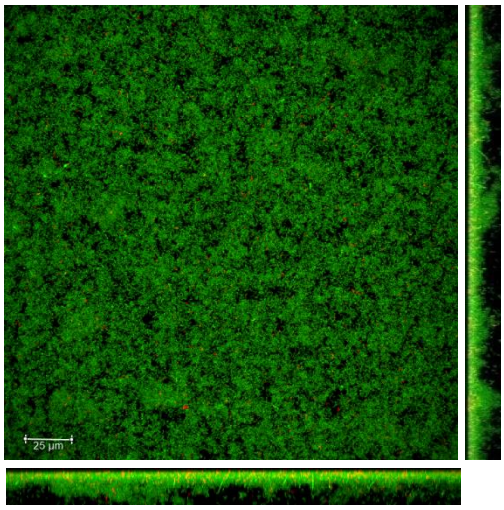


**3 d Δ*pa0290* biofilm**

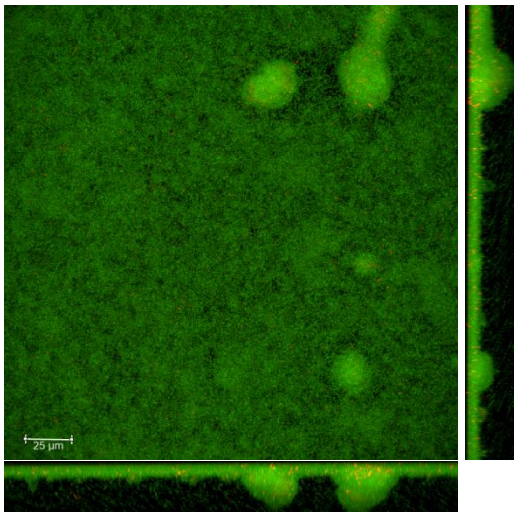


**3 d Δ*pa0338* biofilm**

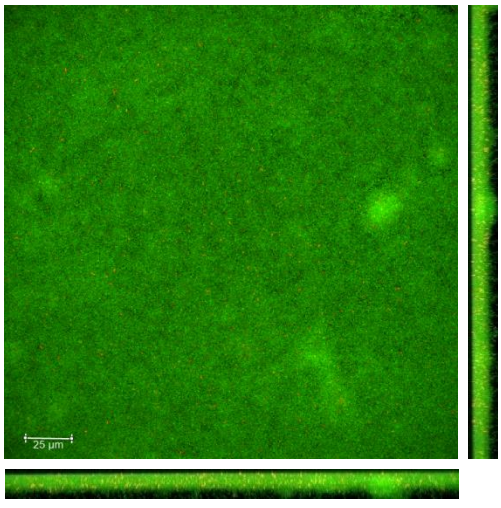

**3 d Δ*pa0575* biofilm**

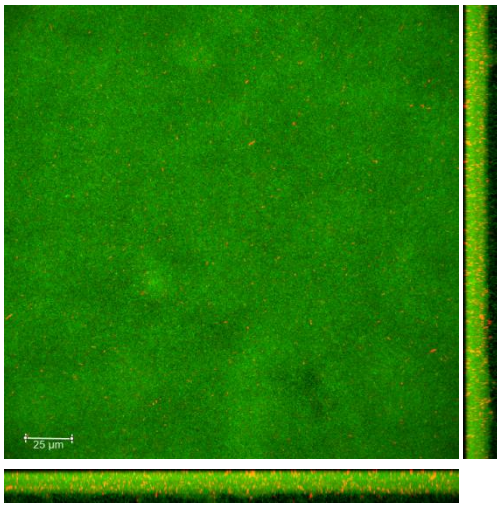


**3 d Δ*pa0847* biofilm**

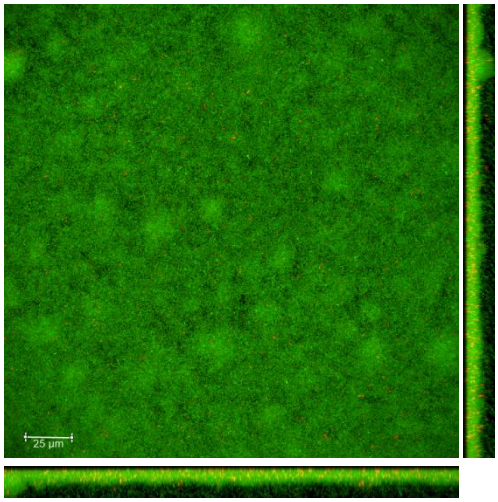


**3 d Δ*rbdA* biofilm**

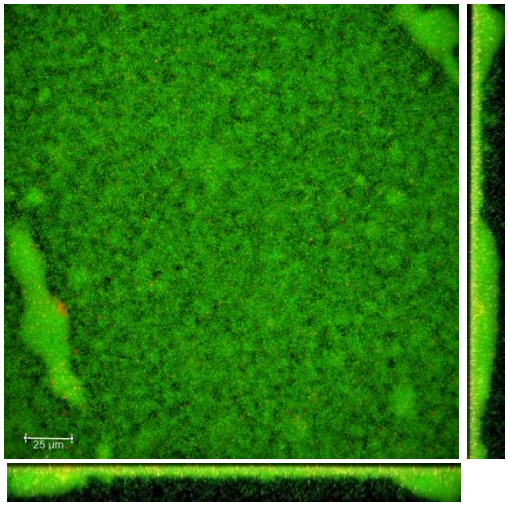


**3 d Δ*yegE* biofilm**

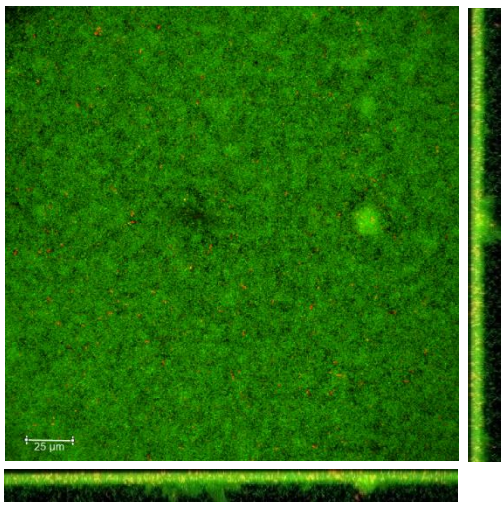


**3 d Δ*bdlA* biofilm**

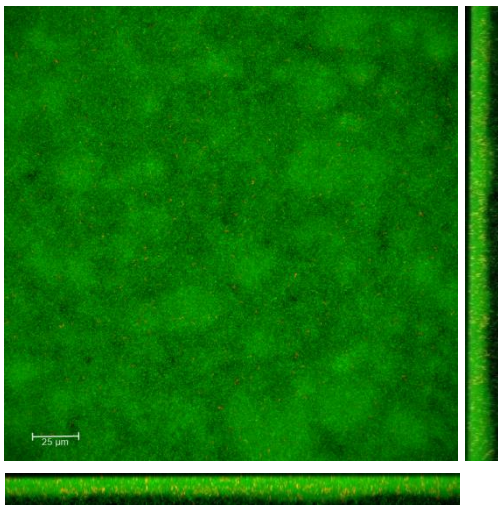


**3 d Δ*mucR* biofilm**

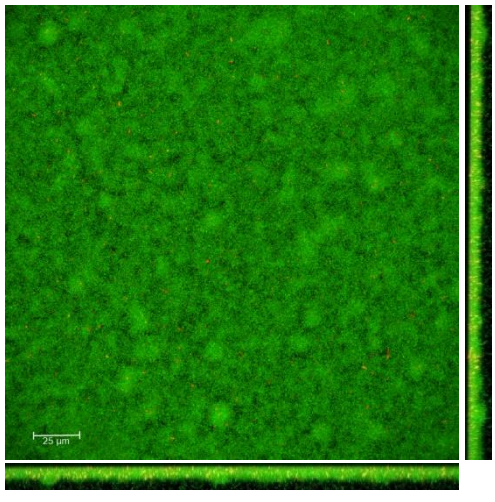

**3 d Δ*nbdA* biofilm**

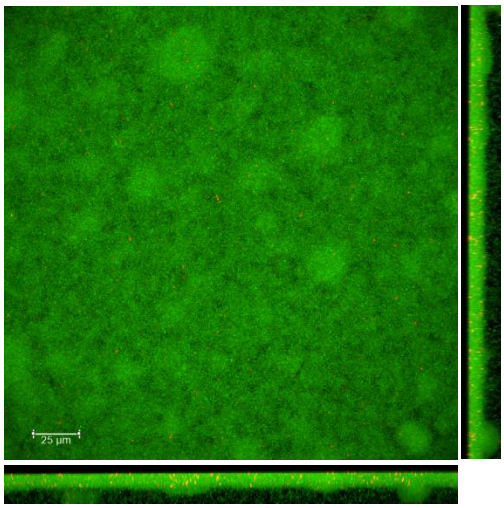


**3 d Δ*morA* biofilm**

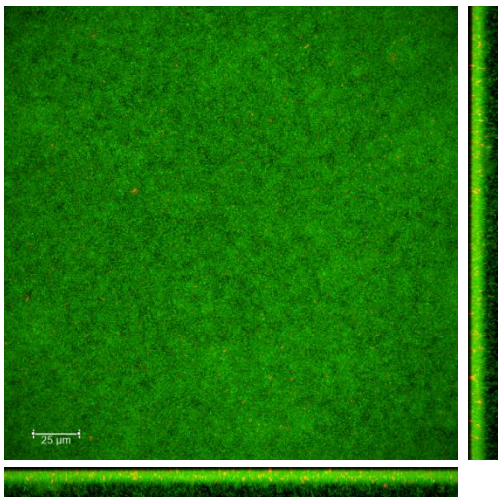


**3 d Δ*fimX* biofilm**

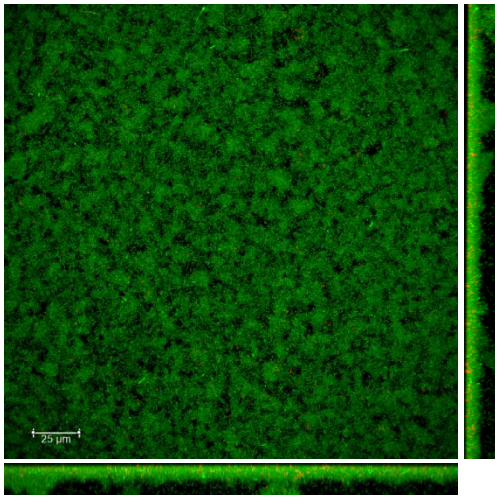


**3 d Δ*dipA* biofilm**

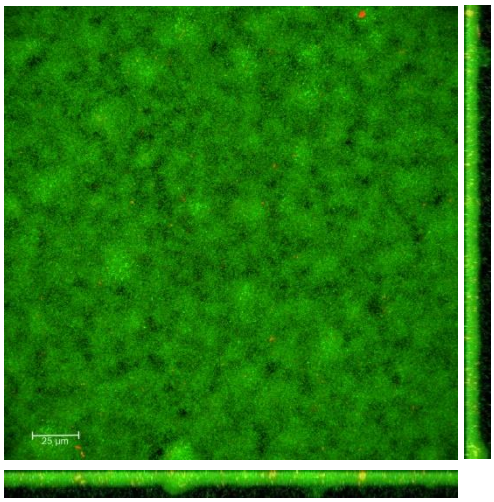


**3 d Δ*pa5442* biofilm**

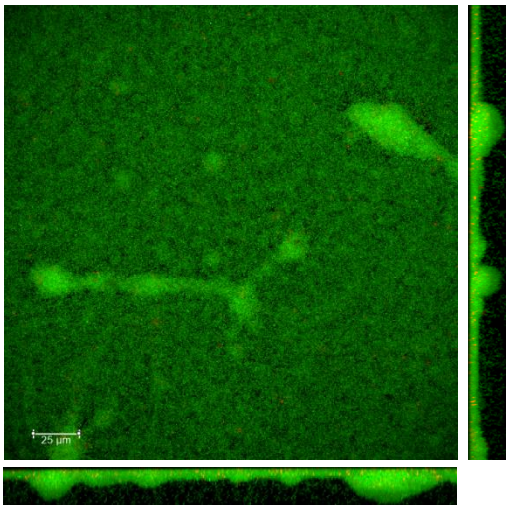


Fig A4. Representative CLSM images of 3 d KO mutants' biofilms. Biofilms are stained using LIVE/DEAD™ *Bac*Light™ Bacterial Viability Kit. Scale bar = 25µm.

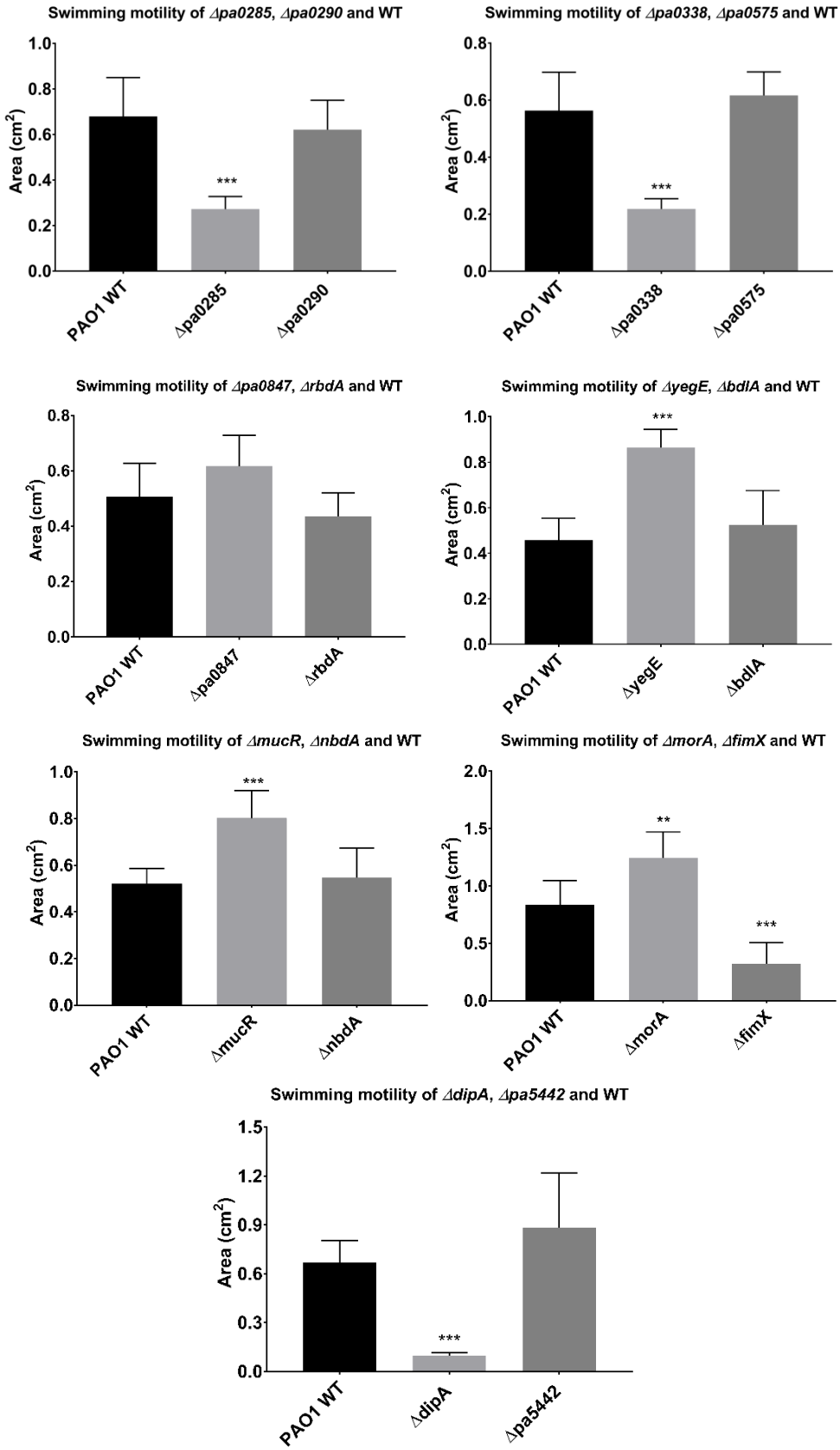


Fig A5. Raw data of swimming assay for 14 KO mutants. Each swimming plate contained 2 KO mutants and 1 PAO1 WT. Data analysis were grouped according to the KO strains on each plate. Measurement of swimming zone areas of KO mutants using ImageJ. n=6 from individual plates. Welch T-test was applied due to large variations. *** represents $p<0.01$, ** represents $0.01<p<0.05$.

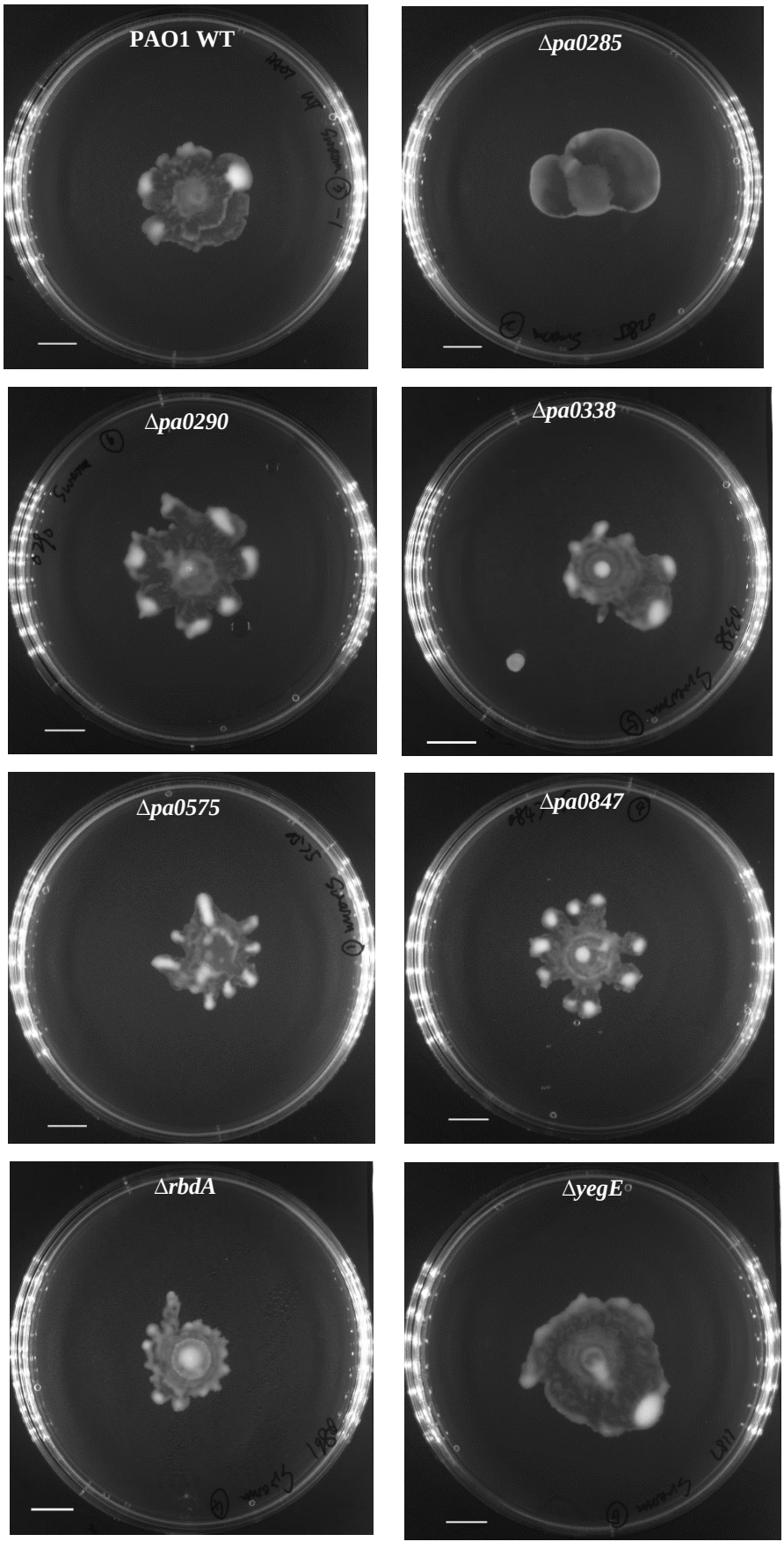
PAO1 WT
Δpa0285
Δpa0290
Δpa0338
Δpa0575
Δpa0847
ΔrbdA
ΔyegE

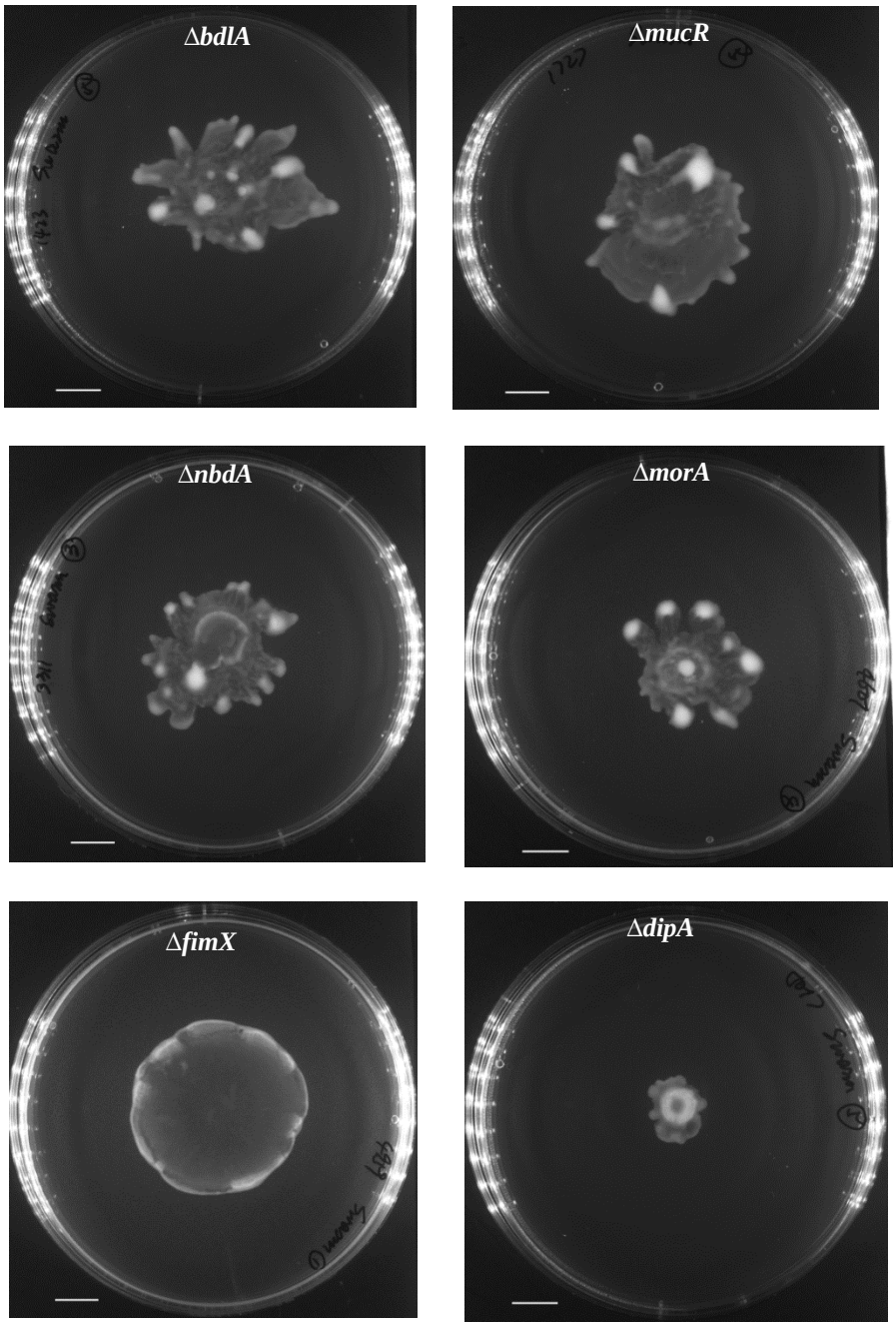


Fig A6. Selective images from swarming plates of 14 KO mutants. Scale bar = 1cm.

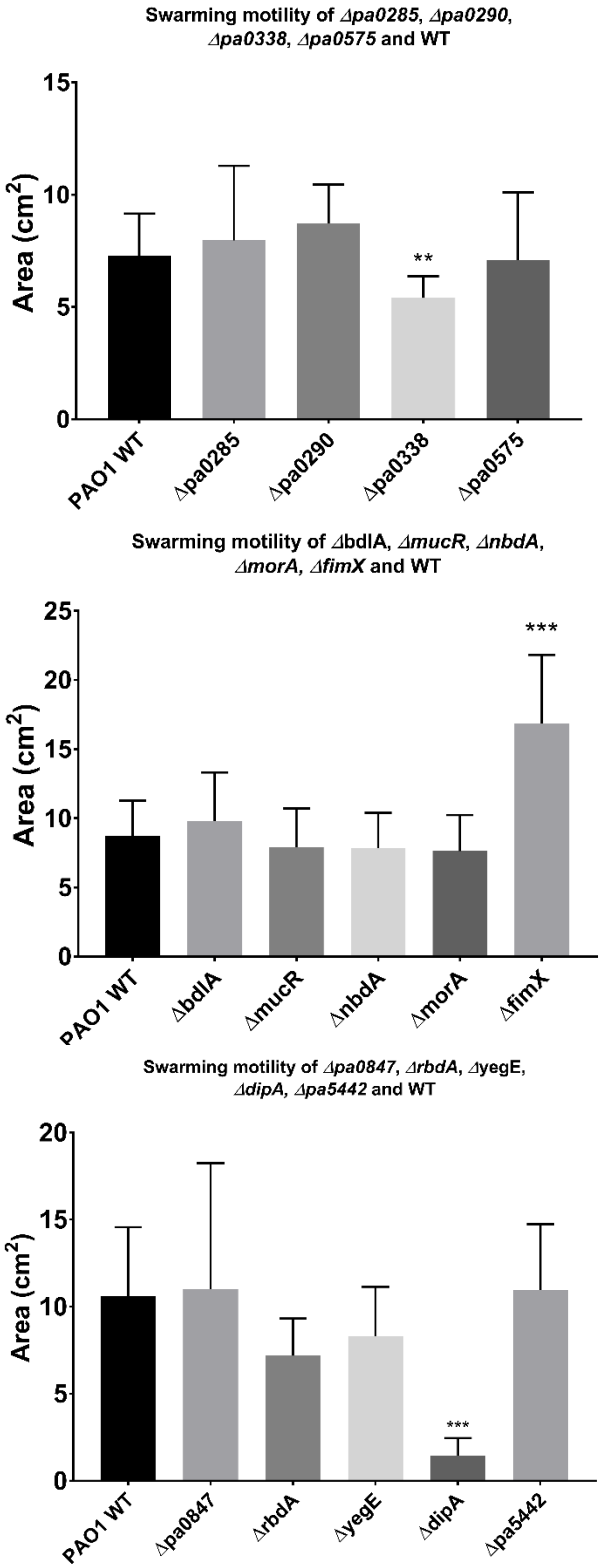


Fig A7. Raw data of swarming assay for 14 KO mutants. Due to the widely accepted inconsistency and less reproducibility of swarming assay, 5 KO strains plus one WT were inoculated into the same batch of agar plates resourced from the same bottle of agar and pouring procedures. Data shown in bar graphs were therefore grouped based on the 5 KO strains used together and compared to the WT within the same batch.

Swarming zone areas were measured using ImageJ. n=6 from individual plates. Welch T-test was applied due to large variations. *** represents $p<0.01$, ** represents $0.01<p<0.05$.

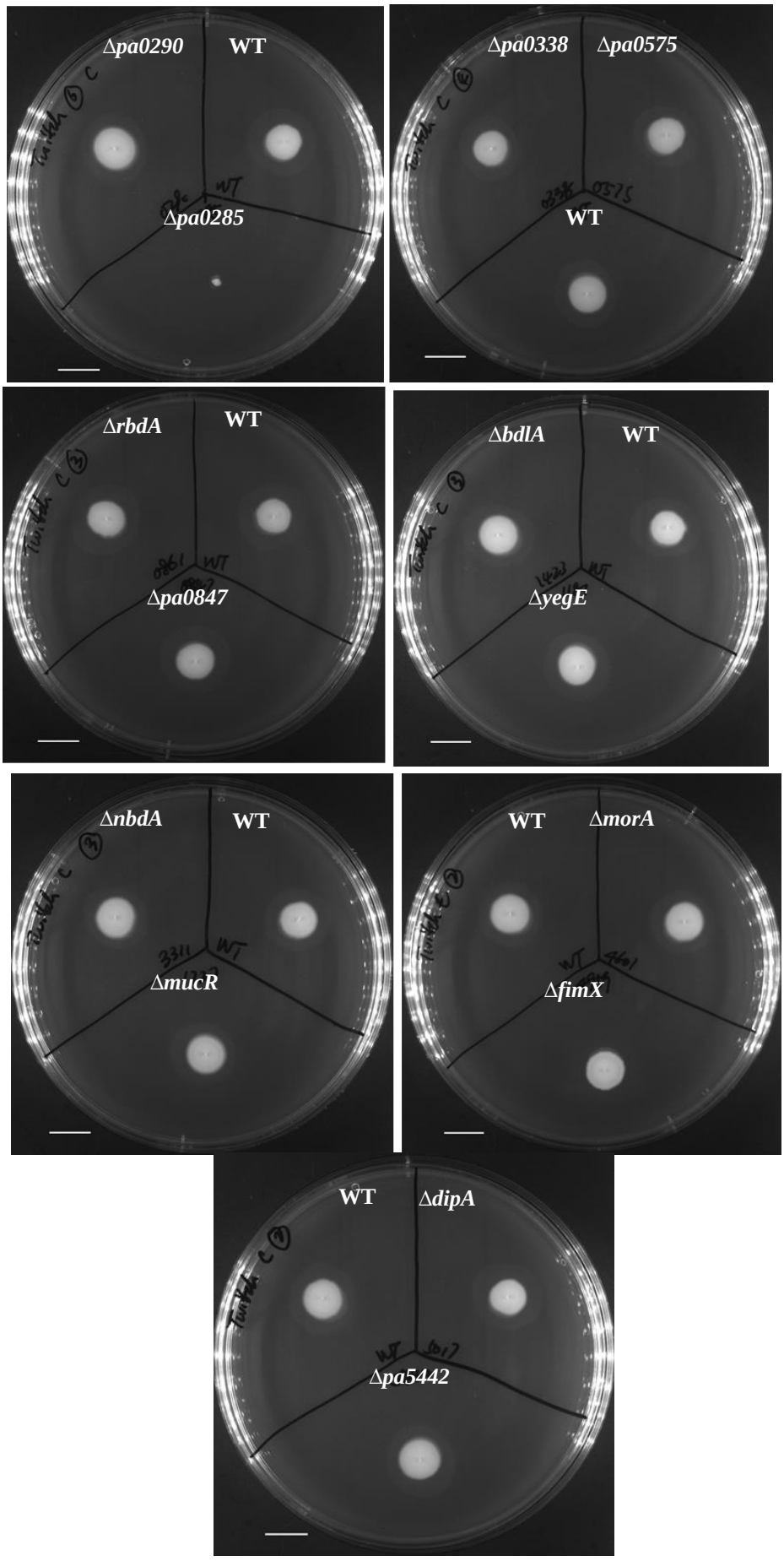
Δpa0290
WT
Δpa0285
Δpa0338
Δpa0575
WT
ΔrbdA
WT
Δpa0847
ΔbdlA
WT
ΔyegE
ΔnbdA
WT
ΔmucR
WT
ΔmorA
ΔfimX
WT
ΔdipA
Δpa5442

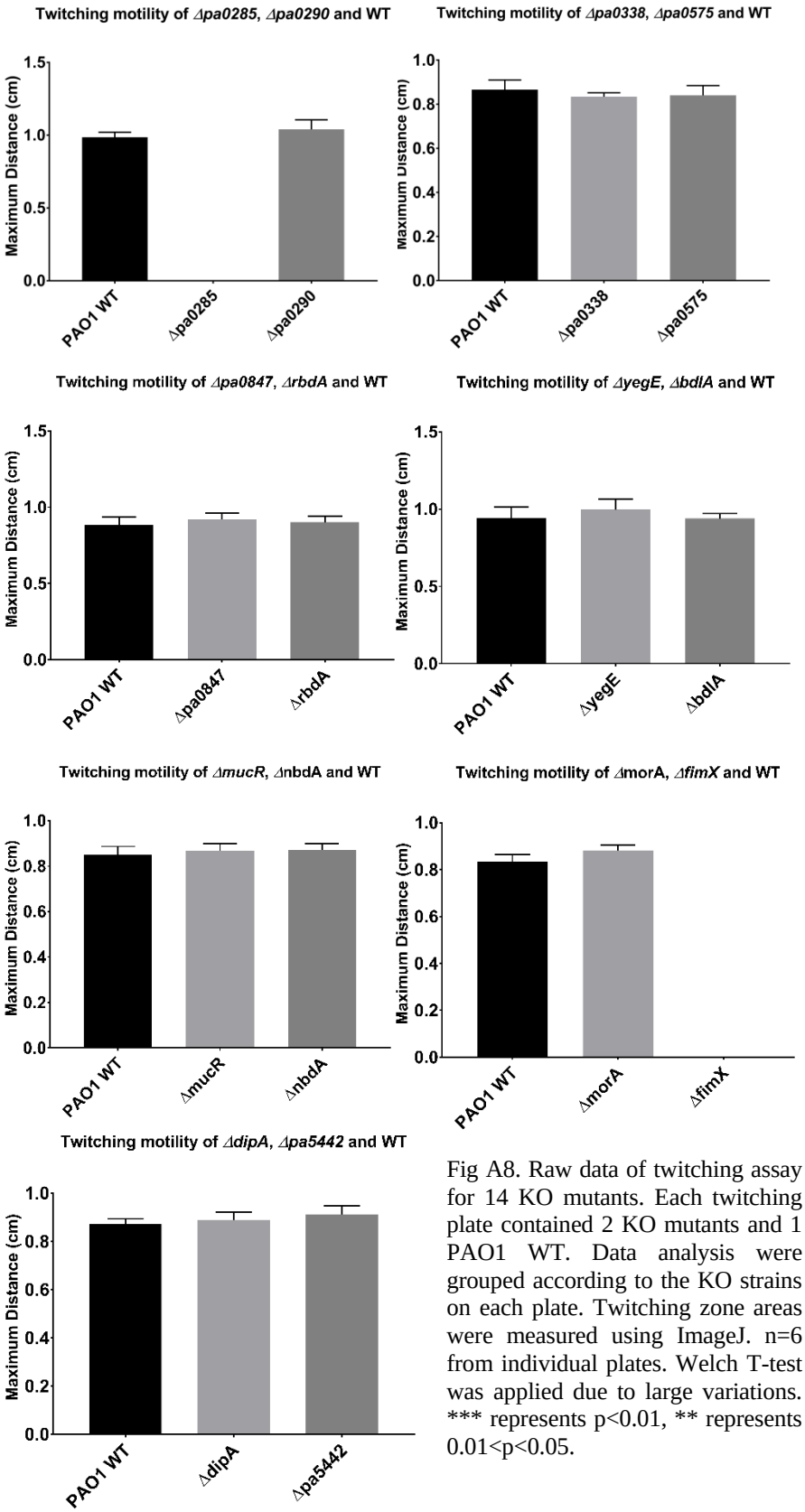


Fig A8. Raw data of twitching assay for 14 KO mutants. Each twitching plate contained 2 KO mutants and 1 PAO1 WT. Data analysis were grouped according to the KO strains on each plate. Twitching zone areas were measured using ImageJ. n=6 from individual plates. Welch T-test was applied due to large variations. *** represents $p<0.01$, ** represents $0.01<p<0.05$.

**2d PAO1 WT biofilm Control**

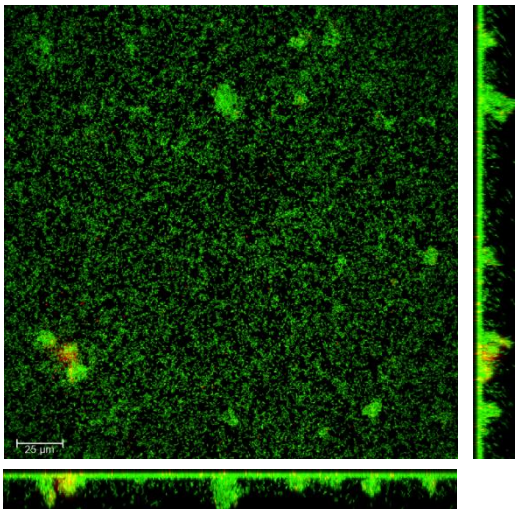


**2d PAO1 WT biofilm 250µM S150**

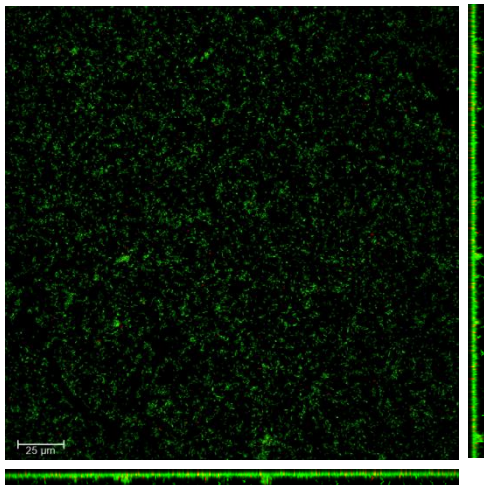


**2d Δ*pa0285* biofilm Control**

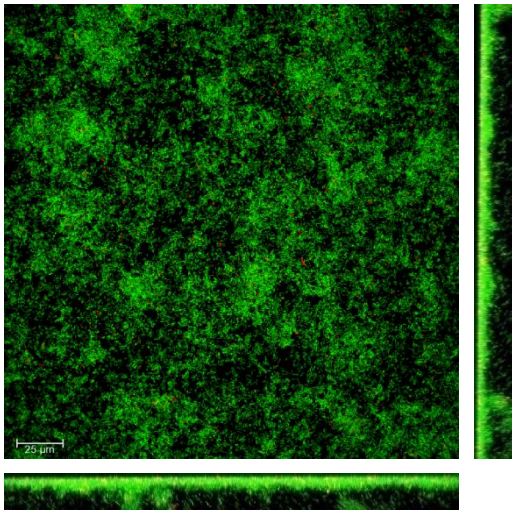


**2d Δ*pa0285* biofilm 250µM S150**

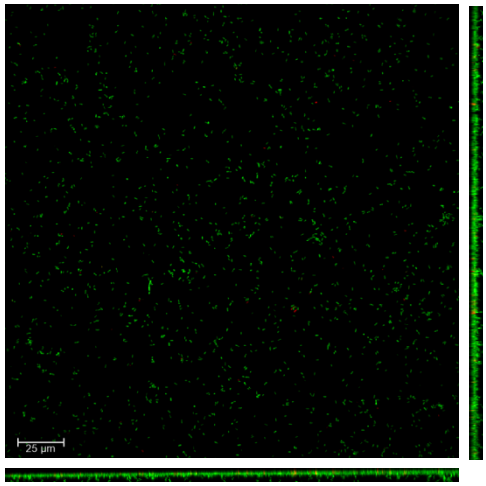


**2d Δ*pa0290* biofilm Control**

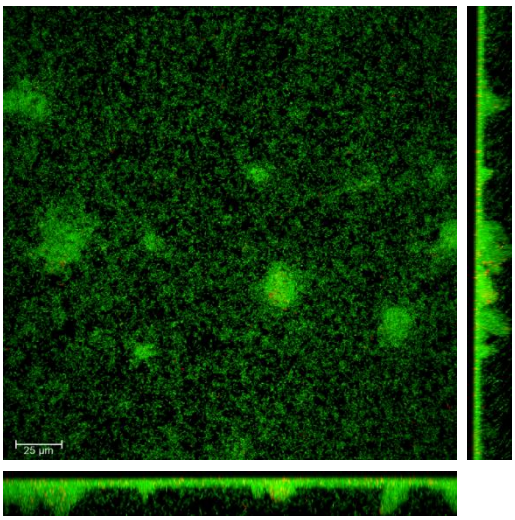


**2d Δ*pa0290* biofilm 250µM S150**

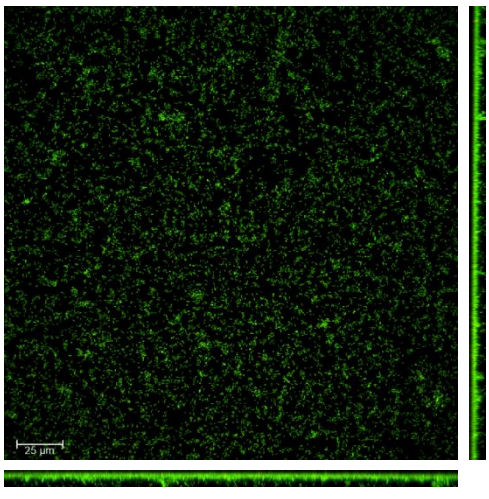

**2d Δ*pa0338* biofilm Control**

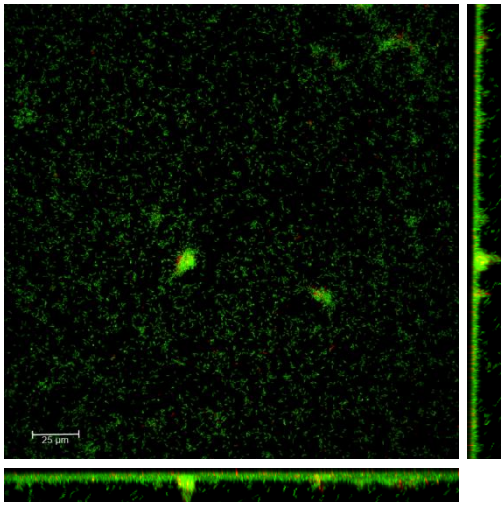


**2d Δ*pa0338* biofilm 250µM S150**

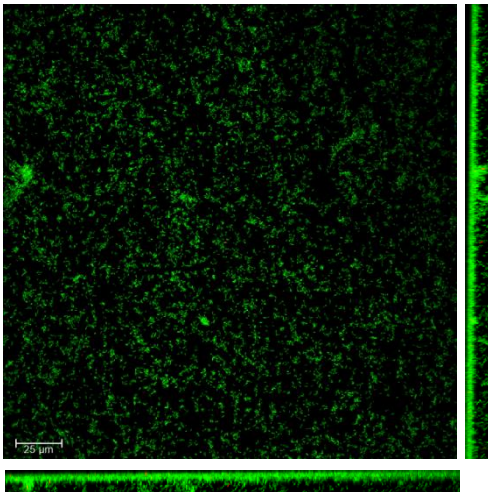


**2d Δ*pa0575* biofilm Control**

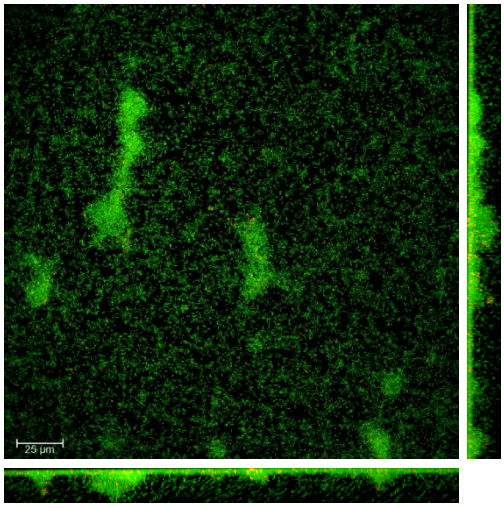


**2d Δ*pa0575* biofilm 250µM S150**

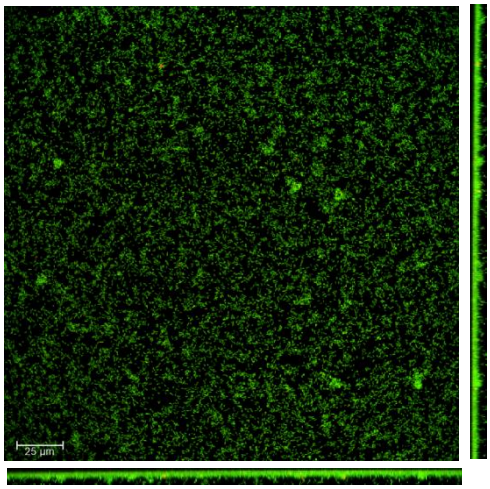


**2d Δ*pa0847* biofilm Control**

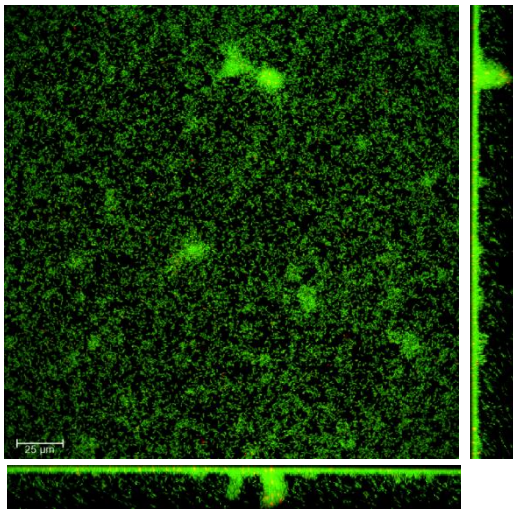


**2d Δ*pa0847* biofilm 250µM S150**

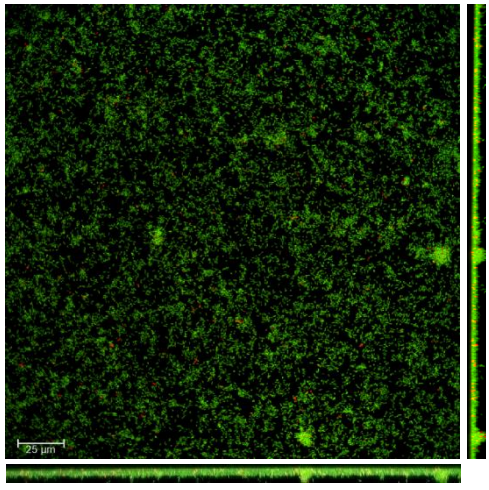

**2d Δ*rbdA* biofilm Control**

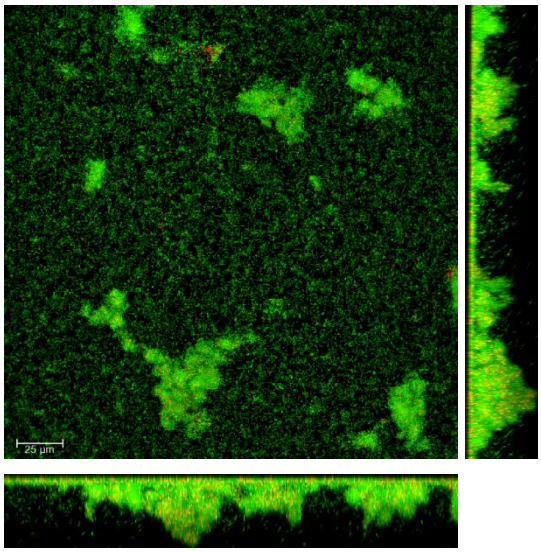


**2d Δ*rbdA* biofilm 250µM S150**

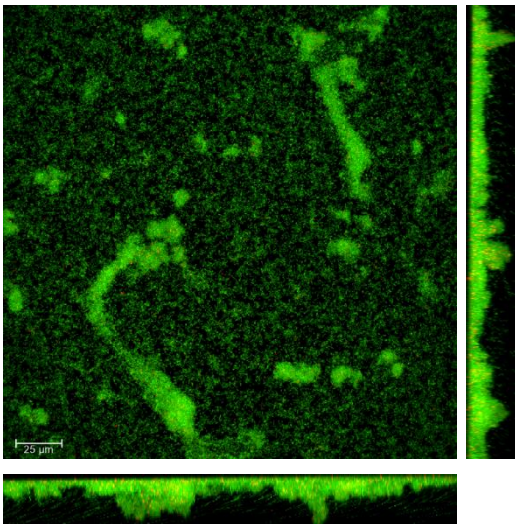


**2d Δ*yegE* biofilm Control**

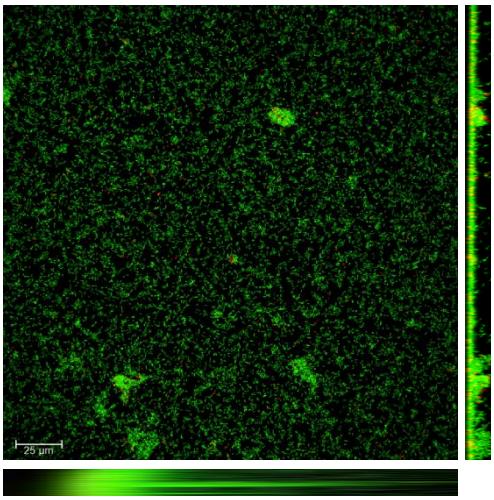


**2d Δ*yegE* biofilm 250µM S150**

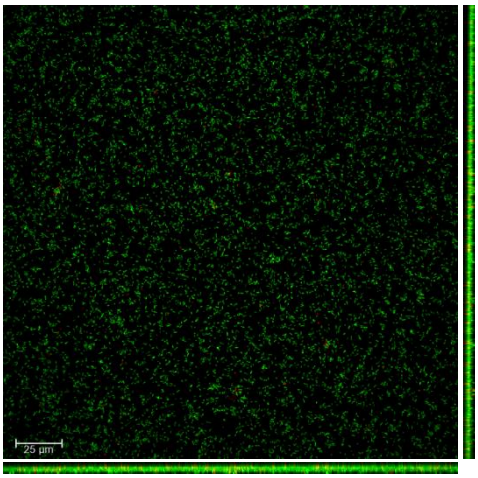


**2d Δ*bdlA* biofilm Control**

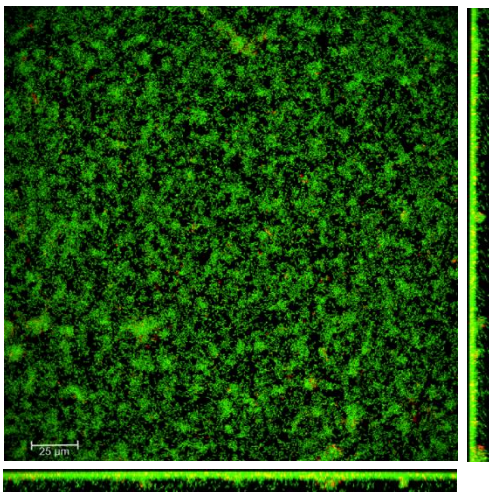


**2d Δ*bdlA* biofilm 250µM S150**

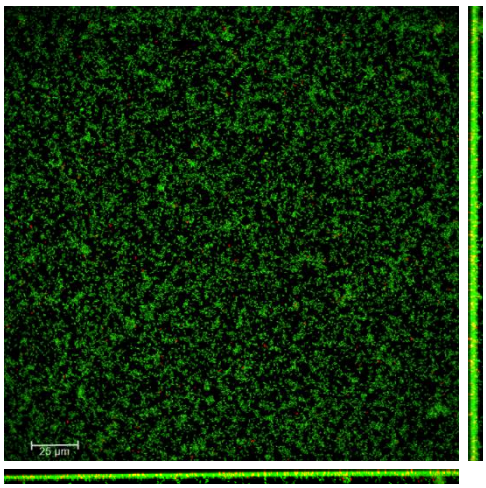

**2d Δ*mucR* biofilm Control**

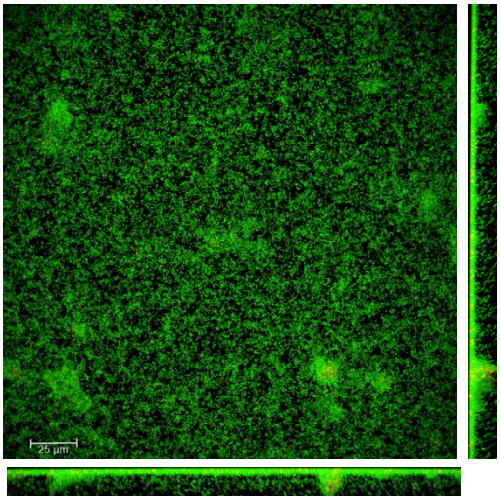


**2d Δ*mucR* biofilm 250µM S150**

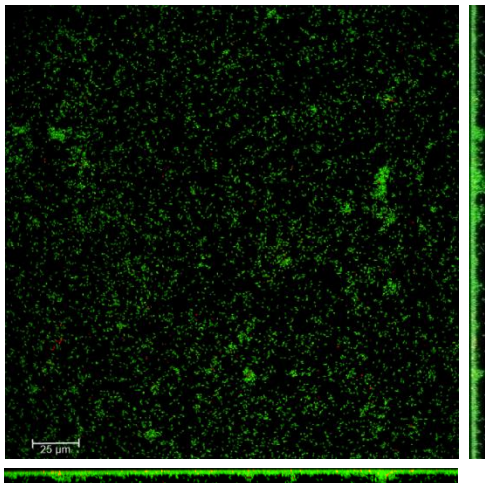


**2d Δ*nbdA* biofilm Control**

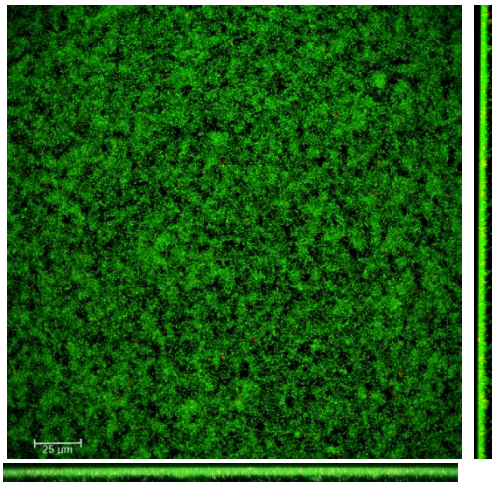


**2d Δ*nbdA* biofilm 250µM S150**

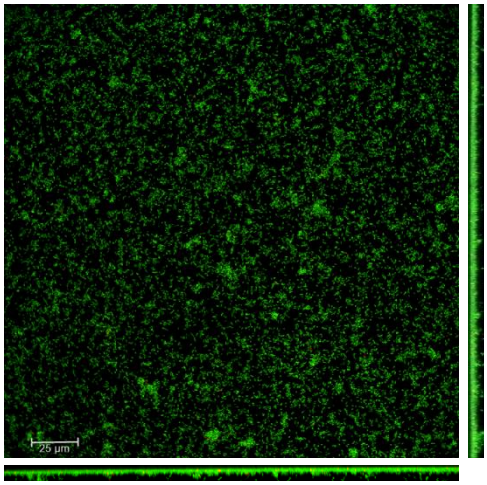


**2d Δ*morA* biofilm Control**

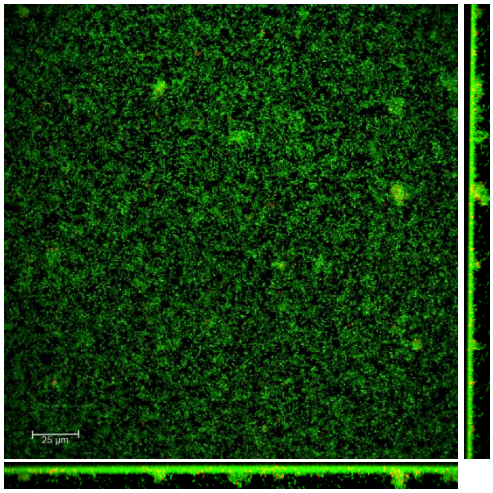


**2d Δ*morA* biofilm 250µM S150**

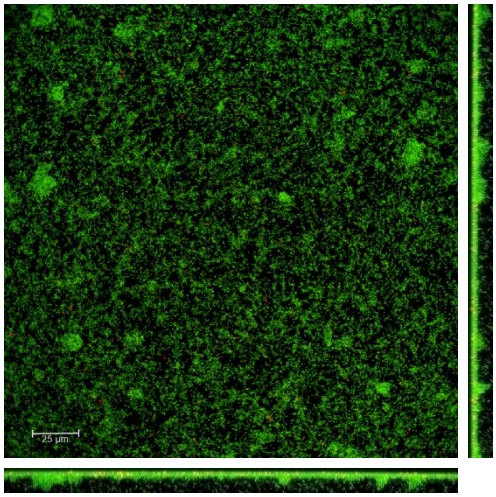

**2d Δ*fimX* biofilm Control**

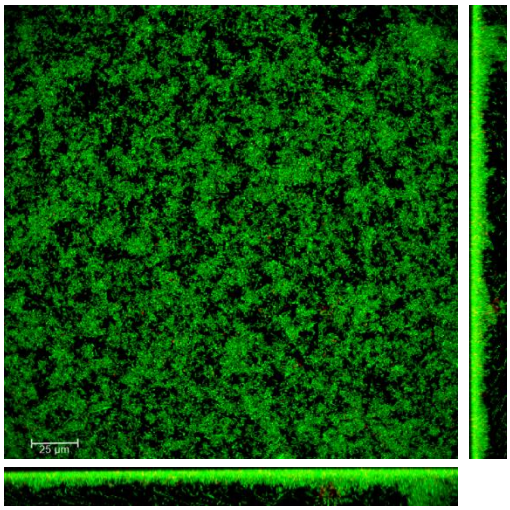


**2d Δ*fimX* biofilm 250µM S150**

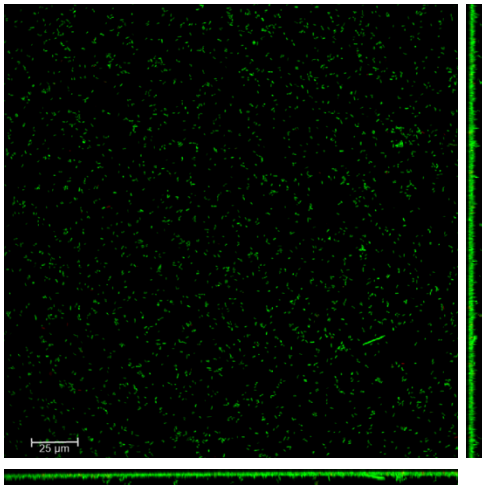


**2d Δ*dipA* biofilm Control**

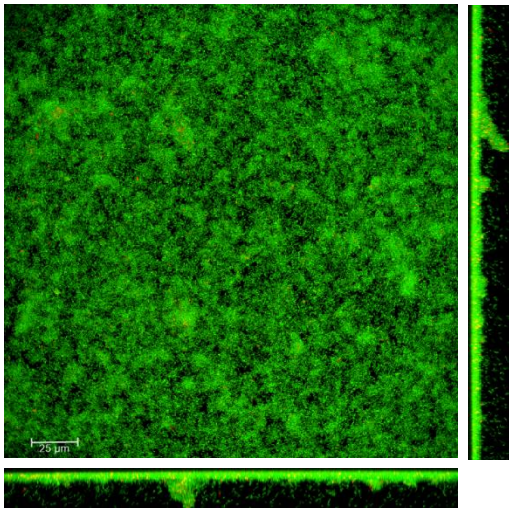


**2d Δ*dipA* biofilm 250µM S150**

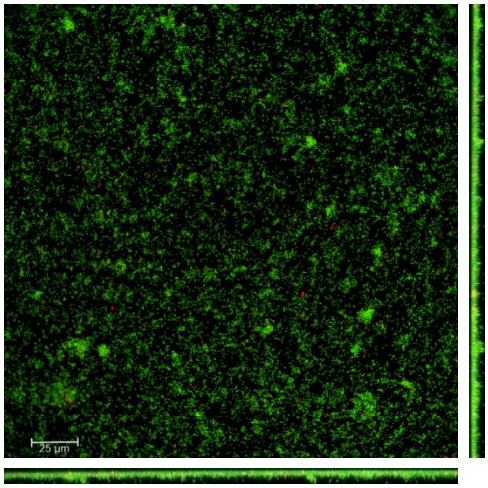


**2d Δ*pa5442* biofilm Control**

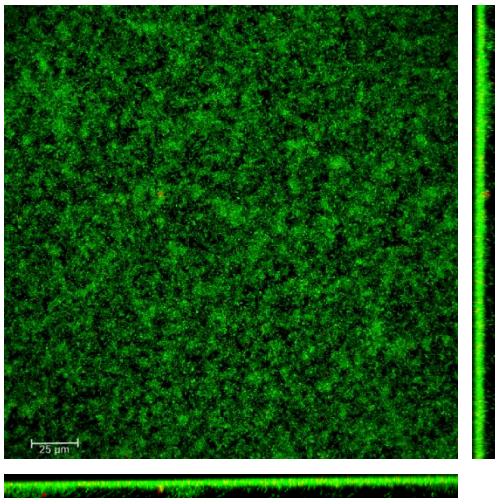


**2d Δ*pa5442* biofilm 250µM S150**

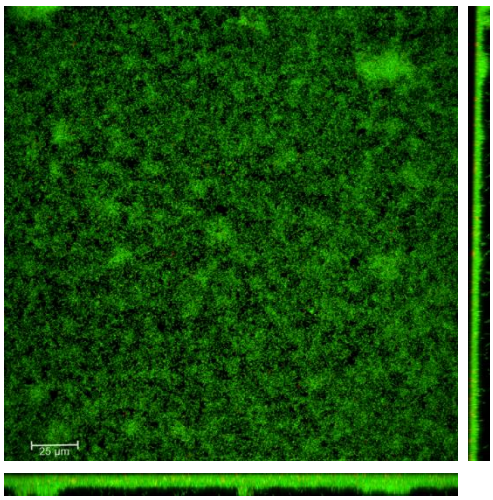


Fig A9. Selective CLSM images of 2 d old KO mutants' biofilms treated with 250µM S150.

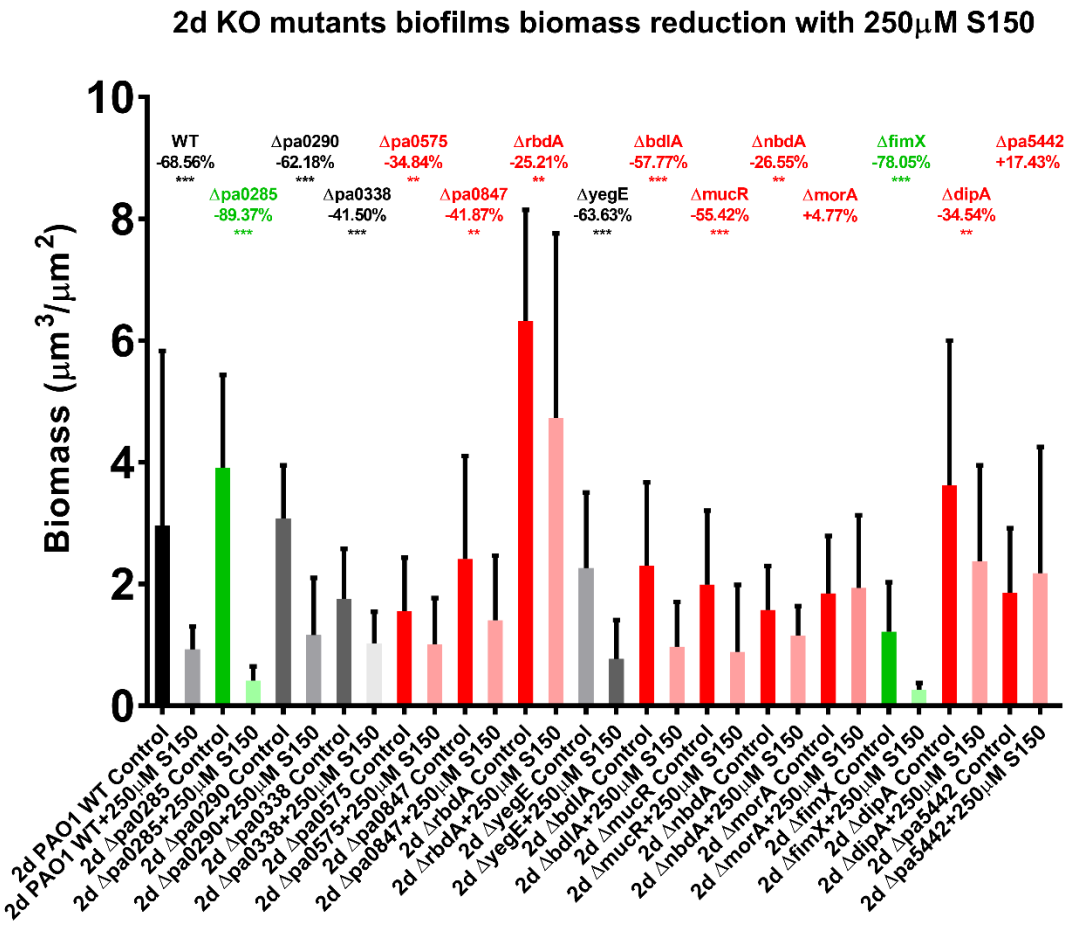


Fig A10. Dispersal effect of 2 hrs 250μM S150 treatment on 2 d old KO mutant biofilms in MatTek plates. Welch T-test was carried out to compare the treated and non-treated groups. Data represents data means of n=6 of 3 biological replicates. *** represents $p<0.01$, ** represents $0.01<p<0.05$.

**3d PAO1 WT biofilm Control**

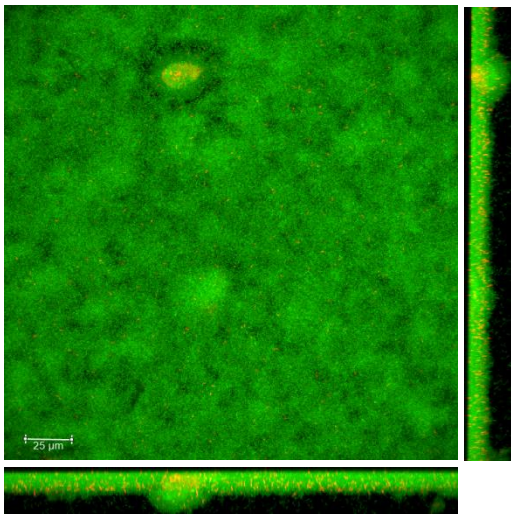


**3d PAO1 WT biofilm 250μM S150**

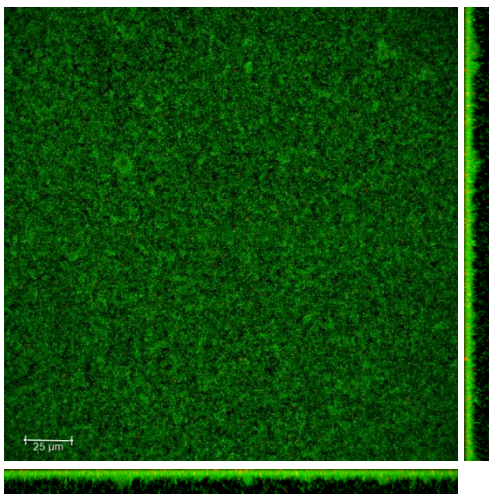

**3d Δ*pa0285* biofilm Control**

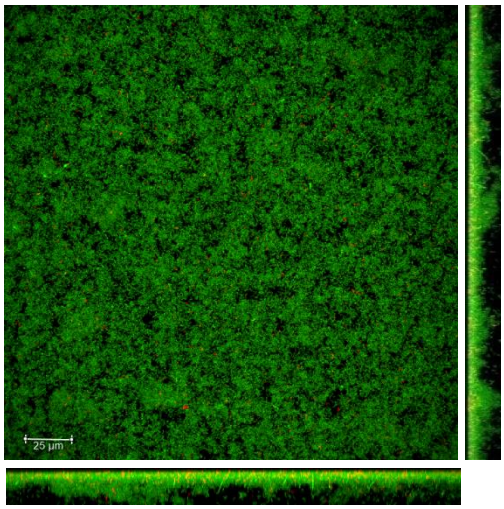


**3d Δ*pa0285* biofilm 250µM S150**

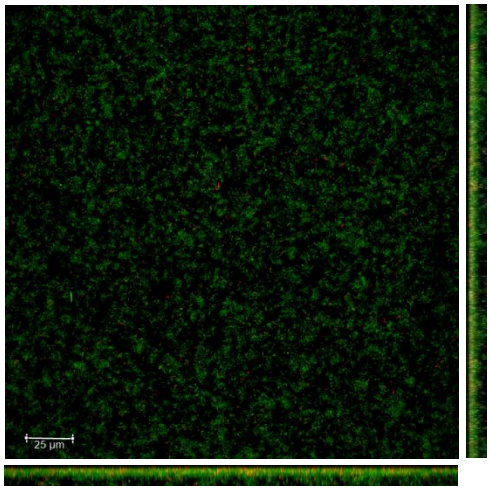


**3d Δ*pa0290* biofilm Control**

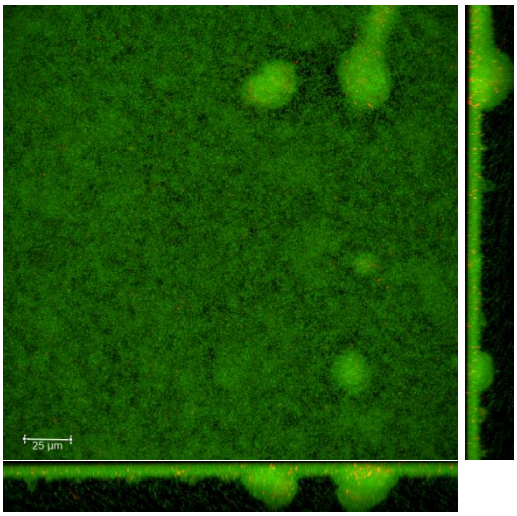


**3d Δ*pa0290* biofilm 250µM S150**

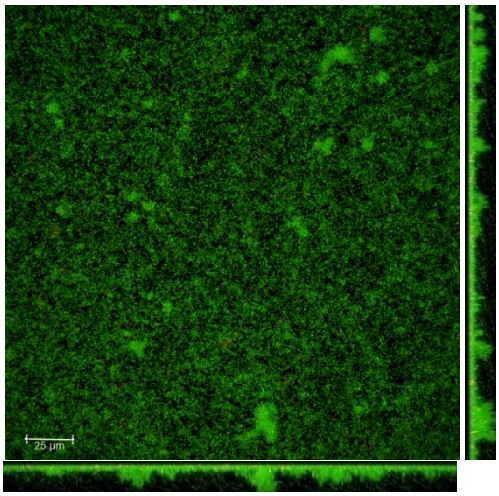


**3d Δ*pa0338* biofilm Control**

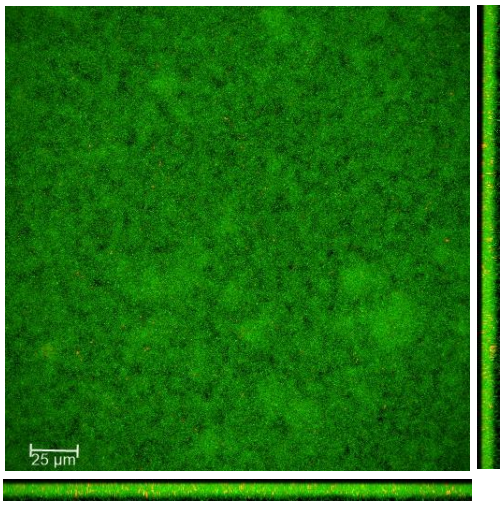


**3d Δ*pa0338* biofilm 250µM S150**

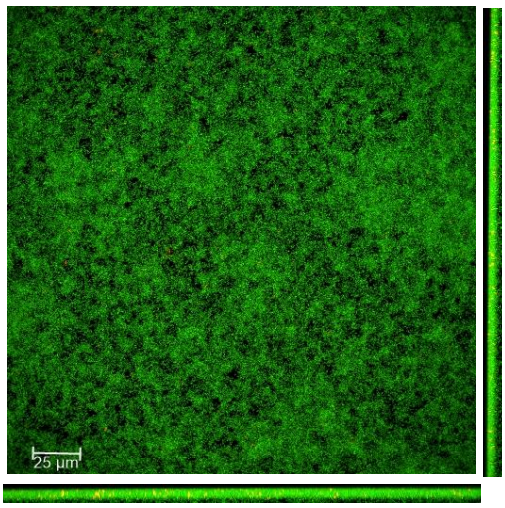

**3d Δ*pa0575* biofilm Control**

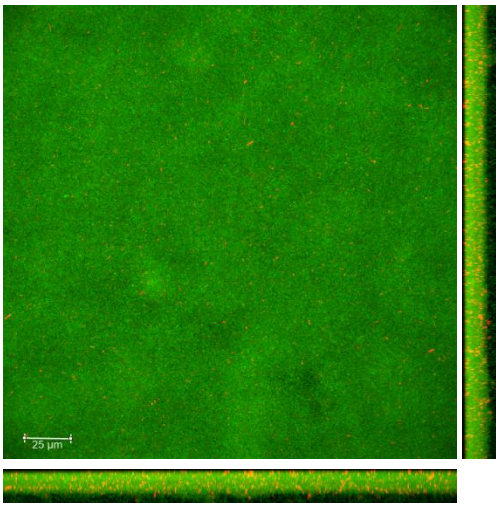


**3d Δ*pa0575* biofilm 250µM S150**

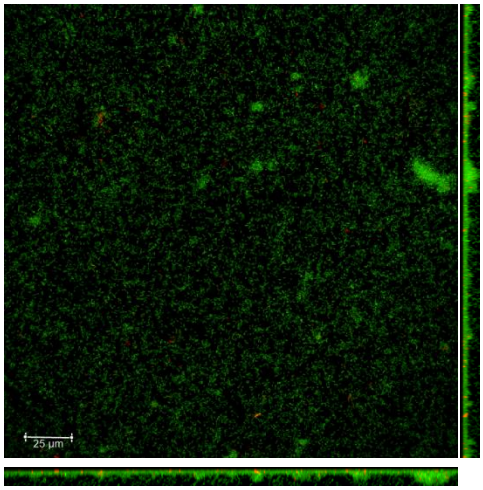


**3d Δ*pa0847* biofilm Control**

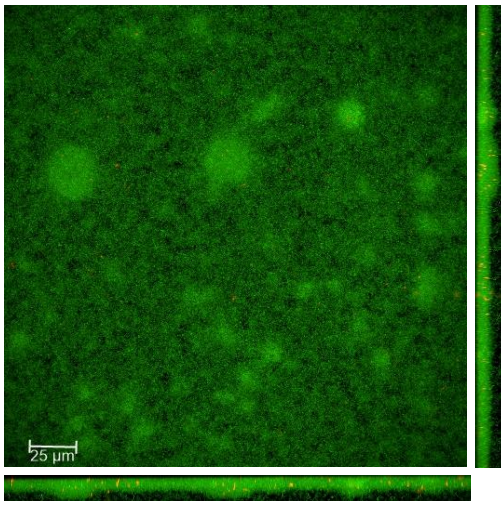


**3d Δ*pa0847* biofilm 250µM S150**

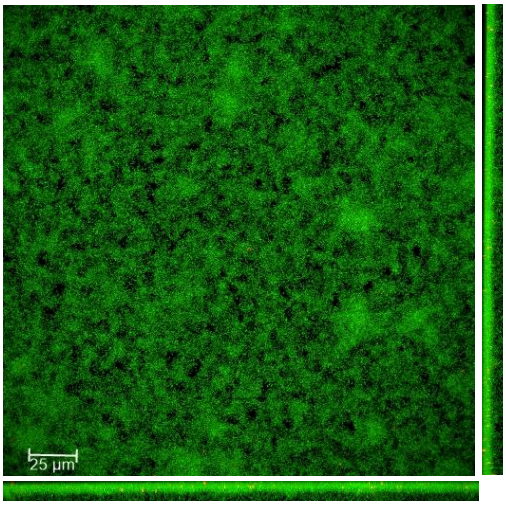


**3d Δ*rbdA* biofilm Control**

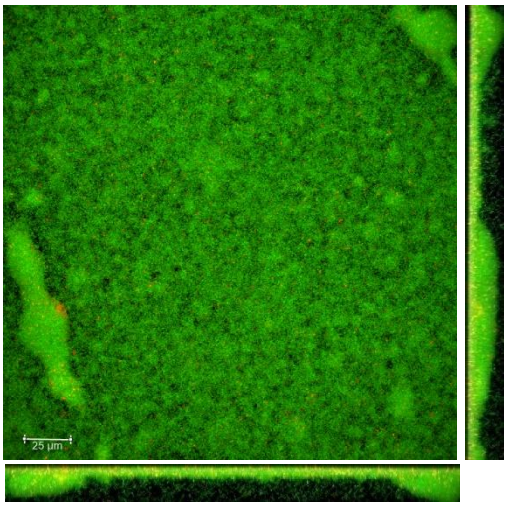


**3d Δ*rbdA* biofilm 250µM S150**

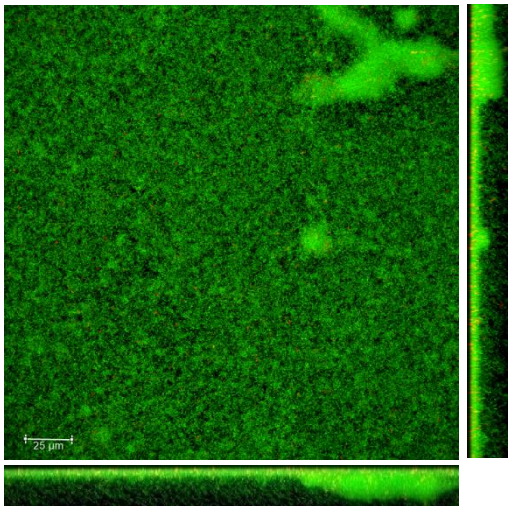

**3d Δ*yegE* biofilm Control**

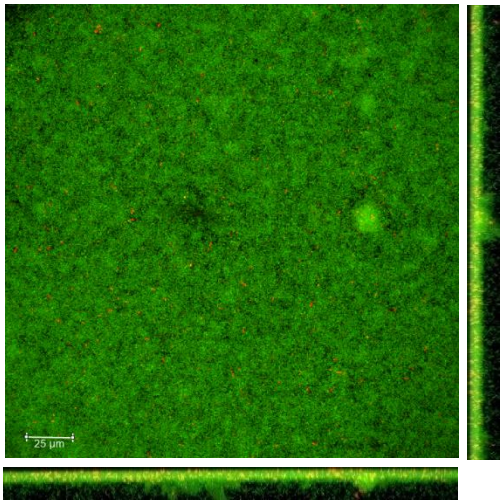


**3d Δ*yegE* biofilm 250µM S150**

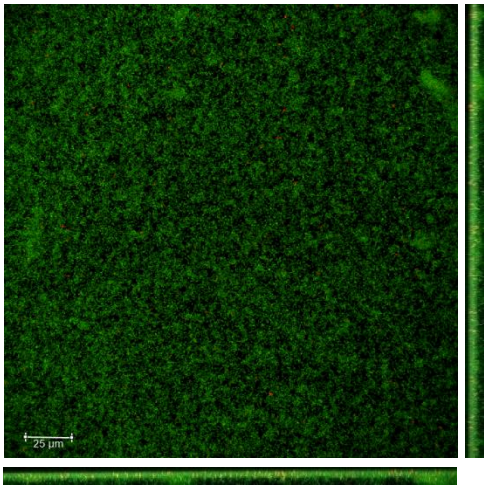


**3d Δ*bdlA* biofilm Control**

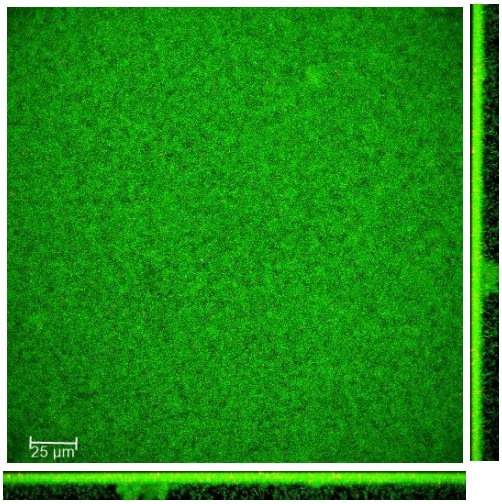


**3d Δ*bdlA* biofilm 250µM S150**

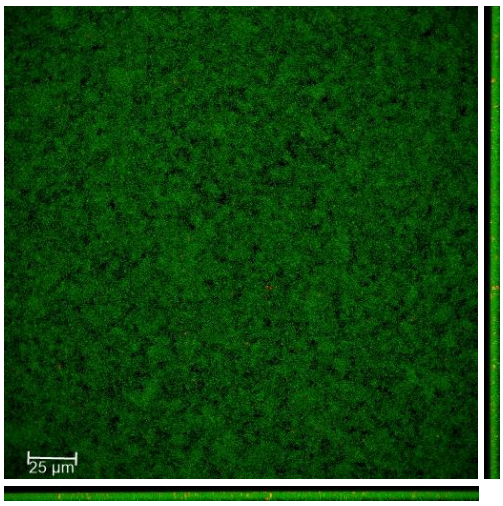


**3d Δ*mucR* biofilm Control**

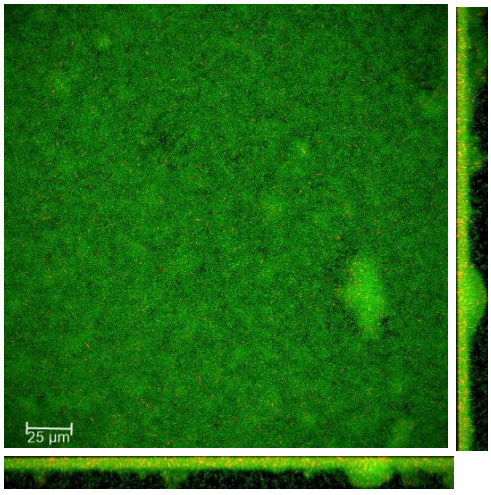


**3d Δ*mucR* biofilm 250µM S150**

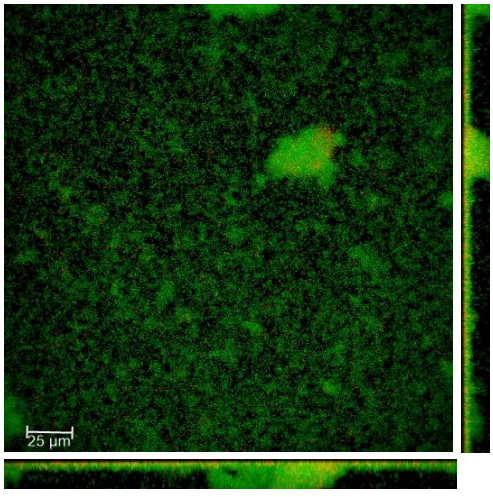

**3d Δ*nbdA* biofilm Control**

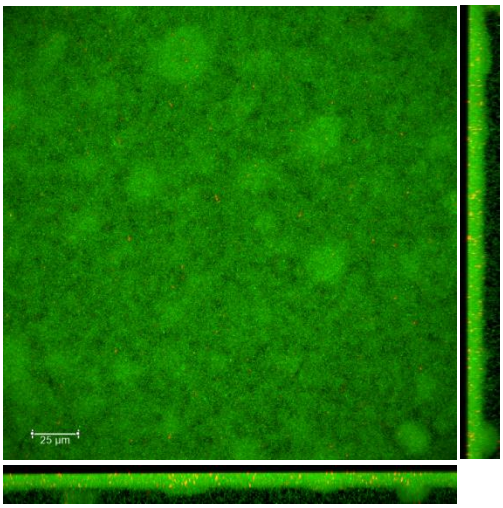


**3d Δ*nbdA* biofilm 250µM S150**

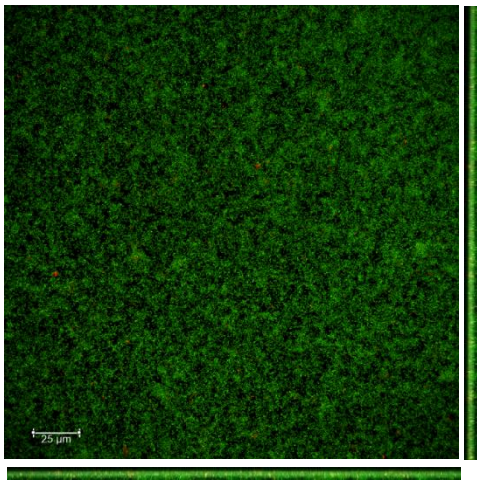


**3d Δ*morA* biofilm Control**

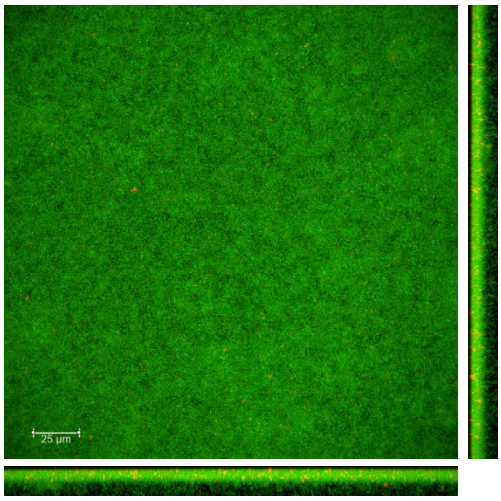


**3d Δ*morA* biofilm 250µM S150**

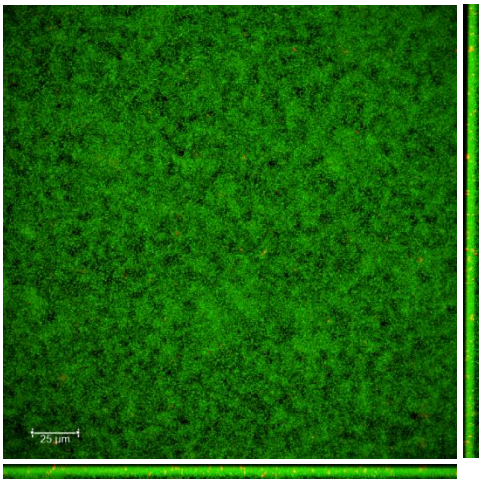


**3d Δ*fimX* biofilm Control**

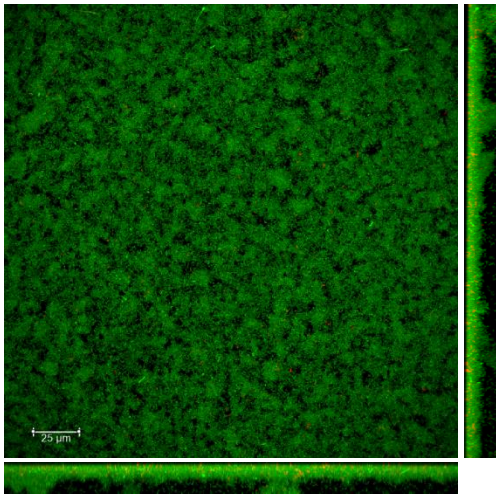


**3d Δ*fimX* biofilm 250µM S150**

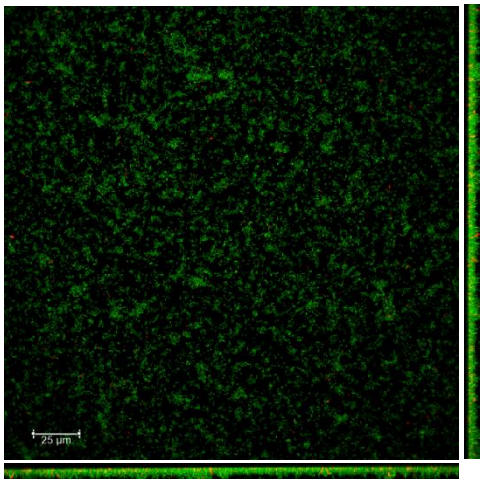

**3d Δ*dipA* biofilm Control**

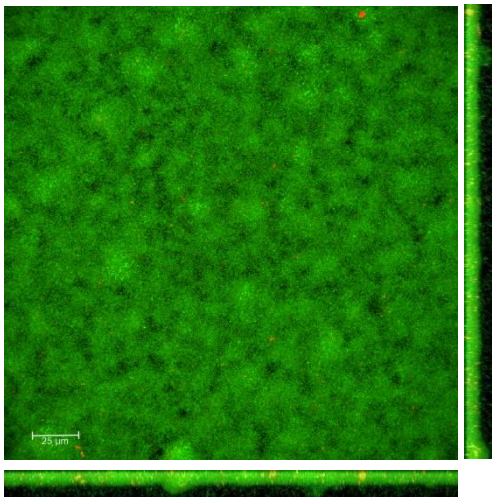


**3d Δ*dipA* biofilm 250µM S150**

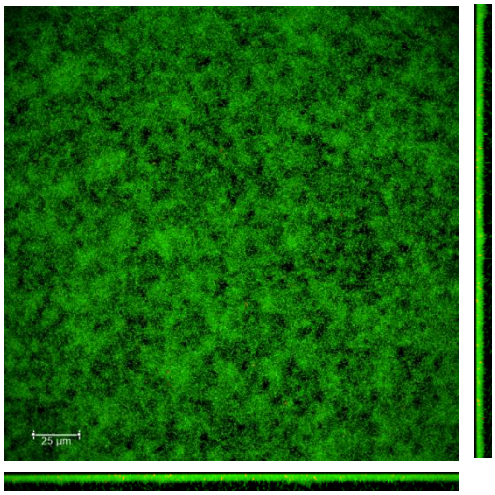


**3d Δ*pa5442* biofilm Control**

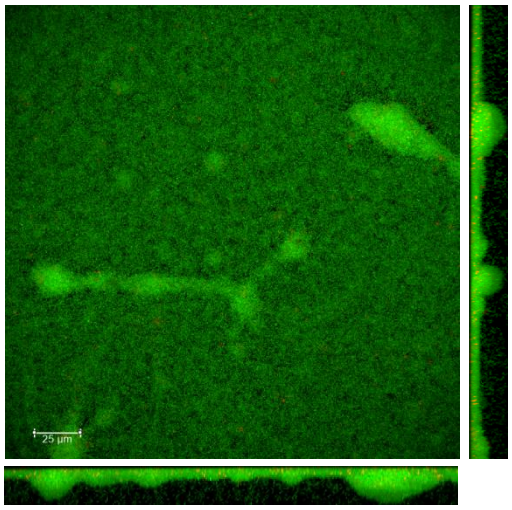


**3d Δ*pa5442* biofilm 250µM S150**

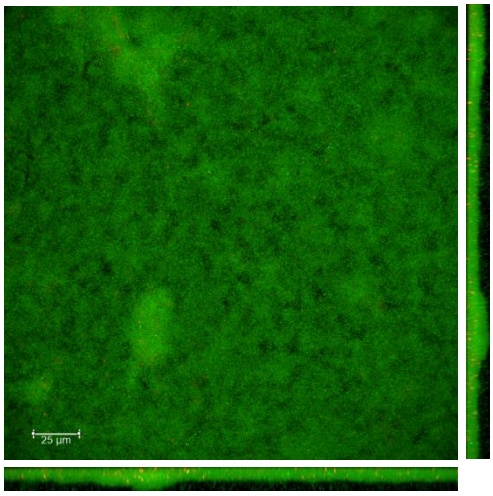


Fig A11. Selective CLSM images of 3 d old KO mutants' biofilms treated with 250µM S150.

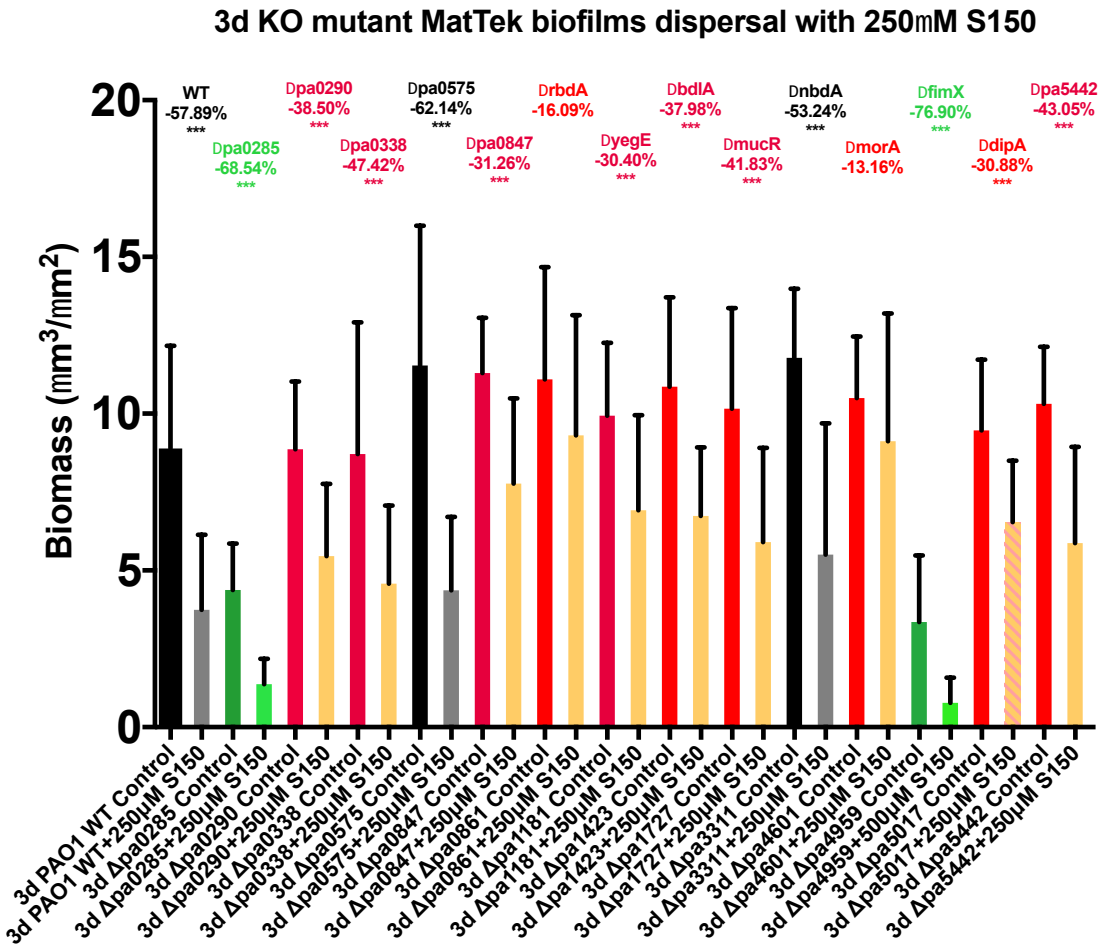


Fig A12. Dispersal effect of 2 hrs 250µM S150 treatment on 3 d old KO mutant biofilms in MatTek plates. Welch T-test was carried out to compare the treated and non-treated groups. Decrease percentages are marked above the bars. Data represents data means of n=6 of 3 biological replicates. *** represents $p<0.01$, ** represents $0.01<p<0.05$.

**A**

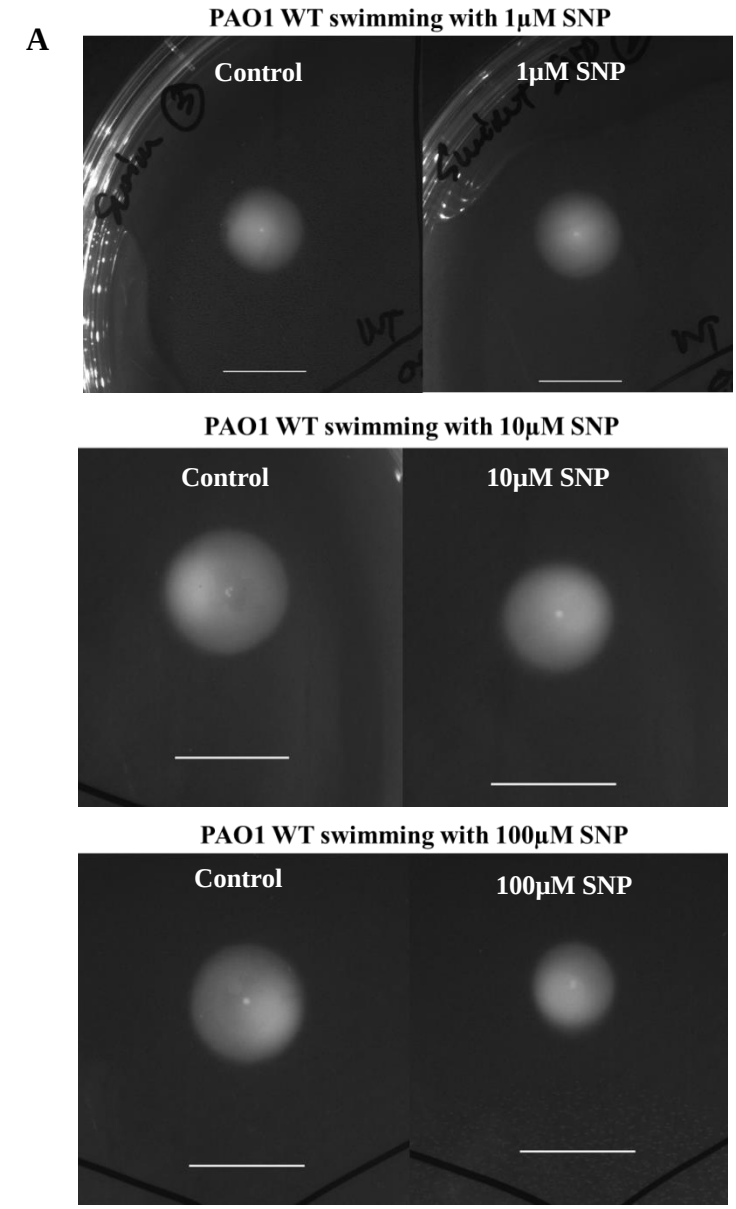
PAO1 WT swimming with 1µM SNP
Control
1µM SNP
PAO1 WT swimming with 10µM SNP
Control
10µM SNP
PAO1 WT swimming with 100µM SNP
Control
100µM SNP

**B**

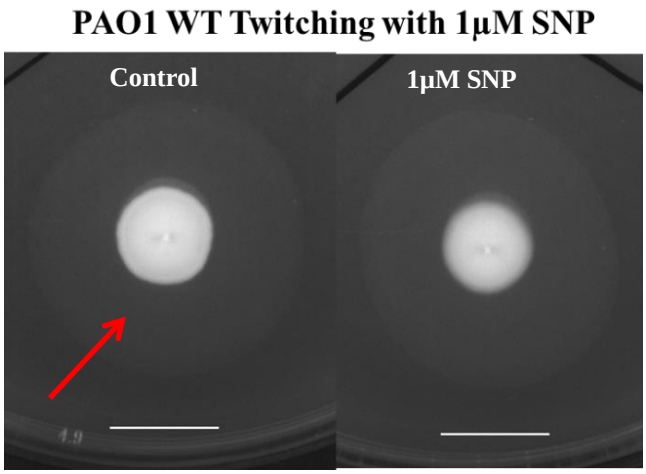
PAO1 WT Twitching with 1µM SNP
Control
1µM SNP

PAO1 WT Twitching with 10µM SNP

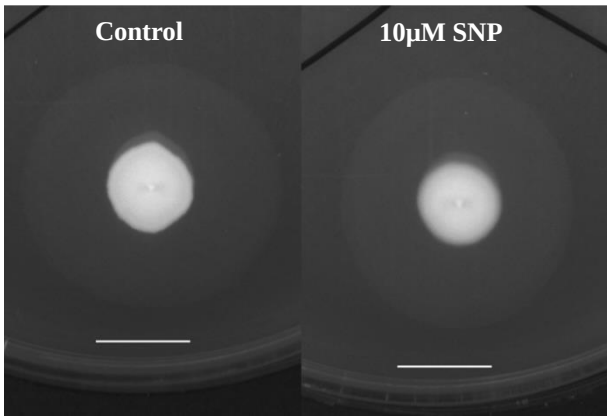


PAO1 WT Twitching with 100µM SNP

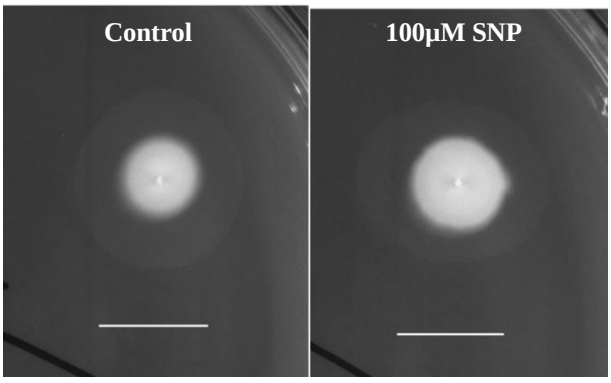


C

PAO1 WT Swarming with 1µM SNP

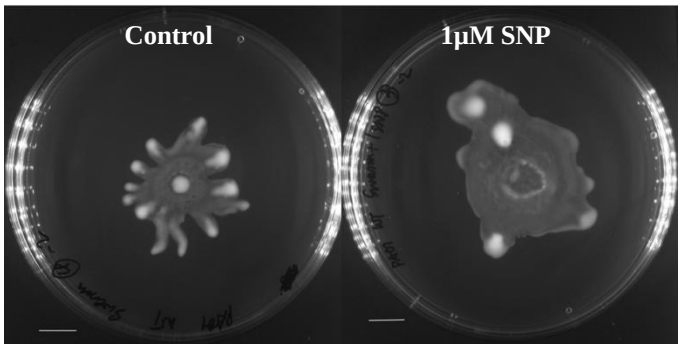


PAO1 WT Swarming with 10µM SNP

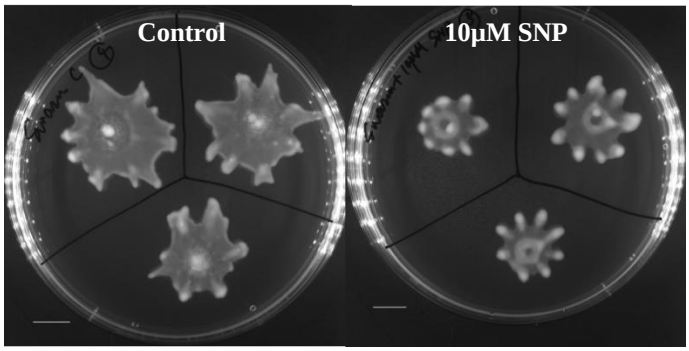

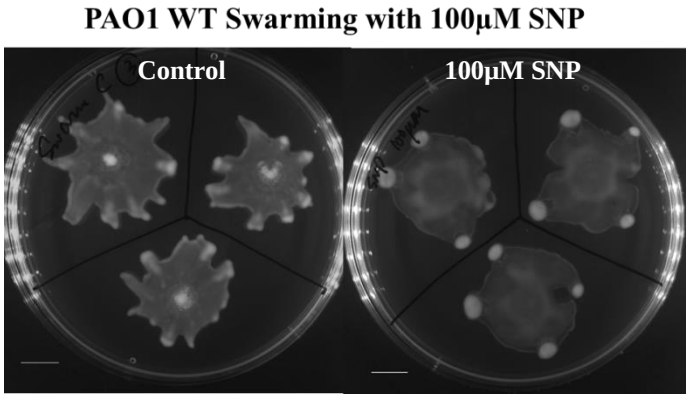
PAO1 WT Swarming with 100µM SNP
Control
100µM SNP

**D**

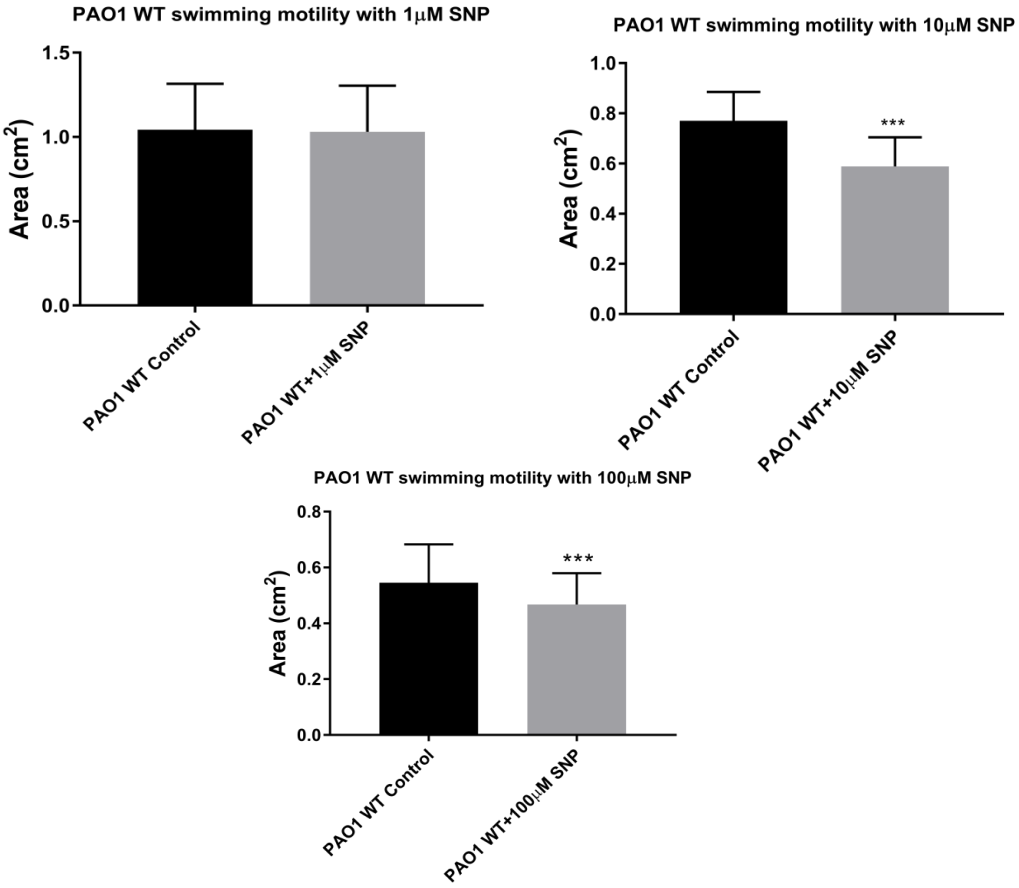
PAO1 WT swimming motility with 1µM SNP
Area (cm2)
1.5
1.0
0.5
0.0
PAO1 WT Control
PAO1 WT+1µM SNP
PAO1 WT swimming motility with 10µM SNP
Area (cm2)
1.0
0.8
0.6
0.4
0.2
0.0
***
PAO1 WT Control
PAO1 WT+10µM SNP
PAO1 WT swimming motility with 100µM SNP
Area (cm2)
0.8
0.6
0.4
0.2
0.0
***
PAO1 WT Control
PAO1 WT+100µM SNP

**E**

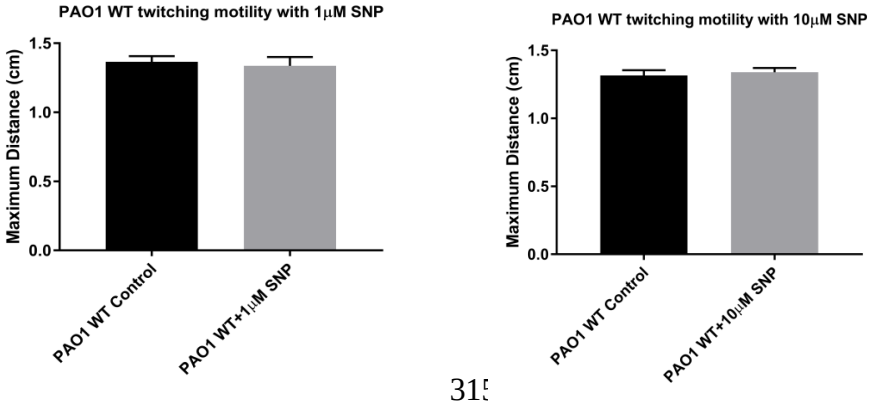
PAO1 WT twitching motility with 1µM SNP
Maximum Distance (cm)
1.5
1.0
0.5
0.0
PAO1 WT Control
PAO1 WT+1µM SNP
PAO1 WT twitching motility with 10µM SNP
Maximum Distance (cm)
1.5
1.0
0.5
0.0
PAO1 WT Control
PAO1 WT+10µM SNP

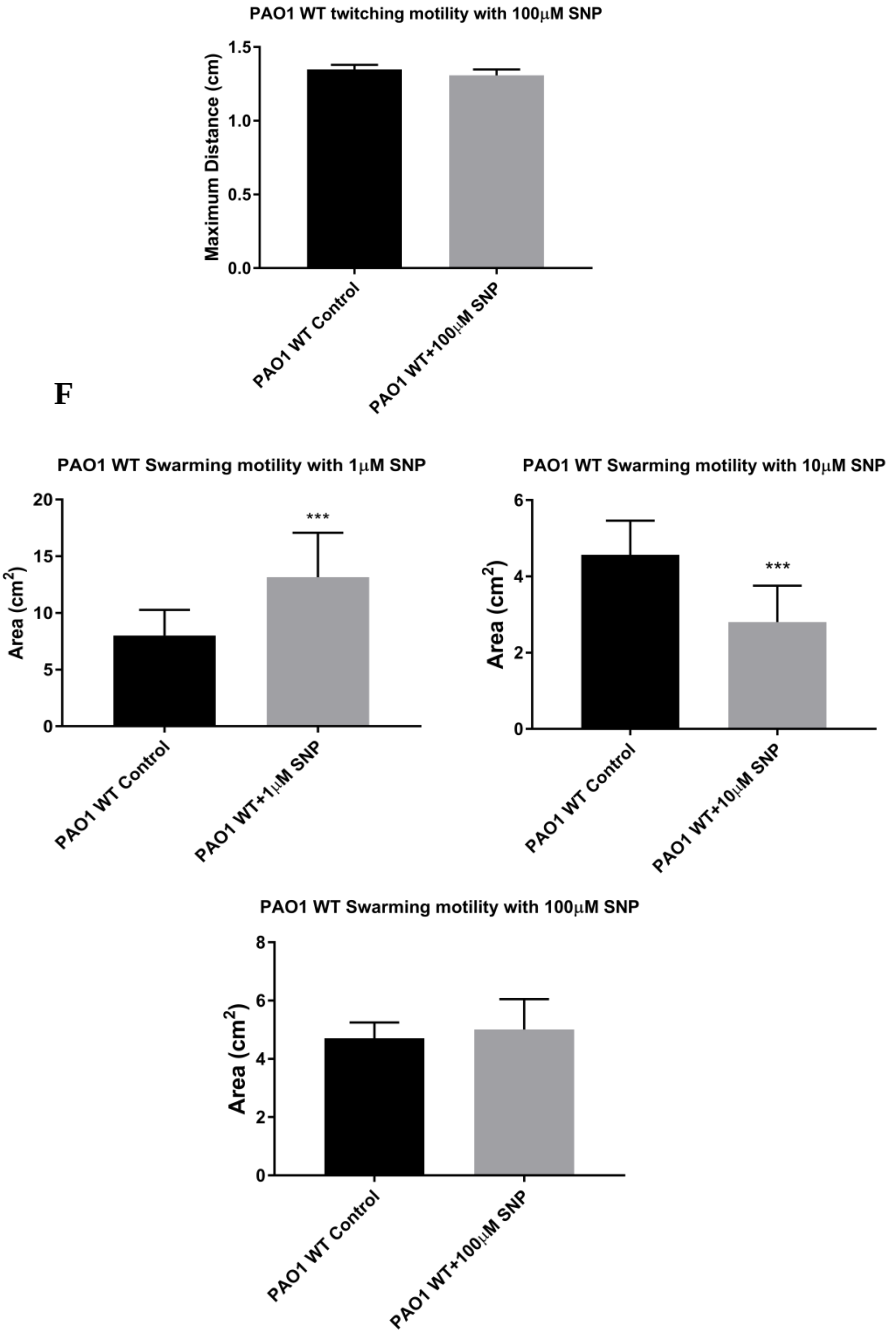


Fig A13 (A)-(C) Selective images of PAO1 WT swimming, swarming and twitching motility agar plates with/without SNP. Twitching zone is the semi-transparent area marked with red arrow. (D) Measurement of swimming zone areas of PAO1 WT with/without SNP using Image J. n=12 from individual plates, Welch T-test was applied due to large variations. *** represents $p<0.01$, ** represents $0.01<p<0.05$. (E) Measurement of twitching zone maximum distance of PAO1 WT with/without SNP using Image J. Maximum distance was applied due to the limitation of software in distinguish twitching zone. n=12 from individual plates, Welch T-test was applied due to large variations. *** represents $p<0.01$, ** represents $0.01<p<0.05$. (F) Measurement of swarming zone areas of PAO1 WT with/without SNP using Image J. n=12 from individual plates, Welch T-test was applied due to large variations. *** represents $p<0.01$, ** represents $0.01<p<0.05$.

**A**

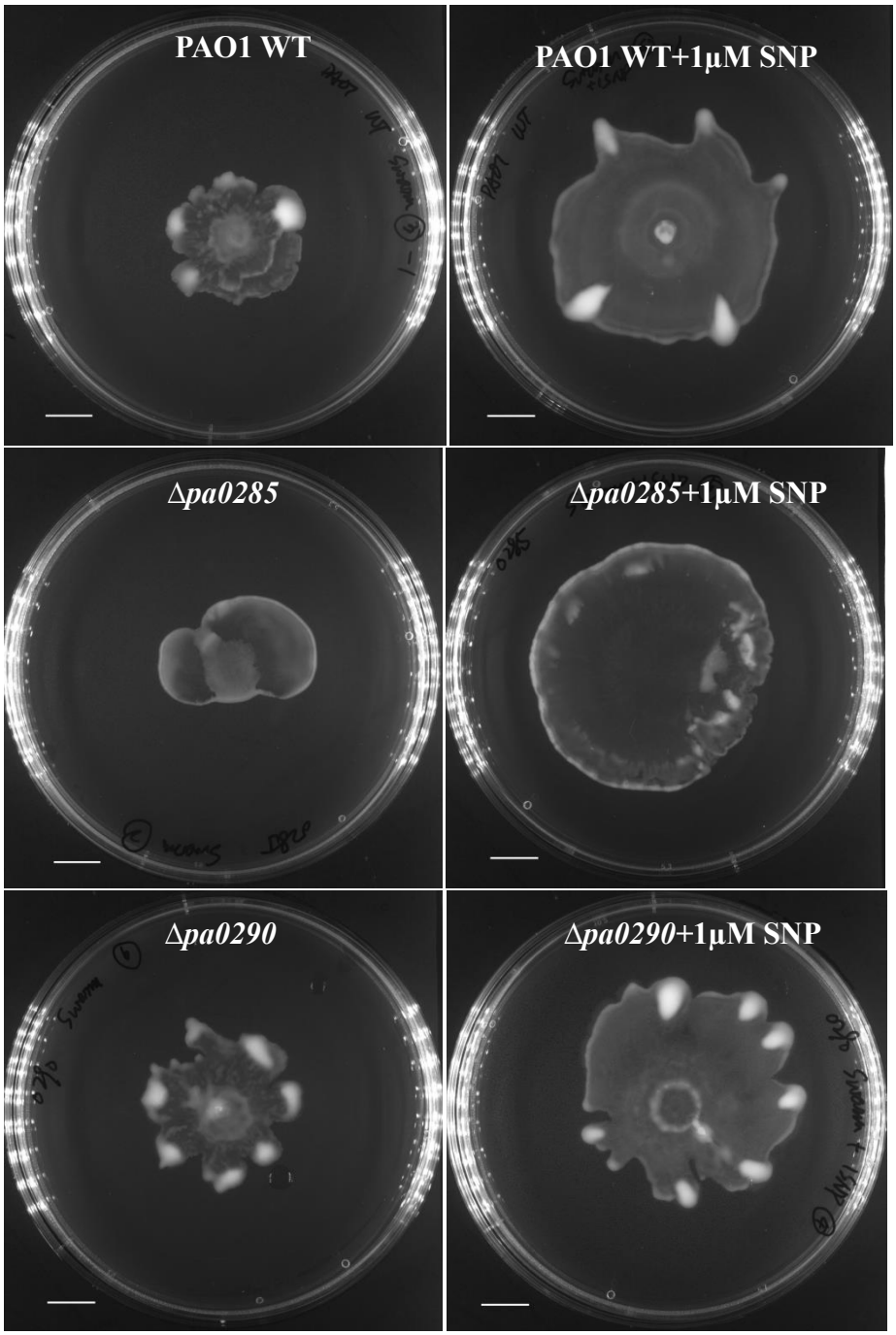
PAO1 WT
PAO1 WT+1μM SNP
Δpa0285
Δpa0285+1μM SNP
Δpa0290
Δpa0290+1μM SNP

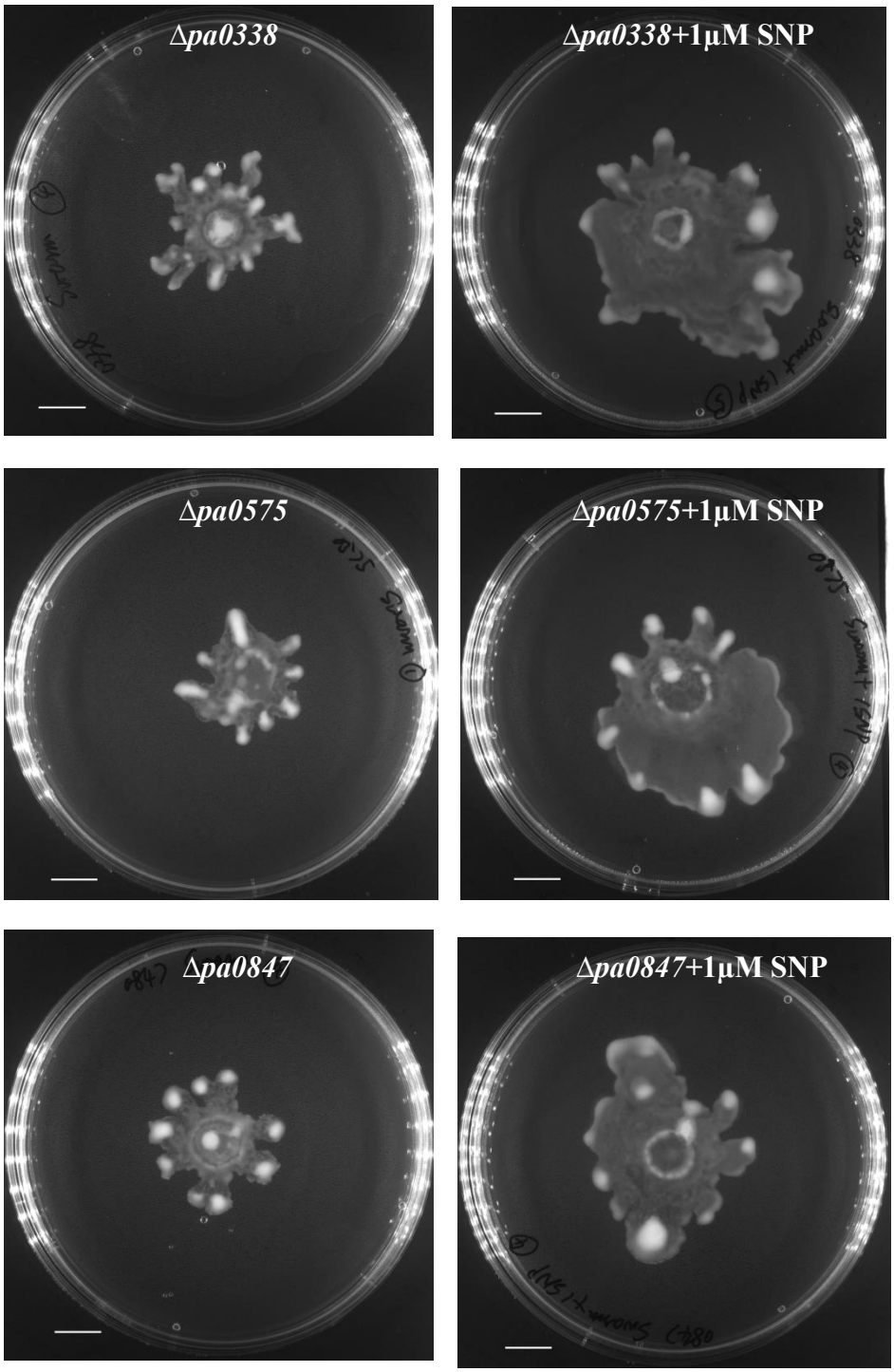
Δpa0338
Δpa0338+1μM SNP
Δpa0575
Δpa0575+1μM SNP
Δpa0847
Δpa0847+1μM SNP

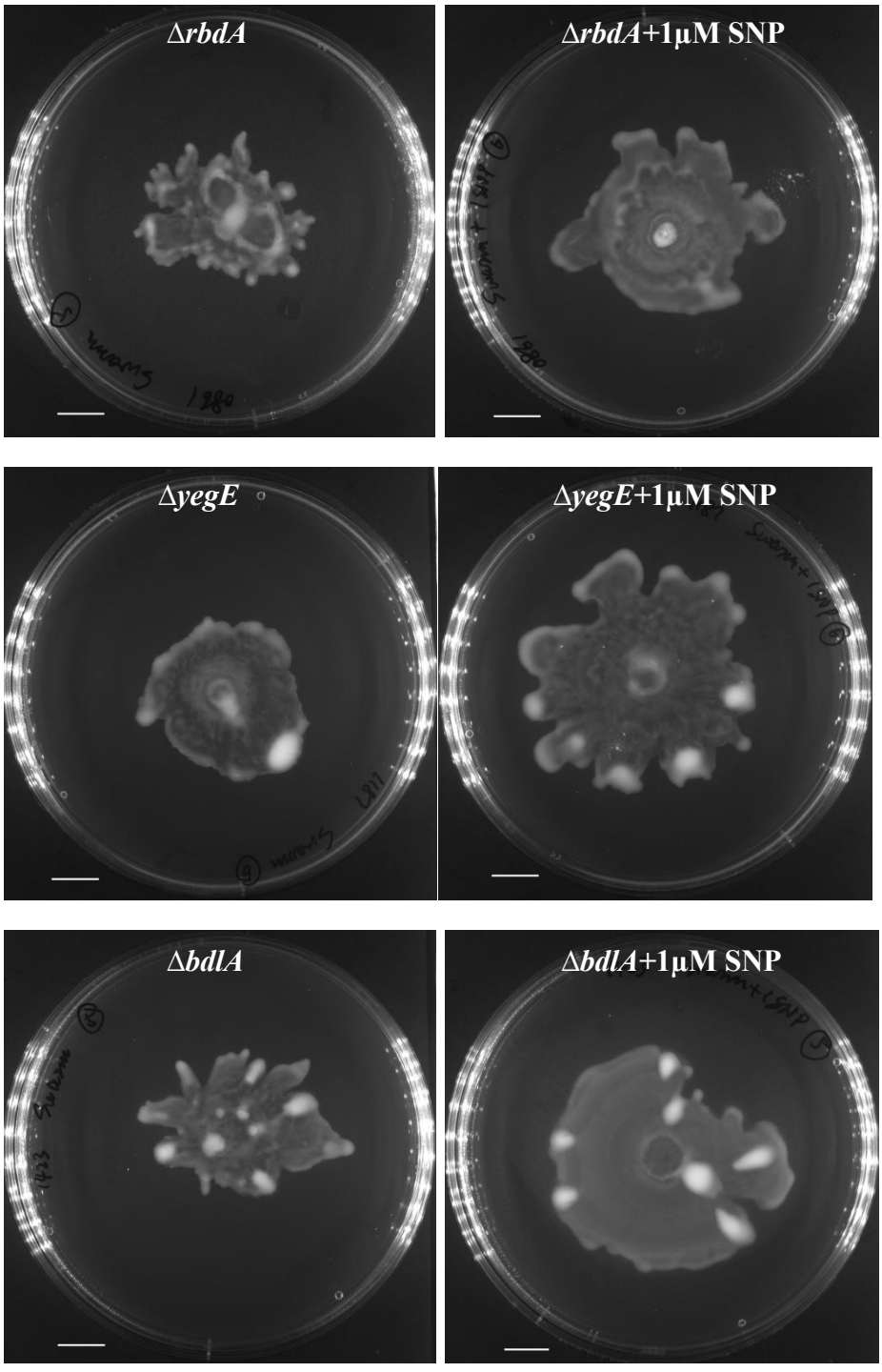
Δ*rbdA*
Δ*rbdA*+1μM SNP
Δ*yegE*
Δ*yegE*+1μM SNP
Δ*bdlA*
Δ*bdlA*+1μM SNP

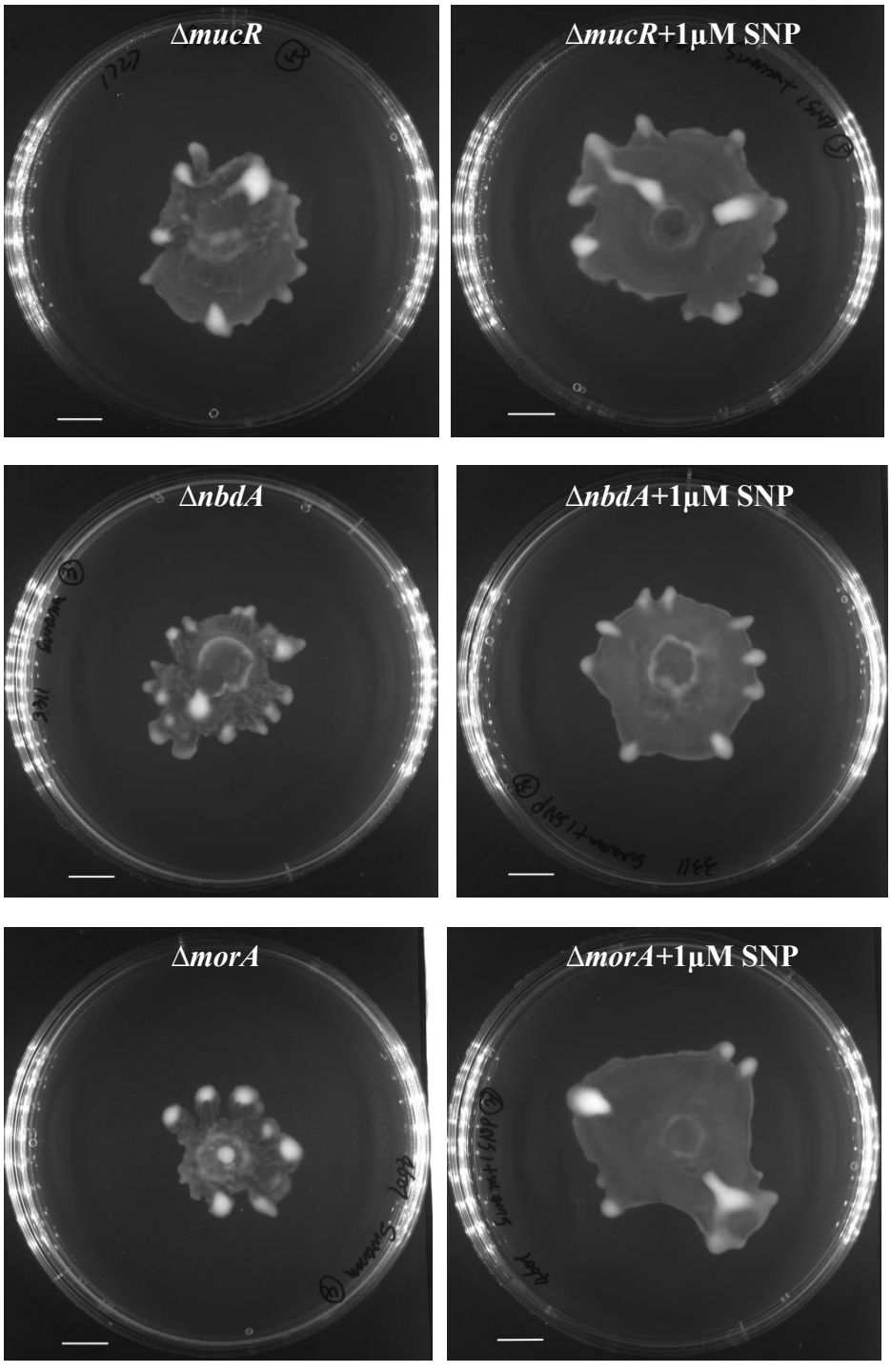
Δ*mucR*
Δ*mucR*+1μM SNP
Δ*nbdA*
Δ*nbdA*+1μM SNP
Δ*morA*
Δ*morA*+1μM SNP

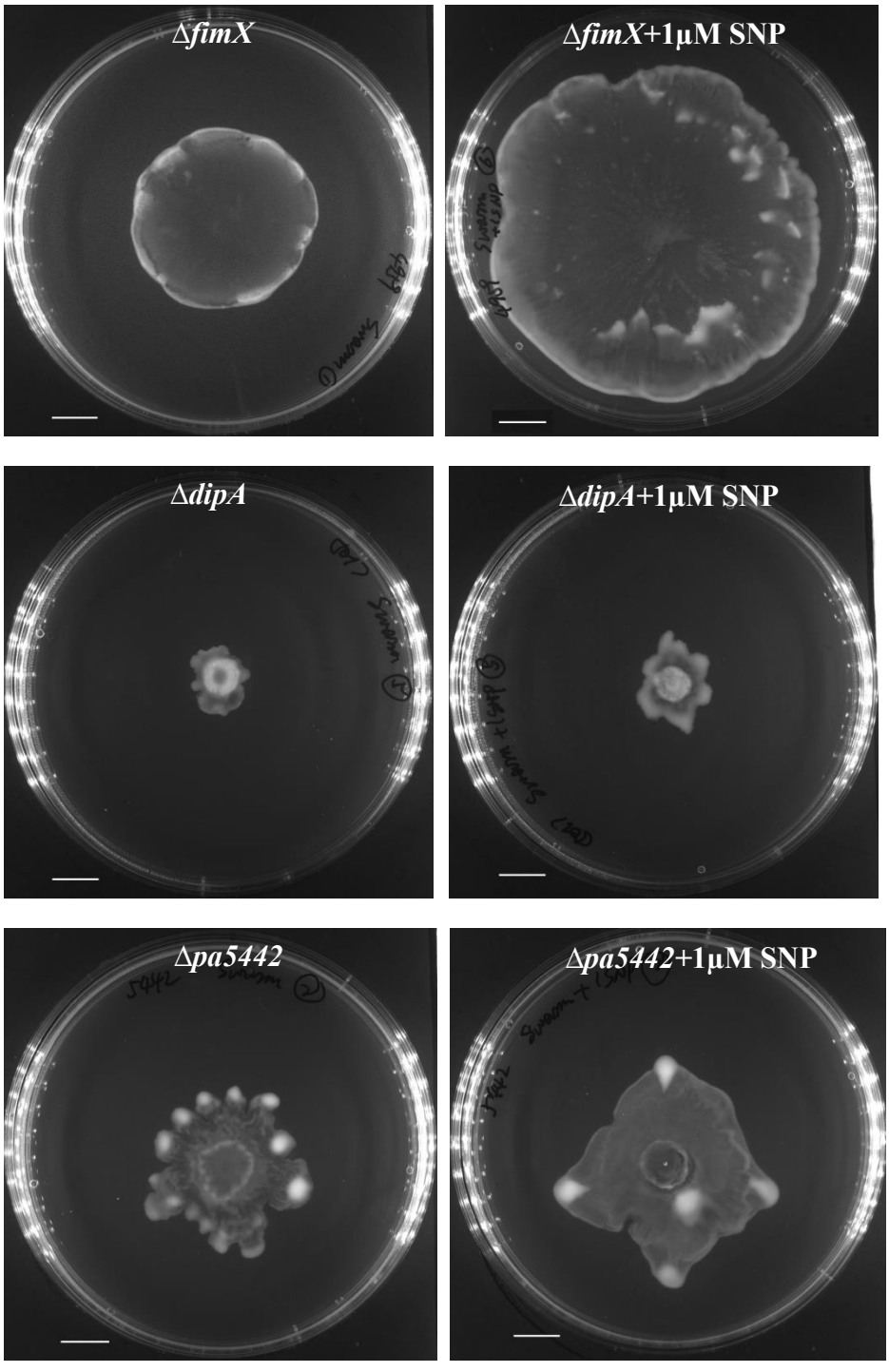
Δ*fimX*
Δ*fimX*+1μM SNP
Δ*dipA*
Δ*dipA*+1μM SNP
Δ*pa5442*
Δ*pa5442*+1μM SNP

**B**

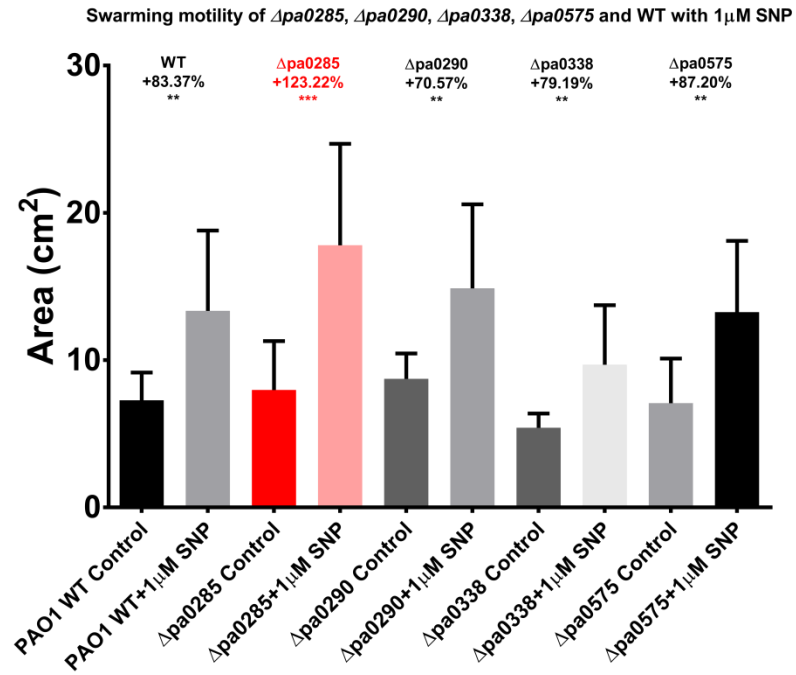
Swarming motility of Δpa0285, Δpa0290, Δpa0338, Δpa0575 and WT with 1μM SNP
WT
+83.37%
**
Δpa0285
+123.22%
***
Δpa0290
+70.57%
**
Δpa0338
+79.19%
**
Δpa0575
+87.20%
**
Area (cm2)
30
20
10
0
PAO1 WT Control
PAO1 WT+1μM SNP
Δpa0285 Control
Δpa0285+1μM SNP
Δpa0290 Control
Δpa0290+1μM SNP
Δpa0338 Control
Δpa0338+1μM SNP
Δpa0575 Control
Δpa0575+1μM SNP

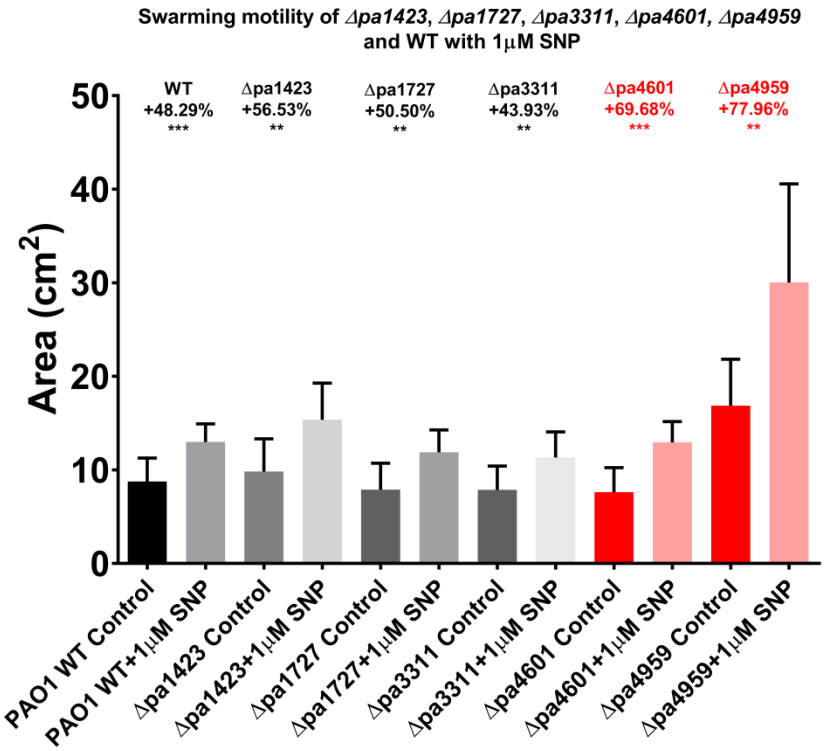
Swarming motility of Δpa1423, Δpa1727, Δpa3311, Δpa4601, Δpa4959
and WT with 1μM SNP
WT
+48.29%
***
Δpa1423
+56.53%
**
Δpa1727
+50.50%
**
Δpa3311
+43.93%
**
Δpa4601
+69.68%
***
Δpa4959
+77.96%
**
Area (cm2)
50
40
30
20
10
0
PAO1 WT Control
PAO1 WT+1μM SNP
Δpa1423 Control
Δpa1423+1μM SNP
Δpa1727 Control
Δpa1727+1μM SNP
Δpa3311 Control
Δpa3311+1μM SNP
Δpa4601 Control
Δpa4601+1μM SNP
Δpa4959 Control
Δpa4959+1μM SNP

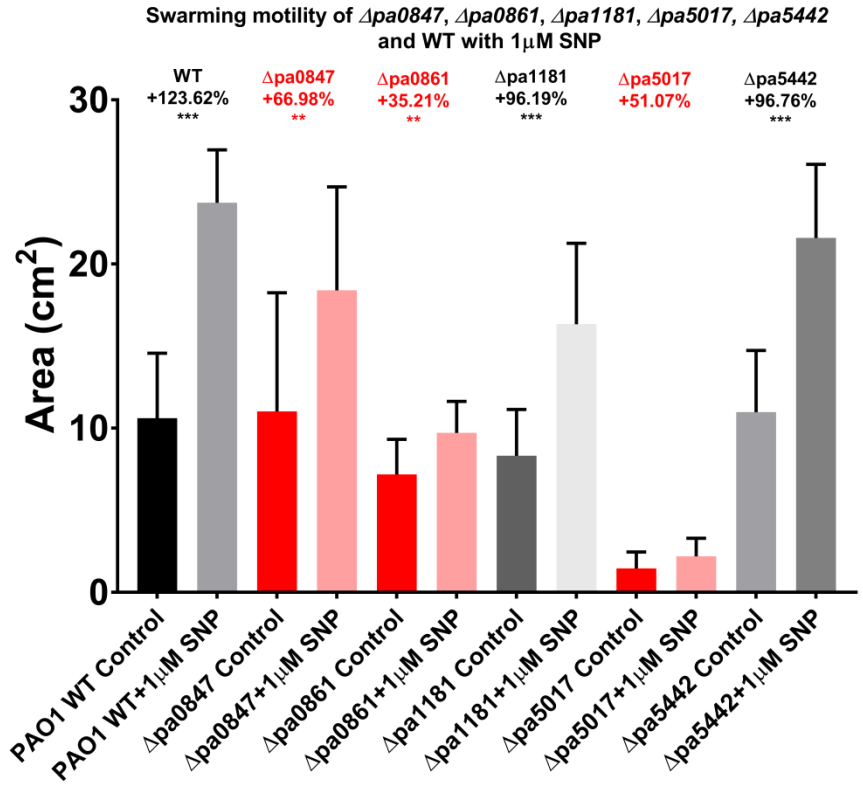


Fig A14 (A) Selective images of KO mutants swarming agar plates with/without SNP. Scale bar = 1cm. (B) Measurement of swarming zone area of KO mutants with/without 1μM SNP using Image J. Due to the widely accepted inconsistency and less reproducibility of swarming assay, 5 KO strains plus one WT were inoculated into the same batch of agar plates resourced from the same bottle of agar and pouring procedures. Data shown in bar graphs were therefore grouped based on the 5 KO strains used together and compared to the WT within the same batch. It can be found that even for PAO1 WT, different batches led to different results. n=6 from individual plates, Welch T-test was applied to compare SNP treatment groups with control due to large variations. *** represents $p<0.01$, ** represents $0.01<p<0.05$. Swarming areas increase percentages were marked above bars.

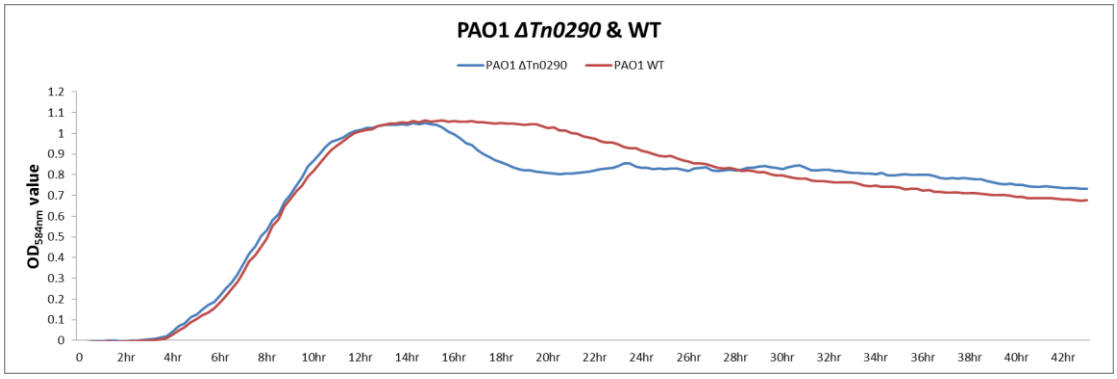

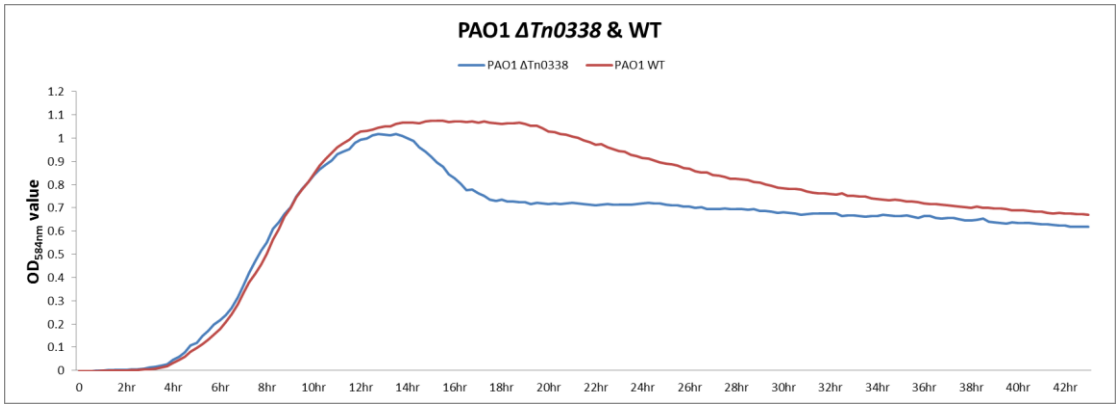
PAO1 ΔTn0338 & WT
PAO1 ΔTn0338
PAO1 WT
OD584nm value
0 0.1 0.2 0.3 0.4 0.5 0.6 0.7 0.8 0.9 1 1.1 1.2
0 2hr 4hr 6hr 8hr 10hr 12hr 14hr 16hr 18hr 20hr 22hr 24hr 26hr 28hr 30hr 32hr 34hr 36hr 38hr 40hr 42hr

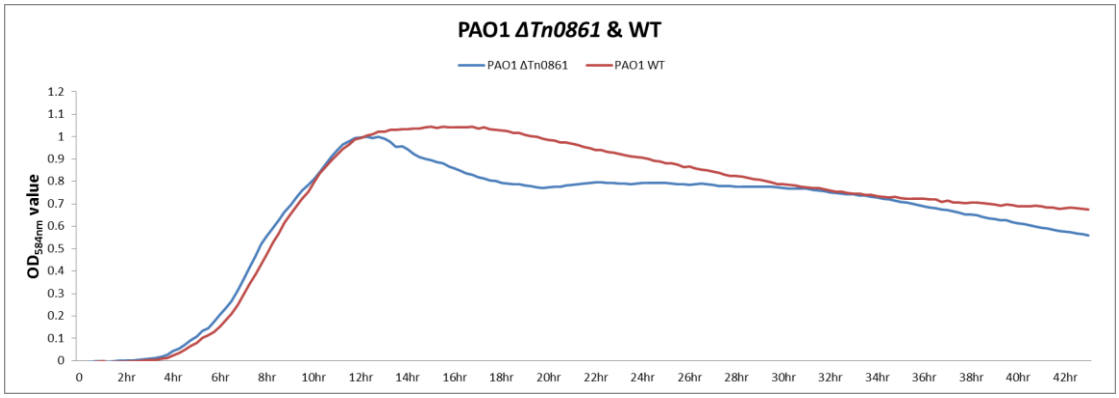
PAO1 ΔTn0861 & WT
PAO1 ΔTn0861
PAO1 WT
OD584nm value
0 0.1 0.2 0.3 0.4 0.5 0.6 0.7 0.8 0.9 1 1.1 1.2
0 2hr 4hr 6hr 8hr 10hr 12hr 14hr 16hr 18hr 20hr 22hr 24hr 26hr 28hr 30hr 32hr 34hr 36hr 38hr 40hr 42hr

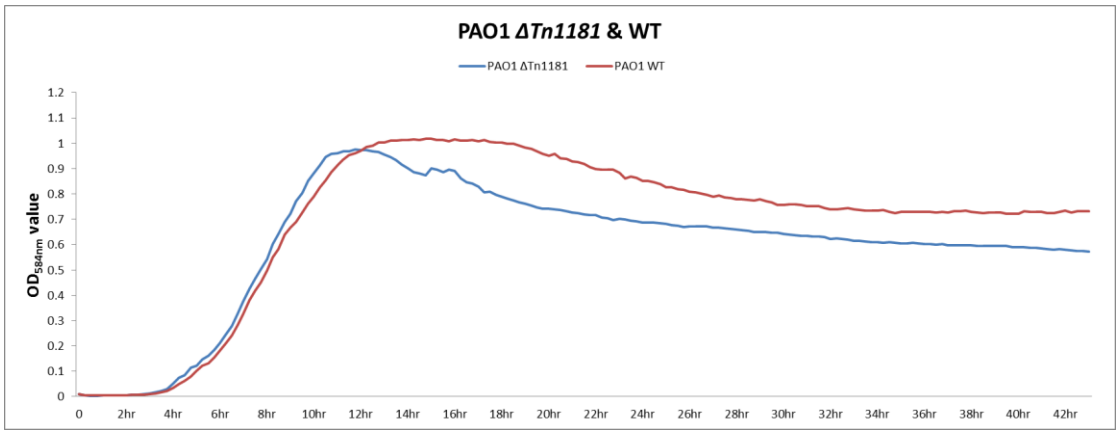
PAO1 ΔTn1181 & WT
PAO1 ΔTn1181
PAO1 WT
OD584nm value
0 0.1 0.2 0.3 0.4 0.5 0.6 0.7 0.8 0.9 1 1.1 1.2
0 2hr 4hr 6hr 8hr 10hr 12hr 14hr 16hr 18hr 20hr 22hr 24hr 26hr 28hr 30hr 32hr 34hr 36hr 38hr 40hr 42hr

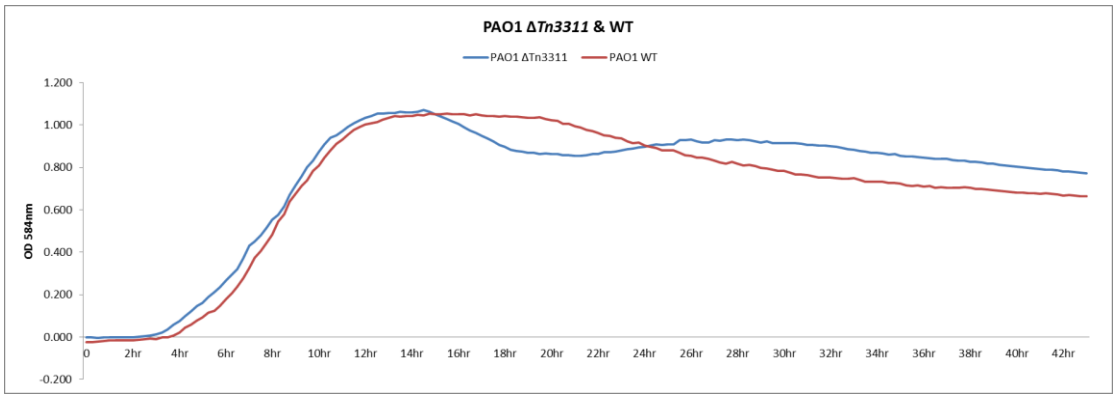
PAO1 ΔTn3311 & WT
PAO1 ΔTn3311
PAO1 WT
OD 584nm
-0.200 0.000 0.200 0.400 0.600 0.800 1.000 1.200
0 2hr 4hr 6hr 8hr 10hr 12hr 14hr 16hr 18hr 20hr 22hr 24hr 26hr 28hr 30hr 32hr 34hr 36hr 38hr 40hr 42hr

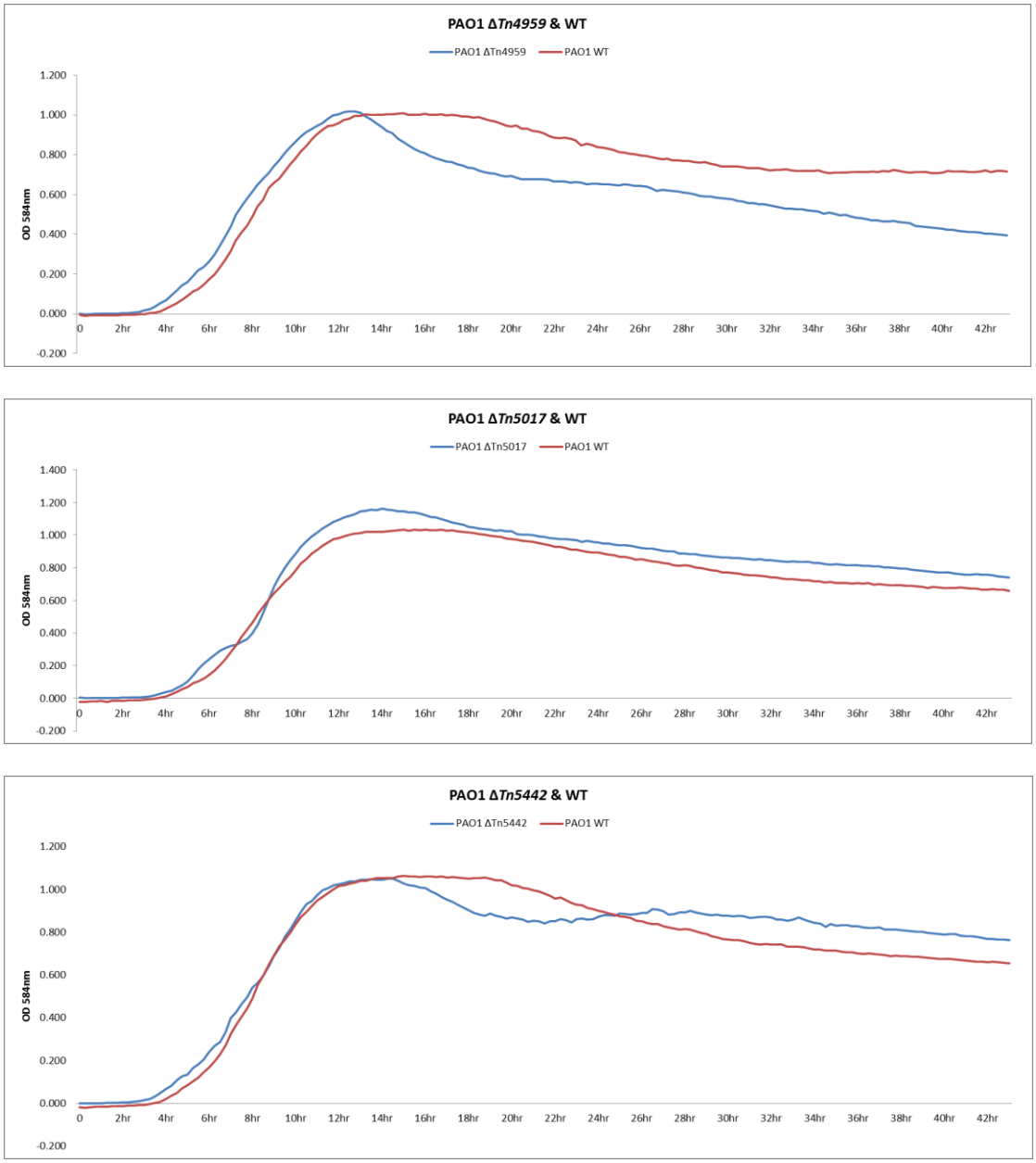


Fig A15. Growth curves of PAO1 WT and Tn mutants

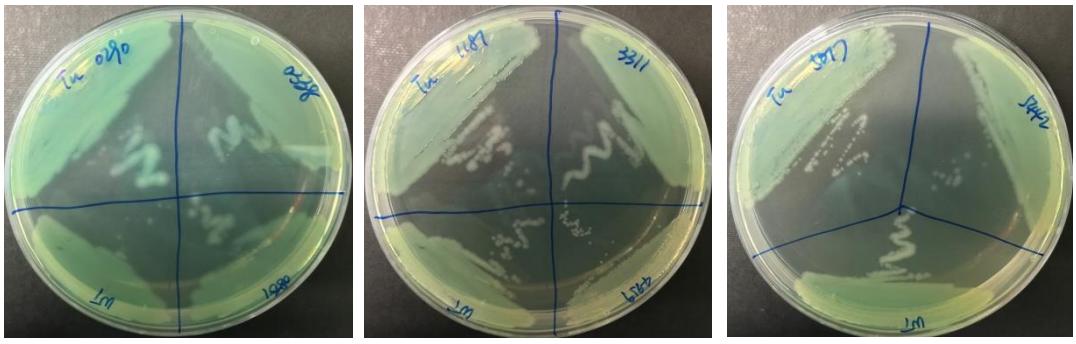

Fig A16. *P. aeruginosa* PAO1 Tn mutants on Cetrimide agar plates. Plates were incubated at 37℃ for 24 hrs.

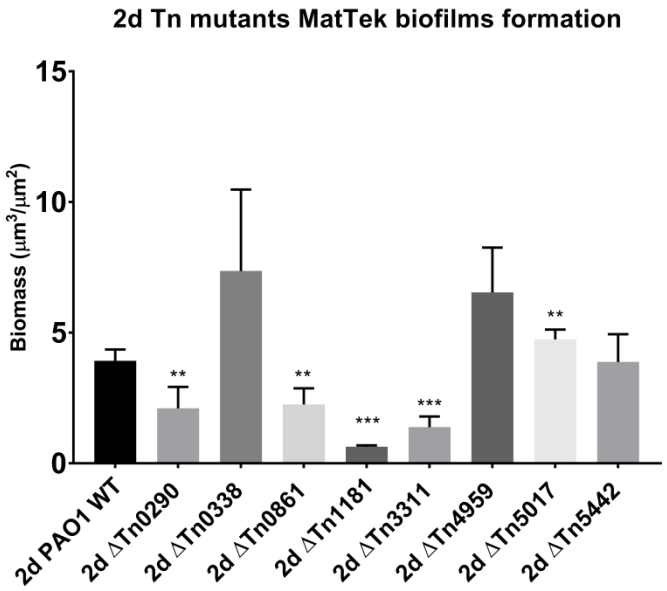


Fig A17. Comparison of biofilm formation abilities of different Tn strains in MatTek plates after 2 d. Welch T-test was carried out to compare the PAO1 WT and Tn mutants. n=3 biological replicates. *** represents $p<0.01$, ** represents $0.01<p<0.05$.